

https://dspace.org/

An in-silico analysis of the glycosylation inhibitors Brefeldin A and Tunicamycin C in colorectal cancer; characterization of novel targets

Naidoo, Vivash

2024

University of the Witwatersrand, Johannesburg

https://hdl.handle.net/10539/43508

Naidoo, Vivash. (2024). An in-silico analysis of the glycosylation inhibitors Brefeldin A and Tunicamycin C in colorectal cancer; characterization of novel targets [PhD thesis, University of the Witwatersrand, Johannesburg].WireDSpace.https://hdl.handle.net/10539/43508

Downloaded from a DSpace repository. https://dspace.org/



An *in-silico* analysis of the glycosylation inhibitors Brefeldin A and Tunicamycin C in colorectal cancer; characterization of novel targets

Vivash Naidoo

Student number: 1353730

Thesis

submitted in fulfilment of the requirements for the degree of a

Doctor of Philosophy

in

Internal Medicine

Faculty of Health Science, University of the Witwatersrand

Johannesburg, South Africa

Supervisor: Prof Clement Penny

Co-Supervisor: Dr Sheefa Mirza

Co-Supervisor: Dr Rodney Hull

2 April 2024

Declaration

I declare that this dissertation is my own unaided work. It is being submitted for the Degree of Doctor of Philosophy in Internal Medicine at the University of the Witwatersrand, Johannesburg. It has not been submitted before for any degree or examination at any other University.



the day of 02-04- 2024

Dedication

This work is dedicated to my late parents Mr. Abboyi Naidoo (Dad) and Mrs. Latchmy Naidoo (Mom) for their courage, knowledge, and wisdom.

Conferences and Workshops

Poster presentation An *In Silico* Investigation of the Anti-Cancer Potential of Brefeldin A and Tunicamycin in Colorectal Cancer
Presented at the Molecular Biosciences Research Thrust Wits (Medical School-Johannesburg) 4 November 2022

Poster presentation An *in silico* Investigation of the Novel Therapeutic Targets and Cellular Pathways Against Brefeldin A and Tunicamycin C in Colon Cancer
Presented at the American Society for Cell Biology (ASCB) Annual Meeting Washington DC,3 -7 December 2022

Poster presentation Brefeldin A and Tunicamycin C A simulated investigation of the therapeutic targets and Cellular Pathways in Colon Cancer
Presented at the Pan African Cancer Research Institute (PACRI) International Cancer Conference, University Pretoria, 26 February- 1 March 2023

Poster presentation Virtual Screening and Molecular Dynamic Simulations of Tunicamycin C as Glycosylation Inhibitor in Colorectal Cancer
Presented at the School of Clinical Medicine SOCM Biennial Research Day, University of the Witwatersrand, Faculty of Health Sciences, 28 September 2023

Publications in Review

Naidoo V, Mirza S, Hull R, Kandhavelu J, Achilonu I, Chihomvu P and Penny C. Computational modeling of Tunicamycin C interaction with potential protein targets: perspectives from inverse docking cum molecular dynamic simulation. (Submitted in Journal of Biomolecular Structure and Dynamics (IF – 4.4)

Naidoo V, Mirza S, Hull R, Kandhavelu J, Achilonu I, Chihomvu P and Penny C. An Evaluation of the Interaction of Brefeldin A with Mitogen-Activated Protein Kinase (MAPK) and Protein Kinase C (PrKC1): Insights from Inverse Docking and Molecular Dynamics Simulation. (Will be submitted in Current Issues in Molecular Biology (IF- 3.1)

Naidoo V, Mirza S, Hull R, Chihomvu P and Penny C. Exploring the Role of Glycosylation in the Pathogenesis and Progression of Colorectal Cancer. (Will be submitted in Frontiers in Oncology (IF- 4.7)

Abstract

Colorectal cancer (CRC), a prevalent malignancy in South Africa, is significantly influenced by posttranslational modifications such as glycosylation. This study investigates the complex interactions between genes, signalling pathways, and cellular processes involved in CRC progression and glycosylation. The glycosylation inhibitors, Tunicamycin and Brefeldin A, are known to hinder colon cancer cell proliferation, migration, and invasion, making them potential therapeutic agents. We used Swiss Target Prediction Software to identify target proteins for both compounds and revealed that Protein Kinase C Alpha (PRKCA), Peroxisome Proliferator-Activated Receptor Gamma (PPARG), and Mitogen-Activated Protein Kinase 1 (MAP2K1) are specific for Brefeldin A, and TK1 and PRKCA for Tunicamycin, respectively. These proteins were selected based on their potential role in the glycosylation process and their role in CRC-related pathways. Further, Kyoto Encyclopedia of Genes and Genomes (KEGG) pathway analysis disclosed significantly enriched pathways, including Epstein-Barr virus infection, cellular senescence, and cancer pathways. The 3D-crystallographic structures of PrKC1 (PDB ID 6ar4), TK1 (PDB ID 1w4r), PrCK1 (PDB ID: 6ar4) and MAPK (PDB ID: 3eqc) were retrieved from RCSB Protein Data Bank. The compounds BSP and EGCG were downloaded from PubChem. All non-relevant co-crystallized molecules, including ions, crystallographic water, and others, were removed. Missing residues in the proteins were filled in using the MODELLER algorithm on the UCSF Chimera Graphic User Interface. Molecular docking of Tunicamycin C and Brefeldin A was performed with UCSF Chimera, and the docked conformations were visualised in Maestro and Chimera.

The complexes with the top docking scores were selected and prepared for molecular dynamics simulation studies to offer structural and dynamic perspectives on the inhibitory potential of the compounds against the target proteins. The Origin Lab software tool was used to post-analyze the docking conformations. Molecular Dynamics simulation was conducted using Graphics Processing Units version of the Particle Mesh Ewald Molecular Dynamics engine in the AMBER18 suite. Our investigation into the dynamic events leading to the proximal binding of Tunicamycin at the pockets of TK1 and PrKC1 suggested that the binding of Tunicamycin induced a conformational perturbation of the 3D structures of these proteins, resulting in a structural deviation that inhibited their activity. Tunicamycin's time-based dynamics indicated a stable pattern, leading to optimal interaction and maximal stabilization in the hydrophobic pockets of TK1 and PrKC1. Binding energy calculations showed a high-affinity interaction of Tunicamycin with these proteins.

Similarly, the structural investigation revealed that the binding of Brefeldin A to Mitogen-Activated Protein Kinase (MAPK) and Protein Kinase C (PrKC1) inhibited their activity. A detailed analysis of active site residues revealed crucial residues that contributed to the binding stabilization of Brefeldin A. It was noted that the Brefeldin A/MAPK complex produced a binding energy of -22.18±4.50Kcal/mol while the Brefeldin A/PrCK1 complex produced a binding energy of -23.90±5.36Kcal/mol. These findings provide crucial insights into designing novel inhibitors of TK1 and PrKC1, potentially blocking glycosylation progression in cancer treatment. This study underscores the potential for exploiting glycosylation inhibition as a therapeutic strategy against CRC, opening avenues to mitigate cancer progression.

Acknowledgments

I am deeply grateful for the success of this endeavor, and I attribute it to my Lord, Jesus Christ, without whom this would not have been successful. I extend my heartfelt appreciation to my esteemed supervisors: Prof. Clement Penny, Dr. Rodney Hull, Dr. Sheefa Mirza, Prof. Ikechukwu Achilonu, Dr. Patience Chihomvu, and Dr. Jeyalakshmi Kandhavelu, whose unwavering support and kindness have been invaluable throughout this journey.

Special recognition goes to Prof. Ikechukwu Achilonu of the Protein Structure-Function Research Unit (PSFRU) for his invaluable assistance in the computational aspects of my work, and to Dr. Patience Chihomvu for her continual contribution and editing of the thesis, manuscripts, motivation, and inspiration. I am also grateful to my colleagues Dr. Aurelie, Dr. Philemon Ubanako, Dr. Aadilah Omar, Prof Duarte, Dr Caroline, Dr Therese, Dr Blessing Oyiogu, Dr, Olalekan Onisuru, Dr, Kiyasha, EGO Office Abe, Denise, Thembeka Mdluli, and Dr Mohammed Patel from UUME Office for their ongoing support. I extend my appreciation to postgraduate students Carlo, Julie, and Zhane, as well as our administrative staff Thiloshni, Janie, Maralese, Donald, Brain, Busi, and Rami for their unwavering support.

Special thanks to Prof. Kalla, Dr. Farzahna Mohamed, and Katekani Ramothwala for their constant support during the toughest days of my PhD journey, and to Dr. Aijaz Ahmad, Dr. Ambar Khan and Sawban for their moral support and guidance.

My heartfelt gratitude goes to my beloved family my son Ethan, brother Shaun, sister Sanusha, nephews Mersan, and Gershon, and my immediate family members Precious, Mekyla, and Pranesh for their unwavering support. I also want to thank Every Nation Online Platform, Pastor Eric, Pastor Ryan, Pastor Simon, Pastor Delight, Pastor David, and Dr. Ajayi for their support and encouragement. Special thanks are extended to my close friends Prof Asare who have been my mentors since 2007, Sarah, Dr Nitta, Princess, Prof. Daniels, Prof. Ballot, Prof. Omole, Prof. Mackuraj, Prof. Amadi, and Dr. Okechi for their steadfast companionship and encouragement throughout this journey. I want to thank all those who have supported me throughout my journey.

Lastly, A very big thank you goes out to my Funders. DAAD Academic Funding, MRC, NRF, FRC and the Departmental Internal Medicine, Division Oncology for the RINC Funding. This research was made possible by all of you.

Table of contents

Declaration.....**i**

Dedication.....**ii**

Conferences and Workshops ..... **iii**

Publications in Review.....**iv**

Abstract..... **v**

Acknowledgments .....**vii**

Table of contents ..... **viii**

List of Abbreviations ..... **xiii**

List of Figures.....**v**

List of Tables .....**vii**

Chapter 1: Introduction **1**

1.1. Colorectal cancer epidemiology and Risk Factors 1

1.2. Colorectal Cancer in South Africa 4

1.3. CRC Pathology 6

1.4. Staging of CRC 7

1.4.1 Duke's Staging or Pathological Staging 7

1.4.2. Clinical Staging.....7

1.4.3. TNM Staging 8

1.4.5. CRC Stage Grouping 9

1.5. Importance of innovative Colorectal Cancer screening 12

1.6. Molecular Biology of CRC 12

1.6.1. Biomarkers 16

1.6.2. Protein Biomarkers 16

1.6.3. Proteomic signatures in CRC 17

1.7. Glycosylation 20

1.7.1. Introduction to Protein Glycosylation.....20

1.7.2. Role of glycosylation in protein modification 22
1.7.3. The Biological Significance of Glycoproteins 25
1.7.4. Glycosylation and Glycoproteins as a Biomarker for CRCs 26
1.7.5. Glycosylation Inhibitors in Cancer 30
1.7.6. Glycosylation Pathways 31
1.7.7. N-linked glycosylation 31
1.7.8. O-glycosylation 32
1.8. Inhibitors of Glycosylation 33
1.8.1. Castanospermine 33
1.8.2. Mannostatin-A 33
1.8.3. Swainsonine 34
1.8.4. Tunicamycin 34
1.8.5. Brefeldin A 37
1.9. Thymidine Kinase 1 40
1.9.1. TK1 and Colorectal Cancer 41
1.9.2. TK1 as a Biomarker in Colorectal Cancer (Diagnostic Biomarker) 41
1.9.3. TK1 as a Therapeutic Target in Colorectal Cancer 41
1.9.4. Thymidine Kinase and Glycosylation: Thymidine kinase in nucleotide sugar synthesis 42
1.9.5. Therapeutic Implications 42
1.10. Protein Kinase C alpha 44
1.10.1. Protein Kinase C and glycosylation 44
1.10.2. PKC-alpha and Colorectal Cancer 45
1.11. The peroxisome proliferator-activated receptor gamma (PPARG) 46
1.11.1. PPARG and colorectal cancer 47
1.11.2. PPARG and Glycosylation 47
1.11.3. Brefeldin A and PPARG 48

1.12. Mitogen-Activated Kinase....49
1.12.1. MAPK and CRC....50
1.12.2. MAPK and Brefeldin A....51
1.12.3. MAPK and glycosylation....52
1.13. *In silico* computer modelling....54
1.13.1. Introduction to in silico Studies....54
1.13.2. The Role of Silico Approaches in Drug Discovery....56
1.13.3. In Silico Approaches....59
1.13.4. Structure-Based Drug Design....59
1.13.5. Molecular Docking....59
1.13.6. Pharmacophore Mapping....62
1.13.7. Ligand-Based Drug-Design....62
1.13.8. Quantitative Structure-Activity Relationship (QSAR). 63
1.14. Molecular Dynamics....63
1.14.1. The Principle of Molecular Mechanics....64
1.14.2. Force field. 65
1.14.3. Molecular dynamics (MD) simulation....66
1.15. Molecular Dynamics Post-Analysis 68
1.15.1. System Stability....68
1.15.2. Conformational Characteristics of the Systems....71
Residue Interaction Network (RIN)....71
1.16. Aims and objectives....72
1.16.1. Problem statement....72
1.16.2. Aim and objectives....72
1.16.3. Objectives....72
Chapter 2: Methodology....74
2.1. Research Design....74

2.2. Drugs targeting glycosylation. 74
2.3. Chemical Entities of Biological Interest/ChEBI database 75
2.4. High-Throughput Docking 75
2.5. Structure preparation of Tunicamycin C and Brefeldin A and Screening of potential glycosylation targets 75
2.6. Pathway identification using KEGG and WIKI 76
2.7. Molecular dynamic modelling of Tunicamycin C and Brefeldin A 77
2.7.1. System Preparation: Retrieval and preparation of systems 77
2.7.2. Molecular Dynamics simulation 78
2.7.4. Thermodynamic Binding Free Energy (BFE) Calculation 80
Chapter 3: Results 82
3.1. Drugs targeting glycosylation. 82
3.1.1 High-Throughput Docking 82
3.2. Protein Target Prediction and Pathway Analysis 83
3.3. Screening glycosylation targets 84
3.4. Estimation of evolving conformational dynamics along the 250 ns MD simulation 90
3.4.1. Comparative evaluation pf structura; drift from their centre of mass 94
3.4.2. Estimation of relative Tunicamycin binding dynamics concerning TK1 and PKC and Brefeldin A with MAPK and PrKC1 97
3.4.3. System-based visualization of ligand interaction 101
3.4.4. Quantitative estimation of implicit interaction contributors 105
3.4.5. Quantification of thermodynamic evaluation of binding affinity 111
Chapter 4: Discussion 112
4.1. Drugs targeting glycosylation. 112
4.2. Potential glycosylation targets for Tunicamycin C 113
4.3. Potential glycosylation targets for Brefeldin A 114
4.4. Pathway Analysis for Tunicamycin C 115

4.5. Molecular dynamic modelling for the interaction between Tunicamycin and the TK1 and PrKC1 target proteins....115

4.6. Molecular dynamic modelling for the interaction between Brefeldin A and MAPK and PrCK1 target proteins....116

4.7. Comparative evaluation of structural drift from their centre of mass....116

Tunicamycin C....118

Brefeldin A....119

4.8. Estimation of relative Tunicamycin C binding dynamics concerning TK1 and PKC and Brefeldin A with MAPK and PrKC1....119

4.8. System-based visualization of ligand interaction....121

4.9. Quantification thermodynamic evaluation of binding affinity....122

Chapter 5: Conclusion....123

Future directions....125

6. References....127

Appendix1: Structures and information of Glycosylation inhibitors in this study....171

Appendix 2: Docking results....175

Appendix 3 Protein Docking....212

Appendix 4 Pathway analysis....214

Appendix 5: Plagiarism report....268

List of Abbreviations

17-DMAG- 17-demethoxygeldanamycin
ADH- Aldehyde dehydrogenase
ADMET- Absorption, distribution, metabolism, excretion, and toxicity
AI- Artificial intelligence
AJCC- American Joint Committee on Cancer
APC- adenomatous polyposis coli
APC/C- anaphase-promoting complex/cyclosome
ARFs- ADP-ribosylation factors
Asn- Asparagine (Asn)
ASR-age-standardised incidence rate
ATF6- activating transcription factor 6
PERK- PKR-like ER kinase
ATM- ataxia-telangiectasia
AURKA- aurora kinase A
BAC-BFA-ADPR conjugate
BCRP- breast cancer resistance protein
BFA- Brefeldin A
BFE- Binding Free Energy
BUB1- Benzimidazoles 1
BUBR1- BUB1-related protein 1
CA 19-9- carbohydrate antigen
CacyBP- calcyclin binding protein
CADD- computer-aided therapeutic design
CAR-T cell- chimeric antigen receptor T-cell
CAS- castanospermine
CAT- catalase
CDG- cancer and glycosylation disorders
CEA- carcinoembryonic antigen
CEA- carcinoembryonic antigen
cfDNA- Cell-free DNA
ChEBI- Chemical Entities of Biological Interest
CIMP- CpG island methylator phenotype
CIN- Chromosomal instability (CIN)
COX2- cyclooxygenase 2 (COX2)
CRC- Colorectal Cancer
CT- computed tomography
ctDNA-circulating DNA
CTNB1- catenin beta-1
DC- dendritic cell
DCC- deleted in colorectal carcinoma
DCCM- Dynamic cross-correlation matrix
DC-SIGN- specific ICAM-3-grabbing non-integrin 1
DDR- DNA damage response
DNMTs- DNA methyltransferases
DSF- differential scanning fluorimetry
dTMP-thymidine monophosphate
ECM- extracellular matrix
ER- endoplasmic reticulum
FasR- FS -7-associated surface antigen
FBDD- fragment-based drug design
FEP- free energy perturbation
FSH- follicle-stimulating hormones
FUT-fucosyltransferases
carcinoembryonic antigen (CEA) or carbohydrate antigen (CA 19-9)
GalNAc- N-acetylgalactose
GAPs- GTPase activating proteins
GEF- guanine-nucleotide exchange factors

GnT-5- glucosaminyltransferase-5
GnT-III- N-acetylglucosaminyltransferase III
GO- Gene Ontology
GPU- Graphical Processor Unit
GR- glutathione reductase
GSK3β- synthase kinase 3 beta
GST- glutathione-S-transferase
HBs- Halogen bonds
HGFR- Hepatocyte growth factor receptor
HGF- hepatocyte growth factor (HGF)
HILIC- hydrophilic interaction liquid chromatography
HIV- Human immune deficiency virus
HIV-IN- HIV integrase inhibitors
HPLC-ESI MS/MS- high-performance liquid chromatography-electrospray ionization mass spectrometry
HSP 40- Heat shock protein 40
HTS- high-throughput screening
HTVS- high-throughput virtual screening
Hyl- hydroxylysine
Hyp- hydroxyproline
IGFBP7- insulin-like growth factor-binding protein 7
IL- interleukins
iNOS/NOS2- inducible nitric oxide synthase
IRE1-inositol-requiring enzyme1
ITC- isothermal titration calorimetry
NMR- nuclear magnetic resonance
iTRAQ- isobaric tag for relative and absolute quantitation
IUCC- International Union Against Cancer
KC- keratinocyte-derived chemokine
KEGG- Kyoto Encyclopedia of Genes and Genomes
KRAS- Kristen Rat Sarcoma
LBDD- ligand-based drug-design
LFQ- label-free quantification
LH- luteinizing hormone
LiSiCA- Ligand Similarity using Clique Algorithm
LMICs- Low- and middle-income countries
MAC- Modified Astler-Coller
MAP2K1-Mitogen-Activated Protein Kinase Kinase 1
MAPK- Mitogen_Activated Protein Kinase
MD- Molecular dynamic
MDR- multi-drug resistance
MGL- macrophage galactose lectin
MIP-2- macrophage inflammatory protein-2
MM- molecular mechanics
MM- Molecular Mechanics
M-metastatic
MM-GBSA- Molecular mechanics generalized Born surface area (MM-GBSA).
MMPs- matrix metalloproteinases
MRI- magnetic resonance imaging
MRM-MS- multiple reaction monitoring-mass spectrometry
MRP-multidrug resistance-associated protein
MS- mass spectrometry

MSI- Microsatellite instability (MSI)
NAP- non-adenomatous polyps
NC- non-cancer
NCE- novel chemical entities
NCR-National Cancer Registry
NM- non-metastatic (NM)
NP- nanoparticles
PBSA- Poisson-Boltzmann Surface Area
PDCD4- Programmed Cell Death Protein 4
PET- positron emission tomography
Pgp- P-glycoprotein
PI3K/Akt- phosphatidylinositol-3-phosphate kinase/protein kinase B
PIK3CA- Phosphatidylinositol-4,5-bisphosphate 3-kinase catalytic subunit alpha
PLK1- polo-like kinase 1
PMEMD- Particle Mesh Ewald Molecular Dynamics
PPARG- Peroxisome Activated Receptor Gama
PrKC1- protein kinase C
PRKCA- Protein Kinase C Alpha
PTM- post-translational modification
QM- quantum mechanical
QPLD- Quantum Polarized Ligand Docking
QSAR- quantitative structure-activity relationship
R&D- research and development
RB-Retinoblastoma
RF-Random Forest (RF)
Rg- Radius of gyration
RIN- Residue Interaction Network
RMSD- Root Mean Square Deviation
RMSF- Root Mean Square Fluctuation
RoG- The radius of Gyration
RTK/Ras- receptor tyrosine kinase/rat sarcoma
SA- South Africa
SAR- structure-activity relationship
SBDD- Structure-based Drug Design
SCKCAT- succinyl-CoA 3-ketoacid coenzyme A transferase
SDHA- Succinate dehydrogenase subunit A (SDHA)
SEA- similarity ensemble approach
Ser- serine
SILAC- Stable isotope labelling by amino acids in cell culture
SMILES- Simplified Molecular Input Line Entry System
SOD- superoxide dismutase
SPR- surface plasmon resonance
SRM-MS- selected reaction monitoring-mass spectrometry
TAS2R31-Taste Receptor Type 2 Member 31
TCA- Tricarboxylic acid
TGFTβ/BMP- transforming growth factor-beta/bone morphogenic protein
TGM2- glutamine gamma-glutamyl transferase 2
Thre-threonine
TI- thermodynamic integration
TICs- tumour-initiating cells
TIMP-1- Metalloproteinase-1

TK1- Thymidine Kinase 1

TMP- thymidine-to-thymidine monophosphate

TMT- tandem mass tag

TNFR1- tumor necrosis factor receptor 1

TNFα- Tumour necrosis factor-alpha (T

TNM- tumour node metastasis

TRAIL- tumour necrosis factor-related apoptosis-inducing ligand

Tyr- tyrosine

UPR- unfolded protein response

VEGF- vascular endothelial growth factor

WHO- World Health Organization

Wnt- Wingless-type

XGBoost- Extreme Gradient Boosting

ML- machine learning

B1-GlcNAc- beta-1 N-acetylglucosamine

List of Figures

Figure 1.1 An illustration of the colon:.....3
Figure 1.2 Molecular Mechanisms of Carcinogenesis in CRC.....6
Figure 1. 3 A typical cartoon representation of the stages of CRC: 11
Figure 1. 4. Wnt Signalling pathway of CIN. 15
Image created using Microsoft PowerPoint.....21
Figure 1.6. Example of glycosylation effect on protein modification. 24
Figure 1. 7. Schematic drawing of N-linked and O-linked glycosylation types.....25
Figure 1. 8. Production of Lewis antigens through the activity of fucosyltransferases. Glucosyltransferases and fucosyltransferases (FUT), encoded by genes FUT1, FUT2, and FUT3, play key roles in the biosynthesis of blood group-related Lewis antigens. Image created using Microsoft PowerPoint 29
Figure 1.9. A schematic illustration of Tunicamycin's mode of action.....36
Figure 1.10. A Schematic illustration of the Effects of Brefeldin A on membrane trafficking between ER and Golgi. 38
Figure 1.11. Mitogen-activated kinase protein signalling pathway.....50
Figure 1.12. *In silico* approaches used in drug design:.....60
Figure 1.13. Illustration of molecular docking between receptor and ligands.....61
Figure 2. 1 Research Design 74
Figure 2.2 A representative illustration of the solvation of a protein molecule 79
Figure 3.1 Chemical structures. 83
Figure 3.2 A representation of the RMSD and RMSF of TK1 and PrKC1 with their corresponding apo.....91
Figure 3.3: An RMSD and RMSF plot of MAPK and PrKC1 with their corresponding apo. 92
Figure 3.4. Docking of Tunicamycin C with protein targets. 93
Figure 3.5. Docking of Brefeldin A with protein targets.....94
Figure 3.6. Rg plots of the interaction between Tunicamycin C withTK1 and PrKC1.....95
Figure 3.7. Rg plots of the interaction between Brefeldin A with MAPK and PrKC1. Rg plot of the global structure of MAPK and PrKC1 with their corresponding apo systems. The Rg plots show the global structure of the proteins compared to the protein interaction with Brefeldin A.....96
Figure 3.8 A descriptive indication of Tunicamycin performance during the MD timeline. ..97
Figure 3.9 A descriptive representation of Brefeldin A properties during the MD timeline...99

Figure 3.10 A time-based structural presentation of ligand conformation and orientation during the MD simulation. 100
Figure 3.11 Time-based illustration of MAPK and PrCK1 structural orientation during the MD simulation.....101
Figure 3. 12 2D interaction representation of Tunicamycin TK1 and PrKC1 complexes. This figure shows the difference between the docking and MD complex environments. A & C depict the complex docking environment, while B& D is the MD environment, which gives an idea of the role of bulk, which depicts a typical physiological environment for better binding interaction stabilization. 102
Figure 3.13 2D interaction representation of Brefeldin A MAPK and PrKC1.....103
Figure 3.14. 2D representation of Tunicamycin C and TK1/PrCK1 interaction diagram for the average PDB. 104
Figure 3.15 2D interaction diagram for the average PDB. 105
This diagram indicates the most dominant contributing residues to the binding stabilization of Brefeldin A.....105
Figure 3.16 Stacked bar charts of side chain interactions and interaction types between tunicamycin and TK1/PrCK1 systems. 106
Figure 3.17 Stacked bar charts of side chains interactions and interaction types between Brefeldin A and MAPK/PrCK1 systems 107
Figure 3.18 Per-residue energy decomposition for the interaction between Tunicamycin C and TK1/PrCK1 systems 109
Figure 3.19. The per-residue energy contribution of MAPK and PrCK1 to the binding of Brefeldin A.....110
Figure A1: Structure of Glycosylation inhibitors in this study:.....172
Figure A3.1 Superimposed pictures of the top 10 binding poses of each ligand.....213

List of Tables

Table 1. 1 Estimate of Cancer incidence and mortality by WHO in 2018 2
Table 1.2 CRC data of incidence rate vs percentage of all cancers in the SA population.....4
Table 1. 3 TNM staging classification of CRC.....9
Table 1. 4 Stage grouping of CRCs in TNM, Dukes and MAC 11
Table 1. 5 A. Proteomic Signatures in CRCs.....19
Table 1. 6 B Proteomic Signatures in CRCs.....20
Table 3.1 Results for High-Throughput Docking 82
Table 3.2 Canonical SMILES Computed by OEChem 2.3.0. 84
Table 3. 3 Top 18 Potential Target Proteins for Brefeldin A and Tunicamycin C 84
Table 3.4 KEGG pathway analysis for targeted proteins for Brefeldin A 86
Table 3.5 KEGG pathway analysis for targeted proteins for Tunicamycin C 89
Table 3.6 Estimated binding energy predictions of Tunicamycin C complexes. 111
Table 3.7 Estimated binding energy predictions of Brefeldin A complexes. 111
Table A1.1. Physical properties of various glycosylation inhibitors in this study 173
Table A2.1. Docking results of Tunicamycin with protein targets.....175
Table A3.1:Top 10 ligand orientations (“binding poses”) within the target.....212
Table A4.1. Pathway analysis for Targeted protein for Brefeldin A 214
Table A4.2: Pathway analysis for Targeted protein for Tunicamycin C 245

Chapter 1: Introduction

Cancer represents a collection of diseases characterized by uncontrolled cell division, posing a significant global health challenge. According to the World Health Organization (WHO), cancer ranks as the second leading cause of death worldwide. In 2018 alone, approximately 18.1 million individuals were diagnosed with cancer, resulting in 9.6 million deaths, with a significant proportion occurring in low- and middle-income countries (LMICs) (World Health Organization, 2020). The global incidence of cancer is anticipated to double by 2040, with a projected increase of 29-37%, the majority of which will occur in LMICs. Among the most prevalent cancer types are lung, breast, colorectal, prostate, stomach, liver, cervical, and thyroid cancers. These cancers collectively contribute to significant morbidity and mortality worldwide. The pathogenesis of cancer involves a multitude of physiological changes over time and space within cancer cells, ultimately culminating in the formation of malignant tumours. The basic hallmark of the cancer is the aberrant proliferation of cells, known as neoplasia. (Hornberg et al., 2006). The main factor contributing to morbidity and mortality in the majority of cancer patients is tumour cell invasion of nearby tissues and distant metastasis (Seyfried and Shelton, 2010). Since 2012, the United States Food and Drug Administration has approved 90 new cancer medications due to the pharmaceutical industry's increased focus on developing, researching, and marketing new oncology drug products to address unmet medical needs (Watch, 2018).

1.1.Colorectal cancer epidemiology and Risk Factors

Colorectal cancer (CRC), also known as colorectal adenocarcinoma, originates from the abnormal growth of tissue (polyps) derived from the glandular epithelial cells lining the colon (see Fig. 1.1). The development of CRC typically involves a sequence of genetic or epigenetic mutations within epithelial cells. These mutations endow the cells with abnormal characteristics such as uncontrolled replication, increased survival, the formation of benign neoplasms, and ultimately progression to adenocarcinomas and metastasis over time (Ewing et al., 2014, Rawla et al., 2019a).

CRC cancer ranks third in global incidence (10.2%) of all cancers (World Health Organization, 2020). It ranks as one of the most commonly diagnosed cancers globally, ranking second among women and third among men. Interestingly, the incidence and mortality rates are approximately 20% lower in women compared to men. (Dekker et al., 2019). The incidence of CRC is on a rapid rise globally, particularly in developing countries influenced by the adoption

of a "Western" lifestyle (Rawla et al., 2019b), and predictions suggest that the incidence rate will peak at 2.5 million new cases by 2035 (Bray et al., 2018, Ferlay et al., 2019).

Table 1. 1 Estimate of Cancer incidence and mortality by WHO in 2018 (World Health Organization, 2018)

Type of Cancer	Incidence (% of all cancers)	Type of Cancer	Mortality (% of all cancers)
Lung	11.6	Lung	18.4
Breast	11.6	Colorectal	9.2
Colorectal	10.2	Stomach	8.2
Prostate	7.1	Liver	8.2
Stomach	5.7	Breast	6.6
Liver	4.7	Oesophagus	5.3
Oesophagus	3.2	Pancreas	4.5
Cervix uteri	3.2	Prostate	3.8
Thyroid	3.1	Cervix uteri	3.3
Bladder	3.0	Leukaemia	3.2
Others	36.7	Others	29.3

The Global burden of Disease Cancer Collaboration, 2017 (Rawla et al., 2019b) has reported that CRC's regional prevalence and incidence varied more than 10-fold worldwide from 1990 to 2015. New Zealand, Australia, North America and Europe had high incidence rates, whereas Southern Central Asia and Africa had the lowest incidence rates.

However, the trend appears to be stabilising and decreasing in highly developed countries such as Europe due to nationwide screening programmes, increasing colonoscopy utilisation, and changing lifestyle and dietary habits (Ouakrim et al., 2015). The development of CRC is influenced by both environmental and genetic factors. Although the most striking increase in risk for CRC is associated with hereditary susceptibility, most cases occur sporadically rather than familially (Chan and Giovannucci, 2010). Age is a significant risk factor for sporadic CRC. The incidence of CRC, especially rectal and left-sided colon cancer, increases in people younger than 50 years (Kasi et al., 2019). In 2018, 880,792 deaths from CRC were reported worldwide, representing 47.62% of the total CRC cases and 9.2% of all cancers (World Health Organization, 2020). The mortality rate from CRC has gradually decreased since the 1980s in the United States of America and many Western countries due to early detection, polyp

removal, and effective treatment procedures (American Cancer Society, 2018). In contrast, the death rate from CRC in people aged > 50 years has increased by 2% each year from 2007 to 2016.

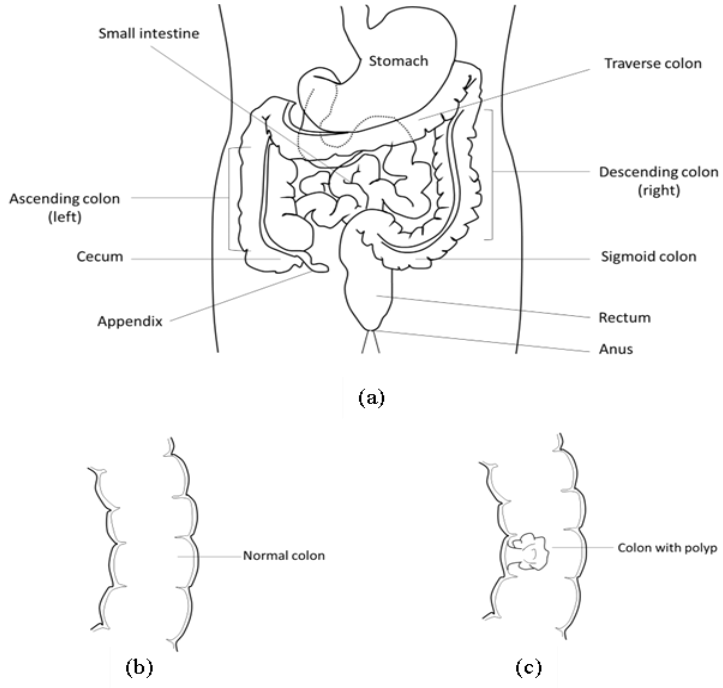


Figure 1.1 An illustration of the colon: (a) Anatomy of the large intestine, (b) cross-sectional view of a normal colon, and (c) cross-sectional view of a colon with polyp Program used Microsoft PowerPoint.

Colorectal cancer is the fourth most commonly diagnosed cancer in South Africa (SA) and ranks second in men and fourth in women. It is the sixth leading cause of death among all cancers in SA (McCabe et al., 2020). According to the South African National Cancer Registry (SANCR), men had a higher risk of developing CRC than women in 2014, with an estimated lifetime risk of 1in 79 (5.28% of all cancers) and 1in 134 (4.29% of all cancers), respectively. This means that 1 in 79 men and 1 in 134 women are at risk of developing CRC, and the risk is higher for people aged > 50 years in both sexes (South African National Cancer Registry, 2014, Sun et al., 2020). The annual crude incidence of CRC in men and women from SA in 2016 was reported to be 7.57 and 6.87 per 100,000, respectively (Singh et al., 2015b). Overall, the prevalence of histologically diagnosed CRC is higher in the white (Caucasian) population (47.68% of all CRC cases), followed by blacks (Africans) (31.25% of all CRC cases), people of mixed ancestry (Coloureds) (14.86% of all CRC cases), and Asians (Indians) (6.18% of all CRC cases) (Singh et al., 2015a). Table 1.2 illustrates the CRC status in SA men and women

in relation to different populations according to the South African National Cancer Registry (NCR) in 2016.

Table 1.2 CRC data of incidence rate vs percentage of all cancers in the SA population

Population	2016 Number of Cases				20016 Incidence Males		Females	
	Males	Females	Total	%	ASR	%	ASR	%
White (Caucasians)	1024	828	1852	47.68	24.89	5.01	17.17	4.99
Black (Africans)	605	609	1214	31.25	4.72	4.53	3.32	3
Mixed Race Ancestry (Coloured)	301	277	578	14.86	6.5	16.52	10.05	5.88
Asian (Indians)	135	105	240	6.18	17.5	13.83	11.26	8.12
All Population	2065	1819	3884	100	11.01	5.29	6.81	4.3

Table 1.2 illustrates the data on the number of CRC cases vs percentage of all CRC cases and age-standardised incidence rate (ASR) of CRC per 100 000 vs percentage of all cancers in SA males and females estimated by the South African National Cancer Registry in 2016. However, these statistics were considered underestimates as the cases reported in the registries are limited only to a few urban areas. The burden of CRC could be far higher if the data is accumulated with cases from all parts of SA. Also, the National Cancer Registry (NCR) is not up to date; hence, there is no data on CRC mortality and survival rates in SA.

1.2. Colorectal Cancer in South Africa

CRC ranks as the third most common cancer type globally, with nearly 2 million cases diagnosed in 2020 alone (Eng and Holowatyj, 2022). Despite the availability of effective screening techniques, CRC remains the second leading cause of cancer-related deaths, resulting in nearly 1 million deaths annually (IARC, 2024). Men have a higher age-standardized incidence rate than women, and after age 50, the incidence rises significantly (Bray et al., 2018). The Westernization of lifestyle has been implicated in the increase in CRC incidence, and factors such as eating habits and decreased physical activity play a significant role (Rawla et al., 2019b).

Environmental, behavioural and genetic risk factors have been associated with the development of CRC. Approximately 20 to 30 percent of CRC cases are attributed to familial or hereditary factors, with Lynch syndrome and familial adenomatous polyposis being the two most prevalent hereditary syndromes (Lichtenstein et al., 2000). High consumption of red and processed meat, obesity, sedentary lifestyle, smoking, and binge drinking are all lifestyle factors linked to an increased risk of CRC (Battaglia et al., 2015)**.** Moreover, several conditions

such as diabetes, inflammatory bowel disease, and a family history of CRC or polyps are recognized to increase the risk of developing CRC (Jurjus et al., 2016).

As a result, the stage at diagnosis primarily determines the type of treatment for CRC, which may include chemotherapy, surgery, targeted therapy, radiation therapy and immunotherapy (Van Cutsem et al., 2011). Surgical resection continues to be the primary curative treatment for localised disease, while chemotherapy and targeted therapies are used as adjuvant or neoadjuvant treatments in conjunction with surgery (Glynne-Jones et al., 2018). A multidisciplinary strategy for metastatic disease includes systemic therapy, surgery, or radiation for localized metastases. On the other hand, lifestyle factors that can be changed are the primary focus of CRC prevention. For example, adopting a healthy diet low in red and processed meats, and rich in fruits, vegetables, and whole grains, has been associated with a reduced risk of CRC (Song and Giovannucci, 2016, Biller and Schrag, 2021). Moreover, abstaining from tobacco use and limiting alcohol intake, maintaining a healthy weight, and participating in regular physical activity can all notably decrease the risk of developing CRC (Faseru et al., 2022).

The posttranslational modification process known as glycosylation plays a crucial part in several biological processes, such as stability, protein folding, and cell-cell interactions (Pinho and Reis, 2015). Abnormal glycosylation has been linked to the development, metastasis, and immune evasion of cancer (Ichikawa et al., 2000). A promising strategy for cancer treatment involves using inhibitors that target particular enzymes connected to glycosylation pathways (Dube and Bertozzi, 2005). An example of an N-linked glycosylation inhibitor is Tunicamycin, which has demonstrated cytotoxic effects in CRC cell lines and has been proposed as a potential therapeutic agent for treating CRC (Hou et al., 2013). Brefeldin A (BFA), a fungal metabolite and a glycosylation inhibitor, has drawn much interest due to its conceivable anticancer effects. Several studies have documented that BFA can disrupt the Golgi apparatus, inhibit cell proliferation, and induce apoptosis in several cancer cell lines (Pommepuy et al., 2003, Yardin et al., 1998). These findings suggest that BFA could be a promising candidate for the development of novel anticancer treatments.

1.3. CRC Pathology

Most colorectal carcinomas occur sporadically, and only < 10% of cases are due to hereditary cancer syndrome. Colorectal carcinomas mainly arises from precursor lesions such as adenomas and transforms into adenocarcinomas or carcinogenesis (Harada and Morlote, 2020, Gian et al., 2018). The molecular mechanisms of CRC can manifest through three different pathways (Figure 1.2), namely: microsatellite instability (MSI), chromosomal instability (CIN) and CpG island methylator phenotype (CIMP). CIN accounts for 85% of CRC, followed by CIMP (17%) and MSI (15%) (Harada and Morlote, 2020). The prognosis of CRC can be determined by several factors, including the stage at which the tumour is located, the location of the tumour, and its histologic subtype. In addition to these factors, detecting the appropriate molecular biomarkers will help determine the prognosis of CRC and response to therapy.

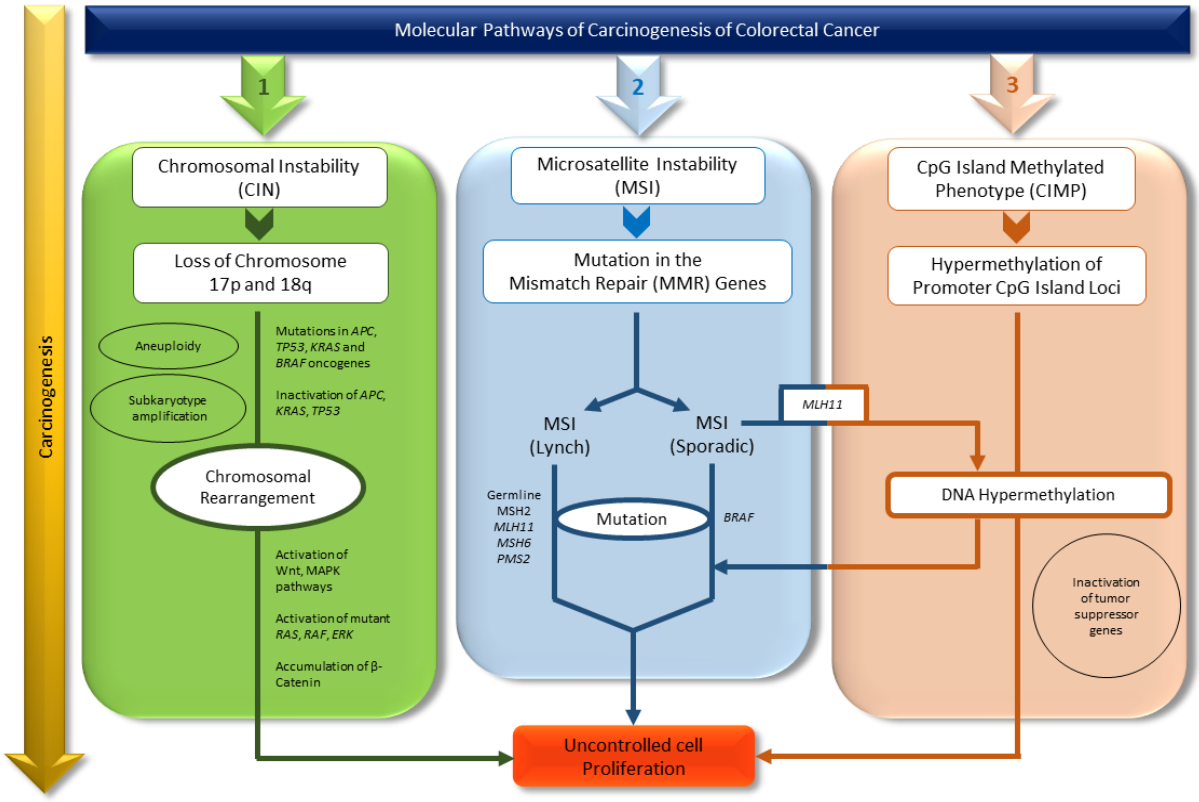


Figure 1.2 Molecular Mechanisms of Carcinogenesis in CRC. Image created using Microsoft PowerPoint.

1.4. Staging of CRC

Staging of CRC is important to determine the severity of the cancer and therapeutic strategies. In addition, staging also helps predict the course and success rate of treatment. It is also a way for a physician to describe the extent of cancer in an individual using various diagnostic procedures, including a simple physical examination, imaging tests such as computed tomography (CT), X-rays, positron emission tomography (PET) scans, magnetic resonance imaging (MRI) and endoscopy, laboratory tests, biopsy and blood tests. Staging of CRC can be done in several ways, including Duke's, pathologic, clinical, and tumour node metastasis (TNM).

1.4.1 Duke's Staging or Pathological Staging

Moreover, Cuthbert E. Dukes (Dukes, 1932) classified CRC based on the histopathology of the carcinoma; that is, those cancers limited to the wall of the rectum are designated as Type A, those have spread directly on to the extra-rectal tissues are designated as Type B, and those in which the metastases are in the regional lymph nodes are designated as Type C. Modifications were made with the Duke's staging system by Kirklin, Dockerty and Waugh in 1949 and further by Astler and Coller in 1954 (Ueno et al., 2004, Astler and Coller, 1954) to differentiate the lesions that are extended through and not through muscularis propria with numerical subscripts along with the Duke's classification and described the modified Astler-Coller (MAC) classification. Later, a designated Stage D was introduced by Rubert B. Turnbull and co-workers (Turnbull Jr et al., 1967) to identify the metastasis of the CRC to the liver, lung, bone and other adjacent organs. The pathological staging of CRC is listed below:

- ***Type A*** – The lesions are limited to the mucosa.
- ***Type B_1*** – The lesions extend into the muscularis propria but do not penetrate through it, with negative lymph nodes.
- ***Type B_2*** – lesions have penetrated the muscularis propria, with negative nodes
- ***Type C_1*** – The lesions have extended into the muscularis propria and have penetrated through, with positive lymph nodes.
- ***Type C_2*** – lesions have penetrated through the muscularis propria with positive nodes
- ***Type D*** lesions metastasized to other adjacent organs, such as the liver, bone, and lung.

1.4.2. Clinical Staging

Clinical staging of CRC is based on the physical examinations and the results of the imaging tests, endoscopies and biopsies, and blood tests before initiating any treatment protocol. This

was mainly used to determine the best treatment procedure and predict the prognosis and therapeutic response. (Nicholls et al., 1982) have proposed a clinical staging system that comprises four stages of the extent of cancer and two stages of the involvement of lymph nodes as below (Nicholls et al., 1982):

- ***Stage 1*** – the tumour is only confined to the rectum.
- ***Stage 2*** – tumour may only be in the rectum or have mildly spread outside of the rectum
- ***Stage 3*** – moderate to extensive spread outside the rectum
- ***Stage 4*** – The tumour might have spread to other organs or unresectable
- ***Node*** – Positive
- ***Node*** – Negative

1.4.3. TNM Staging (Tumour Nodule Metastasis)

The American Joint Committee on Cancer (AJCC), in collaboration with the International Union Against Cancer (IUCC), introduced the TNM cancer staging system in 1987 to provide a more precise classification of cancer stages. TNM system stages cancer based on the depth of the local primary tumour (T), the presence of nodal metastases and their number (N) that tells whether cancer has spread to the lymph nodes or not, and the presence of distant metastases (M) that tells whether cancer has spread to other distant organs or tissues of the body (Hutter, 1987). In each category, a letter or number will be assigned after the main letter T, N, or M, which describes the presence, size, location, and or the spread of cancer into the nearby tissues (For example, TX, T0, Tis, T1, T2, T3, NX, N1, M0, M1). Specific cancers may also have subcategories, and they are designated with a lowercase letter after the primary category (For example, T3a, T3b). The TNM staging system also allows the assessment of the TNM categories based on the histopathological evidence (Duke's staging system) and the other clinical evidence (clinical staging system). Hence, the staging of cancers in TNM has become the most common and widely used cancer staging system worldwide. The 7th edition of the TNM classification of colorectal carcinomas was proposed in 2010 and has now been updated and replaced by the 8th edition, published in 2016 (Bertero et al., 2018). This updated classification system provides more detailed criteria for staging colorectal cancer, as outlined in Table 1.3.

Table 1. 3 TNM staging classification of CRC

T-Primary tumour		
Tx		Primary tumours cannot be assessed.
T0		No evidence of a primary tumour
Tis		Carcinoma in situ: intraepithelial or invasion of lamina propria
T1		Tumour invades submucosa
T2		Tumour invades muscularis propria
T3		Tumour invades through muscularis propria into subserosa or non-peritonealised pericolic or perirectal tissues.
T4	T4a	Tumour directly invades other organs or structures and perforates the visceral peritoneum.
	T4b	The tumour has grown through and attached to other nearby structures or organs
N-Regional lymph nodes		
NX		Regional lymph nodes cannot be assessed.
N0		No regional lymph node metastasis
N1	N1a	Metastasis in one regional lymph node
	N1b	Metastasis in two or three regional lymph nodes
	N1c	Metastasis to the nearby structures and formation of non-lymph nodal nodules
N2	N2a	Metastasis in four to six regional lymph nodes
	N2b	Metastasis in more than six regional lymph nodes
M-Distant metastasis		
MX		Distant metastasis cannot be assessed.
M0		No distant metastasis
M1	M1a	Metastasis to one distal organ
	M1b	Metastasis to more than one distal organ
	M1c	Metastasis into the peritoneal surface

This is based on the American Joint Committee on Cancer and the Union for International Cancer Control (UICC) (Bertero et al., 2018)

1.4.5. CRC Stage Grouping

- Different stages of CRC can be assigned by combining the T, N, and M classifications into groups to identify the status, progression, and severity of cancer and determine the best therapeutic strategy, prognosis, therapeutic response, and time course (American Cancer Society, 2018, Benson et al., 2021, Mehta et al., 1994). A pictorial representation of the different stages of CRC is illustrated in Figure 1.3.

- ***Stage 0 or cancer in situ*** – the tumour is only confined to the mucosa or the inner lining of the colon or rectum.
- ***Stage I*** – the tumour has grown through the mucosa and has invaded the colon or rectum's second layer (muscle) but has not spread to the adjacent tissue and lymph nodes.
- ***Stage II –*** the tumour has wholly grown through the colon or rectal wall.
    - **Stage IIA** – the tumour has completely grown through the colon or rectal wall but has not spread to the adjacent tissue or lymph nodes.
    - **Stage IIB –** the tumour has grown through and reached the visceral peritoneum, the lining of the abdomen, but has not spread to the adjacent tissue or lymph nodes.
    - **Stage IIC** – the tumour has grown through and spread into the surrounding tissue structures but has not spread to the lymph nodes.
- **Stage III –** the tumour has invaded the intestine's layers and spread to the nearby lymph nodes.
    - **Stage IIIA** – the tumour has grown through the intestinal epithelium or muscular layers and has spread into 1 to 3 lymph nodes or the non-lymphatic nodular tumour in the tissues surrounding the colon or rectum. But it has not spread to the other distal organs.
    - **Stage IIIB** – the tumour has grown through the colon or rectal wall, nearby organs and into 1 to 3 lymph nodes or to the non-lymphatic nodular tumour in the tissues around the colon or rectum. But it has not spread to the distal organs.
    - **Stage IIIC** – regardless of the depth, the tumour has grown and spread to 4 or more lymph nodes but not to the other distal organs.
- **Stage IV –** the tumour has metastasized to distant organs of the body.
    - **Stage IVA** – the tumour has spread to a single distal organ, liver or lungs.
    - **Stage IVB** – the tumour has spread to more than one distal organ
    - **Stage IVC** – the tumour has invaded and spread into the peritoneum.

CRC has no symptoms in the early stage and is often diagnosed only at the advanced stages. A comparison of different stage groups of CRCs based on the TNM, Dukes and MAC systems of cancer staging is given in Table 1.4.

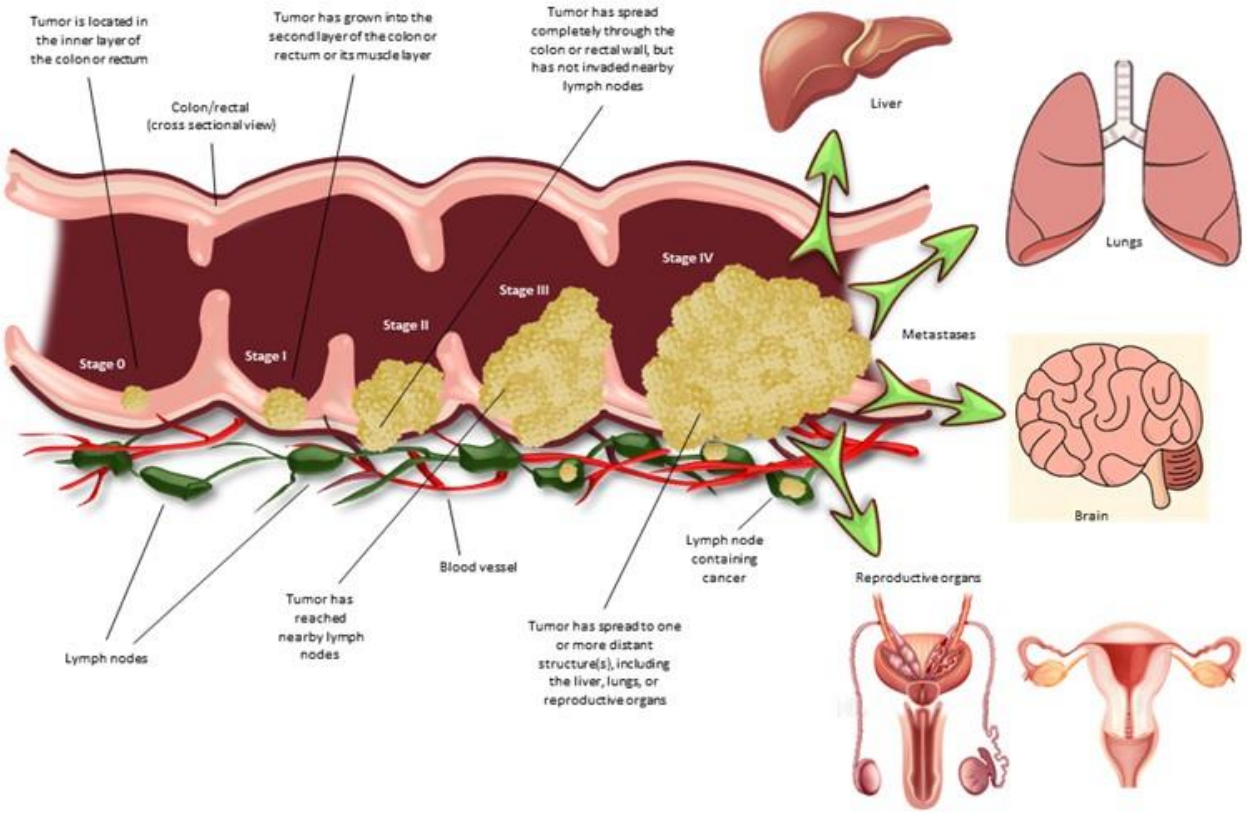


Figure 1. 3 A typical cartoon representation of the stages of CRC: Image created using Microsoft PowerPoint

Table 1. 4 Stage grouping of CRCs in TNM, Dukes, and MAC (Horton and Tepper, 2005)

Stage		T	N	M	Dukes	MAC
0		Tis	N0	M0	-	-
I		T1	N0	M0	A	A
		T2	N0	M0	A	B1
	IIA	T3	N0	M0	B	B2
II	IIB	T4a	N0	M0	B	B3
	IIC	T4b	N0	M0	B	B3
	IIIA	T1, T1–T2	N1/N1c, N2a	M0	C	C1
III	IIIB	T1–T2, T2–T3a–T4a	N1/N1c, N2a, N2b	M0	C	C2/C3
	IIIC	T3–T4a, T4a, T4b	N1–N2, N2a, N2b	M0	C	C1/C2/C3
	IVA	Any T	Any N	M1a	-	D
IV	IVB	Any T	Any N	M1b	-	D
	IVC	Any T	Any N	M1c	-	D

1.5. Importance of innovative Colorectal Cancer screening

The current treatment for CRC typically involves surgery, with histopathological staging guiding the decision for adjuvant chemotherapy, typically administered for a duration of 6 months. (Tie et al., 2022). Patients need to be given the best care. The knowledge of biomarkers and innovative screening that is non-invasive is critical in improving cancer prognosis, especially regarding CRC recurrence.

CRC recurrence risk assessment using circulating DNA (ctDNA) has been actively investigated to improve prognosis. Tie et al. conducted a trial looking at the ctDNA of CRC patients who had undergone surgery and had stage II colon cancer. It was observed that ctDNA-positive patients had a high risk of recurrence if not treated with adjuvant therapy. Patients who tested positive for ctDNA and received oxaliplatin-based therapy demonstrated improved recurrence outcomes, leading to increased recurrence-free survival. With ctDNA-negative CRC patients, it was seen that they had a low risk of recurrence (Tie et al., 2022). Such findings are important in addressing chemotherapy management as liquid biopsy (ctDNA) has a short turnaround time.

As CRC has high morbidity and mortality, it is essential to have a system that can detect cancer at earlier stages. Cell-free DNA (cfDNA), also known as ctDNA from plasma, is one of the most promising early detection and prognosis approaches. Tumours are derived from benign lesions; the malignancy occurs due to acquiring a series of mutations over time (Vogelstein and Kinzler, 2015). In CRC, the mutation process has been studied extensively. There are gatekeeping mutations that allow for selective growth advantage over normal epithelial cells.

1.6. Molecular Biology of CRC

Chromosomal instability (CIN) is the most typical feature of the molecular pathogenesis of CRC, accounting for 65-85% of colon adenocarcinomas (Pino and Chung, 2010, Lengauer et al., 1998). The high chromosomal instability CIN+ tumours are characterized by severe loss of specific chromosomal regions of the entire chromosomes. Despite numerous diagnostic methods available, it is highly complicated to carry out the differential diagnosis of the CIN phenotype. Depending on the chromosomal aberrations that are frequently encountered, CIN+ tumours can be divided into two main groups, namely, CIN-high (CIN-H) and CIN-low (CIN-L) (Kudryavtseva et al., 2016). The most commonly characterized mutations in the tumour suppressor genes such as adenomatous polyposis coli (*APC*), tumour protein 53 (*TP53*/*p53*),

Suppressor of Mothers against Decapentaplegic (*SMAD2/4)* and deleted in colorectal carcinoma (*DCC*) are about 85%, 40-50%, 10-20%, and 5%, respectively. While the mutations in the proto-oncogenes like Kristen Rat Sarcoma (*KRAS*), catenin beta-1 (*CTNB1*) and phosphatidylinositol-4,5-bisphosphate 3-kinase catalytic subunit alpha (*PIK3CA*) are about 30-50%, 5-15%, and 20%, respectively (Pino and Chung, 2010).

Dysregulation of several signaling pathways including the wingless-type integration site (Wnt), receptor tyrosine kinase/rat sarcoma (RTK/Ras), transforming growth factor-beta/bone morphogenetic protein (TGFβ/BMP) and phosphatidylinositol-3-phosphate kinase/protein kinase B (PI3K/Akt) pathways have been identified as primary contributors to most colorectal tumors. The Wnt pathway, in particular, is implicated in over 90% of sporadic CRC cases, where its normal function involves embryonic development as well as regulation of cell proliferation, polarity, and fate (Network, 2012, Schneikert and Behrens, 2007). The ultimate effector molecule of the Wnt pathway is β-catenin, a multifunctional protein encoded by the CTNB1 gene. They are involved in cell-cell adhesion by being a part of cell adhesive protein cadherin and in gene transcription by acting as a signal transducer. It interacts with the transcription factor/lymphoid enhancer-binding factor TCF/LEF family of genes, facilitating the transcriptional activation of numerous proliferative genes, such as Myc (Figure 1.4). In normal cells, they are regulated and degraded by forming a destruction complex with glycogen synthase kinase 3 beta (GSK3β)/Axin/APC proteins to prevent its translocation from the cytoplasm to the nucleus. Wingless-type integration signalling promotes the dissociation of the destruction complex and the release of β-catenin. In addition, the non-availability of normal Anaphase-promoting complex (APC) proteins due to the mutations in the *APC* gene will lead to the accumulation of β-catenin in the cytoplasm, eventual nuclear translocation, and subsequent induction of proliferative molecular mechanisms in CRCs (Network, 2012, Najdi et al., 2011). (APC) deficiency alone cannot be the sole reason for the pathogenesis of CRCs. The mutational activation of *KRAS* and hypermethylation of *APC* promoter may also contribute to tumorigenesis. However, the evidence on the occurrence of CIN in due course of pre- or post-*APC* mutations remains unclear.

The other molecular mechanisms leading to CIN tumour progression are associated with the dysregulation of chromosomal segregation, telomere formation, and DNA repair. These mechanisms involve mutations in the genes related to the cell cycles checkpoint systems, such as budding uninhibited by benzimidazoles 1 (*BUB1*) and or BUB1-related protein 1 (*BUBR1*)

and their protein products leading to impairment in the checkpoints of the chromosome segregation during G2/M cell cycle and inhibits the anaphase-promoting complex/cyclosome (*APC/C*) and cell cycle arrest (Zhao et al., 2014, Herzog et al., 2009). Upregulation of the aurora kinase A (*AURKA*) and polo-like kinase 1 (*PLK1*) genes are also reported in the CRCs (Han et al., 2012, Baba et al., 2009). Centrosomes are essential for various cellular processes, including mitosis induction, assembly of spindle fibers, centrosome duplication, cell division and transition from metaphase to anaphase. Abnormalities in centrosomes, such as the formation of extra microtubule-organizing centers, can contribute to tumorigenesis (Ganem et al., 2009).

Dysfunction of telomeres will cause the amplification of oncogenes in those regions. There are several reports on the shortening of telomere results in CIN and uncontrolled cell proliferation in CR tumours (Baichoo and Boardman, 2014, Bunting and Nussenzweig, 2013, Matsui et al., 2013, Nakamura et al., 2000). One possible molecular mechanism through which CIN can be developed in CRC is the abnormalities in DNA damage response (*DDR*). Cervical intraepithelial neoplasia (CIN) can also develop in the haploinsufficiency of variant histone protein H2AX. When DNA gets damaged, H2AX activates ataxia-telangiectasia (ATM) (Oubaddou et al., 2023). This process can result in chromosome instability due to the DDR-mediated stabilization of the interaction between microtubules and kinetochores, which involves AURKA and PLK1. Ultimately, this can lead to abnormal chromosomal segregation and tumorigenesis (Kobayashi et al., 2009, Bakhoum et al., 2014).

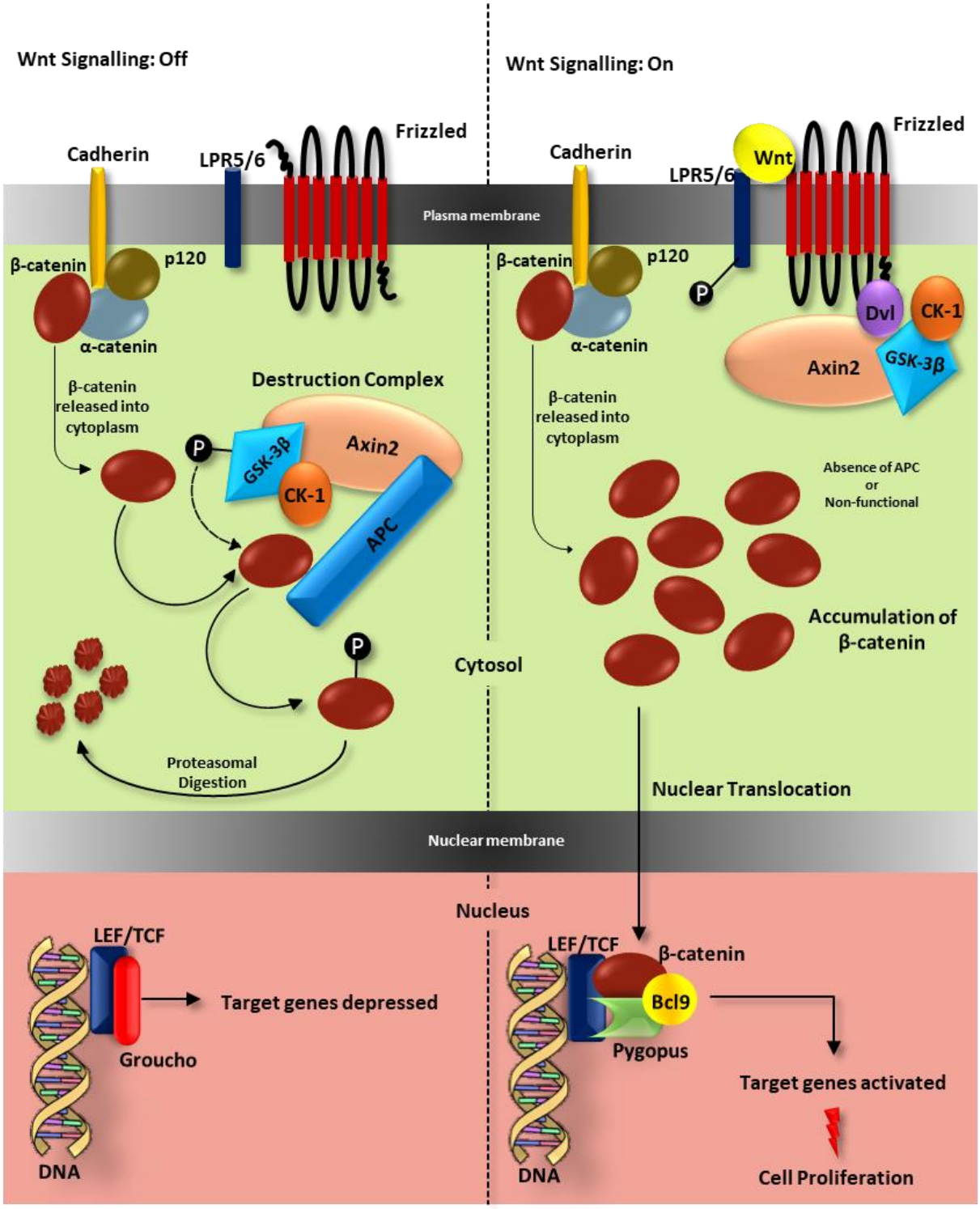


Figure 1. 4. Wnt Signalling pathway of CIN. Image created using Microsoft PowerPoint.

1.6.1. Biomarkers

Biomarkers play a vital role in all stages (diagnostic biomarkers), prognosis (prognostic biomarkers), and opting for the best therapeutic strategies and therapeutic response (predictive biomarkers) of any cancer, including CRC (Henry and Hayes, 2012, Duffy et al., 2011). Biomarkers can be of different types, including nucleic acids, antibodies, proteins and peptides. Most of the studies until the early 20th century focused on the gene mutation statuses as biomarkers, and some of them were used clinically, e.g. specific mutations in *KRAS and UGT1A1*. Targeted therapy for advanced CRCs with cetuximab and panitumumab antibodies that target and inhibit epidermal growth factor receptors (EGFR) signalling pathway becomes ineffective due to specific mutations in the *KRAS* gene (Lièvre et al., 2008, Di Nicolantonio et al., 2008, Di Fiore et al., 2007, Ciardiello and Tortora, 2008, Benvenuti et al., 2007). Similarly, polymorphisms in *UGT1A1* made the drug irinotecan inefficient (Takano and Sugiyama, 2017, Schulz et al., 2009).

1.6.2. Protein Biomarkers

In recent years, the interest in identifying protein biomarkers has been steadily increasing as it has become crucial in clinical practice and personalized medicine. The ultimate aim of proteomics is to study the proteome of the samples from healthy individuals and the potential modifications in the proteome, over-expression, under-expression, up-regulation, down-regulation, post-translational modifications, including methylation, glycosylation, glutathionylation, of the samples from the diseased individuals. The proteomes of the samples, such as blood, tumour biopsy, and stool, are extracted, processed, and quantitatively analysed using mass spectrometry (MS). In clinical proteomics, biomarker identification includes discovery, verification and validation. Each step has a purpose and subset of techniques (Chauvin and Boisvert, 2018). At the discovery stage, a shotgun proteomic approach (tandem mass spectrometry or MS/MS) is used to study a small cohort of samples with the help of techniques like label-free quantification (LFQ), stable isotope labelling by amino acids in cell culture (SILAC), tandem mass tag (TMT), isobaric tag for relative and absolute quantitation (iTRAQ). During the verification stage, a targeted proteomics approach is employed, utilizing techniques such as multiple reaction monitoring-mass spectrometry (MRM-MS), selected reaction monitoring-mass spectrometry (SRM-MS), and sequential window acquisition of all theoretical fragment ion spectra (SWATH) to accurately quantify the target proteins. At the validation step, samples in a large cohort are investigated for their clinical relevance, sensitivity, and specificity.

1.6.3. Proteomic signatures in CRC

In addition, evaluation of the changes in the proteomic profile associated with tumorigenesis will help identify therapeutic targets in the early stage. It is well established that CRC is mediated by signalling and secretory molecules like cytokines, chemokines, growth factors, proteases, and extracellular matrix (ECM) components. Proteins like insulin-like growth factor-binding protein 7 (IGFBP7), glutamine gamma-glutamyl transferase 2 (TGM2), and calcyclin binding protein (CacyBP) were identified as the biomarkers of metastatic CRCs (Kuppusamy et al., 2017, Ghosh et al., 2011, Katayama et al., 2006) while cyclooxygenase 2 (COX2), inducible nitric oxide synthase (iNOS/NOS2), and selenoproteins were identified as the biomarkers of early-stage CRCs (McIntosh, 2008, Bi et al., 2006). Expression of proteins, including enzymes, cytokines, and chemokines, are altered in CRC, which in turn affects the major metabolic pathways like glycolysis, tricarboxylic acid (TCA) cycle, gluconeogenesis, and the minor glucuronic acid pathway. Metabolic enzymes such as triosephosphate isomerase and keratins eight were found to be up-regulated. In contrast, enzymes like succinate dehydrogenase subunit A (SDHA), aldehyde dehydrogenase (ADH), and succinyl-CoA 3-ketoacid coenzyme A transferase (SCKCAT) were found to be down-regulated in CRCs (Di Nicolantonio et al., 2008, Coppedè, 2014, Mao et al., 2012, Sastre et al., 2011). These proteins can be used as diagnostic and prognostic biomarkers of early and metastatic CRCs.

Antioxidants such as superoxide dismutase (SOD), catalase (CAT), glutathione reductase (GR), and glutathione-S-transferase (GST) are crucial for the redox balance of the normal function of the cells, and their levels can be significantly altered during the process of tumorigenesis; thus, they serve as the plasma biomarkers to trace the prognosis of CRC. DNAJB8, a heat shock protein 40 (HSP 40) family member, was found to be over-expressed in colorectal tumorigenesis (Morita et al., 2014). Cell signalling proteins like EGFR, FAK, and c-Met are secreted highly in colon cancer cells that can be regulated by HSP 90 inhibitor 17-demethoxygeldanamycin (17-DMAG), where blocking of HSP 90 will enhance the over-expression of other transcription factors, thus making HSP 90 as an interesting predictive biomarker for the targeted CRC therapy with 17-DMAG.

Cytokines and chemokines play a vital role in the immune-cell infiltration of tumours, tumour cell growth, survival, metastasis, and angiogenesis, and also regulate anti-tumour immunity, especially in CRCs. Secretion of cytokines, including tumour necrosis factor-alpha (TNFα), interleukins (IL) like IL-6 and IL-17 were increased in metastatic colon cancers, where IL17

stimulates the secretion of a variety of angiogenic factors such as vascular endothelial growth factor (VEGF), keratinocyte-derived chemokine (KC), and macrophage inflammatory protein-2 (MIP-2) (Kaler et al., 2014, Wu et al., 2013) leading to angiogenesis in CRCs. Chemokines are low molecular weight cytokines (8-11KDa) and can be divided into C, CC, CXC and CX3 groups. Their functions on various immune cells are distinct. Increased levels of chemokine 25 (CCL25) and its receptor protein chemokine receptor 9 (CCR9) were reported in colon adenomas, while their levels gradually decreased when the adenomas progressed towards invasions and metastases. The involvement of CCL25 and CCR9 in inhibiting CRC invasion and metastasis is well characterized (Chen et al., 2012). Similarly, the levels of chemokines like CCL2, CCL4, CXCL1, and CXCL5 were increased in the malignant colon cancer tissues compared to the normal mucosa. In contrast, the levels of CCL5 decreased towards malignancy (Baier et al., 2005).

Recently, (Saleem et al., 2019) evaluated the proteomic profile in colon cancer progression using high-performance liquid chromatography-electrospray ionization mass spectrometry (HPLC-ESI MS/MS). They identified a list of proteins whose expressions were either up-regulated or down-regulated by examining the tissue biopsies of the colon cells of individuals who are reported to be expected and non-cancer (NC), having non-adenomatous polyps (NAP), non-metastatic (NM), and metastatic (M) tumours (Table 1.5).

Table 1. 5 A. Proteomic Signatures in CRCs Adapted from (Saleem et al., 2019)

Stage	Decreased/Downregulated	Increased/Up-regulated
All Stages	ECM proteins Elastin, Perlecan, Bone marrow proteoglycan, CSPG4, CSPG3, Laminin α, β, & γ subunits, Decorin, Biglycan, Basigin, Nidogen 1 & 2, Collagen α-1(I, IV, V, VI, XIV, XVIII, XXI) chains, Collagen α-2(I, IV, VI) chains, Collagen α-3 (VI) chain, Collagen α-6 (IV) chain, Laminin subunit α-4 & 5, Laminin subunit β-2 Cell adhesion and membrane integrity proteins Integrin α-5 & 6, Integrin β-1 & 5, Annexin A6, A7 & A13, CEACAM1, CEACAM7, CD9, CD48, CD63, CD 81antigens, CD59 glycoprotein, Cell surface A33 antigen, HLA class II histocompatibility antigen γ chain, ADP-ribosyl cyclase/cyclic ADP-ribose hydrolase 1, Guanine nucleotide-binding protein G(Ii) subunit α-2, Peripheral plasma membrane protein CASK, Plasma membrane calcium-transporting ATPase 1 Proteins involved in xenobiotics metabolism UGT2B7, Ras-related protein R-Ras, MCU, Carboxylesterase 3, Liver carboxylesterase 1, Sulfotransferases 1A1 & 1A4, Epoxide hydrolase 1, Estradiol 17-β-dehydrogenase 2 & 8, Corticoid 11-β-dehydrogenase isozyme 2	Cell cycle-related proteins CDC5L, CARP1/CCAR, NASP, ANP32A, ANP32BB, HMG isoforms A1, B1, B2 & B3, SMARCE1 Proteins involved in matrix degradation. Serine protease HTRA3, NGAL, Myeloblastin, Lactotransferrin, MMP-9, ADAMTS4, Neutrophil elastase Proteins involved in remodelling of Cytoskeleton. Nesprin-1, Fascin, Actin-related protein 2/3 complex subunit 4, AIF-1, Protein S100-A8 & A9, Plastin-2CAPG, Neurabin-2, Calponin-2, Twinfilin-1, BAIAP2, Serine/threonine-protein kinase PAK 2 Proteins involved in immunity and inflammations. Fibrinogen α chai, Fibrinogen β & γ chains, Neutrophil defensin 1 & 4

Table 1. 6 B Proteomic Signatures in CRCs Adapted from (Saleem et al., 2019)

Stage	Decreased/Downregulated	Increased/Up-regulated
Malignant and Early Metastatic Stage (TNM Stage II & III)	Proteins associated with various functions Electron transport, Respiratory chain, TCA cycle, Gluconeogenesis including glucagon, Mitochondrial ribosomes, DNA replication, ATP/ADP transport and metabolite trafficking, including ATP synthase G-protein- linked transmembrane signalling Proteins G-protein α, β, & γ subunits, Integrin α (α1, α3, α5, α7, 7 αx) and Integrin β (β1 & β5) subunits, Annexin (A1, A2, A4, A5, A6, A7, A11, & A13), N-Ras, R-Ras, Cav-1	Proteins involved in immunity and inflammation Neutrophil defensin 1 & 4, Fibrinogen α, β, & γ chains, Prothrombin, Protein S100-A8 & A9, Cathepsin E, Coiled-coil domain-containing protein 88B Proteins involved in remodelling of Cytoskeleton Nesprin-1, Fascin, Actin-related Protein 2/3 complex subunit 4, Allograft inflammatory factor 1, Plastin-2, macrophage-capping protein, Neurabin-2, Calpolin-2, twinfilin-1, Brain-specific angiogenesis inhibitor 1-associated protein 2, Serine/threonine-protein kinase PAK, Ubiquitin-like protein degradation proteins
Late Metastatic Stage (TNM Stage III & IV)	Proteins involved in mitochondrial function and membrane transport activity, Mucin-2	Proteins involved in immunity and inflammations Complement C6, Factor H, Syntenin-1, Apoptosis-associated spek-like protein containing CARD, Protein canopy homolog 3, Ubiquitin-conjugating enzyme E2 N, Ubiquitin-1,2 & 4, TP53-binding protein 1, Centrosomal protein 131 kDa

1.7. Glycosylation

1.7.1. Introduction to Protein Glycosylation

Glycosylation is a post-translational modification used in biological systems to explore and diversify proteins (Mann and Jensen, 2003, Walsh et al., 2005, Weerapana and Imperiali, 2006). Glycosylation typically occurs in proteins, with approximately 50% of proteins glycosylated on secreted and transmembrane proteins of eukaryotes, archaea, and prokaryotes (Lehle et al., 2006). Glycosylation, specifically protein glycosylation, is perhaps the most common post-translational modification with significance and complexity in biological processes, given that approximately 50-70% of serum proteins are glycosylated (Holst et al., 2015b). Di Wang *et al.,* 2022 reported that malignant transformation is possible owing to an altered and aberrant glycosylation process, giving credence to glycosylation's significance in cancer therapy. As a biomarker or treatment, aberrant glycosylation is characteristic of various diseases and tumours. Glycoproteins are a class of proteins that contain glycans (oligosaccharide chains) attached to the amino acid side chains by a process known as glycosylation (Hughes, 2014). Glycosylation can occur during protein synthesis (co-translational) or after protein synthesis (post-translational modification, PTM) and can be

classified into many different types, such as N-glycosylation, O-glycosylation, P-glycosylation, C-glycosylation, S-glycosylation, glypiation and glycation. They occur by PTM mechanisms, except for glycation, which occurs randomly in the bloodstream (Ohtsubo and Marth, 2006).

Figure 1.5 depicts glycosylation that is directed through PTM. The first two types identified were widespread. N- or O-linked glycosylation occurs when an asparagine (Asn) residue or a serine (Ser), threonine (Thr), tyrosine (Tyr), hydroxylysine (Hyl), and hydroxyproline (Hyp) residue is attached to an oligosaccharide chain (glycan) (Holst et al., 2015b, Dennis et al., 2009, Brzostek et al., 2009, Roitsch and Lehle, 1989). P-glycosylation happens when the glycan is attached to the phosphorus on a phosphoserine or phosphothreonine. In contrast, the S-glycosylation is achieved by attaching the glycan to the thiol group of the cysteine amino acid. On the other hand, glypiation is a process by which a protein is covalently attached to the glycosylated phosphatidylinositol anchor. One of the most common PTM localizes proteins to the plasma membranes, a type of glycosylation detected on the cell surface glycoproteins of the eukaryotes and archaea.

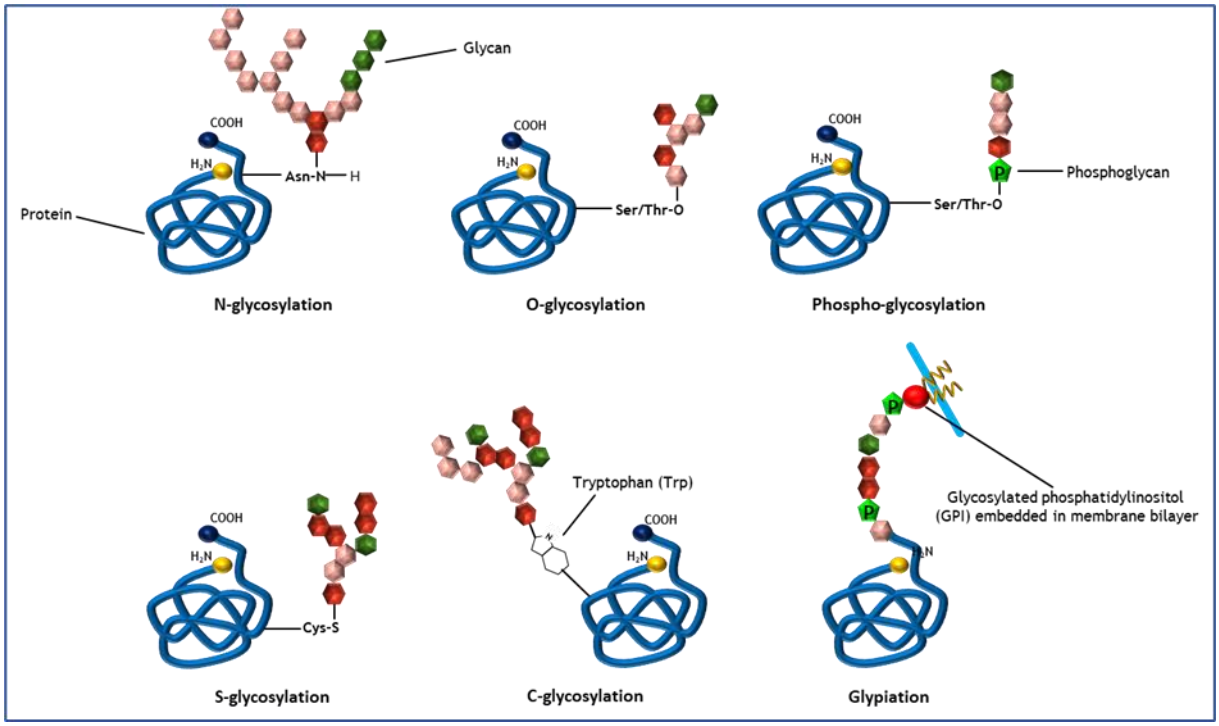


Figure 1. 5. Types of post-translational modification (PTM). Image created using Microsoft PowerPoint

The N-glycosylation is represented by asparagine (Asn) attachment to the protein's oligosaccharide chain. The O- and phospho-glycosylation occur through the attachment of serine (Ser), threonine (Thr), and phosphoglycan to protein. The S-glycosylation happens when a glycan is attached to the thiol group of the cysteine amino. The glypiation occurs through a covalently attached protein to the glycosylated phosphatidylinositol anchor.

1.7.2. Role of glycosylation in protein modification

In every cell, post-translational changes are common and are known to control protein activity by altering their physicochemical properties (Duan and Walther, 2015). Glycosylation, phosphorylation, and methylation are a few changes that can change the thermodynamic, kinetic, and structural characteristics of proteins (Shental-Bechor and Levy, 2009, Solá et al., 2007). Because of this, posttranslational modifications increase the range of protein properties beyond those determined by their sequence, which can be seen as practical means of increasing the diversity of the proteins encoded in the genome (Walsh et al., 2005). The characteristics of the underlying energy landscapes that control protein folding impact the biophysical characteristics of proteins. Joint theoretical and experimental research conducted by different researchers has concluded that proteins fold by navigating an energy landscape focused toward a native state with a defined structure (Fersht and Daggett, 2002) (Walsh et al., 2005). Energy landscapes have a funnelled shape which is a result of sequences affected by interactions that conflict with the natural state of proteins resulting in a high conformational specificity. The reason why protein structure influences folding and binding kinetics is explained by the energy environment present during protein folding.

Numerous experimental findings on the thermodynamics and kinetics of protein folding, including the molecular structure of intermediates and the ensembles of the transition state, have been replicated using the funnelled energy landscape concept where protein structures have been predicted and created (Papoian et al., 2004, Jin et al., 2003, Clementi et al., 2000). Glycosylation is one of the most frequent and significant posttranslational changes during or following protein production (Varki, 1993, Lis and Sharon, 1993). The intricate process of glycosylation, aided by various enzymes, requires the attachment of 13 different forms of monosaccharides to eight different types of amino acid residues (Spiro, 2002). Due to the intrinsic structural differences of glycans, glycosylation is an efficient method of producing a variety of proteins and altering their characteristics.

Glycosylation begins at the endoplasmic reticulum when the ribosome is making proteins. Given that the glycan is added to the unfolded protein while in the translocon complex (Helenius and Aebi, 2004), this may help the protein acquire the proper shape. In the absence of glycans, there is evidence for protein misfolding and aggregation, yet in other instances, removing all or some glycans has no impact on folding. (Mitra et al., 2006). Therefore, this implies that specific glycosylation sites are more critical for folding than others and that glycan effects on folding are probably local. Although glycans can help proteins fold, their removal from folded proteins frequently has little impact on the structure or function of the protein (Shental-Bechor and Levy, 2008, Jayaprakash and Surolia, 2017). The glycans, bulky hydrophilic polymers, are responsible for the protein's high solubility and increased stability against proteolysis. Furthermore, glycans' covalent attachment to protein surfaces may already improve proteins' thermal and kinetic stability (Shental-Bechor and Levy, 2008).

Regarding the role of glycosylation in protein function, the addition of carbohydrates to proteins makes them flexible and mobile inside the confines of the glycoprotein. It is also recognized that these carbohydrates act as a significant stabilizing force for proteins within their microenvironments (Arey, 2012). The role of carbohydrates in ensuring the appropriate three-dimensional structure of glycoproteins is particularly significant. Monosaccharides are added to the protein on particular amino acid residues as they are added to the nascent protein in the endoplasmic reticulum (Shental-Bechor and Levy, 2009). One of the studies conducted by Shental-Bechor and Levy demonstrated the effect of glycosylation on protein folding using thermodynamic stabilization showed how the addition of polysaccharide chains on SH3 protein affects the number of glycosylations and their location on the stability of the protein and its folding mechanism as shown in Figure 1.6 (Shental-Bechor and Levy, 2008)

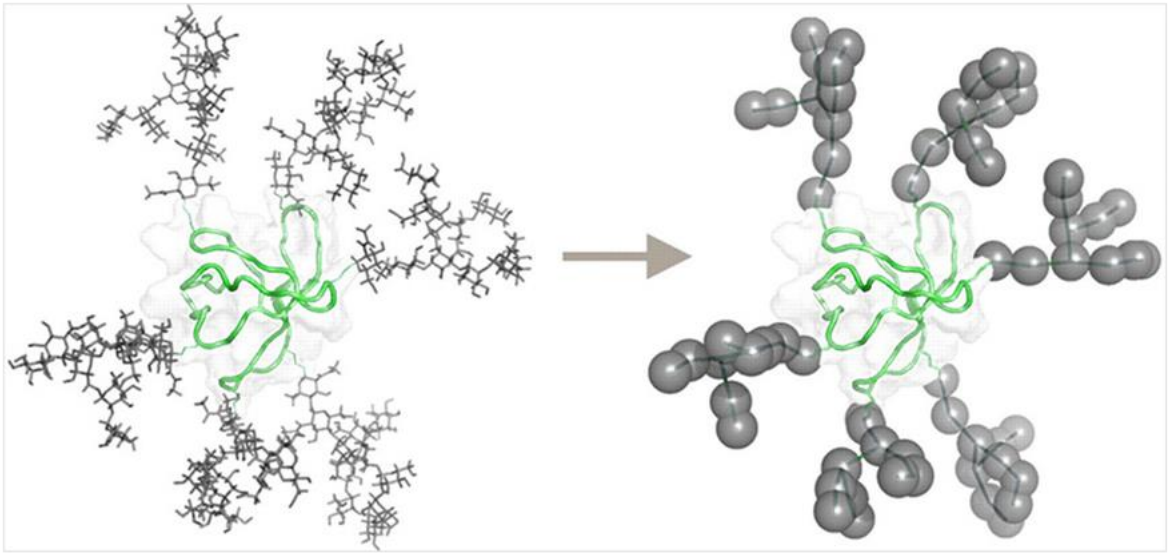


Figure 1.6. Example of glycosylation effect on protein modification. Adapted from (Shental-Bechor and Levy, 2008).

Eight amino acids have been documented to be glycosylated, with N-glycosylation being the most often added carbohydrate residue. The final protein product's proper folding into its three-dimensional and physiologically active conformation can be achieved by glycosylation (Spiro, 2002). However, it has been noted that this is not always the case for many glycoproteins. Interestingly, adding these sugar residues is intricate and little understood, even though the body's various enzymes regulate it. Therefore, these proteins' biological function depends on glycosylation and other secondary protein processing (Shental-Bechor and Levy, 2008) (Arey, 2012).

Glycosylation is vital for regulating secondary protein processes within cells, including modulating intermolecular interactions, preventing aggregation, extending the lifetime of circulating proteins by resisting proteolytic degradation, and intrinsically stabilizing protein structure (Shental-Bechor and Levy, 2009, Varki, 1993). The predominant glycosidic linkages for protein modifications in humans involve N-linked glycosylation, which occurs at asparagine residues via the Asn-X-Thr/Ser recognition sequence, and O-linked glycosylation, which occurs at serine/threonine residues through the attachment to oxygen atoms (Figure 1.7) (Schjoldager and Clausen, 2012, Hossler et al., 2007).

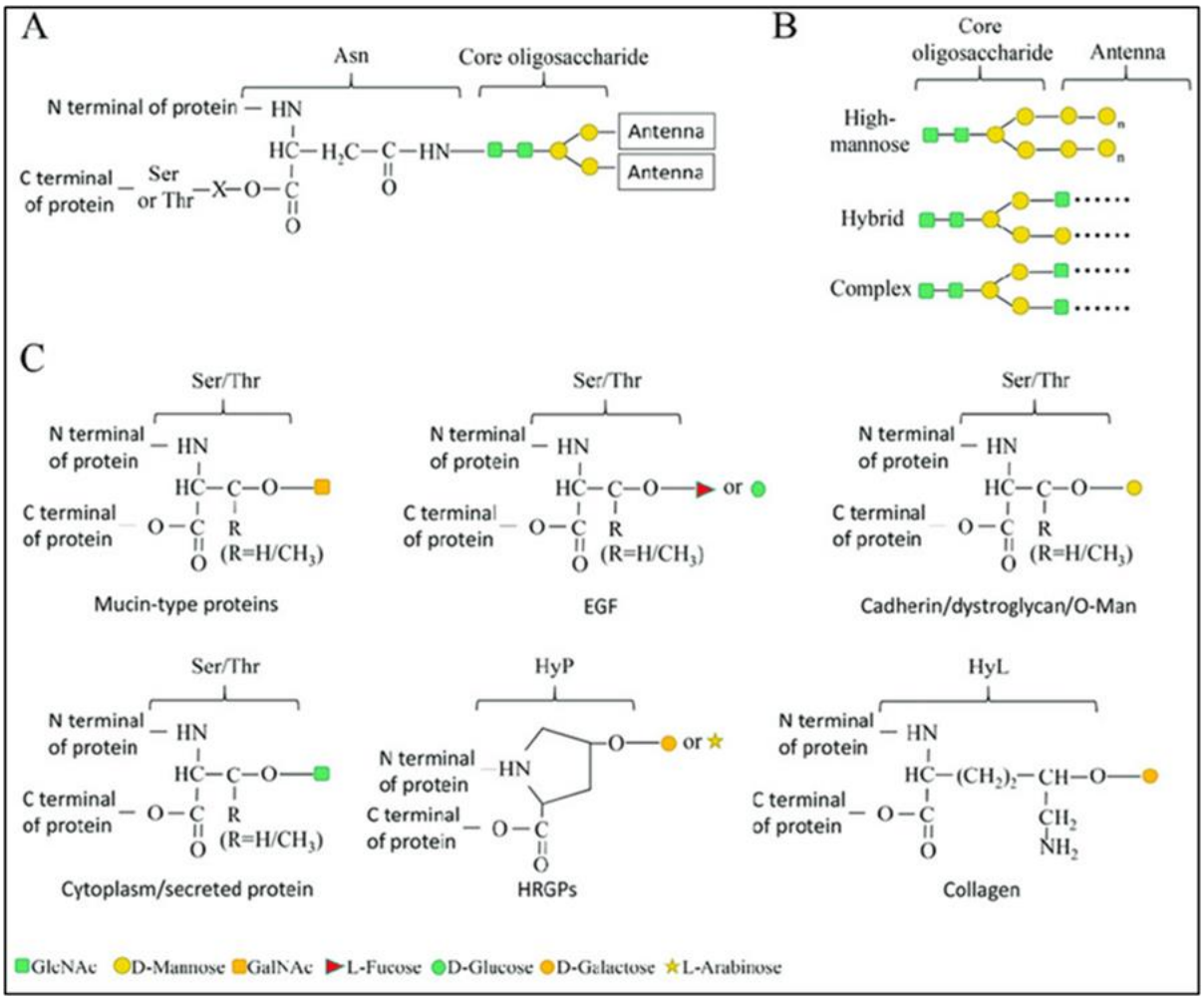


Figure 1. 7. Schematic drawing of N-linked and O-linked glycosylation types. A and B represent N-linked glycoproteins, while C represents O-linked glycoproteins Adapted from (Lin et al., 2020).

1.7.3. The Biological Significance of Glycoproteins

Glycosylation is a highly complex, diverse, regulated, and essential process of protein processing in cells and plays a vital role in determining proteins' structure, function, and stability. Although the mechanism of adding sugars to the proteins is poorly understood, it is known that the process recruits several enzymes to attach the glycans to the proteins. It provides a thermodynamically stabilizing microenvironment and helps the protein to achieve its proper three-dimensional conformation (Dennis et al., 2009, Ruddon and Bedows, 1997).

Adding or removing even a single sugar moiety compromises the thermostability of the protein and could result in misfolding (Shental-Bechor and Levy, 2008). It has also been known for its importance in the protein-protein and protein-ligand interactions. For example, glycosylation of many cytokines alters the recruitment and interaction with their cognate receptors like G-proteins and determines which signalling pathways should be activated. Glycosylation even

helps extend the half-life of many proteins, including cytokines, antibodies, and hormones (Meyer and Möller, 2007). Hormones like luteinizing hormone (LH), follicle-stimulating hormones (FSH), and thyroid-stimulating hormone belong to the glycoprotein hormone family. These hormones, LH and FSH exist as αβ-heterodimers in the circulation, where their degree of glycosylation and complexity varies within their isoforms based on the physiological state of the site where they exert their function (Arey and López, 2011, Ulloa-Aguirre et al., 2003, Ulloa-Aguirre et al., 1995).

The value and importance of glycoproteins have been illustrated in the Human immune deficiency virus (HIV). The HIV viral coat glycoprotein GP120 is well established. GP120 contains 27 heavily glycosylated residues within the protein, contributing to half of the glycoprotein's mass (Meyer and Möller, 2007). It is essential to adhere the virus onto the host cell surface by interacting with the host's CD4 receptor. Subsequently, conformational changes occur within the receptor-co-receptor complex, leading to the fusion of the membranes of the virus particle and the host. Glycosylation in the GP120 is a barrier for the host immune cells and antibodies to recognise and eliminate the virus.

1.7.4. Glycosylation and Glycoproteins as a Biomarker for Colorectal Cancers (CRCs)

Since a characteristic feature of cancer is an alteration in the glycosylation process, which is central to many biological processes, the importance of glycosylation in cancer therapy has been brought into the spotlight and has attracted the attention of researchers because of its enormous potential in cancer research (Costa et al., 2020, Taniguchi and Kizuka, 2015). CRC is a malignancy impacting the colon and rectum, ranking among the top causes of cancer-related mortality globally. Glycans play a critical role in the cellular landscape, residing in the outer layer of the cell and participating in vital biological processes. These include cell adhesion, differentiation, interactions with pathogens, other cells or the extracellular matrix (ECM) as well as cellular transformations seen in cancer development (Schnaar, 2016). Although carcinoembryonic antigen (CEA) and other glycoproteins such as carbohydrate antigens (CA; CA19-9, CA242, CA195, CA50, CA72-2) and tissue inhibitors of metalloproteinase-1 (TIMP-1) are the existing biomarkers of CRC, their low sensitivity and specificity complicate their use for early detection (Qiu et al., 2008). Hence, there is a pressing necessity to discover novel plasma or serum biomarkers capable of early detection of CRC. The N-linked glycans found on the four most abundant serum proteins, IgG, transferrin, haptoglobin, and a1-acid glycoprotein, contribute to the total serum N-glycome, and cancer-

associated changes in glycosylation have been observed, making them an attractive and potential biomarker for the diagnosis of various stages of cancer (Bones et al., 2010).

Alterations in the N-glycosylation profile affect CRC progression and response to chemotherapeutic agents. They often lead to a mechanism of drug resistance. For example, vascular endothelial growth factor receptor (VEFGR) containing aberrant beta-1 N-acetylglucosamine (β1-GlcNAc)-carrying N-glycans activates angiogenic signalling through interaction with galectins, leading to a reduction in the efficacy of anti-VEGF drugs such as bevacizumab (Avastin) and ranibizumab (Lucentis) (Itatani et al., 2018). This abnormality is due to increased expression of abnormal glucosaminyltransferase-5 (GnT-5) in the Golgi apparatus. Where the abnormal GnT-5 produces tri- or tetra-antennary complex glycans by catalyzing the attachment of GlcNAc to the tri-mannosyl core of the N-glycan, this leads to increased production of VEGFR with aberrant β1-GluNAc. Furthermore, altered N-glycosylation in death receptors such as tumour necrosis factor receptor 1 (TNFR1), FS -7-associated surface antigen (FasR), and death receptors (DR4 & DR5) inhibits the induction of apoptosis (Very et al., 2018). N-glycosylation has also been shown to have the potential to stabilize efflux transporters (Marques et al., 2014).

Beta-1 N-acetylglucosamine β1,6-GlcNAc, bisecting GlcNAc and nuclear fucose are the major N-glycan branching structures that directly affect cancer progression, metastasis and therapeutic responses. They are produced by glycosyltransferases (GnT), including GnT-5, GnT-3, and fucosyltransferase 8 (Fut8), which are expressed by MGAT5, MGAT3, and FUT8 genes, respectively (Taniguchi and Kizuka, 2015). The enzymes GnT-5, GnT-3, and Fut8 are associated with cancer metastasis, cancer suppression, and expression of other cancer biomarkers, respectively. The progression of metastasis by GnT-5 is likely mediated by glycosylation of TIMP-1, which affects its binding properties with matrix metalloproteinases (MMPs) (Kim et al., 2008).

It was observed that CRC correlates with five significant alterations in glycosylation: (i) galactosylation – a decrease in mono- and di-galactosylated glycans and an increase in tri- and tetra-galactosylated glycans, (ii) galactosylation – an increase in glycans without galactose residues, (iii) N-acetylgalactose (GalNAc) antennas – a decline in galactosylated and sialylated bi-antennary GalNAc glycans and an rise in highly branched glycans (iv) Sialylation - a reduction in monosialylated glycans and an upsurge in tri- and tetrasialylated glycans (Clerc et al., 2016). In addition to galactosylation, a correlation between fucosylation and CRC was also

found (Osuga et al., 2016). Increased fucosylation was observed in metastasis from CRC. For protein 1 (CDX1), mRNA expression correlated with elevated multi-fucosylation, indicating antenna fucosylation (Holst et al., 2015b).

Antenna fucosylation arises from the action of fucosyltransferases (FUT), which are encoded by genes FUT1 to 7 and 9. This process results in the presentation of blood group-related Lewis antigens (Figure 1.8), which are glycan epitopes found on different glycoproteins and glycolipids (Dotz and Wuhrer, 2016, LE PENDU et al., 2001). More comprehensive details regarding the biological significance of fucosylation have been elaborated in other sources (Becker and Lowe, 2003). Nevertheless, the reports present conflicting views on stage-dependent variations in the expression of fucosylated glycan epitopes in CRC. While some studies suggested a general increase in fucosylation across CRC and other types of cancer (Vajaria and Patel, 2017), recent research indicates a stage-specific reduction in fucosylation, especially Lewis-type antenna fucosylation, in CRC metastases. (Kaprio et al., 2015), (Sethi et al., 2015). While the roles of glycosylation and CDX1 expression in cell differentiation and cancer suppression have been documented in previous studies, there is limited information available on the glycosylation profiles associated with CDX1 (Holst et al., 2015a)**.** Antenna fucosylation on N-glycans has been anticipated as a potential marker of epithelial differentiation in different CRC cell lines (Miyoshi et al., 2012)**.** CDX1 plays a role in the transcriptional regulation of fucosyltransferases (FUTs) involved in antenna fucosylation. This activity leads to a more differentiated and less invasive phenotype in CRC cell lines (Sakuma et al., 2012).

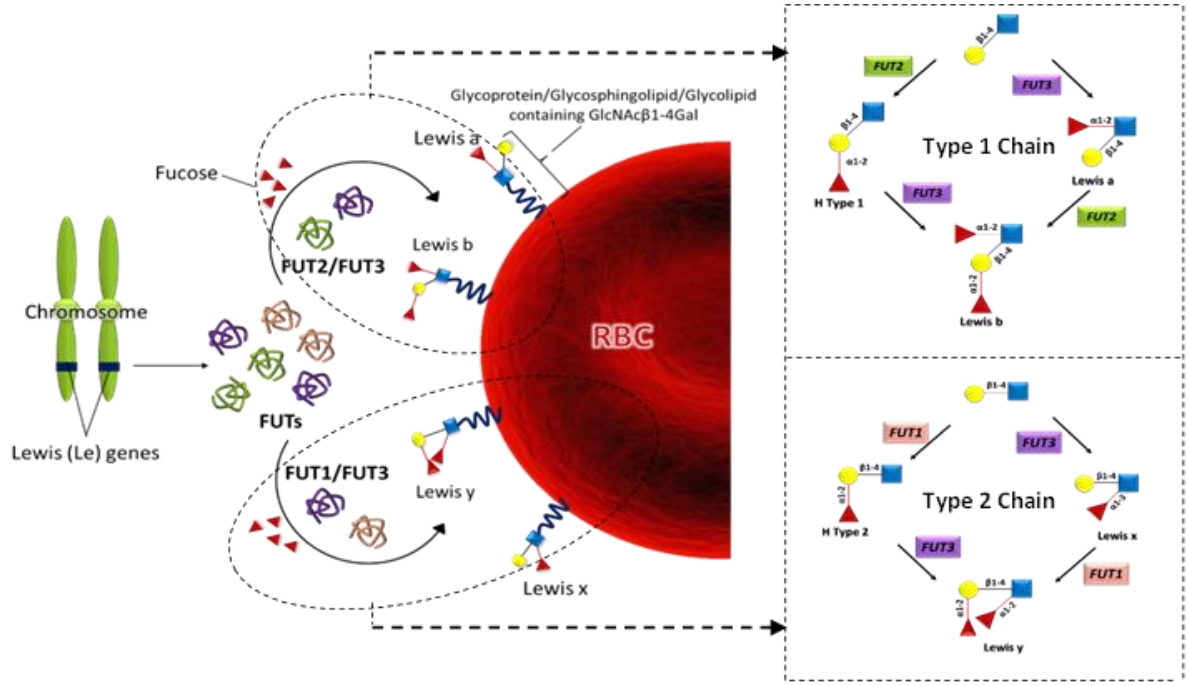


Figure 1. 8. Production of Lewis antigens through the activity of fucosyltransferases. Glucosyltransferases and fucosyltransferases (FUT), encoded by genes FUT1, FUT2, and FUT3, play key roles in the biosynthesis of blood group-related Lewis antigens. Image created using Microsoft PowerPoint

Strikingly, the glycan phenotypes observed in CDX-1 depleted cells resemble those seen in cells undergoing epithelial-mesenchymal transition, during which epithelial markers like E-cadherin are lost and mesenchymal markers like vimentin are acquired. Glycan-associated changes in CRC include a drop in antennal fucosylation and a decline in antennary branching of N-glycans and bisection. Conversely, elevated levels of high-mannose glycans, core fucosylation, and corresponding FUT8 expression, as well as increased 2,6-sialylation and ST6GAL1 gene expression, have been observed (Li et al., 2016a)**.** Glycosylation is pivotal in determining the folding, stability, subcellular localization, and biological functions of glycoproteins. Aberrant glycosylation, a hallmark of cancer, is closely associated with progression, tumor initiation, metastasis and resistance to chemotherapy (Pinho and Reis, 2015, Very et al., 2018). Inhibiting the transfer of UDP-GlcNAc to dolichol phosphate in the endoplasmic reticulum (ER) of eukaryotic cells disrupts protein maturation by blocking N-linked glycosylation (Hakulinen et al., 2017, Surani, 1979).

1.7.5. Glycosylation Inhibitors in Cancer

Cancer-specific glycoprofiles on cell surfaces result in modifications of cell surface receptors, affecting their sensitivity to specific ligands required for cell growth and innovation (Varki et al., 2015b). Increased polysialic acid, sialylation and N-glycan branching, along with the presence of sialylated Lewis antigens in glycolipids and glycoproteins, are identified as terminal modifications that play a role in cancer (Mereiter et al., 2019, Pinho and Reis, 2015). This affects many biological processes, including cancer initiation, progression, metastasis, host antitumour immunity, and chemoresistance (Mereiter et al., 2019).

Galectins, siglecs, selectins, and specific lectins like dendritic cell-specific ICAM-3-grabbing non-integrin 1 (DC-SIGN) and macrophage galactose lectin (MGL) are implicated in various cancer-related processes (Rodriguez et al., 2015). Numerous aspects of cancer progression, such as cell proliferation, immune evasion, extravasation, and invasion, are influenced by glycan-lectin interactions. Clinical trials are underway to explore the potential of specific inhibitors targeting these interactions as a novel treatment strategy for both standalone and combination therapies. The newly exposed tumour glycan field causes unique immunologic interactions mediated by lectins that significantly impact the comprehensive progression of the tumour (Wandall et al., 2021).

A vast protein family, known as lectins, possesses a shared carbohydrate recognition domain (CRD) capable of binding to specific glycosylated structures (Anderluh et al., 2022) (Kremsreiter et al., 2021). Human lectins are categorized based on their subcellular location and structural features (Van Damme, 2022). Lectins can be categorized into various types based on their structural features. These include C-type lectins, I-type lectins (including siglecs), S-type lectins (also referred to as galectins), P-type lectins (also known as selectins), and pentraxins (Raposo et al., 2021). Lectins can also be incorporated into the cell membrane or have a soluble form. They are thought to understand the tumour glycoside that controls immunological tolerance and suppression (Rodriguez et al., 2015). The role of sialic acid is that it is added to the glycan backbone by Gal-2,6-sialyltransferase 1 (ST6GalI), which is upregulated in these cancers (Lise et al., 2000). The sialylated products of ST6GalI, whose increased expression is associated with pro-survival metabolic pathways, can prevent tumour cell apoptosis and activate growth factor pathways (Schultz et al., 2016).

1.7.6. Glycosylation Pathways

Pathway diagrams are important to explore molecular biology because they make complex molecular biological processes understandable. Pathways diagrams offer a useful method for scientists to communicate, integrate, analyze, and visualize 'omics data and are highly cited resources (Kutmon et al., 2016). Pathway databases are used to analyze data from genomics, metagenomics, transcriptomics, proteomics, and metabolomics and are commonly employed to simplify more difficult analytical tasks, including cellular modelling (Sundararaj et al., 2004), flux balance analysis (Orth et al., 2010), gene-set enrichment analysis (Soobrattee et al., 2005), metabolite-set enrichment analysis (Xia and Wishart, 2010), and over-representation analysis. The several different pathways databases include KEGG (Kanehisa et al., 2017), the 'Cyc' databases (Caspi et al., 2016), Reactome (Fabregat et al., 2016), Wikipathways (Kelder et al., 2012), BioCarta (Nishimura, 2001), InnateDB, PharmGKB, and the Pathway Interaction Database.

1.7.7. N-linked glycosylation

Protein modification can occur through the attachment of N-acetylglucosamine (GlcNAc) to the nitrogen atom of the Asn side chain via a β-1N bond. Glycoconjugates linked by Asn comprise a GlcNAc2-mannose (Man) core to which many monosaccharides such as galactosylation, GlcNAclyation, sialylation, and fucosylation can be added or removed (Cherepanova et al., 2016). These additions during protein glycosylation regulate the final structure, which is either a high mannose N-glycan, a hybrid N-glycan, or a complex N-glycan. Since not all possible glycosylation sites are occupied at the same time, the formation of glycoforms with different numbers of attached glycans may occur (Scott et al., 2013). Variability in glycan length, branching pattern, and sequence of monosaccharide sequences can lead to additional structural complexity. In glycoproteins, the terminal ends of these glycans are often further functionalized with chemically charged groups such as phosphates, sulfates, and carboxylic acids, which produce a more complex structural variety (Schnaar, 2016).

Most living organisms are composed of N-glycans, which are essential for various intracellular and extracellular functions. The process of N-glycosylation relies on the development of a lipid precursor in which GlcNAc and Man form a branched carbohydrate structure that is linked to dolichol phosphate on the cytoplasmic side of the endoplasmic reticulum (ER) (Reily et al., 2019). To create a 14-sugar structure known as Glc3Man9GlcNAc2, the lipid precursor is subsequently turned to face the ER lumen. Once the formation of the dolichol phosphate

carbohydrate structure is complete, the addition of a carbohydrate chain to a protein takes place in Asn-X-Ser/Thr site using oligosaccharyltransferase which causes carbohydrate protein conjugate to undergo further processing in the ER (Vasconcelos-Dos-Santos et al., 2015, Fuster and Esko, 2005). The structure then travels to the Golgi apparatus, or the cis-Golgi, where a series of particular mannosidases further trim the carbohydrate structures before transferring them to the medial Golgi for maturation. GlcNAc, galactose, sialic acid, and fucose sugars are added to the medial- and trans-Golgi compartments to create hybrid and complex N-glycans (Helenius and Aebi, 2001, Fisher and Ungar, 2016).

1.7.8. O-glycosylation

Serine (Ser) and threonine (Thr) are the more common amino acids with functional hydroxyl groups on which glycosylation can take place (Varki et al., 2015a). The most frequent sugars in humans connected to Ser or Thr are GlcNAc and N-acetylgalactosamine (GalNAc). Many extracellular and secreted glycoproteins (Bennett et al., 2012, Vasudevan and Haltiwanger, 2014), including mucins, are rich in GalNAc-linked glycans (mucin-type O-glycans). Mucins are an important contact between epithelial cells and the body's exterior mucosal surfaces. Mucins have multiple O-glycosylation sites because of their high Pro, Ser, and Thr content and varying tandem repeats. These locations usually contain prolonged O-glycan cores that produce a gel-like substance that covers glycoproteins and cellular surfaces from external stress, microbial infection, and self-recognition by the immune system (Rangel-Angarita and Malaker, 2021).

The classification of blood-group antigens is based on this class of O-glycans, which includes additional O-linked glycoconjugates. This class of O-glycans has six primary structures, such as terminal GalNAc (Tn) and sialyl-Tn antigens. Polypeptides such as GalNAc Transferases (GALNTs) initiate the synthesis of mucin-type O-glycans (Pirro, 2018). Although they are frequently free, these GALNTs differ in their selectivity for amino acid motifs, adding a layer of regulation to how and where O-glycans are attached. Various carbohydrate structures are produced by the on-template sequential addition of glycans to the initial GalNAc on specific glycoproteins, such as mucins and human immunoglobulin A1 (IgA1) (Khowala et al., 2008). Contrary to N-glycans, these sugars are not subjected to pre- or post-processing modification of the sugar structures already present. Instead, they are added as the protein passes through the cis-, medial-, and trans-Golgi compartments. Different glycosyltransferases alter the

glycopeptide O-glycan chains that allows the addition of galactose, GlcNAc, sialic acid, and occasionally fucose to the structure already in place (Reily et al., 2019).

1.8. Inhibitors of Glycosylation.

1.8.1. Castanospermine

Castanospermine is an indolizidine alkaloid based on a structure named 1,6,7,8-tetrahydroxyoctahydroindolizine. Castanospermine is isolated from the seed of an Australian legume (Hohenschutz et al., 1981) or a black bean or Moreton Bay chestnut tree *Castanospermum australiae*. Castanospermine is a potent inhibitor of glucosidases I and II, which involves obligatory enzyme trimming during the synthesis of N-linked oligosaccharides on glycoproteins (Pili et al., 1995). The 2D chemical structure and the compound summary of Castanospermine are shown in Appendix 1. Castanospermine shows potent inhibition against α-mannosidases and α-glucosidases and inhibits α-glucosidases in the cells by producing vacuolation mainly on renal, thyroid, hepatic, and skeletal muscle cells (Allan et al., 2013). The anticancer activity of castanospermine was confirmed through several *in vitro* cell line studies. It inhibits tumour cell invasion, cell migration, and angiogenesis (Nguyen et al., 1992, Pili et al., 1995). An *in vivo* nude mice study confirmed that castanospermine significantly reduced tumour growth, tumour cell adhesion to the vascular endothelium, and antimetastatic activity (Pili et al., 1995).

1.8.2. Mannostatin-A

Mannostatin A is a glycoprotein processing inhibitor produced by *Streptoverticillium verticillus*, a Gram-positive bacterium. Mannostatin A effectively inhibited the processing of influenza viral hemagglutinin in MDCK cells, resulting in an accumulation of hybrid-type protein-linked oligosaccharides, consistent with blocking the function of Golgi mannosidase II. The 2D chemical structure and the compound summary of Mannostatin A are given in Appendix 1. Mannostatin analogues bind to Golgi alpha-mannosidase II (GMII) (Li et al., 2004). Mannosidase may alter the structure of oligosaccharides to cause malignant potential, according to previous studies. This has been identified in metastatic tumour cell lines showing increased β(1-6) GlcNAc branching oligosaccharides (Handerson et al., 2005). In a study testing several glycosidase inhibitors for tumour inhibitory effect, Ochi *et al.* (1993) reported that B16/F10 cells treated with mannostatin A exhibited a dose-dependent inhibition, and decreased metastatic activity of these cells, which was confirmed in an *in vivo* study using mice (Ochi et al., 1993). The addition of Mannostatin A specifically inhibited α-mannosidase

activity in B16/F10 or K-Ras NIH3T3 cells (Ochi et al., 1993). Mannostatin A has not been extensively studied for its use in CRC, and therefore deserves further investigation, especially in metastatic CRC.

1.8.3. Swainsonine

Swainsonine, a mannosidase inhibitor is extracted from locoweed, a poisonous flowering plant of the *Astragalus* and *Oxytropis* species (Martinez et al., 2019)**.** Swainsonine inhibits the activity of acidic α-mannosidase (Cenci di Bello et al., 1989). The 2D and 3D chemical structure and the compound summary of Swainsonie are given in Appendix 1 and 2. Swainsonine inhibits N-linked, where it inhibits α-mannosidase II, resulting in the formation of hybrid-type glycans. Overexpression of α-1,2 mannosidases is associated with many types of cancers, including liver, renal, and salivary gland larynx cancers (Olszewska et al., 2012). Thus, the ability of swainsonine to inhibit α-mannosidases makes it a feasible anti-tumor agent. Studies indicate that Swainsonine is an effective anti-tumour drug in many cancers by decreasing tumour metastasis invasion and inducing apoptosis (Lv et al., 2020). In mouse embryo fibroblast NIH-3T3 cell, Swainsonine inhibited the proliferation and collagen synthesis via miR-21 decline and suppression of PI3K/AKT and NF-κB pathways (Li et al., 2019). Despite the many evidence from numerous *ex vivo* studies showing that Swainsonine is an effective anti-cancer drug, a recent *in vivo* study showed that Swainsonine contributes to cervical cancer progression by favoring the proliferation and accumulation of myeloid cells in the spleen (Silveira et al., 2019). Swainsonine is reported to reduce 5-fluorouracil tolerance in mouse colon 26 cells and did not show any cytotoxicity regardless of the dosage (Hamaguchi et al., 2007). There are limited studies on the impact of Swainsonine in CRC; hence there is the need to explore it further, given its anti-tumor and chemoprotective effects.

1.8.4. Tunicamycin

Several natural products have been found to alter glycosylation. Tunicamycin (Appendix 1) is a nucleoside antibiotic that inhibits glycosylation, leading to impaired protein folding and the accumulation of misfolded proteins in the endoplasmic reticulum (You et al., 2018). Inhibiting protein glycosylation could induce stress in the endoplasmic reticulum (ER) where nearly a third of all cellular proteins are processed to complete their folding and synthesis
(Chen et al., 2010a). The activity of these protein processing structures is challenged in tumour cells by both intrinsic and extrinsic stresses. These stressess may include oncogenic activation, point mutations, hypoxia, nutrient deprivation, and acidosis (Yadav et al., 2014). The result of

these endoplasmic reticulum perturbations is ER stress. A term which describes altered protein homeostasis, protein misfolding, and the resulting accumulation of misfolded proteins in the endoplasmic reticulum lumen (Oakes, 2020). Endoplasmic Reticulum proteostasis can be restored by the cell, using a range of adaptive mechanisms, known as the unfolded protein response (UPR) which are initiated in response to enoplasmic reticulum stress. These mechanisms include enhanced folding as well as the clearance of misfolded proteins. In order to initiate the UPR, endoplasmic reticulum stress is detected though the action of three stress sensors within the endoplasmic reticulum. These three sensors are; activating transcription factor 6 (ATF6), PKR-like ER kinase (PERK) and inositol-requiring enzyme1 (IRE1) (Le and Kimata, 2021). Although the UPR is initially activated as a cytoprotective response, prolonged ER stress can result in apoptosis (Bjornsti and Houghton, 2004, Urra et al., 2016).

1.8.4.1.Mechanism of action and Anticancer activity of Tunicamycin

It is known that in human prostate cancer cells, Tunicamycin can inhibit growth and promotes apoptosis, by initiating apoptosis mediated by glucose-regulated protein 78 (Miyake et al., 2000, Shiraishi et al., 2005). In addition to this it has been suggested that Tunicamycin can also increase apoptotic signalling via the tumour necrosis factor-related apoptosis-inducing ligand (TRAIL) (Shiraishi et al., 2005). Ling et al. (2009) showed that tunicamycin might activate ER stress (Figure 1.9) and inhibit epidermal growth factor receptor N-glycosylation in human non-small cell lung cancer cells. Studies have also shown that tunicamycin treatment could partially reverse chemoresistance in several cancers (Wojtowicz et al., 2015, Fu et al., 2017).

Many chemo-resistant cancer cells have increased expression of the glycoproteins, P-gp and BCRP, which export the drug from the cell. Tunicamycin treatment can sensitise the cells making them susceptible to chemotherapy-induced death by regulating the function and localization of these proteins (Wojtowicz et al., 2015). endoplasmic reticulum stress can also be activated by the aberrant glycosylation of proteins, a process that can contribute significantly to the development of chemo-resistance (Very et al., 2018, Chakraborty et al., 2018, Yen et al., 2015, Wu et al., 2018, Britain et al., 2018). Dysregulated glycosylation is believed to initiate basal ER stress in multi-drug resistance (MDR) gastric cancer cells and this stress can be further exacerbated by the ability of Tunicamycin to inhibit glycosylation. Recent studies have demonstrated that ER stress can effectively trigger autophagy (Qin et al., 2010, Høyer-Hansen and Jäättelä, 2007, Kouroku et al., 2007).

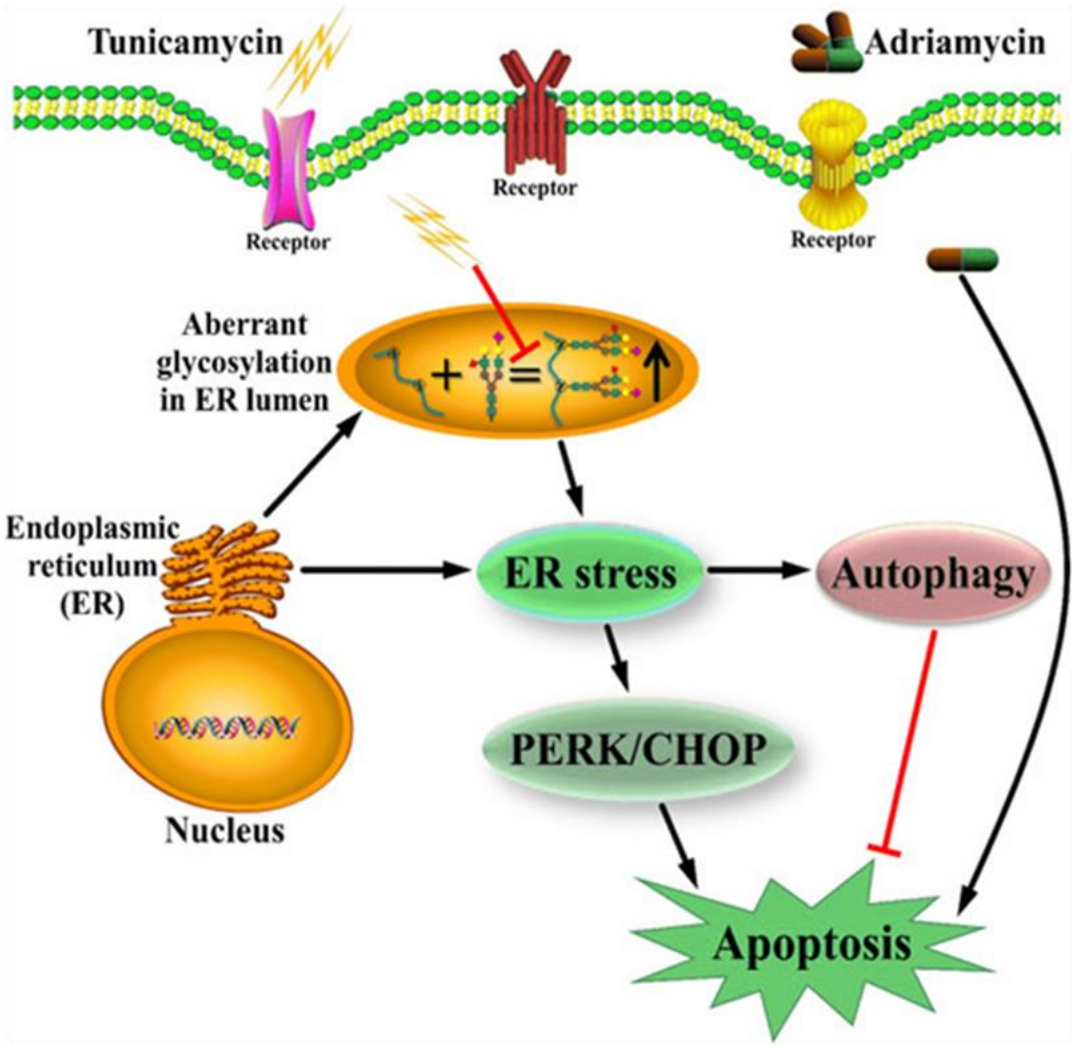


Figure 1.9. A schematic illustration of Tunicamycin's mode of action. Tunicamycin has been shown to specifically exacerbate ER stress and surmount chemoresistance in multidrug-resistant gastric cancer cells by targeting and inhibiting N-glycosylation. Adapted from (Wu et al., 2018)

Tunicamycin can inhibit the growth and aggressiveness of colon cancer cells. Tunicamycin does this by inhibiting the E-cadherin-mediated proliferation and migration of cancer cells by inhibiting N-linked glycosylation (de Freitas Junior et al., 2011). Tunicamycin is also able to inhibit key signalling pathways, including the extracellular signal-regulated kinase (ERK)/c JUN N terminal kinase (JNK) mediated AKT/mammalian target of rapamycin (mTOR) signalling pathway (You et al., 2021). These pathways involve cell proliferation and the aberrant mediation of physiological processes in cancer cells. Research has suggested that inhibition of N-linked glycosylation by tunicamycin may suppress E-cadherin-mediated proliferation, migration, and invasion in human colon cancer cells (de Freitas Junior et al., 2011).

1.8.5. Brefeldin A

Brefeldin A (BFA) was initially isolated from *Penicillium decumbens* in 1958 (Singleton et al., 1958). Because of its anti-cancer (Betina, 1969), antifungal, and antiviral activities, brefeldin A (BFA) has been promoted as a viable lead molecule in the field of drug discovery (Wang et al., 2012). Its ability to disrupt the cis-Golgi apparatus (Lippincott-Schwartz et al., 1989, Dinter and Berger, 1998) and induce apoptosis in many cancer cell lines (Larsson et al., 2010, Moon et al., 2012) allowed scientists to discover more advanced pharmaceutical compounds (APIs) derived from BFA (He et al., 2013).

1.8.5.1. Mechanism of action

Brefeldin A (BFA) is a well-known endoplasmic reticulum stress inducer that alters the Golgi apparatus's structure to cause ER stress responses. Brefeldin A (BFA) targets the SEC7 region of guanine-nucleotide exchange factors (GEF), leading to the activation of ARF (ADP-ribosylation factor) proteins (Chardin and McCormick, 1999). ADP-ribosylation factors (ARFs) are a Ras-family GTPase subfamily suggested as a critical participant in membrane trafficking. ARFs' activities are regulated and controlled by guanine nucleotide exchange factors (GEFs) and GTPase activating proteins (GAPs) (Donaldson and Jackson, 2000, Jackson and Casanova, 2000, Dejgaard and Presley, 2020). Earlier research showed that BFA-induced ADP-ribosylation is a noncanonical two-step process, including the enzymatic production of BFA-ADPR conjugate (BAC) by the ADP-ribosyl cyclase CD38. After BAC synthesis, it is covalently bound to the NAD+-binding pocket of BARS. This ADP-ribosylation alters the shape of BARS, preventing it from interacting with critical interactors and inhibiting BARS fission activity in mitotic Golgi partitioning. Since Golgi complex partitioning is essential for cell cycle completion, it was concluded that they have pharmacological implications for cancer treatment (Colanzi et al., 2013). In the presence of BFA, researchers observed the Golgi apparatus's collapse (Figure 1.10) and protein translocation into the ER. The effects described were rapidly and completely reversed upon discontinuation of the drug (Klausner et al., 1992). The administration of BFA to the Golgi apparatus resulted in the swift formation of membrane tubules due to the suppression of coat protein (-COP) assembly on Golgi cisternae (Klausner et al., 1992), leading to the relocation of various Golgi enzymes to the endoplasmic reticulum (Yardin et al., 1998, Pommepuy et al., 2003). To summarize, BFA has been shown to inhibit the exocytotic pathway of proteins from the endoplasmic reticulum to the Golgi, affecting both secretory and membrane-bound proteins. However, this effect is transient, lasting only briefly (Oda et al., 1990).

Another study looked at the impact of lengthy BFA treatments on overall cell shape, the behaviour of resident and cycling Golgi proteins, and the architecture of the microtubular and actin cytoskeletons. They concluded that BFA could also decrease the activity of critical molecules that regulate the dynamics of the microtubule and actin cytoskeletons (Alvarez and Sztul, 1999).

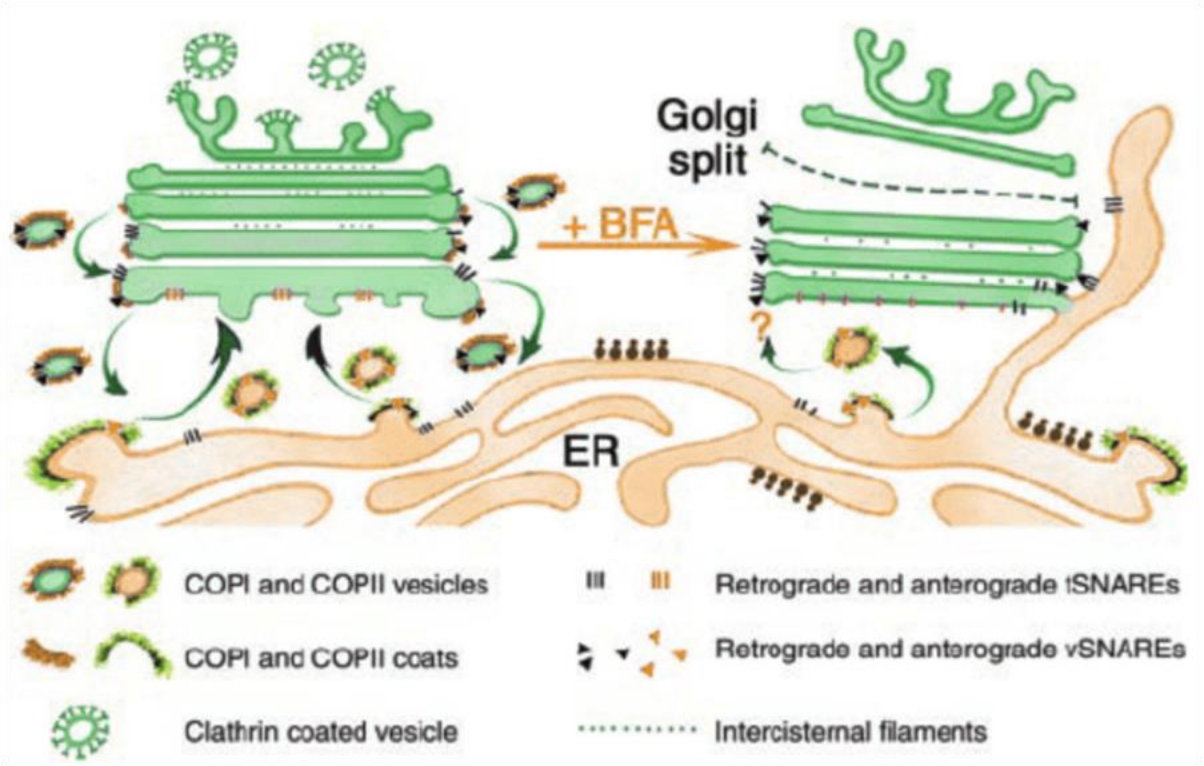


Figure 1.10. A Schematic illustration of the Effects of Brefeldin A on membrane trafficking between ER and Golgi. Under normal conditions, COPII-coated vesicles mediate export from the ER. These anterograde vesicles can fuse Fusion. Depending on the activity of surface proteins such as SNARE and clathrin**.** vesicles that leave the endoplasmic reticulum fuse to the Golgi apparatus from its cis face which contains anterograde *vesicle* or *v-SNAREs*, and *arget* or *t-SNAREs*. vesicles that leave the Golgi apparatus and exit from its trans face are coated with clathrin. Retrograde transport within the Golgi and from the Golgi to the ER depends on the presence of Coat protein complexes (COPI) and retrograde v- and t-SNAREs. BFA treatment results in the inhibition of Arf1, leading to the cessation of all vesiculation at the Golgi. This prevents the splitting off vesicles from the Golgi, effectively blocking ER-to-Golgi transport. Adapted from (Nebenführ et al., 2002)

1.8.5.2. Anticancer properties of Brefeldin A

Brefeldin A (BFA) exhibits anti-cancer properties and has been found to induce apoptosis in human cancer cells based on DNA fragmentation patterns (Shao et al., 1996). Additionally, it has been observed to induce apoptotic cell death in ovarian carcinoma cell lines through the

activation of multiple pathways, including the mitochondrial pathway, as well as the caspase-8 and Bid-dependent pathways (Shao et al., 1996, Wallen et al., 2000, Salles et al., 2004).
Besides, BFA has been shown to impede the action of the multidrug resistance-associated protein (MRP) (Verovski et al., 1996). A study conducted by (Wojtowicz et al., 2016) investigated the impact of brefeldin A (BFA) and castanospermine (CAS) on the activity, stability, and localization of P-glycoprotein (Pgp) and breast cancer resistance protein (BCRP) in various resistant cell lines. The findings suggested that BFA exhibited anti-cancer properties, indicating the potential efficacy of these compounds as adjuncts in cancer therapy.
In another study, the authors synthesized a variety of NO-donating mono- or diester derivatives of brefeldin A, which demonstrated substantial antiproliferative action with low IC_{50} values against human prostate cancer PC-3 cells, human colon carcinoma HT-29 cells and human liver cancer HepG-2 cells (Tian et al., 2017). ADP-ribosylation is a post-translational modification that impacts the activities of numerous target proteins. Research has shown that brefeldin A (Manco et al., 2022) (BFA) triggers ADP-ribosylation of C-terminal-binding protein-1 short-form/BFA-ADP-ribosylation substrate (CtBP1-S/BARS). CtBP1-S/BARS, a bifunctional protein, serves as a transcription factor in the nucleus and regulates membrane fission during intracellular trafficking and mitotic Golgi complex partitioning. The ADP-ribosylation of CtBP1-S/BARS by BFA involves a novel mechanism comprising two steps: Firstly, the ADP-ribosyl cyclase CD38 synthesizes a BFA-ADP-ribose conjugate, which then covalently binds into the CtBP1-S/BARS NAD(+)-binding pocket. This process locks CtBP1-S/BARS in a dimeric conformation, preventing its interaction with molecules involved in membrane fission, thus inhibiting the fission machinery essential for mitotic Golgi partitioning. Consequently, this inhibition may lead to cell cycle arrest in G2. Hence, the development of cell cycle blockers targeting tumour cells expressing high levels of CD38 could hold promise as a potential therapeutic strategy (Colanzi et al., 2013).

Another study revealed that Brefeldin A combined with docetaxel reduced the development of prostate cancer cells in monolayer 3D preparations (Namsa-Aid et al., 2021). Another study found that gemcitabine coupled with BFA at low doses is much more effective against the MIA PaCa-2 cell line than gemcitabine alone. Their findings suggest that the gemcitabine-resistant and 5-FU-resistant pathways may partially overlap. As a result, BFA could be employed as a gemcitabine modulator (Togawa et al., 2003).

1.8.5.3. Brefeldin A role in Colorectal Cancer

CRC is one of the most common neoplastic illnesses in the world, and effective treatment is still problematic. A study by Shao *et al.* (1996) revealed that the macrolide antibiotic brefeldin A (BFA) has significant anti-cancer action both *in vitro* and *in vivo* (Shao et al., 1996). The initiation of total autophagic flux has emerged as a pivotal process in the suppression of colorectal cancer (CRC) induced by BFA. BFA prompts endoplasmic reticulum stress, leading to enhanced production of binding immunoglobulin protein (Bip). This increase in Bip levels facilitates interaction with Akt, resulting in reduced Akt phosphorylation and subsequent activation of autophagy. Notably, inhibition of autophagy or suppression of Bip mitigates BFA-induced cell death, underscoring the importance of Bip-mediated autophagy in the anti-cancer effects exerted by BFA.

BFA works synergistically with paclitaxel or 5-fluorouracil to inhibit CRC. (Zhou et al., 2019) established a crucial molecular foundation for BFA-induced autophagy, implying that the antibiotic BFA could be repositioned as a viable anti-cancer medication for CRC treatment. Another study discovered that BFA inhibited colon cancer cells even at extremely low doses (Tseng et al., 2013). The study revealed that the IC_{50} of BFA was around 15 ng/mL, much lower than the microgram per millilitre range commonly employed in cell biology research to impede endoplasmic reticulum-Golgi transit. Because the RT-PCR results demonstrated that the leading indicators of ER stress response were up-regulated by 15 ng/mL BFA, the researchers concluded that the effects of BFA are most likely mediated via the development of endoplasmic reticulum stress. Their findings suggest that BFA at low concentrations can selectively target CRC stem cells and limit cancer spread with few adverse effects.

1.9. Thymidine Kinase 1

Thymidine kinase 1 (TK1) is an enzyme involved in the nucleotide salvage pathway, crucial for cellular proliferation. Thymidine kinase 1 serves as a significant biomarker for tumor proliferation, detectable in serum samples (Weagel et al., 2018). Human thymidine kinase 1 (hTK1) catalyses the phosphorylation of thymidine (dThd) to thymidine monophosphate (dTMP) in the pyrimidine salvage pathway via the activity of phosphotransferase (Makurat et al., 2021, Tribukait, 2020). Thymidine kinase 1 (TK1) is essential for the nucleoside metabolic process leading to the synthesis of DNA (Fang et al., 2023, Makurat et al., 2022). Many reports have suggested that TK1 is used to predict the recurrence and survival of different kinds of human cancers, and they are equally involved in activities that lead to DNA synthesises and

cell proliferation (Dang et al., 2020). TK1 is usually elevated in the early stages of malignancy in the serum. Hence TK1 is exploited as an early biomarker for detection, and an increase in TK1 levels often corresponds with cancer grade and stage (Weagel et al., 2018). Studies on TK1 have suggested that they are potential immunotherapeutic targets (Weagel et al., 2018).

1.9.1. Thymidine kinase 1 and Colorectal Cancer

CRC is the third most common cancer worldwide (Roshandel et al., 2024), significantly impacting global health. Thymidine kinase 1 (TK1), a cytosolic enzyme responsible for the phosphorylation of thymidine-to-thymidine monophosphate (TMP), has been implicated in the pathogenesis and progression of CRC (Bitter et al., 2020). Overexpression of TK1 has been observed in CRC tumour tissues, and elevated serum TK1 levels have been associated with poor prognosis in CRC patients (Bitter et al., 2020).

1.9.2. Thymidine kinase 1 as a Biomarker in Colorectal Cancer (Diagnostic Biomarker)

Numerous studies have reported elevated serum TK1 levels associated with CRC (Bitter et al., 2020, Velazquez et al., 2020). Serum TK1 activity is significantly higher in CRC patients than in healthy controls, suggesting its potential as a non-invasive diagnostic biomarker for CRC (Bitter et al., 2020).

1.9.3. Thymidine kinase 1 as a Therapeutic Target in Colorectal Cancer

Thymidine kinase 1 (TK1) plays a significant role in the pathogenesis and progression of CRC. Many studies have demonstrated its potential as a diagnostic and prognostic biomarker, and the exploration of TK1 as a therapeutic target shows promise for developing novel CRC treatments (Wang et al., 2018a), Further research is needed to fully understand the molecular mechanisms underlying TK1'sThymidine kinase 1's involvement in CRC and to optimize the use of TK1-targeted therapies in clinical practice. Thymidine kinase (TK) is an enzyme that catalyzes the transfer of a phosphate group from ATP to thymidine, producing thymidine monophosphate. While the primary role of TK1 is to regulate DNA synthesis, it has been shown to play a crucial role in glycosylation. The glycosylation process involves the attachment of carbohydrate molecules to proteins and lipids, and it is essential for numerous biological processes, including cell signalling, immunity, and metabolism.

Thymidine kinase (TK) has two isoforms, TK1 and Thymidine kinase 2, that differ in cellular localization and function. While the role of TK in DNA synthesis is well-established

(Aufderklamm et al., 2012), its possible involvement in glycosylation is a new area of investigation. Glycosylation is a post-translational modification in which carbohydrate moieties are added to proteins, significantly affecting their stability, folding, and function (Schjoldager et al., 2020).

1.9.4. Thymidine Kinase and Glycosylation: Thymidine kinase in nucleotide sugar synthesis

Thymidine kinase may be involved in synthesizing nucleotide sugars, which are essential glycosylation precursors. Nucleotide sugars are required to transfer sugar moieties to proteins during glycosylation (Stanley, 2011). Thymidine kinase activity can influence the availability of nucleotide sugars, potentially affecting glycosylation patterns (He et al., 2010). This suggests that TK may have an indirect role in glycosylation by modulating the levels of nucleotide sugars.

Thymidine kinase is modified by the O-GlcNacylation (Very et al., 2022). This modification is associated with cancer anabolism linking other enzymes involved in the serine biosynthesis pathway and phosphoserine aminotransferase 1 (PSAT1) (Maury et al., 2013). O-GlcNAcylation is another branch of glycosylation. Glycosylation impact on TK1 is also observed through O-GlcNAcylation of c-Myc at Thr58. This PTM stabilizes c-Myc, preventing its ubiquitination and proteosomal degradation. c-Myc is an oncogenic transcription factor that regulates cell metabolism due to its ability to activate the expression of several genes involved in nucleotide, glucose, and glutamine metabolism. These genes include ornithine decarboxylase (ODC), carbamyl-phosphate, and thymidine kinase (TK) (Chiaradonna et al., 2018). TK is indirectly associated with glycosylation in this case through c-Myc been stabilized by O-GlcNacylation. In human prostate cancer, increased O-GlcNacylation of c-Myc has been observed (Itkonen et al., 2013).

1.9.5. Therapeutic Implications

The possibility of thymidine kinase involvement in glycosylation has implications for developing new therapeutic strategies. Targeting TK and its role in glycosylation could lead to novel therapeutic approaches for diseases characterized by abnormal glycosylation, such as cancer and glycosylation disorders (CGD). Targeting TK1 in cancer cells, for example, may disrupt glycosylation patterns linked to tumour progression, potentially inhibiting cancer growth and metastasis (Bitter et al., 2020). Similarly, modulating TK activity might benefit treating CGD by normalizing glycosylation patterns and improving protein function (Very et

al., 2018). The role of thymidine kinase in glycosylation is a growing area of research, with recent studies (Bitter et al., 2020, Pérez-Pérez et al., 2008, Scheper et al., 2023) suggesting its involvement in nucleotide sugar synthesis, protein glycosylation, and interaction with glycosylation-related enzymes. More research into the molecular mechanisms underlying TK's role in glycosylation is required to fully comprehend its implications for human health and disease and investigate its potential therapeutic applications.

It is important to note that currently, in clinical settings, it has been shown that TK1 is elevated in early events of malignancy when looking at patient serums. This observation indicates that TK1 can be an early detection biomarker (O'Neill et al., 2007, Weagel et al., 2018). Furthermore, serum TK1 levels have been observed to be higher in a variety of haematological and solid malignancies, including breast, lung, and CRC, and high serum TK1 levels are frequently associated with cancer grade and stage and increased tumour size (Weagel et al., 2018). It is essential to add that TK-1 levels before and after surgical excision of the tumour might signal neoplasia recurrence and aid in stratifying patients into risk groups and developing a suitable antitumoral treatment. TK-1 can be used to detect relapses early after the tumour has been surgically removed (Ene et al., 2021).

As stated above, thymidine kinase 1 (TK1) plays a crucial role in the DNA salvage pathway, facilitating the regeneration of thymidine necessary for DNA synthesis and repair (Zhang et al., 2022b). Within the cytosol, TK1 converts thymidine into its monophosphate form (dTMP). To understand the significance of elevated TK1 levels in cancer, researchers conducted a study involving p53-null colorectal adenoma HCT-116 cells exposed to radiation or chemotherapeutic agents. An increase followed this in TK1, which promoted cell survival (Bitter et al., 2020). A depletion in TK1 in cells exposed to DNA damage can lead to cell death (Chen et al., 2010b). The increased levels seen in cancer may be due to missing C-terminal (Sheikh et al., 2022). Typically, the C-terminal region of human thymidine kinase 1 (TK1) is recognized and targeted by the Anaphase-Promoting Complex/Cyclosome-Cdh1 complex. This complex marks TK1 for ubiquitin-mediated proteolysis, ultimately resulting in its degradation (Ke and Chang, 2004).

Furthermore, it is important to note that uracil can be an indirect substrate of TK1. This is through uracil methylation (Alexeeva et al., 2019). Methylation of uracil at C5 to form thymine moieties is essential in both DNA synthesis and posttranslational modification of RNA (Mishanina et al., 2012). It is important to mention the structure of tunicamycin C,

characterized by an N-acetylglucosamine moiety linked to an 11-carbon dial dose sugar called tunic amine through a 1,1'-N-glycosidic bond. Additionally, Tunicamycin C contains a uracil base linked to the tunic amine sugar through a 1'-N-glycosidic bond (Astani et al., 2022). The uracil base might be the plausible link that results in tunicamycin interacting with TK1.

1.10. Protein Kinase C alpha

Protein kinase is an enzyme that catalysis the transfer of phosphate groups from ATP to specific amino acids on target proteins, thereby regulating cellular processes such as signal transduction, gene expression, and cell division (Lu and Hunter, 2018). Conversely, glycosylation refers to the process by which sugar molecules are added to proteins and lipids, thereby modulating their function and stability (Thomas et al., 2021). The involvement of protein kinase in glycosylation has been studied extensively in various biological systems, including plants, animals, and bacteria. For example, in *Arabidopsis thaliana*, a plant-specific protein kinase called OST1 (open stomata 1) has been shown to regulate the glycosylation and trafficking of the aquaporin PIP2; 7, which is involved in water transport in plants (Waszczak et al., 2018, Sewelam et al., 2016). Similarly, in human cells, the protein kinase CK2 (casein kinase 2) regulates the glycosylation of the tumour suppressor protein p53, which is involved in cell cycle regulation and apoptosis (Trembley et al., 2023)

1.10.1. Protein Kinase C and glycosylation

Another example of the involvement of protein kinase in glycosylation is the phosphorylation of the enzyme N-acetylglucosaminyltransferase III (GnT-III) by the protein kinase C (PKC) pathway. Enzyme N-acetylglucosaminyltransferase III is responsible for adding a specific sugar residue to the N-glycan structure of glycoproteins, thereby modulating their function and stability. PKC-mediated phosphorylation of enzyme N-acetylglucosaminyltransferase III regulates its activity, leading to changes in glycoprotein glycosylation patterns and biological activities (Ho et al., 2016).

Other studies have also implicated protein kinase in glycosylation regulation. For example, the protein kinase Cdc28 regulates the glycosylation and secretion of the yeast glycoprotein invertase (Little et al., 1994), while the protein kinase CK2 regulates the glycosylation and cell surface expression of the adhesion protein CD44 in human breast cancer cells (Meggio and Pinna, 2003). Protein kinase C alpha (PKCα) is a serine/threonine kinase that participates in vital cellular functions such as cell proliferation, differentiation, apoptosis, and metabolism.

Recent research indicates that PKCα also contributes to the regulation of glycosylation, a post-translational modification of proteins involving the addition of carbohydrate moieties (Cosentino-Gomes et al., 2012, Isakov, 2018). One of the critical roles of PKCα in glycosylation is regulating the expression and activity of glycosyltransferases, enzymes that catalyze the transfer of sugar residues to proteins. PKCα was found to regulate the expression of the glycosyltransferase GnT-V (Zhu et al., 2022), which is involved in the biosynthesis of complex N-glycans. (Zhu et al., 2022) showed that PKCα activation increased GnT-V expression and activity, resulting in enhanced N-glycan branching and altered cell adhesion properties.

Protein kinase C alpha has also been implicated in the regulation of glycoprotein trafficking, sorting and endoplasmic reticulum (ER) to Golgi transportation of the glycoprotein, Thy-1, by modulating the activity of the COPII machinery, which mediates vesicular transport from the ER to the Golgi (Xie et al., 2015). The authors demonstrated that PKCα activation led to increased Thy-1 trafficking and secretion, which was dependent on the activity of the COPII machinery (Xie et al., 2015). PKCα also regulates glycosylation in various disease states, including cancer and diabetes. PKCα regulates the expression of the glycosyltransferase MGAT3, which is involved in the biosynthesis of N-glycans with increased branching (Takahashi et al., 2022). PKCα activation increased MGAT3 expression and enhanced N-glycan branching in breast cancer cells, associated with increased cell migration and invasion (Sun et al., 2024).

In summary, PKCα plays a crucial role in regulating glycosylation through the modulation of glycosyltransferase expression and activity, glycoprotein trafficking and sorting, and its involvement in various disease states. Further research is needed to elucidate the precise mechanisms by which PKCα regulates glycosylation and identify potential therapeutic targets for treating diseases associated with altered glycosylation. Overall, these studies highlight the important role of PKCα in regulating glycosylation and the diverse range of biological processes that are modulated by this regulatory mechanism. Further research in this area may lead to the development of novel therapeutic approaches for various diseases, including cancer and metabolic disorders.

1.10.2. Protein kinase C alpha and Colorectal Cancer

As PKC family was the first found to be activated by phorol-esters which promote carconogen-induced tumorigenesis, they have been of interest in cancers (Yeo et al., 2017). PKC isoforms

appear to impact cancer cell apoptosis both favourably and negatively. PKC, in general, protects cancer cells against apoptosis (He et al., 2022). The role of PKC-alpha in CRC is not fully known. This study will shed insight into the role of P KC-alpha in CRC and glycosylation.

Tunicamycin C has been shown to inhibit the phosphorylation of protein kinase B (Akt) (Feng et al., 2017). This means that tunicamycin C interacted with protein kinase B to elicit the inhibition effect. Another study also revealed that tunicamycin C inhibited the growth of MCF-7 and SKBR-3 breast cell lines through decreasing Akt and NF-κβ expression (Wang et al., 2018b). Protein Kinase B and Protein kinase C-alpha are part of the AGC kinases (Silnitsky et al., 2023). Both kinases have conserved PDK1-interacting fragment (PIF) motifs, and they also share a long 55+ residue largely unstructured c-terminal, that contains the PIF motif (Baffi et al., 2021). Their activation loop is similarly flexible and contains the phosphorylation site (Reinhardt and Leonard, 2023). PDK1 is a master protein kinase that phosphoactivates several critical AGC kinases including AKT1 and PKC isoforms such as PKCα (Gordon et al., 2021). PDK1 phosphorylate through PDK1: AGC heterodimer stabilization facilitated by the PIF interaction (Levina et al., 2022). AKT1 and PKCα are seen to be competing with each other for the PDK1 PIF pocket, but PKCα has a higher affinity (Gordon et al., 2021). As mentioned above, tunicamycin has been demonstrated to interact with AKT1.

1.11. The peroxisome proliferator-activated receptor gamma (PPARG)

Peroxisome proliferator-activated receptor gamma (PPARG) belongs to the nuclear receptor superfamily. It operates on DNA response elements in conjunction with retinoid X receptor (RXR) as a heterodimer (Tyagi et al., 2011). Peroxisome proliferator-activated receptor gamma (PPARG) regulates energy storage, adipocyte differentiation, and glucose metabolism (Lehmann et al., 1995). PPARG has also been implicated in the immune response by virtue of its capability to suppress the expression of inflammatory cytokines and guide the differentiation of immune cells toward anti-inflammatory phenotypes (Martin, 2009). PPARG possesses anti-cancer effects by inhibiting the cell cycle (Grommes et al., 2004). Activation of PPARG has been shown to inhibit the proliferation of malignant cells derived from various cancer types, including breast adenocarcinoma, liposarcoma, colorectal carcinoma, prostate carcinoma, non-small-cell lung carcinoma, bladder cancer, pancreatic carcinoma, glial tumors of the brain and gastric carcinoma (Rubin et al., 2000).

1.11.1. PPARG and colorectal cancer

PPARG immunohistochemical expression can be associated with CRC prognosis (Pancione et al., 2010). PPRAG inhibits the proliferation of malignant cells and it is related to beta-catenin; PPRAG is known for the induction of differentiation similar to beta-catenin (an important molecule in CRC) (Sabatino et al., 2014). Most studies have shown that PPARG has an anti-cancer effect (Esmaeili et al., 2021). The receptor acts intracellularly and depends on the microenvironment (Bandera Merchan et al., 2016). PPARG is epigenetically silenced and no longer functions When the reaches its disease threshold (Villa et al., 2020). Due to epigenetic effects, RNA expressions do not correlate with protein expression as cancer advances (Villa et al., 2020). In CRC, PPRAG could be a new potential and independent marker for CRC survival (Girnun, 2009). PPARG ligands can prevent tumorigenesis, but may not be effective in advanced cancer as a single agent (Ondrey, 2009). PPARG, caspases, Fas, Bax, Bid, APC, antisense hTERT, PUMA, 15-LOX-1, ceramide, butyrate, and tributyrin initiate apoptosis in colon cancer (Rupnarain et al., 2004).

1.11.2. PPARG and Glycosylation

PPARG is derived from four mRNA PPARG1, PPARG2, PPARG3 and PPAGR4; PPARG1, 3, and 4 yield PPARG1 isoforms and PPARG2 protein is translated from PPARG2 (Hernandez-Quiles et al., 2021). PPARG1 mRNA is expressed in skeletal muscle, white and brown adipose tissue, pancreatic β- -cells, liver, macrophages, bone, colon and placenta (Corrales et al., 2018) under physiological conditions (Medina-Gomez et al., 2007). PPARG3 mRNA has been detected in various types of cell lines, including liver hepatocellular cells (HepG2), human intestinal cells (Caco-2), and cervical cancer cells (HeLa) (Martin, 2009). Phosphorylated PPARG1 is implicated in tumour progression (prostate cancer), and PPARG2 is a tumour suppressor (Dong et al., 2022, Salgia et al., 2019).

The variation in PPARG is an indicator that the subclasses under PPARG undergo various post-translation modifications such as phosphorylation, small ubiquitin-like modifier (SUMO)ylation, ubiquitination and glycosylation (Brunmeir and Xu, 2018). Phosphorylation facilitates PPARG activity and in turn, PPARG phosphorylates MAP Kinase and negatively regulates MAP Kinase activation (Carvalho et al., 2021). SUMOylation of PPARG induces the inhibition of NFκB regulating chemokine expression (Lu et al., 2013). In the process of ubiquitination, PPARG interacts with proteins such as developmentally downregulated protein

4 (NEDD4), which stabilizes PPARG and results in the inhibition of proteasomal degradation (Li et al., 2016a).

Beta-O-linked N-acetylglucosamine (O-GlcNAc) glycosylation of PPARG reduces transcriptional activity and terminal adipocyte differentiation. PPARG1 and PPARG2 are modified by O-GlcNAc. β-1,4-Galactosyltransferase I (β1, 4GalT1) mediates the N-glycosylation of PPARG, the N-glycosylation increases PPARG anti-inflammatory activity (Ji et al., 2012). Concerning Treg (T-cell that regulates suppression of anti-inflammatory activity) PPARG activation induces fatty acid oxidation, which gives a by-product that is an essential intermediate to N-glycan branching. N-glycosylation, in this case, occurs in the downstream factor which is a key in the differentiation of Tregs resulting in the regulation of inflammation (Miao et al., 2022). Another example that depicts the role of PPARG in regulating N-glycosylation is seen in monocyte adhesion. Additionally, PPARG activation in endothelial cells mediates the anti-inflammatory effects of PPARG ligand action, inhibiting proinflammatory cytokine-dependent up-regulation of endothelial N-glycans. Monocyte adhesion is regulated by tumour necrosis factor α (TNF α) through the stimulating expression of N-glycans (high mannose or hybrid type) at cell junctions. The N-glycans modulate the rolling and adhesion of monocytes to the endothelium. PPARG activation inhibits TNFα dependent up-regulation of endothelial surface N-glycans (Chacko et al., 2011).

1.11.3. Brefeldin A and PPARG

Brefeldin A has anticancer properties that inhibit cancer cell growth such as HeLa cells and 60 other cancer cell lines (Paek, 2018). No interaction between Brefeldin A and PPARG has been reported. PKC-alpha binds to the Golgi membranes through being induced by phorbol-12-myristate 13-acetate (PMA) (Newton, 2018). The activation of PKC-alpha results in the formation of transport vesicles within the cells (Karunakaran et al., 2013). When a PKC inhibitor interacted with the catalytic domain, vesicle formation was inhibited in Hep2G cells (Westermann et al., 1996). It is important to know that other PKC isoforms can also attach to the Golgi membranes (Goodnight et al., 1995).

As mentioned, brefeldin A (BFA) causes the Golgi stack to disassemble and resident proteins to be transported back into the endoplasmic reticulum. This interferes with forward transport which is the bulk phase. The transport of newly synthesized membrane proteins and secretory proteins is completely inhibited in BFA. Studies have shown that BFA can dissociate β-COP from the Golgi membrane; this protein is one of the coat proteins of non-clathrin-coated

vesicles (Liu et al., 2005). This led to the disintegration of the Golgi complex. PKC-alpha binds to the Golgi membrane thus BFA can interact with PKC-alpha . BFA will exploit the inhibitory mechanism that β-COP used to dissociate β-COP from the Golgi membrane. PKC-alpha shares similar binding motifs as β-COP since it also binds to the Golgi membrane. This means that BFA can displace PKC-α from the Golgi membrane.

1.12. Mitogen-Activated Kinase (MAPK)

Mitogen-activated protein kinase (MAPK) constitutes a family of serine-threonine kinases, which includes extracellular signal-regulated kinases (ERK MAPK, Ras/Raf1/ERK/MEK), c-Jun NH2-terminal kinases (JNK, also known as stress-activated protein kinase SAPK), and p38 (Kim and Choi, 2010, McCubrey et al., 2006). Each MAPK signalling pathway involves at least three components: MAP3K (e.g., ASK, MEKK1, and MLK), MAP2K (e.g., SEK1/MKK4 and MKK7), and MAPK itself, which, through a phosphorylation cascade, triggers MAPK pathway activation (Figure 1.11) (Kim and Choi, 2010). Upon MAPK pathway activation, various substrate proteins such as p53, ELK-1, and c-Jun are activated, leading to cellular responses (Figure 1.11) Conventionally, MAPK signalling pathways are activated by stimuli like growth factors, oxidative stress, and cytokines. This activation triggers intracellular signalling cascades that regulate various cellular processes such as cell proliferation, transformation, differentiation, survival, and apoptosis. (Figure 1.11) (Kim and Choi, 2010) (Torii et al., 2006). Given its involvement in numerous cellular processes, abnormal MAPK signalling, stemming from improper activation and mutations affecting gene expression, has been implicated in various human disorders, including CRC (Fang and Richardson, 2005, Kim and Choi, 2010).

Activating transcription factor 2(ATF-2); ERK, extracellular signal-regulated kinase; JNK, c-Jun NH_2 terminal kinase; MAP, mitogen activate protein; MAPK, MAP kinase; MAPKAP, MAP kinase activated protein kinase; MEF myocyte enhance factor; SAPK, stress-activated protein kinase; MNKs, MARK activating protein kinases; MSKs, mitogen and stress-activated protein kinases; CSBP, cytokine suppressive anti-inflammatory binding protein; RK, reactivating kinase (Hommes et al., 2003).

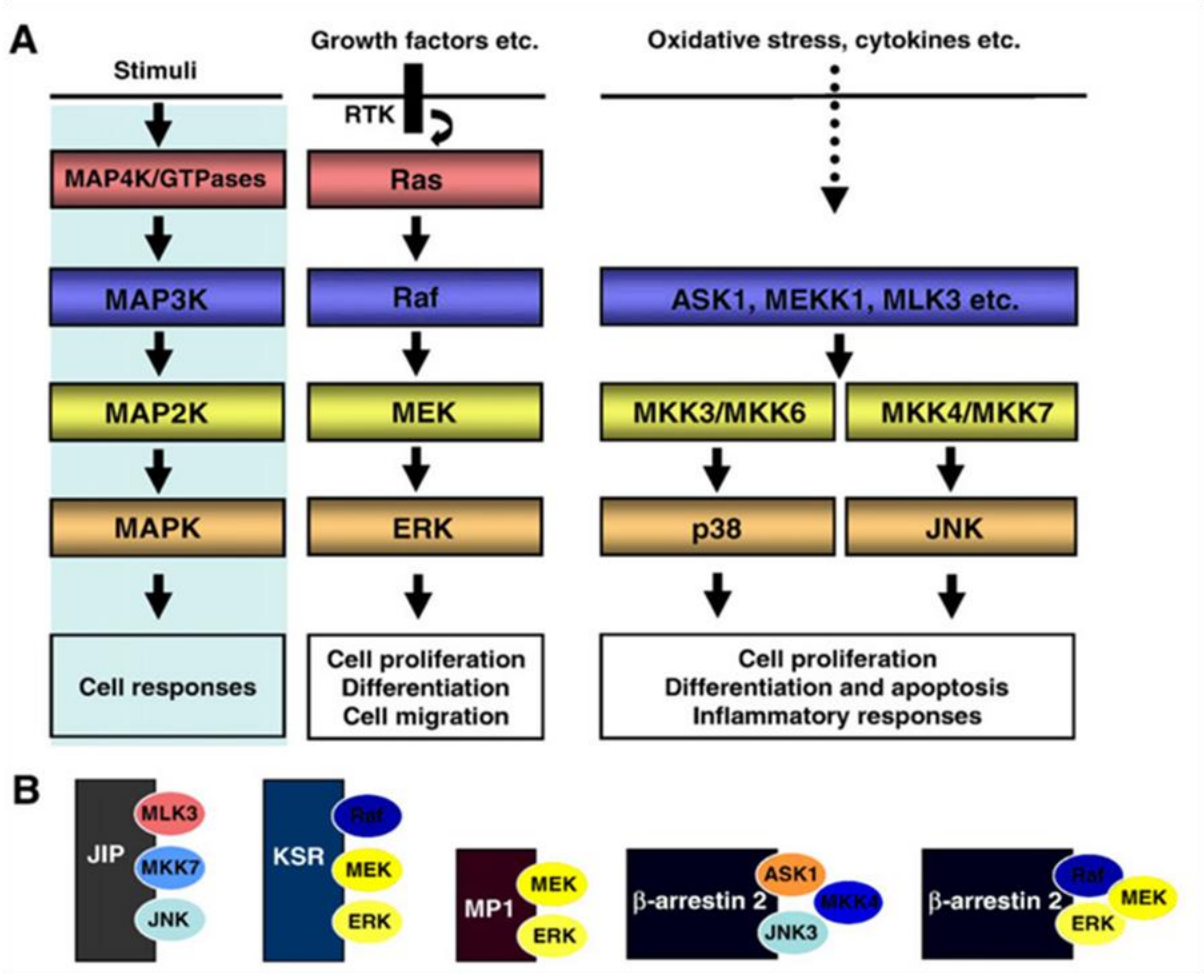


Figure 1.11. Mitogen-activated kinase protein signalling pathway. (Kim and Choi, 2010).

1.12.1. MAPK and CRC

Current research has linked all three subfamilies of MAPK (ERK, c-Jun/SAPK, and p38) with the pathogenesis of CRC (Fang and Richardson, 2005, Stefani et al., 2021). Research conducted by Taupin and Podolsky (1999) has underscored the significance of ERK MAPK in intestinal epithelial differentiation (Podolsky, 1999). Subsequent studies on the ERK MAPK pathway have expanded upon this, linking its inappropriate activation to pathogenic oncogenic effects, mitogenesis (cell cycle entry), and the progression of CRC (Fang and Richardson, 2005, Wang et al., 2004, deFazio et al., 2000, Taupin and Podolsky, 1999). The increased activation of Ras/Raf/ERK/MEK in CRC is characterized by four significant observations: (1) Gain-of-function mutations of Ras, detected in 36% of CRC cases, lead to an imbalance in ERK and JNK activity, contributing to colorectal tumorigenesis. (2) Mutations of BRAF, a serine-threonine kinase related to the Raf family, found in 9-11% of sporadic CRC cases, result in microsatellite instabilities. (3) Activation and phosphorylation of the downstream

transcription factor c-Jun result in increased JNK activity, impacting differentiation and apoptosis. (4) Upregulation of the Epithelial Growth Factor receptor activates the ERK/MAPK signalling pathway, promoting mitogenesis (Davies et al., 2004, Fang and Richardson, 2005, Wisdom et al., 1999). These findings collectively demonstrate the pivotal role of aberrant MAPK signalling in CRC activation.

In addition to its role in CRC activation, aberrant MAPK signalling is implicated in tumour invasion and metastasis. Studies have linked the activation of Ras/Raf/ERK/MEK with elevated levels of vascular endothelial growth factor (VEGF), which is known for its involvement in angiogenesis in CRC patients (Jafari et al., 2022). Besides elevated levels of vascular endothelial growth factor (VEGF), signal transmission through the ERK/MEK pathway has been implicated in activating CRC cell invasion (Zhang et al., 2004). Moreover, urokinase plasminogen activators and integrins are known to heighten basal ERK activity, potentially contributing to CRC invasion and metastasis (Fang and Richardson, 2005). Thus, abnormal MAPK signalling plays a vital role in CRC pathogenesis.

1.12.2. MAPK and Brefeldin A

The involvement of multiple MAPK pathways in CRC development suggests possibilities for more focused therapy with fewer side effects. Brefeldin A (BFA), an anti-cancer therapeutic agent, has shown antitumor activity both *in vitro* and *in vivo* (Zhou et al., 2019). The studies indicate that BFA exhibits promising therapeutic effects in colorectal cancer (CRC) cells. It impedes protein transport and triggers endoplasmic reticulum stress, thereby curtailing cancer stem cell-like attributes and reducing MMP-9 activity in CRC Colo 205 cells. This multifaceted impact suggests BFA's potential cancer progression and invasion in CRC. Further investigations are warranted to elucidate the underlying molecular pathways and assess BFA's therapeutic viability in both preclinical and clinical contexts (Tseng et al., 2013). BFA has the potential to hinder the advancement of colorectal cancer (CRC) during both tumorigenesis and metastasis by stimulating the activation of C/EBP homologous protein (CHOP), thereby initiating apoptosis. This suggests that BFA could serve as a promising therapeutic agent for CRC by targeting key pathways crucial for cancer cell survival and proliferation. Further investigation into its effectiveness and safety profile is required to determine its clinical applicability in CRC treatment (Tseng et al., 2013). BFA can induce cell death in CRC by activating autophagy through the Bip/AKT/PI3K pathways (Zhou et al., 2019, Moon et al., 2012). While the direct impact of Brefeldin A on the MAPK pathway in CRC remains

relatively unexplored, prior research has linked BFA to the suppression of MAPK phosphorylation. This raises questions about whether BFA could elicit similar effects in CRC cells and whether it holds therapeutic promise for targeting the MAPK pathway.(Rizzo et al., 1999)

Brefeldin A, a fungal metabolite with the ability to modulate intracellular trafficking pathways, functions by directly binding to the interface formed by a complex of GDP/GTP exchange factor bound to its substrate Arf-GDP. This binding prevents the exchange of GDP/GTP on the Arf (ADP-ribosylation factors), thereby disrupting essential cellular processes (Wyrozumska et al., 2014). BFA prevents trafficking at the endoplasmic reticulum-Golgi interface, blocking Arf activation (Boal et al., 2010). Arfs are like RAS-related small GTPases, which also can activate MAPK (Zhou et al., 2015). It is well known that RAS activates MAPK in the plasma membrane. It has been documented that RAS signalling down to the MAPK pathway can also happen on the Golgi, the endoplasmic reticulum, endosomes and mitochondria (Zinatizadeh et al., 2022). When Arf activates MAPK, it is localized in the Golgi. The ARF expression enhances the expression of cyclin D1, one of the cell cycle regulators promoted by MAPK for cell proliferation. The MAPK activated by ARF remains at the cytoplasm with its downstream substrates, compared to when activated by Ras, where the MAPK substrates also translocate to the nucleus (Zhou et al., 2015). Since BFA forms a complex with GDP/GTP exchange factor bound to Arf, BFA may associate with MAPK. The association is possible through conserved domain that Arf uses to bind with its substrate.

1.12.3. Mitogen-Activated Protein Kinase (MAPK) and glycosylation

Glycosylation is a crucial post-translational modification that affects over 80% of human proteins and is highly sensitive to nutrient availability (Apweiler et al., 1999). Glycosylation modifications influence proteins, altering their folding, structure, stability, subcellular localization, protein-protein interactions, and overall biological functions (Very et al., 2018). Altered glycosylation patterns, including changes in glycans like carcinoembryonic antigen (CEA) or carbohydrate antigen (CA 19-9), are linked to the initiation and advancement of cancers such as CRC. These glycan alterations serve as biomarkers for the detection and monitoring of CRC (Very et al., 2018). Recent studies have illustrated that glycosylation associated with CRC increases resistance to treatment and progression within cancer cells (Very et al., 2018). End products from advanced glycosylation suppress the proliferation of bone marrow stromal cells in rats by activating the MAPK pathway. Additionally, proper

glycosylation has been associated with maintaining MAPK signal fidelity in *Saccharomyces cerevisiae*. Studies have shown that glycosylation is essential in controlling fidelity in the MAPK pathway. Proper addition of N-glycan moieties to protein (Msb2) played a role in preventing cross-over between signals controlled by MAPK protein. Insufficient glycosylation of Msb2 prevented its role in preventing cross-over between signals. These further highlight the importance of the glycosylation PMT (Lien et al., 2013). Also, of significance and briefly described previously is an association of glycosylation with MAPK signal fidelity in *Saccharomyces cerevisiae*, within the high osmolarity glycerol (HOG) pathway and filamentous growth (FG) pathway. These pathways use MAPKs, such as Hog1 in the HOG pathway and Kss1 in the FG pathway. Each MAPK responds to stimuli and plays distinct roles in the yeasts' response to environmental conditions. In this study, two mutants Mnn10 and Mnn11 were identified, which showed activation of Kss1, an important MAPK involved in the FG pathway. These mutants lacked Mnn10 and Mnn11 genes that encode for mannosyltransferase enzymes, critical Golgi apparatus, and N-glycosylation machinery components. Deleting these genes resulted in the production of N glycosylated proteins with shorter mannan chains. The findings highlight the significance of N glycosylation for maintaining accurate MAPK signalling, mainly to prevent cross-activation between different MAPK pathways. Researchers have identified an N glycosylation site on Msb2 (Asn 30), which, when mutated, led to the activation of Kss1 like that observed in the Mnn11 mutant phenotype. This finding also highlights the significance of N-glycosylation in regulating MAPK signalling for Msb2, a crucial regulator, in the FG pathway (Lien et al., 2013). However, it remains unclear whether glycosylation associated with CRC is linked to the MAPK pathways in humans (Lien et al., 2013).

Previous studies have suggested that PrKC1 and MAPK are involved in glycosylation (Wu et al., 2018, Li et al., 2015b, Arey, 2012, Lien et al., 2013). Protein kinase C (PrKC1) and Mitogen-Activated Protein Kinase (MAPK) have been reported to regulate glycosylation and are worthy therapeutic targets. Protein kinase C (PrKC1) is a serine/threonine kinase family member and plays a vital role in signal transduction (Mackay and Twelves, 2003). They are involved in cell proliferation, differentiation, survival, invasion, migration, apoptosis, angiogenesis, and drug resistance (Kang et al., 2014). Their significant contribution to cell signalling makes them promising therapeutic targets for several diseases with high potential in different cancer types (Kang et al., 2014). PrKC1 is essential for neoplastic transformation, carcinogenesis and tumour cell invasion; therefore, these findings have presented PrKC1 as a

potential target for anticancer therapy (Mackay and Twelves, 2003). Different cellular responses are produced by PrKC1 activation, which is responsible for diverse expressions like growth factors, activation of signalling pathways and improvement of oxidative stress (Lien et al., 2021). Several catalytic and regulatory mechanisms have suggested PrKC1 possesses the potential for drug target design (Edwards and Newton, 1997, Mosior and Newton, 1998, Keranen and Newton, 1997).

Further emphasizing the importance of glycosylation in association with the MAPK pathway, a study by Liu et al. (2017) reported an interaction between glycosylation and the Ras/Raf/MAPK signalling pathway in hepatocellular carcinoma (HCC) cells treated with sorafenib, a multikinase inhibitor. The treatment of HCC cells with sorafenib resulted in modifications to protein glycosylation and changes to glycoprotein binding to lectins. Sorafenib treatment also decreased the expression of Ets 1 (erythroblastosis 26) which is associated with protein glycosylation, suggesting a relationship between Ras/Raf/MAPK signalling and glycosylation within HCC cells (Liu et al., 2017). Furthermore, the study proposes that influencing the sorafenib's Ras/Raf/MAPK signalling pathway indirectly affects protein glycosylation patterns in HCC cells, potentially impacting cancer progression (Liu et al., 2017).

1.13. *In silico* computer modelling

1.13.1. Introduction to in silico Studies

Scientific research continues to represent and advance basic technology in fields such as aeronautics, chemistry, biology, social sciences, artificial intelligence (AI), and physics due to computational experiments such as *in vivo, in vitro, in silico, in virtuo,* and *in mente*, amongst others (Radovic, 2022, Bekisz and Geris, 2020). In biology, computational systems are targeted to improve computational models of biological systems by focusing on efficient algorithms, data structures, visualization, and communication tools that can provide new information on biological models using testable predictions (Barh et al., 2014). Over the years, developments in computer technology have contributed to the completion of the human genome and the structural, chemical, and biological information of novel therapeutic targets needed for drug discovery (Meng et al., 2011). The simulation of the behaviour of biological systems is achieved by building equations that express biological knowledge by performing *in silico* experiments.

Classical methodologies such as high-throughput protein purification, crystallography, and nuclear magnetic resonance spectroscopy have contributed significantly to elucidating the structural characteristics of proteins and protein-ligand interactions (Jorgensen, 2004). Numerous lead compounds have been identified due to the ability to virtually screen compound libraries to improve ligand enrichment through experimental validation. This has led to the development of different computational techniques, such as *in silico* virtual screening or high-throughput virtual screening (HTVS) for further drug discovery using hit identification (Ferreira et al., 2015), Drug-DNA interactions (Agarwal et al., 2015, Agarwal and Mehrotra, 2016), and methods for lead optimization (Shoichet et al., 2002). *In silico* experiments form part of developing different techniques using computer simulation or software to capture, analyze, and assimilate medical data using *in situ, in vivo*, or *in vitro* sources (Ekins et al., 2007). Compared to traditional experimental high-throughput screening (HTS), *in silico* virtual techniques have been preferred because of their ability to make fast predictions based on the compound structure before it is synthesized, increase drug discovery in terms of time, labour, and expense, and vastly contribute to the development of new novel medicinal molecules (Wadood et al., 2013, Shaker et al., 2021).

The continued advancement of bioinformatics has resulted in the ultimate progression of using *in silico* tools and applications. To date, various fields such as biochemistry, nanotechnology, and molecular biology have made use of *in silico* drug design methods (Ratti and Trist, 2001). Chemical principles and theories applied outside the scope of chemistry have given rise to pharmacology as an independent scientific discipline and have a great influence on drug research. In the 20^{th} century, the concept of targeting enzymes and designing drugs as inhibitors had an important influence on drug research, that led to the development of many drugs with a high specificity and low toxicity (Meldrum and Roughton, 1933). Some of the effective drugs, such as Nilotinib and Imatinib, have used CADD techniques and are currently on the market (Druker and Lydon, 2000, Weisberg et al., 2005).

Despite numerous research and development (R&D) efforts, drug discovery has faced delays due to costly and time-consuming processes. Challenges related to absorption, distribution, metabolism, excretion, and toxicity (ADMET), leading to high attrition rates of compounds, have contributed to approximately 50% of expensive failures, prompting a greater emphasis on improving drug discovery processes (Bharath et al., 2011, Parasuraman, 2011, Alomar, 2014). The transition from laboratory-based to computer-based approaches in the search for molecules that bind to target proteins has paved the way for the utilization of in silico tools to improve

the drug discovery process. These tools enable the modelling of the most pertinent absorption, distribution, metabolism, excretion, and toxicity (ADMET) properties, thereby enhancing the efficiency of drug development (Augen, 2002). Continuous advancements in drug discovery are leading to the introduction of innovative and safer medications into the market. This ongoing process remains integral to the growth and success of pharmaceutical companies, catering to a diverse spectrum of diseases (Ratti and Trist, 2001).

1.13.2. The Role of Silico Approaches in Drug Discovery

Drug development is increasingly relying on computer-aided therapeutic design (CADD) approaches are essential for the efficient identification of viable drug candidates. They reduce the usage of animal models in pharmacological research, assist the drug discovery process by rational design of novel and safe drug candidates, and reposition the existing medications (Brogi, Ramalho et al. 2020). Development and validation of GLORY, an innovative tool that predicts the metabolism of molecules and identifies chemical structures of metabolites formed by the cytochrome P450 enzyme family (CYPs) was reported by de Bruyn Kops et al., (2019) (de Bruyn Kops et al., 2019). A pool of CYP-mediated reaction rules based on literature and the prediction of site of metabolism (SoM) are combined in the software stated. This strategy is pertinent because a tool for the *in-silico* prediction of xenobiotic compound metabolism can provide essential knowledge for creating novel chemical entities with enhanced metabolic stability (Brogi et al., 2020). A computational method for forecasting the possible toxicity of compounds while accounting for transporter proteins was described by (Montanari et al., 2019). These proteins, which are produced in the liver are essential for bile flow, play a key role in drug pharmacokinetics, and their blockage may contribute to liver toxicity brought on by drugs.

(Sidorov et al., 2019) dealt with the pharmacological characteristics of several compounds. This study focused on the feasibility of using NCI-ALMANAC data to predict the synergism of cancer therapy combinations. This subject is interesting since medication combinations might be a useful approach to treating cancer. The largest dataset available on anticancer drug synergism was used by the authors to describe an *in-silico* method for examining drug combination synergy (NCI-ALMANAC, with over 290,000 synergy determinations). Random Forest (RF) and Extreme Gradient Boosting (XGBoost), two machine learning (ML) techniques, were applied to the chosen dataset. The evaluation of these computer tools showed that it is possible to predict the synergy of medicines that have never been taken together before.

(Velázquez-Libera et al., 2019) employed both structure- and ligand-based methods to explore the structural criteria dictating the affinity of various molecules for the human Sigma 1 receptor (S1R). Their investigation utilized a combination of ligand- and structure-based approaches to identify potentially promising compounds for targeting this receptor. An effective therapeutic target for the treatment of neuropsychological disorders is S1R. The S1R agonist RC-33, which the authors identified as a promising neuroprotective drug, is a potent S1R agonist. The interactions of RC-33 and its new derivatives within the S1R active site were computationally investigated using several in silico approaches, including docking, interaction fingerprinting, and receptor-guided alignment (3-D-QSAR), to investigate the putative mechanism of action of the created compounds.

(Wu et al., 2020) employed various computational methods, such as de novo protein structure prediction and simulation of ligand-protein interactions, to examine the structural prerequisites of compounds influencing their affinity for the hSK2/calmodulin complex. The study involved creating a homology model of SK2/calmodulin to predict potential binding sites and utilized several computational techniques to investigate ligand-protein interactions. Their findings affirmed the utility of integrating diverse in silico approaches in expediting the drug discovery process.

A study called “Finding Constellations in Chemical Space Through Core Analysis,” conducted by (Naveja and Medina-Franco, 2019) defined a computational approach for selecting lead compounds from large datasets of chemical entities acquired by high-throughput screening (HTS). To improve the information contained in a visual representation and analysis of chemical space, constellation plots were proposed as a universal way for fusing various and complementary molecular representations. This method combined a "classical" coordinate-based representation of chemical space with a substructure-based representation and classification of molecules. A distinctive outcome of this method was the production of groups of compounds, commonly referred to as "constellations," in chemical space as a result of ordering the molecules in an analogue series. Notably, the suggested strategy helped locate, for instance, informative and "bright" SARs in chemical space that are easy to comprehend. The approach was tested using two datasets of DNA methyltransferases (DNMTs) and AKT1 inhibitors.

A computational method described by (Alberca et al., 2019) made it possible to use outdated medications as antimalarial agents. The authors created several ligand-based models that can

locate falcipain-2 inhibitors and experimentally validate them. A virtual screening (VS) campaign used two separate databases that utilized these models (DrugBank and Sweetlead). The authors found four potential hits and submitted them for biological assessment. Two of these, methacycline and odanacatib, were identified as falcipain-2 inhibitors. Falcipain-2 was discovered to be a non-competitive inhibitor in methacycline. Additionally, the effects of both medications on falcipain-2 hemoglobinase activity and *P. falciparum* growth have been researched.

Sirous et al., (2019) created and experimentally verified an *in-silico* method for hit-to-lead optimisation. The authors specifically outlined a computational approach based on an *in-silico* structure-based combinatorial library design technique for micromolar HIV integrase (HIV IN) inhibitors. The approach above helps to integrate Quantum Polarized Ligand Docking (QPLD) and MD simulations with sidechain hopping and combinatorial library construction. The most valuable amendments for a promising scaffold were identified using this technique. Three sample molecules were created and put through *in vitro* experiments using this final set of optimized molecules. One of them was discovered to be a potent HIV-1 inhibitor in the low nanomolar range.

Additionally, the biological evaluation of the chemical revealed that this substance had efficacy comparable to that of raltegravir in its ability to suppress HIV-1 replication and HIV-1 IN strand transfer activity. A novel method for rating the outcomes of high-throughput docking (HTD) techniques was developed by (Cavasotto and Aucar, 2020). The study suggested a quantum mechanical (QM)--based docking scoring algorithm to better characterize protein-ligand interactions and produce more precise HTD results. Ten different drug targets from different families with various binding site properties were used to research this unique method. The results revealed that the performance of HTD approaches might be enhanced by the implementation of the QM scoring function.

The use of molecular mechanics (MM) to describe protein-ligand interactions was described by (Santos et al., 2019). Halogen bonds (XBs) were the subject of a case study. Halogen bonds (HBs) were discovered to be pertinent in CADD even though they are less effective than hydrogen bonds. A molecule's affinity and selectivity toward a potential therapeutic target can be enhanced by XBs. The authors noted that a parametrization of the force-field equations might be considered for refining the definition of XBs due to the limitations of MM approaches

in describing XBs. This review emphasized various recommendations for force-field parametrization to produce accurate results for intricate non-covalent interactions.

1.13.3. In Silico Approaches

The pharmaceutical industry continues recognizing the development of drugs that bind to specific targets as an investment in research and development, leading to a discovery-and-development cycle of drugs (Korycka-Machała et al., 2005). Computer Aided Drug-Design (CADD) approaches are separated into two: Structure-based Drug Design (SBDD) and Ligand-based Drug Design (Figure 1.12) (Arodola and Soliman, 2017).

1.13.4. Structure-Based Drug Design (SBDD)

Multiple steps are taken throughout the SBDD process. The initial step is characterizing the target's structural makeup using experimental techniques like X-ray crystallography, NMR spectroscopy, or homology modelling (Wang et al., 2018a). Analysis can also be done using the 3D structures of numerous proteins and nucleic acids, which have previously been solved and stored in databases (Anderson, 2003). Given the target's 3D structure, screening can be done across several databases to find possible ligands. For biochemical and biological examination, the candidates with the highest scores for affinity and specificity are chosen (Lyne, 2002, Macalino et al., 2015). The target is then investigated in a complex with the most promising chemical to acquire the 3D structure for further optimization or even for the synthesis of novel compounds. The most popular computational SBDD techniques are referred to as molecular docking, molecular dynamics (MD), fragment-based drug design (FBDD), and pharmacophore modelling (Bissaro et al., 2020).

1.13.5. Molecular Docking

Molecular docking, discovered in the early 1980s (Kuntz et al., 1982), is one of the most common *in silico* techniques that uses structure-based methods to predict interactions found in molecules and biological targets (Kitchen et al., 2004). Molecular docking is a method used to find binding sites between two or more molecules to form a stable complex, especially when the 3D structure of the target protein is available (Sousa et al., 2013, Salmaso and Moro, 2018). This method helps examine changes in substrate conformation during complex formation, which helps predict the binding conformation, binding mode, and orientation between a receptor and a ligand (Guedes et al., 2014). For receptor-based virtual screening, molecular

docking is the foundation for exploring how drugs bind to their targets and predicting the drug's affinity and activity (Figure 1.13) (Chaudhary and Mishra, 2016).

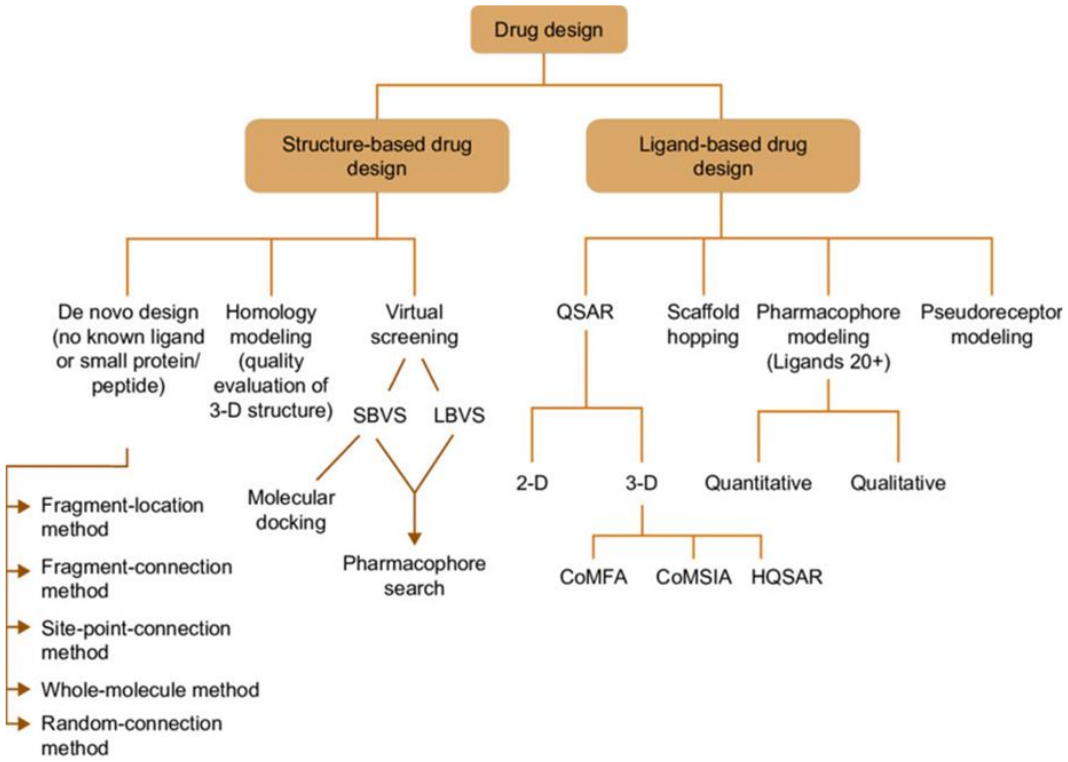


Figure 1.12. ***In silico*** **approaches used in drug design:** SBVS, structure-based virtual screening; QSAR, quantitative structure-activity relationship; HQSAR, hologram quantitative structure-activity relationship; CoMFA, comparative molecular field analysis; LBVS, ligand-based virtual screening; CoMSIA, comparative molecular similarity index analysis. Adapted from (Arodola and Soliman, 2017).

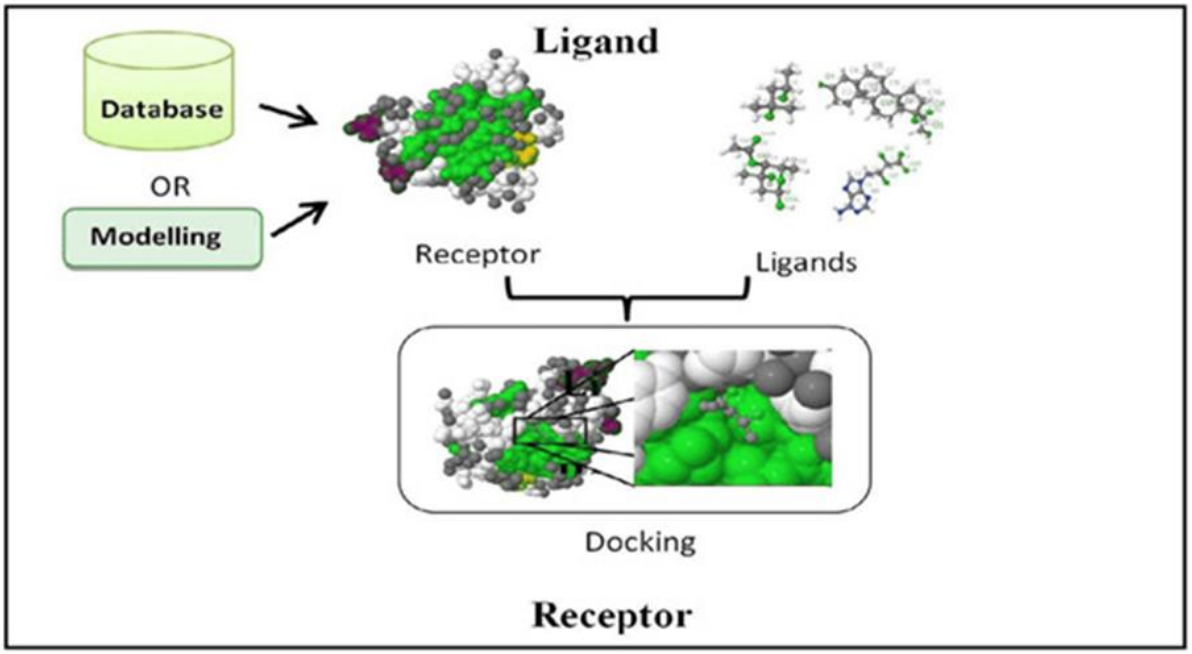


Figure 1.13. Illustration of molecular docking between receptor and ligands. Adapted from (Chaudhary and Mishra, 2016).

The advanced computational resources in drug discovery literature using molecular docking software have increased over the years due to carrying out protein-protein docking, protein-peptide docking, and other large-molecule-related docking problems using biomolecules such as DNA (Zhang et al., 2022a). The ability of the receptor to be flexible during the mechanism of molecular docking permits the modification of rigid receptors while allowing other receptors, like ions and tautomers, to take the shape of the ligands. This results in the formation of rigid docking, semi-flexible docking, and flexible docking (Prieto-Martínez et al., 2018).

In rigid docking, the conformation of the receptor does not change, whereas in semi-flexible docking, the conformation of the fixed receptor remains unchanged while the conformation of the ligand is altered. The flexible docking process allows the complete conformation of receptor and ligand docking to be readily modified, which is mainly preferred due to its accuracy in molecular interactions (Yuriev et al., 2015). Flexible docking ligands employ molecular-dynamics docking of complete molecules (Monte Carlo), in-site combinatorial search, ligand build-up, site mapping, and fragment assembly (Roy et al., 2018).

The prediction of the ligand-receptor complex structure using molecular docking is achieved by using the ligand's sampled conformation algorithms in the protein's active site and ranking these conformations using a scoring function (Meng et al., 2011). The primary function of the

conformation search algorithm is to assist in finding the ideal binding site for the receptor and ligand (Schulz-Gasch and Stahl, 2003), whereas the scoring function is used to measure the strength of binding between the docked molecules (Friesner et al., 2004). More than 100 different docking tools and programs, such as DOCK, AutoDock, FlexX, Surflex, GOLD, ICMGlide, Cdocker, MCDock, FRED, MOE-Dock, LeDock, rDock, UCSF Dock, amongst others, have been developed during the past 20 years for both academic and commercial use (Pagadala et al., 2017). AutoDock Vina, GOLD, and MOE-Dock, Glide (XP) among these programs projected top-ranking poses with approximately 90% accuracy (Wang et al., 2016).

1.13.6. Pharmacophore Mapping

New bioactive compounds against various drug targets have been utilized and designed using a ligand-based pharmacophore mapping approach. A pharmacophore defines all of a chemical compound's functional groups and characteristics that need to be present to engage with its biomolecular target in the best possible way and produce biological activity (van Drie, 2003)**.** An effective pharmacophore has specific chemical characteristics, such as noncovalent interactions or groups necessary for intermolecular interactions, like hydrogen bond donors or acceptors, electronegative or electropositive groups, positive- or negative-charged groups, aromatic rings, lipophilic or hydrophilic groups, and electronegative or electropositive groups (Li et al., 2015a). When there is insufficient knowledge about ligands that have been empirically demonstrated to block or stimulate the activity of a specific therapeutic target, structure-based pharmacophore modelling can be used efficiently. It can also be used to gather more data from the receptor side, giving medicinal chemists a more significant understanding (Sobhy et al., 2019).

1.13.7. Ligand-Based Drug-Design

Three primary techniques are frequently used for discovering novel compounds with the ligand-based drug design (LBDD) methodology. The first is known as "ligand chemical similarity". It is based on the selection of novel molecules with a high degree of similarity to existing active compounds concerning the chemical structure, binding affinity, and physicochemical qualities (Yan et al., 2016). The second method, called “pharmacophore mapping,” identifies the functional groups that interact with the targets so that more potent molecules can be designed. The third method called quantitative structure-activity relationship (QSAR) links several characteristics of a group of chemical compounds to their biological activity for the target under study (Makrynitsa et al., 2018).

1.13.8. Quantitative Structure-Activity Relationship (QSAR).

Quantitative Structure-Activity Relationship (SAR) is a computational or mathematical modelling technique that reveals connections between biological activities and the structural characteristics of chemical substances. The main idea is that diverse biological activities result from changes in structural characteristics (Verma et al., 2010). Biological activities correspond to pharmacokinetic qualities, including absorption, distribution, metabolism, excretion, and toxicity, while structural properties belong to physicochemical properties. As an *in-silico* tool, QSAR modelling aids in prioritizing many compounds in terms of their intended biological activities, significantly reducing the number of candidate chemicals that need to be tested *in vivo*. QSAR modelling has become an important process in the pharmaceutical sector, although there are significant restrictions. Since relationships are determined through *in-situ* experiments, the dataset is assumed to contain some errors (Ma et al., 2015). QSAR data may involve many chemicals (more than hundreds of thousands); a variety of descriptors can represent each chemical; commonly used fingerprints are very sparse (most of the values are zero), and some features are highly correlated (Golbraikh et al., 2014).

1.14. Molecular Dynamics

The induced-fit modelling and conformational selection have superseded Fischer's key-lock paradigm's target-ligand model (Vogt and Di Cera, 2012). It is important to use molecular dynamics modelling to link ligand recognition and a biomolecular system's flexibility. In addition, Molecular dynamics modelling is a helpful tool for locating additional druggable sites, such as allosteric, that are not detectable by other structural techniques, resulting in the formulation of pharmaceutical compounds with greater efficacy (Grant et al., 2011, Nair et al., 2012). Molecular dynamics is a Newtonian mechanics-based computer simulation technique. The atoms and molecules are allowed to interact for a predetermined amount of time providing a glimpse of the dynamic evolution of the system and depicting the motions of atoms and molecules (Hospital et al., 2015).

Theoretical chemistry techniques are integrated into effective computer programs to evaluate the structures and features of molecules and solids. Molecular modelling has become an invaluable and essential device to medicinal chemists in drug design (Nadendla, 2004). Molecular modelling depicts the production, skilful handling, or presentation of three-dimensional molecular structures and related physicochemical properties. It involves various computerized methods established on theoretical chemistry techniques and experimental data

to envision molecular and biological properties (Nadendla, 2004). Two basic molecular modelling principles, Quantum and Molecular Mechanics, are used to describe the conformational and energetic changes to drug-target interaction.

Merging molecular dynamic simulation with these two fundamental principles of molecular modelling stated above will enable thorough investigations of the conformational dynamics of the target and the landscape of the inhibitor binding (Lewars, 2011). The following sections will focus on quantum mechanics, molecular mechanics, and molecular dynamic simulations; they will give insight into the reasons behind the choice of energy descriptors for the research. Computational tools employed in the analysis will be defined by explaining the principle behind Fragment-Based Design

1.14.1. The Principle of Molecular Mechanics

Molecular Mechanics (MM) is a definitive model that applies an algebraic, empirical, and atomistic energy function for chemical schemes. Molecular Mechanics, also called the molecular force field, has grown in application when handling large molecules, necessitating many molecular dynamic calculations (Maseras and Morokuma, 1995). It applies Newtonian mechanics to define large, assorted types of molecules such as hydrocarbons that possess low molecular weight to giant biomolecular complexes such as proteins or membrane fragments (Guvench and MacKerell, 2008, Vanommeslaeghe et al., 2014). Molecular mechanics is established on a mathematical model and views molecules as an assemblage of balls bonded together by strings. In this context, balls refer to atoms, while strings represent bonds. In the confines of this model, the inherent molecular energy alters with geometry due to the springs refusing to be pulled or twisted away from their original length or angle and the resistance from being pulled intimately together (Lewars, 2016). The basis of molecular mechanics presents the energy of a molecule as an aftermath of the refusal of its bond from being stretched or bent as well as the crowding of the atom; it also employs this energy equation to locate the bond lengths, angles, and dihedrals which corresponds to several available potential energy surface minima (Lewars, 2016). The energy's mathematical equation and its parameters make up a force field; this influenced the naming of molecular mechanics method as force field methods (Li et al., 2016b). Molecular mechanics tacitly employs the Born-Oppenheimer approximation on the condition where the nuclei witness some static pulling force from electrons or springs (Born and Oppenheimer, 1927).

1.14.2. Force field.

From a chemistry point of view, a definite potential energy function by which forces are obtained is often termed a force field (Lopes et al., 2015). From a molecular dynamics simulation perspective, the “force field” defines a composite of mathematical equation and related parameters employed to depict proteins energy as something that relate to the protein’s atomic coordinates. Molecular system force field energy can be categorised according to an agreed force field energy equation based on classical Newtonian physics. These mathematical expressions cannot only estimate a system's energy but also calculate the atom types composing the molecule (Jensen, 2017) (Tsai, 2003). Some of the widely applied biomolecular force fields are as follows:

1. Amber (Cornell et al., 1995)
2. CHARMM (MacKerell Jr et al., 1998),
3. GROMOS (Oostenbrink et al., 2004),
4. OPLS-AA (Jorgensen et al., 1996) and
5. NAMD (Phillips et al., 2005).

The energies involved here produce the MM force field and define the energy input of the various atomic forces. The energy expressions are parameterized to tally with experimental and QM information to ensure systems imitate the property of the actual molecules in motion (Durrant and McCammon, 2011). Diverse force fields have been designed with varying methods of parameterisations; force fields are meant to be chosen according to the conditions and the nature of the studied system. The basic functional models of CHARMM, GROMOS, OPLSAA, Amber, and NAMD force fields can be quickly gained insight into by studying the molecular characteristics they stand for (Guvench and MacKerell, 2008, Phillips et al., 2005). These molecular properties can be classified into bonded and nonbonded interactions. The bonded interactions explain bond stretching, valence angle bending and the dihedral angle rotation, whereas nonbonded interaction describes electrostatics, dispersion and Pauli exclusion (also called van der Waals term)(Guvench and MacKerell, 2008). The conventional energy terms for these force fields are:

$$E_{\text{bonded}} = \sum_{\text{bonds}} K_b(b-b_0)^2 + \sum_{\text{angles}} K_\theta(\theta-\theta_0)^2 + \sum_{\text{dihedrals}} K_\chi[1+\cos(n\chi-\sigma)] \quad \text{(Eq 1.6)}$$

and

$$E_{\text{nonbonded}} = \sum_{\substack{\text{nonbonded} \\ \text{pairs } ij}} \left(\varepsilon_{ij} \left[\left(\frac{R_{\min,ij}}{r_{ij}} \right)^{12} - 2 * \left(\frac{R_{\min,ij}}{r_{ij}} \right)^{6} \right] + \frac{q_i q_j}{r_{ij}} \right), \quad \text{(Eq 1.6.1)}$$

Where E_{bonded} denotes bonded interaction total energy while $E_{\text{nonbonded}}$ is the input made by nonbonded interactions. Therefore, the contribution from the bonded and nonbonded interaction can be represented as:

$E_{\text{total}} = E_{\text{bonded}} + E_{\text{nonbonded}} + E_{\text{other}}$, (Eq 1.6.2)

From equation 1.6, the first expression is the summation of the entire bonded pairs of atoms; it explains bond stretching, *b* denotes bond length, while *Kb* and *b*0 describe the stiffness and the bond's equilibrium dimension, respectively.

Equation 1.6.1 is made up of two sections, the first, which is the Lennard-Jones (LJ) equation, is the part in the square bracket together with the prefactor $\varepsilon i\ j$, and it describes attractive dispersion and repulsive Pauli exclusion interactions, and it is generally known as the van der Waals term. The second section is Coulomb's law, which describes the electrostatic interaction between nonbonded pairs of atoms. In this study, the AMBER force field was employed to parameterise the molecular systems.

1.14.3. Molecular dynamics (MD) simulation

Computer simulations are performed to gain insight into the properties of a group of molecules, their structure, and their atomic interactions. Molecular dynamics serves to augment routine experiments by improvising another method of discovering new things. Molecular dynamics involves analytically resolving the classical equations of motion for several atoms using computational tools (Alder and Wainwright, 1957). Estimating molecular dynamics motion is basically conceived to investigate the relaxation following diverse nonequilibrium conditions. This technique comprises accurately solving the simultaneous classical equations of motion of various large particles by application of a speedy computer (Alder and Wainwright, 1957). Apart from the numerical approximations that play a critical role in integrating the equation of motion, two fundamental approximations are implicit in molecular dynamics simulations. Number one is the assumption that atoms adhere to Newton's equations of motion (Meller,

2001). The second approximation is the model employed to define the interactions among the atoms in the system. Here, a generic model which looks at the essential characteristics and the illustrative physics of that specific set of systems is employed. Classical equations of motion controlling the atomic progression of a system in molecular dynamics simulation are resolved numerically based on boundary conditions suitable for the geometry. Molecular dynamics depends on an integrated resolution of Newton's laws of motion that estimates the equation of motion for atoms (Jensen, 2017). Motion can thus be simulated for molecules as their conformations vary over time or when the ligand is bound to them (Lewars, 2011). The time evolution of interacting particles is monitored by solving Newton's equation of motions:

$$\boldsymbol{F}_i = m_i \frac{d^2 \boldsymbol{r}_i(t)}{dt^2} \qquad \text{(Eq 1.7)}$$

Here, $\boldsymbol{F}_i$ denotes the force acting on the particle (i) at the time (t) and mass m of particle i and $r_i(t)$ = (xi(t), yi(t), zi(t)) represents the location vector of the ith particle. Stipulation of the instant forces prevailing on the particles, their initial velocities and positions are needed to integrate the second-order differential equation stated above.

To gain insight into the atomic behaviour of systems from the laws of classical mechanics, molecular dynamics needs a definition of the interactions among the particles as an input. The feature of the output of an molecular dynamics simulation is a product of the efficiency of the interparticle interaction definition, and one possible way of defining this interaction is the involvement of a force field. Molecular dynamics simulation mathematically tries to unravel Newton's equations of motion by applying explicit models of a system of molecules, thereby permitting structural fluctuations to be detected concerning time (Kalyaanamoorthy and Chen, 2014, Karplus and McCammon, 2002b, Karplus and Petsko, 1990). Molecular dynamics simulation techniques are extensively utilised to gain clue of the time evolution of protein conformations in addition to other biological macromolecules (Moraitakis et al., 2003, Karplus and McCammon, 2002b, Norberg and Nilsson, 2002, Cheatham and Kollman, 2000). It is also used to learn about kinetics and thermodynamics. Molecular dynamic simulations can provide in-depth information about the motion of specific atoms at a particular time frame. It may be used to evaluate the features of a protein or other macromolecules at an accuracy and a time scale which alternatively is unattainable. Thus simulation is a suitable device for enhancing the general knowledge of an ideal system (Adcock and McCammon, 2006).

1.15. Molecular Dynamics Post-Analysis

The protein features studied in this thesis were described by analysing and calculating the trajectories generated using the post-dynamic techniques discussed below. The production run of MD simulation creates molecular dynamics trajectories. Molecular dynamics trajectories are snapshots that describe the co-ordinates and the velocities of individual atoms in a simulated system; it also depicts the time progression of the system (Likhachev et al., 2016, Meller, 2001). Analysis of the trajectories obtained during molecular dynamics simulation with a post-dynamics approach is crucial in deciding the following:

1) comparative thermodynamic binding free energies,

2) three-dimensional structure and configurations, and

3) state of thermodynamic equilibrium of the biomolecular system (Karplus and McCammon, 2002a).

1.15.1. System Stability

Convergence

Convergence of molecular dynamics simulation is aimed not only to eliminate residual experimental flaws but also to produce a model dynamical condition of the molecule, which is appropriate for the commencement of a simulation at the particular thermodynamic parameters (Gallo et al., 2009). Convergence, as related to molecular dynamics simulation, is utilised in describing the structural stability of proteins depending on types of bonds and bond angle vibrations in the course of protein motion due to structural unfolding. Proteins are considered glassy systems; thus, the singular acceptable anticipation is to attain thermal equilibration at the unset of the simulation and follow the system's time evolution over ensuing iterations (Gallo et al., 2009). The attainment of equilibrium and the depiction of an absolute energetic and conformational evenness is crucial for an molecular dynamics trajectory to be unambiguous (Amadei et al., 1999). For a group of parameters, the moment of equilibrium is defined as the time required for the pair of data curves to attain an equivalent level (Gallo et al., 2009). This evenness could likely represent a protein-ligand complex demonstration of a conformational energetically stable state.

Root Mean Square Deviation (RMSD)

Root Mean square deviation (RMSD) of atomic positions entails the evaluation of the average distance of the backbone atoms of superimposed proteins. RMSD is estimated as a function of time from the molecular dynamics simulation perspective (Sargsyan et al., 2017, Martínez,

2015). It is an analysis that depicts the close relationship between two structures; it further indicates and identifies the portion of a protein that produces more considerable structural fluctuation (Sargsyan et al., 2017). RSMD quantifies the similarity in the three-dimensional structure of two proteins. The RMSD derived from a trajectory is represented by the equation:

$$\mathbf{RMSD} = \left(\frac{\sum_N (\mathbf{R_i} - \mathbf{R_1^0})^2}{\mathbf{N}}\right)^{\frac{1}{2}} \qquad \text{(Eq 1.7.1)}$$

Here, N denotes the complete number of atoms present in a complex, R_i is the position of the vector of the Cα atom of the particle, and i represents the conformational reference estimated when the structure is aligned to the first conformation by employing the least square fitting protocol. Different ligands can stabilize various conformers. The comparison and the identification of the similarities and disparity in numerous structural ensembles is an integral approach in utilising molecular simulations to understand the conformation and dynamics of complex biomacromolecules (Dixit et al., 2006). Whereas the average structure is frequently used as a depictive of an ensemble of structures in these comparisons. Dynamic molecular systems possess different conformational substrates that demand a more factual representation that contains the total dynamical range of the ensemble, and this is where the use of RMSD becomes imperative (Dixit et al., 2006).

The radius of Gyration (RoG):

The radius of gyration is the mathematical root mean square distance of parts of proteins from their centre of mass or a particular axis based on suitable application (Lobanov et al., 2008). It is a valuable measure of the overall shape of a molecule; it gives a simple measure of asymmetry in a particle. The equation mathematically represents RoG:

$$\mathbf{r^2gyr} = \frac{(\sum_{i-1}^{n} \mathbf{w_i}\,(\mathbf{r_i} - \mathbf{r^-})^2)}{\sum_{i-1}^{n} \mathbf{w_i}} \qquad \text{(Eq 1.7.2)}$$

The radius of gyration does not just want to depict how ordered or disordered a protein is; instead, it tries to show how folded or compact it is (Lobanov et al., 2008). It tries to describe how a secondary structure is compactly packed into a 3D protein structure (Pan and Patterson, 2013, Huang and Paul, 2007). The radius of gyration is calculated to measure a protein structure's compactness; it is an indicator of protein compactness.

Binding free-energy calculations

Molecular energy in combination with the Poisson–Boltzmann or generalized Born and surface area solvation (MM/PBSA and MM/GBSA) technique are attractive applications to evaluate the binding free energy of the binding of ligands to macromolecules (Genheden and Ryde, 2015). Snapshots obtained from trajectories of MD simulation are utilised to estimate individual free energy constituents (Hou et al., 2011). These techniques depend on molecular dynamics simulations of the receptor–ligand interaction and thus are transitional in both precision and computational effort between empirical scoring and firm alchemical perturbation process (Genheden and Ryde, 2015). So far, they have been favourably employed in reproducing and rationalizing experimental discoveries and enhancing virtual screening and docking outcomes. This MM/PBSA technique helps predict ligand binding affinity. When MM/PBSA and MM/GBSA is examined in contrast with free energy perturbation (FEP) as well as thermodynamic integration (TI) methods (Beveridge and Dicapua, 1989), MM/PBSA and MM/GBSA have been ascertained to be highly computationally adequate (Hou et al., 2011). The equation represents the binding free energy between ligand and receptor:

$$\Delta G_{bind} = G_{complex} - G_{receptor} - G_{ligand} \quad \text{(Eq 1.7.3)}$$

$$\Delta G_{bind} = E_{gas} + G_{sol} - TS \quad \text{(Eq 1.7.4)}$$

$$E_{gas} = E_{int} + E_{vdw} + E_{ele} \quad \text{(Eq 1.7.5)}$$

$$G_{sol} = G_{GB} + G_{SA} \quad \text{(Eq 1.7.6)}$$

$$G_{SA} = \gamma SASA \quad \text{(Eq 1.7.7)}$$

The E_{gas} is the gas phase energy, and it consists of the internal energy E_{int}; Coulomb energy $E_{ele,}$ and the van der Waals energies; E_{vdw}. The FF14SB force field expressions were utilized to calculate the E_{gas}. The energy input from the polar states, $G_{GB,}$ and non-polar states, G_{SA} was employed to evaluate solvation-free energy G_{sol}. Solvent accessible surface area (SASA) was utilized to describe the non-polar solvation energy, SA using a water probe radius of 1.4 Å, whereas the polar solvation, G_{GB}, input was described by solving the GB equation.

In the aforementioned equation, Eint represents the internal energy and Egas the gas phase energy. In a similar vein, Eele and Evdw represent the energies of coulomb and van der Waals, respectively. Furthermore, Gsol denotes the free energy of the solvation, and GGB denotes the polar solvation contribution. GSA uses the solvent-accessible surface area (SASA) to describe the non-polar contribution. SASA is computed using a water probe with a radius of 1.4 A and a surface tension constant of 0.0072 kcal/mol A2. A per-residue decomposition analysis was

also carried out to ascertain the different energies that each binding site residue contributed to ligand affinity and stability.

1.15.2. Conformational Characteristics of the Systems

Root Mean Square Fluctuation (RMSF)

Root mean square fluctuation (RMSF) evaluates the displacement of a specific atom or a collection of atoms relative to the reference structure averaged over the number of atoms (Martínez, 2015). RMSF is a comparative dynamical method that measures the similarity score between aligned protein residues. Little and large structural variations directly corresponding to protein functions appear at an extensive range of time scales (Fuglebakk et al., 2012). Methodical examination of the evolutionary preservation of the fluctuation patterns in a protein is mainly hinged on the relationship between the RMSF profiles (Maguid et al., 2008, Maguid et al., 2006). RMSF evaluation indicates the evolutionary preservation of backbone fluctuations (Fuglebakk et al. 2012). RMSF is calculated by the standard equation below:

$$\mathbf{sRMSF} = \frac{(\mathbf{RMSF_i} - \overline{\mathbf{RMSF}})}{\boldsymbol{\sigma}\,(\mathbf{RMSF})} \qquad \text{(Eq 1.7.8)}$$

RMSFi represents the RMSF of the ith residue, from which the mean RMSF is deducted. High RMSF likely demonstrates fluctuation of the entire structure, or it can reflect the considerable flexibility of a unit of the entire structure.

Residue Interaction Network (RIN)

Residual interaction network (RIN)s are a graphical way of representing a protein structural conformation where the nodes denote amino acids, whereas the interactions between two amino acids represent the edges (Contreras-Riquelme et al., 2018). RIN is a computational post-dynamics analysis tool that enables the visualization and comprehension of complex inter-residue interaction (Ndagi et al., 2017, Moonsamy et al., 2016). This technique strongly detects functional residues, defines ligand-induced fluctuation in conformational states of proteins, and regenerates allosteric communication pathways (Stetz and Verkhivker, 2017). It is a classification approach that aids in identifying the interface residue established on the characteristics of a weighted residue interaction network. The result obtained from the residue interaction network can be used to gain insight into the structure-function relationship (Nan and Zhang, 2013). The parameter degree and the community features of the residue interaction network can be employed to predict the hot spot for protein-protein interaction (Nan and Zhang,

2013). The RIN model can be applied in bioinformatics; for instance, in the analysis of protein structural topology (Hu et al., 2013, Huang et al., 2017) or protein evolution (Yan et al., 2014).

1.16. Aims and objectives.

1.16.1. Problem statement

The high incidence and mortality rates associated with CRC both worldwide and in South Africa, despite improvements in screening and treatment, make it a burden on public health. While raising public awareness and promoting early detection is important, developing novel and efficient treatment options for CRC must receive significant attention. The potential application of glycosylation inhibitors in managing CRC is a promising area of research. Targeting glycosylation pathways may offer new therapeutic opportunities for patients who do not respond well to current treatments. Therefore, this study aims to investigate how glycosylation inhibitors could be used to treat CRC.

1.16.2. Aim and objectives.

The crucial posttranslational modification of glycosylation plays a significant role in the initiation and development of CRC. Therefore, inhibiting the glycosylation procedure may reduce CRC growth, invasion, and progression. This study looks at two well-known protein glycosylation inhibitors, Brefeldin A and Tunicamycin C, to see which proteins they may bind to and what role, if any, these proteins play in glycosylation, glycosylation-related processes, or the development of CRC.

1.16.3. Objectives

1. To identify potential targets for the protein glycosylation inhibitors Brefeldin A and Tunicamycin C using the Swiss Target Prediction algorithm.
2. To identify high-level molecular biological roles of the potential target proteins in CRC using Gene Ontology (GO) and the Kyoto Encyclopedia of Genes and Genomes (KEGG) databases analysis to understand their functionality.
3. To computationally analyse the interactions of target proteins for Brefeldin A and Tunicamycin C using molecular modelling, induced-fit docking, and the molecular mechanics generalized Born surface area (MM-GBSA).
4. To assess the dynamics of the target proteins in complex with Tunicamycin C and Brefeldin A by using molecular dynamic (MD) simulations.

Glycosylation pathways are a potential target for CRC intervention. Understanding what glycosylation is, why cells glycosylate proteins, and how glycosylation is related to carcinogenesis are all necessary to comprehend why glycosylation pathways should be targeted. Cancer progression is facilitated by aberrant glycosylation pathways that involve various proteins and enzymes. It has been observed that the interactions of lectins (glycan-binding protein) with tumour-associated glycans facilitate tumour progression in melanomas, lung cancers, neuroblastomas, colon cancers and pancreatic carcinomas. Targeting glycosylation pathways could present new therapeutic opportunities for CRC intervention, given the numerous ways in which glycosylation is linked to cancer development and progression. This study seeks to identify the potential molecular targets for common glycosylation inhibitor drugs. Five drugs were initially selected and screened for potential protein targets. Two of these drugs with the highest number of hits were selected for further study. Brefeldin A and Tunicamycin C were used to search databases for potential targets. Two targets were selected for each drug. These proteins were selected based on their involvement in glycosylation pathways and their role in CRC. The dynamic interaction of these drugs and their target proteins was simulated to gain greater insight into these potential interactions.

Chapter 2: Methodology

2.1. Research Design

The research design for this project involves a comprehensive study of two compounds, Tunicamycin C and Brefeldin A, focusing on their potential as therapeutic targets in CRC. The process begins with analyzing the compounds' unique structures and biological activities, followed by preparing their structures and predicting their protein targets using the Simplified Molecular Input Line Entry System (SMILES) and the SwissTarget web server. The identified protein targets are then screened for their role in glycolysis activity in CRC. Pathways involved in these proteins are identified using the Kyoto Encyclopedia of Genes and Genomes (KEGG) pathway analysis database and the WIKI pathway, supplemented by a literature review to determine previous links to cancer. The final step involves molecular dynamic modelling of the compounds, including system preparation, molecular dynamics, and calculating Thermodynamic Binding Free Energy (BFE) using the Molecular Mechanics/Poisson-Boltzmann Surface Area (MM/PBSA) method.

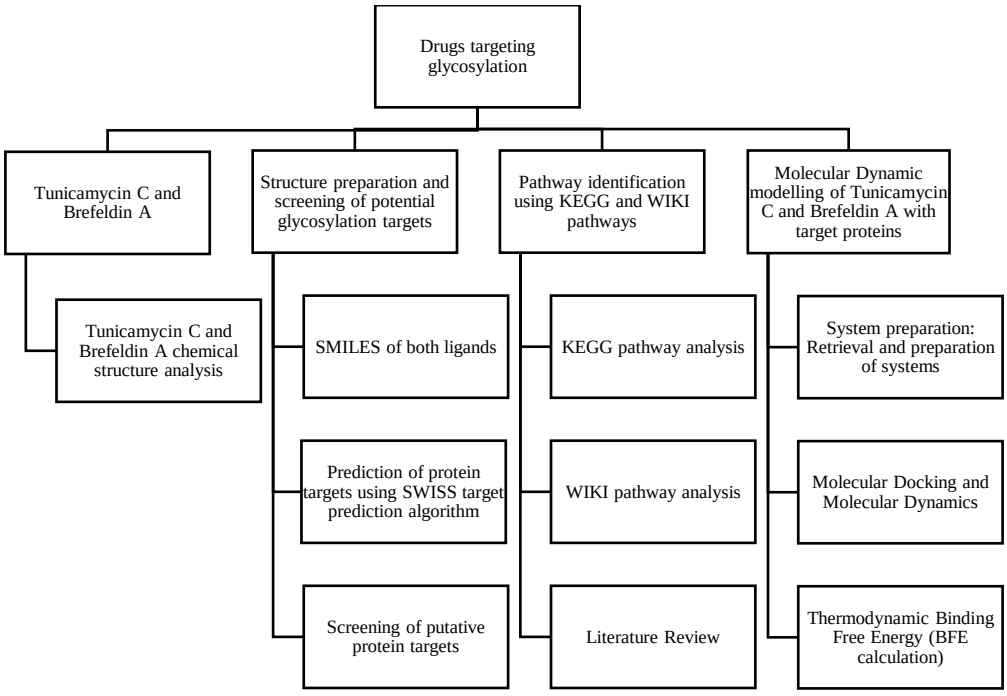


Figure 2. 1 Research Design

2.2. Drugs targeting glycosylation.

In silico analysis is a technique that allows researchers to undertake a theoretical experiment or a computer-simulated experiment utilising bioinformatics-based computational tool. These

strategies are used to determine or select pharmacological targets for *in vitro* or *in vivo* research and to anticipate the outcome/s of other experiments such as knockdown-, gene expression modifications, and drug-ligand interactions. An *in-silico* analysis was performed in this study first to assess whether glycosylation inhibitors (Swainsonine, Brefeldin A, Mannostatin A, Castanospermin, and Tunicamycin C) interact with numerous human proteins, as well as the potential strength of these interactions. Following that, proteins linked to cancer – specifically CRC – were identified, and their role in essential signalling pathways was assessed.

2.3. Chemical Entities of Biological Interest/ChEBI database

The Chemical Entities of Biological Interest (ChEBI) database (https://www.ebi.ac.uk/chebi/) is a website that provides molecular information on small biological chemicals and medications, was used in the preliminary stages of this *in silico* research. The following glycosylation inhibitors, identified from the literature, Swainsonine, Brefeldin A, Mannostatin A, Castanospermin, and Tunicamycin C, were entered into the database to obtain their chemical structures. These results were downloaded as a structural data file (.sdf) for further analysis.

2.4. High-Throughput Docking

The High-Throughput Docking website (https://www.cbligand.org/HTDocking/login.php) was utilized to identify proteins that may interact with the five glycosylation inhibitors and identify the strength of the interactions. The downloaded. sdf. file of each glycosylation inhibitor was uploaded for analysis to the HT-docking site. The two ligands Tunicamycin C and Brefeldin A showed the highest docking scores, and the highest number of potential targets were selected for further studies and analysis. The docking score is used to approximate the binding affinity between the two molecules, with a higher binding score reflecting a higher affinity (Lengauer and Rarey, 1996).

.

2.5. Structure preparation of Tunicamycin C and Brefeldin A and Screening of potential glycosylation targets

The bioinformatics analysis aims to predict protein targets for Tunicamycin C and Brefeldin A. The Simplified Molecular Input Line Entry System (SMILES) of both ligands were obtained from the Chemical Entities of Biological Interest (ChEBI) database, a publicly and freely available dictionary of small compound molecules. The SMILES of both ligands were obtained from the ChEBI database, described above. SMILES is a file format that aims to encode a

ligand's chemical structure in character strings, allowing the easy storing and handling of chemical structures. The prediction of the protein target was performed using SwissTarget, a web server that operates via a graphical interface by the user (Daina et al., 2019). The user submits the ligand's SMILES format, and a workflow is run in the backend that performs the analysis to predict the ligand's most likely macromolecular targets. The chemical information stored in the SMILES format calculated the shape and molecular fingerprint similarity scores of more than 370,000 compounds interacting with more than 3000 protein targets. SwissTargetPrediction returns a CSV report that includes protein target hits ranked according to a score that reflects the probability for a query molecule, assumed as bioactive, to have the listed proteins as biotargets. SwissTargetPrediction can only report on proteins previously identified as binding to at least one chemical compound. In addition to the probability score, SwissTargetPrediction also reports the number of 3D and 2D features; and 2D and 3D similarity values with the most similar known active to the query molecule.

The list of putative protein targets that interact with Tunicamycin C and Brefeldin A was screened for hits that match a crucial role in glycosylation in CRCs. The list was screened thoroughly, and support from biomedical literature was used to verify these types of targets. To further validate the choice, putative protein targets were verified for their available high-quality 3D structure at the Protein Data Bank (PDB).

2.6. Pathway identification using KEGG and WIKI

Kyoto Encyclopaedia of Genes and Genomes (KEGG) illustrates the functionality of genes in the genome by creating a network that informs a researcher about molecules inside a cell with regard to their interdependency (Kanehisa, 2019). KEGG is mostly used in bioinformatics research, especially in genome data analysis, metagenomics, metabolomics, other omics studies, modelling and simulation in systems biology, and translational research in drug development. KEGG was developed in 1995 (Kanehisa, 1997) and is made up of three databases known as pathway maps for interacting molecules, gene catalogues from genome sequences, and ligands (Goto et al., 2000) for enzymes and compounds found in enzymatic reactions (Ogata et al., 1999). The KEGG pathway analysis (https://www.genome.jp/kegg/pathway.html) database was initially used to identify pathways involved in the identified proteins. The KEGG Pathway Database was used for Gene Ontology and KEGG analyses and the $p<0.01$ was deemed statistically significant. However, not all the proteins discovered could be linked to a specific pathway. As a result, the WIKI pathway (https://www.wikipathways.org/index.php/WikiPathways) was employed as a secondary

database to determine the pathway(s) of the remaining proteins. Wiki Pathway was launched in 2018 with 500 pathways to enable high-throughput data analysis and visualization, using transcriptomics and metabolomics initiatives (Pico et al., 2008, Kelder et al., 2012). Wiki pathways consist of over 2300 pathways across 25 different species with the human pathway collection being the largest having increased some 6-fold to include 640 pathways (Kutmon et al., 2014, Kutmon et al., 2016). Wiki pathways provides features for developing and editing pathway maps, visualising expression data from multiple 'omics,' and performing statistical pathway ranking tests (Jennen et al., 2010).

A literature review was then utilised to determine which proteins were connected to cancer, specifically CRC. The goal was to discover proteins that could be used as therapeutic targets, particularly those involved in signalling pathways. This included the use of gene ontogeny terms to identify proteins of interest. One of the primary sources of biological knowledge is the gene ontology pathway since it gives a detailed explanation of how proteins function. Gene Ontology is a restricted and structured vocabulary of words known as GO terms, enabling the analysis of high-throughput molecular data (Ashburner et al., 2000).

2.7. Molecular dynamic modelling of Tunicamycin C and Brefeldin A

2.7.1. System Preparation: Retrieval and preparation of systems

For both compounds, Tunicamycin C and Brefeldin A, the 3D crystallographic structures of their target proteins were retrieved from the RCSB Protein Data Bank (www.rscb.org), this being a database containing three-dimensional structural data of large biological molecules.

For Tunicamycin C, the target proteins were PrKC1 (PDB ID 6ar4) and TK1 (PDB ID 1w4r), while for Brefeldin A, the target proteins were PrCK1 (PDB ID: 6ar4) and MAPK (PDB ID: 3eqc). The compounds themselves were downloaded from PubChem. Any co-crystallized molecules not relevant to the proteins' function, such as ions and crystallographic water, were removed. This was done by opening the topology file with a text editor and removing the data concerning the coordinates of the ligand. The MODELLER algorithm on the UCSF Chimera Graphic User Interface filled in the missing residues in the top protein structures (www.cgl.ucsf.edu/chimera/- this site allows for the interactive visualization and analysis of molecular structures). Molecular docking of Tunicamycin C and Brefeldin A was performed with UCSF Chimera, and the docked conformations were visualised in Maestro and Chimera. The docking scores calculated by Chimera are numerical values that predict the strength and stability of an interaction. It is calculated programs that take factors such as geometric fit and

the energies of the interactions into account. The top docking scores were selected in all cases. These complexes were then prepared for molecular dynamics simulation studies to provide a structural and dynamic perspective into the inhibitory potential of the compounds against the retrieved proteins. Post-analysis was conducted using the Origin Lab software tool (OriginLab - Origin and OriginPro - Data Analysis and Graphing Software)

2.7.2. Molecular Dynamics simulation

2.7.2.1 Desmond Molecular simulation

The protein (TK1, PrKC1, and MAPK): ligand (Brefeldin A and Tunicamycin C) complex were simulated using Molecular Dynamics (MD) to determine its structural stability and interactions. The protein:ligand complexes were immersed in a TIP3P explicitly solvated orthorhombic box using the system builder module, as reported earlier for protein preparation. A 10 Å spacing was maintained between the simulation box boundary and the protein surface. The system was neutralized by adding Na+ and Cl- counterions, and 0.15 M NaCl was used to maintain physiological conditions. MD simulations were carried out for 250 ns in the NPT ensemble using Desmond's default relaxation before simulation, at a temperature of 300 K and a pressure of 1.013 bar. The OPLS2005 force field was used to figure out the system's energy, which was sampled over 1000 frames with 500 ps intervals for each trajectory. To gain insight into the protein and ligand binding stability, MD trajectories of the complexes were analyzed with the Schrodinger Maestro 13.0 ver. The simulation interaction diagram module was used to analyze several parameters such as root-mean-square deviation (RMSD), root-mean-square fluctuation (RMSF), protein-ligand contacts, solvent accessible surface area (SASA), molecular surface area (MSA), and intramolecular hydrogen bonds (intra-HB). In addition, the Simulation Event Analysis Module was used to calculate the systems' radius of gyration (Rg), while the Desmond trajectory clustering tool was used to build 2D and 3D protein-ligand clusters.

2.7.2.2 Amber Molecular Dynamic Simulation for free energy calculation

Molecular Dynamics (MD) simulation for both Tunicamycin C and Brefeldin A was carried out using the Graphical Processor Unit (GPU) version of the Particle Mesh Ewald Molecular Dynamics (PMEMD) engine embedded in the AMBER18 suite, coupled with integrated modules (Case et al., 2023). AMBER (Amber Molecular Dynamics, http://ambermd.org) is a freely available suite of biological simulation programs that consists of two parts, AMBER22 and AMBER23. These refer to molecular and mechanical force fields and a package of

molecular simulator programs. AMBER is downloaded onto a PC for use. Protein parameters were integrated with the FF14SB force field, and the integrated pdb4amber program was used to modify, rename, and protonate the protein. Parameterization and partial charges (Gasteiger-gaff) were generated using the ANTECHAMBER module for both compounds. The LEAP module generated topology and parameter files for the complexes, added counter ions at a constant pH (cpH) to neutralize the system, and solvated the systems in a 10 Å TIP3P water box (Figure 2.2).

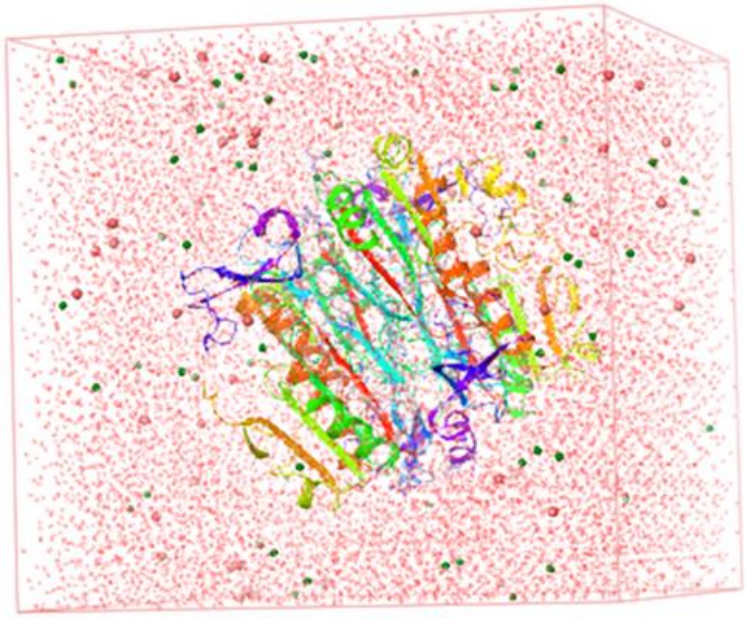


Figure 2.2 A representative illustration of the solvation of a protein molecule: This figure is a depiction of a 10 Å TIP3P water box used to simulate the contribution of the solvation of a protein to its three-dimensional structure. This is a computational description of the exact state of a protein in a physiological system (Grest and Kremer, 1986).

The systems were first partially minimized for 2500 steps using a 500 kcal/mol Å restraint potential, followed by full minimization for 5000 steps with no energy restraints. The Langevin thermostat and a harmonic restraint of 5 kcal/mol $Å^2$ were used to gradually heat the systems from 0 to 300 k in a NVT canonical ensemble for 50 ps. System equilibration was performed at 300 k for 1000 ps without energy restraint, while the Berendsen barostat was used to maintain atmospheric pressure at 1 bar.

Production molecular dynamics run was performed for 250 ns for Tunicamycin C and Brefeldin A, respectively, with the SHAKE algorithm used to restrain all atomic hydrogen bonds. The resulting trajectories were analysed using integrated CPPTRAJ and PTRAJ modules with coordinates. Topology and parameter file generation for the complexes were performed using LEAP module; counter ions were equally added at a constant pH (cpH) with LEAP module in

a bid to neutralize the system, and the systems were finally solvated in a 10 Å TIP3P water box (Figure 2.2). The systems were first partially minimized for 2500 steps using a 500kcal/mol Å restraint potential, followed by complete minimization for 5000 steps with no energy restraints. Langevin thermostat (Grest and Kremer, 1986) and a harmonic restraint of 5 kcal/mol $Å^2$ gradually heat the systems from 0 to 300 K in an NVT canonical ensemble for 50 ps. System equilibration was performed at 300 K for 1000 ps without energy restraint, while the Berendsen barostat was used to maintain atmospheric pressure at 1 bar. Production molecular dynamics run was performed for 25 ns, whereas the SHAKE algorithm was used to restrain all atomic hydrogen bonds. The resulting trajectories were analysed using integrated CPPTRAJ and PTRAJ modules, and coordinates were obtained at every 1 ps while data were plotted and analysed using the Origin data analytical tool (Seifert, 2014). In addition, 3D structural visualization and analyses were carried out on the Graphical User Interface (GUI) of UCSF Chimera.

2.7.3. Post-dynamic analysis

The molecular dynamics simulation studies derived trajectories were viewed relative to post-dynamic analysis using Schrodinger Maestro v13.0 or the Bio-3D R-Statistical package for comparative analysis of protein structures. Succinctly put, both the simulation quality and the alpha carbon atoms' root-mean-square-deviation (RMSD) alongside the ligand with the receptor's RMSD were assessed. In addition, the residue's root-mean-square-fluctuations (RMSF), secondary structures element analysis, and protein-ligand interaction analysis were carried out using the Simulation Interaction Diagram algorithm (implemented in Maestro v13.0). The radius of gyration (Rg) and atomic distance calculations were determined using the Simulation Events Analysis algorithm (also implemented in Maestro v13.0).

2.7.4. Thermodynamic Binding Free Energy (BFE) Calculation

The Thermodynamic Binding Free Energy (BFE) Calculations for Tunicamycin C and Brefeldin A involved the use of the Molecular Mechanics/Poisson-Boltzmann Surface Area (MM/PBSA) method to estimate the binding interaction free energy of these therapeutic molecules with biological macromolecules. The binding interaction free energy was computed from the last 250 ns trajectory for both compounds.

Mathematically, binding free energy is represented by the following equation.

$$\Delta G_{bind} = G_{complex} - G_{receptor} - G_{ligand} \quad (1)$$

$$E_{gas} = E_{int} + E_{vdw} + E_{ele} \quad (2)$$

$$G_{sol} + G_{PB} + G_{SA} \quad (3)$$

$$G_{SA} + \gamma SASA \quad (4)$$

In the aforementioned equation, Eint represents the internal energy and Egas the gas phase energy. In a similar vein, Eele and Evdw represent the energies of coulomb and van der Waals, respectively. Furthermore, Gsol denotes the free energy of solvation, and GGB denotes the polar solvation contribution. G_{SA} uses the solvent-accessible surface area (S_{ASA}) to describe the non-polar contribution. SASA is computed using a water probe with a radius of 1.4 A and a surface tension constant of 0.0072 kcal/mol A2. A per-residue decomposition analysis was also carried out to ascertain the different energies that each binding site residue contributed to ligand affinity and stability.

In addition to these calculations, per residue decomposition analysis was carried out to understand the different energies each binding site residue contributes to ligand affinity and stabilization. This comprehensive approach allows for a detailed understanding of the binding affinities of Tunicamycin C and Brefeldin A.

Chapter 3: Results

3.1. Drugs targeting glycosylation.

3.1.1 High-Throughput Docking

Swainsonine, Brefeldin, Mannostatin A, Castanospermine, and Tunicamycin C were submitted to the HTDocking program (https://www.cbligand.org/HTDocking/search_struct.php) as described below. The structural similarities among the glycosylation inhibitors are minimal. The structures and physical data of all compounds are included in Appendix 1. Table 3.1 summarises the result of the High-Throughput docking.

Table 3.1 Results for High-Throughput Docking

Glycosylation Inhibitor	Number of Target Proteins (Docking Score-minimum 6)	Number of Target Proteins (Docking Score-minimum 7)
Swainsonine	127	1
Brefeldin A	449	234
Mannostatin A	10	0
Castanospermine	167	6
Tunicamycin C	251	168

Table 3.1 represents the target proteins with docking scores greater than 6 and 7, respectively. Brefeldin A had the highest number of target proteins: 449 target proteins with a minimum docking score of 6 and 234 target proteins with a minimum docking score of 7. Tunicamycin also had many target proteins, totalling 251 and 168, with a minimum docking score of 6 and 7, respectively. Manostatin had the least target proteins at 10, with a minimum docking score of 6. Based on these results, Brefeldin A and Tunicamycin C were selected for further protein target prediction and pathway analysis.

Tunicamycin C and Brefeldin A are two distinct compounds with unique structures, which contribute to their biological activities and interactions with target proteins. Tunicamycin C is a nucleoside antibiotic and a member of the Tunicamycin family, consisting of structurally

related compounds. The structure of Tunicamycin C is characterised by an N-acetylglucosamine moiety linked to an 11-carbon dialdose sugar called tunicamine through a 1,1'-N-glycosidic bond. Additionally, Tunicamycin C contains a uracil base linked to the tunicamine sugar through a 1'-N-glycosidic bond (Figure 3.1).

On the other hand, Brefeldin A is a lactone antiviral compound with a unique macrocyclic structure. The structure of Brefeldin A is characterized by a 16-membered lactone ring containing an internal conjugated diene system, along with a flexible seven-membered ring fused to the lactone ring at carbons 7 and 12 (Figure 3.1). The compound also features a cyclopentane ring fused to the lactone ring between carbons 4 and 5. The specific arrangement of these rings and the presence of functional groups, such as the lactone moiety and a highly reactive epoxide group, are crucial for Brefeldin A's biological activity.

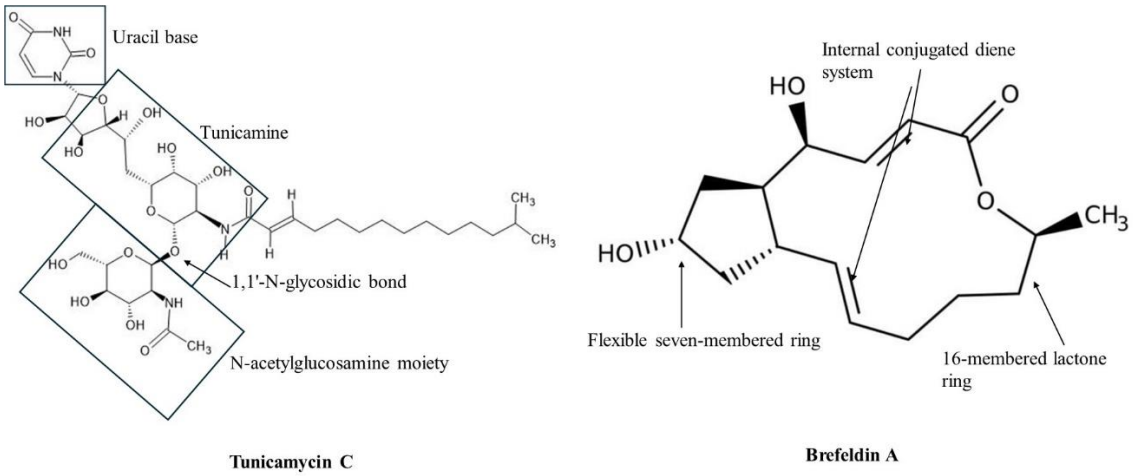


Figure 3.1 Chemical structures. Tunicamycin C and Brefeldin A show structural features. A: structures were drawn and annotated using ACD/Chemscetch freeware 2022.3 (https://www.acdlabs.com/)

3.2. Protein Target Prediction and Pathway Analysis

CRC remains a significant global health concern, with an exceptionally high prevalence and mortality rate in South Africa. (Zhao et al., 2021, Wan et al., 2020, de Freitas Junior et al., 2011, Luesch and Paavilainen, 2020, Kimura and Bugg, 2003)Therefore, to assess the suitability of Tunicamycin C and Brefeldin A as treatments for CRC, their cellular targets were identified, and the affected signalling pathways were examined. Advanced computational approaches were employed, including protein target prediction software, pathway/network analysis, *in silico* analysis, and high throughput docking. These methods facilitate the identification of potential drug targets and allow for a comprehensive understanding of the

molecular interactions between the glycosylation inhibitors and their target proteins. Furthermore, pathway and network analyses revealed the intricate signalling pathways and gene networks modulated by these compounds in colon cancer. This study provides valuable insights into the molecular mechanisms underlying the anticancer activity of these glycosylation inhibitors and informs the development of novel therapeutic strategies targeting CRC.

3.3. Screening glycosylation targets

The SMILES (Simplified Molecular Input Line Entry System) chemical structures of Brefeldin A and Tunicamycin C were utilised in Swiss target protein prediction to identify potential biological targets for these compounds (Table 3.2). The Canonical SMILES obtained from the PubChem database generated the above structures (Figure 3.1).

By representing the molecular structure of these compounds in a standardised format, the input of SMILES data into computational tools can be used for target prediction. This process allowed for systematically evaluating the binding affinity of Brefeldin A and Tunicamycin C to various proteins. Table 3.3 ultimately identifies potential targets for further study and drug development.

Table 3.2 Canonical SMILES Computed by OEChem 2.3.0. (PubChem release 2021.05.07)

Ligand	Canonical SMILES
Tunicamycin C	CC(C)CCCCCCCCC=CC(=O)NC1C(C(C(OC1OC2C(C(C(C(O2)CO)O)O)NC(=O)C)CC(C3C(C(C(O3)N4C=CC(=O)NC4=O)O)O)O)O)O
Brefeldin A	CC1CCCC=CC2CC(CC2C(C=CC(=O)O1)O)O

Table 3. 3 Top 18 Potential Target Proteins for Brefeldin A and Tunicamycin C

Brefeldin A targets	Known actives (3D/2D)	Tunicamycin C	Known actives (3D/2D)
CYP19A1	55/ 69	CDA	0/ 2
ATP12A	03/ 10	PRKCA	2/ 0
RPS6KA5	04/ 03	PDCD4	3/ 0
AR	163 / 56	FNTA/ FNTB	2/0
PRKCA	49/ 203	PYGM	0/ 3
PDCD4	0/8	TK2	0/ 8
PGR	31/ 40	P2RY12	4/ 0
TAS2R31	0/1	ADORA1	0/ 16
PSEN2	66/ 0	TYMP	0/ 6
PPARG	12/ 10	BCL2L1	1/ 0
JAK1	112/ 0	BCL2	1/ 0

CDC25A	8/ 15	HRH3	1/ 0
PDE10A	201/ 0	TK1	0/ 13
MAPK14	118/ 0	PLA2G2A	1/ 0
MAP2K1	133/ 0	PLA2G5	1/ 0
CDK2	85/ 0	PLA2G10	1/ 0
LRRK2	93/ 0	FL23	2/ 0
GABRB3	5/ 0	AURKB	2/ 0

SwissTarget Predict (SwissTargetPrediction) is an *in-silico* protein target prediction software that helps identify potential protein targets for a compound by analysing its structure and evaluating its interactions with proteins. Table 3.3 illustrates the protein targets for Brefeldin A and their respective known actives in 3D and 2D, as the Swiss Protein Predict is a web tool that predicts probable protein. Known actives in 3D and 2D provide insight into the potential interactions and binding affinities between Brefeldin A and the protein targets. A higher number of known actives suggests that the compound may have a stronger affinity for the specific protein target and, thus, a higher likelihood of modulating its function (Daina et al., 2019).

Cytochrome P450 Family 19 Subfamily A Member 1 (CYP19A1) had 55 known actives in 3D and 69 known actives in 2D. The protein ATPase H+/K+ Transporting Non-Gastric Alpha2 Subunit (ATP12A) had 3 known actives in 3D and 10 known actives in 2D. Ribosomal Protein S6 Kinase A5 had 4 known actives in 3D and 3 known actives in 2D. Androgen Receptor (AR) had the highest number of known actives, with 163 known actives in 3D and 56 known actives in 2D. Protein Kinase C Alpha had 49 known actives in 3D and the highest 203 known actives in 2D. Programmed Cell Death Protein 4 (PDCD4) had 0 known actives in 3D and 8 known actives in 2D, and the Progesterone Receptor had 31 known actives in 3D and 40 known actives in 2D (Table 3.3).

Taste Receptor Type 2 Member 31 (TAS2R31) had the least known activities, zero known actives in 3D and 1 known active in 2D. The protein Presenilin 2 had 66 known actives in 3D and zero known actives in 2D. Peroxisome Proliferator-Activated Receptor Gamma (PPARG) had 12 known actives in 3D and 10 known actives in 2D. Another protein of interest was Mitogen-Activated Protein Kinase Kinase 1 (MAP2K1), which had 133 known actives in 3D and zero in 2D. Cyclin-Dependent Kinase 2 had 85 known actives in 3D and zero known actives in 2D. Leucine-Rich Repeat Kinase 2 had 93 known actives in 3D and 0 known actives in 2D. Finally, the Gamma-aminobutyric acid type A receptor beta3 subunit had five known

actives in 3D and 0 known actives in 2D. Swiss Protein Predict for Tunicamycin C results indicate the protein targets and their respective known actives, presented in 3D and 2D formats (Table 3.3).

The protein of interest identified through manual curation was PRKCA (Protein Kinase C Alpha), which had 2 (3D) / zero (2D) known actives; and TK1 (Thymidine Kinase 1, Soluble), which had zero (3D) and 13 (2D) known actives. Combining the Swiss Protein Predict results with further computational and experimental analyses we can gain valuable insights into the molecular mechanisms underlying Brefeldin A's effects on cancer cells. This knowledge will ultimately contribute to developing more effective therapeutic strategies targeting CRC and potentially other types of cancer.

Three target proteins of interest were identified as potential proteins targets through manual curation. For Brefeldin A, PRKCA, PPARG, and MAP2K1 were selected, while PRKCA and TK1 were selected for Tunicamycin C. The three proteins were subjected to pathway analysis using KEGG and WIKI pathway analysis programs., reflecting their involvement in various cellular signalling pathways that regulate essential processes such as cell proliferation, differentiation, survival, and migration. Some of the critical pathways to note are represented in Table 3.3. The listed genes are specific genes of interest that will be further investigated (PRKCA, PPARG, MAP2KI, PRKCA, and TK1.

Table 3.4 KEGG pathway analysis for targeted proteins for Brefeldin A

Term	***p*-value**	**Genes**
Epstein-Barr virus infection	2.49E-15	SYK; PIK_3CD; PIK_3CB; TYK_2; $IRAK_4$; ITGAL; $MAPK_{14}$; IL_6; CDK_6; $CCND_1$; $CCNE_2$; CDK_4; CDK_2; MDM_2; JAK_3; JAK_1
Cellular senescence	2.73E-14	MAP_2K_1; PIK_3CD; PIK_3CB; $MAPK_{14}$; $CDC_{25}A$; IL_6; CDK_6; $CCND_1$; $CCNE_2$; CDK_4; $CHEK_1$; CDK_2; CDK_1; MDM_2
Pathways in cancer	8.34E-14	MAP_2K_1; $ROCK_1$; MMP_1; $ROCK_2$; PIK_3CD; PRKCA; PIK_3CB; AR; IL_6; RPS_6KA_5; CDK_6; $CCND_1$; $CCNE_2$; CDK_4; CDK_2; PIM_1; MDM_2; PPARG; JAK_2; JAK_3; JAK_1
Hepatitis B	1.03E-12	MAP_2K_1; PIK_3CD; PRKCA; PIK_3CB; TYK_2; $IRAK_4$; $MAPK_{14}$; IL_6; $CCNE_2$; CDK_2; JAK_2; JAK_3; JAK_1
PIsK-Akt signalling pathway	1.17E-12	MAP_2K_1; SYK; PIK_3CB; PPP_2CA; GYS_1; IL_6; CDK_6; $CCND_1$; $CCNE_2$; CDK_4; CDK_2; MDM_2; JAK_2; JAK_3; JAK_1
Measles	3.38E-12	IL_6; CDK_6; $CCND_1$; $CCNE_2$; CDK_4; CDK_2; PIK_3CD; PIK_3CB; TYK_2; $IRAK_4$; JAK_3; JAK_1

Human cytomegalovirus infection	4.25E-12	CCR1; MAP_2K_1; $ROCK_1$; $ROCK_2$; PIK_3CD; PRKCA; PIK_3CB; $MAPK_{14}$; IL_6; CDK_6; $CCND_1$; CDK_4; MDM_2; JAK_1
Kaposi sarcoma-associated herpesvirus infection	9.62E-12	CCR_1; MAP_2K_1; SYK; PIK_3CD; TYK_2; MAPK14; IL_6; CDK_6; $CCND_1$; CDK_4; JAK_2; JAK_1
Viral carcinogenesis	1.82E-11	SYK; PIK_3CD, PIK_3CB; CDK_6, $CCND_1$; $CCNE_2$; CDK_4; $CHEK_1$; CDK_2; CDK_1; MDM_2, JAK_3; JAK_1
Cell cycle	2.10E-11	CDK_6; $CCND_1$; $CCNE_2$; PRKDC; CDK_4; $CHEK_1$; CDK_2; CDK_1; MDM_2; CDC_7; $CDC_{25}A$
AGE-RAGE signalling pathway in diabetic complications	5.41E-11	IL_6; $CCND_1$; CDK_4; PIM_1; PIK_3CD; PRKCA; PIK_3CB; JAK_2; $MAPK_{14}$; PRKCZ

The KEGG (Kyoto Encyclopedia of Genes and Genomes) pathway analysis generated a list of significantly enriched pathways in target proteins for Brefeldin A. The lower the *p*-value, the more significant the enrichment of the pathway. The KEGG pathway analysis results show a list of 11 significantly enriched pathways associated with the given gene set. The pathways are related to various biological processes such as viral infections, cellular senescence, cancer, and diabetes complications. The KEGG pathway analysis revealed several significantly enriched pathways associated with the given gene set. The Epstein-Barr virus infection pathway had the lowest *p*-value (2.49E-15), indicating the most robust association among the listed pathways, with genes such as SYK, PIK3CD, and PIK3CB, respectively TYK2, and IRAK4 involved. The Cellular Senescence pathway with a *p*-value of 2.73E-14, included MAP2K1, PIK3CD, PIK3CB, MAPK14, CDC25A, and IL6. Additionally, the Pathways in Cancer showed a p-value of 8.34E-14 and included genes such as MAP2K1, ROCK1, MMP1, ROCK2, PIK3CD, PRKCA, PIK3CB, AR, and IL6 (Table 3.3).

Furthermore, the Hepatitis B pathway, with a p-value of 1.03E-12, included such genes as MAP2K1, PIK3CD, PRKCA, PIK3CB, TYK2, IRAK4, MAPK14, IL6, CCNE2, CDK2, JAK2, JAK3, and JAK1. The PI3K-Akt signalling pathway had a p-value of 1.17E-12 and comprised MAP2K1, SYK, PIK3CB, PPP2CA, GYS1, IL6, CDK6, CCND1, CCNE2, CDK4, CDK2, MDM2, JAK2, JAK3, and JAK1. The Measles Pathway, with a p-value of 3.38E-12, encompassed IL6, CDK6, CCND1, CCNE2, CDK4, CDK2, PIK3CD, PIK3CB, TYK2, IRAK4, JAK3, and JAK1 (Table 3.3).

Moreover, the Human Cytomegalovirus infection pathway had a p-value of 4.25E-12 and included CCR1, MAP2K1, ROCK1, ROCK2, PIK3CD, PRKCA, PIK3CB, MAPK14, IL6, CDK6, CCND1, CDK4, MDM2, and JAK1 (Table 3.3) The Kaposi sarcoma-associated

herpesvirus infection pathway had a p-value of 9.62E-12 and involved genes like CCR1, MAP2K1, SYK, PIK3CD, TYK2, MAPK14, IL6, CDK6, CCND1, CDK4, JAK2, and JAK1. The Viral Carcinogenesis pathway had a p-value of 1.82E-11, and includes genes such as SYK, PIK3CD, PIK3CB, CDK6, CCND1, CCNE2, CDK4, CHEK1, CDK2, CDK1, MDM2, JAK3, and JAK1. Additionally, the Cell Cycle pathway had a p-value of 2.10E-11 and involves genes like CDK6, CCND1, CCNE2, PRKDC, CDK4, CHEK1, CDK2, CDK1, MDM2, CDC7, and CDC25A (Table 3.3). Lastly, the AGE-RAGE Signalling pathway in diabetic complications had a p-value of 5.41E-11, and the associated genes include IL6, CCND1, CDK4, PIM1, PI K3CD, PRKCA, PIK3CB, JAK2, MAPK14, as well as PRKCZ (Table 3.3).

The KEGG pathway analysis in Table 3.4 covered several biological processes, including viral infections, cellular senescence, cancer, and diabetes complications. The genes involved in these pathways vary, with some participating in multiple pathways, suggesting possible overlapping or interconnected biological mechanisms.

Table 3.5 KEGG pathway analysis for targeted proteins for Tunicamycin C

Term	*p*-value	Genes
Neuroactive Ligand-receptor interaction	$5.37E^{-13}$	$P_2RY_{14;}$ $SSTR_{1;}$ $NR_3C_{1;}$ $SSTR_{3;}$ $MCHR_{1;}$ $SSTR_{4;}$ $SSTR_{5;}$ $P_2RY_{6;}$ $CYSLTR_{2;}$ $ADORA_2A$; $HRH_{3;}$ $P_2RY_{4;}$ $ADORA_2B$; $ADORA_{3;}P_2RY_2$ $ADORA_1$
Starch and sucrose metabolism	5.67E-12	MGAM; AMY_2A; AMY_1A; SI; GAA; PYGM; $HK_{2;}$ HK1
Vascular smooth muscle contraction	4.04E-11	ADORA2A; PRKCB; $ADORA_2B$; $ROCK_{2;}$ PRKCE; PRKCD; PLA_2G_5; PRKCA
Carbohydrate digestion and absorption	5.64E-11	MGAM; AMY_2A; AMY_1A; PRKCB; SI; $AKT_{3;}$ $HK_{2;}$ HK
Ras signalling pathway	1.18E-09	$FLT_{3;}$ PRKCB; AKT_3; $PLA_2G_{10;}$ PLA_2G_2A; PRKCA; $PLA_2G_{5;}$ $FGF_{2;}$ VEGFA; BCL_2L_1
HIF – 1 signalling pathway	2.65E-091.18E-09	PRKCB; $AKT_{3,}$ $BCL_{2;}$ PRKCA; GAPDH; EIF_4E; HK_2 $;HK_{1;}$ VEGFA
Proteoglycans in cancer	4.13E-09	PRKCB; $ROCK_{2;}$ $MMP_{2;}$ $AKT_{3;}$ $PDCD_{4;}$ PRKCA; HPSE; PRKACA; $FGF_{2;}$ $MMP_{9;}$ VEGFA
Galactose metabolism	6.98E-09	MGAM; $B_4GALT_{1;}$ SI; GAA; $HK_{2;}$ HK_1
Pyrimidine metabolism	9.00E-09	CDA; $TK_{2,}$ NT_5M; $TK_{1;}$ UMPS; TYMS; TYMP
AGE-Rage signalling pathway in diabetic complications	2.71E-08	PRKCB; $MMP_{2;}$ PRKCE; $AKT_{3;}$ PRKCD; $BCL_{2,}$ PRKCA; VEGFA
Pathways in cancer	3.41E-08	$HSP_{90}AA_{1;}$ $FLT_{3;}$ PRKCB; $ROCK_{2;}$ MMP_2; $FGF_{1;}$ $FGF_{2;}$ $MMP_{9;}$ VEGFA; $CCNE_{2;}$ $AKT_{3,}$ $BCL_{2,}$ PRKCA; BCL_2L_1

The most enriched pathway was the Neuroactive Ligand-receptor interaction pathway which had a *p*-value of 5.37E-13 and included genes such as P2RY14, SSTR1, NR3C1, SSTR3, MCHR1, SSTR4, SSTR5, P2RY6, CYSLTR2, ADORA2A, HRH3, P2RY4, ADORA2B, ADORA3, P2RY2, and ADORA1 (Table 3.5). The Starch and Sucrose Metabolism pathway had a *p*-value of 5.67E-12, with genes comprising MGAM, AMY2A, AMY1A, SI, GAA, PYGM, HK2, and HK1. The Vascular Smooth Muscle Contraction pathway had a *p*-value of 4.04E-11 and was associated with ADORA2A, PRKCB, ADORA2B, ROCK2, PRKCE, PRKCD, PLA2G5, and PRKCA. The Carbohydrate Digestion and Absorption pathway, *p*-value of 5.64E-11, incorporated MGAM, AMY2A, AMY1A, PRKCB, SI, AKT3, HK2, and HK. The Ras signalling pathway, with a p-value of 1.18E-09, encompassed FLT3, PRKCB, AKT3, PLA2G10, PLA2G2A, PRKCA, PLA2G5, FGF2, VEGFA, and BCL2L1 (Table 3.4). The HIF-1 signalling pathway, with p-value of 2.65E-09, included genes PRKCB, AKT3, BCL2, PRKCA, GAPDH, EIF4E, HK2, HK1, and VEGFA. The Proteoglycans in the Cancer pathway had a p-value of 4.13E-09 and involved genes such as PRKCB, ROCK2, MMP2,

AKT3, PDCD4, PRKCA, HPSE, PRKACA, FGF2, MMP9, and VEGFA. The Galactose Metabolism pathway with a p-value of 6.98E-09 comprised genes like MGAM, B4GALT1, SI, GAA, HK2, and HK1 (Table 3.4).

The Pyrimidine Metabolism pathway had a p-value of 9.00E-09 and was associated with CDA, TK2, NT5M, TK1, UMPS, TYMS, and TYMP. The AGE-RAGE Signaling Pathway in Diabetic Complications with a p-value of 2.71E-08 included PRKCB, MMP2, PRKCE, AKT3, PRKCD, BCL2, PRKCA, and VEGFA. Lastly, Pathways in Cancer pathway had a p-value of 3.41E-08 and included genes such as HSP90AA1, FLT3, PRKCB, ROCK2, MMP2, and FGF1, FGF2, MMP9, VEGFA, CCNE2, AKT3, BCL2, PRKCA, and BCL2L1 (Table 3.4).

Altogether, these results show 12 significantly enriched pathways associated with the given gene set, covering various biological processes related to ligand-receptor interactions, metabolism, muscle contraction, signalling pathways, and cancer. The KEGG pathway analyses selected targets to assess their structural stability and conformational changes in the presence of Tunicamycin C (TK1 and PrKC1) and Brefeldin A (MAPK and PrCK1), respectively. These proteins were selected based on their predicted involvement in glycosylation pathways as well as their involvement in numerous pathways that play a role in the development and progression of colon cancer. These dynamic simulations are described below.

3.4. Estimation of evolving conformational dynamics along the 250 ns MD simulation

The structural stability and conformational changes of TK1 and PrKC1 in the presence of Tunicamycin C, as well as MAPK and PrCK1 in the presence of Brefeldin A, were investigated using the C-α root mean square deviation (RMSD) and C-α root mean square fluctuation (RMSF) analyses. For Tunicamycin C, the RMSD analysis, which evaluates the structural stability of proteins through the assessment of their backbone atoms relative to their initial structures during the MD simulation, revealed that both the apo and Tunicamycin C-bound systems closely followed each other, indicating similar structural stability (Figure 3.2). The RMSF analysis related to functional activity showed similar patterns of residue fluctuations for both systems.

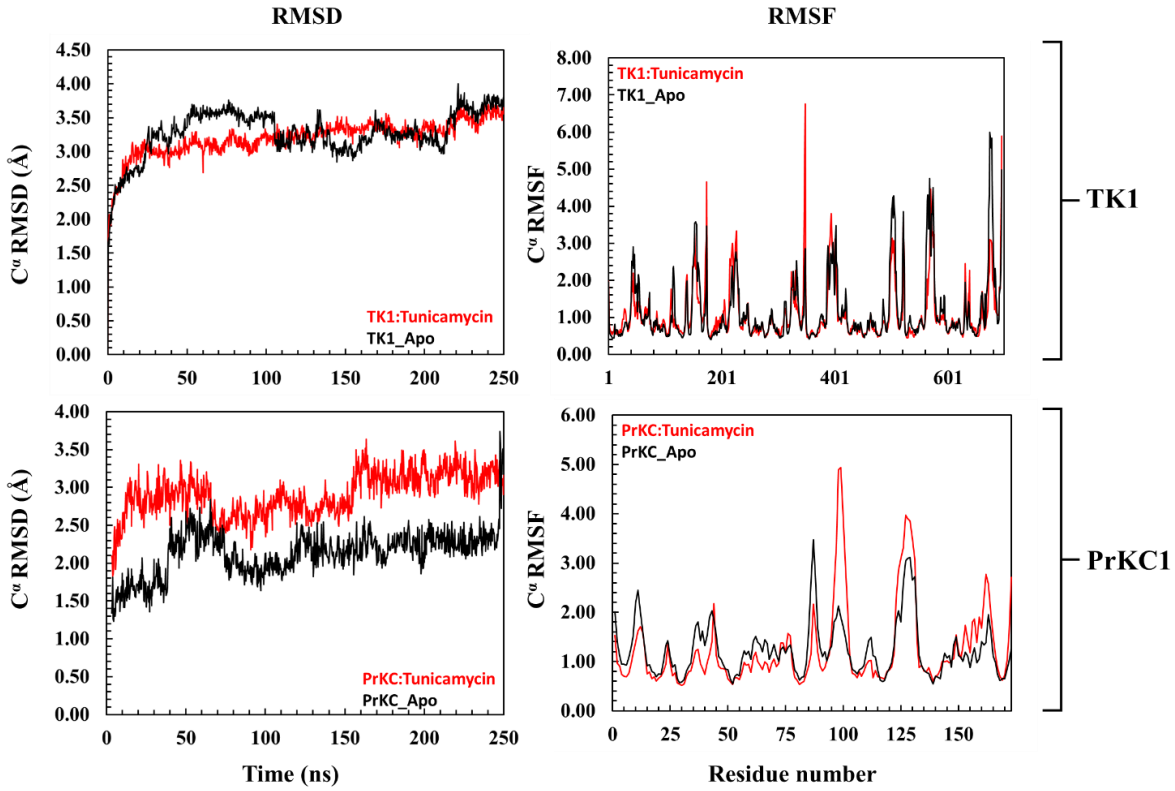


Figure 3.2 A representation of the RMSD and RMSF of TK1 and PrKC1 with their corresponding apo. The upper plots represent the trajectory pattern for TK1, while the lower plots are for PrKC1.

For Brefeldin A, the RMSD plot (Figure 3.3) showed that both the apo and Brefeldin A-bound MAPK trajectories exhibited similar patterns at the start of the MD simulation until 50ns. After this point, the trajectories diverged, with the Brefeldin A-bound MAPK moving upwards and the apo tilting downwards. However, both trajectories maintained a horizontal plot from 75ns toward the end of the MD simulation. The estimated average RMSD of the Brefeldin A-bound MAPK was 3.55±0.58Å, and that of the apo was 2.88±0.31Å.

The RMSF plots of the Brefeldin A-bound MAPK and PrKC1 showed trajectory patterns quite like their corresponding apo systems, indicating similar residue fluctuations and, hence, similar functional activities. The estimated mean RMSF of MAPK was 1.44±1.02Å, while that of the apo was 1.33±0.99Å. For PrCK1, the mean RMSF was 1.47±0.80Å for the Brefeldin A-bound PrKC1, while that of the apo was 1.24±0.55Å.

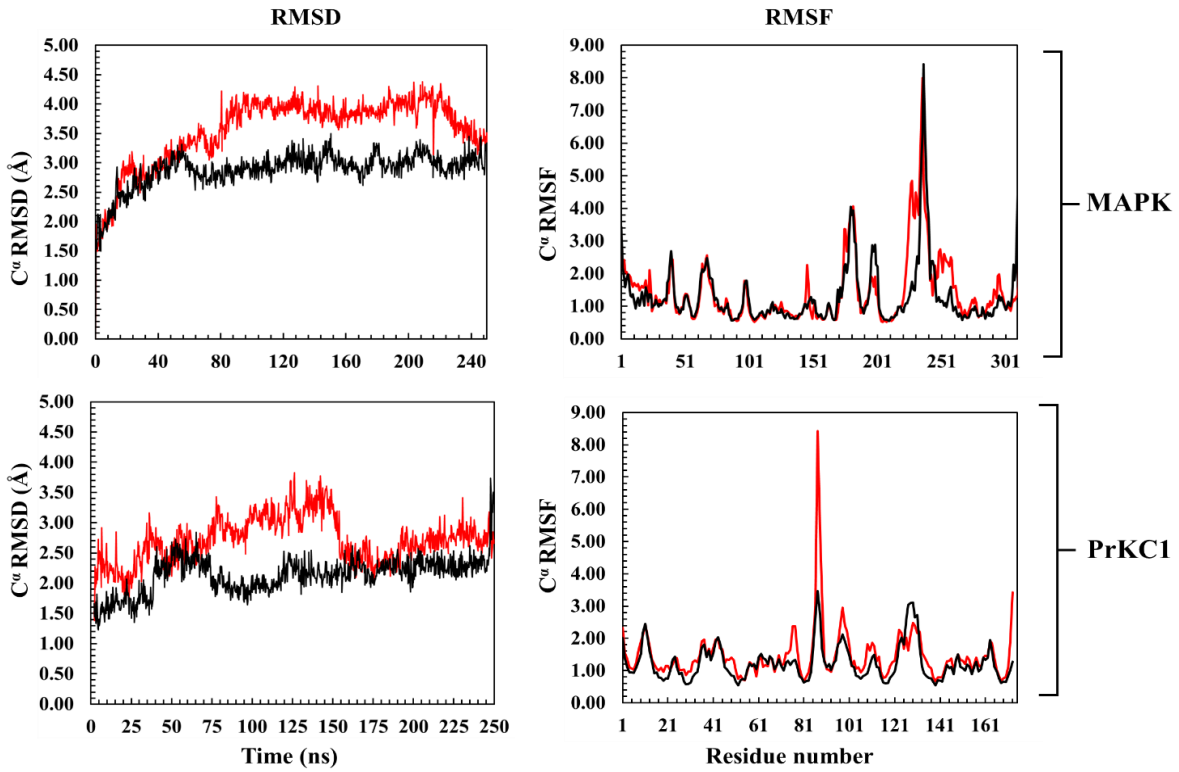


Figure 3.3: An RMSD and RMSF plot of MAPK and PrKC1 with their corresponding apo. The upper plots represent the trajectory pattern for TK1, while the lower plots are for PrKC1.

Tunicamycin C and Brefeldin A showed similar structural stability and functional activities to their respective apo systems, as indicated by the RMSD and RMSF analyses. However, Brefeldin A tended to bind in different pockets, suggesting it may be a weaker binder; thus, further studies are needed to elucidate the underlying mechanisms.

The 3D conformational alignment and orientation of Tunicamycin C and Brefeldin A within their respective binding pockets were investigated. For Tunicamycin C, a 3D image (Figure 3.4) was generated to illustrate how the compound fits within the binding pockets of both TK1 and PrKC1. Both cartoon and surface representations are represented here for a clear and comprehensive view of the ligand's conformational alignment and orientation within the pocket.

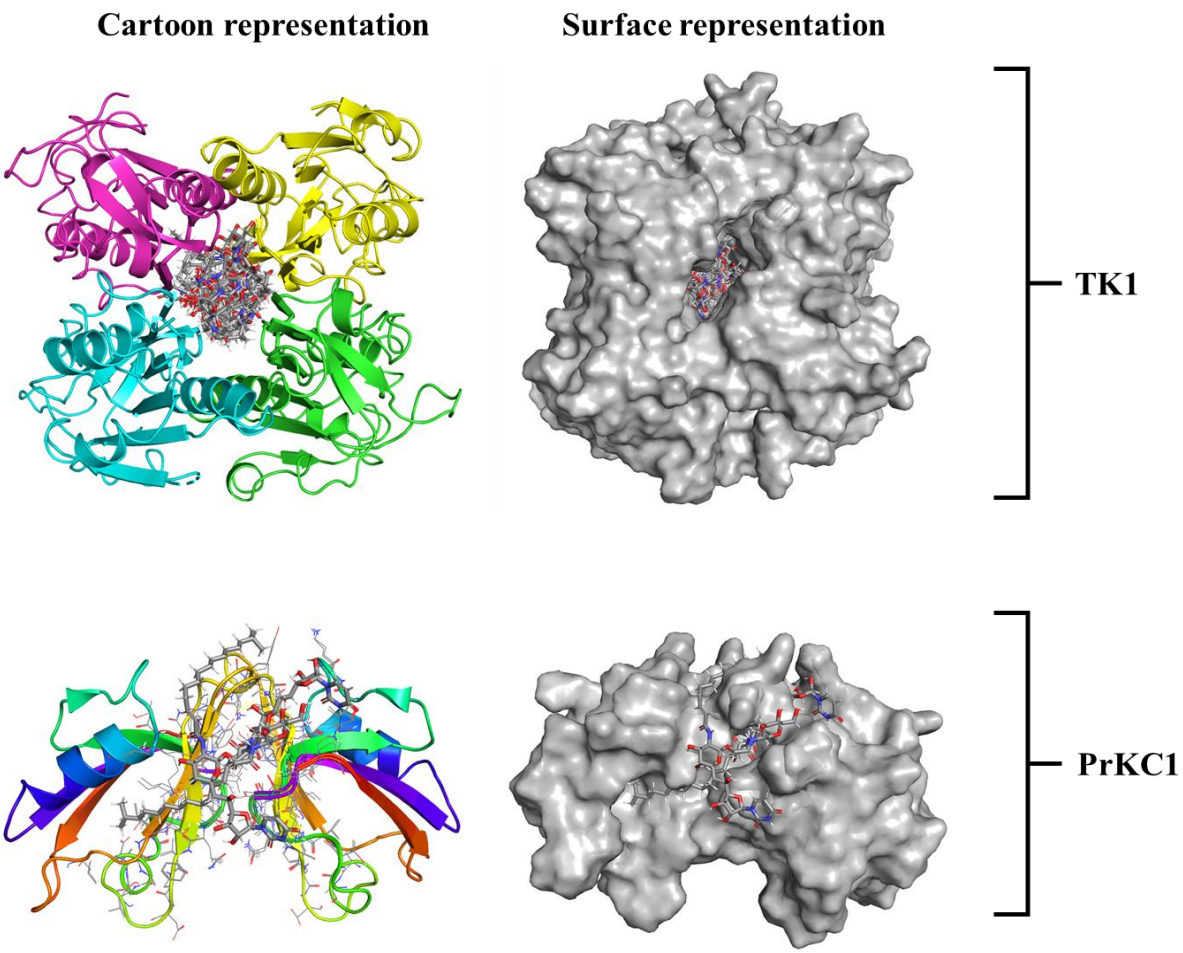


Figure 3.4. Docking of Tunicamycin C with protein targets. An illustrative presentation of Tunicamycin, TK1, and PrKC1 docking complexes. The best binding poses are represented for optimal interactions.

In addition, the binding pattern of Brefeldin A was examined when docked into MAPK and PrCK1. Interestingly, when compared to Tunicamycin, Brefeldin A was found to bind in different pockets of the target proteins (Figure 3.5). This suggests potential flexibility or adaptability in the binding behaviour of Brefeldin A, which could have implications for its interaction dynamics and functional effects. Further studies would be necessary to better understand the implications of this binding behaviour.

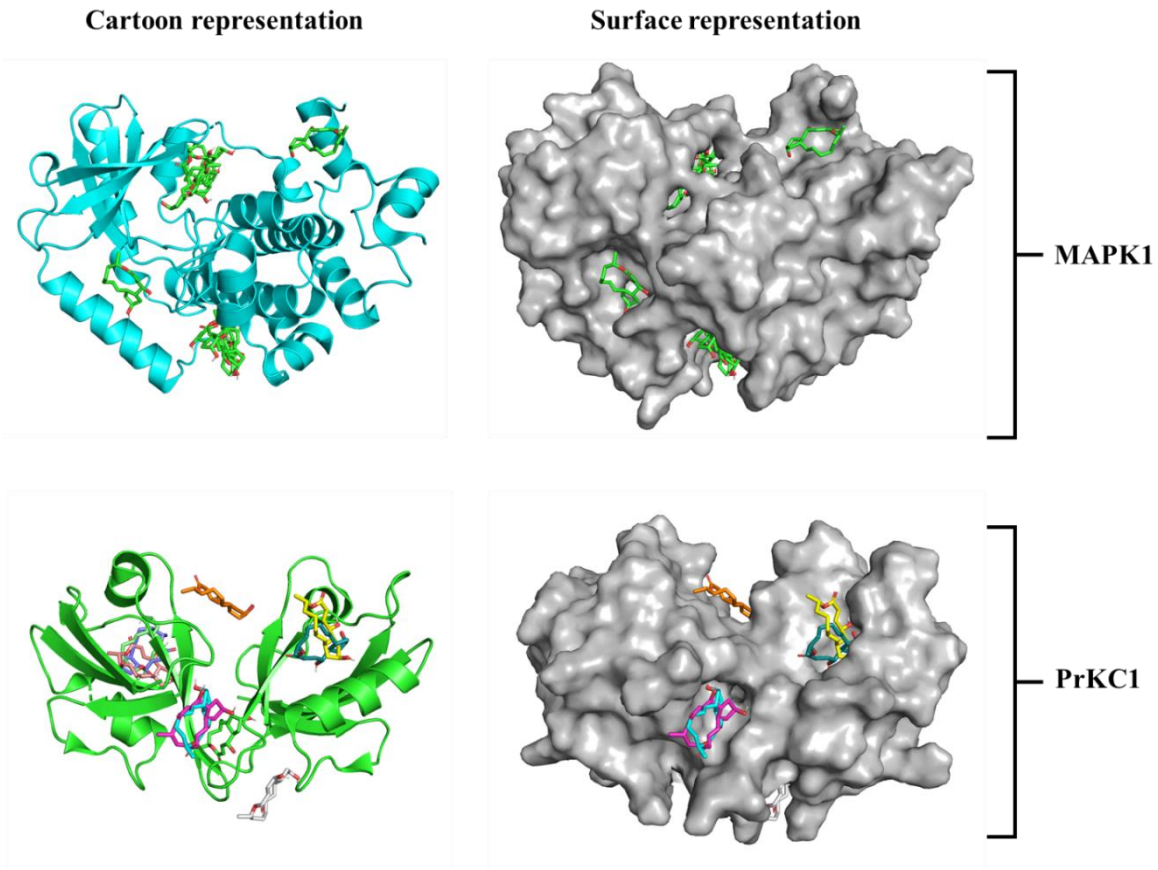


Figure 3.5. Docking of Brefeldin A with protein targets A cartoon and surface representation of Brefeldin A, MAPK, and PrKC1 docking complexes showing the best binding poses conformation for optimal interaction.

3.4.1. Comparative evaluation pf structura; drift from their centre of mass

The Radius of gyration (Rg) is a valuable metric for assessing the mobility of systems, specifically the structural displacement of systems from their centre of mass (Figure 3.6). It measures the degree of structural compactness during the MD simulation. (Emmanuel et al., 2020). The Rg plot for Tunicamycin C (Figure 3.6) produced a trajectory pattern similar to the RMSF plot. There appears to be no noticeable difference between the Tunicamycin C bound TK1 and PrKC1 trajectories and the apo.

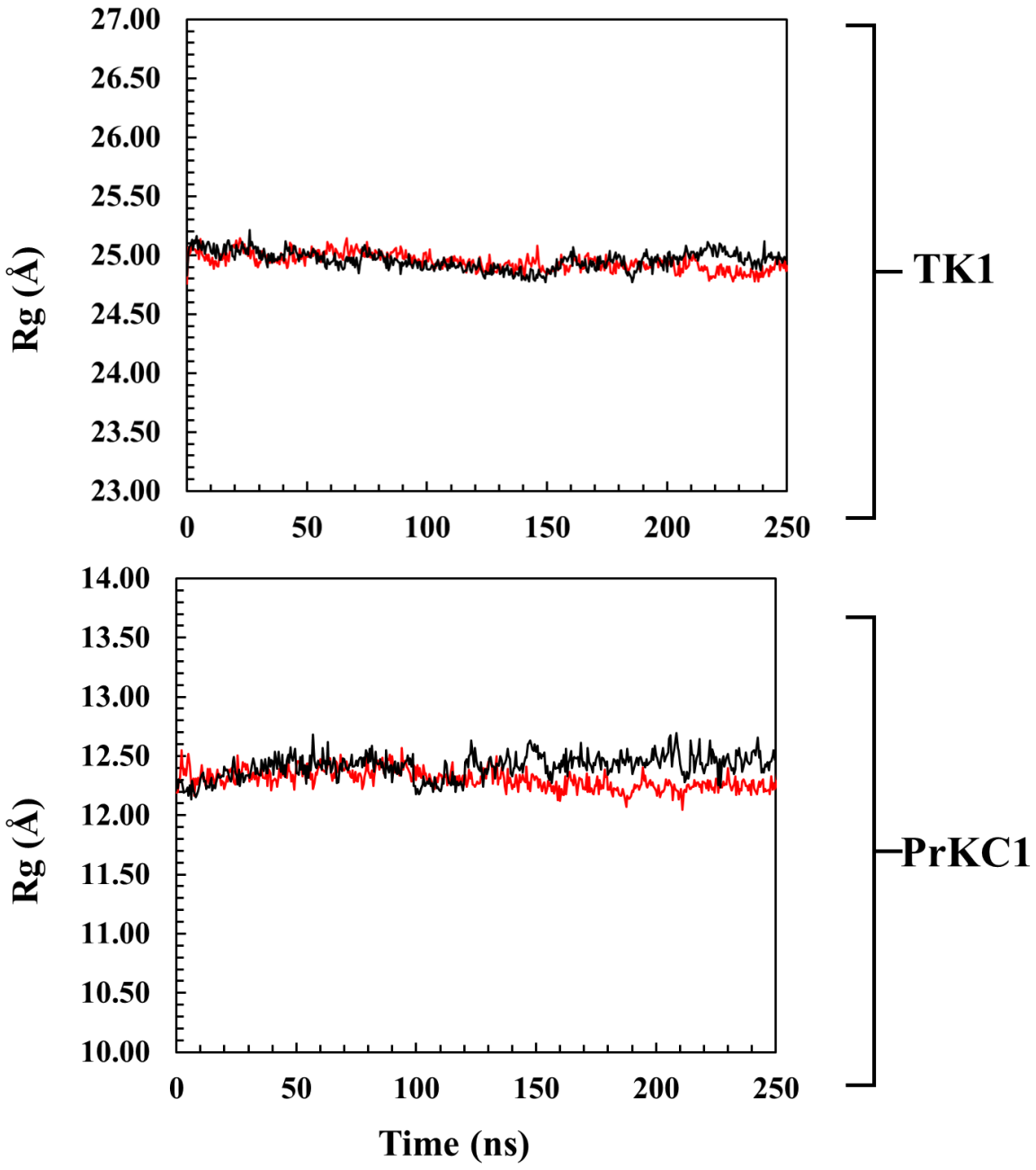


Figure 3.6. Rg plots of the interaction between Tunicamycin C withTK1 and PrKC1.
A pattern representation observed in the Rg plots of the global structure of TK1 and PrKC1 with their corresponding apo systems. The Rg plots show the global structure of the proteins compared to the protein interaction with Tunicamycin C.

The Rg plot for Brefeldin A (Figure 3.7) produced a trajectory pattern like that of the RMSF plot. There appears to be no noticeable difference between the Brefeldin A bound MAPK trajectories and the apo. The estimated mean Rg of the Brefeldin A bound MAPK is 20.09±0.48Å, while that of the apo is 20.02±0.42 Å. In the case of PrCK1, a wide margin of gap was noticed between the Rg of the Brefeldin bound PrCK1 and apo. This indicates that the binding of Brefeldin induced a structurally less compact conformation, which was translated

into a high Rg value relative to the apo. The estimated mean Rg of Brefeldin bound PrCK1 is 18.06±1.15Å, and that of the apo is 12.42±0.09 Å.

The mobility pattern obtained for Brefeldin A bound MAPK did not show a clear case of mobility difference, though the Brefeldin A bound MAPK exhibited Rg pattern higher than that of the apo. In the case of Brefeldin A bound PrKC1, there is a clear difference in mobility between the Brefeldin A bound PrCK1 and the apo, indicating inactivity.

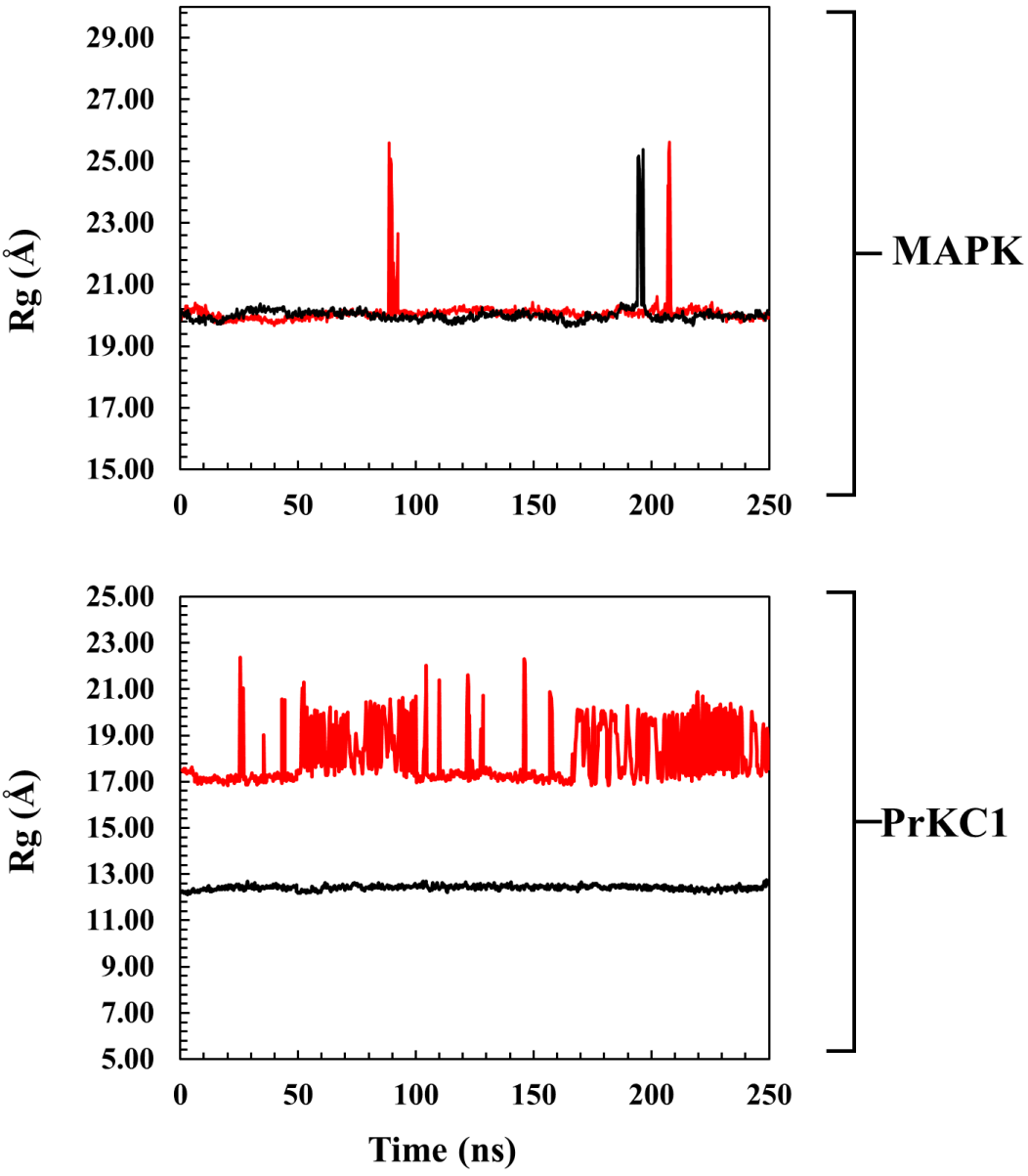


Figure 3.7. Rg plots of the interaction between Brefeldin A with MAPK and PrKC1. Rg plot of the global structure of MAPK and PrKC1 with their corresponding apo systems. The Rg plots show the global structure of the proteins compared to the protein interaction with Brefeldin A

3.4.2. Estimation of relative Tunicamycin binding dynamics concerning TK1 and PKC and Brefeldin A with MAPK and PrKC1

The conformational behaviour of Tunicamycin C and Brefeldin A at the binding pockets of TK1, PKC, MARP, and PrCK1 were extensively analysed here. For Tunicamycin C, the ligand RMSD plot (Figure 3.8) showed that both systems maintained a relatively flat trajectory after reaching equilibrium around 20ns. Around the 140ns mark of the MD simulation, a fluctuation occurred in both systems, but they stabilized once again towards the end of the MD simulation. Other ligand parameters, such as MSA and SASA, have also been studied.

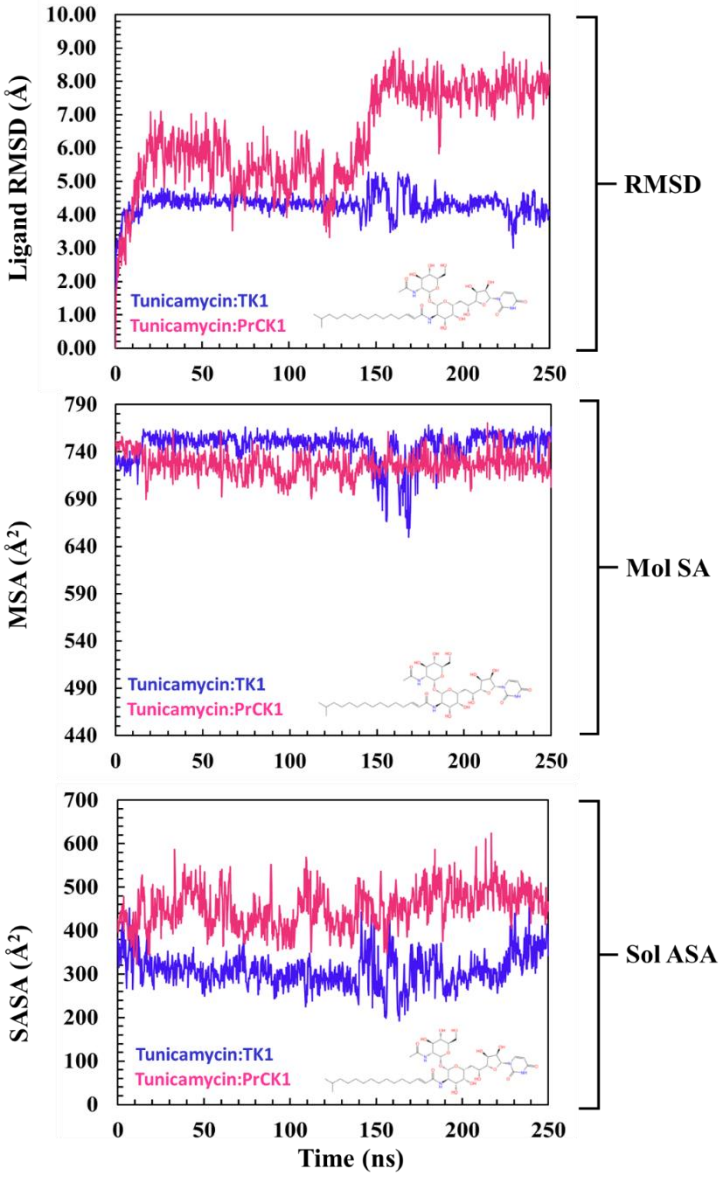


Figure 3.8 A descriptive indication of Tunicamycin performance during the MD timeline. This provides an idea of the ligand's interaction and stabilization pattern.

For Brefeldin A, the ligand RMSD plot (Figure 3.9) shows that Brefeldin A bound quite stably at the respective pockets of MARP and PrCK1, exhibiting a consistent horizontal dynamic from the beginning to the end of the MD simulation. However, a noticeable flip in the trajectory of PrCK1 occurred from 210ns to 230ns of the MD simulation before returning to its initial trajectory pattern. The estimated mean ligand RMSD for MAPK is 3.69±0.43Å, while that of PrCK1 is 6.52±2.04Å.

The Molecular Surface Area (MSA) plot shows that Brefeldin A consistently maintained a similar interaction pattern with MARP and PrCK1 throughout the MD simulation (Figure 3.9). Molecular Surface Area is a quantitative method of calculating the level of interaction established between the ligand and the protein molecular environment. The higher the MSA, the more stable the system is. In this case, the two trajectories for the binding of Brefeldin A to MARP and PrCK1 are quite similar but with high Å2, suggesting that Brefeldin A established an adequate level of interaction, which could result in functional activity or inactivity. The estimated mean MSA of Brefeldin A bound MAPK is 272.56±1.79Å2, while that of the Brefeldin A bound PrCK1 is 272.59±1.93Å2 (Figure 3.9).

The SASA plot shares similarities in trajectory patterns with the ligand RMSD plot. It quantitatively describes the binding dynamics of Brefeldin A in the hydrophobic core of MARP and PrCK1. The trajectory maintained a seemingly horizontal trajectory from the beginning of the MD simulation down to the end. However, a sudden flip occurred between 210 ns to 230 ns of the MD simulation before the trajectory stabilized (Figure 3.9).

For Tunicamycin C, the superposed images in Figure 3.10 show that the orientation of Tunicamycin C in complex with PrKC1 maintained a seemingly steady configuration during the 250ns MD simulation. This observation supports the explanation given to the ligand RMSD plot. The exact figure also shows that Tunicamycin C bound to TK1 established an excellent interaction, resulting in a consistent conformational orientation of Tunicamycin C throughout the 250 ns of the MD simulation.

For Brefeldin A, the 3D presentation in Figure 3.11 shows that the structural packing of Brefeldin A and its conformational configuration remained similar in both MARP and PrCK1 throughout the 250 ns MD simulation. This observation suggests that Brefeldin A maintains a stable interaction with both proteins throughout the simulation.

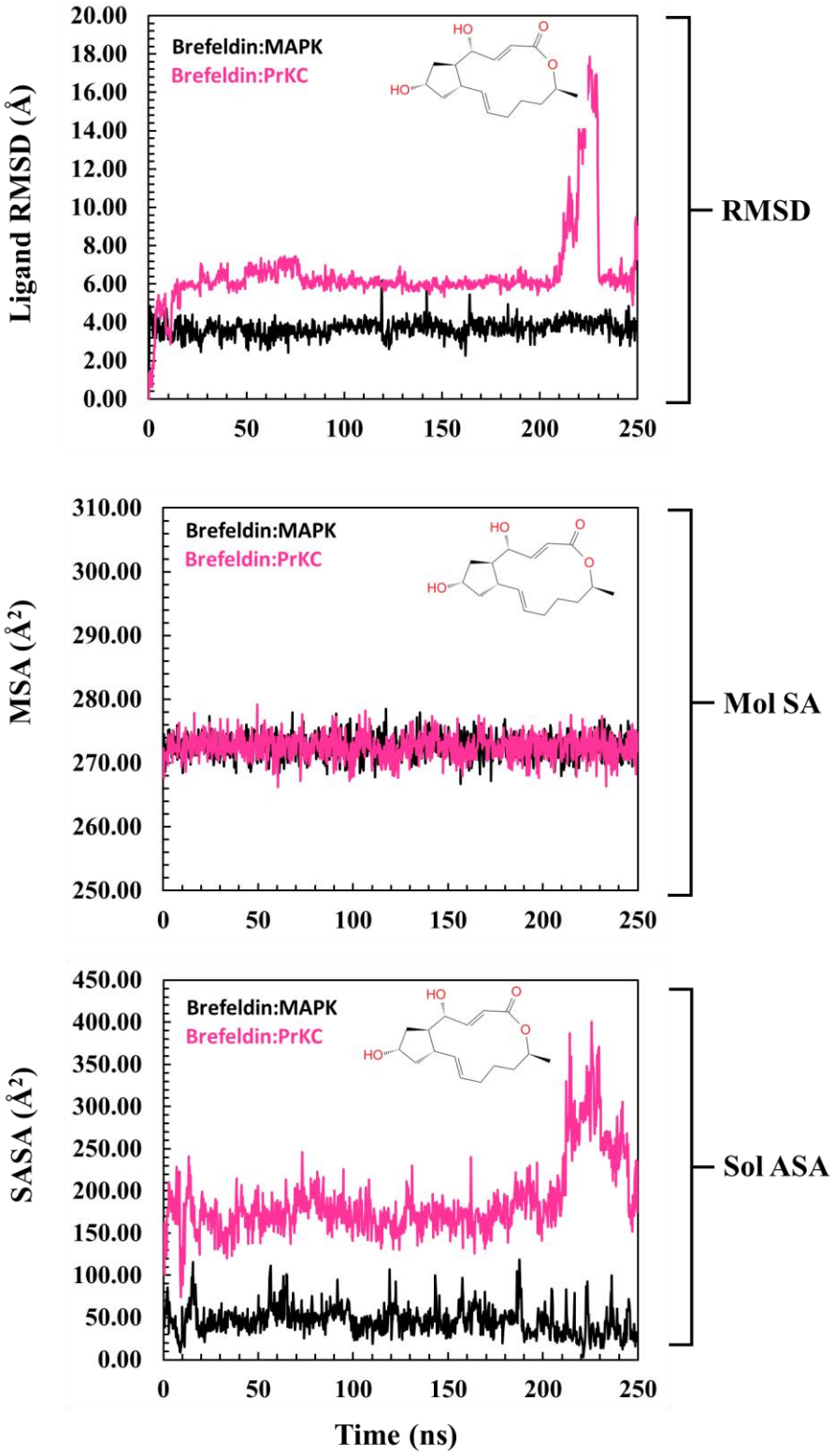


Figure 3.9 A descriptive representation of Brefeldin A properties during the MD timeline. This provides information on the ligand's interaction and stabilization pattern.

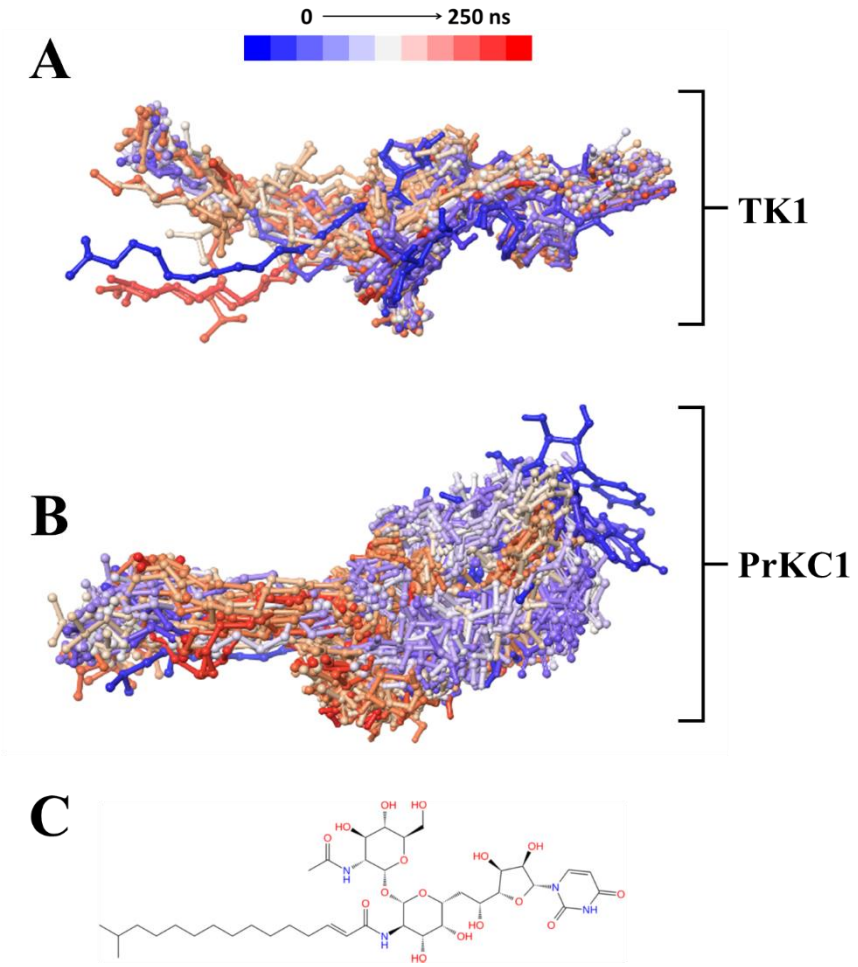


Figure 3.10 A time-based structural presentation of ligand conformation and orientation during the MD simulation. This figure shows the conformational changes that are predicted to occur in Tunicamycin C during the 250 ns interaction with the two protein targets (A) The conformational changes that take place in Tunicamycin C during its binding to TK1 (B) The conformational changes that take place in Tunicamycin C during its binding to PrKC1. The different colours represent the different times of the conformational changes as shown by the key above (C) Representation of the structure of Tunicamycin C.

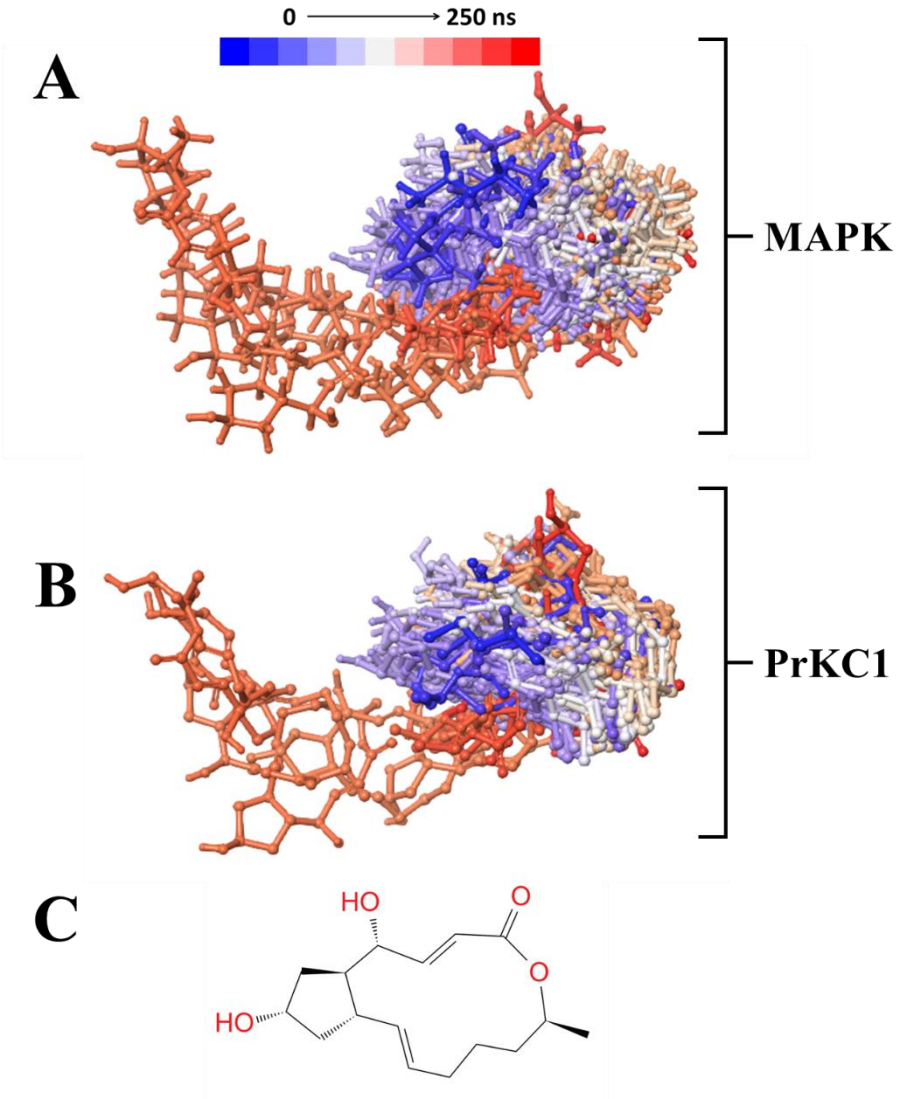


Figure 3.11 Time-based illustration of MAPK and PrCK1 structural orientation during the MD simulation. This figure shows the conformational changes that are predicted to occur in Brefeldin A during the 250ns interaction with the two protein targets (A) The conformational changes that take place in Brefeldin A during its binding to MAPK (B) The conformational changes that take place in Brefeldin A during its binding to PrKC1. The different colours represent the different times of the conformational changes as shown by the key above (C) Representation of the structure of Brefeldin A.

3.4.3. System-based visualization of ligand interaction

The 2D interaction diagrams of Tunicamycin C and Brefeldin A with their respective protein targets provide a comparative view of their interaction patterns in both docking conformation and during the MD simulation.

For Tunicamycin C, the interaction diagram (Figure 3.12) shows a comparative analysis of the interaction patterns of Tunicamycin C with TK1 and PrKC1. Figures 3.12 A & C represent the docking conformation, while Figures 3.12 B & D represent the conformation during the MD run. These diagrams provide insights into the role of bulk water in promoting adequate

interaction of Tunicamycin C with TK1 and PrKC1, presenting its implicit physiological condition.

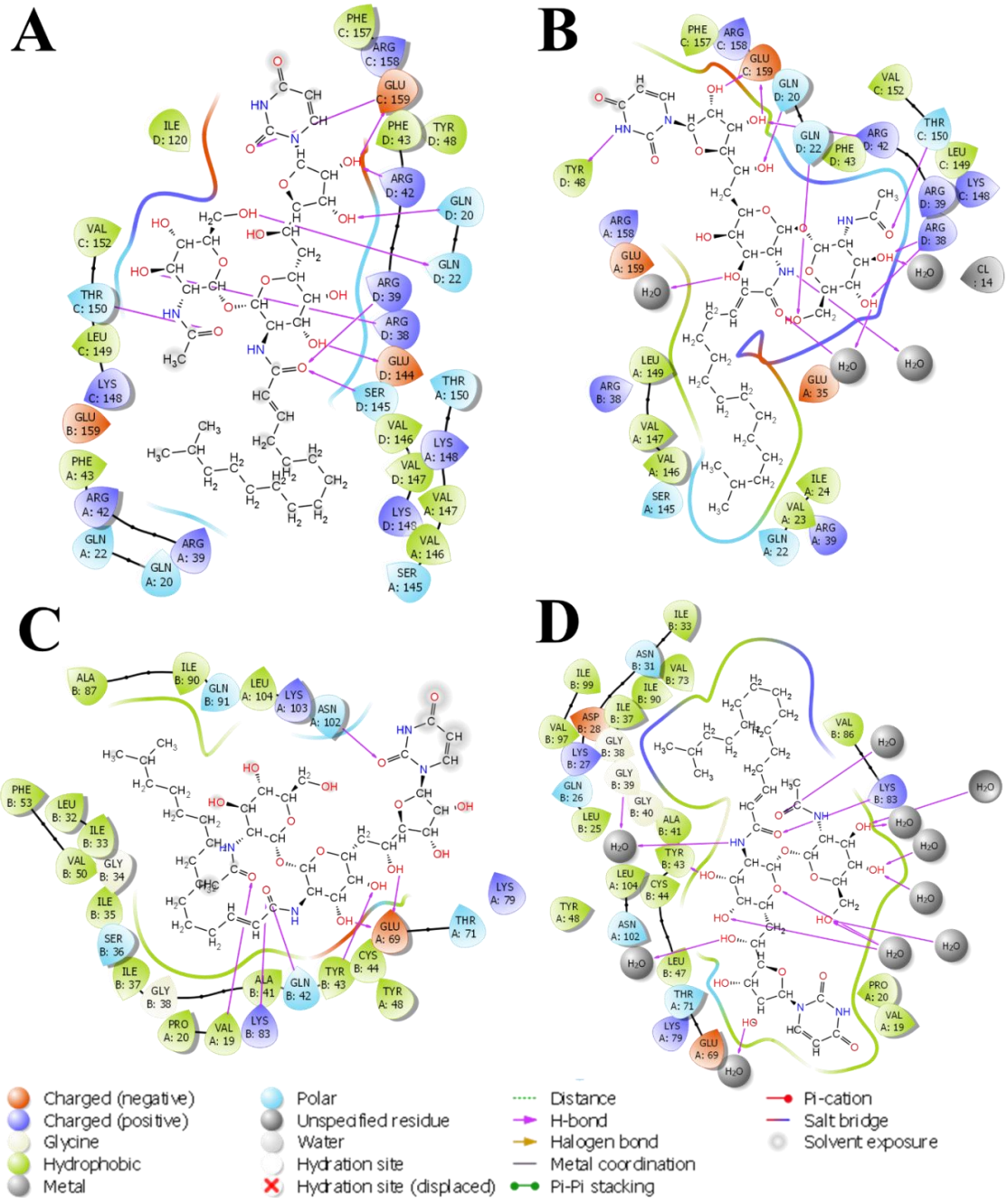


Figure 3. 12 2D interaction representation of Tunicamycin TK1 and PrKC1 complexes. This figure shows the difference between the docking and MD complex environments. A & C depict the complex docking environment, while B& D is the MD environment, which gives an idea of the role of bulk, which depicts a typical physiological environment for better binding interaction stabilization.

For Brefeldin A, a comparative 2D interaction diagram of its binding with MARP/PrCK1 is presented in Figure 3.13. The diagrams in Figure 3.13 B and D represent Brefeldin A in complex with MARP/PrCK1 in a solvent medium (MD simulation), while the diagrams in Figure 3.13A and C represent the same in a non-solvent medium (docking). These diagrams provide a comparative view of the interaction patterns of Brefeldin A with MARP/PrCK1 in different mediums.

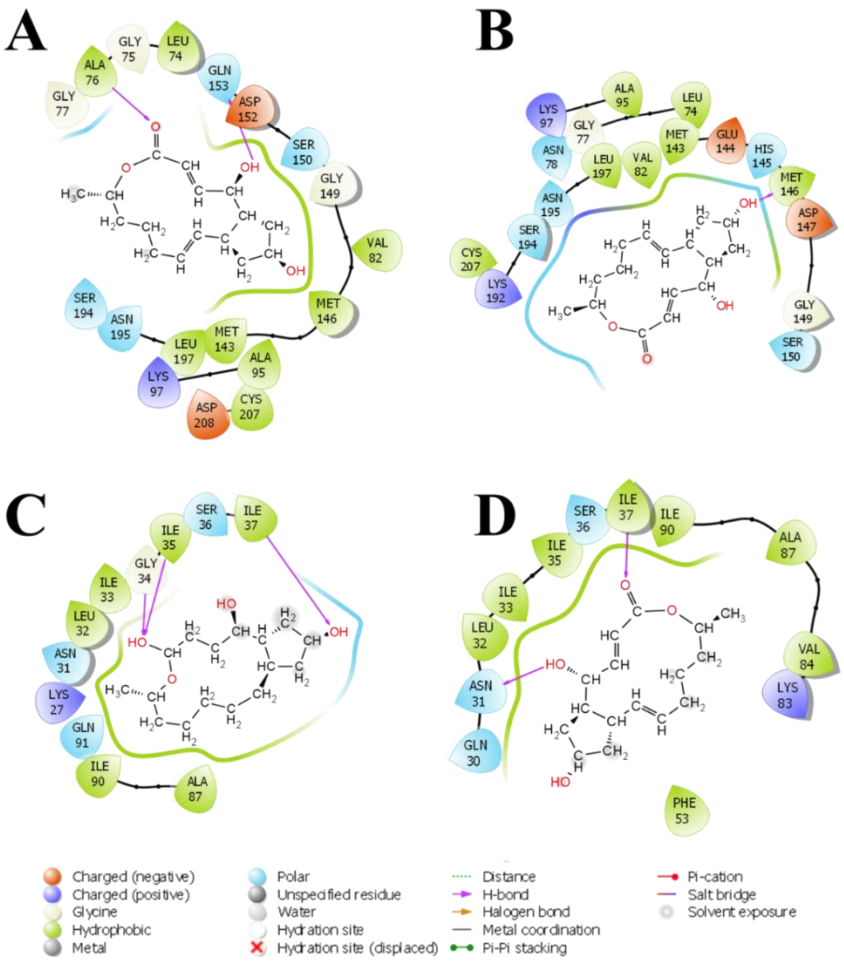


Figure 3.13 2D interaction representation of Brefeldin A MAPK and PrKC1 complexes. This figure shows the difference between the docking and MD complex environment. A and C depict the docking complex environment, while B and D is the MD environment, which gives an idea of the role of bulk, which depicts a typical physiological environment for better binding interaction stabilization.

The interaction of Tunicamycin C and Brefeldin A with their respective protein targets was further analysed to understand the most prominent active site residues that played a critical role in binding stabilization. For Tunicamycin C, the average structural outcome of the complexes during the 250 ns of the MD simulation was analysed by analysing the average PDB. This step

(Figure 3.14) was taken to assess the most prominent active site residues that played a critical role in the binding stabilization of Tunicamycin C at the pockets of TK1 and PrKC1.

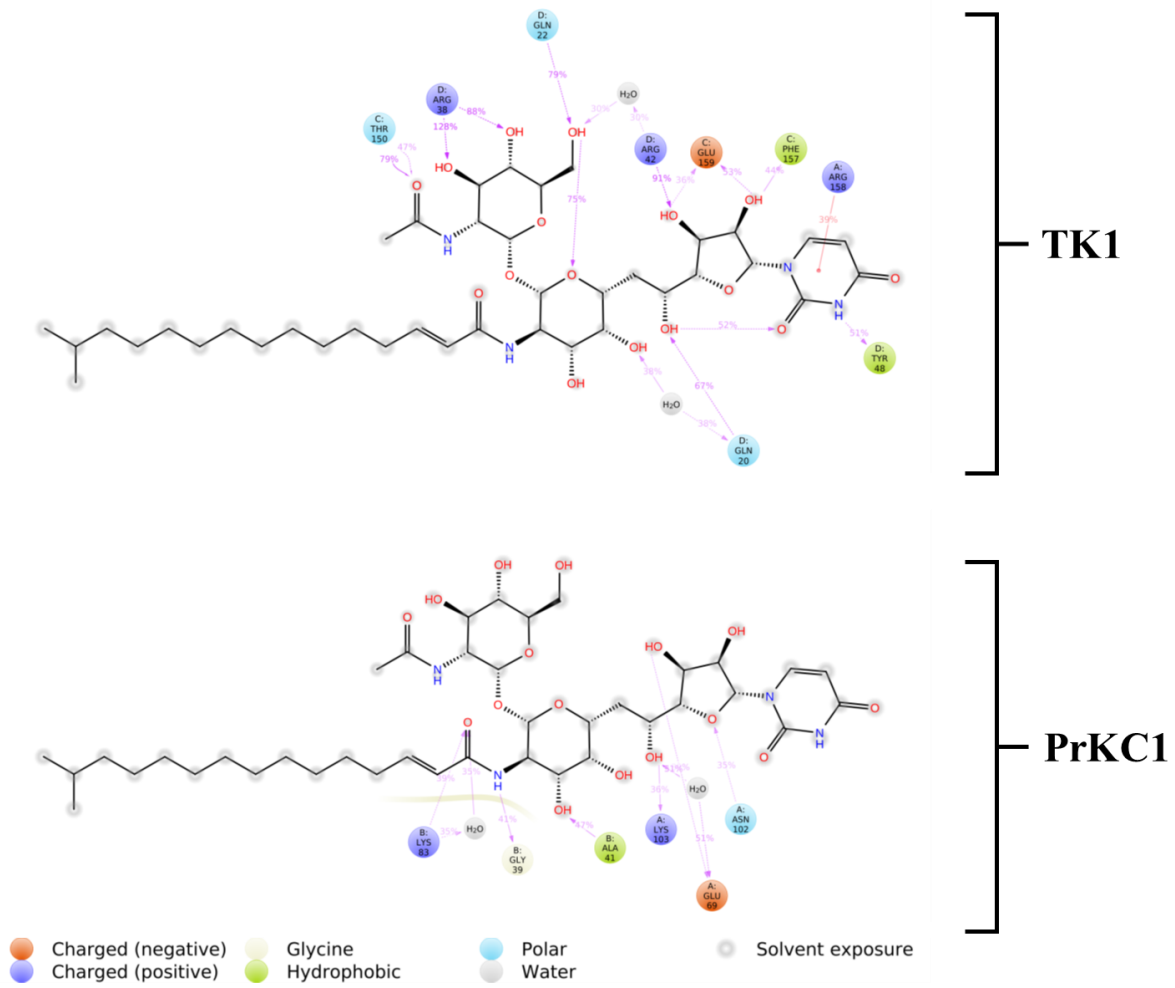


Figure 3.14. 2D representation of Tunicamycin C and TK1/PrCK1 interaction diagram for the average PDB. This figure shows the strongest, most dominant interaction between Tunicamycin C and the target proteins (A) TK1 and (B) PrKC1. It illustrates the different interactions between the Tunicamycin C molecule and the residues of the protein.

For Brefeldin A, the results suggest that bulk water in the MD simulation medium might not have contributed significantly to the dynamics and binding stabilization of Brefeldin A MARP/PrCK1 complexes. The binding and interactions might be produced by other factors that promote molecular recognition and binding interaction.

The average PDB was analysed, which expresses the precise summary of the conformational interaction state assumed by the Brefeldin A complexes (Figure 3.15). The produced hydrogen bond interaction was used as a parameter to predict crucial active site residues necessary for the binding stabilization and molecular recognition of Brefeldin A. For Brefeldin A bound to MAPK, Leu74, and Met146 played prominent roles in the binding stabilization of Brefeldin A,

with average PDBs of 40% for Leu74 and 30% for Met146. The presence of bulk water (H_2O), making a 40% linkage between Leu74 and OH of Brefeldin A, was also noted. For Brefeldin A bound to PrCK1, Gln30, Asn31, Gly34, Ile35, and Ile37 produced average PDBs of 40%, 68%, 61%, 62%, and 77%, respectively, contributing to the binding stabilization of Brefeldin A on MARP/PrCK1. The presence of bulk water contributing 61% and 62% to interactions with Gly34 and Ile34 was also noted.

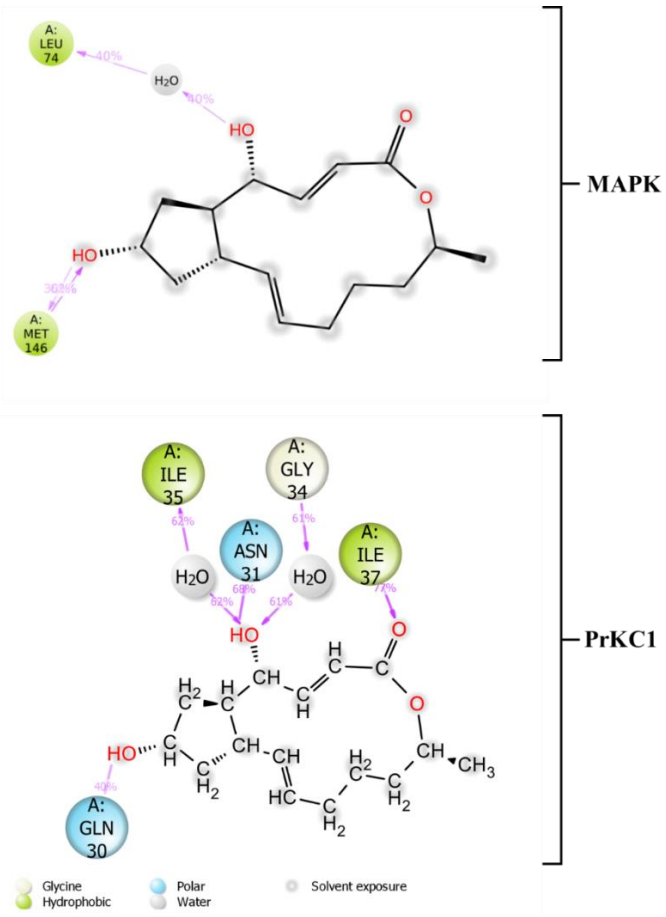


Figure 3.15 2D interaction diagram for the average PDB. This diagram indicates the most dominant contributing residues to the binding stabilization of Brefeldin A**.**

3.4.4. Quantitative estimation of implicit interaction contributors

The binding interactions stabilizing Tunicamycin C and Brefeldin A were evaluated using stacked bar charts (Figures 3.16 and 3.17, respectively).

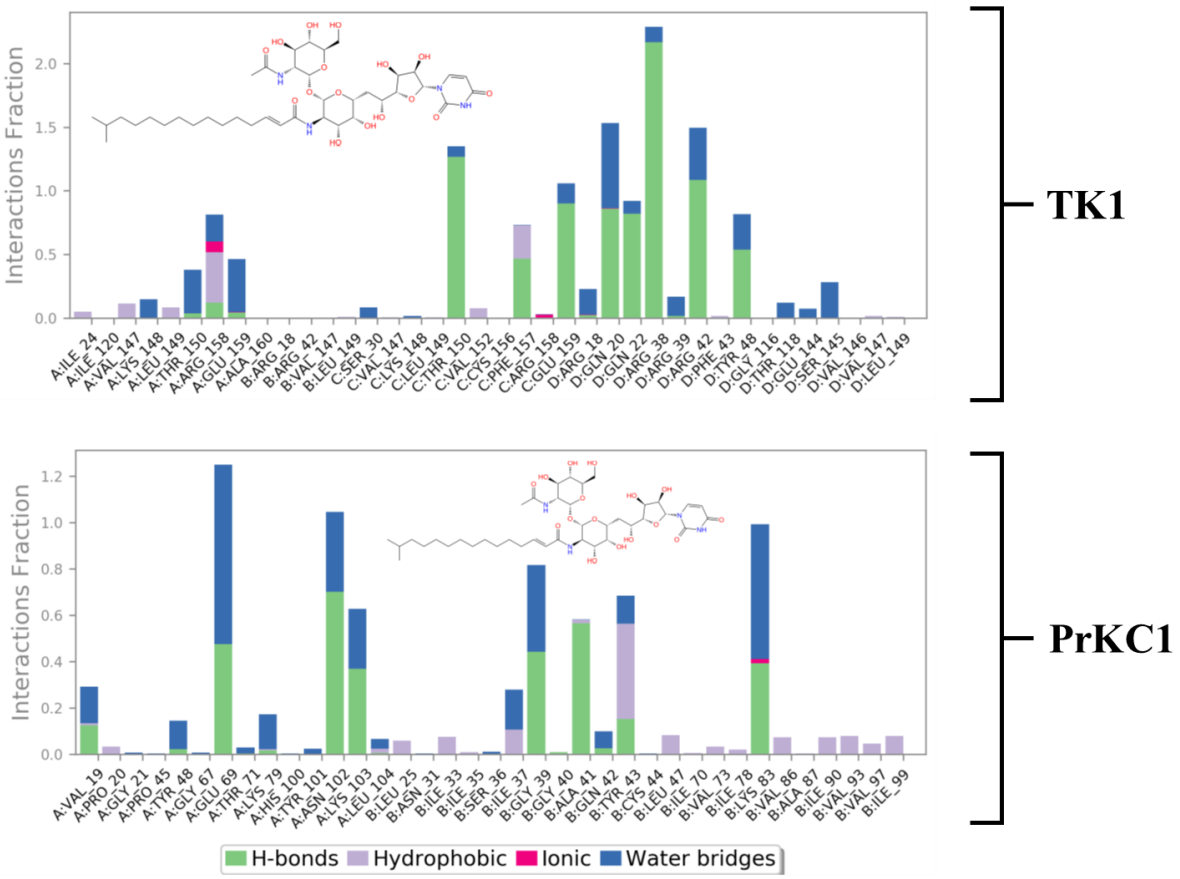


Figure 3.16 Stacked bar charts of side chain interactions and interaction types between tunicamycin and TK1/PrCK1 systems. H-bond is categorised into backbone acceptor; backbone donor; side-chain acceptor; and side-chain donor. Hydrophobic interactions are categorised into p-cation; p-p*, and non-specific interactions.

For Tunicamycin C, the estimation of the most predominant types of binding interaction stabilizing the compound were hydrogen bonds for TK1 and water bridges and hydrogen bonds for PrKC1 as presented in Figure 3.14. For Brefeldin A, the stacked bar chart (Figure 3.16) indicates that water bridge, van der Waals, and H-bond interactions established the binding contacts and complex stabilisation.

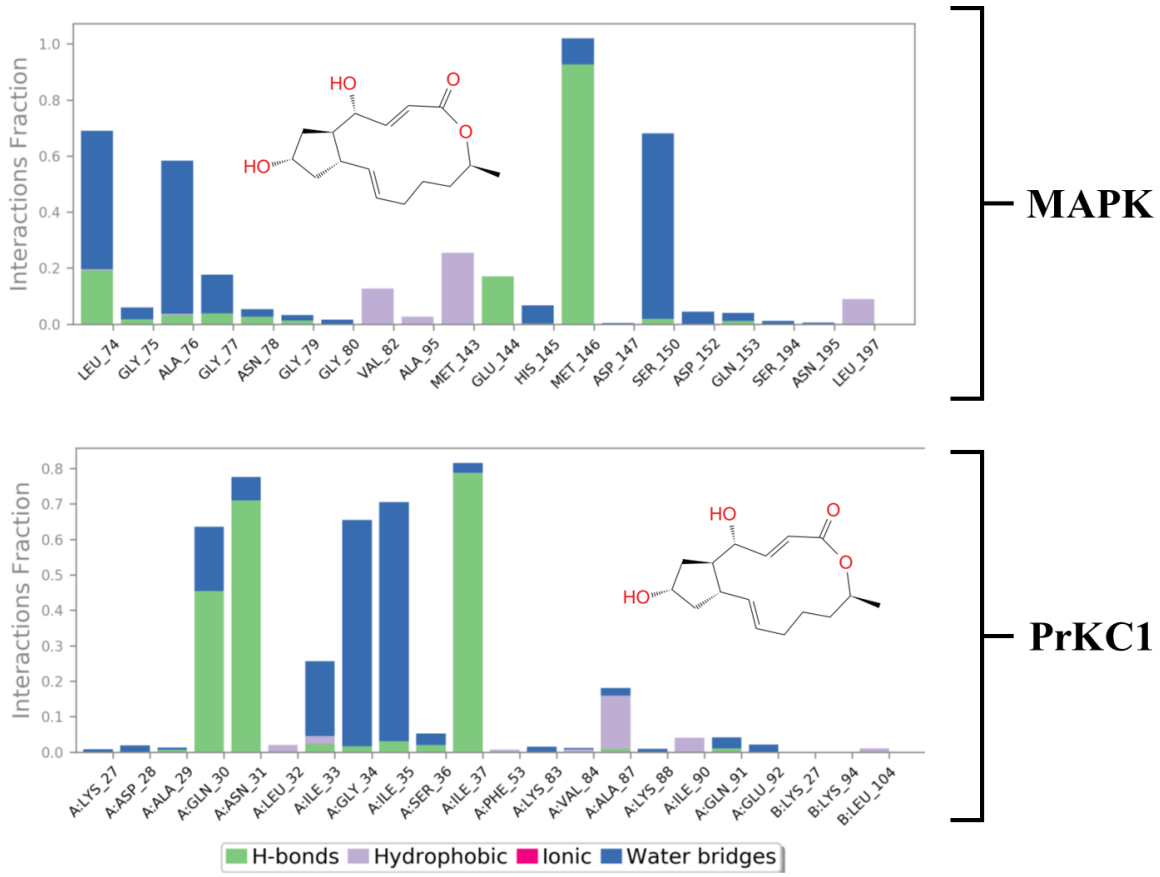


Figure 3.17 Stacked bar charts of side chains interactions and interaction types between Brefeldin A and MAPK/PrCK1 systems. H-bonds are categorised into backbone acceptor; backbone donor; side-chain acceptor; side-chain donor. Hydrophobic interactions are categorised into p-cation; p-p*; and non-specific interactions.

The conformational events leading to the observed structural dynamics of Tunicamycin C and Brefeldin A were explored using different quantitative approaches (Figures 3.16 and 3.17 respectively). These figures indicate that the binding contacts and complex stabilization was established by water bridge, van der Waals and H-bond. In TK1 Glutamine 22 has the highest number of interactions and most of these interactions are due to H bonds as are the majority of the interactions between Tunicamycin C and Leucine 149. In PrKC many of the interactions between the protein residues and Tunicamycin C are due to water bridges with the number of interactions between the most involved residues such as glycine 69 being equally split between water bridges and H bonds. There are fewer residues actively involved in the interactions between Brefeldin A and both MAPK and PrKC with water bridges and H bonds being the most prevalent in the residues with the highest number of interactions.

For Tunicamycin C, further investigation was conducted on nature and types of forces that provided the interactions leading to the binding stabilization of Tunicamycin on TK1 and PrKC1 (Figure 3.18). These stacked bar charts confirmed the previous estimates of the most predominant types of binding interaction stabilizing Tunicamycins interactions with the two protein targets. The figure revealed that the water bridge, van der Waals and H-bond interactions predominantly established the contacts between the ligands and the active site residues.

For Brefeldin A, the quantitative analysis (Figure 3.19) revealed the electrostatic energy contribution to the total energy for binding stabilization. In the case of Brefeldin A binding to MAPK, this contribution was established by Ala76, Gly77, Asn78, Lys97, Asp162, and Asp208. When considering the binding of Brefeldin A to PrCK1, the plot shows that Asp31, Leu32, Ile33, Gly34, Ser36, Ile37, and Lys83 were the key contributors. Quantitative analysis of the binding interactions and dynamics in Figure 3.19 revealed the electrostatic energy contribution to the total energy for the binding stabilization to have been established by Ala76, Gly77, Asn78, Lys97, Asp162, Asp208 in the case of brefeldin A binding to MAPK. On the other hand, when considering the binding of brefeldin A to PrCK1, the plot shows that Asp31, Leu32, Ile33, Gly34, Ser36, Ile37 and Lys83. It can hence be inferred that the roles played by the identified parameters contributed immensely to the binding stabilization of brefeldin A to MARP/PrCK1.

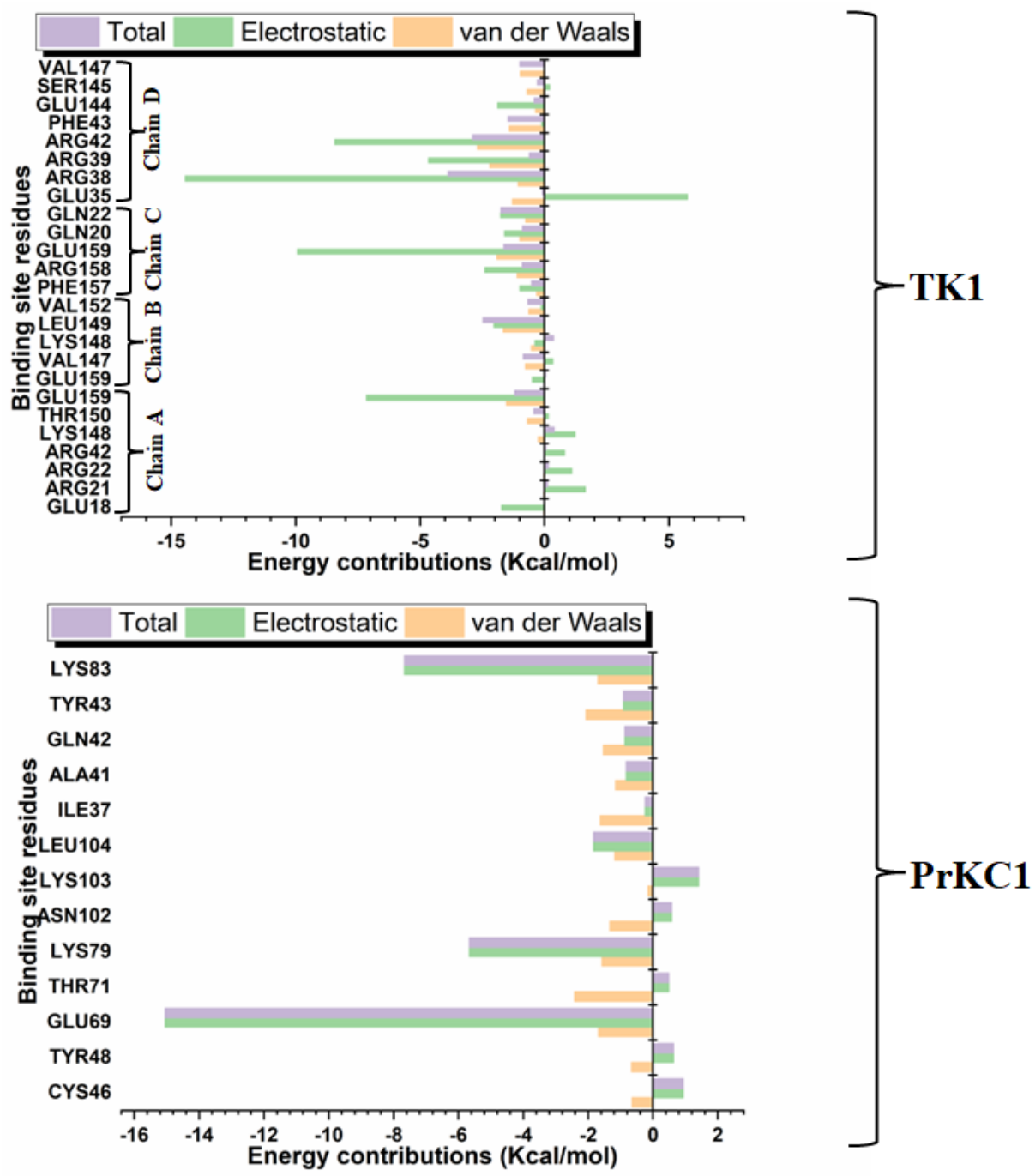


Figure 3.18 Per-residue energy decomposition for the interaction between Tunicamycin C and TK1/PrCK1 systems

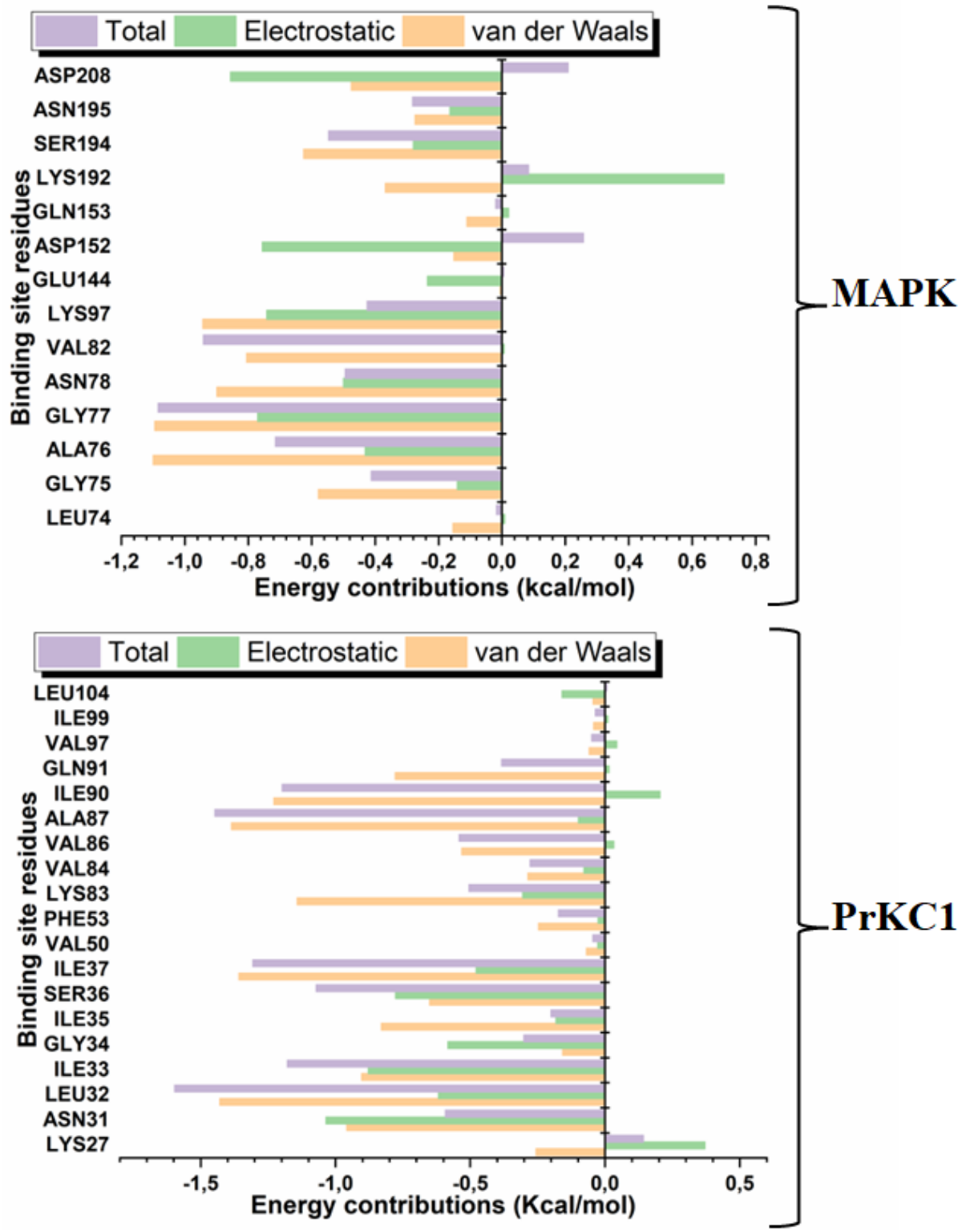


Figure 3.19. The per-residue energy contribution of MAPK and PrCK1 to the binding of Brefeldin A.

3.4.5. Quantification of thermodynamic evaluation of binding affinity

The binding free energy provides insight into the MD simulation timeline's silent interactions and dynamic trends. For Tunicamycin C, the MMDBSA method was employed to gain insight into the binding affinity of Tunicamycin to TK1 and PrKC1. Table 3.6 shows that the estimated ΔG_{bind} for the binding of Tunicamycin C to TK1 is -60.21±9.46 kcal/mol, while that of PrCK1 is -50.37±8.38 kcal/mol.

Table 3.6 Estimated binding energy predictions of Tunicamycin C complexes.

Compounds	Energy components (kcal/mol)				
	ΔE_{vdw}	ΔE_{ele}	ΔG_{gas}	ΔG_{sol}	ΔG_{bind}
TK1_Tunicamycin	-69.13±4.25	-70.08±15.05	-139.20±14.67	78.99±9.96	-60.21±9.46
PrKC1_Tunicamycin	-62.01±6.41	-80.23±13.04	-142.24±13.86	91.87±9.89	-50.37±8.38

For Brefeldin A, the MMGBSA method was also used to investigate the free energy of binding of Brefeldin A to MARP/PrCK1, as tabulated in Table 3.7. This analysis provides an understanding of the favourability of the binding interactions of Brefeldin A to MAPK/PrCK1. The table shows that the estimated ΔG_{bind} for the binding of Brefeldin A to MAPK is –22.18±4.50 kcal/mol, while that of PrCK1 is –23.9±5.36 kcal/mol.

Table 3.7 Estimated binding energy predictions of Brefeldin A complexes.

Compounds	**Energy components (kcal/mol)**				
	ΔE_{vdw}	ΔE_{ele}	ΔG_{gas}	ΔG_{sol}	ΔG_{bind}
MAPK _ Brefeldin A	-28.23±3.24	-11.91±7.52	-40.14±9.14	17.97±5.65	-22.18±4.50
PrKC1_Brefeldin A	-27.44±3.89	-6.31±8.66	-33.75±10.19	9.81±5.82	-23.9±5.36

This shows that Brefeldin A interacted with both protein targets with a nearly identical binding energy. This interaction was much weaker than that seen for the interaction between Tunicamycin with TK1 and PrKC. Therefore, the highest binding energy is the most favourable interaction between Tunicamycin C and TK1. Tunicamycin also interacts more strongly with PrKC than Brefeldin A. This is reflected in the other energy components with stronger Van Der Waals forces and electrostatic interactions observed with Tunicamycin Cs interactions with TK1 and PrKC.

Chapter 4: Discussion

4.1. Drugs targeting glycosylation

Several glycosylation inhibitors, such as Swainsonine, Brefeldin A, Mannostatin A, Castanospermine, and Tunicamycin C, were selected for this study (Table 3.1). The inhibitors were screened using an HTS system to assess their probable docking scores with several human proteins. Docking score measures the binding affinity between a small molecule (like a drug) and a target protein. A higher docking score generally indicates a stronger or more favourable interaction. Tunicamycin C and Brefeldin A were selected for further evaluation due to their high number of target proteins at both docking score thresholds. Therefore, this suggests that these compounds have a broad range of potential targets and could have wide-ranging effects on cellular processes. Tunicamycin C interacted with 251 target proteins at a minimum docking score of 6 and 168 target proteins at a minimum docking score of 7 (Table 3.1). This indicates that Tunicamycin C has a relatively high binding affinity for many proteins.

Brefeldin A interacted with an even more significant number of target proteins: 449 at a minimum docking score of 6 and 234 at a minimum docking score of 7 (Table 3.1). Therefore, this suggests that Brefeldin A may have a broader range of potential targets than Tunicamycin C. The selection of these two compounds for further study was also influenced by other factors, such as their known biological activities, availability, or chemical properties. For example, both Tunicamycin C and Brefeldin A are known to inhibit protein glycosylation, which is crucial for protein function and cellular homeostasis. Tunicamycin (Figure 3.1) is an antibiotic derived from Streptomyces clavuligerus and Streptomyces lysosuperficus bacteria, among other species, and has been intriguing to scientists for its complex biosynthetic pathway. However, despite the extensive knowledge of its physical properties, there remains a significant lack of information concerning tunicamycin's pharmacodynamics, absorption, protein binding, metabolism, toxicity, affected organisms, and its effects in human clinical trials (Dawood and Altobje, 2020).

In molecular terms, Tunicamycin, as depicted in Figure 3.1, is an analogue of UDP-N-acetylglucosamine. Tunicamycin interferes with the formation of dolichol pyrophosphate-acetylglucosamine, which is crucial for the N-glycosidic linkage of core oligosaccharides to asparagine residues on glycoproteins (Price and Tsvetanova, 2007). The bacteria synthesize Tunicamycin utilizes enzymes in the tun gene cluster (TunA-N). This antibiotic might disrupt the glycosylation of various cellular glycoproteins, such as fetuin, corneal proteoglycan,

thyroglobulin, and immunoglobulins, which contain asparagine-linked and serine or threonine-linked oligosaccharides. Moreover, tunicamycin can cause endoplasmic reticulum stress in cells by inhibiting the initial step in the biosynthesis of N-linked glycans in proteins, leading to an increase in misfolded proteins. When Tunicamycin obstructs N-glycans' glycosylation, it causes cell cycle arrest at the G1 phase in human cells (Dawood, 2023). Research has indicated the potential use of tunicamycin as a therapeutic drug against human colon or prostate cancer cells by inducing apoptosis (Cortez et al., 2024). Furthermore, it inhibits the glycosylation of the structural glycoproteins in several viruses, including alphaviruses, bunyaviruses, herpes viruses, myxoviruses, and all other viruses possessing glycoprotein envelopes It has been proposed that inhibiting N-glycosylation biosynthesis by Tunicamycin could provide an effective treatment strategy, potentially heightening the sensitivity of cancer cells to trastuzumab (Dawood and Altobje, 2020).

Brefeldin A (BFA) (Figure 3.1), a compound sourced from *Penicillium brefeldianum*, is recognized for hindering protein transportation from the endoplasmic reticulum (ER) to the Golgi apparatus. This inhibition occurs due to BFA's ability to prevent COP-I assembly, which influences protein glycosylation by barring nascent ER glycoproteins from reaching the glycosylation processes in the Golgi apparatus. Despite its potent blocking effect on protein secretion and the transportation of glycoproteins to the cell surface, the use of such inhibitors as BFA as global glycosylation inhibitors to investigate glycans' biological functions is limited. More selective pan-inhibitors of sialyltransferase and fucosyltransferase isoenzymes have been developed to tackle this challenge based on fluorinated sugar mimetics (Rillahan et al., 2012). These inhibitors offer the advantage of enabling a more specific deletion of glycan capping, thereby offering a more focused approach to studying the biological roles of glycans (Sørensen et al., 2023).

4.2. Potential glycosylation targets for Tunicamycin C

As reported in the present study Tunicamycin C and Brefeldin A both target PRKC1. Tunicamycin C also targets Thymidine kinase (TK) (Table 3.3), which plays a role in the salvage pathway of nucleotide synthesis (Xu et al., 2015). Thymidine kinase's primary function is to catalyse the phosphorylation of thymidine into thymidine monophosphate (TMP), which is then converted into thymidine triphosphate (TTP)—an essential precursor for DNA synthesis (Bitter et al., 2020). There are two types of thymidine kinase: thymidine kinase 1 (TK1), found in the cytoplasm, and thymidine kinase 2 (TK2), located in the mitochondria. TK1 and TK2

enzymes are important in cellular proliferation and DNA repair (Bitter et al., 2020). Elevated levels of TK1 have been linked to tumour development and progression. For example, CRC tissues have previously been shown to have increased levels of TK1, which is associated with a poor prognosis (Desterke et al., 2024). This elevation supports the hypothesis that TK might contribute to excessive DNA synthesis and replication necessary for rapid tumour cell growth (Hannigan et al., 1993).

4.3. Potential glycosylation targets for Brefeldin A

Three potential glycosylation targets identified for Brefeldin A are PKRCA, PPARG, and MAP2K1 (Table 3.3). These target proteins have crucial roles in various cellular processes and signalling pathways related to CRC and glycosylation. One of the proteins we identified as a Brefeldin A target is PRKCA, also known as Protein Kinase C Alpha. PRKCA belongs to the protein kinase C (PKC) family of serine/threonine kinases and regulates cell proliferation, differentiation, apoptosis, and migration (Black and Black, 2021).

Abnormal activation of PRKCA has been linked to enhanced cell proliferation and survival, as well as angiogenesis and resistance to apoptosis in multiple cancer types, including CRC (Rosenberg et al., 2018). Other proteins that Brefeldin A targets are PPARG or Peroxisome Proliferator Activated Receptor Gamma. PPARG functions as a transcription factor and a nuclear receptor that regulates gene expression in lipid metabolism, inflammation, and cell differentiation (Hu et al., 2023). Interestingly, PPARG can exhibit tumour-promoting and suppressive effects depending on the cellular context and specific ligands present (Kaur et al., 2019). The third protein target we identified is Mitogen-Activated Protein Kinase 1(MAP2K1), or MEK1. MAP2K1 is a dual specificity kinase because it phosphorylates and activates MAPK/ERK proteins in the MAPK signalling pathway. This pathway regulates cell proliferation, differentiation, survival, and migration (Guo et al., 2020). Dysregulation of MAPK signalling has been associated with the development and progression of CRC. As a result, heightened MAP2K1 activity promotes cell proliferation, survival, and resistance to apoptosis. Glycosylation processes may be indirectly affected by changes in MAPK signalling. MAPK potentially alters the glycosylation pattern of proteins and contributes to CRC progression (Lake et al., 2016).

4.4. Pathway Analysis for Tunicamycin C

The target protein for Tunicamycin C, PRKCA, is also involved in the downstream signalling cascade activated by the Ras protein in the Ras signalling pathway. Ras proteins are small GTPases that play a central role in regulating cell growth, differentiation, and survival in response to extracellular signals (Berthon et al., 2015). Upon activation by RTKs, Ras proteins can activate the Raf/MEK/ERK pathway (Table 3.4), the PI3K/Akt pathway, and the PLC/PKC pathway. PRKCA, as a member of the PKC family, is one of the critical effectors of the PLC/PKC pathway. Activation of PRKCA can lead to the phosphorylation and regulation of various target proteins involved in cellular processes, such as cell proliferation and migration, which can contribute to cancer development and progression (Song et al., 2023).

Another pathway that was identified is 'Proteoglycans in cancer,' The target protein, PRKCA, plays a role in regulating the functions of proteoglycans, which are complex macromolecules composed of core protein and glycosaminoglycan (GAG) side chains (Reily et al., 2019, Nakashima, 2002). Proteoglycans are essential components of the extracellular matrix (ECM) and are involved in various aspects of cell behaviour, such as adhesion, migration, and signalling. Dysregulation of proteoglycans can lead to cancer progression, invasion, and metastasis (Wight et al., 1992).

4.5. Molecular dynamic modelling for the interaction between Tunicamycin and the TK1 and PrKC1 target proteins

From Figure 3.4, apo systems exhibited subtle movement, whereas the tunicamycin-bound system was slightly stable relative to the apo. The estimated mean RMSD for the tunicamycin bound system is 3,20± 0.28Å whereas that of the apo is 3.27±0.35Å. A critical examination of this RMSD pattern suggests that the binding of this tunicamycin could not produce a marked reduction or increase in RMSD even when the binding reduced trajectory fluctuation, which could suggest favourable binding interaction. Having previously mentioned that high RMSD correlates with instability while low RMSD indicates stability, comparing the obtained results wherein the binding of tunicamycin produced neither a marked reduction nor an increase in RMSD, conclusions cannot be drawn. However, in evaluating the plot, the minor difference in conformational deviation does not adequately represent stability. However, it can be adjudged as structural instability, which correlates to functional inactivity. Thus, tunicamycin binding resulted in TK1 inactivity which could presumably halt cancer cell proliferation. The plots of the RMSF (Figure 3.2) depict a rigid fluctuation pattern in both cases of TK1 and PrKC1, considering the near similar trajectory pattern between the tunicamycin bound systems (with

mean RMSF value of 1.10±0.77Å) and the apo (with mean RMSF value of 1.17±0.90Å). Comparing this to the result obtained for the RMSD plot, the binding of tunicamycin induced a structurally rigid system, which further indicates inhibition of TK1 activities. Progressing into the binding/dynamic landscape for the tunicamycin relative to PrKC1 (Figure 3.2), the inhibition proficiency of tunicamycin on PrKC1 concerning cancer cell proliferation is evident. The RMSD plot indicates that the tunicamycin binding produced a perturbation that induced a significant 3D structural deviation of the PrKC1. This vast difference in the trajectory of the tunicamycin-bound PrKC1 is relative to the apo, wherein the tunicamycin-bound PKC exhibited higher RMSD, clearly indicates functional inactivity. It can, therefore, be deduced that the binding of tunicamycin resulted in a structural deviation, which could presumably lead to halting of cancer cell progression. The estimated mean RMSD of the tunicamycin-bound PrKC1 is 2.89±0.33 Å while that of the apo is 2.12±0.31 Å. On evaluating the trajectory of the RMSF plots of the PrKC1 and TK1, there is a similarity between these, where very little difference was obtained in the fluctuation patterns of tunicamycin bound TK1 and PrKC1, relative to their respective apos. Thus, similar to TK1, binding of tunicamycin induced residue rigidity, in PrKC1. This is reflected in the mean RMSF of tunicamycin bound PrKC1 is 1.25±0.84 Å while that of apo is 1.24±0.55 Å; indicating little variation. In summary, the binding of tunicamycin produced negative structural deviations, which could inhibit the activities of both proteins with the effect of halting cancer cell proliferation. This is corroborated in the cartoon and surface representations which demonstrate that tunicamycin is well aligned in the binding grooves of TK1 and PrKC1, to create the interactions resulting in the dynamics described here.

4.6. Molecular dynamic modelling for the interaction between Brefeldin A and MAPK and PrCK1 target proteins

Brefeldin A analysis provides important insights into the structural variations of protein structures during the 250 ns Molecular Dynamics (MD) simulations, where the Root Mean Square Deviation (RMSD) and Root Mean Square Fluctuation (RMSF) analyses were utilized to evaluate these changes (Figure 3.3). The RMSD analysis, as indicated by the plot in Figure 3.3, demonstrates that both the apo (unbound) and Brefeldin A-bound Mitogen-Activated Protein Kinase (MAPK) displayed similar trajectory patterns during the early phase of the MD simulation up to 50ns. Post this time point, the trajectories diverged with the Brefeldin A-bound MAPK trending upwards, while the apo moved slightly downwards. However, they both remained relatively steady from 75ns onwards till the end of the MD simulation. The Brefeldin

A-bound MAPK trajectory then trends downwards towards the apo trajectory. The estimated average RMSD values were 3.55±0.58Å for the Brefeldin A-bound MAPK and 2.88±0.31Å for the apo, indicating a degree of structural stability.
In observing PrCK1's conformation, the binding of Brefeldin A appears to increase the RMSD value, as indicated by an upward deviation from the apo trajectory. The estimated average RMSD was 2.70±0.40Å for Brefeldin A-bound PrCK1 and 2.12±0.13Å for the apo, suggesting that Brefeldin A binding possibly contributes to increased structural fluctuation. Interestingly, the binding pattern of Brefeldin A to both MAPK and PrCK1 shows that it binds in different pockets, suggesting its potential as a weak binder, leading to instability at one pocket and consequent binding at alternate sites. Further studies are needed to better elucidate this.

The RMSF plots show that the fluctuation patterns of Brefeldin A-bound MARP and PrKC1 are similar to their apo counterparts, indicating comparable structural dynamics between the bound and unbound states (Figure 3.5). The mean RMSF values for the bound MAPK and PrKC1 are 1.44±1.02Å and 1.47±0.80Å, respectively, while for the apoenzymes, they are 1.33±0.99Å and 1.24±0.55Å, respectively. These findings suggest that Brefeldin A binding has a discernible impact on the structural dynamics of these proteins, which could influence their biological functions. However, these preliminary observations need to be substantiated with more extensive studies.

Brefeldin A in contrast to Tunicamycin exhibited a different binding pattern when docked into Mitogen-Activated Protein Kinase (MAPK) and Protein Related C Kinase 1 (PrCK1). As illustrated in Figure 3.5, Brefeldin A intriguingly binds in different pockets, implying a certain degree of flexibility or adaptability in its binding behaviour. This variability may have significant repercussions for Brefeldin A's interaction dynamics and functional effects, potentially altering the protein's activity or regulation. However, these findings are preliminary, and it is essential to note that a complete understanding of the implications of this binding behaviour requires further investigation. Future research might include detailed computational modelling or experimental studies to elucidate the exact dynamics and consequences of these binding interactions. Such studies could provide valuable drug design and discovery information, particularly in developing glycosylation-targeted therapies.

4.7. Comparative evaluation of structural drift from their centre of mass

Tunicamycin C

Visual inspection of the Rg plot in Figure 3.6 shows the trajectory of both the Tunicamycin bound TK1 and the apo projects a similar trajectory trend. However, the tunicamycin-bound TK1 system appears to be exhibiting a lower trajectory trend towards the end of the MD simulation. The estimated mean Rg of the tunicamycin bound TK1 is 24.97±0.10Å while that of the apo is 25.00±0.13Å. The inference that can be drawn from both the plot and the mean Rg value is that the binding of tunicamycin could not induce much perturbation in the 3D structure of TK1. This could be the mechanism of action of TK1 as it can be noticed that the observed deviation of tunicamycin-bound TK1 did not reveal much structural difference relative to that of the apo. Moving forward to the estimate, the Rg of PrKC1 reveals trajectory patterns similar to those of TK1, wherein the binding of tunicamycin bound PrKC1 and the apo trail each with an Rg trajectory that cannot seemly be termed compactness. The mean Rg value of the tunicamycin bound PrKC1 is 12.27±0.08Å while that of the apo is 12.42±0.09Å. In most dynamic studies, the binding of ligands usually produces a trajectory pattern whereby the ligand-bound system exhibits lower RMSD and Rg, which are quite distinct from that of the apo; this indicates stability, which suggests functional activation. However, in our study, the ligand-bound systems exhibited a trajectory that trails that of the apos; it cannot readily be concluded as conformational stability but rather instability, which indicates inactivity. Thus, it can be inferred that the binding of the ligands induces a conformational variation that results in structural inactivity, producing inhibition of TK1 and PKC, which halts cancer cell proliferation.

The mean ligand RMSD of the tunicamycin/TK1 system is 4.31±0.35Å, and that of the tunicamycin/PrCK1 system is 6.32±1.44Å. However, looking at the trajectory of tunicamycin bound PrCK1, the fluctuation was more significant; this could presumably be due to the reorientation of the large tunicamycin molecule to conform to the correctly initially reported conformational fitness/orientation at the pocket of PrKC1 which has a smaller 3D structure relative to TK1 (Figure 3.6). Figure 3.6 shows that the pharmacophoric region of tunicamycin maintained similarity in orientation. As depicted in Figure 3.6, the higher ligand RMSD of the PrKC1 relative to TK1 suggests a higher inactivity performance in PrKC1 than TK1. This drift of TK1 and PKC at this 140 ns of the MD run could be a product of the internal dynamics of the systems, though this is beyond the scope of this study.

Brefeldin A

For Brefeldin A-bound Mitogen-Activated Protein Kinase (MAPK), the Rg plot (Figure 3.7) reveals a trajectory pattern akin to the Root Mean Square Fluctuation (RMSF) plot. Interestingly, there seems to be no substantial difference between the trajectories of Brefeldin A-bound MAPK and the unbound (apo) state. The estimated mean Rg values of 20.09±0.48Å for the Brefeldin A-bound MAPK and 20.02±0.42Å for the apo state suggest minor variations, pointing towards similar compactness in both states. In contrast, Protein Related C Kinase 1 (PrCK1) displays a significant gap between the Rg of the Brefeldin A-bound and apo states. This difference suggests that Brefeldin A binding provokes a less compact conformation in PrCK1, resulting in a higher Rg value. The estimated mean Rg of the Brefeldin A-bound PrCK1 is 18.06±1.15Å, considerably more extensive than that of the apo state at 12.42±0.09Å. Regarding protein mobility, the Brefeldin A-bound MAPK does not show a significant mobility difference compared to the apo state, although a slightly higher Rg pattern is observed in the Brefeldin A-bound state. However, for PrCK1, there is a clear difference in mobility between the Brefeldin A-bound state and the apo state, suggesting a potential loss of activity upon binding to Brefeldin A.

4.8. Estimation of relative Tunicamycin C binding dynamics concerning TK1 and PKC and Brefeldin A with MAPK and PrKC1

The MSA plot in Figure 3.8 portrays a similar trajectory trend in both cases of tunicamycin bound TK1 and PrKC1 with mean MSA of 746±16Å^2 for and 726±12Å^2 for PrCK1. The plot shows that the overall dynamics of the polar surface of the ligand remained constant across the two proteins throughout molecular dynamics simulation. The obtained MSA could suggest an adequately established hydrophobic interaction promoting ligand binding.

The SASA result in Figure 3.8 reveals that the surface exposure of atoms in TK1 bound tunicamycin was immensely lowered (mean SASA 310±39 Å^2) relative to that of PrKC1 (mean SASA 454±45 Å^2) across the MD simulation time. The results obtained for ligand RMSD and SASA suggest that tunicamycin is a better binder with PRKC1 than TK1. The SASA indicates and equally reveals hydrophobic interaction and hydrophobicity, which promotes ligand interactions. The plots show that the trajectory of the SASA plots of the binding of tunicamycin to TK1 and PrKC1 maintained a presumably steady type of motion throughout the MD simulation time. It did not exhibit a wide flip in trajectory, which suggests that there was no

time when the ligands tried to move out of the pockets, which interpreted the obtained steady configurational orientation shown in Figure 3.10 for the ligands, which depicts ligand stability at the pocket. The trajectory of this plot indicates that the buried surface-exposed moieties of tunicamycin were transitioned to the hydrophobic core in TK1 but not in PrKC1. This effectively promotes the interaction of tunicamycin, and this trajectory remained constant at the timeline of the MD simulation. This suggests steadily sustained ligand binding interaction at the pockets of TK1 rather than PrKC1.

The analysis of Brefeldin A binding in terms of Ligand Root Mean Square Deviation (RMSD), Molecular Surface Area (MSA), and Solvent Accessible Surface Area (SASA) offers valuable insights into the nature of ligand-protein interactions. From the Ligand RMSD plot (Figure 3.9), it can be inferred that Brefeldin A binds stably in the respective pockets of Mitogen-Activated Protein Kinase (MAPK) and Protein Related C Kinase 1 (PrCK1). The RMSD trajectories remained horizontally throughout the Molecular Dynamics (MD) simulation, indicative of stable binding. However, before reverting to its initial pattern, an unexpected fluctuation in the PrCK1 trajectory between 210ns and 230ns hints at a temporary shift in Brefeldin A's position. The estimated mean ligand RMSD for MAPK is 3.69±0.43 Å, and for PrCK1, it is 6.52±2.04 Å, denoting more significant positional fluctuation in PrCK1.

The MSA plot (Figure 3.9) reveals that Brefeldin A maintains consistent interactions with MAPK and PrCK1 throughout the simulation. The MSA quantifies the degree of interaction between the ligand and the protein's molecular environment, with a higher MSA indicating a more stable system. The trajectories for Brefeldin A binding to both MAPK and PrCK1 are similar with high $Å^2$ values, suggesting substantial interaction, which could influence functional activity or inactivity. The mean MSA for Brefeldin A-bound MAPK is 272.56±1.79Å2, and for PrCK1, it is 272.59±1.93$Å^2$.

The SASA plot (Figure 3.9), which quantitatively describes Brefeldin A's binding dynamics in the hydrophobic cores of MAPK and PrCK1, exhibits similar patterns to the ligand RMSD plot. The trajectory remains consistent throughout most of the MD simulation, with a sudden fluctuation occurring between 210ns and 230ns before stabilizing and mirroring the RMSD trajectory pattern. These results suggest that Brefeldin A establishes stable binding with both MAPK and PrCK1, maintaining consistent interactions throughout the simulation, except for a brief period of positional fluctuation in PrCK1. Future studies are needed to elucidate the functional consequences of these binding behaviours.

The 3D representations of Tunicamycin C and Brefeldin A complexed with their respective proteins offer valuable insights into these ligand-protein interactions' stability and conformational consistency over a 250 ns Molecular Dynamics (MD) simulation. The superimposed images of Tunicamycin C bound to Protein Related C Kinase 1 (PrKC1) and Thymidine Kinase 1 (TK1) (as shown in Figure 3.10) illustrate a stable and consistent orientation throughout the simulation period. This steady configuration aligns with observations made from the ligand RMSD plot and suggests a well-established and stable interaction between Tunicamycin C and both proteins.

Similarly, the 3D presentation of Brefeldin A in complex with Mitogen-Activated Protein Kinase (MAPK) and PrKC1 (depicted in Figure 3.11) reveals that the structural packing and conformational configuration of Brefeldin A remains consistent in both proteins throughout the molecular dynamics simulation. This finding implies that Brefeldin A sustains a stable interaction with both proteins, likely affecting the biological activity or inactivity of these proteins. These results underline the significance of stable and consistent ligand-protein interactions in maintaining the functional efficacy of the bound proteins. Further research, however, is needed to unravel the precise implications of these steady interactions on the proteins' biological functions and potential therapeutic applications.

4.9. System-based visualization of ligand interaction

The present study provides a comprehensive understanding of the interactions between Tunicamycin C and Brefeldin A with their respective protein targets. For Tunicamycin C, a significant observation from Figure 3.12 is that bulk water encourages a higher formation of hydrogen bonds than the docked complexes, enhancing ligand interaction, molecular recognition, and protein targeting. This provides and supports the importance of water molecules in protein-ligand interaction and stability. Figure 3.12 also identifies the critical active site residues contributing to Tunicamycin C binding stability in TK1 and PrKC1, with various occupancy degrees. The stacked bar charts in Figure 3.16 reveal the dominant role of water bridge, van der Waals, and H-bond interactions in stabilising these complexes.

Figure 3.4 reveals specific residues in TK1 and PrKC1 contributing significantly to the electrostatic energy essential for Tunicamycin C's binding stabilization. The MMDBSA results further confirm a highly favourable binding interaction, indicated by the negative binding energy values for both TK1 and PrKC1. Whereas, Brefeldin A, the 2D interaction diagrams and comparative analysis in Figures 3.13A, and 3.13B clearly show its binding and interaction

patterns with MAPK and PrCK1 in different mediums. Figure 3.3 also identifies the active site residues crucial for the binding stabilization of Brefeldin A to both MAPK and PrCK1, with noted contributions from bulk water in both interactions. However, the results suggest that for Brefeldin A, bulk water might not significantly contribute to the binding stabilization of MARP/PrCK1 complexes. Other factors might have a more significant role in promoting molecular recognition and binding interaction. These findings highlight the intricacy of ligand-protein interactions, influenced by various factors, including bulk water, electrostatic interactions, and specific amino acid residues within the binding pocket. The significant contribution of water molecules in these interactions emphasizes the importance of considering the role of the solvent environment in studying protein-ligand dynamics and in the drug design process.

4.1.0 Quantification thermodynamic evaluation of binding affinity

Table 3.6 presents the estimated binding energy predictions of Tunicamycin C when in complex with Thymidine Kinase 1 (TK1) and Protein Related C Kinase 1 (PrKC1). Binding energy is a crucial factor in understanding the stability and affinity of ligand-protein complexes. For Tunicamycin C, the binding free energy (ΔG_{bind}) with Thymidine Kinase 1 (TK1) is estimated to be -60.21±9.46 kcal/mol, and with Protein Related C Kinase 1 (PrKC1), it is -50.37±8.38 kcal/mol.

In comparison, Brefeldin A's ΔG_{bind} with Mitogen-Activated Protein Kinase (MAPK) is estimated to be -22.18±4.50 kcal/mol, and with PrKC1, it is -23.9±5.36 kcal/mol. From these results, Tunicamycin C appears to have more negative (and hence more favourable) binding free energy values than Brefeldin A for both proteins, indicating stronger binding interactions. In the case of TK1 and MAPK, Tunicamycin C shows a markedly stronger binding affinity. However, when comparing the binding of the two ligands to PrKC1, Tunicamycin C still shows a stronger affinity, but the difference is not as pronounced. Binding affinity is just one aspect of a potential drug's effectiveness. Other factors, such as drug metabolism, distribution, toxicity, and the ability to reach the target site in the body, also play crucial roles in determining a drug's therapeutic potential.

Chapter 5: Conclusion

This study explored the binding dynamics and interaction patterns of two glycosylation inhibitors, Tunicamycin C and Brefeldin A, with their respective protein targets, Thymidine Kinase 1 (TK1), Protein Related C Kinase 1 (PrKC1), and Mitogen-Activated Protein Kinase (MAPK). Molecular dynamics simulations and binding energy calculations reveal critical insights into these ligand-protein interactions' complex stability and potential biological effects. Notably, Tunicamycin C showed solid and consistent binding interactions with TK1 and PrKC1, and the presence of bulk water was crucial in promoting hydrogen bonding and overall complex stability. Similarly, Brefeldin A maintained stable interactions with MAPK and PrKC1 throughout the simulations. However, Brefeldin A's binding to these proteins showed lower estimated binding free energy values than Tunicamycin C, suggesting less favourable binding (Figure 5.1).

In comparing the binding energies of Tunicamycin C and Brefeldin A, Tunicamycin C demonstrated more favourable binding free energy values for both proteins, indicating stronger binding interactions. This difference in binding affinity was more pronounced in comparison with TK1 and MAPK, while it was less significant in the case of PrKC1. However, while these results provide valuable theoretical insights into the binding dynamics of these bioactive compounds, it is critical to remember that these are computational predictions and would need further validation through experimental studies.

Target proteins for these compounds were found using SwissTargetPrediction Software. Peroxisome Proliferator-Activated Receptor Gamma (PPARG), Protein Kinase C Alpha (PRKC/A) and Mitogen-Activated Protein Kinase Kinase 1 (MAP2K1) were targets for Brefeldin A, whereas TK1 and PRKCA were targets for Tunicamycin. Furthermore, KEGG pathway analysis revealed significantly enriched pathways such as Epstein-Barr virus infection, cellular senescence, and general cancer pathways. 3D crystallographic structures of proteins TK1, PrKC1, PrCK1, and MAPK were analysed after retrieval from the RCSB Protein Data Bank. Molecular docking studies and MD simulations were conducted to understand the inhibitory capability of the compounds against these proteins. The study found that binding Tunicamycin C and Brefeldin A to their respective targets led to a conformational change inhibiting protein activity, suggesting their potential as novel inhibitors for cancer treatment by blocking glycosylation progression.

While the roles of these proteins in glycosylation are not fully understood, multiple studies have indicated that they play an indirect role in this process. The role of these proteins in glycosylation and colon cancer is summarised in Figure 5.1, TK1 for instance contributes to the pool of raw materials used in glycosylation in the form of nucleotide sugars formed in Pyrimidine metabolism. It is predicted that TK1 will be tightly bound by Tunicamycin C, indicated by the thicker red arrow in figure 5.1. The inhibition of TK1 by Tunicamycin C can potentially inhibit CRC progression in several ways based on current understanding. Firstly, it can hinder the formation of raw materials necessary for DNA synthesis, thereby impeding the growth and replication of tumor cells. Secondly, it can inhibit glycolysis, which is upregulated due to TK1 activity, thereby preventing the metabolic shift required for increased energy utilization in cancer cells. Thirdly, and significantly in this study, the inhibition of glycolysis results from the absence of nucleoside sugars normally provided by TK1 activity. Both Tunicamycin C and BFA are predicted to bind to PrKCA, with Tunicamycin C being the stronger interactor of the two. This study also predicts that BFA can bind to and inhibit the function of MAPK. PrKCA and MAPK both regulate the upstream signalling pathways involved in glycosylation. Additionally, both proteins play crucial roles in the development and progression of CRC (Figure 5.1). PrKCA functions upstream of MAPK in all three of the signaling pathways activated by PrKCA, including the Raf-1 and AKT pathways, as well as the function of the glucotransferase enzyme required for glycosylation. The regulation of glucotransferase is also under the control of MAPK, while many upstream regulators of the MAPK cascade are glycosylated to perform their function. The activation of the AKT pathway occurs downstream of PrKCA, and thus both Tunicamycin C and BFA may inhibit this activity. Moreover, the MAPK cascade is involved downstream in this pathway, and the ability of BFA to inhibit components of the cascade may impede the functioning of this pathway, reducing the ability of cancer cells to evade apoptosis. The Raf-1 pathway also involves upstream regulation by PrKCA and requires downstream MAPK cascade signalling to initiate angiogenesis and ECM degradation. Once again, Tunicamycin can inhibit this pathway by binding to and inhibiting PrKCA. BFA can also bind to PrKCA but with weaker binding energy than Tunicamycin does. BFA can then also inhibit this pathway downstream by binding to and inhibiting MAPK cascade signalling. Additionally, the Raf-1 and AKT pathways function together to initiate invasion and migration of tumor cells. Thus, both Brefeldin A and Tunicamycin may serve as lead compounds for the development of new treatment strategies for managing CRC.

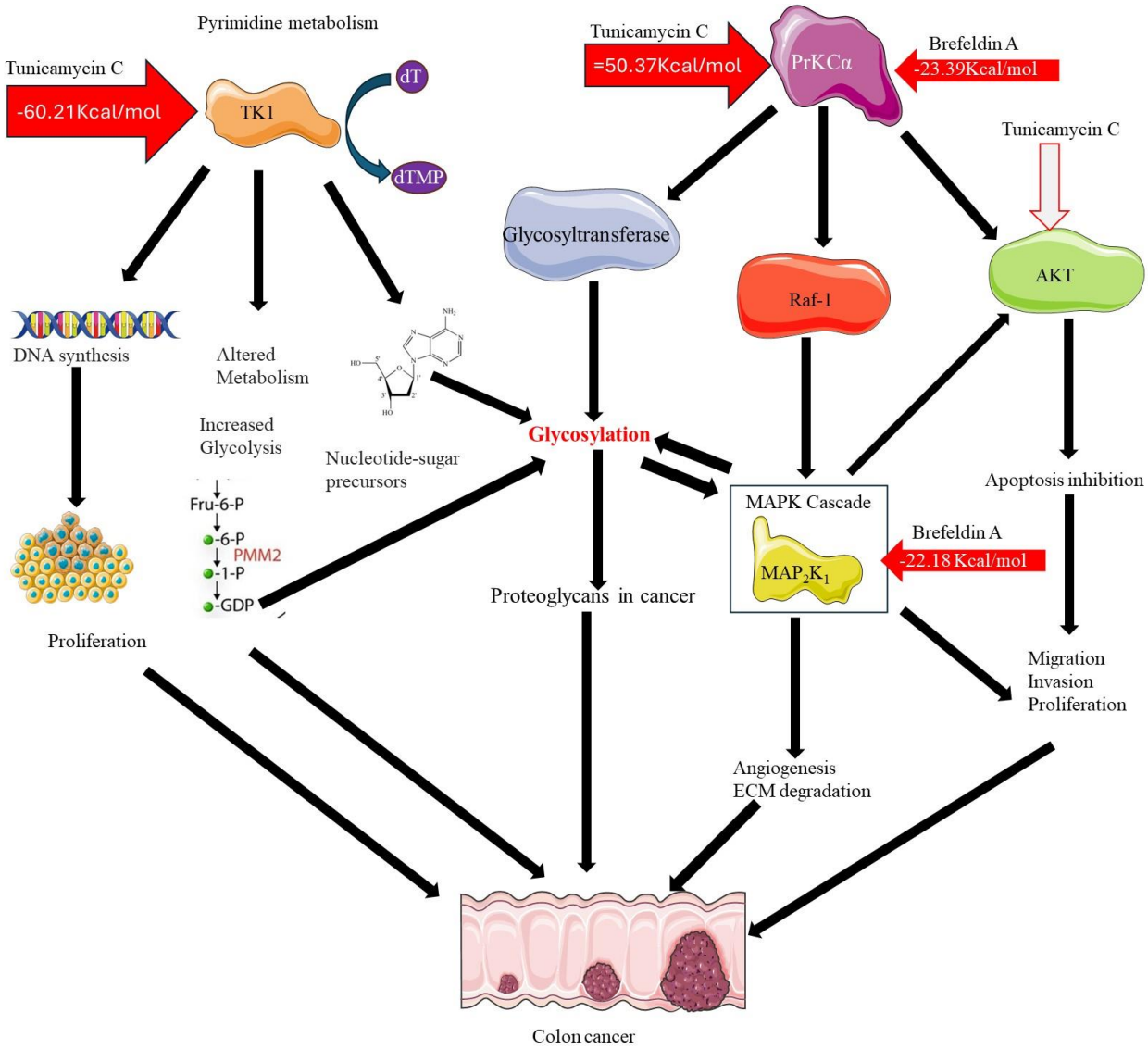


Figure 5.1. Illustration of the possible roles Tunicamycin C and Brefeldin A may play in CRC. Based on previous studies it is known that TK1, PrKCA and MAP2K1 all play a role in the development and progression of CRC. However, they are also thought to play a role in glycosylation through its regulation or by contributing to the building blocks used in the glycosylation process. The figure above shows the points in these pathways where these drugs bind to their respective targets, with the thickness of the red arrows representing the strength of the predicted interaction with the ΔG values of the interaction indicated in the arrow in Kcal/mol.

Future directions

It is possible to enhance and broaden the scope of this research by taking several additional steps. Firstly, validation through experimentation by carrying out wet lab techniques, including biochemical or cell-based assays to confirm tunicamycin's and brefeldin A's inhibition of target proteins; and to validate the proposed mechanism of action. Also, one can investigate other potential glycosylation inhibitors and evaluate their interactions with glycosylation targets, allowing for a more comprehensive understanding of potential therapeutic agents. Furthermore,

selectivity and off-target effects can be determined. In this regard, the selectivity of Tunicamycin C and Brefeldin A and other potential TK1, MAPK, and PrKC1 inhibitors could be compared to other proteins to minimize off-target effects and the likelihood of adverse side effects in potential therapeutic applications.

Structure-activity relationships (SAR) can also be investigated to assess the relationship between Tunicamycin C and Brefeldin, A chemical structure with other potential inhibitors' biological activities, to identify key features that contribute to the effective inhibition of target proteins. Drug enhancement can also be evaluated to optimize the chemical structures of Tunicamycin C and Brefeldin A inhibitors based on SAR analysis to improve their potency, selectivity, and pharmacokinetic properties, ultimately improving their therapeutic potential. Following this assessment of the efficacy, safety, and pharmacokinetics of the optimized inhibitors in an *in vivo* physiological setting can provide additional evidence for their therapeutic potential. Finally, with promising preclinical results, the optimized inhibitors can be tested in human clinical trials to determine their safety, tolerability, and efficacy in treating CRC and potentially other types of cancer.

6. References

Adcock, S. A. & Mccammon, J. A. 2006. Molecular dynamics: survey of methods for simulating the activity of proteins. *Chemical reviews,* 106**,** 1589-1615.

Agarwal, S. & Mehrotra, R. 2016. An overview of molecular docking. *JSM chem,* 4**,** 1024-1028.

Agarwal, S., Ray, B. & Mehrotra, R. 2015. SERS as an advanced tool for investigating chloroethyl nitrosourea derivatives complexation with DNA. *International journal of biological macromolecules,* 81**,** 891-7.

Alberca, L. N., Chuguransky, S. R., Álvarez, C. L., Talevi, A. & Salas-Sarduy, E. 2019. In silico Guided Drug Repurposing: Discovery of New Competitive and Non-competitive Inhibitors of Falcipain-2. *Frontiers in chemistry,* 7**,** 534.

Alder, B. J. & Wainwright, T. E. 1957. Phase transition for a hard sphere system. *The Journal of chemical physics,* 27**,** 1208.

Alexeeva, M., Moen, M. N., Grøsvik, K., Tesfahun, A. N., Xu, X. M., Muruzábal-Lecumberri, I., Olsen, K. M., Rasmussen, A., Ruoff, P., Kirpekar, F., Klungland, A. & Bjelland, S. 2019. Excision of uracil from DNA by hSMUG1 includes strand incision and processing. *Nucleic Acids Res,* 47**,** 779-793.

Allan, G., Ouadid-Ahidouch, H., Sanchez-Fernandez, E. M., Risquez-Cuadro, R., Fernandez, J. M., Ortiz-Mellet, C. & Ahidouch, A. 2013. New castanospermine glycoside analogues inhibit breast cancer cell proliferation and induce apoptosis without affecting normal cells. *PloS one,* 8**,** e76411.

Alomar, M. J. 2014. Factors affecting the development of adverse drug reactions (Review article). *Saudi pharmaceutical journal : SPJ : the official publication of the Saudi Pharmaceutical Society,* 22**,** 83-94.

Alvarez, C. & Sztul, E. S. 1999. Brefeldin A (BFA) disrupts the organization of the microtubule and the actin cytoskeletons. *European journal of cell biology,* 78**,** 1-14.

Amadei, A., Ceruso, M. A. & Di Nola, A. 1999. On the convergence of the conformational coordinates basis set obtained by the essential dynamics analysis of proteins' molecular dynamics simulations. *Proteins,* 36**,** 419-24.

American Cancer Society. 2018. *Colorectal Cancer Stages* [Online]. 250 Williams Street NW

Atlanta, GA 30303. Available: https://www.cancer.org/about-us/online-help/contact-us.html [Accessed 7 July 2023].

Anderluh, M., Berti, F., Bzducha-Wróbel, A., Chiodo, F., Colombo, C., Compostella, F., Durlik, K., Ferhati, X., Holmdahl, R., Jovanovic, D., Kaca, W., Lay, L., Marinovic-Cincovic, M., Marradi, M., Ozil, M., Polito, L., Reina, J. J., Reis, C. A., Sackstein, R., Silipo, A., Švajger, U., Vaněk, O., Yamamoto, F., Richichi, B. & Van Vliet, S. J. 2022. Recent advances on smart glycoconjugate vaccines in infections and cancer. *The FEBS journal,* 289**,** 4251-4303.

Anderson, A. C. 2003. The process of structure-based drug design. *Chemistry & biology,* 10**,** 787-97.

Apweiler, R., Hermjakob, H. & Sharon, N. 1999. On the frequency of protein glycosylation, as deduced from analysis of the SWISS-PROT database. *Biochimica et biophysica acta,* 1473**,** 4-8.

Arey, B. 2012. The role of glycosylation in receptor signaling. *Glycosylation,* 26**,** 50262.

Arey, B. J. & López, F. J. 2011. Are circulating gonadotropin isoforms naturally occurring biased agonists? Basic and therapeutic implications. *Reviews in endocrine & metabolic disorders,* 12**,** 275-88.

Arodola, O. A. & Soliman, M. E. 2017. Quantum mechanics implementation in drug-design workflows: does it really help? *Drug Des Devel Ther,* 11**,** 2551-2564.

Ashburner, M., Ball, C. A., Blake, J. A., Botstein, D., Butler, H., Cherry, J. M., Davis, A. P., Dolinski, K., Dwight, S. S., Eppig, J. T., Harris, M. A., Hill, D. P., Issel-Tarver, L., Kasarskis, A., Lewis, S., Matese, J. C., Richardson, J. E., Ringwald, M., Rubin, G. M. & Sherlock, G. 2000. Gene ontology: tool for the unification of biology. The Gene Ontology Consortium. *Nature genetics,* 25**,** 25-9.

Astani, E. K., Malek Zadeh, S., Hsu, N. S., Lin, K. H., Sardari, S. & Li, T. L. 2022. Intermolecular Interactions of Nucleoside Antibiotic Tunicamycin with On-Target MraY(CB)-TUN and Off-Target DPAGT1-TUN in the Active Sites Delineated by Quantum Mechanics/Molecular Mechanics Calculations. *ACS Omega,* 7**,** 32970-32987.

Astler, V. B. & Coller, F. A. 1954. The prognostic significance of direct extension of carcinoma of the colon and rectum. *Annals of surgery,* 139**,** 846-846.

Aufderklamm, S., Todenhöfer, T., Gakis, G., Kruck, S., Hennenlotter, J., Stenzl, A. & Schwentner, C. 2012. Thymidine kinase and cancer monitoring. *Cancer letters,* 316**,** 6-10.

Augen, J. 2002. The evolving role of information technology in the drug discovery process. *Drug discovery today,* 7**,** 315-23.

Baba, Y., Nosho, K., Shima, K., Irahara, N., Kure, S., Toyoda, S., Kirkner, G. J., Goel, A., Fuchs, C. S. & Ogino, S. 2009. Aurora-A expression is independently associated with chromosomal instability in colorectal cancer. *Neoplasia (New York, N.Y.),* 11**,** 418-25.

Baffi, T. R., Lordén, G., Wozniak, J. M., Feichtner, A., Yeung, W., Kornev, A. P., King, C. C., Del Rio, J. C., Limaye, A. J. & Bogomolovas, J. 2021. mTORC2 controls the activity of PKC and Akt by phosphorylating a conserved TOR interaction motif. *Science signaling,* 14**,** eabe4509.

Baichoo, E. & Boardman, L. A. 2014. Toward a molecular classification of colorectal cancer: the role of telomere length. *Frontiers in oncology,* 4**,** 158.

Baier, P. K., Eggstein, S., Wolff-Vorbeck, G., Baumgartner, U. & Hopt, U. T. 2005. Chemokines in human colorectal carcinoma. *Anticancer research,* 25**,** 3581-4.

Bakhoum, S. F., Kabeche, L., Murnane, J. P., Zaki, B. I. & Compton, D. A. 2014. DNA-damage response during mitosis induces whole-chromosome missegregation. *Cancer discovery,* 4**,** 1281-9.

Bandera Merchan, B., Tinahones, F. J. & Macías-González, M. 2016. Commonalities in the Association between PPARG and Vitamin D Related with Obesity and Carcinogenesis. *PPAR research,* 2016**,** 2308249.

Barh, D., Chaitankar, V., Yiannakopoulou, E. C., Salawu, E. O., Chowbina, S., Ghosh, P. & Azevedo, V. 2014. In silico models: from simple networks to complex diseases. *Animal biotechnology*. Elsevier.

Battaglia, T. A., Gunn, C. M., Mccoy, M. E., Mu, H. H., Baranoski, A. S., Chiao, E. Y., Kachnic, L. A. & Stier, E. A. 2015. Beliefs About Anal Cancer among HIV-Infected Women: Barriers and Motivators to Participation in Research. *Women's health issues : official publication of the Jacobs Institute of Women's Health,* 25**,** 720-6.

Becker, D. J. & Lowe, J. B. 2003. Fucose: biosynthesis and biological function in mammals. *Glycobiology,* 13**,** 41R-53R.

Bekisz, S. & Geris, L. J. J. O. C. S. 2020. Cancer modeling: From mechanistic to data-driven approaches, and from fundamental insights to clinical applications. 46**,** 101198.

Bennett, E. P., Mandel, U., Clausen, H., Gerken, T. A., Fritz, T. A. & Tabak, L. A. 2012. Control of mucin-type O-glycosylation: a classification of the polypeptide GalNAc-transferase gene family. *Glycobiology,* 22**,** 736-56.

Benson, A. B., Venook, A. P., Al-Hawary, M. M., Arain, M. A., Chen, Y.-J., Ciombor, K. K., Cohen, S., Cooper, H. S., Deming, D. & Farkas, L. 2021. Colon cancer, version 2.2021, NCCN clinical practice guidelines in oncology. *Journal of the National Comprehensive Cancer Network,* 19**,** 329-359.

Benvenuti, S., Sartore-Bianchi, A., Di Nicolantonio, F., Zanon, C., Moroni, M., Veronese, S., Siena, S. & Bardelli, A. 2007. Oncogenic activation of the RAS/RAF signaling pathway impairs the response of metastatic colorectal cancers to anti–epidermal growth factor receptor antibody therapies. *Cancer research,* 67**,** 2643-2648.

Bertero, L., Massa, F., Metovic, J., Zanetti, R., Castellano, I., Ricardi, U., Papotti, M. & Cassoni, P. 2018. Eighth Edition of the UICC Classification of Malignant Tumours: an overview of the changes in the pathological TNM classification criteria-What has changed and why? *Virchows Archiv : an international journal of pathology,* 472**,** 519-531.

Berthon, A. S., Szarek, E. & Stratakis, C. A. 2015. PRKACA: the catalytic subunit of protein kinase A and adrenocortical tumors. *Frontiers in cell and developmental biology,* 3**,** 26.

Betina, V. 1969. Effects of the macrolide antibiotic cyanein on HeLa cells growth and metabolism. *Neoplasma,* 16**,** 23-32.

Beveridge, D. L. & Dicapua, F. M. 1989. Free energy via molecular simulation: applications to chemical and biomolecular systems. *Annual review of biophysics and biophysical chemistry,* 18**,** 431-492.

Bharath, E., Manjula, S. & Vijaychand, A. J. I. J. P. P. S. 2011. In silico drug design tool for overcoming the innovation deficit in the drug discovery process. 3**,** 8-12.

Bi, X., Lin, Q., Foo, T. W., Joshi, S., You, T., Shen, H.-M., Ong, C. N., Cheah, P. Y., Eu, K. W. & Hew, C.-L. 2006. Proteomic analysis of colorectal cancer reveals alterations in metabolic pathways: mechanism of tumorigenesis. *Molecular & cellular proteomics,* 5**,** 1119-1130.

Biller, L. H. & Schrag, D. 2021. Diagnosis and Treatment of Metastatic Colorectal Cancer: A Review. *Jama,* 325**,** 669-685.

Bissaro, M., Sturlese, M. & Moro, S. 2020. The rise of molecular simulations in fragment-based drug design (FBDD): an overview. *Drug discovery today,* 25**,** 1693-1701.

Bitter, E. E., Townsend, M. H., Erickson, R., Allen, C. & O'neill, K. L. 2020. Thymidine kinase 1 through the ages: a comprehensive review. *Cell & bioscience,* 10**,** 138.

Bjornsti, M. A. & Houghton, P. J. 2004. The TOR pathway: a target for cancer therapy. *Nature reviews. Cancer,* 4**,** 335-48.

Black, A. R. & Black, J. D. 2021. The complexities of PKCα signaling in cancer. *Advances in biological regulation,* 80**,** 100769.

Boal, F., Guetzoyan, L., Sessions, R. B., Zeghouf, M., Spooner, R. A., Lord, J. M., Cherfils, J., Clarkson, G. J., Roberts, L. M. & Stephens, D. J. 2010. LG186: An inhibitor of GBF1 function that causes Golgi disassembly in human and canine cells. *Traffic,* 11**,** 1537-1551.

Bones, J., Mittermayr, S., O'donoghue, N., Guttman, A. & Rudd, P. M. 2010. Ultra performance liquid chromatographic profiling of serum N-glycans for fast and efficient identification of cancer associated alterations in glycosylation. *Analytical chemistry,* 82**,** 10208-15.

Born, M. & Oppenheimer, R. 1927. Zur Quantentheorie der Molekeln *Annalen der Physik,* 84.

Bray, F., Ferlay, J., Soerjomataram, I., Siegel, R. L., Torre, L. A. & Jemal, A. 2018. Global cancer statistics 2018: GLOBOCAN estimates of incidence and mortality worldwide for 36 cancers in 185 countries. *CA: a cancer journal for clinicians,* 68**,** 394-424.

Britain, C. M., Holdbrooks, A. T., Anderson, J. C., Willey, C. D. & Bellis, S. L. 2018. Sialylation of EGFR by the ST6Gal-I sialyltransferase promotes EGFR activation and resistance to gefitinib-mediated cell death. *Journal of ovarian research,* 11**,** 12.

Brogi, S., Ramalho, T. C., Kuca, K., Medina-Franco, J. L. & Valko, M. 2020. Editorial: In silico Methods for Drug Design and Discovery. *Frontiers in chemistry,* 8**,** 612.

Brunmeir, R. & Xu, F. 2018. Functional regulation of PPARs through post-translational modifications. *International journal of molecular sciences,* 19**,** 1738.

Brzostek, A., Pawelczyk, J., Rumijowska-Galewicz, A., Dziadek, B. & Dziadek, J. 2009. Mycobacterium tuberculosis is able to accumulate and utilize cholesterol. *Journal of bacteriology,* 191**,** 6584-91.

Bunting, S. F. & Nussenzweig, A. 2013. End-joining, translocations and cancer. *Nature reviews Cancer,* 13**,** 443-454.

Carvalho, M. V. D., Gonçalves-De-Albuquerque, C. F. & Silva, A. R. 2021. PPAR gamma: from definition to molecular targets and therapy of lung diseases. *International journal of molecular sciences,* 22**,** 805.

Case, D. A., Aktulga, H. M., Belfon, K., Cerutti, D. S., Cisneros, G. A., Cruzeiro, V. W. D., Forouzesh, N., Giese, T. J., Götz, A. W., Gohlke, H., Izadi, S., Kasavajhala, K., Kaymak, M. C., King, E., Kurtzman, T., Lee, T.-S., Li, P., Liu, J., Luchko, T., Luo, R., Manathunga, M., Machado, M. R., Nguyen, H. M., O'hearn, K. A., Onufriev, A. V., Pan, F., Pantano, S., Qi, R., Rahnamoun, A., Risheh, A., Schott-Verdugo, S., Shajan,

A., Swails, J., Wang, J., Wei, H., Wu, X., Wu, Y., Zhang, S., Zhao, S., Zhu, Q., Cheatham, T. E., Iii, Roe, D. R., Roitberg, A., Simmerling, C., York, D. M., Nagan, M. C. & Merz, K. M., Jr. 2023. AmberTools. *Journal of chemical information and modeling,* 63**,** 6183-6191.

Caspi, R., Billington, R., Ferrer, L., Foerster, H., Fulcher, C. A., Keseler, I. M., Kothari, A., Krummenacker, M., Latendresse, M., Mueller, L. A., Ong, Q., Paley, S., Subhraveti, P., Weaver, D. S. & Karp, P. D. 2016. The MetaCyc database of metabolic pathways and enzymes and the BioCyc collection of pathway/genome databases. *Nucleic Acids Res,* 44**,** D471-80.

Cavasotto, C. N. & Aucar, M. G. 2020. High-Throughput Docking Using Quantum Mechanical Scoring. *Frontiers in chemistry,* 8**,** 246.

Cenci Di Bello, I., Fleet, G., Namgoong, S. K., Tadano, K. & Winchester, B. 1989. Structure-activity relationship of swainsonine. Inhibition of human alpha-mannosidases by swainsonine analogues. *The Biochemical journal,* 259**,** 855-61.

Chacko, B. K., Scott, D. W., Chandler, R. T. & Patel, R. P. 2011. Endothelial Surface N-Glycans Mediate Monocyte Adhesion and Are Targets for Anti-inflammatory Effects of Peroxisome Proliferator-activated Receptor γ Ligands*. *Journal of Biological Chemistry,* 286**,** 38738-38747.

Chakraborty, A., Dorsett, K. A., Trummell, H. Q., Yang, E. S., Oliver, P. G., Bonner, J. A., Buchsbaum, D. J. & Bellis, S. L. 2018. ST6Gal-I sialyltransferase promotes chemoresistance in pancreatic ductal adenocarcinoma by abrogating gemcitabine-mediated DNA damage. *The Journal of biological chemistry,* 293**,** 984-994.

Chan, A. T. & Giovannucci, E. L. 2010. Primary prevention of colorectal cancer. *Gastroenterology,* 138**,** 2029-2043.

Chardin, P. & Mccormick, F. 1999. Brefeldin A: the advantage of being uncompetitive. *Cell,* 97**,** 153-5.

Chaudhary, K. K. & Mishra, N. J. D. 2016. A review on molecular docking: novel tool for drug discovery. 3**,** 1029.

Chauvin, A. & Boisvert, F.-M. 2018. Clinical proteomics in colorectal cancer, a promising tool for improving personalised medicine. *Proteomes,* 6**,** 49-49.

Cheatham, T. E., 3rd & Kollman, P. A. 2000. Molecular dynamics simulation of nucleic acids. *Annual review of physical chemistry,* 51**,** 435-71.

Chen, H. J., Edwards, R., Tucci, S., Bu, P., Milsom, J., Lee, S., Edelmann, W., Gümüs, Z. H., Shen, X. & Lipkin, S. 2012. Chemokine 25–induced signaling suppresses colon cancer invasion and metastasis. *The Journal of clinical investigation,* 122**,** 3184-3196.

Chen, X., Karnovsky, A., Sans, M. D., Andrews, P. C. & Williams, J. A. 2010a. Molecular characterization of the endoplasmic reticulum: insights from proteomic studies. *Proteomics,* 10**,** 4040-4052.

Chen, Y. L., Eriksson, S. & Chang, Z. F. 2010b. Regulation and functional contribution of thymidine kinase 1 in repair of DNA damage. *The Journal of biological chemistry,* 285**,** 27327-27335.

Cherepanova, N., Shrimal, S. & Gilmore, R. 2016. N-linked glycosylation and homeostasis of the endoplasmic reticulum. *Current opinion in cell biology,* 41**,** 57-65.

Chiaradonna, F., Ricciardiello, F. & Palorini, R. 2018. The Nutrient-Sensing Hexosamine Biosynthetic Pathway as the Hub of Cancer Metabolic Rewiring. *Cells,* 7.

Ciardiello, F. & Tortora, G. 2008. EGFR antagonists in cancer treatment. *New England Journal of Medicine,* 358**,** 1160-1174.

Clementi, C., Nymeyer, H. & Onuchic, J. N. 2000. Topological and energetic factors: what determines the structural details of the transition state ensemble and "en-route" intermediates for protein folding? An investigation for small globular proteins. *Journal of molecular biology,* 298**,** 937-53.

Clerc, F., Reiding, K. R., Jansen, B. C., Kammeijer, G. S., Bondt, A. & Wuhrer, M. 2016. Human plasma protein N-glycosylation. *Glycoconjugate journal,* 33**,** 309-43.

Colanzi, A., Grimaldi, G., Catara, G., Valente, C., Cericola, C., Liberali, P., Ronci, M., Lalioti, V. S., Bruno, A., Beccari, A. R., Urbani, A., De Flora, A., Nardini, M., Bolognesi, M., Luini, A. & Corda, D. 2013. Molecular mechanism and functional role of brefeldin A-mediated ADP-ribosylation of CtBP1/BARS. *Proceedings of the National Academy of Sciences of the United States of America,* 110**,** 9794-9.

Contreras-Riquelme, S., Garate, J. A., Perez-Acle, T. & Martin, A. J. M. 2018. RIP-MD: a tool to study residue interaction networks in protein molecular dynamics. *PeerJ,* 6**,** e5998.

Coppedè, F. 2014. Epigenetic biomarkers of colorectal cancer: Focus on DNA methylation. *Cancer letters,* 342**,** 238-247.

Cornell, W. D., Cieplak, P., Bayly, C. I., Gould, I. R., Merz, K. M., Ferguson, D. M., Spellmeyer, D. C., Fox, T., Caldwell, J. W. & Kollman, P. A. 1995. A second generation force field for the simulation of proteins, nucleic acids, and organic molecules. *Journal of the American Chemical Society,* 117**,** 5179-5197.

Corrales, P., Izquierdo-Lahuerta, A. & Medina-Gómez, G. 2018. Maintenance of Kidney Metabolic Homeostasis by PPAR Gamma. *International journal of molecular sciences,* 19.

Cortez, N., Villegas, C., Burgos, V., Ortiz, L., Cabrera-Pardo, J. R. & Paz, C. 2024. Therapeutic Potential of Chlorogenic Acid in Chemoresistance and Chemoprotection in Cancer Treatment. *International journal of molecular sciences,* 25.

Cosentino-Gomes, D., Rocco-Machado, N. & Meyer-Fernandes, J. R. 2012. Cell signaling through protein kinase C oxidation and activation. *International journal of molecular sciences,* 13**,** 10697-10721.

Costa, A. F., Campos, D., Reis, C. A. & Gomes, C. 2020. Targeting glycosylation: a new road for cancer drug discovery. *Trends in cancer,* 6**,** 757-766.

Daina, A., Michielin, O. & Zoete, V. 2019. SwissTargetPrediction: updated data and new features for efficient prediction of protein targets of small molecules. *Nucleic Acids Res,* 47**,** W357-w364.

Dang, L., Ma, H., Hei, A., Xu, S., Zhou, J., He, E. & Skog, S. 2020. A meta-analysis of serological thymidine kinase 1 as a marker for colorectal benign and malignant tumor risk assessment. *Molecular and clinical oncology,* 12**,** 440-450.

Davies, C. C., Mason, J., Wakelam, M. J., Young, L. S. & Eliopoulos, A. G. 2004. Inhibition of phosphatidylinositol 3-kinase- and ERK MAPK-regulated protein synthesis reveals the pro-apoptotic properties of CD40 ligation in carcinoma cells. *The Journal of biological chemistry,* 279**,** 1010-9.

Dawood, A. A. 2023. Determination of binding affinity of tunicamycin with SARS-CoV-2 proteins: Proteinase, protease, nsp2, nsp9, ORF3a, ORF7a, ORF8, ORF9b, envelope and RBD of spike glycoprotein. *Vacunas,* 24**,** 1-12.

Dawood, A. A. & Altobje, M. A. 2020. Inhibition of N-linked glycosylation by tunicamycin may contribute to the treatment of SARS-CoV-2. *Microbial Pathogenesis,* 149**,** 104586-104586.

De Bruyn Kops, C., Stork, C., Šícho, M., Kochev, N., Svozil, D., Jeliazkova, N. & Kirchmair, J. 2019. GLORY: Generator of the Structures of Likely Cytochrome P450 Metabolites Based on Predicted Sites of Metabolism. *Frontiers in chemistry,* 7**,** 402.

De Freitas Junior, J. C., Silva Bdu, R., De Souza, W. F., De Araújo, W. M., Abdelhay, E. S. & Morgado-Díaz, J. A. 2011. Inhibition of N-linked glycosylation by tunicamycin induces E-cadherin-mediated cell-cell adhesion and inhibits cell proliferation in

undifferentiated human colon cancer cells. *Cancer chemotherapy and pharmacology,* 68**,** 227-38.

Defazio, A., Chiew, Y. E., Sini, R. L., Janes, P. W. & Sutherland, R. L. 2000. Expression of c-erbB receptors, heregulin and oestrogen receptor in human breast cell lines. *International journal of cancer,* 87**,** 487-98.

Dejgaard, S. Y. & Presley, J. F. 2020. Class II Arfs require a brefeldin-A-sensitive factor for Golgi association. *Biochemical and biophysical research communications,* 530**,** 301-306.

Dekker, E., Tanis, P. J., Vleugels, J. L. A., Kasi, P. M. & Wallace, M. B. 2019. Colorectal cancer. *The Lancet,* 394**,** 1467-1480.

Dennis, J. W., Nabi, I. R. & Demetriou, M. 2009. Metabolism, cell surface organization, and disease. *Cell,* 139**,** 1229-41.

Desterke, C., Jaulin, F. & Dornier, E. 2024. Hypermethylated Colorectal Cancer Tumours Present a Myc-Driven Hypermetabolism with a One-Carbon Signature Associated with Worsen Prognosis. *Biomedicines,* 12.

Di Fiore, F., Blanchard, F., Charbonnier, F., Le Pessot, F., Lamy, A., Galais, M. P., Bastit, L., Killian, A., Sesboüé, R. & Tuech, J. J. 2007. Clinical relevance of KRAS mutation detection in metastatic colorectal cancer treated by Cetuximab plus chemotherapy. *British journal of cancer,* 96**,** 1166-1169.

Di Nicolantonio, F., Martini, M., Molinari, F., Sartore Bianchi, A., Arena, S., Saletti, P., De Dosso, S., Mazzucchelli, L., Frattini, M. & Siena, S. 2008. Wild-type BRAF is required for response to panitumumab or cetuximab in metastatic colorectal cancer. *Journal of clinical oncology,* 26**,** 5705-5712.

Dinter, A. & Berger, E. G. 1998. Golgi-disturbing agents. *Histochemistry and cell biology,* 109**,** 571-90.

Dixit, S. B., Ponomarev, S. Y. & Beveridge, D. L. 2006. Root mean square deviation probability analysis of molecular dynamics trajectories on DNA. *Journal of chemical information and modeling,* 46**,** 1084-1093.

Donaldson, J. G. & Jackson, C. L. 2000. Regulators and effectors of the ARF GTPases. *Current opinion in cell biology,* 12**,** 475-82.

Dong, F. L., Liu, D. M., Lu, T. T., Li, F., Zhang, C., E, Q. & Zhang, Y. H. 2022. PPARγ2 functions as a tumor suppressor in a translational mouse model of human prostate cancer. *Asian journal of andrology,* 24**,** 90-96.

Dotz, V. & Wuhrer, M. 2016. Histo-blood group glycans in the context of personalized medicine. *Biochimica et biophysica acta,* 1860**,** 1596-607.

Druker, B. J. & Lydon, N. B. 2000. Lessons learned from the development of an abl tyrosine kinase inhibitor for chronic myelogenous leukemia. *The Journal of clinical investigation,* 105**,** 3-7.

Duan, G. & Walther, D. 2015. The roles of post-translational modifications in the context of protein interaction networks. *PLoS computational biology,* 11**,** e1004049.

Dube, D. H. & Bertozzi, C. R. 2005. Glycans in cancer and inflammation — potential for therapeutics and diagnostics. *Nature Reviews Drug Discovery,* 4**,** 477-488.

Duffy, M. J., O'donovan, N. & Crown, J. 2011. Use of molecular markers for predicting therapy response in cancer patients. *Cancer treatment reviews,* 37**,** 151-159.

Dukes, C. E. 1932. The classification of cancer of the rectum. *The Journal of Pathology and Bacteriology,* 35**,** 323-332.

Durrant, J. D. & Mccammon, J. A. 2011. Molecular dynamics simulations and drug discovery. *BMC biology,* 9**,** 1-9.

Edwards, A. S. & Newton, A. C. 1997. Phosphorylation at conserved carboxyl-terminal hydrophobic motif regulates the catalytic and regulatory domains of protein kinase C. *Journal of biological chemistry,* 272**,** 18382-18390.

Ekins, S., Mestres, J. & Testa, B. 2007. In silico pharmacology for drug discovery: methods for virtual ligand screening and profiling. *British journal of pharmacology,* 152**,** 9-20.

Emmanuel, I. A., Olotu, F. A., Agoni, C. & Soliman, M. E. S. 2020. In Silico Repurposing of J147 for Neonatal Encephalopathy Treatment: Exploring Molecular Mechanisms of Mutant Mitochondrial ATP Synthase. *Current pharmaceutical biotechnology,* 21**,** 1551-1566.

Ene, C. D., Penescu, M. N., Georgescu, S. R., Tampa, M. & Nicolae, I. 2021. Posttranslational Modifications Pattern in Clear Cell Renal Cell Carcinoma. *Metabolites,* 11**,** 10.

Eng, C. & Holowatyj, A. N. 2022. Colorectal Cancer Genomics by Genetic Ancestry. *Cancer discovery,* 12**,** 1187-1188.

Esmaeili, S., Salari, S., Kaveh, V., Ghaffari, S. H. & Bashash, D. 2021. Alteration of PPAR-GAMMA (PPARG; PPARγ) and PTEN gene expression in acute myeloid leukemia patients and the promising anticancer effects of PPARγ stimulation using pioglitazone on AML cells. *Molecular genetics & genomic medicine,* 9**,** e1818.

Ewing, I., Hurley, J. J., Josephides, E. & Millar, A. 2014. The molecular genetics of colorectal cancer. *Frontline gastroenterology,* 5**,** 26-30.

Fabregat, A., Sidiropoulos, K., Garapati, P., Gillespie, M., Hausmann, K., Haw, R., Jassal, B., Jupe, S., Korninger, F., Mckay, S., Matthews, L., May, B., Milacic, M., Rothfels, K., Shamovsky, V., Webber, M., Weiser, J., Williams, M., Wu, G., Stein, L., Hermjakob, H. & D'eustachio, P. 2016. The Reactome pathway Knowledgebase. *Nucleic Acids Res,* 44**,** D481-7.

Fang, J. Y. & Richardson, B. C. 2005. The MAPK signalling pathways and colorectal cancer. *The Lancet. Oncology,* 6**,** 322-7.

Fang, Y., Skog, S., Ou, Q., Chen, Z., Liu, S., Hei, A., Li, J., Zhou, J., He, E. & Wan, D. 2023. Is serum thymidine kinase 1 a prognostic biomarker in primary tumor location of colorectal carcinomas? *Discover Oncology,* 14**,** 21.

Faseru, B., Fagan, P. & Okuyemi, K. S. 2022. Additional Benefits of Maintaining a Healthy Lifestyle After Quitting Smoking. *JAMA network open,* 5**,** e2232784.

Feng, B., Huang, X., Jiang, D., Hua, L., Zhuo, Y. & Wu, D. 2017. Endoplasmic Reticulum Stress Inducer Tunicamycin Alters Hepatic Energy Homeostasis in Mice. *International journal of molecular sciences,* 18.

Ferlay, J., Colombet, M., Soerjomataram, I., Mathers, C., Parkin, D. M., Piñeros, M., Znaor, A. & Bray, F. 2019. Estimating the global cancer incidence and mortality in 2018: GLOBOCAN sources and methods. *International journal of cancer,* 144**,** 1941-1953.

Ferreira, L. G., Dos Santos, R. N., Oliva, G. & Andricopulo, A. D. 2015. Molecular docking and structure-based drug design strategies. *Molecules (Basel, Switzerland),* 20**,** 13384-421.

Fersht, A. R. & Daggett, V. 2002. Protein folding and unfolding at atomic resolution. *Cell,* 108**,** 573-82.

Fisher, P. & Ungar, D. 2016. Bridging the Gap between Glycosylation and Vesicle Traffic. *Frontiers in cell and developmental biology,* 4**,** 15.

Friesner, R. A., Banks, J. L., Murphy, R. B., Halgren, T. A., Klicic, J. J., Mainz, D. T., Repasky, M. P., Knoll, E. H., Shelley, M., Perry, J. K., Shaw, D. E., Francis, P. & Shenkin, P. S. 2004. Glide: a new approach for rapid, accurate docking and scoring. 1. Method and assessment of docking accuracy. *Journal of medicinal chemistry,* 47**,** 1739-49.

Fu, Y. F., Liu, X., Gao, M., Zhang, Y. N. & Liu, J. 2017. Endoplasmic reticulum stress induces autophagy and apoptosis while inhibiting proliferation and drug resistance in multiple myeloma through the PI3K/Akt/mTOR signaling pathway. *Oncotarget,* 8**,** 61093-61106.

Fuglebakk, E., Echave, J. & Reuter, N. 2012. Measuring and comparing structural fluctuation patterns in large protein datasets. *Bioinformatics (Oxford, England),* 28**,** 2431-2440.

Fuster, M. M. & Esko, J. D. 2005. The sweet and sour of cancer: glycans as novel therapeutic targets. *Nature reviews. Cancer,* 5**,** 526-42.

Gallo, M. T., Grant, B. J., Teodoro, M. L., Melton, J., Cieplak, P., Phillips Jr, G. N. & Stec, B. 2009. Novel procedure for thermal equilibration in molecular dynamics simulation. *Molecular simulation,* 35**,** 349-357.

Ganem, N. J., Godinho, S. A. & Pellman, D. 2009. A mechanism linking extra centrosomes to chromosomal instability. *Nature,* 460**,** 278-282.

Genheden, S. & Ryde, U. 2015. The MM/PBSA and MM/GBSA methods to estimate ligand-binding affinities. *Expert opinion on drug discovery,* 10**,** 449-461.

Ghosh, D., Yu, H., Tan, X. F., Lim, T. K., Zubaidah, R. M., Tan, H. T., Chung, M. C. M. & Lin, Q. 2011. Identification of key players for colorectal cancer metastasis by iTRAQ quantitative proteomics profiling of isogenic SW480 and SW620 cell lines. *Journal of proteome research,* 10**,** 4373-4387.

Gian, L. D. A., Lorena, B., Cinzia, A., Gioacchino, L., Federica, G. & Francesca, N. 2018. Microsatellite instability in colorectal cancer. *Acta Bio Medica: Atenei Parmensis,* 89**,** 97-97.

Girnun, G. 2009. PPARG: a new independent marker for colorectal cancer survival. *Gastroenterology,* 136**,** 1157-1160.

Glynne-Jones, R., Hall, M. R., Lopes, A., Pearce, S., Goh, V., Bosompem, S., Bridgewater, J., Chau, I., Wasan, H., Moran, B., Melcher, L., West, N. P., Quirke, P., Wong, W. L., Beare, S., Hava, N., Duggan, M. & Harrison, M. 2018. BACCHUS: A randomised non-comparative phase II study of neoadjuvant chemotherapy (NACT) in patients with locally advanced rectal cancer (LARC). *Heliyon,* 4**,** e00804.

Golbraikh, A., Muratov, E., Fourches, D. & Tropsha, A. 2014. Data set modelability by QSAR. *Journal of chemical information and modeling,* 54**,** 1-4.

Goodnight, J. A., Mischak, H., Kolch, W. & Mushinski, J. F. 1995. Immunocytochemical localization of eight protein kinase C isozymes overexpressed in NIH 3T3 fibroblasts. Isoform-specific association with microfilaments, Golgi, endoplasmic reticulum, and nuclear and cell membranes. *The Journal of biological chemistry,* 270**,** 9991-10001.

Gordon, M. T., Ziemba, B. P. & Falke, J. J. 2021. Single-molecule studies reveal regulatory interactions between master kinases PDK1, AKT1, and PKC. *Biophysical journal,* 120**,** 5657-5673.

Goto, S., Nishioka, T. & Kanehisa, M. 2000. LIGAND: chemical database of enzyme reactions. *Nucleic Acids Res,* 28**,** 380-2.

Grant, B. J., Lukman, S., Hocker, H. J., Sayyah, J., Brown, J. H., Mccammon, J. A. & Gorfe, A. A. 2011. Novel allosteric sites on Ras for lead generation. *PloS one,* 6**,** e25711.

Grest, G. S. & Kremer, K. 1986. Molecular dynamics simulation for polymers in the presence of a heat bath. *Physical Review A,* 33**,** 3628-3628.

Grommes, C., Landreth, G. E. & Heneka, M. T. 2004. Antineoplastic effects of peroxisome proliferatoractivated receptor γ agonists. *The lancet oncology,* 5**,** 419-429.

Guedes, I. A., De Magalhães, C. S. & Dardenne, L. E. 2014. Receptor-ligand molecular docking. *Biophysical reviews,* 6**,** 75-87.

Guo, N., Xiao, Y., Chen, D. & Wang, J. 2020. Antiproliferative effects of Norartocarpetin isoflavone in human lung carcinoma cells are mediated via targeting Ras/Raf/MAPK signalling pathway, mitochondrial mediated apoptosis, S-phase cell cycle arrest and suppression of cell migration and invasion. *Journal of B.U.ON. : official journal of the Balkan Union of Oncology,* 25**,** 855-861.

Guvench, O. & Mackerell, A. D., Jr. 2008. Comparison of protein force fields for molecular dynamics simulations. *Methods in molecular biology (Clifton, N.J.),* 443**,** 63-88.

Hakulinen, J. K., Hering, J., Brändén, G., Chen, H., Snijder, A., Ek, M. & Johansson, P. 2017. MraY-antibiotic complex reveals details of tunicamycin mode of action. *Nature chemical biology,* 13**,** 265-267.

Hamaguchi, J., Nakagawa, H., Takahashi, M., Kudo, T., Kamiyama, N., Sun, B., Oshima, T., Sato, Y., Deguchi, K., Todo, S. & Nishimura, S. 2007. Swainsonine reduces 5-fluorouracil tolerance in the multistage resistance of colorectal cancer cell lines. *Molecular cancer,* 6**,** 58.

Han, D. P., Zhu, Q. L., Cui, J. T., Wang, P. X., Qu, S., Cao, Q. F., Zong, Y. P., Feng, B., Zheng, M. H. & Lu, A. G. 2012. Polo-like kinase 1 is overexpressed in colorectal cancer and participates in the migration and invasion of colorectal cancer cells. *Medical science monitor : international medical journal of experimental and clinical research,* 18**,** Br237-46.

Handerson, T., Camp, R., Harigopal, M., Rimm, D. & Pawelek, J. 2005. Beta1,6-branched oligosaccharides are increased in lymph node metastases and predict poor outcome in breast carcinoma. *Clinical cancer research : an official journal of the American Association for Cancer Research,* 11**,** 2969-73.

Hannigan, B. M., Barnett, Y. A., Armstrong, D. B., Mckelvey-Martin, V. J. & Mckenna, P. G. 1993. Thymidine kinases: the enzymes and their clinical usefulness. *Cancer biotherapy,* 8**,** 189-97.

Harada, S. & Morlote, D. 2020. Molecular pathology of colorectal cancer. *Advances in anatomic pathology,* 27**,** 20-26.

He, B., Wang, Y., Zheng, Y., Chen, W. & Zhu, Q. 2013. Synthesis and cytotoxic evaluation of acylated brefeldin a derivatives as potential anticancer agents. *Chemical biology & drug design,* 82**,** 307-16.

He, E., Xu, X. H., Guan, H., Chen, Y., Chen, Z. H., Pan, Z. L., Tang, L. L., Hu, G. Z., Li, Y., Zhang, M., Zhou, J., Eriksson, S., Fornander, T. & Skog, S. 2010. Thymidine kinase 1 is a potential marker for prognosis and monitoring the response to treatment of patients with breast, lung, and esophageal cancer and non-Hodgkin's lymphoma. *Nucleosides, nucleotides & nucleic acids,* 29**,** 352-8.

He, S., Li, Q., Huang, Q. & Cheng, J. 2022. Targeting protein kinase C for cancer therapy. *Cancers,* 14**,** 1104-1104.

Heasley, B. J. C. O. C. 2014. Recent developments in the stereocontrolled synthesis of highly substituted cyclopentane core structures: from drug discovery research to natural product synthesis. 18**,** 641-686.

Helenius, A. & Aebi, M. 2001. Intracellular functions of N-linked glycans. *Science (New York, N.Y.),* 291**,** 2364-9.

Helenius, A. & Aebi, M. 2004. Roles of N-linked glycans in the endoplasmic reticulum. *Annual review of biochemistry,* 73**,** 1019-49.

Henry, N. L. & Hayes, D. F. 2012. Cancer biomarkers. *Molecular oncology,* 6**,** 140-146.

Hernandez-Quiles, M., Broekema, M. F. & Kalkhoven, E. 2021. PPARgamma in metabolism, immunity, and cancer: unified and diverse mechanisms of action. *Frontiers in endocrinology,* 12**,** 624112.

Herzog, F., Primorac, I., Dube, P., Lenart, P., Sander, B., Mechtler, K., Stark, H. & Peters, J. M. 2009. Structure of the anaphase-promoting complex/cyclosome interacting with a mitotic checkpoint complex. *Science (New York, N.Y.),* 323**,** 1477-81.

Ho, W. L., Hsu, W. M., Huang, M. C., Kadomatsu, K. & Nakagawara, A. 2016. Protein glycosylation in cancers and its potential therapeutic applications in neuroblastoma. *Journal of hematology & oncology,* 9**,** 100.

Hohenschutz, L. D., Bell, E. A., Jewess, P. J., Leworthy, D. P., Pryce, R. J., Arnold, E. & Clardy, J. 1981. Castanospermine, A 1,6,7,8-tetrahydroxyoctahydroindolizine alkaloid, from seeds of Castanospermum australe. *Phytochemistry,* 20**,** 811-814.

Holst, S., Wuhrer, M. & Rombouts, Y. 2015a. Glycosylation characteristics of colorectal cancer. *Advances in cancer research,* 126**,** 203-56.

Holst, S., Wuhrer, M. & Rombouts, Y. 2015b. Glycosylation characteristics of colorectal cancer. *Advances in cancer research,* 126**,** 203-256.

Hommes, D. W., Peppelenbosch, M. P. & Van Deventer, S. J. 2003. Mitogen activated protein (MAP) kinase signal transduction pathways and novel anti-inflammatory targets. *Gut,* 52**,** 144-51.

Hornberg, J. J., Bruggeman, F. J., Westerhoff, H. V. & Lankelma, J. 2006. Cancer: a Systems Biology disease. *Bio Systems,* 83**,** 81-90.

Horton, J. K. & Tepper, J. E. 2005. Staging of colorectal cancer: past, present, and future. *Clinical colorectal cancer,* 4**,** 302-12.

Hospital, A., Goñi, J. R., Orozco, M. & Gelpí, J. L. 2015. Molecular dynamics simulations: advances and applications. *Advances and applications in bioinformatics and chemistry : AABC,* 8**,** 37-47.

Hossler, P., Mulukutla, B. C. & Hu, W. S. 2007. Systems analysis of N-glycan processing in mammalian cells. *PloS one,* 2**,** e713.

Hou, N., Huo, D. & Dignam, J. J. 2013. Prevention of colorectal cancer and dietary management. *Chinese clinical oncology,* 2**,** 13.

Hou, T., Wang, J., Li, Y. & Wang, W. 2011. Assessing the performance of the MM/PBSA and MM/GBSA methods. 1. The accuracy of binding free energy calculations based on molecular dynamics simulations. *Journal of chemical information and modeling,* 51**,** 69-82.

Høyer-Hansen, M. & Jäättelä, M. 2007. Connecting endoplasmic reticulum stress to autophagy by unfolded protein response and calcium. *Cell death and differentiation,* 14**,** 1576-82.

Hu, G., Zhou, J., Yan, W., Chen, J. & Shen, B. 2013. The topology and dynamics of protein complexes: insights from intra–molecular network theory. *Current Protein and Peptide Science,* 14**,** 121-132.

Hu, P., Li, K., Peng, X., Kan, Y., Li, H., Zhu, Y., Wang, Z., Li, Z., Liu, H. Y. & Cai, D. 2023. Nuclear Receptor PPARα as a Therapeutic Target in Diseases Associated with Lipid Metabolism Disorders. *Nutrients,* 15.

Huang, H., Liu, T., Guo, J., Yu, L., Wu, X., He, Y., Li, D., Liu, J., Zhang, K., Zheng, X. & Goodin, S. 2017. Brefeldin A enhances docetaxel-induced growth inhibition and apoptosis in prostate cancer cells in monolayer and 3D cultures. *Bioorganic & medicinal chemistry letters,* 27**,** 2286-2291.

Huang, Y. & Paul, D. 2007. Effect of molecular weight and temperature on physical aging of thin glassy poly (2, 6-dimethyl-1, 4-phenylene oxide) films. *Journal of Polymer Science Part B: Polymer Physics,* 45**,** 1390-1398.

Hughes, R. C. 2014. Membrane glycoproteins: a review of structure and function.

Hutter, R. V. P. 1987. At last—worldwide agreement on the staging of cancer: presidential address. *Archives of surgery,* 122**,** 1235-1239.

Iarc. 2024. *Colorectal Cancer* [Online]. World Health Organisation. Available: https://www.iarc.who.int/cancer-type/colorectal-cancer/ [Accessed].

Ichikawa, D., Kitamura, K., Tani, N., Nishida, S., Tsurutome, H., Hakomori, S., Ikeda, E., Mutoh, F., Kurioka, H. & Yamagishi, H. 2000. Molecular detection of disseminated cancer cells in the peripheral blood and expression of sialylated antigens in colon cancers. *Journal of surgical oncology,* 75**,** 98-102.

Isakov, N. 2018. Protein kinase C (PKC) isoforms in cancer, tumor promotion and tumor suppression. *Seminars in cancer biology,* 48**,** 36-52.

Itatani, Y., Kawada, K. & Sakai, Y. 2018. Treatment of Elderly Patients with Colorectal Cancer. *BioMed research international,* 2018**,** 2176056.

Itkonen, H. M., Minner, S., Guldvik, I. J., Sandmann, M. J., Tsourlakis, M. C., Berge, V., Svindland, A., Schlomm, T. & Mills, I. G. 2013. O-GlcNAc transferase integrates metabolic pathways to regulate the stability of c-MYC in human prostate cancer cells. *Cancer research,* 73**,** 5277-87.

Jackson, C. L. & Casanova, J. E. 2000. Turning on ARF: the Sec7 family of guanine-nucleotide-exchange factors. *Trends in cell biology,* 10**,** 60-7.

Jafari, M., Laraqui, A., Baba, W., Benmokhtar, S., Zaitouni, S. E., Ali, A. A., Bounaim, A., Moujahid, M., Tanz, R., Mahfoud, T., Sbitti, Y., Annaz, H. E., Abi, R., Tagajdid, M. R., Kochri, S. E., Lahlou, I. A., Hsaini, H. E., Belayachi, L., Benjouad, A., Ichou, M., En-Nya, A. & Ennibi, K. 2022. Prevalence and patterns of mutations in RAS/RAF/MEK/ERK/MAPK signaling pathway in colorectal cancer in North Africa. *BMC cancer,* 22**,** 1142.

Jayaprakash, N. G. & Surolia, A. 2017. Role of glycosylation in nucleating protein folding and stability. *The Biochemical journal,* 474**,** 2333-2347.

Jennen, D. G., Gaj, S., Giesbertz, P. J., Van Delft, J. H., Evelo, C. T. & Kleinjans, J. C. 2010. Biotransformation pathway maps in WikiPathways enable direct visualization of drug metabolism related expression changes. *Drug discovery today,* 15**,** 851-8.

Jensen, F. 2017. *Introduction to computational chemistry*, John wiley & sons.

Ji, S., Park, S. Y., Roth, J., Kim, H. S. & Cho, J. W. 2012. O-GlcNAc modification of PPARγ reduces its transcriptional activity. *Biochemical and biophysical research communications,* 417**,** 1158-1163.

Jin, W., Kambara, O., Sasakawa, H., Tamura, A. & Takada, S. 2003. De novo design of foldable proteins with smooth folding funnel: automated negative design and experimental verification. *Structure (London, England : 1993),* 11**,** 581-90.

Jorgensen, W. L. 2004. The many roles of computation in drug discovery. *Science (New York, N.Y.),* 303**,** 1813-8.

Jorgensen, W. L., Maxwell, D. S. & Tirado-Rives, J. 1996. Development and testing of the OPLS all-atom force field on conformational energetics and properties of organic liquids. *Journal of the American Chemical Society,* 118**,** 11225-11236.

Jurjus, A., Eid, A., Al Kattar, S., Zeenny, M. N., Gerges-Geagea, A., Haydar, H., Hilal, A., Oueidat, D., Matar, M., Tawilah, J., Hussein, I. H., Schembri-Wismayer, P., Cappello, F., Tomasello, G., Leone, A. & Jurjus, R. A. 2016. Inflammatory bowel disease, colorectal cancer and type 2 diabetes mellitus: The links. *BBA clinical,* 5**,** 16-24.

Kaler, P., Owusu, B. Y., Augenlicht, L. & Klampfer, L. 2014. The role of STAT1 for crosstalk between fibroblasts and colon cancer cells. *Frontiers in oncology,* 4**,** 88-88.

Kalyaanamoorthy, S. & Chen, Y.-P. P. 2014. Modelling and enhanced molecular dynamics to steer structure-based drug discovery. *Progress in biophysics and molecular biology,* 114**,** 123-136.

Kanehisa, M. 1997. Linking databases and organisms: GenomeNet resources in Japan. *Trends in biochemical sciences,* 22**,** 442-4.

Kanehisa, M. 2019. Toward understanding the origin and evolution of cellular organisms. *Protein science : a publication of the Protein Society,* 28**,** 1947-1951.

Kanehisa, M., Furumichi, M., Tanabe, M., Sato, Y. & Morishima, K. 2017. KEGG: new perspectives on genomes, pathways, diseases and drugs. *Nucleic Acids Res,* 45**,** D353-d361.

Kang, K.-W., Lee, M.-J., Song, J., Jeong, J.-Y., Kim, Y.-K., Lee, C., Kim, T.-H., Kwak, K.-B., Kim, O.-J. & An, H. J. 2014. Overexpression of goosecoid homeobox is associated

with chemoresistance and poor prognosis in ovarian carcinoma. *Oncology reports,* 32**,** 189-198.

Kaprio, T., Satomaa, T., Heiskanen, A., Hokke, C. H., Deelder, A. M., Mustonen, H., Hagström, J., Carpen, O., Saarinen, J. & Haglund, C. 2015. N-glycomic profiling as a tool to separate rectal adenomas from carcinomas. *Molecular & cellular proteomics : MCP,* 14**,** 277-88.

Karplus, M. & Mccammon, J. A. 2002a. Molecular dynamics simulations of biomolecules. *Nature structural biology,* 9**,** 646-52.

Karplus, M. & Mccammon, J. A. 2002b. Molecular dynamics simulations of biomolecules. *Nature structural biology,* 9**,** 646-652.

Karplus, M. & Petsko, G. A. 1990. Molecular dynamics simulations in biology. *Nature,* 347**,** 631-9.

Karunakaran, D., Kockx, M., Owen, D. M., Burnett, J. R., Jessup, W. & Kritharides, L. 2013. Protein kinase C controls vesicular transport and secretion of apolipoprotein E from primary human macrophages. *The Journal of biological chemistry,* 288**,** 5186-97.

Kasi, P. M., Shahjehan, F., Cochuyt, J. J., Li, Z., Colibaseanu, D. T. & Merchea, A. 2019. Rising proportion of young individuals with rectal and colon cancer. *Clinical colorectal cancer,* 18**,** e87-e95.

Katayama, M., Nakano, H., Ishiuchi, A., Wu, W., Oshima, R., Sakurai, J., Nishikawa, H., Yamaguchi, S. & Otsubo, T. 2006. Protein pattern difference in the colon cancer cell lines examined by two-dimensional differential in-gel electrophoresis and mass spectrometry. *Surgery today,* 36**,** 1085-1093.

Kaur, S., Nag, A., Gangenahalli, G. & Sharma, K. 2019. Peroxisome Proliferator Activated Receptor Gamma Sensitizes Non-small Cell Lung Carcinoma to Gamma Irradiation Induced Apoptosis. *Frontiers in genetics,* 10**,** 554.

Ke, P. Y. & Chang, Z. F. 2004. Mitotic degradation of human thymidine kinase 1 is dependent on the anaphase-promoting complex/cyclosome-CDH1-mediated pathway. *Mol Cell Biol,* 24**,** 514-26.

Kelder, T., Van Iersel, M. P., Hanspers, K., Kutmon, M., Conklin, B. R., Evelo, C. T. & Pico, A. R. 2012. WikiPathways: building research communities on biological pathways. *Nucleic acids research,* 40**,** D1301-D1307.

Keranen, L. M. & Newton, A. C. 1997. Ca2+ differentially regulates conventional protein kinase Cs' membrane interaction and activation. *Journal of Biological Chemistry,* 272**,** 25959-25967.

Khowala, S., Verma, D. & Banik, S. P. 2008. BIOMOLECULES:(INTRODUCTION, STRUCTURE & FUNCTION). *Indian Institute of Chemical Biology***,** 3-92.

Kim, E. K. & Choi, E. J. 2010. Pathological roles of MAPK signaling pathways in human diseases. *Biochimica et biophysica acta,* 1802**,** 396-405.

Kim, H. H., Lee, Y., Eun, H. C. & Chung, J. H. 2008. Eicosapentaenoic acid inhibits TNF-alpha-induced matrix metalloproteinase-9 expression in human keratinocytes, HaCaT cells. *Biochemical and biophysical research communications,* 368**,** 343-9.

Kimura, K. & Bugg, T. D. 2003. Recent advances in antimicrobial nucleoside antibiotics targeting cell wall biosynthesis. *Natural product reports,* 20**,** 252-73.

Kitchen, D. B., Decornez, H., Furr, J. R. & Bajorath, J. 2004. Docking and scoring in virtual screening for drug discovery: methods and applications. *Nature reviews. Drug discovery,* 3**,** 935-49.

Klausner, R. D., Donaldson, J. G. & Lippincott-Schwartz, J. 1992. Brefeldin A: insights into the control of membrane traffic and organelle structure. *The Journal of cell biology,* 116**,** 1071-80.

Kobayashi, J., Tauchi, H., Chen, B., Bruma, S., Tashiro, S., Matsuura, S., Tanimoto, K., Chen, D. J. & Komatsu, K. 2009. Histone H2AX participates the DNA damage-induced ATM activation through interaction with NBS1. *Biochemical and biophysical research communications,* 380**,** 752-757.

Korycka-Machała, M., Rumijowska-Galewicz, A. & Dziadek, J. 2005. The effect of ethambutol on mycobacterial cell wall permeability to hydrophobic compounds. *Polish journal of microbiology,* 54**,** 5-11.

Kouroku, Y., Fujita, E., Tanida, I., Ueno, T., Isoai, A., Kumagai, H., Ogawa, S., Kaufman, R. J., Kominami, E. & Momoi, T. 2007. ER stress (PERK/eIF2alpha phosphorylation) mediates the polyglutamine-induced LC3 conversion, an essential step for autophagy formation. *Cell death and differentiation,* 14**,** 230-9.

Kremsreiter, S. M., Kroell, A. H., Weinberger, K. & Boehm, H. 2021. Glycan-Lectin Interactions in Cancer and Viral Infections and How to Disrupt Them. *International journal of molecular sciences,* 22.

Kudryavtseva, A. V., Lipatova, A. V., Zaretsky, A. R., Moskalev, A. A., Fedorova, M. S., Rasskazova, A. S., Shibukhova, G. A., Snezhkina, A. V., Kaprin, A. D. & Alekseev, B. Y. 2016. Important molecular genetic markers of colorectal cancer. *Oncotarget,* 7**,** 53959-53959.

Kuntz, I. D., Blaney, J. M., Oatley, S. J., Langridge, R. & Ferrin, T. E. 1982. A geometric approach to macromolecule-ligand interactions. *Journal of molecular biology,* 161**,** 269-88.

Kuppusamy, P., Govindan, N., Yusoff, M. M. & Ichwan, S. J. A. 2017. Proteins are potent biomarkers to detect colon cancer progression. *Saudi journal of biological sciences,* 24**,** 1212-1221.

Kutmon, M., Lotia, S., Evelo, C. T. & Pico, A. R. 2014. WikiPathways App for Cytoscape: Making biological pathways amenable to network analysis and visualization. *F1000Research,* 3**,** 152.

Kutmon, M., Riutta, A., Nunes, N., Hanspers, K., Willighagen, E. L., Bohler, A., Mélius, J., Waagmeester, A., Sinha, S. R., Miller, R., Coort, S. L., Cirillo, E., Smeets, B., Evelo, C. T. & Pico, A. R. 2016. WikiPathways: capturing the full diversity of pathway knowledge. *Nucleic Acids Res,* 44**,** D488-94.

Lake, D., Corrêa, S. A. & Müller, J. 2016. Negative feedback regulation of the ERK1/2 MAPK pathway. *Cellular and molecular life sciences : CMLS,* 73**,** 4397-4413.

Larsson, D. E., Wickström, M., Hassan, S., Oberg, K. & Granberg, D. 2010. The cytotoxic agents NSC-95397, brefeldin A, bortezomib and sanguinarine induce apoptosis in neuroendocrine tumors in vitro. *Anticancer research,* 30**,** 149-56.

Le Pendu, J., Marionneau, S., Cailleau-Thomas, A., Rocher, J., Le Moullac-Vaidye, B. & Clément, M. 2001. ABH and Lewis histo-blood group antigens in cancer. *APMIS,* 109**,** 9-26.

Le, Q. G. & Kimata, Y. 2021. Multiple ways for stress sensing and regulation of the endoplasmic reticulum-stress sensors. *Cell Structure and Function,* 46**,** 37-49.

Lehle, L., Strahl, S. & Tanner, W. 2006. Protein glycosylation, conserved from yeast to man: a model organism helps elucidate congenital human diseases. *Angewandte Chemie (International ed. in English),* 45**,** 6802-18.

Lehmann, J. M., Moore, L. B., Smith-Oliver, T. A., Wilkison, W. O., Willson, T. M. & Kliewer, S. A. 1995. An antidiabetic thiazolidinedione is a high affinity ligand for peroxisome proliferator-activated receptor gamma (PPAR gamma). *The Journal of biological chemistry,* 270**,** 12953-6.

Lengauer, C., Kinzler, K. W. & Vogelstein, B. 1998. Genetic instabilities in human cancers. *Nature,* 396**,** 643-649.

Lengauer, T. & Rarey, M. 1996. Computational methods for biomolecular docking. *Current opinion in structural biology,* 6**,** 402-406.

Levina, A., Fleming, K. D., Burke, J. E. & Leonard, T. A. 2022. Activation of the essential kinase PDK1 by phosphoinositide-driven trans-autophosphorylation. *Nature communications,* 13**,** 1874.

Lewars, E. 2011. Computational chemistry. *Introduction to the theory and applications of molecular and quantum mechanics,* 318.

Lewars, E. G. 2016. Molecular mechanics. *Computational Chemistry: Introduction to the Theory and Applications of Molecular and Quantum Mechanics***,** 51-99.

Li, B., Kawatkar, S. P., George, S., Strachan, H., Woods, R. J., Siriwardena, A., Moremen, K. W. & Boons, G. J. 2004. Inhibition of Golgi mannosidase II with mannostatin A analogues: synthesis, biological evaluation, and structure-activity relationship studies. *Chembiochem : a European journal of chemical biology,* 5**,** 1220-7.

Li, C., Wang, P., Fu, Z., Li, Y. & Li, S. 2019. Swainsonine inhibits proliferation and collagen synthesis of NIH-3T3 cells by declining miR-21. *Artificial cells, nanomedicine, and biotechnology,* 47**,** 2256-2264.

Li, J. J., Wang, R., Lama, R., Wang, X., Floyd, Z. E., Park, E. A. & Liao, F.-F. 2016a. Ubiquitin ligase NEDD4 regulates PPARγ stability and adipocyte differentiation in 3T3-L1 cells. *Scientific reports,* 6**,** 38550.

Li, R. J., Wang, Y. L., Wang, Q. H., Wang, J. & Cheng, M. S. 2015a. In silico design of human IMPDH inhibitors using pharmacophore mapping and molecular docking approaches. *Computational and mathematical methods in medicine,* 2015**,** 418767.

Li, Y., Li, H., Chan, M. K., Sankaranarayanan, S. & Rouxb, B. 2016b. Methodology of parameterization of molecular mechanics force field from quantum chemistry calculations using genetic algorithm: A case study of methanol. *arXiv preprint arXiv:*. 04188.

Li, Y., Lv, Z., He, G., Wang, J., Zhang, X., Lu, G., Ren, X., Wang, F., Zhu, X., Ding, Y., Liao, W., Ding, Y. & Liang, L. 2015b. The SOX17/miR-371-5p/SOX2 axis inhibits EMT, stem cell properties and metastasis in colorectal cancer. *Oncotarget,* 6**,** 9099-9112.

Lichtenstein, P., Holm, N. V., Verkasalo, P. K., Iliadou, A., Kaprio, J., Koskenvuo, M., Pukkala, E., Skytthe, A. & Hemminki, K. 2000. Environmental and heritable factors in the causation of cancer--analyses of cohorts of twins from Sweden, Denmark, and Finland. *The New England journal of medicine,* 343**,** 78-85.

Lien, C.-F., Chen, S.-J., Tsai, M.-C. & Lin, C.-S. 2021. Potential role of protein kinase C in the pathophysiology of diabetes-associated atherosclerosis. *Frontiers in pharmacology,* 12**,** 716332-716332.

Lien, E. C., Nagiec, M. J. & Dohlman, H. G. 2013. Proper protein glycosylation promotes mitogen-activated protein kinase signal fidelity. *Biochemistry,* 52**,** 115-24.

Lièvre, A., Bachet, J. B., Boige, V., Cayre, A., Le Corre, D., Buc, E., Ychou, M., Bouché, O., Landi, B., Louvet, C., André, T., Bibeau, F., Diebold, M. D., Rougier, P., Ducreux, M., Tomasic, G., Emile, J. F., Penault-Llorca, F. & Laurent-Puig, P. 2008. KRAS mutations as an independent prognostic factor in patients with advanced colorectal cancer treated with cetuximab. *Journal of clinical oncology : official journal of the American Society of Clinical Oncology,* 26**,** 374-9.

Likhachev, I. V., Balabaev, N. K. & Galzitskaya, O. V. 2016. Available instruments for analyzing molecular dynamics trajectories. *The open biochemistry journal,* 10**,** 1-1.

Lin, B., Qing, X., Liao, J. & Zhuo, K. 2020. Role of Protein Glycosylation in Host-Pathogen Interaction. *Cells,* 9.

Lippincott-Schwartz, J., Yuan, L. C., Bonifacino, J. S. & Klausner, R. D. 1989. Rapid redistribution of Golgi proteins into the ER in cells treated with brefeldin A: evidence for membrane cycling from Golgi to ER. *Cell,* 56**,** 801-13.

Lis, H. & Sharon, N. 1993. Protein glycosylation. Structural and functional aspects. *European journal of biochemistry,* 218**,** 1-27.

Lise, M., Belluco, C., Perera, S. P., Patel, R., Thomas, P. & Ganguly, A. 2000. Clinical correlations of alpha2,6-sialyltransferase expression in colorectal cancer patients. *Hybridoma,* 19**,** 281-6.

Little, E., Ramakrishnan, M., Roy, B., Gazit, G. & Lee, A. S. 1994. The glucose-regulated proteins (GRP78 and GRP94): functions, gene regulation, and applications. *Critical reviews in eukaryotic gene expression,* 4**,** 1-18.

Liu, T., Liu, R., Zhang, S., Guo, K., Zhang, Q., Li, W. & Liu, Y. 2017. Sorafenib induced alteration of protein glycosylation in hepatocellular carcinoma cells. *Oncol Lett,* 14**,** 517-524.

Liu, W., Duden, R., Phair, R. D. & Lippincott-Schwartz, J. 2005. ArfGAP1 dynamics and its role in COPI coat assembly on Golgi membranes of living cells. *The Journal of cell biology,* 168**,** 1053-1063.

Lobanov, M. Y., Bogatyreva, N. S. & Galzitskaya, O. V. 2008. Radius of gyration as an indicator of protein structure compactness. *Molecular Biology,* 42**,** 623-628.

Lopes, P. E., Guvench, O. & Mackerell, A. D., Jr. 2015. Current status of protein force fields for molecular dynamics simulations. *Methods in molecular biology (Clifton, N.J.),* 1215**,** 47-71.

Lu, Y., Zhou, Q., Shi, Y., Liu, J., Zhong, F., Hao, X., Li, C., Chen, N. & Wang, W. 2013. SUMOylation of PPARγ by rosiglitazone prevents LPS-induced NCoR degradation mediating down regulation of chemokines expression in renal proximal tubular cells. *PloS one,* 8**,** e79815.

Lu, Z. & Hunter, T. 2018. Metabolic Kinases Moonlighting as Protein Kinases. *Trends in biochemical sciences,* 43**,** 301-310.

Luesch, H. & Paavilainen, V. O. 2020. Natural products as modulators of eukaryotic protein secretion. *Natural product reports,* 37**,** 717-736.

Lv, H., Zhang, S. & Hao, X. 2020. Swainsonine protects H9c2 cells against lipopolysaccharide-induced apoptosis and inflammatory injury via down-regulating miR-429. *Cell cycle (Georgetown, Tex.),* 19**,** 207-217.

Lyne, P. D. 2002. Structure-based virtual screening: an overview. *Drug discovery today,* 7**,** 1047-1055.

Ma, J., Sheridan, R. P., Liaw, A., Dahl, G. E. & Svetnik, V. 2015. Deep neural nets as a method for quantitative structure-activity relationships. *Journal of chemical information and modeling,* 55**,** 263-74.

Macalino, S. J., Gosu, V., Hong, S. & Choi, S. 2015. Role of computer-aided drug design in modern drug discovery. *Archives of pharmacal research,* 38**,** 1686-701.

Mackay, H. J. & Twelves, C. J. 2003. Protein kinase C: a target for anticancer drugs? *Endocrine-related cancer,* 10**,** 389-96.

Mackerell Jr, A. D., Bashford, D., Bellott, M., Dunbrack Jr, R. L., Evanseck, J. D., Field, M. J., Fischer, S., Gao, J., Guo, H. & Ha, S. 1998. All-atom empirical potential for molecular modeling and dynamics studies of proteins. *The journal of physical chemistry B,* 102**,** 3586-3616.

Maguid, S., Fernandez-Alberti, S. & Echave, J. 2008. Evolutionary conservation of protein vibrational dynamics. *Gene,* 422**,** 7-13.

Maguid, S., Fernández-Alberti, S., Parisi, G. & Echave, J. 2006. Evolutionary conservation of protein backbone flexibility. *Journal of molecular evolution,* 63**,** 448-457.

Makrynitsa, G. I., Lykouras, M., Spyroulias, G. A. & Matsoukas, M.-T. 2018. In silico drug design. *eLS***,** 1-7.

Makurat, S., Cournia, Z. & Rak, J. 2021. Inactive-to-active transition of human thymidine kinase 1 revealed by molecular dynamics simulations. *Journal of chemical information and modeling,* 62**,** 142-149.

Makurat, S., Cournia, Z. & Rak, J. 2022. Inactive-to-Active Transition of Human Thymidine Kinase 1 Revealed by Molecular Dynamics Simulations. *Journal of chemical information and modeling,* 62**,** 142-149.

Manco, G., Lacerra, G., Porzio, E. & Catara, G. 2022. ADP-Ribosylation Post-Translational Modification: An Overview with a Focus on RNA Biology and New Pharmacological Perspectives. *Biomolecules,* 12.

Mann, M. & Jensen, O. N. 2003. Proteomic analysis of post-translational modifications. *Nature biotechnology,* 21**,** 255-61.

Mao, C., Yang, Z. Y., Hu, X. F., Chen, Q. & Tang, J. L. 2012. PIK3CA exon 20 mutations as a potential biomarker for resistance to anti-EGFR monoclonal antibodies in KRAS wild-type metastatic colorectal cancer: a systematic review and meta-analysis. *Annals of oncology,* 23**,** 1518-1525.

Marques, I., Colaço, A. R., Costa, P. J., Busschaert, N., Gale, P. A. & Félix, V. 2014. Tris-thiourea tripodal-based molecules as chloride transmembrane transporters: insights from molecular dynamics simulations. *Soft matter,* 10**,** 3608-21.

Martin, H. 2009. Role of PPAR-gamma in inflammation. Prospects for therapeutic intervention by food components. *Mutation Research/Fundamental and Molecular Mechanisms of Mutagenesis,* 669**,** 1-7.

Martinez, A., Robles, C. A., Roper, J. M., Gardner, D. R., Neyaz, M. S., Joelson, N. Z. & Cook, D. 2019. Detection of swainsonine-producing endophytes in Patagonian Astragalus species. *Toxicon : official journal of the International Society on Toxinology,* 171**,** 1-6.

Martínez, L. 2015. Automatic identification of mobile and rigid substructures in molecular dynamics simulations and fractional structural fluctuation analysis. *PloS one,* 10**,** e0119264-e0119264.

Maseras, F. & Morokuma, K. 1995. IMOMM: A new integrated ab initio+ molecular mechanics geometry optimization scheme of equilibrium structures and transition states. *Journal of computational chemistry,* 16**,** 1170-1179.

Matsui, A., Ihara, T., Suda, H., Mikami, H. & Semba, K. 2013. Gene amplification: mechanisms and involvement in cancer. *Biomolecular concepts,* 4**,** 567-582.

Maury, J. J., Chan, K. K., Zheng, L., Bardor, M. & Choo, A. B. 2013. Excess of O-linked N-acetylglucosamine modifies human pluripotent stem cell differentiation. *Stem Cell Res,* 11**,** 926-37.

Mccabe, M., Perner, Y., Magobo, R., Mirza, S. & Penny, C. 2020. Descriptive epidemiological study of South African colorectal cancer patients at a Johannesburg Hospital Academic

institution. *JGH open : an open access journal of gastroenterology and hepatology,* 4**,** 360-367.

Mccubrey, J. A., Lahair, M. M. & Franklin, R. A. 2006. Reactive oxygen species-induced activation of the MAP kinase signaling pathways. *Antioxidants & redox signaling,* 8**,** 1775-89.

Mcintosh, G. H. 2008. Influence of selenised dairy proteins on biomarkers of colon cancer risk. *Nutrition & Dietetics,* 65**,** S33-S36.

Medina-Gomez, G., Gray, S. & Vidal-Puig, A. 2007. Adipogenesis and lipotoxicity: role of peroxisome proliferator-activated receptor γ (PPARγ) and PPARγcoactivator-1 (PGC1). *Public health nutrition,* 10**,** 1132-1137.

Meggio, F. & Pinna, L. A. 2003. One-thousand-and-one substrates of protein kinase CK2? *FASEB journal : official publication of the Federation of American Societies for Experimental Biology,* 17**,** 349-68.

Mehta, S., Johnson, R. J. & Schofield, P. F. 1994. Staging of colorectal cancer. *Clinical radiology,* 49**,** 515-523.

Meldrum, N. U. & Roughton, F. J. 1933. Carbonic anhydrase. Its preparation and properties. *The Journal of physiology,* 80**,** 113-42.

Meller, J. 2001. Molecular dynamics. *Encyclopedia of life sciences,* 18.

Meng, X. Y., Zhang, H. X., Mezei, M. & Cui, M. 2011. Molecular docking: a powerful approach for structure-based drug discovery. *Current computer-aided drug design,* 7**,** 146-57.

Mereiter, S., Balmaña, M., Campos, D., Gomes, J. & Reis, C. A. 2019. Glycosylation in the era of cancer-targeted therapy: where are we heading? *Cancer cell,* 36**,** 6-16.

Meyer, B. & Möller, H. 2007. *Conformation of glycopeptides and glycoproteins,* Springer.

Miao, Y., Zhang, C., Yang, L., Zeng, X., Hu, Y., Xue, X., Dai, Y. & Wei, Z. 2022. The activation of PPARγ enhances Treg responses through up-regulating CD36/CPT1-mediated fatty acid oxidation and subsequent N-glycan branching of TβRII/IL-2Rα. *Cell Communication and Signaling,* 20**,** 48.

Mishanina, T. V., Koehn, E. M. & Kohen, A. 2012. Mechanisms and inhibition of uracil methylating enzymes. *Bioorganic chemistry,* 43**,** 37-43.

Mitra, N., Sinha, S., Ramya, T. N. & Surolia, A. 2006. N-linked oligosaccharides as outfitters for glycoprotein folding, form and function. *Trends in biochemical sciences,* 31**,** 156-63.

Miyake, H., Hara, I., Arakawa, S. & Kamidono, S. 2000. Stress protein GRP78 prevents apoptosis induced by calcium ionophore, ionomycin, but not by glycosylation inhibitor, tunicamycin, in human prostate cancer cells. *Journal of cellular biochemistry,* 77**,** 396-408.

Miyoshi, E., Terao, M. & Kamada, Y. 2012. Physiological roles of N-acetylglucosaminyltransferase V(GnT-V) in mice. *BMB reports,* 45**,** 554-9.

Montanari, F., Knasmüller, B., Kohlbacher, S., Hillisch, C., Baierová, C., Grandits, M. & Ecker, G. F. 2019. Vienna LiverTox Workspace-A Set of Machine Learning Models for Prediction of Interactions Profiles of Small Molecules With Transporters Relevant for Regulatory Agencies. *Frontiers in chemistry,* 7**,** 899.

Moon, J. L., Kim, S. Y., Shin, S. W. & Park, J. W. 2012. Regulation of brefeldin A-induced ER stress and apoptosis by mitochondrial $NADP^+$-dependent isocitrate dehydrogenase. *Biochemical and biophysical research communications,* 417**,** 760-4.

Moonsamy, S., Bhakat, S., Walker, R. C. & Soliman, M. E. S. 2016. Single active site mutation causes serious resistance of HIV reverse transcriptase to lamivudine: insight from multiple molecular dynamics simulations. *Cell biochemistry and biophysics,* 74**,** 35-48.

Moraitakis, G., Purkiss, A. G. & Goodfellow, J. M. 2003. Simulated dynamics and biological macromolecules. *Reports on Progress in Physics,* 66**,** 383-383.

Morita, R., Nishizawa, S., Torigoe, T., Takahashi, A., Tamura, Y., Tsukahara, T., Kanaseki, T., Sokolovskaya, A., Kochin, V. & Kondo, T. 2014. Heat shock protein DNAJB 8 is a novel target for immunotherapy of colon cancer-initiating cells. *Cancer science,* 105**,** 389-395.

Mosior, M. & Newton, A. C. 1998. Mechanism of the apparent cooperativity in the interaction of protein kinase C with phosphatidylserine. *Biochemistry,* 37**,** 17271-9.

Nadendla, R. R. 2004. Molecular modeling: A powerful tool for drug design and molecular docking. *Resonance,* 9**,** 51-60.

Nair, P. C., Malde, A. K., Drinkwater, N. & Mark, A. E. 2012. Missing fragments: detecting cooperative binding in fragment-based drug design. *ACS medicinal chemistry letters,* 3**,** 322-6.

Najdi, R., Holcombe, R. F. & Waterman, M. L. 2011. Wnt signaling and colon carcinogenesis: beyond APC. *Journal of carcinogenesis,* 10.

Nakamura, K., Furugori, E., Esaki, Y., Arai, T., Sawabe, M., Okayasu, I., Fujiwara, M., Kammori, M., Mafune, K., Kato, M., Oshimura, M., Sasajima, K. & Takubo, K. 2000.

Correlation of telomere lengths in normal and cancers tissue in the large bowel. *Cancer letters,* 158**,** 179-84.

Nakashima, S. 2002. Protein kinase C alpha (PKC alpha): regulation and biological function. *Journal of biochemistry,* 132**,** 669-75.

Namsa-Aid, M., Wiyakrutta, S., Prachya, S., Namsa-Aid, A. & Suksamrarn, A. 2021. Structural modification of the macrolide brefeldin a to analogues with enhanced cytotoxicity against KB cells. *Trends in Sciences,* 18**,** 44-44.

Nan, D. & Zhang, X. Prediction of hot regions in protein-protein interactions based on complex network and community detection. 2013 2013. IEEE, 17-23.

Naveja, J. J. & Medina-Franco, J. L. 2019. Finding Constellations in Chemical Space Through Core Analysis. *Frontiers in chemistry,* 7**,** 510.

Ndagi, U., Mhlongo, N. N. & Soliman, M. E. 2017. The impact of Thr91 mutation on c-Src resistance to UM-164: molecular dynamics study revealed a new opportunity for drug design. *Molecular bioSystems,* 13**,** 1157-1171.

Nebenführ, A., Ritzenthaler, C. & Robinson, D. G. 2002. Brefeldin A: deciphering an enigmatic inhibitor of secretion. *Plant physiology,* 130**,** 1102-8.

Network, C. G. A. 2012. Comprehensive molecular characterization of human colon and rectal cancer. *Nature,* 487**,** 330-330.

Newton, A. C. 2018. Protein kinase C: perfectly balanced. *Crit Rev Biochem Mol Biol,* 53**,** 208-230.

Nguyen, M., Folkman, J. & Bischoff, J. 1992. 1-Deoxymannojirimycin inhibits capillary tube formation in vitro. Analysis of N-linked oligosaccharides in bovine capillary endothelial cells. *The Journal of biological chemistry,* 267**,** 26157-65.

Nicholls, R. J., Mason, A. Y., Morson, B. C., Dixon, A. K. & Fry, I. K. 1982. The clinical staging of rectal cancer. *Journal of British Surgery,* 69**,** 404-409.

Nishimura, D. 2001. BioCarta. *Biotech Software Internet Report: The Computer Software Journal for Scient,* 2**,** 117-120.

Norberg, J. & Nilsson, L. 2002. Molecular dynamics applied to nucleic acids. *Accounts of chemical research,* 35**,** 465-472.

O'neill, K., Zhang, F., Li, H., Fuja, D. & Murray, B. 2007. Thymidine kinase 1–a prognostic and diagnostic indicator in ALL and AML patients. *Leukemia,* 21**,** 560-563.

Oakes, S. A. 2020. Endoplasmic reticulum stress signaling in cancer cells. *The American journal of pathology,* 190**,** 934-946.

Ochi, Y., Atsumi, S., Aoyagi, T. & Umezawa, K. 1993. Inhibition of tumor cell invasion in the Boyden chamber assay by a mannosidase inhibitor, mannostatin A. *Anticancer research,* 13**,** 1421-4.

Oda, K., Fujiwara, T. & Ikehara, Y. 1990. Brefeldin A arrests the intracellular transport of viral envelope proteins in primary cultured rat hepatocytes and HepG2 cells. *The Biochemical journal,* 265**,** 161-7.

Ogata, H., Goto, S., Sato, K., Fujibuchi, W., Bono, H. & Kanehisa, M. 1999. KEGG: Kyoto Encyclopedia of Genes and Genomes. *Nucleic Acids Res,* 27**,** 29-34.

Ohtsubo, K. & Marth, J. D. 2006. Glycosylation in cellular mechanisms of health and disease. *Cell,* 126**,** 855-67.

Olszewska, E., Borzym-Kluczyk, M., Rzewnicki, I., Wojtowicz, J., Rogowski, M., Pietruski, J. K., Czajkowska, A. & Sieskiewicz, A. 2012. Possible role of α-mannosidase and β-galactosidase in larynx cancer. *Contemporary oncology (Poznan, Poland),* 16**,** 154-8.

Ondrey, F. 2009. Peroxisome proliferator-activated receptor γ pathway targeting in carcinogenesis: implications for chemoprevention. *Clinical Cancer Research,* 15**,** 2-8.

Oostenbrink, C., Villa, A., Mark, A. E. & Van Gunsteren, W. F. 2004. A biomolecular force field based on the free enthalpy of hydration and solvation: the GROMOS force-field parameter sets 53A5 and 53A6. *Journal of computational chemistry,* 25**,** 1656-1676.

Orth, J. D., Thiele, I. & Palsson, B. 2010. What is flux balance analysis? *Nature biotechnology,* 28**,** 245-8.

Osuga, T., Takimoto, R., Ono, M., Hirakawa, M., Yoshida, M., Okagawa, Y., Uemura, N., Arihara, Y., Sato, Y., Tamura, F., Sato, T., Iyama, S., Miyanishi, K., Takada, K., Hayashi, T., Kobune, M. & Kato, J. 2016. Relationship Between Increased Fucosylation and Metastatic Potential in Colorectal Cancer. *Journal of the National Cancer Institute,* 108.

Ouakrim, D. A., Pizot, C., Boniol, M., Malvezzi, M., Boniol, M., Negri, E., Bota, M., Jenkins, M. A., Bleiberg, H. & Autier, P. 2015. Trends in colorectal cancer mortality in Europe: retrospective analysis of the WHO mortality database. *BMJ (Clinical research ed.),* 351.

Oubaddou, Y., Oukabli, M., Fenniche, S., Elktaibi, A., Elochi, M. R., Al Bouzidi, A., Qmichou, Z., Dakka, N., Diorio, C., Richter, A., Bakri, Y. & Ameziane El Hassani, R. 2023. BRCA1 Promoter Hypermethylation in Malignant Breast Tumors and in the Histologically Normal Adjacent Tissues to the Tumors: Exploring Its Potential as a Biomarker and Its Clinical Significance in a Translational Approach. *Genes,* 14.

Paek, S. M. 2018. Recent Synthesis and Discovery of Brefeldin A Analogs. *Marine drugs,* 16.

Pagadala, N. S., Syed, K. & Tuszynski, J. 2017. Software for molecular docking: a review. *Biophysical reviews,* 9**,** 91-102.

Pan, L. & Patterson, J. C. 2013. Molecular dynamics study of Zn (aβ) and Zn (aβ) 2. *PloS one,* 8**,** e70681-e70681.

Pancione, M., Sabatino, L., Fucci, A., Carafa, V., Nebbioso, A., Forte, N., Febbraro, A., Parente, D., Ambrosino, C. & Normanno, N. 2010. Epigenetic silencing of peroxisome proliferator-activated receptor γ is a biomarker for colorectal cancer progression and adverse patients' outcome. *PloS one,* 5**,** e14229.

Papoian, G. A., Ulander, J., Eastwood, M. P., Luthey-Schulten, Z. & Wolynes, P. G. 2004. Water in protein structure prediction. *Proceedings of the National Academy of Sciences of the United States of America,* 101**,** 3352-7.

Parasuraman, S. 2011. Toxicological screening. *Journal of pharmacology & pharmacotherapeutics,* 2**,** 74-9.

Pérez-Pérez, M. J., Priego, E. M., Hernández, A. I., Familiar, O., Camarasa, M. J., Negri, A., Gago, F. & Balzarini, J. 2008. Structure, physiological role, and specific inhibitors of human thymidine kinase 2 (TK2): present and future. *Medicinal research reviews,* 28**,** 797-820.

Phillips, J. C., Braun, R., Wang, W., Gumbart, J., Tajkhorshid, E., Villa, E., Chipot, C., Skeel, R. D., Kalé, L. & Schulten, K. 2005. Scalable molecular dynamics with NAMD. *Journal of computational chemistry,* 26**,** 1781-802.

Pico, A. R., Kelder, T., Van Iersel, M. P., Hanspers, K., Conklin, B. R. & Evelo, C. 2008. WikiPathways: pathway editing for the people. *PLoS biology,* 6**,** e184.

Pili, R., Chang, J., Partis, R. A., Mueller, R. A., Chrest, F. J. & Passaniti, A. 1995. The alpha-glucosidase I inhibitor castanospermine alters endothelial cell glycosylation, prevents angiogenesis, and inhibits tumor growth. *Cancer research,* 55**,** 2920-6.

Pinho, S. S. & Reis, C. A. 2015. Glycosylation in cancer: mechanisms and clinical implications. *Nature Reviews Cancer,* 15**,** 540-555.

Pino, M. S. & Chung, D. C. 2010. The chromosomal instability pathway in colon cancer. *Gastroenterology,* 138**,** 2059-2072.

Pirro, M. 2018. Gl coproteomics-based signatures of cancer cell lines. *J chemistry,* 399**,** 649-659.

Podolsky, D. K. 1999. Inflammatory bowel disease 1999: present and future promises. *Current opinion in gastroenterology,* 15**,** 283-4.

Pommepuy, I., Terro, F., Petit, B., Trimoreau, F., Bellet, V., Robert, S., Hugon, J., Labrousse, F. & Yardin, C. 2003. Brefeldin A induces apoptosis and cell cycle blockade in glioblastoma cell lines. *Oncology,* 64**,** 459-67.

Price, N. P. & Tsvetanova, B. 2007. Biosynthesis of the tunicamycins: a review. *The Journal of antibiotics,* 60**,** 485-91.

Prieto-Martínez, F. D., Arciniega, M. & Medina-Franco, J. L. 2018. Molecular docking: current advances and challenges. *TIP. Revista especializada en ciencias químico-biológi cas,* 21.

Qin, L., Wang, Z., Tao, L. & Wang, Y. 2010. ER stress negatively regulates AKT/TSC/mTOR pathway to enhance autophagy. *Autophagy,* 6**,** 239-47.

Qiu, W., Zhou, G., Zhai, Y., Zhang, X., Xie, W., Zhang, H., Yang, H., Zhi, L., Yuan, X., Zhang, X. & He, F. 2008. No association of MMP-7, MMP-8, and MMP-21 polymorphisms with the risk of hepatocellular carcinoma in a Chinese population. *Cancer epidemiology, biomarkers & prevention : a publication of the American Association for Cancer Research, cosponsored by the American Society of Preventive Oncology,* 17**,** 2514-8.

Radovic, T. 2022. History of in silico biology.

Rangel-Angarita, V. & Malaker, S. A. 2021. Mucinomics as the Next Frontier of Mass Spectrometry. *ACS chemical biology,* 16**,** 1866-1883.

Raposo, C. D., Canelas, A. B. & Barros, M. T. 2021. Human Lectins, Their Carbohydrate Affinities and Where to Find Them. *Biomolecules,* 11.

Ratti, E. & Trist, D. 2001. Continuing evolution of the drug discovery process in the pharmaceutical industry. *Pure applied chemistry,* 73**,** 67-75.

Rawla, P., Barsouk, A., Hadjinicolaou, A. V. & Barsouk, A. 2019a. Immunotherapies and targeted therapies in the treatment of metastatic colorectal cancer. *Medical sciences,* 7**,** 83-83.

Rawla, P., Sunkara, T. & Barsouk, A. 2019b. Epidemiology of colorectal cancer: incidence, mortality, survival, and risk factors. *Gastroenterology Review/Przegląd Gastroenterologiczny,* 14**,** 89-103.

Reily, C., Stewart, T. J., Renfrow, M. B. & Novak, J. 2019. Glycosylation in health and disease. *Nature reviews. Nephrology,* 15**,** 346-366.

Reinhardt, R. & Leonard, T. A. 2023. A critical evaluation of protein kinase regulation by activation loop autophosphorylation. *Elife,* 12.

Rillahan, C. D., Antonopoulos, A., Lefort, C. T., Sonon, R., Azadi, P., Ley, K., Dell, A., Haslam, S. M. & Paulson, J. C. 2012. Global metabolic inhibitors of sialyl- and fucosyltransferases remodel the glycome. *Nature chemical biology,* 8**,** 661-8.

Rizzo, M. A., Shome, K., Vasudevan, C., Stolz, D. B., Sung, T. C., Frohman, M. A., Watkins, S. C. & Romero, G. 1999. Phospholipase D and its product, phosphatidic acid, mediate agonist-dependent raf-1 translocation to the plasma membrane and the activation of the mitogen-activated protein kinase pathway. *The Journal of biological chemistry,* 274**,** 1131-9.

Rodriguez, M. C., Yegorova, S., Pitteloud, J. P., Chavaroche, A. E., André, S., Ardá, A., Minond, D., Jiménez-Barbero, J., Gabius, H. J. & Cudic, M. 2015. Thermodynamic Switch in Binding of Adhesion/Growth Regulatory Human Galectin-3 to Tumor-Associated TF Antigen (CD176) and MUC1 Glycopeptides. *Biochemistry,* 54**,** 4462-74.

Roitsch, T. & Lehle, L. 1989. Structural requirements for protein N-glycosylation. Influence of acceptor peptides on cotranslational glycosylation of yeast invertase and site-directed mutagenesis around a sequon sequence. *European journal of biochemistry,* 181**,** 525-9.

Rosenberg, S., Simeonova, I., Bielle, F., Verreault, M., Bance, B., Le Roux, I., Daniau, M., Nadaradjane, A., Gleize, V., Paris, S., Marie, Y., Giry, M., Polivka, M., Figarella-Branger, D., Aubriot-Lorton, M. H., Villa, C., Vasiljevic, A., Lechapt-Zalcman, E., Kalamarides, M., Sharif, A., Mokhtari, K., Pagnotta, S. M., Iavarone, A., Lasorella, A., Huillard, E. & Sanson, M. 2018. A recurrent point mutation in PRKCA is a hallmark of chordoid gliomas. *Nature communications,* 9**,** 2371.

Roshandel, G., Ghasemi-Kebria, F. & Malekzadeh, R. 2024. Colorectal Cancer: Epidemiology, Risk Factors, and Prevention. *Cancers,* 16.

Roy, S., Narang, B. K., Gupta, M. K., Abbot, V., Singh, V. & Rawal, R. K. 2018. Molecular Docking Studies on Isocytosine Analogues as Xanthine Oxidase Inhibitors. *Drug research,* 68**,** 395-402.

Rubin, G. L., Zhao, Y., Kalus, A. M. & Simpson, E. R. 2000. Peroxisome proliferator-activated receptor γ ligands inhibit estrogen biosynthesis in human breast adipose tissue: possible implications for breast cancer therapy. *Cancer research,* 60**,** 1604-1608.

Ruddon, R. W. & Bedows, E. 1997. Assisted protein folding. *The Journal of biological chemistry,* 272**,** 3125-8.

Rupnarain, C., Dlamini, Z., Naicker, S. & Bhoola, K. 2004. Colon cancer: genomics and apoptotic events. *Biological chemistry,* 385**,** 449-64.

Sabatino, L., Pancione, M., Votino, C., Colangelo, T., Lupo, A., Novellino, E., Lavecchia, A. & Colantuoni, V. 2014. Emerging role of the β-catenin-PPARγ axis in the pathogenesis of colorectal cancer. *World journal of gastroenterology,* 20**,** 7137-7151.

Sakuma, K., Aoki, M. & Kannagi, R. 2012. Transcription factors c-Myc and CDX2 mediate E-selectin ligand expression in colon cancer cells undergoing EGF/bFGF-induced epithelial-mesenchymal transition. *Proceedings of the National Academy of Sciences of the United States of America,* 109**,** 7776-81.

Saleem, S., Tariq, S., Aleem, I., Shaheed, S.-U., Tahseen, M., Atiq, A., Hassan, S., Abu Bakar, M., Khattak, S. & Syed, A. A. 2019. Proteomics analysis of colon cancer progression. *Clinical proteomics,* 16**,** 1-17.

Salgia, M. M., Elix, C. C., Pal, S. K. & Jones, J. O. 2019. Different roles of peroxisome proliferator-activated receptor gamma isoforms in prostate cancer. *American journal of clinical and experimental urology,* 7**,** 98.

Salles, F. T., Hespanhol, A. M., Jaeger, R. G. & Marques, M. M. 2004. Brefeldin-A induces apoptosis in human adenoid cystic carcinoma cultured cells. *Oral oncology,* 40**,** 585-90.

Salmaso, V. & Moro, S. 2018. Bridging Molecular Docking to Molecular Dynamics in Exploring Ligand-Protein Recognition Process: An Overview. *Frontiers in pharmacology,* 9**,** 923.

Santos, L. A., Prandi, I. G. & Ramalho, T. C. 2019. Could Quantum Mechanical Properties Be Reflected on Classical Molecular Dynamics? The Case of Halogenated Organic Compounds of Biological Interest. *Frontiers in chemistry,* 7**,** 848.

Sargsyan, K., Grauffel, C. & Lim, C. 2017. How molecular size impacts RMSD applications in molecular dynamics simulations. *Journal of chemical theory and computation,* 13**,** 1518-1524.

Sastre, J., Aranda, E., Grávalos, C., Massutí, B., Varella-Garcia, M., Rivera, F., Soler, G., Carrato, A., Manzano, J. L. & Díaz-Rubio, E. 2011. First-line single-agent cetuximab in elderly patients with metastatic colorectal cancer. A phase II clinical and molecular study of the Spanish group for digestive tumor therapy (TTD). *Critical reviews in oncology/hematology,* 77**,** 78-84.

Scheper, A. F., Schofield, J., Bohara, R., Ritter, T. & Pandit, A. 2023. Understanding glycosylation: Regulation through the metabolic flux of precursor pathways. *Biotechnology Advances,* 67**,** 108184.

Schjoldager, K. T. & Clausen, H. 2012. Site-specific protein O-glycosylation modulates proprotein processing - deciphering specific functions of the large polypeptide GalNAc-transferase gene family. *Biochimica et biophysica acta,* 1820**,** 2079-94.

Schjoldager, K. T., Narimatsu, Y., Joshi, H. J. & Clausen, H. 2020. Global view of human protein glycosylation pathways and functions. *Nature Reviews Molecular Cell Biology,* 21**,** 729-749.

Schnaar, R. L. 2016. Glycobiology simplified: diverse roles of glycan recognition in inflammation. *Journal of leukocyte biology,* 99**,** 825-38.

Schneikert, J. & Behrens, J. 2007. The canonical Wnt signalling pathway and its APC partner in colon cancer development. *Gut,* 56**,** 417-425.

Schultz, M. J., Holdbrooks, A. T., Chakraborty, A., Grizzle, W. E., Landen, C. N., Buchsbaum, D. J., Conner, M. G., Arend, R. C., Yoon, K. J., Klug, C. A., Bullard, D. C., Kesterson, R. A., Oliver, P. G., O'connor, A. K., Yoder, B. K. & Bellis, S. L. 2016. The Tumor-Associated Glycosyltransferase ST6Gal-I Regulates Stem Cell Transcription Factors and Confers a Cancer Stem Cell Phenotype. *Cancer research,* 76**,** 3978-88.

Schulz-Gasch, T. & Stahl, M. 2003. Binding site characteristics in structure-based virtual screening: evaluation of current docking tools. *Journal of molecular modeling,* 9**,** 47-57.

Schulz, C., Heinemann, V., Schalhorn, A., Moosmann, N., Zwingers, T., Boeck, S., Giessen, C. & Stemmler, H.-J. 2009. UGT1A1 gene polymorphism: impact on toxicity and efficacy of irinotecan-based regimens in metastatic colorectal cancer. *World Journal of Gastroenterology: WJG,* 15**,** 5058-5058.

Scott, R. A., Park, K. & Panitch, A. 2013. Water soluble polymer films for intravascular drug delivery of antithrombotic biomolecules. *European journal of pharmaceutics and biopharmaceutics : official journal of Arbeitsgemeinschaft fur Pharmazeutische Verfahrenstechnik e.V,* 84**,** 125-31.

Seifert, E. 2014. OriginPro 9.1: scientific data analysis and graphing software-software review. *Journal of chemical information and modeling,* 54**,** 1552-1552.

Sethi, M. K., Kim, H., Park, C. K., Baker, M. S., Paik, Y. K., Packer, N. H., Hancock, W. S., Fanayan, S. & Thaysen-Andersen, M. 2015. In-depth N-glycome profiling of paired colorectal cancer and non-tumorigenic tissues reveals cancer-, stage- and EGFR-specific protein N-glycosylation. *Glycobiology,* 25**,** 1064-78.

Sewelam, N., Kazan, K. & Schenk, P. M. 2016. Global Plant Stress Signaling: Reactive Oxygen Species at the Cross-Road. *Frontiers in plant science,* 7**,** 187.

Seyfried, T. N. & Shelton, L. M. 2010. Cancer as a metabolic disease. *Nutrition & metabolism,* 7**,** 7.

Shaker, B., Ahmad, S., Lee, J., Jung, C. & Na, D. 2021. In silico methods and tools for drug discovery. *Computers in biology and medicine,* 137**,** 104851.

Shao, R. G., Shimizu, T. & Pommier, Y. 1996. Brefeldin A is a potent inducer of apoptosis in human cancer cells independently of p53. *Experimental cell research,* 227**,** 190-6.

Sheikh, E., Tran, T., Vranic, S., Levy, A. & Bonfil, R. D. 2022. Role and significance of c-KIT receptor tyrosine kinase in cancer: A review. *Bosnian Journal of Basic Medical Sciences,* 22**,** 683.

Shental-Bechor, D. & Levy, Y. 2008. Effect of glycosylation on protein folding: a close look at thermodynamic stabilization. *Proceedings of the National Academy of Sciences of the United States of America,* 105**,** 8256-61.

Shental-Bechor, D. & Levy, Y. 2009. Folding of glycoproteins: toward understanding the biophysics of the glycosylation code. *Current opinion in structural biology,* 19**,** 524-33.

Shiraishi, T., Yoshida, T., Nakata, S., Horinaka, M., Wakada, M., Mizutani, Y., Miki, T. & Sakai, T. 2005. Tunicamycin enhances tumor necrosis factor–related apoptosis-inducing ligand–induced apoptosis in human prostate cancer cells. *Cancer research,* 65**,** 6364-6370.

Shoichet, B. K., Mcgovern, S. L., Wei, B. & Irwin, J. J. 2002. Lead discovery using molecular docking. *Current opinion in chemical biology,* 6**,** 439-46.

Sidorov, P., Naulaerts, S., Ariey-Bonnet, J., Pasquier, E. & Ballester, P. J. 2019. Predicting Synergism of Cancer Drug Combinations Using NCI-ALMANAC Data. *Frontiers in chemistry,* 7**,** 509.

Silnitsky, S., Rubin, S. J., Zerihun, M. & Qvit, N. 2023. An Update on Protein Kinases as Therapeutic Targets—Part I: Protein Kinase C Activation and Its Role in Cancer and Cardiovascular Diseases. *International journal of molecular sciences,* 24**,** 17600.

Silveira, C. R. F., Cipelli, M., Manzine, C., Rabelo-Santos, S. H., Zeferino, L. C., Rodríguez Rodríguez, G., De Assis, J. B., Hebster, S., Bernadinelli, I., Laginha, F., Boccardo, E., Villa, L. L., Termini, L. & Lepique, A. P. 2019. Swainsonine, an alpha-mannosidase inhibitor, may worsen cervical cancer progression through the increase in myeloid derived suppressor cells population. *PloS one,* 14**,** e0213184.

Singh, E., Underwood, J. M., Nattey, C., Babb, C., Sengayi, M. & Kellett, P. 2015a. South African National Cancer Registry: Effect of withheld data from private health systems

on cancer incidence estimates. *South African medical journal = Suid-Afrikaanse tydskrif vir geneeskunde,* 105**,** 107-9.

Singh, E., Underwood, J. M., Nuttey, C., Babb, C., Sengayi, M. & Kellett, P. 2015b. South African National Cancer Registry: Effect of withheld data from private health systems on cancer incidence estimates. *South African Medical Journal,* 105.

Singleton, V. L., Bohonos, N. & Ullstrup, A. J. 1958. Decumbin, a new compound from a species of Penicillium. *Nature,* 181**,** 1072-3.

Sobhy, M. K., Mowafy, S., Lasheen, D. S., Farag, N. A. & Abouzid, K. a. M. 2019. 3D-QSAR pharmacophore modelling, virtual screening and docking studies for lead discovery of a novel scaffold for VEGFR 2 inhibitors: Design, synthesis and biological evaluation. *Bioorganic chemistry,* 89**,** 102988.

Solá, R. J., Rodríguez-Martínez, J. A. & Griebenow, K. 2007. Modulation of protein biophysical properties by chemical glycosylation: biochemical insights and biomedical implications. *Cellular and molecular life sciences : CMLS,* 64**,** 2133-52.

Song, M. & Giovannucci, E. 2016. Preventable Incidence and Mortality of Carcinoma Associated With Lifestyle Factors Among White Adults in the United States. *JAMA oncology,* 2**,** 1154-61.

Song, Y., Bi, Z., Liu, Y., Qin, F., Wei, Y. & Wei, X. 2023. Targeting RAS-RAF-MEK-ERK signaling pathway in human cancer: Current status in clinical trials. *Genes & diseases,* 10**,** 76-88.

Soobrattee, M. A., Neergheen, V. S., Luximon-Ramma, A., Aruoma, O. I. & Bahorun, T. 2005. Phenolics as potential antioxidant therapeutic agents: mechanism and actions. *Mutation research,* 579**,** 200-13.

Sørensen, D. M., Büll, C., Madsen, T. D., Lira-Navarrete, E., Clausen, T. M., Clark, A. E., Garretson, A. F., Karlsson, R., Pijnenborg, J. F. A., Yin, X., Miller, R. L., Chanda, S. K., Boltje, T. J., Schjoldager, K. T., Vakhrushev, S. Y., Halim, A., Esko, J. D., Carlin, A. F., Hurtado-Guerrero, R., Weigert, R., Clausen, H. & Narimatsu, Y. 2023. Identification of global inhibitors of cellular glycosylation. *Nature communications,* 14**,** 948.

Sousa, S. F., Ribeiro, A. J., Coimbra, J. T., Neves, R. P., Martins, S. A., Moorthy, N. S., Fernandes, P. A. & Ramos, M. J. 2013. Protein-ligand docking in the new millennium--a retrospective of 10 years in the field. *Current medicinal chemistry,* 20**,** 2296-314.

South African National Cancer Registry 2014. Cancer in South Africa. Johannesburg.

Spiro, R. G. 2002. Protein glycosylation: nature, distribution, enzymatic formation, and disease implications of glycopeptide bonds. *Glycobiology,* 12**,** 43r-56r.

Stanley, P. 2011. Golgi glycosylation. *Cold Spring Harb Perspect Biol,* 3.

Stefani, C., Miricescu, D., Stanescu, S., Ii, Nica, R. I., Greabu, M., Totan, A. R. & Jinga, M. 2021. Growth Factors, PI3K/AKT/mTOR and MAPK Signaling Pathways in Colorectal Cancer Pathogenesis: Where Are We Now? *International journal of molecular sciences,* 22.

Stetz, G. & Verkhivker, G. M. 2017. Computational analysis of residue interaction networks and coevolutionary relationships in the Hsp70 chaperones: A community-hopping model of allosteric regulation and communication. *PLoS computational biology,* 13**,** e1005299-e1005299.

Sun, D., Li, H., Cao, M., He, S., Lei, L., Peng, J. & Chen, W. 2020. Cancer burden in China: trends, risk factors and prevention. *Cancer Biology & Medicine,* 17**,** 879-879.

Sun, Y., Wu, T. & Gu, J. 2024. An emerging role of N-glycosylation in cancer chemoresistance. *Carbohydrate research,* 539**,** 109107.

Sundararaj, S., Guo, A., Habibi-Nazhad, B., Rouani, M., Stothard, P., Ellison, M. & Wishart, D. S. 2004. The CyberCell Database (CCDB): a comprehensive, self-updating, relational database to coordinate and facilitate in silico modeling of Escherichia coli. *Nucleic Acids Res,* 32**,** D293-5.

Surani, M. A. 1979. Glycoprotein synthesis and inhibition of glycosylation by tunicamycin in preimplantation mouse embryos: compaction and trophoblast adhesion. *Cell,* 18**,** 217-27.

Takahashi, M., Hasegawa, Y., Maeda, K., Kitano, M. & Taniguchi, N. 2022. Role of glycosyltransferases in carcinogenesis; growth factor signaling and EMT/MET programs. *Glycoconjugate journal,* 39**,** 167-176.

Takano, M. & Sugiyama, T. 2017. UGT1A1 polymorphisms in cancer: impact on irinotecan treatment. *Pharmacogenomics and personalized medicine***,** 61-68.

Taniguchi, N. & Kizuka, Y. 2015. Glycans and cancer: role of N-glycans in cancer biomarker, progression and metastasis, and therapeutics. *Advances in cancer research,* 126**,** 11-51.

Taupin, D. & Podolsky, D. K. 1999. Mitogen-activated protein kinase activation regulates intestinal epithelial differentiation. *Gastroenterology,* 116**,** 1072-80.

Thomas, D., Rathinavel, A. K. & Radhakrishnan, P. 2021. Altered glycosylation in cancer: A promising target for biomarkers and therapeutics. *Biochimica et Biophysica Acta (BBA)-Reviews on Cancer,* 1875**,** 188464-188464.

Tian, K., Xu, F., Gao, X., Han, T., Li, J., Pan, H., Zang, L., Li, D., Li, Z., Uchita, T., Gao, M. & Hua, H. 2017. Nitric oxide-releasing derivatives of brefeldin A as potent and highly selective anticancer agents. *European journal of medicinal chemistry,* 136**,** 131-143.

Tie, J., Cohen, J. D., Lahouel, K., Lo, S. N., Wang, Y., Kosmider, S., Wong, R., Shapiro, J., Lee, M. & Harris, S. 2022. Circulating tumor DNA analysis guiding adjuvant therapy in stage II colon cancer. *New England Journal of Medicine,* 386**,** 2261-2272.

Togawa, A., Ito, H., Kimura, F., Shimizu, H., Ohtsuka, M., Shimamura, F., Yoshidome, H., Katoh, A. & Miyazaki, M. 2003. Establishment of gemcitabine-resistant human pancreatic cancer cells and effect of brefeldin-a on the resistant cell line. *Pancreas,* 27**,** 220-4.

Torii, S., Yamamoto, T., Tsuchiya, Y. & Nishida, E. 2006. ERK MAP kinase in G cell cycle progression and cancer. *Cancer science,* 97**,** 697-702.

Trembley, J. H., Kren, B. T., Afzal, M., Scaria, G. A., Klein, M. A. & Ahmed, K. 2023. Protein kinase CK2 - diverse roles in cancer cell biology and therapeutic promise. *Molecular and cellular biochemistry,* 478**,** 899-926.

Tribukait, B. 2020. Early prediction of pathologic response to neoadjuvant treatment of breast cancer: use of a cell-loss metric based on serum thymidine kinase 1 and tumour volume. *BMC cancer,* 20**,** 1-11.

Tsai, C. S. 2003. *An introduction to computational biochemistry*, John Wiley & Sons.

Tseng, C. N., Huang, C. F., Cho, C. L., Chang, H. W., Huang, C. W., Chiu, C. C. & Chang, Y. F. 2013. Brefeldin a effectively inhibits cancer stem cell-like properties and MMP-9 activity in human colorectal cancer Colo 205 cells. *Molecules (Basel, Switzerland),* 18**,** 10242-53.

Turnbull Jr, R. B., Kyle, K., Watson, F. R. & Spratt, J. 1967. Cancer of the colon: the influence of the no-touch isolation technic on survival rates. *Annals of surgery,* 166**,** 420-420.

Tyagi, S., Gupta, P., Saini, A. S., Kaushal, C. & Sharma, S. 2011. The peroxisome proliferator-activated receptor: A family of nuclear receptors role in various diseases. *Journal of advanced pharmaceutical technology & research,* 2**,** 236.

Ueno, H., Mochizuki, H., Hashiguchi, Y., Shimazaki, H., Aida, S., Hase, K., Matsukuma, S., Kanai, T., Kurihara, H. & Ozawa, K. 2004. Risk factors for an adverse outcome in early invasive colorectal carcinoma. *Gastroenterology,* 127**,** 385-394.

Ulloa-Aguirre, A., Midgley, A. R., Jr., Beitins, I. Z. & Padmanabhan, V. 1995. Follicle-stimulating isohormones: characterization and physiological relevance. *Endocrine reviews,* 16**,** 765-87.

Ulloa-Aguirre, A., Timossi, C., Barrios-De-Tomasi, J., Maldonado, A. & Nayudu, P. 2003. Impact of carbohydrate heterogeneity in function of follicle-stimulating hormone: studies derived from in vitro and in vivo models. *Biology of reproduction,* 69**,** 379-89.

Urra, H., Dufey, E., Avril, T., Chevet, E. & Hetz, C. 2016. Endoplasmic Reticulum Stress and the Hallmarks of Cancer. *Trends in cancer,* 2**,** 252-262.

Vajaria, B. N. & Patel, P. S. 2017. Glycosylation: a hallmark of cancer? *Glycoconjugate journal,* 34**,** 147-156.

Van Cutsem, E., Kohne, C. H., Lang, I., Folprecht, G., Nowacki, M. P., Cascinu, S., Shchepotin, I., Maurel, J., Cunningham, D., Tejpar, S., Schlichting, M., Zubel, A., Celik, I., Rougier, P. & Ciardiello, F. 2011. Cetuximab plus irinotecan, fluorouracil, and leucovorin as first-line treatment for metastatic colorectal cancer: updated analysis of overall survival according to tumor KRAS and BRAF mutation status. *Journal of clinical oncology : official journal of the American Society of Clinical Oncology,* 29**,** 2011-9.

Van Damme, E. J. M. 2022. 35 years in plant lectin research: a journey from basic science to applications in agriculture and medicine. *Glycoconjugate journal,* 39**,** 83-97.

Van Drie, J. H. 2003. Pharmacophore discovery--lessons learned. *Current pharmaceutical design,* 9**,** 1649-64.

Vanommeslaeghe, K., Guvench, O. & Mackerell, A. D., Jr. 2014. Molecular mechanics. *Current pharmaceutical design,* 20**,** 3281-92.

Varki, A. 1993. Biological roles of oligosaccharides: all of the theories are correct. *Glycobiology,* 3**,** 97-130.

Varki, A., Cummings, R. D., Aebi, M., Packer, N. H., Seeberger, P. H., Esko, J. D., Stanley, P., Hart, G., Darvill, A., Kinoshita, T., Prestegard, J. J., Schnaar, R. L., Freeze, H. H., Marth, J. D., Bertozzi, C. R., Etzler, M. E., Frank, M., Vliegenthart, J. F., Lütteke, T., Perez, S., Bolton, E., Rudd, P., Paulson, J., Kanehisa, M., Toukach, P., Aoki-Kinoshita, K. F., Dell, A., Narimatsu, H., York, W., Taniguchi, N. & Kornfeld, S. 2015a. Symbol Nomenclature for Graphical Representations of Glycans. *Glycobiology,* 25**,** 1323-4.

Varki, A., Kannagi, R., Toole, B. & Stanley, P. 2015b. Glycosylation Changes in Cancer. *In:* VARKI, A., CUMMINGS, R. D., ESKO, J. D., STANLEY, P., HART, G. W., AEBI, M., DARVILL, A. G., KINOSHITA, T., PACKER, N. H., PRESTEGARD, J. H., SCHNAAR, R. L. & SEEBERGER, P. H. (eds.) *Essentials of Glycobiology.* Cold Spring Harbor (NY): Cold Spring Harbor Laboratory Press

Copyright 2015-2017 by The Consortium of Glycobiology Editors, La Jolla, California. All rights reserved.

Vasconcelos-Dos-Santos, A., Oliveira, I. A., Lucena, M. C., Mantuano, N. R., Whelan, S. A., Dias, W. B. & Todeschini, A. R. 2015. Biosynthetic Machinery Involved in Aberrant Glycosylation: Promising Targets for Developing of Drugs Against Cancer. *Frontiers in oncology,* 5**,** 138.

Vasudevan, D. & Haltiwanger, R. S. 2014. Novel roles for O-linked glycans in protein folding. *Glycoconjugate journal,* 31**,** 417-26.

Velázquez-Libera, J. L., Rossino, G., Navarro-Retamal, C., Collina, S. & Caballero, J. 2019. Docking, Interaction Fingerprint, and Three-Dimensional Quantitative Structure-Activity Relationship (3D-QSAR) of Sigma1 Receptor Ligands, Analogs of the Neuroprotective Agent RC-33. *Frontiers in chemistry,* 7**,** 496.

Velazquez, E. J., Brindley, T. D., Shrestha, G., Bitter, E. E., Cress, J. D., Townsend, M. H., Berges, B. K., Robison, R. A., Weber, K. S. & O'neill, K. L. 2020. Novel monoclonal antibodies against thymidine kinase 1 and their potential use for the immunotargeting of lung, breast and colon cancer cells. *Cancer Cell Int,* 20**,** 127.

Verma, J., Khedkar, V. M. & Coutinho, E. C. 2010. 3D-QSAR in drug design--a review. *Current topics in medicinal chemistry,* 10**,** 95-115.

Verovski, V. N., Van Den Berge, D. L., Delvaeye, M. M., Scheper, R. J., De Neve, W. J. & Storme, G. A. 1996. Low-level doxorubicin resistance in P-glycoprotein-negative human pancreatic tumour PSN1/ADR cells implicates a brefeldin A-sensitive mechanism of drug extrusion. *British journal of cancer,* 73**,** 596-602.

Very, N., Hardivillé, S., Decourcelle, A., Thévenet, J., Djouina, M., Page, A., Vergoten, G., Schulz, C., Kerr-Conte, J., Lefebvre, T., Dehennaut, V. & El Yazidi-Belkoura, I. 2022. Thymidylate synthase O-GlcNAcylation: a molecular mechanism of 5-FU sensitization in colorectal cancer. *Oncogene,* 41**,** 745-756.

Very, N., Lefebvre, T. & El Yazidi-Belkoura, I. 2018. Drug resistance related to aberrant glycosylation in colorectal cancer. *Oncotarget,* 9**,** 1380-1402.

Villa, A. L. P., Parra, R. S., Feitosa, M. R., Camargo, H. P. D., Machado, V. F., Tirapelli, D. P. D. C., Rocha, J. J. R. D. & Feres, O. 2020. PPARG expression in colorectal cancer and its association with staging and clinical evolution. *Acta cirurgica brasileira,* 35.

Vogelstein, B. & Kinzler, K. W. 2015. The path to cancer—three strikes and you're out. *The New England journal of medicine,* 373**,** 1895-1898.

Vogt, A. D. & Di Cera, E. 2012. Conformational selection or induced fit? A critical appraisal of the kinetic mechanism. *Biochemistry,* 51**,** 5894-902.

Wadood, A., Ahmed, N., Shah, L., Ahmad, A., Hassan, H. & Shams, S. J. O. D. D. D. 2013. In-silico drug design: An approach which revolutionarised the drug discovery process. 1**,** 3.

Wallen, E., Sellers, R. G. & Peehl, D. M. 2000. Brefeldin A induces p53-independent apoptosis in primary cultures of human prostatic cancer cells. *The Journal of urology,* 164**,** 836-41.

Walsh, C. T., Garneau-Tsodikova, S. & Gatto, G. J., Jr. 2005. Protein posttranslational modifications: the chemistry of proteome diversifications. *Angewandte Chemie (International ed. in English),* 44**,** 7342-72.

Wan, M. L., Wang, Y., Zeng, Z., Deng, B., Zhu, B. S., Cao, T., Li, Y. K., Xiao, J., Han, Q. & Wu, Q. 2020. Colorectal cancer (CRC) as a multifactorial disease and its causal correlations with multiple signaling pathways. *Bioscience reports,* 40.

Wandall, H. H., Nielsen, M. a. I., King-Smith, S., De Haan, N. & Bagdonaite, I. 2021. Global functions of O-glycosylation: promises and challenges in O-glycobiology. *The FEBS journal,* 288**,** 7183-7212.

Wang, X., Song, K., Li, L. & Chen, L. 2018a. Structure-Based Drug Design Strategies and Challenges. *Current topics in medicinal chemistry,* 18**,** 998-1006.

Wang, X., Wang, Q., Hu, W. & Evers, B. M. 2004. Regulation of phorbol ester-mediated TRAF1 induction in human colon cancer cells through a PKC/RAF/ERK/NF-kappaB-dependent pathway. *Oncogene,* 23**,** 1885-95.

Wang, X., Xiong, W. & Tang, Y. 2018b. Tunicamycin suppresses breast cancer cell growth and metastasis via regulation of the protein kinase B/nuclear factor-κB signaling pathway. *Oncol Lett,* 15**,** 4137-4142.

Wang, Y. J., Wu, Y. F., Xue, F., Wu, Z. X., Xue, Y. P., Zheng, Y. G. & Shen, Y. C. 2012. Isolation of brefeldin A from Eupenicillium brefeldianum broth using macroporous resin adsorption chromatography. *Journal of chromatography. B, Analytical technologies in the biomedical and life sciences,* 895-896**,** 146-53.

Wang, Z., Sun, H., Yao, X., Li, D., Xu, L., Li, Y., Tian, S. & Hou, T. 2016. Comprehensive evaluation of ten docking programs on a diverse set of protein-ligand complexes: the prediction accuracy of sampling power and scoring power. *Physical chemistry chemical physics : PCCP,* 18**,** 12964-75.

Waszczak, C., Carmody, M. & Kangasjärvi, J. 2018. Reactive oxygen species in plant signaling. *Annual review of plant biology,* 69**,** 209-236.

Watch, C. 2018. *FDA approved drugs for oncology* [Online]. [Accessed].

Weagel, E. G., Burrup, W., Kovtun, R., Velazquez, E. J., Felsted, A. M., Townsend, M. H., Ence, Z. E., Suh, E., Piccolo, S. R. & Weber, K. S. 2018. Membrane expression of thymidine kinase 1 and potential clinical relevance in lung, breast, and colorectal malignancies. *Cancer Cell International,* 18**,** 1-14.

Weerapana, E. & Imperiali, B. 2006. Asparagine-linked protein glycosylation: from eukaryotic to prokaryotic systems. *Glycobiology,* 16**,** 91r-101r.

Weisberg, E., Manley, P. W., Breitenstein, W., Brüggen, J., Cowan-Jacob, S. W., Ray, A., Huntly, B., Fabbro, D., Fendrich, G., Hall-Meyers, E., Kung, A. L., Mestan, J., Daley, G. Q., Callahan, L., Catley, L., Cavazza, C., Azam, M., Neuberg, D., Wright, R. D., Gilliland, D. G. & Griffin, J. D. 2005. Characterization of AMN107, a selective inhibitor of native and mutant Bcr-Abl. *Cancer cell,* 7**,** 129-41.

Westermann, P., Knoblich, M., Maier, O., Lindschau, C. & Haller, H. 1996. Protein kinase C bound to the Golgi apparatus supports the formation of constitutive transport vesicles. *The Biochemical journal,* 320 (Pt 2)**,** 651-8.

Wight, T. N., Kinsella, M. G. & Qwarnström, E. E. 1992. The role of proteoglycans in cell adhesion, migration and proliferation. *Current opinion in cell biology,* 4**,** 793-801.

Wisdom, R., Johnson, R. S. & Moore, C. 1999. c-Jun regulates cell cycle progression and apoptosis by distinct mechanisms. *The EMBO journal,* 18**,** 188-97.

Wojtowicz, K., Januchowski, R., Nowicki, M. & Zabel, M. 2015. Inhibition of protein glycosylation reverses the MDR phenotype of cancer cell lines. *Biomedicine & Pharmacotherapy,* 74**,** 49-56.

Wojtowicz, K., Januchowski, R., Sosińska, P., Nowicki, M. & Zabel, M. 2016. Effect of brefeldin A and castanospermine on resistant cell lines as supplements in anticancer therapy. *Oncology reports,* 35**,** 2896-906.

World Health Organization 2018. Lastest global cancer data. 12/9/2018 ed. Geneva, Switerland: International Agency for Research on Cancer.

World Health Organization 2020. WHO report on cancer: setting priorities, investing wisely and providing care for all. *World Health Organization***,** 399-438 (2003).

Wu, D., Wu, P., Huang, Q., Liu, Y., Ye, J. & Huang, J. 2013. Interleukin-17: a promoter in colorectal cancer progression. *Clinical and Developmental Immunology,* 2013.

Wu, J., Chen, S., Liu, H., Zhang, Z., Ni, Z., Chen, J., Yang, Z., Nie, Y. & Fan, D. 2018. Tunicamycin specifically aggravates ER stress and overcomes chemoresistance in multidrug-resistant gastric cancer cells by inhibiting N-glycosylation. *Journal of experimental & clinical cancer research : CR,* 37**,** 272.

Wu, Y., Lou, L. & Xie, Z. R. 2020. A Pilot Study of All-Computational Drug Design Protocol-From Structure Prediction to Interaction Analysis. *Frontiers in chemistry,* 8**,** 81.

Wyrozumska, P., Ashley, J. W., Ramanadham, S., Liu, Q., Garvey, W. T. & Sztul, E. 2014. Novel effects of Brefeldin A (BFA) in signaling through the insulin receptor (IR) pathway and regulating FoxO1-mediated transcription. *Cellular logistics,* 4**,** e27732.

Xia, J. & Wishart, D. S. 2010. MSEA: a web-based tool to identify biologically meaningful patterns in quantitative metabolomic data. *Nucleic Acids Res,* 38**,** W71-7.

Xie, S., Naslavsky, N. & Caplan, S. 2015. Diacylglycerol kinases in membrane trafficking. *Cellular logistics,* 5**,** e1078431.

Xu, J., Zhang, L., Yang, D. L., Li, Q. & He, Z. 2015. Thymidine kinases share a conserved function for nucleotide salvage and play an essential role in Arabidopsis thaliana growth and development. *The New phytologist,* 208**,** 1089-103.

Yadav, R. K., Chae, S.-W., Kim, H.-R. & Chae, H. J. 2014. Endoplasmic reticulum stress and cancer. *Journal of cancer prevention,* 19**,** 75.

Yan, W., Sun, M., Hu, G., Zhou, J., Zhang, W., Chen, J., Chen, B. & Shen, B. 2014. Amino acid contact energy networks impact protein structure and evolution. *Journal of theoretical biology,* 355**,** 95-104.

Yan, X., Liao, C., Liu, Z., Hagler, A. T., Gu, Q. & Xu, J. 2016. Chemical Structure Similarity Search for Ligand-based Virtual Screening: Methods and Computational Resources. *Current drug targets,* 17**,** 1580-1585.

Yardin, C., Terro, F., Esclaire, F., Rigaud, M. & Hugon, J. 1998. Brefeldin A-induced apoptosis is expressed in rat neurons with dephosphorylated tau protein. *Neuroscience letters,* 250**,** 1-4.

Yen, H. Y., Liu, Y. C., Chen, N. Y., Tsai, C. F., Wang, Y. T., Chen, Y. J., Hsu, T. L., Yang, P. C. & Wong, C. H. 2015. Effect of sialylation on EGFR phosphorylation and resistance to tyrosine kinase inhibition. *Proceedings of the National Academy of Sciences of the United States of America,* 112**,** 6955-60.

Yeo, M. K., Kim, J. Y., Seong, I. O., Kim, J. M. & Kim, K. H. 2017. Phosphorylated Protein Kinase C (Zeta/Lambda) Expression in Colorectal Adenocarcinoma and Its Correlation

with Clinicopathologic Characteristics and Prognosis. *Journal of Cancer,* 8**,** 3371-3377.

You, S., Li, W. & Guan, Y. 2018. Tunicamycin inhibits colon carcinoma growth and aggressiveness via modulation of the ERK-JNK-mediated AKT/mTOR signaling pathway. *Molecular medicine reports,* 17**,** 4203-4212.

You, Z., He, L. & Yan, N. 2021. Tunicamycin-Induced Endoplasmic Reticulum Stress Promotes Breast Cancer Cell MDA-MB-231 Apoptosis through Inhibiting Wnt/β-Catenin Signaling Pathway. *Journal of healthcare engineering,* 2021**,** 6394514.

Yuriev, E., Holien, J. & Ramsland, P. A. 2015. Improvements, trends, and new ideas in molecular docking: 2012-2013 in review. *Journal of molecular recognition : JMR,* 28**,** 581-604.

Zhang, B., Li, H., Yu, K. & Jin, Z. 2022a. Molecular docking-based computational platform for high-throughput virtual screening. *CCF transactions on high performance computing,* 4**,** 63-74.

Zhang, C., Ma, S., Hao, X., Wang, Z. & Sun, Z. 2022b. Methylation status of TK1 correlated with immune infiltrates in prostate cancer. *Frontiers in genetics,* 13**,** 899384.

Zhang, J., Anastasiadis, P. Z., Liu, Y., Thompson, E. A. & Fields, A. P. 2004. Protein kinase C (PKC) betaII induces cell invasion through a Ras/Mek-, PKC iota/Rac 1-dependent signaling pathway. *The Journal of biological chemistry,* 279**,** 22118-23.

Zhao, H., Wu, L., Yan, G., Chen, Y., Zhou, M., Wu, Y. & Li, Y. 2021. Inflammation and tumor progression: signaling pathways and targeted intervention. *Signal transduction and targeted therapy,* 6**,** 263.

Zhao, Y., Ando, K., Oki, E., Ikawa-Yoshida, A., Ida, S., Kimura, Y., Saeki, H., Kitao, H., Morita, M. & Maehara, Y. 2014. Aberrations of BUBR1 and TP53 gene mutually associated with chromosomal instability in human colorectal cancer. *Anticancer research,* 34**,** 5421-5427.

Zhou, F., Dong, C., Davis, J. E., Wu, W. H., Surrao, K. & Wu, G. 2015. The mechanism and function of mitogen-activated protein kinase activation by ARF1. *Cell Signal,* 27**,** 2035-2044.

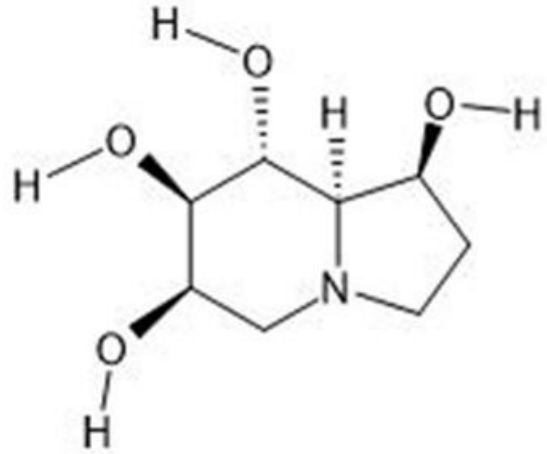
Zhou, L., Gao, W., Wang, K., Huang, Z., Zhang, L., Zhang, Z., Zhou, J., Nice, E. C. & Huang, C. 2019. Brefeldin A inhibits colorectal cancer growth by triggering Bip/Akt-regulated autophagy. *FASEB journal : official publication of the Federation of American Societies for Experimental Biology,* 33**,** 5520-5534.

Zhu, X., Al-Danakh, A., Zhang, L., Sun, X., Jian, Y., Wu, H., Feng, D., Wang, S. & Yang, D. 2022. Glycosylation in Renal Cell Carcinoma: Mechanisms and Clinical Implications. *Cells,* 11.

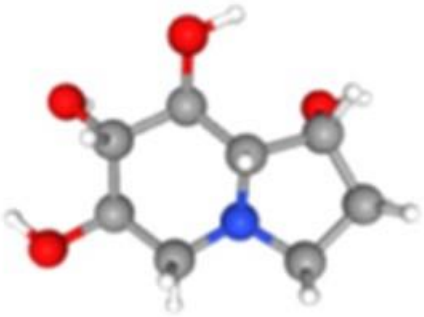
Zinatizadeh, M. R., Zarandi, P. K., Keshavarz-Fathi, M., Yousefi, M. H. & Rezaei, N. 2022. The role of ral signaling and post translational modifications (PTMs) of Ras in cancer. *Genome Instability & Disease,* 3**,** 22-32.

Appendix1: Structures and information of Glycosylation inhibitors in this study

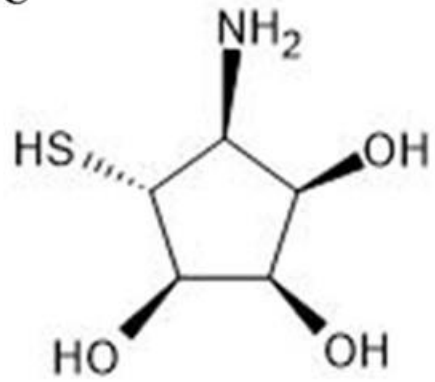
A



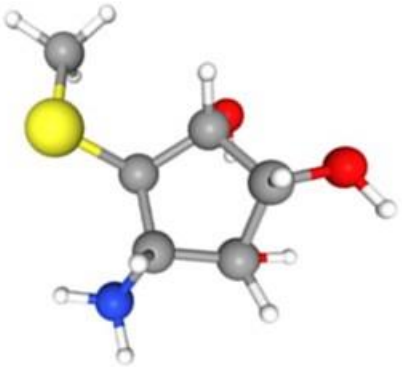
B



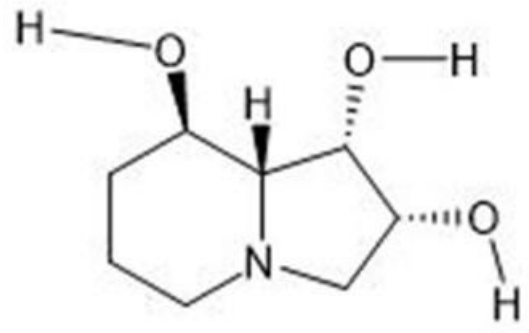
C



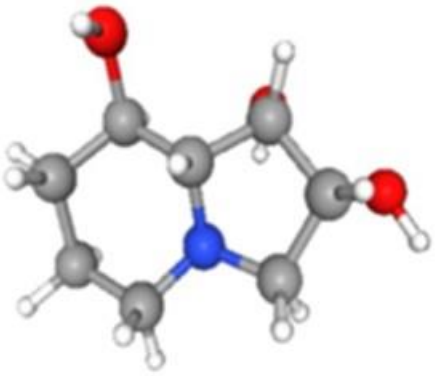
D



E



F



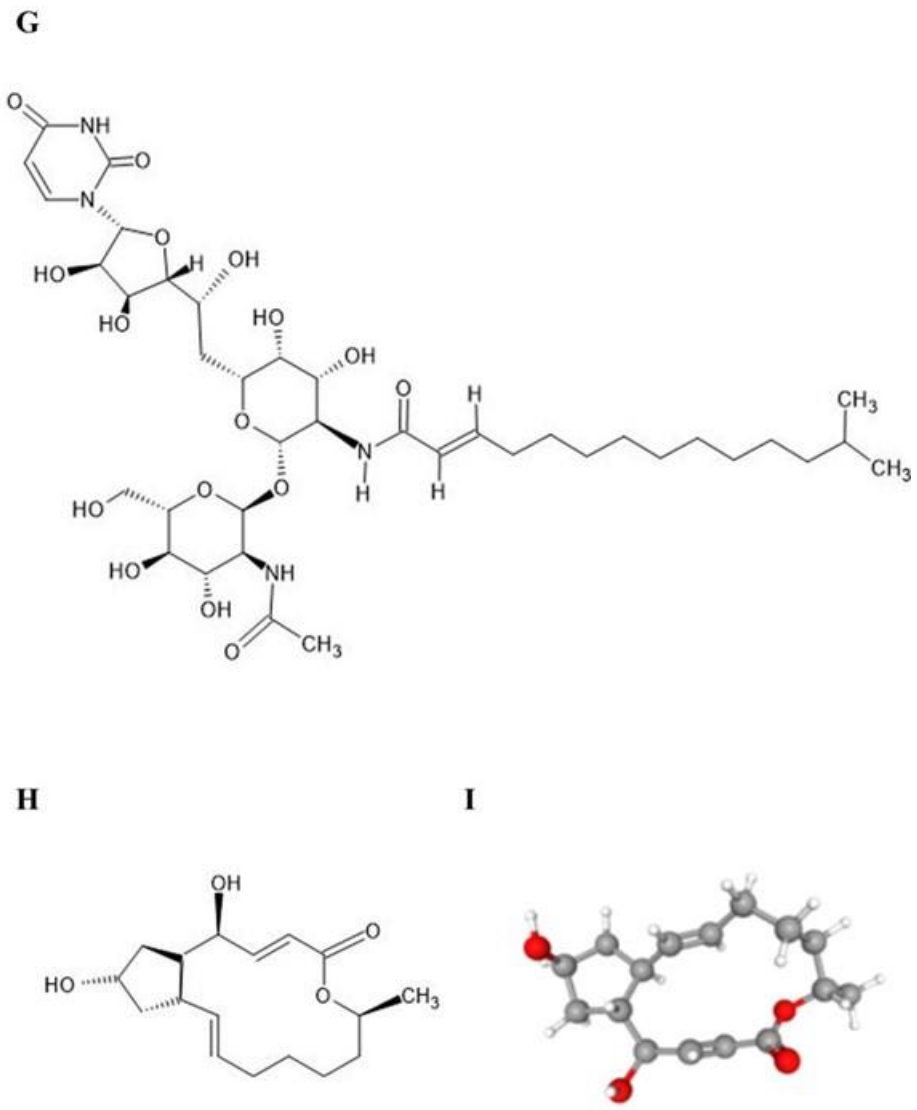


Figure A1: Structure of Glycosylation inhibitors in this study:
(A and B) Castanospermine – [a] 2D structure; [b] 3D structure (PubChem CID: 54445). (C and D) Mannostatin-A – [C] 2D structure; [D] 3D structure (PubChem CID: 124189). (E and F) Chemical structure of Swainsonine – [E] 2D structure; [F] 3D structure (PubChem CID: 51683). (G) Chemical structure of Tunicamycin 2D structure (PubChem CID: 145720586). No 3D structure is available due to there being too many atoms, too flexible, and too many undefined stereocenters. (H and I) Brefeldin A [H] 2D structure; [I] 3D structure (PubChem CID: 5287620). This natural product has a unique trisubstituted cyclopentane skeleton with a 13-membered macrolactone ring containing two trans-alkene moieties (Heasley, 2014).

Table A1.1. Physical properties of various glycosylation inhibitors in this study

Compound Name	Castanospermine	Mannostatin A	Swainsonine	Tunicamycin	Brefeldin A
Molecular Formula	$C_8H_{15}NO_4$	$C_6H_{13}NO_3S$	$C_{38}H_{62}N_4O_{16}$	$C_{38}H_{62}N_4O_{16}$	$C_{16}H_{24}O_4$
Molecular Weight	189.21	179.24	830.9	830.9	280.36
IUPAC Name	((1*S*,6*S*,7*R*,8*R*,8a*R*)-Octahydroindolizine-1,6,7,8-tetro	(1R,2R,3R,4S,5R)-4-amino-5-methylsulfanylcyclo-pentane-1,2,3-triol	(1*S*,2*R*,8*R*,8a*R*)-Octahydroindolizine-1,2,8-trio	(E)-N-[(2S,3R,4R,5R,6R)-2-[(2S,3S,4S,5R,6S)-3-acetamido-4,5-dihydroxy-6-(hydroxymethyl)oxan-2-yl]oxy-6-[(2R)-2-[(2R,3S, 4R,5R)-5-(2,4-dioxo pyrimidin-1-yl)-3,4-dihy droxyoxolan-2-yl]-2-hydr oxyethyl]-4,5-dihydr oxyoxan-3-yl]-13-methyl tetradec-2-enamide	(1R,2R,3E,7S,11E,13S,15S)-2,15-dihydroxy-7-methyl-6-oxabicyclo [11.3.0] hexadeca-3,11-dien-5-one
XLogP3-AA	-2.2	-2	-1.3	0.2	2
Hydrogen Bond Donor Count	4	4	3	11	2
Hydrogen Bond Acceptor Count	5	5	4	16	4
Rotatable Bond Count	0	1	0	20	0
Topological Polar Surface Area	84.2 Å²	112 Å²	63.9 Å²	306 Å²	66.8 Å²
Heavy Atom Count	13	11	12	58	20
Formal Charge	0	0	0	0	0
Complexity	201	146	176	1420	388
Isotope Atom Count	0	0	0	0	0

Defined Atom Stereocenter Count	5	5	4	15	5
Undefined Atom Stereocenter Count	0	0	0	0	0
Defined Bond Stereocenter Count	0	0	0	1	2
Undefined Bond Stereocenter Count	0	0	0	0	0
Covalently Bonded Unit Count	1	1	1	1	1
Compound Is Canonicalized	Yes	Yes	Yes	Yes	Yes

Appendix 2: Docking results

Table A2.1. Docking results of Tunicamycin with protein targets

PDB ID	Protein	Docking Score
2h26	T-cell surface glycoprotein CD1b (CD1B_HUMAN)	11
2r59	Leukotriene A-4 hydrolase (LKHA4_HUMAN)	10.6
2vqq	Histone deacetylase 4 (HDAC4_HUMAN)	10.2
2gvj	Nicotinamide phosphoribosyltransferase (NAMPT_HUMAN)	10.1
1s9i	Dual specificity mitogen-activated protein kinase kinase 2 (MP2K2_HUMAN)	9.9
2po6	T-cell surface glycoprotein CD1d (CD1D_HUMAN)	9.8
2f38	Aldo-keto reductase family 1 member C3 (AK1C3_HUMAN)	9.7
2h44	cGMP-specific 3',5'-cyclic phosphodiesterase (PDE5A_HUMAN)	9.6
2hh5	Cathepsin S (CATS_HUMAN)	9.6
2w4q	Prostaglandin reductase 2 (PTGR2_HUMAN)	9.6
1e9a	Thymidylate kinase (KTHY_HUMAN)	9.5
1ros	Macrophage metalloelastase (MMP12_HUMAN)	9.5
1ohk	Dihydrofolate reductase (DYR_HUMAN)	9.4
1d1j	Profilin-2 (PROF2_HUMAN)	9.2
1egc	Medium-chain specific acyl-CoA dehydrogenase, mitochondrial (ACADM_HUMAN)	9.2
1ezf	Squalene synthetase (FDFT_HUMAN)	9.2
1kkq	Nuclear receptor corepressor 2 (NCOR2_HUMAN)	9.2
1mc5	Alcohol dehydrogenase class-3 (ADHX_HUMAN)	9.2
1t46	Mast/stem cell growth factor receptor (KIT_HUMAN)	9.2
1w78	Bifunctional protein folC (FOLC_ECOLI)	9.2
1wuu	Galactokinase(GALK1_HUMAN)	9.2
2abj	Branched-chain-amino-acid aminotransferase, cytosolic (BCAT1_HUMAN)	9.2
2fv5	ADAM 17 (ADA17_HUMAN)	9.2
2ewy	Beta-secretase 2 (BACE2_HUMAN)	9.1
2nni	Cytochrome P450 2C8 (CP2C8_HUMAN)	9.1
2rjp	A disintegrin and metalloproteinase with thrombospondin motifs 4 (ATS4_HUMAN)	9.1
1ksw	Proto-oncogene tyrosine-protein kinase Src (SRC_HUMAN)	9
1kws	Galactosylgalactosylxylosylprotein 3-beta-glucuronosyltransferase 3	9
1sg0	Ribosyldihydronicotinamide dehydrogenase [quinone] (NQO2_HUMAN)	9
2hi4	Cytochrome P450 1A2 (CP1A2_HUMAN)	9
2w0b	Cytochrome P450 51 (CP51_MYCTU)	9
2wax	Probable ATP-dependent RNA helicase DDX6 (DDX6_HUMAN)	9
1ish	ADP-ribosyl cyclase 2 (BST1_HUMAN)	8.9
1qu3	Isoleucyl-tRNA synthetase (SYI1_STAAU)	8.9
1s9j	Dual specificity mitogen-activated protein kinase kinase 1(MP2K1_HUMAN)	8.9
2fb8	B-Raf proto-oncogene serine/threonine-protein kinase(BRAF1_HUMAN)	8.9
2ovz	Matrix metalloproteinase-9 (MMP9_HUMAN)	8.9
1h22	Acetylcholinesterase (ACES_TORCA)	8.8
1imb	Inositol monophosphatase (IMPA1_HUMAN)	8.8
1onq	T-cell surface glycoprotein CD1a (CD1A_HUMAN)	8.8
1qip	Lactoylglutathione lyase (LGUL_HUMAN)	8.8
1so2	cGMP-inhibited 3',5'-cyclic phosphodiesterase B (PDE3B_HUMAN)	8.8
2nru	Interleukin-1 receptor-associated kinase 4 (IRAK4_HUMAN)	8.8
2x6v	T-box transcription factor TBX5 (TBX5_HUMAN)	8.8
1byg	Tyrosine-protein kinase CSK(CSK_HUMAN)	8.7
1og5	Cytochrome P450 2C9 (CP2C9_HUMAN)	8.7
2c0i	Tyrosine-protein kinase HCK (HCK_HUMAN)	8.7
2e3r	Collagen type IV alpha-3-binding protein (C43BP_HUMAN)	8.7
2oc2	Angiotensin-converting enzyme (ACE_HUMAN)	8.7
2x7h	Zinc-binding alcohol dehydrogenase domain-containing protein 2 (ZADH2_HUMAN)	8.7
3ant	Epoxide hydrolase 2 (HYES_HUMAN)	8.7
1r4l	Angiotensin-converting enzyme 2 (ACE2_HUMAN)	8.6
1zdt	Steroidogenic factor 1 (STF1_HUMAN)	8.6
2bdm	Cytochrome P450 2B4 (CP2B4_RABIT)	8.6
2bil	Proto-oncogene serine/threonine-protein kinase Pim-1 (PIM1_HUMAN)	8.6
2jev	Diamine acetyltransferase 1 (SAT1_HUMAN)	8.6

2q7r	Arachidonate 5-lipoxygenase-activating protein (AL5AP_HUMAN)	8.6
2qg6	Nicotinamide riboside kinase 1(NRK1_HUMAN)	8.6
2vn9	Calcium/calmodulin-dependent protein kinase type II delta chain (KCC2D_HUMAN)	8.6
2woe	ADP-ribosyl-[dinitrogen reductase] glycohydrolase (DRAG_RHORU)	8.6
2xbj	Serine/threonine-protein kinase Chk2 (CHK2_HUMAN)	8.6
1gnj	Serum albumin (ALBU_HUMAN)	8.5
1ogu	Cyclin-A2 (CCNA2_HUMAN)	8.5
1s8c	Heme oxygenase 1 (HMOX1_HUMAN)	8.5
2z65	Lymphocyte antigen 96 Toll-like receptor 4(LY96_HUMAN/TLR4_HUMAN)	8.5
1d4l	Gag-Pol polyprotein (POL_HV1A2)	8.4
1rgy	Beta-lactamase (AMPC_CITFR)	8.4
1rne	Renin (RENI_HUMAN)	8.4
2jiv	Epidermal growth factor receptor (EGFR_HUMAN)	8.4
2r3v	Mevalonate kinase(KIME_HUMAN)	8.4
2vgq	Mitochondrial antiviral-signaling protein (MAVS_HUMAN)	8.4
2vz6	Calcium/calmodulin-dependent protein kinase type II alpha chain (KCC2A_HUMAN)	8.4
3a4o	Tyrosine-protein kinase Lyn(LYN_HUMAN)	8.4
1esv	Gelsolin (GELS_HUMAN)	8.3
1k9s	Purine nucleoside phosphorylase deoD-type (DEOD_ECOLI)	8.3
1lqv	Endothelial protein C receptor Vitamin K-dependent protein	8.3
1pk0	Calmodulin (CALM_HUMAN)	8.3
1pl6	Sorbitol dehydrogenase (DHSO_HUMAN)	8.3
1t40	Aldose reductase (ALDR_HUMAN)	8.3
2gz5	Methionine aminopeptidase 1 (AMPM1_HUMAN)	8.3
2jed	Protein kinase C theta type (KPCT_HUMAN)	8.3
2ntj	Enoyl-[acyl-carrier-protein] reductase [NADH] (INHA_MYCTU)	8.3
2qpj	Neprilysin (NEP_HUMAN)	8.3
2qt0	Nicotinamide riboside kinase 1 (NRK1_HUMAN)	8.3
1bbp	Bilin-binding protein (BBP_PIEBR)	8.2
1d8d	GTPase KRas (RASK_HUMAN)	8.2
1fm9	Peroxisome proliferator-activated receptor gamma (PPARG_HUMAN)	8.2
1hh4	Ras-related C3 botulinum toxin substrate 1 (RAC1_HUMAN)	8.2
1qzy	Methionine aminopeptidase 2 (AMPM2_HUMAN)	8.2
1s5o	Carnitine O-acetyltransferase (CACP_HUMAN)	8.2
1ysw	Apoptosis regulator Bcl-2 (BCL2_HUMAN)	8.2
2iwi	Serine/threonine-protein kinase Pim-2 (PIM2_HUMAN)	8.2
1caq	Stromelysin-1 (MMP3_HUMAN)	8.1
1i4f	HLA class I histocompatibility antigen, A-2 alpha chain Melanoma-associated antigen 4(1A02_HUMAN/MAGA4_HUMAN)	8.1
1iz2	Alpha-1-antitrypsin (A1AT_HUMAN)	8.1
1nf7	Inosine-5'-monophosphate dehydrogenase 2 (IMDH2_HUMAN)	8.1
1rc1	Trifunctional purine biosynthetic protein adenosine-3 (PUR2_HUMAN)	8.1
2cke	Death-associated protein kinase 2 (DAPK2_HUMAN)	8.1
2cmw	Casein kinase I isoform gamma-1 (KC1G1_HUMAN)	8.1
2dr6	Acriflavine resistance protein B (ACRB_ECOLI)	8.1
2hw7	MAP kinase-interacting serine/threonine-protein kinase 2(MKNK2_HUMAN)	8.1
2io6	Wee1-like protein kinase (WEE1_HUMAN)	8.1
2ouq	cAMP and cAMP-inhibited cGMP 3',5'-cyclic phosphodiesterase 10A	8.1
2v5x	Histone deacetylase 8 (HDAC8_HUMAN)	8.1
2vct	Glutathione S-transferase A2 (GSTA2_HUMAN)	8.1
2vx3	Dual specificity tyrosine-phosphorylation-regulated kinase 1A (DYR1A_HUMAN)	8.1
2z8i	Gamma-glutamyltranspeptidase (GGT_ECOLI)	8.1
1tu6	Cathepsin K (CATK_HUMAN)	8
2jih	A disintegrin and metalloproteinase with thrombospondin motifs 1 (ATS1_HUMAN)	8
2q32	Heme oxygenase 2 (HMOX2_HUMAN)	8
2vc2	Integrin alpha-IIb Integrin beta-3(ITA2B_HUMAN/ITB3_HUMAN)	8
2xef	Glutamate carboxypeptidase 2 (FOLH1_HUMAN)	8
1dmw	Phenylalanine-4-hydroxylase (PH4H_HUMAN)	7.9
1s0x	Nuclear receptor ROR-alpha (RORA_HUMAN)	7.9
1zrz	Protein kinase C iota type (KPCI_HUMAN)	7.9
2.00E+82	D-amino-acid oxidase (OXDA_HUMAN)	7.9
2ojj	Mitogen-activated protein kinase 1 (MK01_HUMAN)	7.9
2qrn	Deoxycytidine kinase(DCK_HUMAN)	7.9
2v3e	Glucosylceramidase (GLCM_HUMAN)	7.9

2vle	Aldehyde dehydrogenase, mitochondrial (ALDH2_HUMAN)	7.9
1fco	Beta-lactamase (AMPC_ECOLI)	7.8
1ib1	14-3-3 protein zeta/delta (1433Z_HUMAN)	7.8
1nue	Nucleoside diphosphate kinase B(NDKB_HUMAN)	7.8
1pmn	Mitogen-activated protein kinase 10 (MK10_HUMAN)	7.8
1skx	Nuclear receptor subfamily 1 group I member 2 (NR1I2_HUMAN)	7.8
1tuf	Diaminopimelate decarboxylase (DCDA_METJA)	7.8
1z11	Cytochrome P450 2A6 (CP2A6_HUMAN)	7.8
2bu7	[Pyruvate dehydrogenase [lipoamide]] kinase isozyme 2, mitochondrial (PDK2_HUMAN)	7.8
2clq	Mitogen-activated protein kinase kinase kinase 5(M3K5_HUMAN)	7.8
2eal	Galectin-9 (LEG9_HUMAN)	7.8
2euf	Cell division protein kinase 6 (CDK6_HUMAN)	7.8
2v4m	Glucosamine--fructose-6-phosphate aminotransferase [isomerizing] 1	7.8
2vag	Dual specificity protein kinase CLK1 (CLK1_HUMAN)	7.8
2vd5	Myotonin-protein kinase (DMPK_HUMAN)	7.8
2xb7	ALK tyrosine kinase receptor (ALK_HUMAN)	7.8
3acl	Pirin (PIR_HUMAN)	7.8
1a5h	Tissue-type plasminogen activator (TPA_HUMAN)	7.7
1dgh	Catalase (CATA_HUMAN)	7.7
1k4t	DNA topoisomerase 1 (TOP1_HUMAN)	7.7
1nd5	Prostatic acid phosphatase (PPAP_HUMAN)	7.7
1p4r	Bifunctional purine biosynthesis protein PURH (PUR9_HUMAN)	7.7
2fs8	Tryptase beta-2 (TRYB2_HUMAN)	7.7
2h6i	Protein farnesyltransferase/geranylgeranyltransferase type-1 subunit alpha (FNTA_HUMAN)	7.7
2jam	Calcium/calmodulin-dependent protein kinase type 1G (KCC1G_HUMAN)	7.7
2nyr	NAD-dependent deacetylase sirtuin-5 (SIRT5_HUMAN)	7.7
2obd	Cholesteryl ester transfer protein (CETP_HUMAN)	7.7
2x7o	TGF-beta receptor type-1 (TGFR1_HUMAN)	7.7
2y7j	Phosphorylase b kinase gamma catalytic chain, testis/liver isoform	7.7
3agm	cAMP-dependent protein kinase catalytic subunit alpha (KAPCA_HUMAN)	7.7
1a2n	UDP-N-acetylglucosamine 1-carboxyvinyltransferase (MURA_ECOLI)	7.6
1gnp	GTPase HRas (RASH_HUMAN)	7.6
1rv1	E3 ubiquitin-protein ligase Mdm2 (MDM2_HUMAN)	7.6
1ucn	Nucleoside diphosphate kinase A(NDKA_HUMAN)	7.6
1unl	Cyclin-dependent kinase 5 activator 1 Cell division protein kinase 5	7.6
2g0e	HTH-type transcriptional regulator qacR (QACR_STAHA)	7.6
2gl6	Creatine kinase, sarcomeric mitochondrial(KCRS_HUMAN)	7.6
2hy8	Serine/threonine-protein kinase PAK 1 (PAK1_HUMAN)	7.6
2qmj	Maltase-glucoamylase, intestinal (MGA_HUMAN)	7.6
2uym	Kinesin-like protein KIF11 (KIF11_HUMAN)	7.6
1byd	Beta-amylase (AMYB_SOYBN)	7.5
1qvn	Interleukin-2 (IL2_HUMAN)	7.5
1u59	Tyrosine-protein kinase ZAP-70(ZAP70_HUMAN)	7.5
1xdd	Integrin alpha-L (ITAL_HUMAN)	7.5
1zsl	Coagulation factor XI (FA11_HUMAN)	7.5
2chl	Casein kinase I isoform gamma-3 (KC1G3_HUMAN)	7.5
2dq7	Proto-oncogene tyrosine-protein kinase Fyn(FYN_HUMAN)	7.5
2i6a	Adenosine kinase (ADK_HUMAN)	7.5
2px6	Fatty acid synthase (FAS_HUMAN)	7.5
2q5g	Peroxisome proliferator-activated receptor delta (PPARD_HUMAN)	7.5
2shp	Tyrosine-protein phosphatase non-receptor type 11 (PTN11_HUMAN)	7.5
2v7o	Calcium/calmodulin-dependent protein kinase type II gamma chain	7.5
2vwu	Ephrin type-B receptor 4 (EPHB4_HUMAN)	7.5
2zv2	Calcium/calmodulin-dependent protein kinase kinase 2 (KKCC2_HUMAN)	7.5
1csb	Cathepsin B (CATB_HUMAN)	7.4
1doa	Cell division control protein 42 homolog (CDC42_HUMAN)	7.4
1ek6	UDP-glucose 4-epimerase (GALE_HUMAN)	7.4
1h27	Cyclin-A2@Cyclin-dependent kinase inhibitor	7.4
1hmr	Fatty acid-binding protein, heart (FABPH_HUMAN)	7.4
1j96	Aldo-keto reductase family 1 member C2 (AK1C2_HUMAN)	7.4
1kfy	Fumarate reductase flavoprotein subunit (FRDA_ECOLI)	7.4
1nde	Estrogen receptor beta (ESR2_HUMAN)	7.4

1p7c	Thymidine kinase (KITH_HHV11)	7.4
1q5h	Deoxyuridine 5'-triphosphate nucleotidohydrolase, mitochondrial (DUT_HUMAN)	7.4
1rm8	Matrix metalloproteinase-16 (MMP16_HUMAN)	7.4
1y6q	5'-methylthioadenosine/S-adenosylhomocysteine nucleosidase (MTNN_ECOLI)	7.4
1yfh	Methylated-DNA--protein-cysteine methyltransferase (MGMT_HUMAN)	7.4
2ayr	Estrogen receptor (ESR1_HUMAN)	7.4
2buj	Serine/threonine-protein kinase 16(STK16_HUMAN)	7.4
2bxr	Amine oxidase [flavin-containing] A (AOFA_HUMAN)	7.4
2f57	Serine/threonine-protein kinase PAK 7 (PAK7_HUMAN)	7.4
2q80	Geranylgeranyl pyrophosphate synthetase (GGPPS_HUMAN)	7.4
2w4o	Calcium/calmodulin-dependent protein kinase type IV (KCC4_HUMAN)	7.4
3a7h	Serine/threonine-protein kinase 24(STK24_HUMAN)	7.4
1b86	Hemoglobin subunit alpha beta(HBA_HUMAN/HBB_HUMAN)	7.3
1cm8	Mitogen-activated protein kinase 12(MK12_HUMAN)	7.3
1i7b	S-adenosylmethionine decarboxylase proenzyme (DCAM_HUMAN)	7.3
1lpg	Coagulation factor X (FA10_HUMAN)	7.3
1mrl	Streptogramin A acetyltransferase (VATD_ENTFC)	7.3
1nny	Tyrosine-protein phosphatase non-receptor type 1 (PTN1_HUMAN)	7.3
1qhy	Chloramphenicol 3-O phosphotransferase (CPT_STRVL)	7.3
1xd0	Pancreatic alpha-amylase (AMYP_HUMAN)	7.3
2byi	Heat shock protein HSP 90-alpha (HS90A_HUMAN)	7.3
2eva	Mitogen-activated protein kinase kinase kinase 7(M3K7_HUMAN)	7.3
2fgi	Basic fibroblast growth factor receptor 1 (FGFR1_HUMAN)	7.3
2gv7	Suppressor of tumorigenicity protein 14 (ST14_HUMAN)	7.3
2hz6	Serine/threonine-protein kinase/endoribonuclease IRE1(ERN1_HUMAN)	7.3
2oat	Ornithine aminotransferase, mitochondrial (OAT_HUMAN)	7.3
2p4j	Beta-secretase 1 (BACE1_HUMAN)	7.3
2q6b	3-hydroxy-3-methylglutaryl-coenzyme A reductase (HMDH_HUMAN)	7.3
2qu6	Vascular endothelial growth factor receptor 2 (VGFR2_HUMAN)	7.3
2vdy	Corticosteroid-binding globulin (CBG_HUMAN)	7.3
2xk4	Serine/threonine-protein kinase Nek2 (NEK2_HUMAN)	7.3
3a60	Ribosomal protein S6 kinase beta-1(KS6B1_HUMAN)	7.3
1hak	Annexin A5 (ANXA5_HUMAN)	7.2
1itu	Dipeptidase 1 (DPEP1_HUMAN)	7.2
1x89	Neutrophil gelatinase-associated lipocalin (NGAL_HUMAN)	7.2
2ivu	Proto-oncogene tyrosine-protein kinase receptor ret (RET_HUMAN)	7.2
2p4i	Angiopoietin-1 receptor (TIE2_HUMAN)	7.2
2x4z	Serine/threonine-protein kinase PAK 4 (PAK4_HUMAN)	7.2
2zoq	Mitogen-activated protein kinase 3(MK03_HUMAN)	7.2
1c4y	Prothrombin (THRB_HUMAN)	7.1
1kgi	Transthyretin (TTHY_RAT)	7.1
1li4	Adenosylhomocysteinase (SAHH_HUMAN)	7.1
1rwx	Caspase-1 (CASP1_HUMAN)	7.1
2afu	Glutaminyl-peptide cyclotransferase (QPCT_HUMAN)	7.1
2az5	Tumor necrosis factor (TNFA_HUMAN)	7.1
2wu7	Dual specificity protein kinase CLK3 (CLK3_HUMAN)	7.1
1a4q	Neuraminidase (NRAM_INBBE)	7
1aj2	Dihydropteroate synthase (DHPS_ECOLI)	7
1b0f	Leukocyte elastase (ELNE_HUMAN)	7
1ec1	Gag-Pol polyprotein (POL_HV1B1)	7
1h9u	Retinoic acid receptor RXR-beta (RXRB_HUMAN)	7
1jls	Uracil phosphoribosyltransferase (UPP_TOXGO)	7
1lpa	Pancreatic triacylglycerol lipase (LIPP_HUMAN)	7
1nun	Fibroblast growth factor 10 (FGF10_HUMAN)	7
1vj9	Urokinase-type plasminogen activator (UROK_HUMAN)	7
2ar9	Caspase-9 (CASP9_HUMAN)	7
2gi7	Platelet glycoprotein VI (GPVI_HUMAN)	7
2jc6	Calcium/calmodulin-dependent protein kinase type 1D (KCC1D_HUMAN)	7
2x7k	Peptidyl-prolyl cis-trans isomerase-like 1 (PPIL1_HUMAN)	7
2zdx	[Pyruvate dehydrogenase [lipoamide]] kinase isozyme 4, mitochondrial	7
3a7e	Catechol O-methyltransferase (COMT_HUMAN)	7
1rhu	Caspase-3 (CASP3_HUMAN)	6.9
1w7n	Kynurenine--oxoglutarate transaminase 1 (KAT1_HUMAN)	6.9
2e9p	Serine/threonine-protein kinase Chk1 (CHK1_HUMAN)	6.9

2i6l	Mitogen-activated protein kinase 6(MK06_HUMAN)	6.9
2oyc	Pyridoxal phosphate phosphatase (PLPP_HUMAN)	6.9
2qnj	MAP/microtubule affinity-regulating kinase 3(MARK3_HUMAN)	6.9
1fdq	Fatty acid-binding protein, brain (FABP7_HUMAN)	6.8
1ghm	Beta-lactamase (BLAC_STAAU)	6.8
1wkw	Eukaryotic translation initiation factor 4E-binding protein 1 (4EBP1_HUMAN)	6.8
1yb1	Estradiol 17-beta-dehydrogenase 11 (DHB11_HUMAN)	6.8
1zs6	Nucleoside diphosphate kinase 3(NDK3_HUMAN)	6.8
2dyl	Dual specificity mitogen-activated protein kinase kinase 7(MP2K7_HUMAN)	6.8
2i0e	Protein kinase C beta type (KPCB_HUMAN)	6.8
2onb	Thymidylate synthase (TYSY_HUMAN)	6.8
2q8g	[Pyruvate dehydrogenase [lipoamide]] kinase isozyme 1, mitochondrial	6.8
2xhd	Glutamate receptor 2 (GRIA2_HUMAN)	6.8
1eba	Erythropoietin receptor (EPOR_HUMAN)	6.7
1k3a	Insulin receptor substrate 1 (IRS1_HUMAN)	6.7
1rs0	Complement factor B (CFAB_HUMAN)	6.7
1t31	Chymase (CMA1_HUMAN)	6.7
1t5c	Centromeric protein E (CENPE_HUMAN)	6.7
1z6j	Coagulation factor VII Tissue factor(FA7_HUMAN/TF_HUMAN)	6.7
2hv8	Ras-related protein Rab-11A (RB11A_HUMAN)	6.7
2wex	Apolipoprotein M (APOM_HUMAN)	6.7
1j78	Vitamin D-binding protein (VTDB_HUMAN)	6.6
1mmr	Matrilysin (MMP7_HUMAN)	6.6
1mq0	Cytidine deaminase (CDD_HUMAN)	6.6
1t32	Cathepsin G (CATG_HUMAN)	6.6
2ewp	Estrogen-related receptor gamma (ERR3_HUMAN)	6.6
2jaj	N(G),N(G)-dimethylarginine dimethylaminohydrolase 1 (DDAH1_HUMAN)	6.6
2on3	Ornithine decarboxylase (DCOR_HUMAN)	6.6
1d5z	HLA class II histocompatibility antigen, DRB1-4 beta chain (2B14_HUMAN)	6.5
1wda	Protein-arginine deiminase type-4 (PADI4_HUMAN)	6.5
1x70	Dipeptidyl peptidase 4 (DPP4_HUMAN)	6.5
2hw6	MAP kinase-interacting serine/threonine-protein kinase 1(MKNK1_HUMAN)	6.5
2oju	Peptidyl-prolyl cis-trans isomerase-like 3 (PPIL3_HUMAN)	6.5
2z7x	Toll-like receptor 1 Toll-like receptor 2(TLR1_HUMAN/TLR2_HUMAN)	6.5
1i0e	Creatine kinase M-type(KCRM_HUMAN)	6.4
1kpe	Histidine triad nucleotide-binding protein 1 (HINT1_HUMAN)	6.4
1nuh	Glucose-6-phosphate isomerase (G6PI_HUMAN)	6.4
1zcm	Calpain-1 catalytic subunit (CAN1_HUMAN)	6.4
2ofv	Proto-oncogene tyrosine-protein kinase LCK (LCK_HUMAN)	6.4
2q8i	[Pyruvate dehydrogenase [lipoamide]] kinase isozyme 3, mitochondrial	6.4
2rew	Peroxisome proliferator-activated receptor alpha (PPARA_HUMAN)	6.4
2v62	Serine/threonine-protein kinase VRK2(VRK2_HUMAN)	6.4
2v77	Carboxypeptidase A1 (CBPA1_HUMAN)	6.4
1bnq	Carbonic anhydrase 2 (CAH2_HUMAN)	6.3
1cf0	Profilin-1 (PROF1_HUMAN)	6.3
1qha	Hexokinase-1(HXK1_HUMAN)	6.3
1xd3	Ubiquitin carboxyl-terminal hydrolase isozyme L3 (UCHL3_HUMAN)	6.3
2ipk	HLA class II histocompatibility antigen, DRB1-1 beta chain (2B11_HUMAN)	6.3
2nzt	Hexokinase-2(HXK2_HUMAN)	6.3
2uzp	Protein kinase C gamma type (KPCG_HUMAN)	6.3
2vpg	B-cell CLL/lymphoma 9 protein Pygopus homolog 1	6.3
2wal	Growth arrest and DNA-damage-inducible protein GADD45 gamma	6.3
1qgi	Chitosanase (CHIS_BACCI)	6.2
1w6f	Arylamine N-acetyltransferase (NAT_MYCSM)	6.2
2jii	Serine/threonine-protein kinase VRK3(VRK3_HUMAN)	6.2
2nnq	Fatty acid-binding protein, adipocyte (FABP4_HUMAN)	6.2
2nwg	Stromal cell-derived factor 1 (SDF1_HUMAN)	6.2
2vwi	Serine/threonine-protein kinase OSR1(OXSR1_HUMAN)	6.2
1e2s	Arylsulfatase A (ARSA_HUMAN)	6.1
1osh	Bile acid receptor (NR1H4_HUMAN)	6.1
1r55	ADAM 33 (ADA33_HUMAN)	6.1
2c47	Casein kinase I isoform gamma-2 (KC1G2_HUMAN)	6.1
2vgb	Pyruvate kinase isozymes R/L(KPYR_HUMAN)	6.1
2wo1	Ephrin type-A receptor 4 (EPHA4_HUMAN)	6.1

1d1q	Low molecular weight phosphotyrosine protein phosphatase (PPAL_YEAST)	6
2odb	Cell division control protein 42 homolog@Serine/threonine-protein kinase PAK 6	6
1jr1	Inosine-5'-monophosphate dehydrogenase 2 (IMDH2_CRIGR)	5.9
2f0z	Sialidase-2 (NEUR2_HUMAN)	5.9
2hy3	Receptor-type tyrosine-protein phosphatase gamma (PTPRG_HUMAN)	5.9
2obf	Phenylethanolamine N-methyltransferase (PNMT_HUMAN)	5.9
2wqn	Serine/threonine-protein kinase Nek7(NEK7_HUMAN)	5.9
1cza	Hexokinase-1(HXK1_HUMAN)	5.8
1efn	Proto-oncogene tyrosine-protein kinase Fyn (FYN_HUMAN)	5.8
1hkn	Heparin-binding growth factor 1 (FGF1_HUMAN)	5.8
1j86	High affinity immunoglobulin epsilon receptor subunit alpha (FCERA_HUMAN)	5.8
1s1s	Cell division protein zipA (ZIPA_ECOLI)	5.8
1sr5	Antithrombin-III (ANT3_HUMAN)	5.8
1tev	UMP-CMP kinase(KCY_HUMAN)	5.8
1u4l	C-C motif chemokine 5 (CCL5_HUMAN)	5.8
2ggu	Pulmonary surfactant-associated protein D (SFTPD_HUMAN)	5.8
2xfo	Amine oxidase [flavin-containing] B (AOFB_HUMAN)	5.8
1mg4	Serine/threonine-protein kinase DCLK1(DCLK1_HUMAN)	5.7
2aeb	Arginase-1 (ARGI1_HUMAN)	5.7
2wor	Protein S100-A7 (S10A7_HUMAN)	5.7
1w80	Synaptojanin-1 (SYNJ1_HUMAN)	5.6
1xr9	HLA class I histocompatibility antigen, B-15 alpha chain (1B15_HUMAN)	5.6
2i3i	Baculoviral IAP repeat-containing protein 7 (BIRC7_HUMAN)	5.6
1dfp	Complement factor D (CFAD_HUMAN)	5.5
1t83	Low affinity immunoglobulin gamma Fc region receptor III-B (FCG3B_HUMAN)	5.4
2qou	30S ribosomal protein S9 (RS9_ECOLI)	5.4
2zks	Granzyme M (GRAM_HUMAN)	5.4
1g1s	P-selectin (LYAM3_HUMAN)	5.3
1l5g	Integrin alpha-V (ITAV_HUMAN)	5.3
2bo9	Carboxypeptidase A4 Latexin(CBPA4_HUMAN/LXN_HUMAN)	5.3
2r2n	Kynurenine/alpha-aminoadipate aminotransferase mitochondrial (AADAT_HUMAN)	5.3
1auq	von Willebrand factor (VWF_HUMAN)	5.2
1dx4	Acetylcholinesterase (ACES_DROME)	5.1
1elv	Complement C1s subcomponent (C1S_HUMAN)	5.1
1kjr	Galectin-3 (LEG3_HUMAN)	5.1
2hxs	Ras-related protein Rab-28 (RAB28_HUMAN)	5.1
2prh	Dihydroorotate dehydrogenase, mitochondrial (PYRD_HUMAN)	5.1
2uz9	Guanine deaminase (GUAD_HUMAN)	5.1
1aii	Annexin A3 (ANXA3_HUMAN)	5
1bm7	Transthyretin (TTHY_HUMAN)	5
1czs	Coagulation factor V (FA5_HUMAN)	5
1g86	Eosinophil lysophospholipase (LPPL_HUMAN)	5
1l9n	Protein-glutamine gamma-glutamyltransferase E (TGM3_HUMAN)	5
2f8z	Farnesyl pyrophosphate synthetase (FPPS_HUMAN)	5
2wr6	Retinol-binding protein 4 (RET4_HUMAN)	4.9
2x8b	Acetylcholinesterase (ACES_HUMAN)	4.9
2xwc	Tumor protein p73 (P73_HUMAN)	4.9
1h0c	Serine--pyruvate aminotransferase (SPYA_HUMAN)	4.8
2huw	Growth factor receptor-bound protein 2 (GRB2_HUMAN)	4.8
1ft4	Tumor necrosis factor receptor superfamily member 1A (TNR1A_HUMAN)	4.7
1nrp	Proteinase-activated receptor 1 (PAR1_HUMAN)	4.7
2har	Vitamin D3 receptor (VDR_HUMAN)	4.7
1n7d	Low-density lipoprotein receptor (LDLR_HUMAN)	4.6
1pq6	Oxysterols receptor LXR-beta (NR1H2_HUMAN)	4.6
2v8e	Complement factor H (CFAH_HUMAN)	4.6
1nbf	Ubiquitin carboxyl-terminal hydrolase 7 (UBP7_HUMAN)	4.3
2r4b	Receptor tyrosine-protein kinase erbB-4 (ERBB4_HUMAN)	4.3
1au1	Interferon beta (IFNB_HUMAN)	4.2
1rqd	Deoxyhypusine synthase (DHYS_HUMAN)	4.2
1lgp	E3 ubiquitin-protein ligase CHFR (CHFR_HUMAN)	4.1
2dyb	Neutrophil cytosol factor 4 (NCF4_HUMAN)	4.1
2qkh	Gastric inhibitory polypeptide receptor Gastric inhibitory polypeptide)	4.1
1w70	Neutrophil cytosol factor 1 (NCF1_HUMAN)	4
1k5r	65 kDa Yes-associated protein (YAP1_HUMAN)	3.9

1f9p	Platelet basic protein (CXCL7_HUMAN)	3.7
1lhy	Sex hormone-binding globulin (SHBG_HUMAN)	3.7
2ayo	Ubiquitin carboxyl-terminal hydrolase 14 (UBP14_HUMAN)	3.7
2ra4	C-C motif chemokine 13 (CCL13_HUMAN)	3.7
2e1q	Xanthine dehydrogenase/oxidase (XDH_HUMAN)	3.3
2hrq	Liver carboxylesterase 1 (EST1_HUMAN)	3.3
2ibi	Ubiquitin carboxyl-terminal hydrolase 2 (UBP2_HUMAN)	3.3
1fga	Heparin-binding growth factor 2 (FGF2_HUMAN)	3.2
1hy3	Estrogen sulfotransferase (ST1E1_HUMAN)	3.2
2a3r	Sulfotransferase 1A3/1A4 (ST1A3_HUMAN)	2.6
1sr7	Progesterone receptor (PRGR_HUMAN)	2.3
1xap	Retinoic acid receptor beta (RARB_HUMAN)	1.2
1uou	Thymidine phosphorylase (TYPH_HUMAN)	0.7
2pnu	Androgen receptor (ANDR_HUMAN)	0.7
2wnv	Complement C1q subcomponent subunit A B C	0.6
2a3i	Mineralocorticoid receptor (MCR_HUMAN)	-0.6
1u3u	Alcohol dehydrogenase 1B (ADH1B_HUMAN)	-0.9
1w6k	Lanosterol synthase (ERG7_HUMAN)	-1.2
2qcg	Uridine 5'-monophosphate synthase (PYR5_HUMAN)	-1.6
1u3t	Alcohol dehydrogenase 1A (ADH1A_HUMAN)	-2.2
2pqt	Arylamine N-acetyltransferase 1 (ARY1_HUMAN)	-2.4
1lyb	Cathepsin D (CATD_HUMAN)	-2.5
1xvp	Nuclear receptor subfamily 1 group I member 3 (NR1I3_HUMAN)	-2.7
1a7c	Plasminogen activator inhibitor 1 (PAI1_HUMAN)	-3.6
2gwh	Sulfotransferase 1C4 (ST1C4_HUMAN)	-3.8
1exa	Retinoic acid receptor gamma (RARG_HUMAN)	-4
2znt	Glutamate receptor, ionotropic kainate 1 (GRIK1_HUMAN)	-4.1
2qro	Deoxycytidine kinase (DCK_HUMAN)	-4.8
1ls6	Sulfotransferase 1A1 (ST1A1_HUMAN)	-6
1w4n	Phenylethylamine oxidase (PAOX_ARTGO)	-10.8
2q3z	Protein-glutamine gamma-glutamyltransferase 2 (TGM2_HUMAN)	-10.8
1.00E+51	Delta-aminolevulinic acid dehydratase (HEM2_HUMAN)	-10.9
1p49	Steryl-sulfatase (STS_HUMAN)	-12
2p8u	Hydroxymethylglutaryl-CoA synthase, cytoplasmic (HMCS1_HUMAN)	-13
1fsu	Arylsulfatase B (ARSB_HUMAN)	-17.6
2c11	Membrane primary amine oxidase (AOC3_HUMAN)	-18.3
1m5b	Glutamate receptor 2 (GRIA2_RAT)	-19.8
1ym9	M-phase inducer phosphatase 2 (MPIP2_HUMAN)	-24.5
2hhj	Bisphosphoglycerate mutase (PMGE_HUMAN)	-25.2
2hei	Ras-related protein Rab-5B (RAB5B_HUMAN)	-42
2pfg	Carbonyl reductase [NADPH] 1 (CBR1_HUMAN)	-43.4
1evu	Coagulation factor XIII A chain (F13A_HUMAN)	-46
1stf	Cystatin-B (CYTB_HUMAN)	-56.8

Table A2.2. Docking results of Brefeldin with protein targets

PDB ID	Protein	Docking Score
2xfo	Amine oxidase [flavin-containing] B (AOFB_HUMAN)	9.8
1s0x	Nuclear receptor ROR-alpha (RORA_HUMAN)	9.5
3g7w	Islet amyloid polypeptide (IAPP_HUMAN)	9.3
1ohk	Dihydrofolate reductase (DYR_HUMAN)	9.2
2g0e	HTH-type transcriptional regulator qacR (QACR_STAHA)	9.2
1pq6	Oxysterols receptor LXR-beta (NR1H2_HUMAN)	9.1
1sr7	Progesterone receptor (PRGR_HUMAN)	9
1w6k	Lanosterol synthase (ERG7_HUMAN)	9
1xvp	Nuclear receptor subfamily 1 group I member 3 (NR1I3_HUMAN)	9

2uym	Kinesin-like protein KIF11 (KIF11_HUMAN)	9
1onq	T-cell surface glycoprotein CD1a (CD1A_HUMAN)	8.9
2f38	Aldo-keto reductase family 1 member C3 (AK1C3_HUMAN)	8.9
2rew	Peroxisome proliferator-activated receptor alpha (PPARA_HUMAN)	8.9
3fc6	Retinoic acid receptor RXR-alpha (RXRA_HUMAN)	8.9
3jsx	NAD(P)H dehydrogenase [quinone] 1 (NQO1_HUMAN)	8.9
3o3u	Advanced glycosylation end product-specific receptor (RAGE_HUMAN)	8.8
1sg0	Ribosyldihydronicotinamide dehydrogenase [quinone] (NQO2_HUMAN)	8.7
2vgq	Mitochondrial antiviral-signaling protein (MAVS_HUMAN)	8.7
2x7h	Zinc-binding alcohol dehydrogenase domain-containing protein 2 (ZADH2_HUMAN)	8.7
3dl9	Vitamin D 25-hydroxylase (CP2R1_HUMAN)	8.7
3gkj	Niemann-Pick C1 protein (NPC1_HUMAN)	8.7
2jed	Protein kinase C theta type (KPCT_HUMAN)	8.6
3ipq	Oxysterols receptor LXR-alpha (NR1H3_HUMAN)	8.6
1lhv	Sex hormone-binding globulin (SHBG_HUMAN)	8.5
1s5o	Carnitine O-acetyltransferase (CACP_HUMAN)	8.5
2w4q	Prostaglandin reductase 2 (PTGR2_HUMAN)	8.5
3mtf	Activin receptor type-1 (ACVR1_HUMAN)	8.5
3my0	Serine/threonine-protein kinase receptor R3(ACVL1_HUMAN)	8.5
1j96	Aldo-keto reductase family 1 member C2 (AK1C2_HUMAN)	8.4
2ayr	Estrogen receptor (ESR1_HUMAN)	8.4
2bxr	Amine oxidase [flavin-containing] A (AOFA_HUMAN)	8.4
2e3r	Collagen type IV alpha-3-binding protein (C43BP_HUMAN)	8.4
2jiv	Epidermal growth factor receptor (EGFR_HUMAN)	8.4
3fzm	BAG family molecular chaperone regulator 1 (BAG1_HUMAN)	8.4
1kkq	Nuclear receptor corepressor 2 (NCOR2_HUMAN)	8.3
1nde	Estrogen receptor beta (ESR2_HUMAN)	8.3
2har	Vitamin D3 receptor (VDR_HUMAN)	8.3
2pnu	Androgen receptor (ANDR_HUMAN)	8.3
2v3e	Glucosylceramidase (GLCM_HUMAN)	8.3
3dh4	Sodium/glucose cotransporter (SGLT_VIBPA)	8.3
1dgh	Catalase (CATA_HUMAN)	8.2
1h22	Acetylcholinesterase (ACES_TORCA)	8.2
1h27	Cyclin-A2@Cyclin-dependent kinase inhibitor 1B(CCNA2_HUMAN/CDN1B_HUMAN)	8.2
1hmr	Fatty acid-binding protein, heart (FABPH_HUMAN)	8.2
1imb	Inositol monophosphatase (IMPA1_HUMAN)	8.2
1xd0	Pancreatic alpha-amylase (AMYP_HUMAN)	8.2
2nyr	NAD-dependent deacetylase sirtuin-5 (SIRT5_HUMAN)	8.2
2vqq	Histone deacetylase 4 (HDAC4_HUMAN)	8.2
3fap	Peptidyl-prolyl cis-trans isomerase FKBP1A (FKB1A_HUMAN)	8.2
3gqy	Pyruvate kinase isozymes M1/M2 (KPYM_HUMAN)	8.2
3l0j	Nuclear receptor ROR-gamma (RORG_HUMAN)	8.2
3mvh	RAC-alpha serine/threonine-protein kinase (AKT1_HUMAN)	8.2
1d4l	Gag-Pol polyprotein (POL_HV1A2)	8.1
1fm9	Peroxisome proliferator-activated receptor gamma (PPARG_HUMAN)	8.1
1ish	ADP-ribosyl cyclase 2 (BST1_HUMAN)	8.1

2euf	Cell division protein kinase 6 (CDK6_HUMAN)	8.1
2ewy	Beta-secretase 2 (BACE2_HUMAN)	8.1
2oc2	Angiotensin-converting enzyme (ACE_HUMAN)	8.1
2p4i	Angiopoietin-1 receptor (TIE2_HUMAN)	8.1
2r59	Leukotriene A-4 hydrolase (LKHA4_HUMAN)	8.1
3d94	Insulin-like growth factor 1 receptor (IGF1R_HUMAN)	8.1
3ldp	78 kDa glucose-regulated protein (GRP78_HUMAN)	8.1
1e9a	Thymidylate kinase (KTHY_HUMAN)	8
1gnj	Serum albumin (ALBU_HUMAN)	8
1kfy	Fumarate reductase flavoprotein subunit (FRDA_ECOLI)	8
1kgi	Transthyretin (TTHY_RAT)	8
1rne	Renin (RENI_HUMAN)	8
1xap	Retinoic acid receptor beta (RARB_HUMAN)	8
1z11	Cytochrome P450 2A6 (CP2A6_HUMAN)	8
2a3i	Mineralocorticoid receptor (MCR_HUMAN)	8
2az5	Tumor necrosis factor (TNFA_HUMAN)	8
2h44	cGMP-specific 3',5'-cyclic phosphodiesterase (PDE5A_HUMAN)	8
2q80	Geranylgeranyl pyrophosphate synthetase (GGPPS_HUMAN)	8
2r2n	Kynurenine/alpha-aminoadipate aminotransferase mitochondrial (AADAT_HUMAN)	8
3e8d	RAC-beta serine/threonine-protein kinase Glycogen synthase kinase-3 beta(AKT2_HUMAN/GSK3B_HUMAN)	8
3eml	Adenosine receptor A2a (AA2AR_HUMAN)	8
3hf8	Tryptophan 5-hydroxylase 1 (TPH1_HUMAN)	8
3kq0	Alpha-1-acid glycoprotein 1 (A1AG1_HUMAN)	8
3nxu	Cytochrome P450 3A4 (CP3A4_HUMAN)	8
3pbl	D(3) dopamine receptor (DRD3_HUMAN)	8
1cm8	Mitogen-activated protein kinase 12(MK12_HUMAN)	7.9
1eba	Erythropoietin receptor (EPOR_HUMAN)	7.9
1fdq	Fatty acid-binding protein, brain (FABP7_HUMAN)	7.9
1ksw	Proto-oncogene tyrosine-protein kinase Src (SRC_HUMAN)	7.9
1mc5	Alcohol dehydrogenase class-3 (ADHX_HUMAN)	7.9
1xdd	Integrin alpha-L (ITAL_HUMAN)	7.9
2jc6	Calcium/calmodulin-dependent protein kinase type 1D (KCC1D_HUMAN)	7.9
2jev	Diamine acetyltransferase 1 (SAT1_HUMAN)	7.9
2xb7	ALK tyrosine kinase receptor (ALK_HUMAN)	7.9
3bkb	Proto-oncogene tyrosine-protein kinase Fes/Fps(FES_HUMAN)	7.9
3e5a	Targeting protein for Xklp2 (TPX2_HUMAN)	7.9
3ff6	Acetyl-CoA carboxylase 2 (ACACB_HUMAN)	7.9
3nyn	G protein-coupled receptor kinase 6 (GRK6_HUMAN)	7.9
1ezf	Squalene synthetase (FDFT_HUMAN)	7.8
1jr1	Inosine-5'-monophosphate dehydrogenase 2 (IMDH2_CRIGR)	7.8
1mrl	Streptogramin A acetyltransferase (VATD_ENTFC)	7.8
1nd5	Prostatic acid phosphatase (PPAP_HUMAN)	7.8
2q32	Heme oxygenase 2 (HMOX2_HUMAN)	7.8
2r3v	Mevalonate kinase(KIME_HUMAN)	7.8
2vx3	Dual specificity tyrosine-phosphorylation-regulated kinase 1A (DYR1A_HUMAN)	7.8
3frj	Corticosteroid 11-beta-dehydrogenase isozyme 1 (DHI1_HUMAN)	7.8

3ld6	Cytochrome P450 51A1 (CP51A_HUMAN)	7.8
3n7r	Calcitonin gene-related peptide type 1 receptor Receptor activity-modifying protein 1(CALRL_HUMAN/RAMP1_HUMAN)	7.8
1byd	Beta-amylase (AMYB_SOYBN)	7.7
1csb	Cathepsin B (CATB_HUMAN)	7.7
1ec1	Gag-Pol polyprotein (POL_HV1B1)	7.7
1p4r	Bifunctional purine biosynthesis protein PURH (PUR9_HUMAN)	7.7
1qip	Lactoylglutathione lyase (LGUL_HUMAN)	7.7
1t40	Aldose reductase (ALDR_HUMAN)	7.7
2dq7	Proto-oncogene tyrosine-protein kinase Fyn(FYN_HUMAN)	7.7
2nni	Cytochrome P450 2C8 (CP2C8_HUMAN)	7.7
2nnq	Fatty acid-binding protein, adipocyte (FABP4_HUMAN)	7.7
2obd	Cholesteryl ester transfer protein (CETP_HUMAN)	7.7
2oju	Peptidyl-prolyl cis-trans isomerase-like 3 (PPIL3_HUMAN)	7.7
2xef	Glutamate carboxypeptidase 2 (FOLH1_HUMAN)	7.7
2z65	Lymphocyte antigen 96 Toll-like receptor 4(LY96_HUMAN/TLR4_HUMAN)	7.7
3a4o	Tyrosine-protein kinase Lyn(LYN_HUMAN)	7.7
3b6h	Prostacyclin synthase (PTGIS_HUMAN)	7.7
3djy	Cholinesterase (CHLE_HUMAN)	7.7
3nr9	Dual specificity protein kinase CLK2 (CLK2_HUMAN)	7.7
3ov6	T-cell surface glycoprotein CD1c (CD1C_HUMAN)	7.7
3pm0	Cytochrome P450 1B1 (CP1B1_HUMAN)	7.7
1dmw	Phenylalanine-4-hydroxylase (PH4H_HUMAN)	7.6
1efn	Proto-oncogene tyrosine-protein kinase Fyn (FYN_HUMAN)	7.6
1qu3	Isoleucyl-tRNA synthetase (SYI1_STAAU)	7.6
1unl	Cyclin-dependent kinase 5 activator 1 Cell division protein kinase 5(CD5R1_HUMAN/CDK5_HUMAN)	7.6
1zdt	Steroidogenic factor 1 (STF1_HUMAN)	7.6
2bil	Proto-oncogene serine/threonine-protein kinase Pim-1 (PIM1_HUMAN)	7.6
2gvj	Nicotinamide phosphoribosyltransferase (NAMPT_HUMAN)	7.6
2ntj	Enoyl-[acyl-carrier-protein] reductase [NADH] (INHA_MYCTU)	7.6
2v7o	Calcium/calmodulin-dependent protein kinase type II gamma chain (KCC2G_HUMAN)	7.6
2wu7	Dual specificity protein kinase CLK3 (CLK3_HUMAN)	7.6
3e7g	Nitric oxide synthase, inducible (NOS2_HUMAN)	7.6
3h10	Serine/threonine-protein kinase 6 (STK6_HUMAN)	7.6
3k23	Glucocorticoid receptor (GCR_HUMAN)	7.6
3ljr	Glutathione S-transferase theta-2 (GSTT2_HUMAN)	7.6
3lq5	Cyclin-T1 Cell division protein kinase 9 Cell division protein kinase 9(CCNT1_HUMAN/CDK9_HUMAN)	7.6
3ndm	Rho-associated protein kinase 1 (ROCK1_HUMAN)	7.6
1d1j	Profilin-2 (PROF2_HUMAN)	7.5
1og5	Cytochrome P450 2C9 (CP2C9_HUMAN)	7.5
1pl6	Sorbitol dehydrogenase (DHSO_HUMAN)	7.5
1u59	Tyrosine-protein kinase ZAP-70(ZAP70_HUMAN)	7.5
2w0b	Cytochrome P450 51 (CP51_MYCTU)	7.5
2x6v	T-box transcription factor TBX5 (TBX5_HUMAN)	7.5
2x7k	Peptidyl-prolyl cis-trans isomerase-like 1 (PPIL1_HUMAN)	7.5
3e7e	Mitotic checkpoint serine/threonine-protein kinase BUB1(BUB1_HUMAN)	7.5
3odu	C-X-C chemokine receptor type 4 (CXCR4_HUMAN)	7.5

4ald	Fructose-bisphosphate aldolase A (ALDOA_HUMAN)	7.5
1d8d	GTPase KRas (RASK_HUMAN)	7.4
1gnp	GTPase HRas (RASH_HUMAN)	7.4
1hy3	Estrogen sulfotransferase (ST1E1_HUMAN)	7.4
1r4l	Angiotensin-converting enzyme 2 (ACE2_HUMAN)	7.4
1s8c	Heme oxygenase 1 (HMOX1_HUMAN)	7.4
2chl	Casein kinase I isoform gamma-3 (KC1G3_HUMAN)	7.4
2fs8	Tryptase beta-2 (TRYB2_HUMAN)	7.4
2i0e	Protein kinase C beta type (KPCB_HUMAN)	7.4
2vc2	Integrin alpha-IIb Integrin beta-3(ITA2B_HUMAN/ITB3_HUMAN)	7.4
2vd5	Myotonin-protein kinase (DMPK_HUMAN)	7.4
2vz6	Calcium/calmodulin-dependent protein kinase type II alpha chain (KCC2A_HUMAN)	7.4
2wax	Probable ATP-dependent RNA helicase DDX6 (DDX6_HUMAN)	7.4
2wnv	Complement C1q subcomponent subunit A B C(C1QA_HUMAN/C1QB_HUMAN/C1QC_HUMAN)	7.4
2x7o	TGF-beta receptor type-1 (TGFR1_HUMAN)	7.4
3agm	cAMP-dependent protein kinase catalytic subunit alpha (KAPCA_HUMAN)	7.4
3ant	Epoxide hydrolase 2 (HYES_HUMAN)	7.4
3eqm	Cytochrome P450 19A1 (CP19A_HUMAN)	7.4
3g3n	High affinity cAMP-specific 3',5'-cyclic phosphodiesterase 7A (PDE7A_HUMAN)	7.4
3iw4	Protein kinase C alpha type (KPCA_HUMAN)	7.4
3kvw	Dual specificity tyrosine-phosphorylation-regulated kinase 2 (DYRK2_HUMAN)	7.4
3op5	Serine/threonine-protein kinase VRK1 (VRK1_HUMAN)	7.4
3pkj	Mono-ADP-ribosyltransferase sirtuin-6 (SIRT6_HUMAN)	7.4
1a2n	UDP-N-acetylglucosamine 1-carboxyvinyltransferase (MURA_ECOLI)	7.3
1nf7	Inosine-5'-monophosphate dehydrogenase 2 (IMDH2_HUMAN)	7.3
1skx	Nuclear receptor subfamily 1 group I member 2 (NR1I2_HUMAN)	7.3
1w7n	Kynurenine--oxoglutarate transaminase 1 (KAT1_HUMAN)	7.3
1wuu	Galactokinase(GALK1_HUMAN)	7.3
1yb1	Estradiol 17-beta-dehydrogenase 11 (DHB11_HUMAN)	7.3
1zrz	Protein kinase C iota type (KPCI_HUMAN)	7.3
2abj	Branched-chain-amino-acid aminotransferase, cytosolic (BCAT1_HUMAN)	7.3
2aeb	Arginase-1 (ARGI1_HUMAN)	7.3
2c47	Casein kinase I isoform gamma-2 (KC1G2_HUMAN)	7.3
2ouq	cAMP and cAMP-inhibited cGMP 3',5'-cyclic phosphodiesterase 10A (PDE10_HUMAN)	7.3
2qnj	MAP/microtubule affinity-regulating kinase 3(MARK3_HUMAN)	7.3
2uzp	Protein kinase C gamma type (KPCG_HUMAN)	7.3
2z8i	Gamma-glutamyltranspeptidase (GGT_ECOLI)	7.3
3dyl	High affinity cGMP-specific 3',5'-cyclic phosphodiesterase 9A (PDE9A_HUMAN)	7.3
3eta	Insulin receptor (INSR_HUMAN)	7.3
3fcl	Uracil-DNA glycosylase (UNG_HUMAN)	7.3
3iec	Serine/threonine-protein kinase MARK2(MARK2_HUMAN)	7.3
3o2m	Mitogen-activated protein kinase 8 (MK08_HUMAN)	7.3
1byg	Tyrosine-protein kinase CSK(CSK_HUMAN)	7.2
1egc	Medium-chain specific acyl-CoA dehydrogenase, mitochondrial (ACADM_HUMAN)	7.2
1ogu	Cyclin-A2 (CCNA2_HUMAN)	7.2
1so2	cGMP-inhibited 3',5'-cyclic phosphodiesterase B (PDE3B_HUMAN)	7.2

2dyl	Dual specificity mitogen-activated protein kinase kinase 7(MP2K7_HUMAN)	7.2
2f57	Serine/threonine-protein kinase PAK 7 (PAK7_HUMAN)	7.2
2hh5	Cathepsin S (CATS_HUMAN)	7.2
2z7x	Toll-like receptor 1 Toll-like receptor 2(TLR1_HUMAN/TLR2_HUMAN)	7.2
3b6r	Creatine kinase B-type (KCRB_HUMAN)	7.2
3bz3	Focal adhesion kinase 1 (FAK1_HUMAN)	7.2
3e4a	Insulin-degrading enzyme (IDE_HUMAN)	7.2
3enm	Dual specificity mitogen-activated protein kinase kinase 6(MP2K6_HUMAN)	7.2
3hhm	Phosphatidylinositol 3-kinase regulatory subunit alpha Phosphatidylinositol-4,5-bisphosphate 3-kinase catalytic subunit alpha isoform(P85A_HUMAN/PK3CA_HUMAN)	7.2
3hm8	Hexokinase-3(HXK3_HUMAN)	7.2
3iad	cAMP-specific 3',5'-cyclic phosphodiesterase 4D (PDE4D_HUMAN)	7.2
3kec	Collagenase 3 (MMP13_HUMAN)	7.2
1a5h	Tissue-type plasminogen activator (TPA_HUMAN)	7.1
1d5z	HLA class II histocompatibility antigen, DRB1-4 beta chain (2B14_HUMAN)	7.1
1esv	Gelsolin (GELS_HUMAN)	7.1
1ghm	Beta-lactamase (BLAC_STAAU)	7.1
1ib1	14-3-3 protein zeta/delta (1433Z_HUMAN)	7.1
1jls	Uracil phosphoribosyltransferase (UPP_TOXGO)	7.1
1p49	Steryl-sulfatase (STS_HUMAN)	7.1
1pmn	Mitogen-activated protein kinase 10 (MK10_HUMAN)	7.1
2gl6	Creatine kinase, sarcomeric mitochondrial(KCRS_HUMAN)	7.1
2gz5	Methionine aminopeptidase 1 (AMPM1_HUMAN)	7.1
2hi4	Cytochrome P450 1A2 (CP1A2_HUMAN)	7.1
2hw7	MAP kinase-interacting serine/threonine-protein kinase 2(MKNK2_HUMAN)	7.1
2io6	Wee1-like protein kinase (WEE1_HUMAN)	7.1
2jih	A disintegrin and metalloproteinase with thrombospondin motifs 1 (ATS1_HUMAN)	7.1
2on3	Ornithine decarboxylase (DCOR_HUMAN)	7.1
2vct	Glutathione S-transferase A2 (GSTA2_HUMAN)	7.1
2vn9	Calcium/calmodulin-dependent protein kinase type II delta chain (KCC2D_HUMAN)	7.1
2w4o	Calcium/calmodulin-dependent protein kinase type IV (KCC4_HUMAN)	7.1
3coi	Mitogen-activated protein kinase 13(MK13_HUMAN)	7.1
3cok	Serine/threonine-protein kinase PLK4(PLK4_HUMAN)	7.1
3csh	Glutathione S-transferase P (GSTP1_HUMAN)	7.1
3e3b	Casein kinase II subunit alpha' (CSK22_HUMAN)	7.1
3eu7	Breast cancer type 2 susceptibility protein (BRCA2_HUMAN)	7.1
3g7e	DNA gyrase subunit B (GYRB_ECOLI)	7.1
3imx	Glucokinase (HXK4_HUMAN)	7.1
3ocs	Tyrosine-protein kinase BTK (BTK_HUMAN)	7.1
1i4f	HLA class I histocompatibility antigen, A-2 alpha chain Melanoma-associated antigen 4(1A02_HUMAN/MAGA4_HUMAN)	7
1kws	Galactosylgalactosylxylosylprotein 3-beta-glucuronosyltransferase 3 (B3GA3_HUMAN)	7
1lpg	Coagulation factor X (FA10_HUMAN)	7
1nun	Fibroblast growth factor 10 (FGF10_HUMAN)	7
1rhu	Caspase-3 (CASP3_HUMAN)	7
1ros	Macrophage metalloelastase (MMP12_HUMAN)	7
1rv1	E3 ubiquitin-protein ligase Mdm2 (MDM2_HUMAN)	7

2cke	Death-associated protein kinase 2 (DAPK2_HUMAN)	7
2dr6	Acriflavine resistance protein B (ACRB_ECOLI)	7
2f8z	Farnesyl pyrophosphate synthetase (FPPS_HUMAN)	7
2fgi	Basic fibroblast growth factor receptor 1 (FGFR1_HUMAN)	7
2h6i	Protein farnesyltransferase/geranylgeranyltransferase type-1 subunit alpha (FNTA_HUMAN)	7
2hy8	Serine/threonine-protein kinase PAK 1 (PAK1_HUMAN)	7
2i6a	Adenosine kinase (ADK_HUMAN)	7
2ojj	Mitogen-activated protein kinase 1 (MK01_HUMAN)	7
2prh	Dihydroorotate dehydrogenase, mitochondrial (PYRD_HUMAN)	7
2rjp	A disintegrin and metalloproteinase with thrombospondin motifs 4 (ATS4_HUMAN)	7
2vdy	Corticosteroid-binding globulin (CBG_HUMAN)	7
2xbj	Serine/threonine-protein kinase Chk2 (CHK2_HUMAN)	7
3com	Serine/threonine-protein kinase 4(STK4_HUMAN)	7
3gu8	Death-associated protein kinase 1 (DAPK1_HUMAN)	7
3jwe	Monoglyceride lipase (MGLL_HUMAN)	7
3krr	Tyrosine-protein kinase JAK2 (JAK2_HUMAN)	7
3nos	Nitric oxide synthase, endothelial (NOS3_HUMAN)	7
1dx4	Acetylcholinesterase (ACES_DROME)	6.9
1nny	Tyrosine-protein phosphatase non-receptor type 1 (PTN1_HUMAN)	6.9
1osh	Bile acid receptor (NR1H4_HUMAN)	6.9
2nru	Interleukin-1 receptor-associated kinase 4 (IRAK4_HUMAN)	6.9
2qg6	Nicotinamide riboside kinase 1(NRK1_HUMAN)	6.9
2v4m	Glucosamine--fructose-6-phosphate aminotransferase [isomerizing] 1 (GFPT1_HUMAN)	6.9
2vag	Dual specificity protein kinase CLK1 (CLK1_HUMAN)	6.9
2woe	ADP-ribosyl-[dinitrogen reductase] glycohydrolase (DRAG_RHORU)	6.9
2x4z	Serine/threonine-protein kinase PAK 4 (PAK4_HUMAN)	6.9
3a60	Ribosomal protein S6 kinase beta-1(KS6B1_HUMAN)	6.9
3fqe	Tyrosine-protein kinase SYK (KSYK_HUMAN)	6.9
3g7b	DNA gyrase subunit B (GYRB_STAAU)	6.9
3gd7	Cystic fibrosis transmembrane conductance regulator (CFTR_HUMAN)	6.9
3gp0	Mitogen-activated protein kinase 11 (MK11_HUMAN)	6.9
3iqv	14-3-3 protein sigma RAF proto-oncogene serine/threonine-protein kinase(1433S_HUMAN/RAF1_HUMAN)	6.9
3lco	Macrophage colony-stimulating factor 1 receptor (CSF1R_HUMAN)	6.9
3lxe	Carbonic anhydrase 1 (CAH1_HUMAN)	6.9
1a4q	Neuraminidase (NRAM_INBBE)	6.8
1c4y	Prothrombin (THRB_HUMAN)	6.8
1caq	Stromelysin-1 (MMP3_HUMAN)	6.8
1iz2	Alpha-1-antitrypsin (A1AT_HUMAN)	6.8
1tu6	Cathepsin K (CATK_HUMAN)	6.8
1w78	Bifunctional protein folC (FOLC_ECOLI)	6.8
1wkw	Eukaryotic translation initiation factor 4E-binding protein 1 (4EBP1_HUMAN)	6.8
1x89	Neutrophil gelatinase-associated lipocalin (NGAL_HUMAN)	6.8
1zcm	Calpain-1 catalytic subunit (CAN1_HUMAN)	6.8
1zs6	Nucleoside diphosphate kinase 3(NDK3_HUMAN)	6.8
2afu	Glutaminyl-peptide cyclotransferase (QPCT_HUMAN)	6.8
2bdm	Cytochrome P450 2B4 (CP2B4_RABIT)	6.8

2clq	Mitogen-activated protein kinase kinase kinase 5(M3K5_HUMAN)	6.8
2ewp	Estrogen-related receptor gamma (ERR3_HUMAN)	6.8
2h26	T-cell surface glycoprotein CD1b (CD1B_HUMAN)	6.8
2ovz	Matrix metalloproteinase-9 (MMP9_HUMAN)	6.8
2p4j	Beta-secretase 1 (BACE1_HUMAN)	6.8
2po6	T-cell surface glycoprotein CD1d (CD1D_HUMAN)	6.8
2q5g	Peroxisome proliferator-activated receptor delta (PPARD_HUMAN)	6.8
2q6b	3-hydroxy-3-methylglutaryl-coenzyme A reductase (HMDH_HUMAN)	6.8
2qu6	Vascular endothelial growth factor receptor 2 (VGFR2_HUMAN)	6.8
2v5x	Histone deacetylase 8 (HDAC8_HUMAN)	6.8
2v62	Serine/threonine-protein kinase VRK2(VRK2_HUMAN)	6.8
3b8z	A disintegrin and metalloproteinase with thrombospondin motifs 5 (ATS5_HUMAN)	6.8
3bho	Cleavage and polyadenylation specificity factor subunit 5 (CPSF5_HUMAN)	6.8
3c2l	DNA polymerase beta (DPOLB_HUMAN)	6.8
3dpf	Neutrophil collagenase (MMP8_HUMAN)	6.8
3e7v	Serine/threonine-protein kinase haspin (HASP_HUMAN)	6.8
3eqc	Dual specificity mitogen-activated protein kinase kinase 1 (MP2K1_HUMAN)	6.8
3g33	G1/S-specific cyclin-D3@Cell division protein kinase 4(CCND3_HUMAN/CDK4_HUMAN)	6.8
3gvu	Tyrosine-protein kinase ABL2 (ABL2_HUMAN)	6.8
3i8v	cAMP-specific 3',5'-cyclic phosphodiesterase 4A (PDE4A_HUMAN)	6.8
3iol	Glucagon (GLUC_HUMAN)	6.8
3lmg	Receptor tyrosine-protein kinase erbB-3(ERBB3_HUMAN)	6.8
3m9k	Thioredoxin (THIO_HUMAN)	6.8
1d1q	Low molecular weight phosphotyrosine protein phosphatase (PPAL_YEAST)	6.7
1i7b	S-adenosylmethionine decarboxylase proenzyme (DCAM_HUMAN)	6.7
1k4t	DNA topoisomerase 1 (TOP1_HUMAN)	6.7
1k9s	Purine nucleoside phosphorylase deoD-type (DEOD_ECOLI)	6.7
1rgy	Beta-lactamase (AMPC_CITFR)	6.7
1t46	Mast/stem cell growth factor receptor (KIT_HUMAN)	6.7
1ysw	Apoptosis regulator Bcl-2 (BCL2_HUMAN)	6.7
2cmw	Casein kinase I isoform gamma-1 (KC1G1_HUMAN)	6.7
2fv5	ADAM 17 (ADA17_HUMAN)	6.7
2gv7	Suppressor of tumorigenicity protein 14 (ST14_HUMAN)	6.7
2i6l	Mitogen-activated protein kinase 6(MK06_HUMAN)	6.7
2oat	Ornithine aminotransferase, mitochondrial (OAT_HUMAN)	6.7
2pqt	Arylamine N-acetyltransferase 1 (ARY1_HUMAN)	6.7
2qrn	Deoxycytidine kinase(DCK_HUMAN)	6.7
2qt0	Nicotinamide riboside kinase 1 (NRK1_HUMAN)	6.7
2wqn	Serine/threonine-protein kinase Nek7(NEK7_HUMAN)	6.7
2zv2	Calcium/calmodulin-dependent protein kinase kinase 2 (KKCC2_HUMAN)	6.7
3a7h	Serine/threonine-protein kinase 24(STK24_HUMAN)	6.7
3bpr	Proto-oncogene tyrosine-protein kinase MER (MERTK_HUMAN)	6.7
3cm2	Baculoviral IAP repeat-containing protein 4 (XIAP_HUMAN)	6.7
3d9s	Aquaporin-5 (AQP5_HUMAN)	6.7
3da2	Carbonic anhydrase 13 (CAH13_HUMAN)	6.7
3dwb	Endothelin-converting enzyme 1 (ECE1_HUMAN)	6.7

3f7b	Carbonic anhydrase 4 (CAH4_HUMAN)	6.7
3g5k	Peptide deformylase, mitochondrial (DEFM_HUMAN)	6.7
3glt	NAD-dependent deacetylase sirtuin-3, mitochondrial (SIRT3_HUMAN)	6.7
3n0t	Dipeptidyl-peptidase 2 (DPP2_HUMAN)	6.7
3nc0	GTP-binding nuclear protein Ran (RAN_HUMAN)	6.7
3npc	Mitogen-activated protein kinase 9 (MK09_HUMAN)	6.7
1bbp	Bilin-binding protein (BBP_PIEBR)	6.6
1ek6	UDP-glucose 4-epimerase (GALE_HUMAN)	6.6
1j78	Vitamin D-binding protein (VTDB_HUMAN)	6.6
1lpa	Pancreatic triacylglycerol lipase (LIPP_HUMAN)	6.6
1lqv	Endothelial protein C receptor Vitamin K-dependent protein C(EPCR_HUMAN/PROC_HUMAN)	6.6
1pk0	Calmodulin (CALM_HUMAN)	6.6
1rc1	Trifunctional purine biosynthetic protein adenosine-3 (PUR2_HUMAN)	6.6
1rs0	Complement factor B (CFAB_HUMAN)	6.6
1s9j	Dual specificity mitogen-activated protein kinase kinase 1(MP2K1_HUMAN)	6.6
1w6f	Arylamine N-acetyltransferase (NAT_MYCSM)	6.6
1x70	Dipeptidyl peptidase 4 (DPP4_HUMAN)	6.6
2eva	Mitogen-activated protein kinase kinase kinase 7(M3K7_HUMAN)	6.6
2fb8	B-Raf proto-oncogene serine/threonine-protein kinase(BRAF1_HUMAN)	6.6
2hz6	Serine/threonine-protein kinase/endoribonuclease IRE1(ERN1_HUMAN)	6.6
2jam	Calcium/calmodulin-dependent protein kinase type 1G (KCC1G_HUMAN)	6.6
2p8u	Hydroxymethylglutaryl-CoA synthase, cytoplasmic (HMCS1_HUMAN)	6.6
2qpj	Neprilysin (NEP_HUMAN)	6.6
3dls	PAS domain-containing serine/threonine-protein kinase(PASK_HUMAN)	6.6
3dzi	ADP-ribosyl cyclase 1 (CD38_HUMAN)	6.6
3e0p	Prostasin (PRSS8_HUMAN)	6.6
3eqr	Activated CDC42 kinase 1 (ACK1_HUMAN)	6.6
3eyg	Tyrosine-protein kinase JAK1 (JAK1_HUMAN)	6.6
1aj2	Dihydropteroate synthase (DHPS_ECOLI)	6.5
1bnq	Carbonic anhydrase 2 (CAH2_HUMAN)	6.5
1mq0	Cytidine deaminase (CDD_HUMAN)	6.5
1s9i	Dual specificity mitogen-activated protein kinase kinase 2 (MP2K2_HUMAN)	6.5
2buj	Serine/threonine-protein kinase 16(STK16_HUMAN)	6.5
2iwi	Serine/threonine-protein kinase Pim-2 (PIM2_HUMAN)	6.5
2nzt	Hexokinase-2(HXK2_HUMAN)	6.5
2q7r	Arachidonate 5-lipoxygenase-activating protein (AL5AP_HUMAN)	6.5
3acl	Pirin (PIR_HUMAN)	6.5
3deg	30S ribosomal protein S12 (RS12_ECOLI)	6.5
3efj	Hepatocyte growth factor receptor (MET_HUMAN)	6.5
3f96	Platelet-activating factor acetylhydrolase (PAFA_HUMAN)	6.5
3fme	Dual specificity mitogen-activated protein kinase kinase 6(MP2K6_HUMAN)	6.5
3gzn	NEDD8-activating enzyme E1 regulatory subunit (ULA1_HUMAN)	6.5
3hnb	Coagulation factor VIII (FA8_HUMAN)	6.5
3iar	Adenosine deaminase (ADA_HUMAN)	6.5
3kn5	Ribosomal protein S6 kinase alpha-5(KS6A5_HUMAN)	6.5
3mdz	Carbonic anhydrase 7 (CAH7_HUMAN)	6.5

1cza	Hexokinase-1(HXK1_HUMAN)	6.4
1doa	Cell division control protein 42 homolog (CDC42_HUMAN)	6.4
1fco	Beta-lactamase (AMPC_ECOLI)	6.4
1yfh	Methylated-DNA--protein-cysteine methyltransferase (MGMT_HUMAN)	6.4
2ar9	Caspase-9 (CASP9_HUMAN)	6.4
2hy3	Receptor-type tyrosine-protein phosphatase gamma (PTPRG_HUMAN)	6.4
2q8i	[Pyruvate dehydrogenase [lipoamide]] kinase isozyme 3, mitochondrial (PDK3_HUMAN)	6.4
2vle	Aldehyde dehydrogenase, mitochondrial (ALDH2_HUMAN)	6.4
2vwu	Ephrin type-B receptor 4 (EPHB4_HUMAN)	6.4
2zoq	Mitogen-activated protein kinase 3(MK03_HUMAN)	6.4
3cbp	Histone-lysine N-methyltransferase SETD7 (SETD7_HUMAN)	6.4
3dko	Ephrin type-A receptor 7 (EPHA7_HUMAN)	6.4
3g45	cAMP-specific 3',5'-cyclic phosphodiesterase 4B (PDE4B_HUMAN)	6.4
3hng	Vascular endothelial growth factor receptor 1 (VGFR1_HUMAN)	6.4
3ibe	Phosphatidylinositol-4,5-bisphosphate 3-kinase catalytic subunit gamma isoform (PK3CG_HUMAN)	6.4
3kjn	Caspase-8 (CASP8_HUMAN)	6.4
1hak	Annexin A5 (ANXA5_HUMAN)	6.3
1itu	Dipeptidase 1 (DPEP1_HUMAN)	6.3
1nrp	Proteinase-activated receptor 1 (PAR1_HUMAN)	6.3
2byi	Heat shock protein HSP 90-alpha (HS90A_HUMAN)	6.3
2c0i	Tyrosine-protein kinase HCK (HCK_HUMAN)	6.3
2wr6	Retinol-binding protein 4 (RET4_HUMAN)	6.3
3ddu	Prolyl endopeptidase (PPCE_HUMAN)	6.3
3gur	Glutathione S-transferase Mu 2 (GSTM2_HUMAN)	6.3
3i1h	Bcl-2 homologous antagonist/killer (BAK_HUMAN)	6.3
3ks9	Metabotropic glutamate receptor 1 (GRM1_HUMAN)	6.3
3osh	Phospholipase A2 isoform 3 (PA23_NAJSG)	6.3
1cf0	Profilin-1 (PROF1_HUMAN)	6.2
1e2s	Arylsulfatase A (ARSA_HUMAN)	6.2
1k3a	Insulin receptor substrate 1 (IRS1_HUMAN)	6.2
1mmr	Matrilysin (MMP7_HUMAN)	6.2
1p7c	Thymidine kinase (KITH_HHV11)	6.2
1qvn	Interleukin-2 (IL2_HUMAN)	6.2
1rwx	Caspase-1 (CASP1_HUMAN)	6.2
1t5c	Centromeric protein E (CENPE_HUMAN)	6.2
1tev	UMP-CMP kinase(KCY_HUMAN)	6.2
1z6j	Coagulation factor VII Tissue factor(FA7_HUMAN/TF_HUMAN)	6.2
1zsl	Coagulation factor XI (FA11_HUMAN)	6.2
2f0z	Sialidase-2 (NEUR2_HUMAN)	6.2
2hv8	Ras-related protein Rab-11A (RB11A_HUMAN)	6.2
2y7j	Phosphorylase b kinase gamma catalytic chain, testis/liver isoform (PHKG2_HUMAN)	6.2
3pty	Probable arabinosyltransferase C (EMBC_MYCTU)	6.2
1rm8	Matrix metalloproteinase-16 (MMP16_HUMAN)	6.1
1t31	Chymase (CMA1_HUMAN)	6.1
1tuf	Diaminopimelate decarboxylase (DCDA_METJA)	6.1
1xr9	HLA class I histocompatibility antigen, B-15 alpha chain (1B15_HUMAN)	6.1

2ipk	HLA class II histocompatibility antigen, DRB1-1 beta chain (2B11_HUMAN)	6.1
2vwi	Serine/threonine-protein kinase OSR1(OXSR1_HUMAN)	6.1
3bhh	Calcium/calmodulin-dependent protein kinase type II beta chain (KCC2B_HUMAN)	6.1
3c0z	Histone deacetylase 7 (HDAC7_HUMAN)	6.1
3ckl	Sulfotransferase family cytosolic 1B member 1 (ST1B1_HUMAN)	6.1
3e6i	Cytochrome P450 2E1 (CP2E1_HUMAN)	6.1
3fzt	Protein tyrosine kinase 2 beta (FAK2_HUMAN)	6.1
3kvf	Ubiquitin carboxyl-terminal hydrolase isozyme L1 (UCHL1_HUMAN)	6.1
3lxk	Tyrosine-protein kinase JAK3 (JAK3_HUMAN)	6.1
3max	Histone deacetylase 2 (HDAC2_HUMAN)	6.1
3p0g	Beta-2 adrenergic receptor (ADRB2_HUMAN)	6.1
1b86	Hemoglobin subunit alpha beta(HBA_HUMAN/HBB_HUMAN)	6
1kpe	Histidine triad nucleotide-binding protein 1 (HINT1_HUMAN)	6
1li4	Adenosylhomocysteinase (SAHH_HUMAN)	6
1lyb	Cathepsin D (CATD_HUMAN)	6
1nue	Nucleoside diphosphate kinase B(NDKB_HUMAN)	6
1vj9	Urokinase-type plasminogen activator (UROK_HUMAN)	6
2e9p	Serine/threonine-protein kinase Chk1 (CHK1_HUMAN)	6
2eal	Galectin-9 (LEG9_HUMAN)	6
2gi7	Platelet glycoprotein VI (GPVI_HUMAN)	6
2ivu	Proto-oncogene tyrosine-protein kinase receptor ret (RET_HUMAN)	6
2q8g	[Pyruvate dehydrogenase [lipoamide]] kinase isozyme 1, mitochondrial (PDK1_HUMAN)	6
2r4b	Receptor tyrosine-protein kinase erbB-4 (ERBB4_HUMAN)	6
2wo1	Ephrin type-A receptor 4 (EPHA4_HUMAN)	6
3bhy	Death-associated protein kinase 3 (DAPK3_HUMAN)	6
3hdn	Serine/threonine-protein kinase Sgk1 (SGK1_HUMAN)	6
3k8o	Purine nucleoside phosphorylase (PNPH_HUMAN)	6
3krx	Beta-adrenergic receptor kinase 1 (ARBK1_HUMAN)	6
3mhj	Tankyrase-2 (TNKS2_HUMAN)	6
3q4t	Activin receptor type-2A (AVR2A_HUMAN)	6
1dfp	Complement factor D (CFAD_HUMAN)	5.9
1fsu	Arylsulfatase B (ARSB_HUMAN)	5.9
1nuh	Glucose-6-phosphate isomerase (G6PI_HUMAN)	5.9
1qhy	Chloramphenicol 3-O phosphotransferase (CPT_STRVL)	5.9
1t32	Cathepsin G (CATG_HUMAN)	5.9
2hrq	Liver carboxylesterase 1 (EST1_HUMAN)	5.9
2huw	Growth factor receptor-bound protein 2 (GRB2_HUMAN)	5.9
2hw6	MAP kinase-interacting serine/threonine-protein kinase 1(MKNK1_HUMAN)	5.9
2px6	Fatty acid synthase (FAS_HUMAN)	5.9
2qmj	Maltase-glucoamylase, intestinal (MGA_HUMAN)	5.9
2x8b	Acetylcholinesterase (ACES_HUMAN)	5.9
2xk4	Serine/threonine-protein kinase Nek2 (NEK2_HUMAN)	5.9
3ap4	Galectin-8 (LEG8_HUMAN)	5.9
3fwl	Penicillin-binding protein 1B (PBPB_ECOLI)	5.9
3h1p	Caspase-7 (CASP7_HUMAN)	5.9
3kmz	Nuclear receptor corepressor 1 Retinoic acid receptor alpha(NCOR1_HUMAN/RARA_HUMAN)	5.9

3lc5	Coagulation factor IX (FA9_HUMAN)	5.9
3ooy	Transketolase (TKT_HUMAN)	5.9
3oui	Egl nine homolog 1 (EGLN1_HUMAN)	5.9
1exa	Retinoic acid receptor gamma (RARG_HUMAN)	5.8
1hkn	Heparin-binding growth factor 1 (FGF1_HUMAN)	5.8
2e82	D-amino-acid oxidase (OXDA_HUMAN)	5.8
2odb	Cell division control protein 42 homolog@Serine/threonine-protein kinase PAK 6 (CDC42_HUMAN@PAK6_HUMAN)	5.8
2oyc	Pyridoxal phosphate phosphatase (PLPP_HUMAN)	5.8
2v77	Carboxypeptidase A1 (CBPA1_HUMAN)	5.8
2vpg	B-cell CLL/lymphoma 9 protein Pygopus homolog 1(BCL9_HUMAN/PYGO1_HUMAN)	5.8
2zdx	[Pyruvate dehydrogenase [lipoamide]] kinase isozyme 4, mitochondrial (PDK4_HUMAN)	5.8
3ll6	Cyclin G-associated kinase(GAK_HUMAN)	5.8
1h9u	Retinoic acid receptor RXR-beta (RXRB_HUMAN)	5.7
1i0e	Creatine kinase M-type(KCRM_HUMAN)	5.7
1l5g	Integrin alpha-V (ITAV_HUMAN)	5.7
1l9n	Protein-glutamine gamma-glutamyltransferase E (TGM3_HUMAN)	5.7
1qgi	Chitosanase (CHIS_BACCI)	5.7
1qzy	Methionine aminopeptidase 2 (AMPM2_HUMAN)	5.7
1r55	ADAM 33 (ADA33_HUMAN)	5.7
1xd3	Ubiquitin carboxyl-terminal hydrolase isozyme L3 (UCHL3_HUMAN)	5.7
2onb	Thymidylate synthase (TYSY_HUMAN)	5.7
3ecr	Porphobilinogen deaminase (HEM3_HUMAN)	5.7
3eyc	Lipocalin-1 (LCN1_HUMAN)	5.7
3h54	Alpha-N-acetylgalactosaminidase (NAGAB_HUMAN)	5.7
3hcm	Protein S100-B (S100B_HUMAN)	5.7
3l5t	Macrophage migration inhibitory factor (MIF_HUMAN)	5.7
3lbj	Protein Mdm4 (MDM4_HUMAN)	5.7
3mng	Peroxiredoxin-5, mitochondrial (PRDX5_HUMAN)	5.7
1h0c	Serine--pyruvate aminotransferase (SPYA_HUMAN)	5.6
1q5h	Deoxyuridine 5'-triphosphate nucleotidohydrolase, mitochondrial (DUT_HUMAN)	5.6
1t83	Low affinity immunoglobulin gamma Fc region receptor III-B (FCG3B_HUMAN)	5.6
1ucn	Nucleoside diphosphate kinase A(NDKA_HUMAN)	5.6
1w80	Synaptojanin-1 (SYNJ1_HUMAN)	5.6
1wda	Protein-arginine deiminase type-4 (PADI4_HUMAN)	5.6
2nwg	Stromal cell-derived factor 1 (SDF1_HUMAN)	5.6
2xwc	Tumor protein p73 (P73_HUMAN)	5.6
3dtc	Mitogen-activated protein kinase kinase kinase 9 (M3K9_HUMAN)	5.6
3lo9	Neutrophil defensin 1 (DEF1_HUMAN)	5.6
1b0f	Leukocyte elastase (ELNE_HUMAN)	5.5
1qha	Hexokinase-1(HXK1_HUMAN)	5.5
2uz9	Guanine deaminase (GUAD_HUMAN)	5.5
3i68	Dihydroorotate dehydrogenase homolog, mitochondrial (PYRD_PLAF7)	5.5
3i97	Neuropilin-1 (NRP1_HUMAN)	5.5
3leo	Leukotriene C4 synthase (LTC4S_HUMAN)	5.5
3n22	Protein S100-A2 (S10A2_HUMAN)	5.5
2hxs	Ras-related protein Rab-28 (RAB28_HUMAN)	5.4

2obf	Phenylethanolamine N-methyltransferase (PNMT_HUMAN)	5.4
2xhd	Glutamate receptor 2 (GRIA2_HUMAN)	5.4
2zks	Granzyme M (GRAM_HUMAN)	5.4
3i4w	Disks large homolog 4 (DLG4_HUMAN)	5.4
3l6b	Serine racemase (SRR_HUMAN)	5.4
3lbz	B-cell lymphoma 6 protein (BCL6_HUMAN)	5.4
1j86	High affinity immunoglobulin epsilon receptor subunit alpha (FCERA_HUMAN)	5.3
2vgb	Pyruvate kinase isozymes R/L(KPYR_HUMAN)	5.3
3a7e	Catechol O-methyltransferase (COMT_HUMAN)	5.3
3ibd	Cytochrome P450 2B6 (CP2B6_HUMAN)	5.3
3mk8	Induced myeloid leukemia cell differentiation protein Mcl-1 (MCL1_HUMAN)	5.3
1g1s	P-selectin (LYAM3_HUMAN)	5.2
1g86	Eosinophil lysophospholipase (LPPL_HUMAN)	5.2
1hh4	Ras-related C3 botulinum toxin substrate 1 (RAC1_HUMAN)	5.2
1s1s	Cell division protein zipA (ZIPA_ECOLI)	5.2
2bo9	Carboxypeptidase A4 Latexin(CBPA4_HUMAN/LXN_HUMAN)	5.2
2bu7	[Pyruvate dehydrogenase [lipoamide]] kinase isozyme 2, mitochondrial (PDK2_HUMAN)	5.2
2dyb	Neutrophil cytosol factor 4 (NCF4_HUMAN)	5.2
3c5t	Glucagon-like peptide 1 receptor (GLP1R_HUMAN)	5.2
3f81	Dual specificity protein phosphatase 3 (DUS3_HUMAN)	5.2
3fxw	MAP kinase-activated protein kinase 3 (MAPK3_HUMAN)	5.2
1mg4	Serine/threonine-protein kinase DCLK1(DCLK1_HUMAN)	5.1
2ggu	Pulmonary surfactant-associated protein D (SFTPD_HUMAN)	5.1
2i3i	Baculoviral IAP repeat-containing protein 7 (BIRC7_HUMAN)	5.1
2jii	Serine/threonine-protein kinase VRK3(VRK3_HUMAN)	5.1
2ra4	C-C motif chemokine 13 (CCL13_HUMAN)	5.1
2wal	Growth arrest and DNA-damage-inducible protein GADD45 gamma (GA45G_HUMAN)	5.1
2wor	Protein S100-A7 (S10A7_HUMAN)	5.1
3bxz	Protein translocase subunit secA (SECA_ECOLI)	5.1
3f1o	Aryl hydrocarbon receptor nuclear translocator Endothelial PAS domain-containing protein 1(ARNT_HUMAN/EPAS1_HUMAN)	5.1
3oyw	Galectin-1 (LEG1_HUMAN)	5.1
1aii	Annexin A3 (ANXA3_HUMAN)	5
1sr5	Antithrombin-III (ANT3_HUMAN)	5
1uou	Thymidine phosphorylase (TYPH_HUMAN)	5
2a3r	Sulfotransferase 1A3/1A4 (ST1A3_HUMAN)	5
2jaj	N(G),N(G)-dimethylarginine dimethylaminohydrolase 1 (DDAH1_HUMAN)	5
2qou	30S ribosomal protein S9 (RS9_ECOLI)	5
1auq	von Willebrand factor (VWF_HUMAN)	4.9
1u4l	C-C motif chemokine 5 (CCL5_HUMAN)	4.9
1y6q	5'-methylthioadenosine/S-adenosylhomocysteine nucleosidase (MTNN_ECOLI)	4.9
2shp	Tyrosine-protein phosphatase non-receptor type 11 (PTN11_HUMAN)	4.9
3nax	3-phosphoinositide-dependent protein kinase 1 (PDPK1_HUMAN)	4.9
1bm7	Transthyretin (TTHY_HUMAN)	4.8
1kjr	Galectin-3 (LEG3_HUMAN)	4.8
2qkh	Gastric inhibitory polypeptide receptor Gastric inhibitory polypeptide(GIPR_HUMAN/GIP_HUMAN)	4.8
2v8e	Complement factor H (CFAH_HUMAN)	4.8

2wex	Apolipoprotein M (APOM_HUMAN)	4.8
3d5k	Outer membrane protein oprM (OPRM_PSEAE)	4.8
1czs	Coagulation factor V (FA5_HUMAN)	4.7
1elv	Complement C1s subcomponent (C1S_HUMAN)	4.7
1f9p	Platelet basic protein (CXCL7_HUMAN)	4.6
1n7d	Low-density lipoprotein receptor (LDLR_HUMAN)	4.6
1nbf	Ubiquitin carboxyl-terminal hydrolase 7 (UBP7_HUMAN)	4.6
2gwh	Sulfotransferase 1C4 (ST1C4_HUMAN)	4.6
2ofv	Proto-oncogene tyrosine-protein kinase LCK (LCK_HUMAN)	4.6
2q3z	Protein-glutamine gamma-glutamyltransferase 2 (TGM2_HUMAN)	4.6
3gal	Galectin-7 (LEG7_HUMAN)	4.6
3gxt	Alpha-galactosidase A (AGAL_HUMAN)	4.6
3ihp	Ubiquitin carboxyl-terminal hydrolase 5 (UBP5_HUMAN)	4.6
1rqd	Deoxyhypusine synthase (DHYS_HUMAN)	4.5
1ft4	Tumor necrosis factor receptor superfamily member 1A (TNR1A_HUMAN)	4.4
1u3t	Alcohol dehydrogenase 1A (ADH1A_HUMAN)	4.4
2ayo	Ubiquitin carboxyl-terminal hydrolase 14 (UBP14_HUMAN)	4.4
2qro	Deoxycytidine kinase (DCK_HUMAN)	4.4
1lgp	E3 ubiquitin-protein ligase CHFR (CHFR_HUMAN)	4.3
2znt	Glutamate receptor, ionotropic kainate 1 (GRIK1_HUMAN)	4.2
1k5r	65 kDa Yes-associated protein (YAP1_HUMAN)	4.1
3gxe	Collagen alpha-1(I) chain (CO1A1_HUMAN)	4.1
1au1	Interferon beta (IFNB_HUMAN)	4
1fga	Heparin-binding growth factor 2 (FGF2_HUMAN)	4
1u3u	Alcohol dehydrogenase 1B (ADH1B_HUMAN)	4
1w70	Neutrophil cytosol factor 1 (NCF1_HUMAN)	4
2e1q	Xanthine dehydrogenase/oxidase (XDH_HUMAN)	3.9
2qcg	Uridine 5'-monophosphate synthase (PYR5_HUMAN)	3.9
2ibi	Ubiquitin carboxyl-terminal hydrolase 2 (UBP2_HUMAN)	3.8
3d67	Carboxypeptidase B2 (CBPB2_HUMAN)	3.6
1a7c	Plasminogen activator inhibitor 1 (PAI1_HUMAN)	2.7
3p71	Leucine carboxyl methyltransferase 1 (LCMT1_HUMAN)	1.6
1ls6	Sulfotransferase 1A1 (ST1A1_HUMAN)	-0.3
1w4n	Phenylethylamine oxidase (PAOX_ARTGO)	-0.3
1m5b	Glutamate receptor 2 (GRIA2_RAT)	-1.6
2c11	Membrane primary amine oxidase (AOC3_HUMAN)	-2
2hei	Ras-related protein Rab-5B (RAB5B_HUMAN)	-3.6
1e51	Delta-aminolevulinic acid dehydratase (HEM2_HUMAN)	-3.9
2hhj	Bisphosphoglycerate mutase (PMGE_HUMAN)	-8.2
3hqr	Hypoxia-inducible factor 1 alpha (HIF1A_HUMAN)	-8.7
3i3t	Ubiquitin carboxyl-terminal hydrolase 21 (UBP21_HUMAN)	-10.7
2pfg	Carbonyl reductase [NADPH] 1 (CBR1_HUMAN)	-14.3
6jdw	Glycine amidinotransferase, mitochondrial (GATM_HUMAN)	-16.3
1ym9	M-phase inducer phosphatase 2 (MPIP2_HUMAN)	-22.3
1evu	Coagulation factor XIII A chain (F13A_HUMAN)	-29
1stf	Cystatin-B (CYTB_HUMAN)	-30.7

3kfq	Cathepsin L2 Cystatin-A(CATL2_HUMAN/CYTA_HUMAN)	-43.1
607/607		

Table A2.3. Docking results of Swainsonine with protein targets

PDB ID	Protein	Docking Score
1m5b	Glutamate receptor 2 (GRIA2_RAT)	7.4
3b8z	A disintegrin and metalloproteinase with thrombospondin motifs 5 (ATS5_HUMAN)	7.2
1ros	Macrophage metalloelastase (MMP12_HUMAN)	7.1
1itu	Dipeptidase 1 (DPEP1_HUMAN)	7
2fv5	ADAM 17 (ADA17_HUMAN)	7
2qcg	Uridine 5'-monophosphate synthase (PYR5_HUMAN)	6.9
2xhd	Glutamate receptor 2 (GRIA2_HUMAN)	6.9
1q5h	Deoxyuridine 5'-triphosphate nucleotidohydrolase, mitochondrial (DUT_HUMAN)	6.8
2gz5	Methionine aminopeptidase 1 (AMPM1_HUMAN)	6.8
2h44	cGMP-specific 3',5'-cyclic phosphodiesterase (PDE5A_HUMAN)	6.8
1h22	Acetylcholinesterase (ACES_TORCA)	6.7
1imb	Inositol monophosphatase (IMPA1_HUMAN)	6.7
1uou	Thymidine phosphorylase (TYPH_HUMAN)	6.7
2ovz	Matrix metalloproteinase-9 (MMP9_HUMAN)	6.7
2vgb	Pyruvate kinase isozymes R/L(KPYR_HUMAN)	6.7
2wnv	Complement C1q subcomponent subunit A B C(C1QA_HUMAN/C1QB_HUMAN/C1QC_HUMAN)	6.7
2xfo	Amine oxidase [flavin-containing] B (AOFB_HUMAN)	6.7
1bbp	Bilin-binding protein (BBP_PIEBR)	6.6
1caq	Stromelysin-1 (MMP3_HUMAN)	6.6
1i7b	S-adenosylmethionine decarboxylase proenzyme (DCAM_HUMAN)	6.6
1w78	Bifunctional protein folC (FOLC_ECOLI)	6.6
2gwh	Sulfotransferase 1C4 (ST1C4_HUMAN)	6.6
2p8u	Hydroxymethylglutaryl-CoA synthase, cytoplasmic (HMCS1_HUMAN)	6.6
2uzp	Protein kinase C gamma type (KPCG_HUMAN)	6.6
2znt	Glutamate receptor, ionotropic kainate 1 (GRIK1_HUMAN)	6.6
3d67	Carboxypeptidase B2 (CBPB2_HUMAN)	6.6
1dgh	Catalase (CATA_HUMAN)	6.5
1t32	Cathepsin G (CATG_HUMAN)	6.5
1w4n	Phenylethylamine oxidase (PAOX_ARTGO)	6.5
1w6k	Lanosterol synthase (ERG7_HUMAN)	6.5
1z6j	Coagulation factor VII Tissue factor(FA7_HUMAN/TF_HUMAN)	6.5
2aeb	Arginase-1 (ARGI1_HUMAN)	6.5
2gv7	Suppressor of tumorigenicity protein 14 (ST14_HUMAN)	6.5
2har	Vitamin D3 receptor (VDR_HUMAN)	6.5
2v4m	Glucosamine--fructose-6-phosphate aminotransferase [isomerizing] 1 (GFPT1_HUMAN)	6.5
3ant	Epoxide hydrolase 2 (HYES_HUMAN)	6.5
1dmw	Phenylalanine-4-hydroxylase (PH4H_HUMAN)	6.4
1j96	Aldo-keto reductase family 1 member C2 (AK1C2_HUMAN)	6.4
1qzy	Methionine aminopeptidase 2 (AMPM2_HUMAN)	6.4
1sg0	Ribosyldihydronicotinamide dehydrogenase [quinone] (NQO2_HUMAN)	6.4

1y6q	5'-methylthioadenosine/S-adenosylhomocysteine nucleosidase (MTNN_ECOLI)	6.4
1ysw	Apoptosis regulator Bcl-2 (BCL2_HUMAN)	6.4
2cke	Death-associated protein kinase 2 (DAPK2_HUMAN)	6.4
2jiv	Epidermal growth factor receptor (EGFR_HUMAN)	6.4
2nzt	Hexokinase-2(HXK2_HUMAN)	6.4
2pnu	Androgen receptor (ANDR_HUMAN)	6.4
2q7r	Arachidonate 5-lipoxygenase-activating protein (AL5AP_HUMAN)	6.4
3c0z	Histone deacetylase 7 (HDAC7_HUMAN)	6.4
3ckl	Sulfotransferase family cytosolic 1B member 1 (ST1B1_HUMAN)	6.4
1a4q	Neuraminidase (NRAM_INBBE)	6.3
1cza	Hexokinase-1(HXK1_HUMAN)	6.3
1dx4	Acetylcholinesterase (ACES_DROME)	6.3
1esv	Gelsolin (GELS_HUMAN)	6.3
1hy3	Estrogen sulfotransferase (ST1E1_HUMAN)	6.3
1kfy	Fumarate reductase flavoprotein subunit (FRDA_ECOLI)	6.3
1li4	Adenosylhomocysteinase (SAHH_HUMAN)	6.3
1ls6	Sulfotransferase 1A1 (ST1A1_HUMAN)	6.3
1tuf	Diaminopimelate decarboxylase (DCDA_METJA)	6.3
1zsl	Coagulation factor XI (FA11_HUMAN)	6.3
2afu	Glutaminyl-peptide cyclotransferase (QPCT_HUMAN)	6.3
2e1q	Xanthine dehydrogenase/oxidase (XDH_HUMAN)	6.3
2e82	D-amino-acid oxidase (OXDA_HUMAN)	6.3
2jih	A disintegrin and metalloproteinase with thrombospondin motifs 1 (ATS1_HUMAN)	6.3
2v3e	Glucosylceramidase (GLCM_HUMAN)	6.3
2w4q	Prostaglandin reductase 2 (PTGR2_HUMAN)	6.3
3cbp	Histone-lysine N-methyltransferase SETD7 (SETD7_HUMAN)	6.3
1a5h	Tissue-type plasminogen activator (TPA_HUMAN)	6.2
1d8d	GTPase KRas (RASK_HUMAN)	6.2
1lhv	Sex hormone-binding globulin (SHBG_HUMAN)	6.2
1lpa	Pancreatic triacylglycerol lipase (LIPP_HUMAN)	6.2
1qu3	Isoleucyl-tRNA synthetase (SYI1_STAAU)	6.2
1rc1	Trifunctional purine biosynthetic protein adenosine-3 (PUR2_HUMAN)	6.2
1t5c	Centromeric protein E (CENPE_HUMAN)	6.2
1vj9	Urokinase-type plasminogen activator (UROK_HUMAN)	6.2
2eal	Galectin-9 (LEG9_HUMAN)	6.2
2f38	Aldo-keto reductase family 1 member C3 (AK1C3_HUMAN)	6.2
2f8z	Farnesyl pyrophosphate synthetase (FPPS_HUMAN)	6.2
2fs8	Tryptase beta-2 (TRYB2_HUMAN)	6.2
2g0e	HTH-type transcriptional regulator qacR (QACR_STAHA)	6.2
2hi4	Cytochrome P450 1A2 (CP1A2_HUMAN)	6.2
2woe	ADP-ribosyl-[dinitrogen reductase] glycohydrolase (DRAG_RHORU)	6.2
1aj2	Dihydropteroate synthase (DHPS_ECOLI)	6.1
1byd	Beta-amylase (AMYB_SOYBN)	6.1
1cm8	Mitogen-activated protein kinase 12(MK12_HUMAN)	6.1
1gnp	GTPase HRas (RASH_HUMAN)	6.1
1jr1	Inosine-5'-monophosphate dehydrogenase 2 (IMDH2_CRIGR)	6.1

1lpg	Coagulation factor X (FA10_HUMAN)	6.1
1mrl	Streptogramin A acetyltransferase (VATD_ENTFC)	6.1
1nf7	Inosine-5'-monophosphate dehydrogenase 2 (IMDH2_HUMAN)	6.1
1nuh	Glucose-6-phosphate isomerase (G6PI_HUMAN)	6.1
1ohk	Dihydrofolate reductase (DYR_HUMAN)	6.1
1s0x	Nuclear receptor ROR-alpha (RORA_HUMAN)	6.1
1s5o	Carnitine O-acetyltransferase (CACP_HUMAN)	6.1
1t46	Mast/stem cell growth factor receptor (KIT_HUMAN)	6.1
1xr9	HLA class I histocompatibility antigen, B-15 alpha chain (1B15_HUMAN)	6.1
2e3r	Collagen type IV alpha-3-binding protein (C43BP_HUMAN)	6.1
2fb8	B-Raf proto-oncogene serine/threonine-protein kinase(BRAF1_HUMAN)	6.1
2obf	Phenylethanolamine N-methyltransferase (PNMT_HUMAN)	6.1
2q6b	3-hydroxy-3-methylglutaryl-coenzyme A reductase (HMDH_HUMAN)	6.1
2vct	Glutathione S-transferase A2 (GSTA2_HUMAN)	6.1
2vgq	Mitochondrial antiviral-signaling protein (MAVS_HUMAN)	6.1
2vqq	Histone deacetylase 4 (HDAC4_HUMAN)	6.1
2wal	Growth arrest and DNA-damage-inducible protein GADD45 gamma (GA45G_HUMAN)	6.1
2wax	Probable ATP-dependent RNA helicase DDX6 (DDX6_HUMAN)	6.1
2xef	Glutamate carboxypeptidase 2 (FOLH1_HUMAN)	6.1
1eba	Erythropoietin receptor (EPOR_HUMAN)	6
1exa	Retinoic acid receptor gamma (RARG_HUMAN)	6
1hak	Annexin A5 (ANXA5_HUMAN)	6
1ish	ADP-ribosyl cyclase 2 (BST1_HUMAN)	6
1kkq	Nuclear receptor corepressor 2 (NCOR2_HUMAN)	6
1nde	Estrogen receptor beta (ESR2_HUMAN)	6
1so2	cGMP-inhibited 3',5'-cyclic phosphodiesterase B (PDE3B_HUMAN)	6
1t40	Aldose reductase (ALDR_HUMAN)	6
2a3r	Sulfotransferase 1A3/1A4 (ST1A3_HUMAN)	6
2ewy	Beta-secretase 2 (BACE2_HUMAN)	6
2gvj	Nicotinamide phosphoribosyltransferase (NAMPT_HUMAN)	6
2ipk	HLA class II histocompatibility antigen, DRB1-1 beta chain (2B11_HUMAN)	6
2ofv	Proto-oncogene tyrosine-protein kinase LCK (LCK_HUMAN)	6
2ouq	cAMP and cAMP-inhibited cGMP 3',5'-cyclic phosphodiesterase 10A (PDE10_HUMAN)	6
2prh	Dihydroorotate dehydrogenase, mitochondrial (PYRD_HUMAN)	6
2qro	Deoxycytidine kinase (DCK_HUMAN)	6
2r4b	Receptor tyrosine-protein kinase erbB-4 (ERBB4_HUMAN)	6
2wr6	Retinol-binding protein 4 (RET4_HUMAN)	6
2x8b	Acetylcholinesterase (ACES_HUMAN)	6
2y7j	Phosphorylase b kinase gamma catalytic chain, testis/liver isoform (PHKG2_HUMAN)	6
3acl	Pirin (PIR_HUMAN)	6

Table A2. Docking results of Casantospermine with protein targets

PDB ID	Protein	Docking Score

1m5b	Glutamate receptor 2 (GRIA2_RAT)	7.4
3b8z	A disintegrin and metalloproteinase with thrombospondin motifs 5 (ATS5_HUMAN)	7.2
1ros	Macrophage metalloelastase (MMP12_HUMAN)	7.1
3mhj	Tankyrase-2 (TNKS2_HUMAN)	7.1
1itu	Dipeptidase 1 (DPEP1_HUMAN)	7
2fv5	ADAM 17 (ADA17_HUMAN)	7
3ldp	78 kDa glucose-regulated protein (GRP78_HUMAN)	7
2qcg	Uridine 5'-monophosphate synthase (PYR5_HUMAN)	6.9
2xhd	Glutamate receptor 2 (GRIA2_HUMAN)	6.9
1q5h	Deoxyuridine 5'-triphosphate nucleotidohydrolase, mitochondrial (DUT_HUMAN)	6.8
1uou	Thymidine phosphorylase (TYPH_HUMAN)	6.8
2gz5	Methionine aminopeptidase 1 (AMPM1_HUMAN)	6.8
2h44	cGMP-specific 3',5'-cyclic phosphodiesterase (PDE5A_HUMAN)	6.8
3fzm	BAG family molecular chaperone regulator 1 (BAG1_HUMAN)	6.8
1h22	Acetylcholinesterase (ACES_TORCA)	6.7
1imb	Inositol monophosphatase (IMPA1_HUMAN)	6.7
2ovz	Matrix metalloproteinase-9 (MMP9_HUMAN)	6.7
2vgb	Pyruvate kinase isozymes R/L(KPYR_HUMAN)	6.7
2wnv	Complement C1q subcomponent subunit A B C(C1QA_HUMAN/C1QB_HUMAN/C1QC_HUMAN)	6.7
2xfo	Amine oxidase [flavin-containing] B (AOFB_HUMAN)	6.7
3b6r	Creatine kinase B-type (KCRB_HUMAN)	6.7
3lc5	Coagulation factor IX (FA9_HUMAN)	6.7
1bbp	Bilin-binding protein (BBP_PIEBR)	6.6
1caq	Stromelysin-1 (MMP3_HUMAN)	6.6
1i7b	S-adenosylmethionine decarboxylase proenzyme (DCAM_HUMAN)	6.6
1w78	Bifunctional protein folC (FOLC_ECOLI)	6.6
2gwh	Sulfotransferase 1C4 (ST1C4_HUMAN)	6.6
2p8u	Hydroxymethylglutaryl-CoA synthase, cytoplasmic (HMCS1_HUMAN)	6.6
2uzp	Protein kinase C gamma type (KPCG_HUMAN)	6.6
2znt	Glutamate receptor, ionotropic kainate 1 (GRIK1_HUMAN)	6.6
3d67	Carboxypeptidase B2 (CBPB2_HUMAN)	6.6
3eta	Insulin receptor (INSR_HUMAN)	6.6
3frj	Corticosteroid 11-beta-dehydrogenase isozyme 1 (DHI1_HUMAN)	6.6
3glt	NAD-dependent deacetylase sirtuin-3, mitochondrial (SIRT3_HUMAN)	6.6
3k8o	Purine nucleoside phosphorylase (PNPH_HUMAN)	6.6
3p71	Leucine carboxyl methyltransferase 1 (LCMT1_HUMAN)	6.6
3pm0	Cytochrome P450 1B1 (CP1B1_HUMAN)	6.6
1dgh	Catalase (CATA_HUMAN)	6.5
1t32	Cathepsin G (CATG_HUMAN)	6.5
1w4n	Phenylethylamine oxidase (PAOX_ARTGO)	6.5
1w6k	Lanosterol synthase (ERG7_HUMAN)	6.5
1z6j	Coagulation factor VII Tissue factor(FA7_HUMAN/TF_HUMAN)	6.5
2aeb	Arginase-1 (ARGI1_HUMAN)	6.5
2gv7	Suppressor of tumorigenicity protein 14 (ST14_HUMAN)	6.5
2har	Vitamin D3 receptor (VDR_HUMAN)	6.5
2v4m	Glucosamine--fructose-6-phosphate aminotransferase [isomerizing] 1 (GFPT1_HUMAN)	6.5

3ant	Epoxide hydrolase 2 (HYES_HUMAN)	6.5
3hf8	Tryptophan 5-hydroxylase 1 (TPH1_HUMAN)	6.5
1dmw	Phenylalanine-4-hydroxylase (PH4H_HUMAN)	6.4
1j96	Aldo-keto reductase family 1 member C2 (AK1C2_HUMAN)	6.4
1qzy	Methionine aminopeptidase 2 (AMPM2_HUMAN)	6.4
1sg0	Ribosyldihydronicotinamide dehydrogenase [quinone] (NQO2_HUMAN)	6.4
1y6q	5'-methylthioadenosine/S-adenosylhomocysteine nucleosidase (MTNN_ECOLI)	6.4
1ysw	Apoptosis regulator Bcl-2 (BCL2_HUMAN)	6.4
2cke	Death-associated protein kinase 2 (DAPK2_HUMAN)	6.4
2jiv	Epidermal growth factor receptor (EGFR_HUMAN)	6.4
2nzt	Hexokinase-2(HXK2_HUMAN)	6.4
2pnu	Androgen receptor (ANDR_HUMAN)	6.4
2q7r	Arachidonate 5-lipoxygenase-activating protein (AL5AP_HUMAN)	6.4
2v3e	Glucosylceramidase (GLCM_HUMAN)	6.4
3c0z	Histone deacetylase 7 (HDAC7_HUMAN)	6.4
3ckl	Sulfotransferase family cytosolic 1B member 1 (ST1B1_HUMAN)	6.4
3dyl	High affinity cGMP-specific 3',5'-cyclic phosphodiesterase 9A (PDE9A_HUMAN)	6.4
3i8v	cAMP-specific 3',5'-cyclic phosphodiesterase 4A (PDE4A_HUMAN)	6.4
1a4q	Neuraminidase (NRAM_INBBE)	6.3
1cza	Hexokinase-1(HXK1_HUMAN)	6.3
1dx4	Acetylcholinesterase (ACES_DROME)	6.3
1hy3	Estrogen sulfotransferase (ST1E1_HUMAN)	6.3
1kfy	Fumarate reductase flavoprotein subunit (FRDA_ECOLI)	6.3
1li4	Adenosylhomocysteinase (SAHH_HUMAN)	6.3
1ls6	Sulfotransferase 1A1 (ST1A1_HUMAN)	6.3
1t5c	Centromeric protein E (CENPE_HUMAN)	6.3
1tuf	Diaminopimelate decarboxylase (DCDA_METJA)	6.3
1zsl	Coagulation factor XI (FA11_HUMAN)	6.3
2afu	Glutaminyl-peptide cyclotransferase (QPCT_HUMAN)	6.3
2e1q	Xanthine dehydrogenase/oxidase (XDH_HUMAN)	6.3
2e82	D-amino-acid oxidase (OXDA_HUMAN)	6.3
2jih	A disintegrin and metalloproteinase with thrombospondin motifs 1 (ATS1_HUMAN)	6.3
3cbp	Histone-lysine N-methyltransferase SETD7 (SETD7_HUMAN)	6.3
3g7w	Islet amyloid polypeptide (IAPP_HUMAN)	6.3
3gu8	Death-associated protein kinase 1 (DAPK1_HUMAN)	6.3
3m9k	Thioredoxin (THIO_HUMAN)	6.3
3n7r	Calcitonin gene-related peptide type 1 receptor Receptor activity-modifying protein 1(CALRL_HUMAN/RAMP1_HUMAN)	6.3
3p0g	Beta-2 adrenergic receptor (ADRB2_HUMAN)	6.3
3pkj	Mono-ADP-ribosyltransferase sirtuin-6 (SIRT6_HUMAN)	6.3
1aj2	Dihydropteroate synthase (DHPS_ECOLI)	6.2
1d8d	GTPase KRas (RASK_HUMAN)	6.2
1lhv	Sex hormone-binding globulin (SHBG_HUMAN)	6.2
1lpa	Pancreatic triacylglycerol lipase (LIPP_HUMAN)	6.2
1nuh	Glucose-6-phosphate isomerase (G6PI_HUMAN)	6.2
1rc1	Trifunctional purine biosynthetic protein adenosine-3 (PUR2_HUMAN)	6.2
1vj9	Urokinase-type plasminogen activator (UROK_HUMAN)	6.2

2eal	Galectin-9 (LEG9_HUMAN)	6.2
2f38	Aldo-keto reductase family 1 member C3 (AK1C3_HUMAN)	6.2
2f8z	Farnesyl pyrophosphate synthetase (FPPS_HUMAN)	6.2
2fs8	Tryptase beta-2 (TRYB2_HUMAN)	6.2
2g0e	HTH-type transcriptional regulator qacR (QACR_STAHA)	6.2
2hi4	Cytochrome P450 1A2 (CP1A2_HUMAN)	6.2
2woe	ADP-ribosyl-[dinitrogen reductase] glycohydrolase (DRAG_RHORU)	6.2
3enm	Dual specificity mitogen-activated protein kinase kinase 6(MP2K6_HUMAN)	6.2
3fc6	Retinoic acid receptor RXR-alpha (RXRA_HUMAN)	6.2
3hng	Vascular endothelial growth factor receptor 1 (VGFR1_HUMAN)	6.2
1a5h	Tissue-type plasminogen activator (TPA_HUMAN)	6.1
1byd	Beta-amylase (AMYB_SOYBN)	6.1
1cm8	Mitogen-activated protein kinase 12(MK12_HUMAN)	6.1
1esv	Gelsolin (GELS_HUMAN)	6.1
1gnp	GTPase HRas (RASH_HUMAN)	6.1
1jr1	Inosine-5'-monophosphate dehydrogenase 2 (IMDH2_CRIGR)	6.1
1lpg	Coagulation factor X (FA10_HUMAN)	6.1
1mrl	Streptogramin A acetyltransferase (VATD_ENTFC)	6.1
1ohk	Dihydrofolate reductase (DYR_HUMAN)	6.1
1s0x	Nuclear receptor ROR-alpha (RORA_HUMAN)	6.1
1s5o	Carnitine O-acetyltransferase (CACP_HUMAN)	6.1
1t46	Mast/stem cell growth factor receptor (KIT_HUMAN)	6.1
1xr9	HLA class I histocompatibility antigen, B-15 alpha chain (1B15_HUMAN)	6.1
2e3r	Collagen type IV alpha-3-binding protein (C43BP_HUMAN)	6.1
2fb8	B-Raf proto-oncogene serine/threonine-protein kinase(BRAF1_HUMAN)	6.1
2obf	Phenylethanolamine N-methyltransferase (PNMT_HUMAN)	6.1
2q6b	3-hydroxy-3-methylglutaryl-coenzyme A reductase (HMDH_HUMAN)	6.1
2vct	Glutathione S-transferase A2 (GSTA2_HUMAN)	6.1
2vgq	Mitochondrial antiviral-signaling protein (MAVS_HUMAN)	6.1
2vqq	Histone deacetylase 4 (HDAC4_HUMAN)	6.1
2w4q	Prostaglandin reductase 2 (PTGR2_HUMAN)	6.1
2wal	Growth arrest and DNA-damage-inducible protein GADD45 gamma (GA45G_HUMAN)	6.1
2wax	Probable ATP-dependent RNA helicase DDX6 (DDX6_HUMAN)	6.1
2xef	Glutamate carboxypeptidase 2 (FOLH1_HUMAN)	6.1
3eml	Adenosine receptor A2a (AA2AR_HUMAN)	6.1
3f1o	Aryl hydrocarbon receptor nuclear translocator Endothelial PAS domain-containing protein 1(ARNT_HUMAN/EPAS1_HUMAN)	6.1
3g45	cAMP-specific 3',5'-cyclic phosphodiesterase 4B (PDE4B_HUMAN)	6.1
3i68	Dihydroorotate dehydrogenase homolog, mitochondrial (PYRD_PLAF7)	6.1
3lco	Macrophage colony-stimulating factor 1 receptor (CSF1R_HUMAN)	6.1
3my0	Serine/threonine-protein kinase receptor R3(ACVL1_HUMAN)	6.1
3nax	3-phosphoinositide-dependent protein kinase 1 (PDPK1_HUMAN)	6.1
3nc0	GTP-binding nuclear protein Ran (RAN_HUMAN)	6.1
3oui	Egl nine homolog 1 (EGLN1_HUMAN)	6.1
4ald	Fructose-bisphosphate aldolase A (ALDOA_HUMAN)	6.1
1eba	Erythropoietin receptor (EPOR_HUMAN)	6
1exa	Retinoic acid receptor gamma (RARG_HUMAN)	6

1hak	Annexin A5 (ANXA5_HUMAN)	6
1ish	ADP-ribosyl cyclase 2 (BST1_HUMAN)	6
1nde	Estrogen receptor beta (ESR2_HUMAN)	6
1nf7	Inosine-5'-monophosphate dehydrogenase 2 (IMDH2_HUMAN)	6
1qip	Lactoylglutathione lyase (LGUL_HUMAN)	6
1so2	cGMP-inhibited 3',5'-cyclic phosphodiesterase B (PDE3B_HUMAN)	6
1t40	Aldose reductase (ALDR_HUMAN)	6
2a3r	Sulfotransferase 1A3/1A4 (ST1A3_HUMAN)	6
2ewy	Beta-secretase 2 (BACE2_HUMAN)	6
2gvj	Nicotinamide phosphoribosyltransferase (NAMPT_HUMAN)	6
2ipk	HLA class II histocompatibility antigen, DRB1-1 beta chain (2B11_HUMAN)	6
2ofv	Proto-oncogene tyrosine-protein kinase LCK (LCK_HUMAN)	6
2ouq	cAMP and cAMP-inhibited cGMP 3',5'-cyclic phosphodiesterase 10A (PDE10_HUMAN)	6
2prh	Dihydroorotate dehydrogenase, mitochondrial (PYRD_HUMAN)	6
2qro	Deoxycytidine kinase (DCK_HUMAN)	6
2r4b	Receptor tyrosine-protein kinase erbB-4 (ERBB4_HUMAN)	6
2wr6	Retinol-binding protein 4 (RET4_HUMAN)	6
2x8b	Acetylcholinesterase (ACES_HUMAN)	6
2y7j	Phosphorylase b kinase gamma catalytic chain, testis/liver isoform (PHKG2_HUMAN)	6
3acl	Pirin (PIR_HUMAN)	6
3e7e	Mitotic checkpoint serine/threonine-protein kinase BUB1(BUB1_HUMAN)	6
3eqc	Dual specificity mitogen-activated protein kinase kinase 1 (MP2K1_HUMAN)	6
3ff6	Acetyl-CoA carboxylase 2 (ACACB_HUMAN)	6
3gqy	Pyruvate kinase isozymes M1/M2 (KPYM_HUMAN)	6
3hm8	Hexokinase-3(HXK3_HUMAN)	6
3jsx	NAD(P)H dehydrogenase [quinone] 1 (NQO1_HUMAN)	6
3kec	Collagenase 3 (MMP13_HUMAN)	6
3lxk	Tyrosine-protein kinase JAK3 (JAK3_HUMAN)	6
3osh	Phospholipase A2 isoform 3 (PA23_NAJSG)	6
1e9a	Thymidylate kinase (KTHY_HUMAN)	5.9
1efn	Proto-oncogene tyrosine-protein kinase Fyn (FYN_HUMAN)	5.9
1egc	Medium-chain specific acyl-CoA dehydrogenase, mitochondrial (ACADM_HUMAN)	5.9
1ib1	14-3-3 protein zeta/delta (1433Z_HUMAN)	5.9
1kgi	Transthyretin (TTHY_RAT)	5.9
1kkq	Nuclear receptor corepressor 2 (NCOR2_HUMAN)	5.9
1kws	Galactosylgalactosylxylosylprotein 3-beta-glucuronosyltransferase 3 (B3GA3_HUMAN)	5.9
1mmr	Matrilysin (MMP7_HUMAN)	5.9
1mq0	Cytidine deaminase (CDD_HUMAN)	5.9
1pk0	Calmodulin (CALM_HUMAN)	5.9
1pq6	Oxysterols receptor LXR-beta (NR1H2_HUMAN)	5.9
1qu3	Isoleucyl-tRNA synthetase (SYI1_STAAU)	5.9
1rm8	Matrix metalloproteinase-16 (MMP16_HUMAN)	5.9
1unl	Cyclin-dependent kinase 5 activator 1 Cell division protein kinase 5(CD5R1_HUMAN/CDK5_HUMAN)	5.9
2a3i	Mineralocorticoid receptor (MCR_HUMAN)	5.9
2bxr	Amine oxidase [flavin-containing] A (AOFA_HUMAN)	5.9
2gl6	Creatine kinase, sarcomeric mitochondrial(KCRS_HUMAN)	5.9

2h6i	Protein farnesyltransferase/geranylgeranyltransferase type-1 subunit alpha (FNTA_HUMAN)	5.9
2hh5	Cathepsin S (CATS_HUMAN)	5.9
2jc6	Calcium/calmodulin-dependent protein kinase type 1D (KCC1D_HUMAN)	5.9
2nnq	Fatty acid-binding protein, adipocyte (FABP4_HUMAN)	5.9
2q5g	Peroxisome proliferator-activated receptor delta (PPARD_HUMAN)	5.9
2qpj	Neprilysin (NEP_HUMAN)	5.9
2r2n	Kynurenine/alpha-aminoadipate aminotransferase mitochondrial (AADAT_HUMAN)	5.9
2wu7	Dual specificity protein kinase CLK3 (CLK3_HUMAN)	5.9
2z7x	Toll-like receptor 1 Toll-like receptor 2(TLR1_HUMAN/TLR2_HUMAN)	5.9
3dl9	Vitamin D 25-hydroxylase (CP2R1_HUMAN)	5.9
3dtc	Mitogen-activated protein kinase kinase kinase 9 (M3K9_HUMAN)	5.9
3g3n	High affinity cAMP-specific 3',5'-cyclic phosphodiesterase 7A (PDE7A_HUMAN)	5.9
3g5k	Peptide deformylase, mitochondrial (DEFM_HUMAN)	5.9
3g7e	DNA gyrase subunit B (GYRB_ECOLI)	5.9
3gvu	Tyrosine-protein kinase ABL2 (ABL2_HUMAN)	5.9
3iad	cAMP-specific 3',5'-cyclic phosphodiesterase 4D (PDE4D_HUMAN)	5.9
3krx	Beta-adrenergic receptor kinase 1 (ARBK1_HUMAN)	5.9
3mvh	RAC-alpha serine/threonine-protein kinase (AKT1_HUMAN)	5.9
3o3u	Advanced glycosylation end product-specific receptor (RAGE_HUMAN)	5.9
1a2n	UDP-N-acetylglucosamine 1-carboxyvinyltransferase (MURA_ECOLI)	5.8
1c4y	Prothrombin (THRB_HUMAN)	5.8
1d4l	Gag-Pol polyprotein (POL_HV1A2)	5.8
1ek6	UDP-glucose 4-epimerase (GALE_HUMAN)	5.8
1k9s	Purine nucleoside phosphorylase deoD-type (DEOD_ECOLI)	5.8
1ksw	Proto-oncogene tyrosine-protein kinase Src (SRC_HUMAN)	5.8
1lqv	Endothelial protein C receptor Vitamin K-dependent protein C(EPCR_HUMAN/PROC_HUMAN)	5.8
1mc5	Alcohol dehydrogenase class-3 (ADHX_HUMAN)	5.8
1ogu	Cyclin-A2 (CCNA2_HUMAN)	5.8
1p4r	Bifunctional purine biosynthesis protein PURH (PUR9_HUMAN)	5.8
1r4l	Angiotensin-converting enzyme 2 (ACE2_HUMAN)	5.8
1rs0	Complement factor B (CFAB_HUMAN)	5.8
1s9i	Dual specificity mitogen-activated protein kinase kinase 2 (MP2K2_HUMAN)	5.8
1s9j	Dual specificity mitogen-activated protein kinase kinase 1(MP2K1_HUMAN)	5.8
1t31	Chymase (CMA1_HUMAN)	5.8
1tu6	Cathepsin K (CATK_HUMAN)	5.8
1xvp	Nuclear receptor subfamily 1 group I member 3 (NR1I3_HUMAN)	5.8
1zcm	Calpain-1 catalytic subunit (CAN1_HUMAN)	5.8
2euf	Cell division protein kinase 6 (CDK6_HUMAN)	5.8
2h26	T-cell surface glycoprotein CD1b (CD1B_HUMAN)	5.8
2jaj	N(G),N(G)-dimethylarginine dimethylaminohydrolase 1 (DDAH1_HUMAN)	5.8
2nyr	NAD-dependent deacetylase sirtuin-5 (SIRT5_HUMAN)	5.8
2p4j	Beta-secretase 1 (BACE1_HUMAN)	5.8
2po6	T-cell surface glycoprotein CD1d (CD1D_HUMAN)	5.8
2vag	Dual specificity protein kinase CLK1 (CLK1_HUMAN)	5.8
3dpf	Neutrophil collagenase (MMP8_HUMAN)	5.8
3e4a	Insulin-degrading enzyme (IDE_HUMAN)	5.8

3e7v	Serine/threonine-protein kinase haspin (HASP_HUMAN)	5.8
3gkj	Niemann-Pick C1 protein (NPC1_HUMAN)	5.8
3lxe	Carbonic anhydrase 1 (CAH1_HUMAN)	5.8
1doa	Cell division control protein 42 homolog (CDC42_HUMAN)	5.7
1fm9	Peroxisome proliferator-activated receptor gamma (PPARG_HUMAN)	5.7
1nd5	Prostatic acid phosphatase (PPAP_HUMAN)	5.7
1onq	T-cell surface glycoprotein CD1a (CD1A_HUMAN)	5.7
1rgy	Beta-lactamase (AMPC_CITFR)	5.7
1sr7	Progesterone receptor (PRGR_HUMAN)	5.7
1u3u	Alcohol dehydrogenase 1B (ADH1B_HUMAN)	5.7
1xap	Retinoic acid receptor beta (RARB_HUMAN)	5.7
1z11	Cytochrome P450 2A6 (CP2A6_HUMAN)	5.7
1zs6	Nucleoside diphosphate kinase 3(NDK3_HUMAN)	5.7
2ar9	Caspase-9 (CASP9_HUMAN)	5.7
2bil	Proto-oncogene serine/threonine-protein kinase Pim-1 (PIM1_HUMAN)	5.7
2c0i	Tyrosine-protein kinase HCK (HCK_HUMAN)	5.7
2hrq	Liver carboxylesterase 1 (EST1_HUMAN)	5.7
2jam	Calcium/calmodulin-dependent protein kinase type 1G (KCC1G_HUMAN)	5.7
2oc2	Angiotensin-converting enzyme (ACE_HUMAN)	5.7
2q80	Geranylgeranyl pyrophosphate synthetase (GGPPS_HUMAN)	5.7
2r3v	Mevalonate kinase(KIME_HUMAN)	5.7
2r59	Leukotriene A-4 hydrolase (LKHA4_HUMAN)	5.7
2rjp	A disintegrin and metalloproteinase with thrombospondin motifs 4 (ATS4_HUMAN)	5.7
2vz6	Calcium/calmodulin-dependent protein kinase type II alpha chain (KCC2A_HUMAN)	5.7
2x7o	TGF-beta receptor type-1 (TGFR1_HUMAN)	5.7
3bkb	Proto-oncogene tyrosine-protein kinase Fes/Fps(FES_HUMAN)	5.7
3c2l	DNA polymerase beta (DPOLB_HUMAN)	5.7
3da2	Carbonic anhydrase 13 (CAH13_HUMAN)	5.7
3dh4	Sodium/glucose cotransporter (SGLT_VIBPA)	5.7
3dzi	ADP-ribosyl cyclase 1 (CD38_HUMAN)	5.7
3e8d	RAC-beta serine/threonine-protein kinase Glycogen synthase kinase-3 beta(AKT2_HUMAN/GSK3B_HUMAN)	5.7
3fqe	Tyrosine-protein kinase SYK (KSYK_HUMAN)	5.7
3gp0	Mitogen-activated protein kinase 11 (MK11_HUMAN)	5.7
3ipq	Oxysterols receptor LXR-alpha (NR1H3_HUMAN)	5.7
3jwe	Monoglyceride lipase (MGLL_HUMAN)	5.7
3ljr	Glutathione S-transferase theta-2 (GSTT2_HUMAN)	5.7
3nos	Nitric oxide synthase, endothelial (NOS3_HUMAN)	5.7
3nyn	G protein-coupled receptor kinase 6 (GRK6_HUMAN)	5.7
3odu	C-X-C chemokine receptor type 4 (CXCR4_HUMAN)	5.7
3ooy	Transketolase (TKT_HUMAN)	5.7
1csb	Cathepsin B (CATB_HUMAN)	5.6
1gnj	Serum albumin (ALBU_HUMAN)	5.6
1hh4	Ras-related C3 botulinum toxin substrate 1 (RAC1_HUMAN)	5.6
1hmr	Fatty acid-binding protein, heart (FABPH_HUMAN)	5.6
1j86	High affinity immunoglobulin epsilon receptor subunit alpha (FCERA_HUMAN)	5.6
1kpe	Histidine triad nucleotide-binding protein 1 (HINT1_HUMAN)	5.6

1nun	Fibroblast growth factor 10 (FGF10_HUMAN)	5.6
1p7c	Thymidine kinase (KITH_HHV11)	5.6
1rne	Renin (RENI_HUMAN)	5.6
1s8c	Heme oxygenase 1 (HMOX1_HUMAN)	5.6
1wuu	Galactokinase(GALK1_HUMAN)	5.6
1xd0	Pancreatic alpha-amylase (AMYP_HUMAN)	5.6
2ayr	Estrogen receptor (ESR1_HUMAN)	5.6
2az5	Tumor necrosis factor (TNFA_HUMAN)	5.6
2byi	Heat shock protein HSP 90-alpha (HS90A_HUMAN)	5.6
2c47	Casein kinase I isoform gamma-2 (KC1G2_HUMAN)	5.6
2dr6	Acriflavine resistance protein B (ACRB_ECOLI)	5.6
2hw7	MAP kinase-interacting serine/threonine-protein kinase 2(MKNK2_HUMAN)	5.6
2i6a	Adenosine kinase (ADK_HUMAN)	5.6
2io6	Wee1-like protein kinase (WEE1_HUMAN)	5.6
2jed	Protein kinase C theta type (KPCT_HUMAN)	5.6
2jev	Diamine acetyltransferase 1 (SAT1_HUMAN)	5.6
2jii	Serine/threonine-protein kinase VRK3(VRK3_HUMAN)	5.6
2nru	Interleukin-1 receptor-associated kinase 4 (IRAK4_HUMAN)	5.6
2ntj	Enoyl-[acyl-carrier-protein] reductase [NADH] (INHA_MYCTU)	5.6
2ojj	Mitogen-activated protein kinase 1 (MK01_HUMAN)	5.6
2on3	Ornithine decarboxylase (DCOR_HUMAN)	5.6
2qg6	Nicotinamide riboside kinase 1(NRK1_HUMAN)	5.6
2qt0	Nicotinamide riboside kinase 1 (NRK1_HUMAN)	5.6
2rew	Peroxisome proliferator-activated receptor alpha (PPARA_HUMAN)	5.6
2vpg	B-cell CLL/lymphoma 9 protein Pygopus homolog 1(BCL9_HUMAN/PYGO1_HUMAN)	5.6
3b6h	Prostacyclin synthase (PTGIS_HUMAN)	5.6
3djy	Cholinesterase (CHLE_HUMAN)	5.6
3eqr	Activated CDC42 kinase 1 (ACK1_HUMAN)	5.6
3eyg	Tyrosine-protein kinase JAK1 (JAK1_HUMAN)	5.6
3fxw	MAP kinase-activated protein kinase 3 (MAPK3_HUMAN)	5.6
3gzn	NEDD8-activating enzyme E1 regulatory subunit (ULA1_HUMAN)	5.6
3hnb	Coagulation factor VIII (FA8_HUMAN)	5.6
3ibd	Cytochrome P450 2B6 (CP2B6_HUMAN)	5.6
3k23	Glucocorticoid receptor (GCR_HUMAN)	5.6
3l0j	Nuclear receptor ROR-gamma (RORG_HUMAN)	5.6
3lmg	Receptor tyrosine-protein kinase erbB-3(ERBB3_HUMAN)	5.6
3mdz	Carbonic anhydrase 7 (CAH7_HUMAN)	5.6
3op5	Serine/threonine-protein kinase VRK1 (VRK1_HUMAN)	5.6
1d5z	HLA class II histocompatibility antigen, DRB1-4 beta chain (2B14_HUMAN)	5.5
1ec1	Gag-Pol polyprotein (POL_HV1B1)	5.5
1fco	Beta-lactamase (AMPC_ECOLI)	5.5
1iz2	Alpha-1-antitrypsin (A1AT_HUMAN)	5.5
1k4t	DNA topoisomerase 1 (TOP1_HUMAN)	5.5
1qvn	Interleukin-2 (IL2_HUMAN)	5.5
1yb1	Estradiol 17-beta-dehydrogenase 11 (DHB11_HUMAN)	5.5
2e9p	Serine/threonine-protein kinase Chk1 (CHK1_HUMAN)	5.5

2ewp	Estrogen-related receptor gamma (ERR3_HUMAN)	5.5
2i0e	Protein kinase C beta type (KPCB_HUMAN)	5.5
2nni	Cytochrome P450 2C8 (CP2C8_HUMAN)	5.5
2p4i	Angiopoietin-1 receptor (TIE2_HUMAN)	5.5
2q8i	[Pyruvate dehydrogenase [lipoamide]] kinase isozyme 3, mitochondrial (PDK3_HUMAN)	5.5
2uym	Kinesin-like protein KIF11 (KIF11_HUMAN)	5.5
2vx3	Dual specificity tyrosine-phosphorylation-regulated kinase 1A (DYR1A_HUMAN)	5.5
2wex	Apolipoprotein M (APOM_HUMAN)	5.5
2x4z	Serine/threonine-protein kinase PAK 4 (PAK4_HUMAN)	5.5
2x7h	Zinc-binding alcohol dehydrogenase domain-containing protein 2 (ZADH2_HUMAN)	5.5
2z8i	Gamma-glutamyltranspeptidase (GGT_ECOLI)	5.5
3a7e	Catechol O-methyltransferase (COMT_HUMAN)	5.5
3bhy	Death-associated protein kinase 3 (DAPK3_HUMAN)	5.5
3cm2	Baculoviral IAP repeat-containing protein 4 (XIAP_HUMAN)	5.5
3e5a	Targeting protein for Xklp2 (TPX2_HUMAN)	5.5
3e6i	Cytochrome P450 2E1 (CP2E1_HUMAN)	5.5
3e7g	Nitric oxide synthase, inducible (NOS2_HUMAN)	5.5
3efj	Hepatocyte growth factor receptor (MET_HUMAN)	5.5
3eu7	Breast cancer type 2 susceptibility protein (BRCA2_HUMAN)	5.5
3h10	Serine/threonine-protein kinase 6 (STK6_HUMAN)	5.5
3hdn	Serine/threonine-protein kinase Sgk1 (SGK1_HUMAN)	5.5
3hqr	Hypoxia-inducible factor 1 alpha (HIF1A_HUMAN)	5.5
3imx	Glucokinase (HXK4_HUMAN)	5.5
3iw4	Protein kinase C alpha type (KPCA_HUMAN)	5.5
3krr	Tyrosine-protein kinase JAK2 (JAK2_HUMAN)	5.5
3ndm	Rho-associated protein kinase 1 (ROCK1_HUMAN)	5.5
3ov6	T-cell surface glycoprotein CD1c (CD1C_HUMAN)	5.5
3pbl	D(3) dopamine receptor (DRD3_HUMAN)	5.5
1bnq	Carbonic anhydrase 2 (CAH2_HUMAN)	5.4
1byg	Tyrosine-protein kinase CSK(CSK_HUMAN)	5.4
1dfp	Complement factor D (CFAD_HUMAN)	5.4
1ezf	Squalene synthetase (FDFT_HUMAN)	5.4
1ft4	Tumor necrosis factor receptor superfamily member 1A (TNR1A_HUMAN)	5.4
1ghm	Beta-lactamase (BLAC_STAAU)	5.4
1jls	Uracil phosphoribosyltransferase (UPP_TOXGO)	5.4
1osh	Bile acid receptor (NR1H4_HUMAN)	5.4
1qha	Hexokinase-1(HXK1_HUMAN)	5.4
1u3t	Alcohol dehydrogenase 1A (ADH1A_HUMAN)	5.4
1w6f	Arylamine N-acetyltransferase (NAT_MYCSM)	5.4
2abj	Branched-chain-amino-acid aminotransferase, cytosolic (BCAT1_HUMAN)	5.4
2dq7	Proto-oncogene tyrosine-protein kinase Fyn(FYN_HUMAN)	5.4
2eva	Mitogen-activated protein kinase kinase kinase 7(M3K7_HUMAN)	5.4
2f0z	Sialidase-2 (NEUR2_HUMAN)	5.4
2hv8	Ras-related protein Rab-11A (RB11A_HUMAN)	5.4
2iwi	Serine/threonine-protein kinase Pim-2 (PIM2_HUMAN)	5.4
2obd	Cholesteryl ester transfer protein (CETP_HUMAN)	5.4

2q8g	[Pyruvate dehydrogenase [lipoamide]] kinase isozyme 1, mitochondrial (PDK1_HUMAN)	5.4
2qrn	Deoxycytidine kinase(DCK_HUMAN)	5.4
2qu6	Vascular endothelial growth factor receptor 2 (VGFR2_HUMAN)	5.4
2vc2	Integrin alpha-IIb Integrin beta-3(ITA2B_HUMAN/ITB3_HUMAN)	5.4
2w4o	Calcium/calmodulin-dependent protein kinase type IV (KCC4_HUMAN)	5.4
2xb7	ALK tyrosine kinase receptor (ALK_HUMAN)	5.4
2xbj	Serine/threonine-protein kinase Chk2 (CHK2_HUMAN)	5.4
2xk4	Serine/threonine-protein kinase Nek2 (NEK2_HUMAN)	5.4
2zdx	[Pyruvate dehydrogenase [lipoamide]] kinase isozyme 4, mitochondrial (PDK4_HUMAN)	5.4
3a4o	Tyrosine-protein kinase Lyn(LYN_HUMAN)	5.4
3a60	Ribosomal protein S6 kinase beta-1(KS6B1_HUMAN)	5.4
3d94	Insulin-like growth factor 1 receptor (IGF1R_HUMAN)	5.4
3dls	PAS domain-containing serine/threonine-protein kinase(PASK_HUMAN)	5.4
3fcl	Uracil-DNA glycosylase (UNG_HUMAN)	5.4
3g7b	DNA gyrase subunit B (GYRB_STAAU)	5.4
3iqv	14-3-3 protein sigma RAF proto-oncogene serine/threonine-protein kinase(1433S_HUMAN/RAF1_HUMAN)	5.4
3l5t	Macrophage migration inhibitory factor (MIF_HUMAN)	5.4
3ld6	Cytochrome P450 51A1 (CP51A_HUMAN)	5.4
3mtf	Activin receptor type-1 (ACVR1_HUMAN)	5.4
3n0t	Dipeptidyl-peptidase 2 (DPP2_HUMAN)	5.4
3nr9	Dual specificity protein kinase CLK2 (CLK2_HUMAN)	5.4
3ocs	Tyrosine-protein kinase BTK (BTK_HUMAN)	5.4
3q4t	Activin receptor type-2A (AVR2A_HUMAN)	5.4
1i0e	Creatine kinase M-type(KCRM_HUMAN)	5.3
1j78	Vitamin D-binding protein (VTDB_HUMAN)	5.3
1l5g	Integrin alpha-V (ITAV_HUMAN)	5.3
1pl6	Sorbitol dehydrogenase (DHSO_HUMAN)	5.3
1wda	Protein-arginine deiminase type-4 (PADI4_HUMAN)	5.3
1yfh	Methylated-DNA--protein-cysteine methyltransferase (MGMT_HUMAN)	5.3
1zrz	Protein kinase C iota type (KPCI_HUMAN)	5.3
2fgi	Basic fibroblast growth factor receptor 1 (FGFR1_HUMAN)	5.3
2ivu	Proto-oncogene tyrosine-protein kinase receptor ret (RET_HUMAN)	5.3
2odb	Cell division control protein 42 homolog@Serine/threonine-protein kinase PAK 6 (CDC42_HUMAN@PAK6_HUMAN)	5.3
2uz9	Guanine deaminase (GUAD_HUMAN)	5.3
2vd5	Myotonin-protein kinase (DMPK_HUMAN)	5.3
2zv2	Calcium/calmodulin-dependent protein kinase kinase 2 (KKCC2_HUMAN)	5.3
3bpr	Proto-oncogene tyrosine-protein kinase MER (MERTK_HUMAN)	5.3
3bz3	Focal adhesion kinase 1 (FAK1_HUMAN)	5.3
3coi	Mitogen-activated protein kinase 13(MK13_HUMAN)	5.3
3dwb	Endothelin-converting enzyme 1 (ECE1_HUMAN)	5.3
3e0p	Prostasin (PRSS8_HUMAN)	5.3
3e3b	Casein kinase II subunit alpha' (CSK22_HUMAN)	5.3
3ecr	Porphobilinogen deaminase (HEM3_HUMAN)	5.3
3eqm	Cytochrome P450 19A1 (CP19A_HUMAN)	5.3
3fzt	Protein tyrosine kinase 2 beta (FAK2_HUMAN)	5.3
3gd7	Cystic fibrosis transmembrane conductance regulator (CFTR_HUMAN)	5.3

3gxt	Alpha-galactosidase A (AGAL_HUMAN)	5.3
3i4w	Disks large homolog 4 (DLG4_HUMAN)	5.3
3kmz	Nuclear receptor corepressor 1 Retinoic acid receptor alpha(NCOR1_HUMAN/RARA_HUMAN)	5.3
3l6b	Serine racemase (SRR_HUMAN)	5.3
3ll6	Cyclin G-associated kinase(GAK_HUMAN)	5.3
3lq5	Cyclin-T1 Cell division protein kinase 9 Cell division protein kinase 9(CCNT1_HUMAN/CDK9_HUMAN)	5.3
1d1j	Profilin-2 (PROF2_HUMAN)	5.2
1e2s	Arylsulfatase A (ARSA_HUMAN)	5.2
1fsu	Arylsulfatase B (ARSB_HUMAN)	5.2
1h27	Cyclin-A2@Cyclin-dependent kinase inhibitor 1B(CCNA2_HUMAN/CDN1B_HUMAN)	5.2
1og5	Cytochrome P450 2C9 (CP2C9_HUMAN)	5.2
1p49	Steryl-sulfatase (STS_HUMAN)	5.2
1pmn	Mitogen-activated protein kinase 10 (MK10_HUMAN)	5.2
1r55	ADAM 33 (ADA33_HUMAN)	5.2
1x70	Dipeptidyl peptidase 4 (DPP4_HUMAN)	5.2
2c11	Membrane primary amine oxidase (AOC3_HUMAN)	5.2
2chl	Casein kinase I isoform gamma-3 (KC1G3_HUMAN)	5.2
2i6l	Mitogen-activated protein kinase 6(MK06_HUMAN)	5.2
2oat	Ornithine aminotransferase, mitochondrial (OAT_HUMAN)	5.2
2oyc	Pyridoxal phosphate phosphatase (PLPP_HUMAN)	5.2
2pqt	Arylamine N-acetyltransferase 1 (ARY1_HUMAN)	5.2
2qnj	MAP/microtubule affinity-regulating kinase 3(MARK3_HUMAN)	5.2
2v7o	Calcium/calmodulin-dependent protein kinase type II gamma chain (KCC2G_HUMAN)	5.2
2vdy	Corticosteroid-binding globulin (CBG_HUMAN)	5.2
2x6v	T-box transcription factor TBX5 (TBX5_HUMAN)	5.2
2x7k	Peptidyl-prolyl cis-trans isomerase-like 1 (PPIL1_HUMAN)	5.2
2zoq	Mitogen-activated protein kinase 3(MK03_HUMAN)	5.2
3agm	cAMP-dependent protein kinase catalytic subunit alpha (KAPCA_HUMAN)	5.2
3ap4	Galectin-8 (LEG8_HUMAN)	5.2
3bho	Cleavage and polyadenylation specificity factor subunit 5 (CPSF5_HUMAN)	5.2
3csh	Glutathione S-transferase P (GSTP1_HUMAN)	5.2
3f7b	Carbonic anhydrase 4 (CAH4_HUMAN)	5.2
3fap	Peptidyl-prolyl cis-trans isomerase FKBP1A (FKB1A_HUMAN)	5.2
3fme	Dual specificity mitogen-activated protein kinase kinase 6(MP2K6_HUMAN)	5.2
3g33	G1/S-specific cyclin-D3@Cell division protein kinase 4(CCND3_HUMAN/CDK4_HUMAN)	5.2
3hhm	Phosphatidylinositol 3-kinase regulatory subunit alpha Phosphatidylinositol-4,5-bisphosphate 3-kinase catalytic subunit alpha isoform(P85A_HUMAN/PK3CA_HUMAN)	5.2
3iec	Serine/threonine-protein kinase MARK2(MARK2_HUMAN)	5.2
3kn5	Ribosomal protein S6 kinase alpha-5(KS6A5_HUMAN)	5.2
3ks9	Metabotropic glutamate receptor 1 (GRM1_HUMAN)	5.2
3npc	Mitogen-activated protein kinase 9 (MK09_HUMAN)	5.2
3nxu	Cytochrome P450 3A4 (CP3A4_HUMAN)	5.2
3o2m	Mitogen-activated protein kinase 8 (MK08_HUMAN)	5.2
1l9n	Protein-glutamine gamma-glutamyltransferase E (TGM3_HUMAN)	5.1
1nue	Nucleoside diphosphate kinase B(NDKB_HUMAN)	5.1
1qgi	Chitosanase (CHIS_BACCI)	5.1
1skx	Nuclear receptor subfamily 1 group I member 2 (NR1I2_HUMAN)	5.1

1ucn	Nucleoside diphosphate kinase A(NDKA_HUMAN)	5.1
1x89	Neutrophil gelatinase-associated lipocalin (NGAL_HUMAN)	5.1
1xd3	Ubiquitin carboxyl-terminal hydrolase isozyme L3 (UCHL3_HUMAN)	5.1
2cmw	Casein kinase I isoform gamma-1 (KC1G1_HUMAN)	5.1
2f57	Serine/threonine-protein kinase PAK 7 (PAK7_HUMAN)	5.1
2oju	Peptidyl-prolyl cis-trans isomerase-like 3 (PPIL3_HUMAN)	5.1
2v77	Carboxypeptidase A1 (CBPA1_HUMAN)	5.1
2vwu	Ephrin type-B receptor 4 (EPHB4_HUMAN)	5.1
2w0b	Cytochrome P450 51 (CP51_MYCTU)	5.1
2wqn	Serine/threonine-protein kinase Nek7(NEK7_HUMAN)	5.1
3bhh	Calcium/calmodulin-dependent protein kinase type II beta chain (KCC2B_HUMAN)	5.1
3com	Serine/threonine-protein kinase 4(STK4_HUMAN)	5.1
3f96	Platelet-activating factor acetylhydrolase (PAFA_HUMAN)	5.1
3i97	Neuropilin-1 (NRP1_HUMAN)	5.1
3kq0	Alpha-1-acid glycoprotein 1 (A1AG1_HUMAN)	5.1
1b86	Hemoglobin subunit alpha beta(HBA_HUMAN/HBB_HUMAN)	5
1cf0	Profilin-1 (PROF1_HUMAN)	5
1fdq	Fatty acid-binding protein, brain (FABP7_HUMAN)	5
1h9u	Retinoic acid receptor RXR-beta (RXRB_HUMAN)	5
1k3a	Insulin receptor substrate 1 (IRS1_HUMAN)	5
1mg4	Serine/threonine-protein kinase DCLK1(DCLK1_HUMAN)	5
1nny	Tyrosine-protein phosphatase non-receptor type 1 (PTN1_HUMAN)	5
1nrp	Proteinase-activated receptor 1 (PAR1_HUMAN)	5
1rhu	Caspase-3 (CASP3_HUMAN)	5
1u59	Tyrosine-protein kinase ZAP-70(ZAP70_HUMAN)	5
1xdd	Integrin alpha-L (ITAL_HUMAN)	5
1zdt	Steroidogenic factor 1 (STF1_HUMAN)	5
2bu7	[Pyruvate dehydrogenase [lipoamide]] kinase isozyme 2, mitochondrial (PDK2_HUMAN)	5
2buj	Serine/threonine-protein kinase 16(STK16_HUMAN)	5
2clq	Mitogen-activated protein kinase kinase kinase 5(M3K5_HUMAN)	5
2q32	Heme oxygenase 2 (HMOX2_HUMAN)	5
2v5x	Histone deacetylase 8 (HDAC8_HUMAN)	5
2vwi	Serine/threonine-protein kinase OSR1(OXSR1_HUMAN)	5
3a7h	Serine/threonine-protein kinase 24(STK24_HUMAN)	5
3dko	Ephrin type-A receptor 7 (EPHA7_HUMAN)	5
3h1p	Caspase-7 (CASP7_HUMAN)	5
3h54	Alpha-N-acetylgalactosaminidase (NAGAB_HUMAN)	5
3kjn	Caspase-8 (CASP8_HUMAN)	5
3kvw	Dual specificity tyrosine-phosphorylation-regulated kinase 2 (DYRK2_HUMAN)	5
1qhy	Chloramphenicol 3-O phosphotransferase (CPT_STRVL)	4.9
1rwx	Caspase-1 (CASP1_HUMAN)	4.9
1tev	UMP-CMP kinase(KCY_HUMAN)	4.9
2dyl	Dual specificity mitogen-activated protein kinase kinase 7(MP2K7_HUMAN)	4.9
2hy3	Receptor-type tyrosine-protein phosphatase gamma (PTPRG_HUMAN)	4.9
2hy8	Serine/threonine-protein kinase PAK 1 (PAK1_HUMAN)	4.9
2vn9	Calcium/calmodulin-dependent protein kinase type II delta chain (KCC2D_HUMAN)	4.9

2z65	Lymphocyte antigen 96 Toll-like receptor 4(LY96_HUMAN/TLR4_HUMAN)	4.9
3cok	Serine/threonine-protein kinase PLK4(PLK4_HUMAN)	4.9
3ddu	Prolyl endopeptidase (PPCE_HUMAN)	4.9
3ibe	Phosphatidylinositol-4,5-bisphosphate 3-kinase catalytic subunit gamma isoform (PK3CG_HUMAN)	4.9
3iol	Glucagon (GLUC_HUMAN)	4.9
1d1q	Low molecular weight phosphotyrosine protein phosphatase (PPAL_YEAST)	4.8
2hxs	Ras-related protein Rab-28 (RAB28_HUMAN)	4.8
2hz6	Serine/threonine-protein kinase/endoribonuclease IRE1(ERN1_HUMAN)	4.8
2vle	Aldehyde dehydrogenase, mitochondrial (ALDH2_HUMAN)	4.8
2xwc	Tumor protein p73 (P73_HUMAN)	4.8
2zks	Granzyme M (GRAM_HUMAN)	4.8
3c5t	Glucagon-like peptide 1 receptor (GLP1R_HUMAN)	4.8
3d9s	Aquaporin-5 (AQP5_HUMAN)	4.8
2bdm	Cytochrome P450 2B4 (CP2B4_RABIT)	4.7
2hw6	MAP kinase-interacting serine/threonine-protein kinase 1(MKNK1_HUMAN)	4.7
3deg	30S ribosomal protein S12 (RS12_ECOLI)	4.7
3gur	Glutathione S-transferase Mu 2 (GSTM2_HUMAN)	4.7
3i1h	Bcl-2 homologous antagonist/killer (BAK_HUMAN)	4.7
3iar	Adenosine deaminase (ADA_HUMAN)	4.7
3kvf	Ubiquitin carboxyl-terminal hydrolase isozyme L1 (UCHL1_HUMAN)	4.7
1e51	Delta-aminolevulinic acid dehydratase (HEM2_HUMAN)	4.6
1g1s	P-selectin (LYAM3_HUMAN)	4.6
1i4f	HLA class I histocompatibility antigen, A-2 alpha chain Melanoma-associated antigen 4(1A02_HUMAN/MAGA4_HUMAN)	4.6
1rv1	E3 ubiquitin-protein ligase Mdm2 (MDM2_HUMAN)	4.6
1sr5	Antithrombin-III (ANT3_HUMAN)	4.6
1w7n	Kynurenine--oxoglutarate transaminase 1 (KAT1_HUMAN)	4.6
1wkw	Eukaryotic translation initiation factor 4E-binding protein 1 (4EBP1_HUMAN)	4.6
2onb	Thymidylate synthase (TYSY_HUMAN)	4.6
2qou	30S ribosomal protein S9 (RS9_ECOLI)	4.6
3max	Histone deacetylase 2 (HDAC2_HUMAN)	4.6
3pty	Probable arabinosyltransferase C (EMBC_MYCTU)	4.6
1hkn	Heparin-binding growth factor 1 (FGF1_HUMAN)	4.5
1u4l	C-C motif chemokine 5 (CCL5_HUMAN)	4.5
1w80	Synaptojanin-1 (SYNJ1_HUMAN)	4.5
2i3i	Baculoviral IAP repeat-containing protein 7 (BIRC7_HUMAN)	4.5
2px6	Fatty acid synthase (FAS_HUMAN)	4.5
2qmj	Maltase-glucoamylase, intestinal (MGA_HUMAN)	4.5
2shp	Tyrosine-protein phosphatase non-receptor type 11 (PTN11_HUMAN)	4.5
3eyc	Lipocalin-1 (LCN1_HUMAN)	4.5
3lo9	Neutrophil defensin 1 (DEF1_HUMAN)	4.5
3n22	Protein S100-A2 (S10A2_HUMAN)	4.5
1auq	von Willebrand factor (VWF_HUMAN)	4.4
1b0f	Leukocyte elastase (ELNE_HUMAN)	4.4
1n7d	Low-density lipoprotein receptor (LDLR_HUMAN)	4.4
2ggu	Pulmonary surfactant-associated protein D (SFTPD_HUMAN)	4.4
2ibi	Ubiquitin carboxyl-terminal hydrolase 2 (UBP2_HUMAN)	4.4

2nwg	Stromal cell-derived factor 1 (SDF1_HUMAN)	4.4
2v62	Serine/threonine-protein kinase VRK2(VRK2_HUMAN)	4.4
2wo1	Ephrin type-A receptor 4 (EPHA4_HUMAN)	4.4
3fwl	Penicillin-binding protein 1B (PBPB_ECOLI)	4.4
3mk8	Induced myeloid leukemia cell differentiation protein Mcl-1 (MCL1_HUMAN)	4.4
3mng	Peroxiredoxin-5, mitochondrial (PRDX5_HUMAN)	4.4
3oyw	Galectin-1 (LEG1_HUMAN)	4.4
1aii	Annexin A3 (ANXA3_HUMAN)	4.3
1g86	Eosinophil lysophospholipase (LPPL_HUMAN)	4.3
1t83	Low affinity immunoglobulin gamma Fc region receptor III-B (FCG3B_HUMAN)	4.3
2gi7	Platelet glycoprotein VI (GPVI_HUMAN)	4.3
2hhj	Bisphosphoglycerate mutase (PMGE_HUMAN)	4.3
3f81	Dual specificity protein phosphatase 3 (DUS3_HUMAN)	4.3
3i3t	Ubiquitin carboxyl-terminal hydrolase 21 (UBP21_HUMAN)	4.3
1bm7	Transthyretin (TTHY_HUMAN)	4.2
1czs	Coagulation factor V (FA5_HUMAN)	4.2
1lgp	E3 ubiquitin-protein ligase CHFR (CHFR_HUMAN)	4.2
2bo9	Carboxypeptidase A4 Latexin(CBPA4_HUMAN/LXN_HUMAN)	4.2
2huw	Growth factor receptor-bound protein 2 (GRB2_HUMAN)	4.1
3hcm	Protein S100-B (S100B_HUMAN)	4.1
3lbj	Protein Mdm4 (MDM4_HUMAN)	4.1
3leo	Leukotriene C4 synthase (LTC4S_HUMAN)	4.1
1h0c	Serine--pyruvate aminotransferase (SPYA_HUMAN)	4
1kjr	Galectin-3 (LEG3_HUMAN)	4
1lyb	Cathepsin D (CATD_HUMAN)	4
1nbf	Ubiquitin carboxyl-terminal hydrolase 7 (UBP7_HUMAN)	4
1s1s	Cell division protein zipA (ZIPA_ECOLI)	4
2ayo	Ubiquitin carboxyl-terminal hydrolase 14 (UBP14_HUMAN)	4
3bxz	Protein translocase subunit secA (SECA_ECOLI)	4
3d5k	Outer membrane protein oprM (OPRM_PSEAE)	4
3gal	Galectin-7 (LEG7_HUMAN)	4
3lbz	B-cell lymphoma 6 protein (BCL6_HUMAN)	4
1elv	Complement C1s subcomponent (C1S_HUMAN)	3.9
1f9p	Platelet basic protein (CXCL7_HUMAN)	3.9
2dyb	Neutrophil cytosol factor 4 (NCF4_HUMAN)	3.9
2q3z	Protein-glutamine gamma-glutamyltransferase 2 (TGM2_HUMAN)	3.9
1k5r	65 kDa Yes-associated protein (YAP1_HUMAN)	3.8
2qkh	Gastric inhibitory polypeptide receptor Gastric inhibitory polypeptide(GIPR_HUMAN/GIP_HUMAN)	3.8
2ra4	C-C motif chemokine 13 (CCL13_HUMAN)	3.8
3ihp	Ubiquitin carboxyl-terminal hydrolase 5 (UBP5_HUMAN)	3.8
1rqd	Deoxyhypusine synthase (DHYS_HUMAN)	3.7
2wor	Protein S100-A7 (S10A7_HUMAN)	3.7
3gxe	Collagen alpha-1(I) chain (CO1A1_HUMAN)	3.6
2v8e	Complement factor H (CFAH_HUMAN)	3.5
1au1	Interferon beta (IFNB_HUMAN)	3.4
1a7c	Plasminogen activator inhibitor 1 (PAI1_HUMAN)	3.3

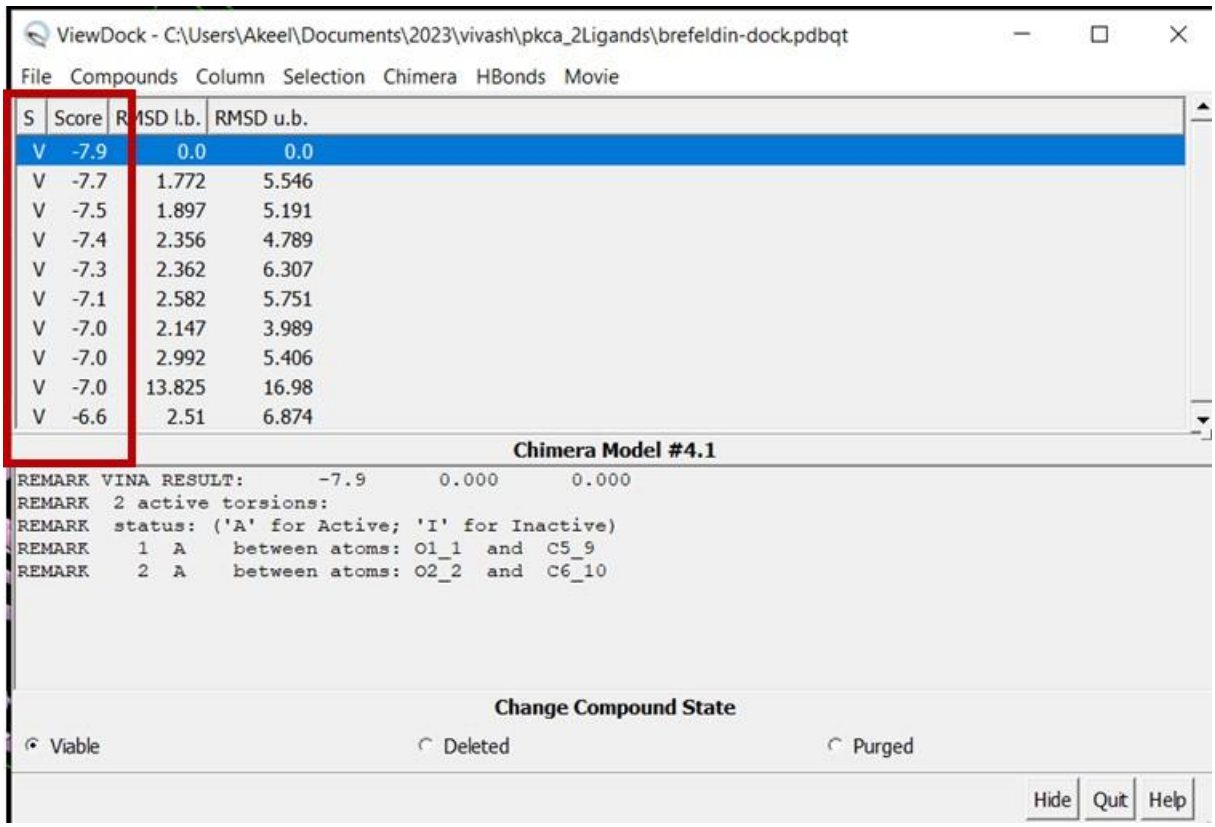
1fga	Heparin-binding growth factor 2 (FGF2_HUMAN)	3.2
2hei	Ras-related protein Rab-5B (RAB5B_HUMAN)	3.2
1w70	Neutrophil cytosol factor 1 (NCF1_HUMAN)	2.8
1ym9	M-phase inducer phosphatase 2 (MPIP2_HUMAN)	2.7
2pfg	Carbonyl reductase [NADPH] 1 (CBR1_HUMAN)	2.6
6jdw	Glycine amidinotransferase, mitochondrial (GATM_HUMAN)	2.1
1evu	Coagulation factor XIII A chain (F13A_HUMAN)	0.2
1stf	Cystatin-B (CYTB_HUMAN)	-3.5
3kfq	Cathepsin L2 Cystatin-A(CATL2_HUMAN/CYTA_HUMAN)	-9.8

Appendix 3 Protein Docking

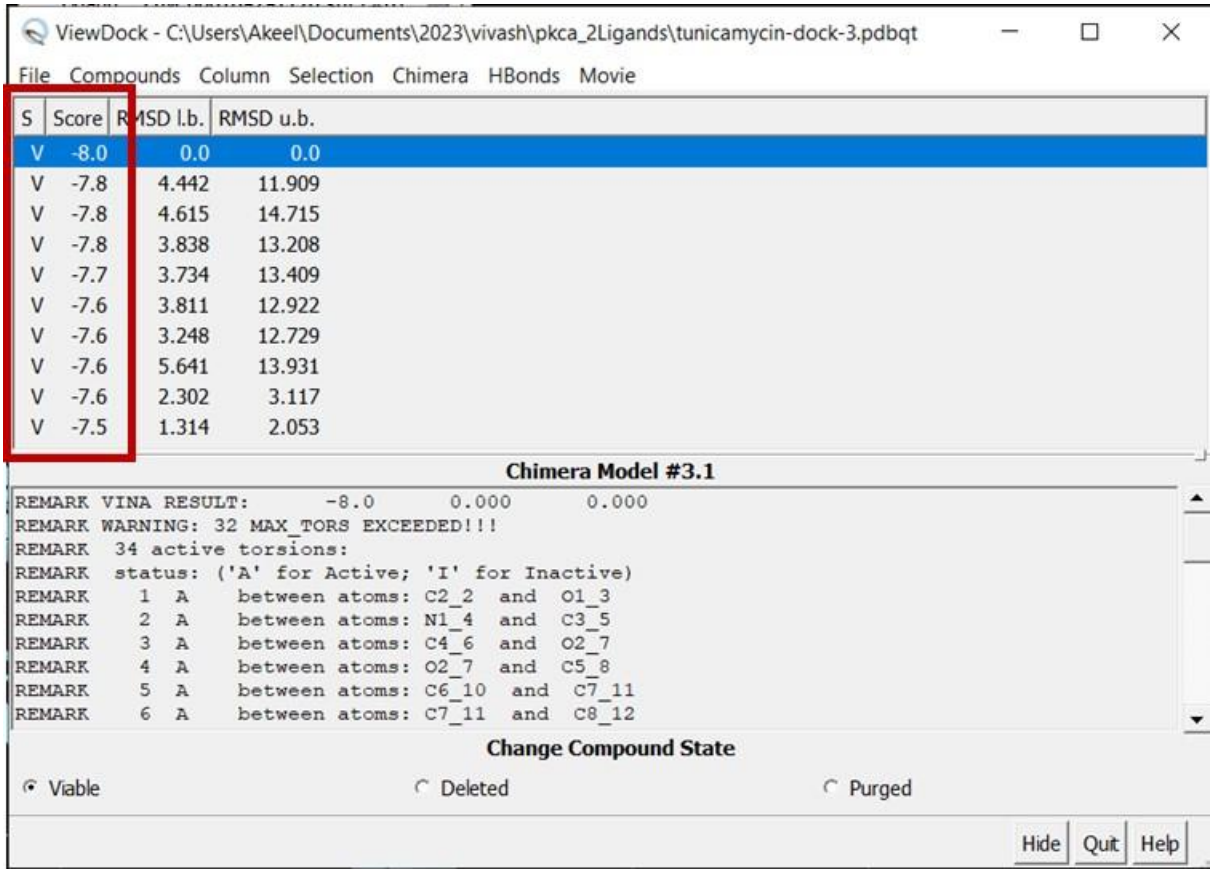
Docking Brefeldin and Tunicamycin C with protein kinase C alpha

Table A3.1:Top 10 ligand orientations (“binding poses”) within the target.

Brefeldin A



Tunicamycin C



The binding poses are ranked from best docking score (in kcal/mol) to worst.

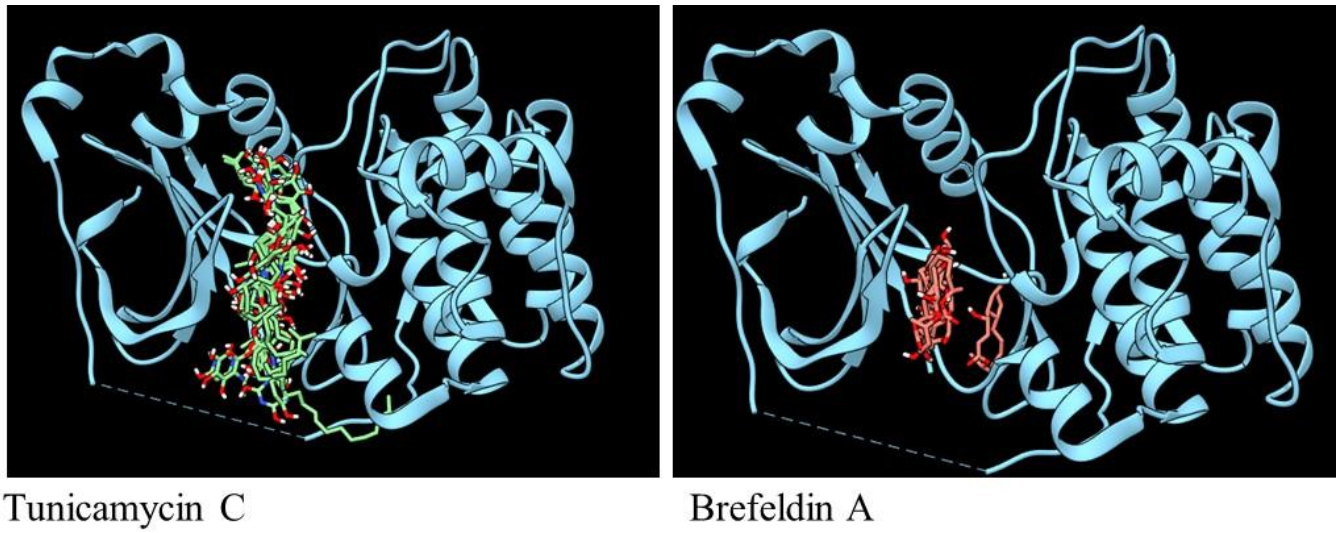


Figure A3.1 Superimposed pictures of the top 10 binding poses of each ligand.

Appendix 4 Pathway analysis

Table A4.1. Pathway analysis for Targeted protein for Brefeldin A

Swiss Target

Target	Common name	Uniprot ID	ChEMBL ID	Target Class	Probability*	Known actives (3D/2D)
Cytochrome P450 19A1	CYP19A1	P11511	CHEMBL1978	Cytochrome P450	0.108771	55 / 69Â Â Â Â Â
Potassium-transporting ATPase alpha chain 2	ATP12A	P54707	CHEMBL2933	Primary active transporter	0.100579	3 / 10Â Â Â Â Â
Ribosomal protein S6 kinase alpha 5	RPS6KA5	O75582	CHEMBL4237	Kinase	0.100579	4 / 3Â Â Â Â Â
Androgen Receptor	AR	P10275	CHEMBL1871	Nuclear receptor	0.100579	163 / 56Â Â Â Â Â
Protein kinase C alpha	PRKCA	P17252	CHEMBL299	Kinase	0.100579	49 / 203Â Â Â Â Â
Programmed cell death protein 4	PDCD4	Q53EL6	CHEMBL1781868	Unclassified protein	0.100579	0 / 8Â Â Â Â Â
Progesterone receptor	PGR	P06401	CHEMBL208	Nuclear receptor	0.100579	31 / 40Â Â Â Â Â
Taste receptor type 2 member 31	TAS2R31	P59538	CHEMBL2034804	Taste family G protein-coupled receptor	0.100579	0 / 1Â Â Â Â Â
Gamma-secretase	PSEN2 PSENEN NCSTN APH1A PSEN1 APH1B	P49810 Q9NZ42 Q92542 Q96BI3 P49768 Q8WW43	CHEMBL2094135	Protease	0.100579	66 / 0Â Â Â Â Â
Peroxisome proliferator-activated receptor gamma	PPARG	P37231	CHEMBL235	Nuclear receptor	0.100579	12 / 10Â Â Â Â Â
Tyrosine-protein kinase JAK1	JAK1	P23458	CHEMBL2835	Kinase	0.100579	112 / 0Â Â Â Â Â
Dual specificity phosphatase Cdc25A	CDC25A	P30304	CHEMBL3775	Phosphatase	0.100579	8 / 15Â Â Â Â Â
Phosphodiesterase 10A	PDE10A	Q9Y233	CHEMBL4409	Phosphodiesterase	0.100579	201 / 0Â Â Â Â Â
MAP kinase p38 alpha	MAPK14	Q16539	CHEMBL260	Kinase	0.100579	118 / 0Â Â Â Â Â
Dual specificity mitogen-activated protein kinase kinase 1	MAP2K1	Q02750	CHEMBL3587	Kinase	0.100579	133 / 0Â Â Â Â Â
Cyclin-dependent kinase 2	CDK2	P24941	CHEMBL301	Kinase	0.100579	85 / 0Â Â Â Â Â
Leucine-rich repeat serine/threonine-protein kinase 2	LRRK2	Q5S007	CHEMBL1075104	Kinase	0.100579	93 / 0Â Â Â Â Â

GABA-A receptor; alpha-3/beta-3/gamma-2	GABRB3 GABRA3 GABRG2	P28472 P34903 P18507	CHEMBL2094120	Ligand-gated ion channel	0.100579	5 / 0Â Â Â Â Â
GABA-A receptor; alpha-1/beta-3/gamma-2	GABRB3 GABRG2 GABRA1	P28472 P18507 P14867	CHEMBL2094121	Ligand-gated ion channel	0.100579	5 / 0Â Â Â Â Â
GABA-A receptor; alpha-5/beta-3/gamma-2	GABRB3 GABRG2 GABRA5	P28472 P18507 P31644	CHEMBL2094122	Ligand-gated ion channel	0.100579	7 / 0Â Â Â Â Â
GABA-A receptor; alpha-2/beta-3/gamma-2	GABRA2 GABRB3 GABRG2	P47869 P28472 P18507	CHEMBL2094130	Ligand-gated ion channel	0.100579	5 / 0Â Â Â Â Â
Tubulin--tyrosine ligase	TTL	Q8NG68	CHEMBL5549	Enzyme	0.100579	6 / 12Â Â Â Â Â
Testis-specific androgen-binding protein	SHBG	P04278	CHEMBL3305	Secreted protein	0.100579	24 / 7Â Â Â Â Â
Corticosteroid binding globulin	SERPINA6	P08185	CHEMBL2421	Secreted protein	0.100579	12 / 5Â Â Â Â Â
Cyclin-dependent kinase 6	CDK6	Q00534	CHEMBL2508	Kinase	0.100579	3 / 0Â Â Â Â Â
Cyclin-dependent kinase 1	CDK1	P06493	CHEMBL308	Kinase	0.100579	94 / 0Â Â Â Â Â
Cyclin-dependent kinase 9	CDK9	P50750	CHEMBL3116	Kinase	0.100579	17 / 0Â Â Â Â Â
Cyclin-dependent kinase 4	CDK4	P11802	CHEMBL331	Kinase	0.100579	9 / 0Â Â Â Â Â
Cyclin-dependent kinase 5/CDK5 activator 1	CDK5	Q00535	CHEMBL4036	Kinase	0.100579	8 / 0Â Â Â Â Â
Cyclin-dependent kinase 3	CDK3	Q00526	CHEMBL4442	Kinase	0.100579	2 / 0Â Â Â Â Â
Tyrosine-protein kinase JAK2	JAK2	O60674	CHEMBL2971	Kinase	0.100579	128 / 0Â Â Â Â Â
Phospholipase A2 group IIA	PLA2G2A	P14555	CHEMBL3474	Enzyme	0.100579	13 / 8Â Â Â Â Â
Tyrosine-protein kinase JAK3	JAK3	P52333	CHEMBL2148	Kinase	0.100579	87 / 0Â Â Â Â Â
Glucocorticoid receptor	NR3C1	P04150	CHEMBL2034	Nuclear receptor	0.100579	106 / 13Â Â Â Â Â
Inosine-5'-monophosphate dehydrogenase 1	IMPDH1	P20839	CHEMBL1822	Oxidoreductase	0.100579	5 / 0Â Â Â Â Â
Inosine-5'-monophosphate dehydrogenase 2	IMPDH2	P12268	CHEMBL2002	Oxidoreductase	0.100579	22 / 0Â Â Â Â Â
Hormone sensitive lipase	LIPE	Q05469	CHEMBL3590	Enzyme	0.100579	5 / 0Â Â Â Â Â
Serine/threonine-protein kinase PIM1	PIM1	P11309	CHEMBL2147	Kinase	0.100579	73 / 0Â Â Â Â Â
CDK8/Cyclin C	CCNC CDK8	P24863 P49336	CHEMBL3038474	Kinase	0.100579	8 / 0Â Â Â Â Â
Serine/threonine-protein kinase PIM3	PIM3	Q86V86	CHEMBL5407	Kinase	0.100579	35 / 0Â Â Â Â Â

Cell division protein kinase 8	CDK8	P49336	CHEMBL5719	Kinase	0.100579	9 / 0Â Â Â Â Â
Myeloperoxidase	MPO	P05164	CHEMBL2439	Enzyme	0.100579	7 / 0Â Â Â Â Â
Liver glycogen phosphorylase	PYGL	P06737	CHEMBL2568	Enzyme	0.100579	85 / 0Â Â Â Â Â
Serine/threonine-protein kinase Chk1	CHEK1	O14757	CHEMBL4630	Kinase	0.100579	82 / 0Â Â Â Â Â
Carbonic anhydrase II	CA2	P00918	CHEMBL205	Lyase	0.100579	66 / 0Â Â Â Â Â
C-C chemokine receptor type 1	CCR1	P32246	CHEMBL2413	Family A G protein-coupled receptor	0.100579	88 / 0Â Â Â Â Â
Orexin receptor 2	HCRTR2	O43614	CHEMBL4792	Family A G protein-coupled receptor	0.100579	16 / 0Â Â Â Â Â
Orexin receptor 1	HCRTR1	O43613	CHEMBL5113	Family A G protein-coupled receptor	0.100579	10 / 0Â Â Â Â Â
Phosphodiesterase 7A	PDE7A	Q13946	CHEMBL3012	Phosphodiesterase	0.100579	18 / 0Â Â Â Â Â
Muscle glycogen synthase	GYS1	P13807	CHEMBL4000	Enzyme	0.100579	5 / 0Â Â Â Â Â
Mineralocorticoid receptor	NR3C2	P08235	CHEMBL1994	Nuclear receptor	0.100579	10 / 17Â Â Â Â Â
Pregnane X receptor	NR1I2	O75469	CHEMBL3401	Nuclear receptor	0.100579	6 / 0Â Â Â Â Â
p53-binding protein Mdm-2	MDM2	Q00987	CHEMBL5023	Other nuclear protein	0.100579	106 / 0Â Â Â Â Â
LIM domain kinase 2	LIMK2	P53671	CHEMBL5932	Kinase	0.100579	7 / 0Â Â Â Â Â
HMG-CoA reductase (by homology)	HMGCR	P04035	CHEMBL402	Oxidoreductase	0.100579	153 / 74Â Â Â Â Â
Phosphodiesterase 3	PDE3A	Q14432	CHEMBL241	Phosphodiesterase	0.100579	9 / 0Â Â Â Â Â
Phosphodiesterase 4B	PDE4B	Q07343	CHEMBL275	Phosphodiesterase	0.100579	14 / 0Â Â Â Â Â
DNA-dependent protein kinase	PRKDC	P78527	CHEMBL3142	Kinase	0.100579	45 / 0Â Â Â Â Â
Poly [ADP-ribose] polymerase-1	PARP1	P09874	CHEMBL3105	Enzyme	0.100579	70 / 0Â Â Â Â Â
Biotin--protein ligase	HLCS	P50747	CHEMBL2062354	Enzyme	0.100579	1 / 0Â Â Â Â Â
Serine/threonine-protein kinase PAK 1	PAK1	Q13153	CHEMBL4600	Kinase	0.100579	5 / 0Â Â Â Â Â
Cyclin-dependent kinase 2/cyclin A	CDK2 CCNA1 CCNA2	P24941 P78396 P20248	CHEMBL2094128	Other cytosolic protein	0.100579	26 / 0Â Â Â Â Â
Interleukin-8 receptor A	CXCR1	P25024	CHEMBL4029	Family A G protein-coupled receptor	0.100579	10 / 2Â Â Â Â Â
Tyrosine-protein kinase receptor UFO	AXL	P30530	CHEMBL4895	Kinase	0.100579	19 / 0Â Â Â Â Â
Tyrosine-protein kinase receptor TYRO3	TYRO3	Q06418	CHEMBL5314	Kinase	0.100579	27 / 0Â Â Â Â Â
Proto-oncogene tyrosine-protein kinase MER	MERTK	Q12866	CHEMBL5331	Kinase	0.100579	30 / 0Â Â Â Â Â
Carbonic anhydrase VII	CA7	P43166	CHEMBL2326	Lyase	0.100579	14 / 0Â Â Â Â Â

Rho-associated protein kinase 2	ROCK2	O75116	CHEMBL2973	Kinase	0.100579	30 / 0Â Â Â Â Â
Rho-associated protein kinase 1	ROCK1	Q13464	CHEMBL3231	Kinase	0.100579	12 / 0Â Â Â Â Â
Cyclin-dependent kinase 4/cyclin D1	CCND1 CDK4	P24385 P11802	CHEMBL1907601	Kinase	0.100579	36 / 0Â Â Â Â Â
PI3-kinase p110-delta subunit	PIK3CD	O00329	CHEMBL3130	Enzyme	0.100579	67 / 0Â Â Â Â Â
PI3-kinase p110-beta subunit	PIK3CB	P42338	CHEMBL3145	Enzyme	0.100579	74 / 0Â Â Â Â Â
Serine/threonine protein phosphatase 2A, catalytic subunit, alpha isoform	PPP2CA	P67775	CHEMBL4703	Phosphatase	0.100579	0 / 8Â Â Â Â Â
P2X purinoceptor 7	P2RX7	Q99572	CHEMBL4805	Ligand-gated ion channel	0.100579	18 / 0Â Â Â Â Â
Protein-tyrosine phosphatase 1B	PTPN1	P18031	CHEMBL335	Phosphatase	0.100579	44 / 40Â Â Â Â Â
Isoleucyl-tRNA synthetase	IARS	P41252	CHEMBL3235	Enzyme	0.100579	0 / 1Â Â Â Â Â
Cyclin-dependent kinase 5/CDK5 activator 1	CDK5R1 CDK5	Q15078 Q00535	CHEMBL1907600	Kinase	0.100579	35 / 0Â Â Â Â Â
11-beta-hydroxysteroid dehydrogenase 1	HSD11B1	P28845	CHEMBL4235	Enzyme	0.100579	175 / 22Â Â Â Â Â
Tyrosine-protein kinase TYK2	TYK2	P29597	CHEMBL3553	Kinase	0.100579	39 / 0Â Â Â Â Â
DNA polymerase alpha subunit	POLA1	P09884	CHEMBL1828	Transferase	0.100579	11 / 9Â Â Â Â Â
Cathepsin K	CTSK	P43235	CHEMBL268	Protease	0.100579	30 / 0Â Â Â Â Â
Cathepsin S	CTSS	P25774	CHEMBL2954	Protease	0.100579	33 / 0Â Â Â Â Â
Phosphodiesterase 4D	PDE4D	Q08499	CHEMBL288	Phosphodiesterase	0.100579	5 / 8Â Â Â Â Â
Interleukin-6	IL6	P05231	CHEMBL1795129	Secreted protein	0.100579	1 / 0Â Â Â Â Â
Dopamine D3 receptor	DRD3	P35462	CHEMBL234	Family A G protein-coupled receptor	0.100579	107 / 0Â Â Â Â Â
Protein kinase C (PKC)	PRKCZ	Q05513	CHEMBL3438	Kinase	0.100579	2 / 0Â Â Â Â Â
ADAM17	ADAM17	P78536	CHEMBL3706	Protease	0.100579	64 / 0Â Â Â Â Â
Cathepsin L	CTSL	P07711	CHEMBL3837	Protease	0.100579	20 / 0Â Â Â Â Â
Glutamine synthetase	GLUL	P15104	CHEMBL4612	Ligase	0.100579	1 / 0Â Â Â Â Â
G-protein coupled bile acid receptor 1	GPBAR1	Q8TDU6	CHEMBL5409	Family A G protein-coupled receptor	0.100579	1 / 0Â Â Â Â Â
Fatty acid-binding protein, liver (by homology)	FABP1	P07148	CHEMBL5421	Fatty acid binding protein family	0.100579	1 / 0Â Â Â Â Â
Intercellular adhesion molecule (ICAM-1), Integrin alpha-L/beta-2	ITGAL ICAM1 ITGB2	P20701 P05362 P05107	CHEMBL2096661	Membrane receptor	0.100579	8 / 0Â Â Â Â Â
Thymidine kinase, cytosolic	TK1	P04183	CHEMBL2883	Transferase	0.100579	6 / 0Â Â Â Â Â
Matrix metalloproteinase 1	MMP1	P03956	CHEMBL332	Protease	0.100579	93 / 0Â Â Â Â Â

Cyclin-dependent kinase 2/cyclin E	CCNE2 CDK2 CCNE1	O96020 P24941 P24864	CHEMBL2094126	Other cytosolic protein	0.100579	35 / 0Â Â Â Â Â
Interleukin-1 receptor-associated kinase 4	IRAK4	Q9NWZ3	CHEMBL3778	Kinase	0.100579	20 / 0Â Â Â Â Â
CDC7/DBF4 (Cell division cycle 7-related protein kinase/Activator of S phase kinase)	CDC7	O00311	CHEMBL5443	Kinase	0.100579	16 / 0Â Â Â Â Â
Acid ceramidase (by homology)	ASAH1	Q13510	CHEMBL5463	Enzyme	0.100579	3 / 0Â Â Â Â Â
Phospholipase A2 group 1B	PLA2G1B	P04054	CHEMBL4426	Enzyme	0.100579	0 / 4Â Â Â Â Â
Tyrosine-protein kinase SYK	SYK	P43405	CHEMBL2599	Kinase	0.100579	57 / 0Â Â Â Â Â

Wiki pathways

Term	Overlap	P-value	Adjusted P-value	Odds Ratio	Combined Score	Genes
Retinoblastoma gene in cancer WP2446	Dec-87	1.10E-14	3.70E-12	37.32329	1199.478	POLA1;CDK6;CCND1;CCNE2;PRKDC;CDK4;CHEK1;CDK2;CDK1;MDM2;CDC7;CDC25A
DNA damage response WP707	Nov-68	2.38E-14	3.98E-12	44.53407	1397.033	CDK6;CCND1;CCNE2;CDK5;PRKDC;CDK4;CHEK1;CDK2;CDK1;MDM2;CDC25A
miRNA regulation of DNA damage response WP1530	Nov-71	3.92E-14	4.38E-12	42.30097	1305.784	CDK6;CCND1;CCNE2;CDK5;PRKDC;CDK4;CHEK1;CDK2;CDK1;MDM2;CDC25A
PI3K-Akt signaling pathway WP4172	17/340	6.12E-13	5.13E-11	12.88158	362.2564	MAP2K1;SYK;PIK3CD;PRKCA;PIK3CB;PPP2CA;GYS1;IL6;CDK6;CCND1;CCNE2;CDK4;CDK2;MDM2;JAK2;JAK3;JAK1
Glioblastoma signaling pathways WP2261	Oct-82	7.18E-12	4.81E-10	31.65868	812.3539	MAP2K1;CDK6;CCND1;CDK4;CDK2;MDM2;PIK3CD;PRKCA;PIK3CB;PRKCZ
Integrated breast cancer pathway WP1984	12/152	9.80E-12	5.47E-10	19.92908	505.1839	AR;PAK1;CCND1;CDK4;MMP1;CHEK1;CDK2;MDM2;HMGCR;CYP19A1;CDC25A;JAK1
Cell cycle WP179	11/120	1.47E-11	7.01E-10	23.22744	579.4341	CDK6;CCND1;CCNE2;PRKDC;CDK4;CHEK1;CDK2;CDK1;MDM2;CDC7;CDC25A
Oncostatin M Signaling Pathway WP2374	Sep-65	2.60E-11	1.09E-09	36.24655	883.4849	MAP2K1;MMP1;CDK2;PRKCA;TYK2;JAK2;MAPK14;JAK3;JAK1
Integrated Cancer Pathway WP1971	Aug-44	3.50E-11	1.30E-09	49.60549	1194.264	MMP1;CDK4;CHEK1;CDK2;CDK1;MDM2;CDC25A;JAK1
Hepatitis B infection WP4666	11/152	1.93E-10	6.45E-09	17.92693	401.0372	MAP2K1;IL6;PIK3CD;PRKCA;PIK3CB;TYK2;IRAK4;JAK2;MAPK14;JAK3;JAK1
EGFR Tyrosine Kinase Inhibitor Resistance WP4806	Sep-84	2.77E-10	8.44E-09	27.03818	595.0009	MAP2K1;IL6;CCND1;AXL;PIK3CD;PRKCA;PIK3CB;JAK2;JAK1
G1 to S cell cycle control WP45	Aug-64	8.08E-10	2.26E-08	31.85714	666.9812	CDK6;CCND1;CCNE2;CDK4;CDK2;CDK1;MDM2;CDC25A

Melanoma WP4685	Aug-68	1.33E-09	3.42E-08	29.72734	607.6152	MAP2K1;PAK1;CDK6;CCND1;CDK4;MDM2;PIK3CD;PIK3CB
Non-small cell lung cancer WP4255	Aug-72	2.12E-09	5.06E-08	27.86376	556.5378	MAP2K1;CDK6;CCND1;CDK4;PIK3CD;PRKCA;PIK3CB;JAK3
Translation inhibitors in chronically activated PDGFRA cells WP4566	Jul-46	2.32E-09	5.19E-08	39.61481	787.5538	MAP2K1;RPS6KA5;PIM1;PDCD4;PRKCA;PIK3CB;MAPK14
Leptin signaling pathway WP2034	Aug-76	3.28E-09	6.87E-08	26.21943	512.1933	PTPN1;MAP2K1;CCND1;ROCK1;ROCK2;JAK2;MAPK14;JAK1
Insulin Signaling WP481	10/160	5.60E-09	1.10E-07	15.1364	287.5972	LIPE;GYS1;PTPN1;MAP2K1;RPS6KA5;PIK3CD;PRKCA;PIK3CB;MAPK14;PRKCZ
EGF/EGFR signaling pathway WP437	10/162	6.31E-09	1.18E-07	14.93572	281.9935	MAP2K1;PAK1;RPS6KA5;ROCK1;LIMK2;PRKCA;JAK2;MAPK14;PRKCZ;JAK1
Chemokine signaling pathway WP3929	10/164	7.11E-09	1.23E-07	14.74026	276.5595	CCR1;MAP2K1;PAK1;ROCK1;ROCK2;PIK3CD;PIK3CB;JAK2;PRKCZ;JAK3
MicroRNAs in cardiomyocyte hypertrophy WP1544	Aug-84	7.35E-09	1.23E-07	23.45003	439.1826	CDK9;MAP2K1;ROCK1;ROCK2;PLA2G2A;PIK3CD;PIK3CB;MAPK14
Pancreatic adenocarcinoma pathway WP4263	Aug-89	1.17E-08	1.86E-07	21.99695	401.7921	MAP2K1;PAK1;CDK6;CCND1;CDK4;PIK3CD;PIK3CB;JAK1
AGE/RAGE pathway WP2324	Jul-66	3.12E-08	4.55E-07	26.1597	452.0788	MAP2K1;ROCK1;PRKCA;IRAK4;JAK2;MAPK14;PRKCZ
Thyroid stimulating hormone (TSH) signaling pathway WP2032	Jul-66	3.12E-08	4.55E-07	26.1597	452.0788	MAP2K1;CDK4;PDE4D;CDK2;JAK2;MAPK14;JAK1
Brain-derived neurotrophic factor (BDNF) signaling pathway WP2380	9/144	3.37E-08	4.71E-07	14.97576	257.6494	GABRB3;PPP2CA;MAP2K1;ADAM17;RPS6KA5;CDK5;JAK2;MAPK14;CDK5R1
Bladder cancer WP2828	Jun-40	3.74E-08	5.01E-07	38.5307	658.9502	MAP2K1;RPS6KA5;CCND1;MMP1;CDK4;MDM2
Gastrin signaling pathway WP4659	8/114	8.24E-08	1.05E-06	16.78779	273.8373	MAP2K1;PAK1;CCND1;ROCK1;PRKCA;PPARG;JAK2;MAPK14
Prolactin Signaling Pathway WP2037	Jul-76	8.43E-08	1.05E-06	22.35717	364.1697	PTPN1;MAP2K1;PAK1;PIK3CB;JAK2;MAPK14;JAK1
Spinal Cord Injury WP2431	8/118	1.08E-07	1.29E-06	16.17406	259.4795	IL6;CCND1;CDK4;ROCK2;CDK2;PLA2G2A;CDK1;PRKCA
Hepatitis C and Hepatocellular Carcinoma WP3646	Jun-49	1.32E-07	1.52E-06	30.45234	482.4932	IL6;CCND1;CXCR1;MMP1;MAPK14;JAK1
Ebola Virus Pathway on Host WP4217	8/129	2.15E-07	2.40E-06	14.69551	225.6114	ADAM17;PAK1;CTSL;AXL;TYRO3;PIK3CD;PIK3CB;MERTK
IL-4 signaling pathway WP395	Jun-54	2.38E-07	2.49E-06	27.27335	415.9236	PIK3CD;TYK2;JAK2;MAPK14;JAK3;JAK1
Interferon type I signaling pathways WP585	Jun-54	2.38E-07	2.49E-06	27.27335	415.9236	RPS6KA5;PDCD4;PIK3CD;TYK2;MAPK14;JAK1
Focal Adhesion-PI3K-Akt-mTOR-signaling pathway WP3932	11/303	2.52E-07	2.56E-06	8.590355	130.5231	PPP2CA;LIPE;GYS1;MAP2K1;MDM2;PIK3CD;PIK3CB;ITGAL;JAK2;JAK3;JAK1

ErbB signaling pathway WP673	Jul-91	2.94E-07	2.90E-06	18.35093	275.9769	MAP2K1;PAK1;CCND1;MDM2;PIK3CD;PRKCA;PIK3CB
ncRNAs involved in STAT3 signaling in hepatocellular carcinoma WP4337	13-Apr	3.59E-07	3.44E-06	95.07288	1410.765	IL6;JAK2;JAK3;JAK1
Small cell lung cancer WP4658	Jul-96	4.25E-07	3.95E-06	17.31561	254.0462	CDK6;CCND1;CCNE2;CDK4;CDK2;PIK3CD;PIK3CB
Mammary gland development pathway - Pregnancy and lactation (Stage 3 of 4) WP2817	May-32	4.39E-07	3.97E-06	40.00805	585.6745	PTPN1;CCND1;PGR;NR3C1;JAK2
Prader-Willi and Angelman Syndrome WP3998	Jun-61	4.98E-07	4.39E-06	23.79381	345.2973	GABRB3;CDK6;CCND1;CDK4;MDM2;PRKCZ
mBDNF and proBDNF regulation of GABA neurotransmission WP4829	May-38	1.07E-06	8.95E-06	32.72398	449.9088	GABRB3;GABRA2;ROCK1;PIK3CB;JAK2
Nuclear receptors WP170	May-38	1.07E-06	8.95E-06	32.72398	449.9088	AR;NR1I2;PPARG;PGR;NR3C1
IL-9 signaling pathway WP22	17-Apr	1.18E-06	9.60E-06	65.80645	898.3291	CDK9;MAP2K1;JAK3;JAK1
VEGFA-VEGFR2 Signaling Pathway WP3888	12/432	1.20E-06	9.60E-06	6.548908	89.26541	PPP2CA;PTPN1;MAP2K1;PAK1;RPS6KA5;CCND1;ROCK1;ROCK2;MDM2;PRKCA;MAPK14;PRKCZ
Non-genomic actions of 1,25 dihydroxyvitamin D3 WP4341	Jun-71	1.24E-06	9.63E-06	20.12308	273.7445	IL6;PRKCA;TYK2;MAPK14;PRKCZ;JAK1
ATM Signaling Pathway WP2516	May-40	1.39E-06	1.06E-05	30.85093	416.041	CHEK1;CDK2;CDK1;MDM2;CDC25A
Osteoblast differentiation WP4787	7/118	1.72E-06	1.28E-05	13.86827	184.0493	PRKDC;PIK3CD;PRKCA;PPARG;PIK3CB;MAPK14;PRKCZ
IL-6 signaling pathway WP364	May-43	2.01E-06	1.46E-05	28.41104	372.6562	MAP2K1;IL6;TYK2;JAK2;JAK1
DNA IR-damage and cellular response via ATR WP4016	Jun-80	2.50E-06	1.77E-05	17.66766	227.8688	PARP1;PRKDC;CHEK1;CDK2;CDK1;MDM2
ATM Signaling Network in Development and Disease WP3878	May-45	2.53E-06	1.77E-05	26.98777	347.7603	CDK5;PRKDC;CHEK1;CDK1;CDK5R1
Thymic Stromal LymphoPoietin (TSLP) Signaling Pathway WP2203	May-47	3.16E-06	2.16E-05	25.70005	325.5158	MAP2K1;IL6;JAK2;MAPK14;JAK1
Angiopoietin Like Protein 8 Regulatory Pathway WP3915	7/132	3.65E-06	2.39E-05	12.30631	154.0994	GYS1;PTPN1;MAP2K1;RPS6KA5;PIK3CD;PIK3CB;MAPK14

TGF-beta Signaling Pathway WP366	7/132	3.65E-06	2.39E-05	12.30631	154.0994	MAP2K1;CCND1;ROCK1;MMP1;LIMK2;CDK1;MAPK14
IL-3 signaling pathway WP286	May-49	3.89E-06	2.51E-05	24.5294	305.5378	MAP2K1;SYK;PIK3CD;JAK2;JAK1
Androgen receptor signaling pathway WP138	Jun-90	4.99E-06	3.15E-05	15.55651	189.9137	AR;CCND1;ROCK1;ROCK2;LIMK2;MDM2
Regulation of toll-like receptor signaling pathway WP1449	7/139	5.13E-06	3.19E-05	11.64958	141.8865	MAP2K1;IL6;SYK;PIK3CD;PIK3CB;IRAK4;MAPK14
Focal Adhesion WP306	8/198	5.45E-06	3.32E-05	9.326079	113.0304	MAP2K1;PAK1;CCND1;ROCK1;ROCK2;PIK3CD;PRKCA;PIK3CB
Phosphodiesterases in neuronal function WP4222	May-53	5.77E-06	3.45E-05	22.48075	271.1756	PDE10A;PDE4D;PDE4B;PDE3A;PDE7A
IL-7 signaling pathway WP205	25-Apr	6.08E-06	3.46E-05	40.72094	489.0694	MAP2K1;CCND1;JAK3;JAK1
Relationship between inflammation, COX-2 and EGFR WP4483	25-Apr	6.08E-06	3.46E-05	40.72094	489.0694	MMP1;PIK3CD;PIK3CB;CYP19A1
Circadian rhythm related genes WP3594	8/201	6.09E-06	3.46E-05	9.179717	110.2413	IL6;PRKDC;CDK4;ROCK2;PPARG;DRD3;HCRTR2;HCRTR1
Cardiac Hypertrophic Response WP2795	May-55	6.94E-06	3.81E-05	21.57935	256.3141	CDK9;MAP2K1;PLA2G2A;PRKCA;MAPK14
DNA IR-double strand breaks and cellular response via ATM WP3959	May-55	6.94E-06	3.81E-05	21.57935	256.3141	PARP1;CDK5;PRKDC;CHEK1;MDM2
PPAR-alpha pathway WP2878	26-Apr	7.16E-06	3.87E-05	38.86804	460.4669	FABP1;CCND1;CDK4;CDK1
MET in type 1 papillary renal cell carcinoma WP4205	May-59	9.84E-06	5.23E-05	19.97685	230.3135	MAP2K1;PAK1;PIK3CD;PIK3CB;JAK3
Breast cancer pathway WP4262	7/154	1.01E-05	5.27E-05	10.45291	120.2715	MAP2K1;CDK6;CCND1;PARP1;CDK4;PIK3CD;PGR
Toll-like Receptor Signaling Pathway WP75	6/103	1.09E-05	5.62E-05	13.46278	153.8421	MAP2K1;IL6;PIK3CD;PIK3CB;IRAK4;MAPK14
PDGFR-beta pathway WP3972	29-Apr	1.12E-05	5.71E-05	34.19871	389.7	MAP2K1;PRKCA;JAK2;JAK1
miRNA regulation of prostate cancer signaling pathways WP3981	Apr-33	1.91E-05	9.41E-05	29.47571	320.284	AR;MAP2K1;CCND1;MDM2
Resistin as a regulator of inflammation WP4481	Apr-33	1.91E-05	9.41E-05	29.47571	320.284	IL6;PIK3CD;PIK3CB;MAPK14

AMP-activated protein kinase (AMPK) signaling WP1403	May-69	2.13E-05	1.03E-04	16.84698	181.2505	GYS1;LIPE;PIK3CD;PIK3CB;HMGCR
Overview of interferons-mediated signaling pathway WP4558	Apr-37	3.04E-05	1.45E-04	25.89769	269.392	PRKCA;TYK2;JAK2;JAK1
Ras signaling WP4223	7/184	3.18E-05	1.50E-04	8.668048	89.76003	MAP2K1;PAK1;PLA2G1B;PLA2G2A;PIK3CD;PRKCA;PIK3CB
Sleep regulation WP3591	Apr-38	3.38E-05	1.57E-04	25.13472	258.7533	IL6;DRD3;HCRTR2;HCRTR1
G13 Signaling Pathway WP524	Apr-39	3.75E-05	1.68E-04	24.41536	248.7962	ROCK1;ROCK2;PIK3CD;PIK3CB
Kisspeptin/kisspeptin receptor system in the ovary WP4871	Apr-39	3.75E-05	1.68E-04	24.41536	248.7962	MAP2K1;PIK3CD;PRKCA;PIK3CB
Regulatory circuits of the STAT3 signaling pathway WP4538	May-78	3.86E-05	1.68E-04	14.76325	150.0328	TYK2;JAK2;MAPK14;JAK3;JAK1
Cancer immunotherapy by CTLA4 blockade WP4582	14-Mar	3.87E-05	1.68E-04	57.71373	586.3187	PPP2CA;PIK3CD;PIK3CB
H19 action Rb-E2F1 signaling and CDK-Beta-catenin activity WP3969	14-Mar	3.87E-05	1.68E-04	57.71373	586.3187	CDK8;CCND1;CDK4
IL-5 signaling pathway WP127	Apr-40	4.16E-05	1.78E-04	23.73596	239.4603	MAP2K1;SYK;JAK2;JAK1
miRNAs involved in DNA damage response WP1545	15-Mar	4.82E-05	2.05E-04	52.9016	525.8134	CDK6;CCND1;CDC25A
IL-2 signaling pathway WP49	Apr-42	5.05E-05	2.12E-04	22.48444	222.4427	MAP2K1;SYK;JAK3;JAK1
Interleukin-11 Signaling Pathway WP2332	Apr-44	6.08E-05	2.52E-04	21.35806	207.3368	MAP2K1;TYK2;JAK2;JAK1
Acute viral myocarditis WP4298	May-86	6.17E-05	2.52E-04	13.29979	128.9091	IL6;CCND1;PARP1;ITGAL;JAK1
Regulation of Microtubule Cytoskeleton WP2038	Apr-46	7.26E-05	2.93E-04	20.33897	193.851	PAK1;ROCK1;CDK1;PRKCA
TNF-alpha signaling pathway WP231	May-92	8.52E-05	3.40E-04	12.37881	115.9947	PPP2CA;IL6;PYGL;GLUL;PRKCZ
G Protein Signaling Pathways WP35	May-93	8.97E-05	3.53E-04	12.23752	114.0413	PDE4D;PDE4B;PRKCA;PDE7A;PRKCZ
Regulation of Actin Cytoskeleton WP51	6/150	9.07E-05	3.53E-04	9.047161	84.20627	MAP2K1;PAK1;ROCK1;ROCK2;PIK3CD;PIK3CB

Structural Pathway of Interleukin 1 (IL-1) WP2637	Apr-49	9.32E-05	3.59E-04	18.98017	176.1553	MAP2K1;RPS6KA5;IRAK4;MAPK14
Serotonin Receptor 4/6/7 and NR3C Signaling WP734	19-Mar	1.01E-04	3.86E-04	39.66822	364.8515	MAP2K1;RPS6KA5;NR3C1
Wnt Signaling Pathway WP363	Apr-52	1.18E-04	4.43E-04	17.79122	160.9579	CDK6;CCND1;PRKCA;PPARG
Integrin-mediated Cell Adhesion WP185	5/101	1.33E-04	4.94E-04	11.2132	100.1127	MAP2K1;PAK1;ROCK1;ROCK2;ITGAL
Wnt signaling pathway and pluripotency WP399	5/102	1.39E-04	5.11E-04	11.09704	98.56021	PPP2CA;CCND1;LRRK2;PRKCA;PRKCZ
IL-1 signaling pathway WP195	Apr-55	1.47E-04	5.28E-04	16.74215	147.7865	MAP2K1;IRAK4;MAPK14;PRKCZ
RANKL/RANK signaling pathway WP2018	Apr-55	1.47E-04	5.28E-04	16.74215	147.7865	MAP2K1;SYK;CTSK;MAPK14
Transcription factor regulation in adipogenesis WP3599	22-Mar	1.59E-04	5.62E-04	33.39978	292.0764	IL6;PPARG;NR3C1
Vitamin D in inflammatory diseases WP4482	22-Mar	1.59E-04	5.62E-04	33.39978	292.0764	IL6;NR3C1;MAPK14
Immune response to tuberculosis WP4197	23-Mar	1.83E-04	6.37E-04	31.72819	273.1358	TYK2;JAK2;JAK1
Kit receptor signaling pathway WP304	Apr-59	1.93E-04	6.66E-04	15.52141	132.7624	MAP2K1;PRKCA;JAK2;MAPK14
Notch Signaling Pathway Netpath WP61	Apr-61	2.20E-04	7.50E-04	14.97529	126.1532	ADAM17;CCND1;PSEN2;JAK2
Endometrial cancer WP4155	Apr-63	2.49E-04	8.42E-04	14.46619	120.0579	MAP2K1;CCND1;PIK3CD;PIK3CB
FGFR3 signaling in chondrocyte proliferation and terminal differentiation WP4767	27-Mar	2.97E-04	9.77E-04	26.43484	214.6755	PPP2CA;MAP2K1;MAPK14
Follicle Stimulating Hormone (FSH) signaling pathway WP2035	27-Mar	2.97E-04	9.77E-04	26.43484	214.6755	PRKCA;MAPK14;CYP19A1
Association Between Physico-Chemical Features and Toxicity Associated Pathways WP3680	Apr-66	2.98E-04	9.77E-04	13.76413	111.7611	PPP2CA;MAP2K1;PAK1;ROCK2
Nanoparticle-mediated activation of receptor signaling WP2643	28-Mar	3.32E-04	0.001079	25.37617	203.2914	MAP2K1;PIK3CD;MAPK14
Glycerophospholipid Biosynthetic Pathway WP2533	30-Mar	4.08E-04	0.001315	23.49409	183.338	PLA2G2A;PIK3CD;PIK3CB
Head and Neck Squamous Cell Carcinoma WP4674	Apr-73	4.38E-04	0.001397	12.36341	95.611	CDK6;CCND1;CDK4;PIK3CB
Type I interferon induction and signaling during SARS-CoV-2 infection WP4868	31-Mar	4.50E-04	0.001424	22.65388	174.5551	IRAK4;TYK2;JAK1
Peptide GPCRs WP24	Apr-74	4.61E-04	0.001444	12.18618	93.60824	CCR1;CXCR1;HCRTR2;HCRTR1

Ovarian infertility WP34	Mar-32	4.95E-04	0.001536	21.87161	166.4513	CDK4;PGR;CYP19A1
Host-pathogen interaction of human coronaviruses - interferon induction WP4880	Mar-33	5.43E-04	0.001669	21.14149	158.954	TYK2;MAPK14;JAK1
The influence of laminopathies on Wnt signaling WP4844	Mar-35	6.47E-04	0.001952	19.81815	145.5369	CDK6;CCND1;PPARG
Photodynamic therapy-induced NF-kB survival signaling WP3617	Mar-35	6.47E-04	0.001952	19.81815	145.5369	IL6;CCND1;MMP1
Alzheimer's disease WP2059	Apr-83	7.13E-04	0.002131	10.79298	78.21232	ADAM17;CDK5;PSEN2;CDK5R1
miRNAs involvement in the immune response in sepsis WP4329	Mar-37	7.62E-04	0.00226	18.6505	133.8931	IL6;IRAK4;MAPK14
Parkinson's disease pathway WP2371	Mar-38	8.25E-04	0.002424	18.11672	128.6347	CCNE2;LRRK2;MAPK14
Nuclear Receptors Meta-Pathway WP2882	7/319	9.27E-04	0.002696	4.883796	34.10702	FABP1;CCND1;CDK4;NR1I2;CDK1;PDE4B;NR3C1
Glycogen Synthesis and Degradation WP500	Mar-40	9.59E-04	0.002696	17.13571	119.0819	PPP2CA;GYS1;PYGL
Microglia Pathogen Phagocytosis Pathway WP3937	Mar-40	9.59E-04	0.002696	17.13571	119.0819	SYK;PIK3CD;PIK3CB
Neural Crest Cell Migration during Development WP4564	Mar-40	9.59E-04	0.002696	17.13571	119.0819	PAK1;PIK3CD;PIK3CB
PDGF Pathway WP2526	Mar-40	9.59E-04	0.002696	17.13571	119.0819	PAK1;MAP2K1;JAK1
T-cell receptor (TCR) signaling pathway WP69	Apr-90	9.66E-04	0.002696	9.910978	68.80967	MAP2K1;PAK1;IL6;MAPK14
Myometrial relaxation and contraction pathways WP289	5/156	9.80E-04	0.002713	7.109128	49.25204	IL6;PDE4D;PDE4B;PRKCA;PRKCZ
Type III interferon signaling WP2113	10-Feb	0.001021	0.002805	52.35526	360.5482	TYK2;JAK1
Fibrin Complement Receptor 3 Signaling Pathway WP4136	Mar-41	0.001031	0.002809	16.68393	114.733	IL6;SYK;IRAK4
Corticotropin-releasing hormone signaling pathway WP2355	Apr-93	0.001091	0.00292	9.57545	65.30908	MAP2K1;PARP1;PRKCA;MAPK14
Epithelial to mesenchymal transition in CRC WP4239	5/160	0.001097	0.00292	6.924264	47.18863	MAP2K1;PAK1;PIK3CD;PIK3CB;MAPK14
DNA Replication WP466	Mar-42	0.001107	0.00292	16.25532	110.6379	POLA1;CDK2;CDC7
Fas ligand pathway and stress induction of heat shock proteins WP314	Mar-42	0.001107	0.00292	16.25532	110.6379	PAK1;PARP1;PRKDC
Thyroid hormones production and their peripheral downstream signaling effects WP4746	Apr-95	0.001181	0.003079	9.364055	63.1263	MAP2K1;MDM2;PPARG;MAPK14

Neural Crest Cell Migration in Cancer WP4565	Mar-43	0.001186	0.003079	15.84814	106.7759	PAK1;PIK3CD;PIK3CB
NAD metabolism, sirtuins and aging WP3630	11-Feb	0.001244	0.003207	46.53567	311.28	PARP1;PPARG
MAPK Signaling Pathway WP382	6/246	0.001267	0.003239	5.401923	36.03859	MAP2K1;PAK1;RPS6KA5;LRRK2;PRKCA;MAPK14
IL-10 Anti-inflammatory Signaling Pathway WP4495	12-Feb	0.001489	0.003778	41.88	272.6346	IL6;JAK1
Senescence and Autophagy in Cancer WP615	4/105	0.001709	0.004305	8.432663	53.73032	MAP2K1;IL6;MDM2;MAPK14
Mammary gland development pathway - Puberty (Stage 2 of 4) WP2814	13-Feb	0.001754	0.004384	38.07081	241.5976	CCND1;PGR
Photodynamic therapy-induced AP-1 survival signaling. WP3611	Mar-50	0.001838	0.00456	13.48302	84.93419	IL6;CCND1;MAPK14
DNA damage response (only ATM dependent) WP710	4/110	0.002027	0.004992	8.032867	49.81468	CCND1;MDM2;PIK3CD;PIK3CB
Copper homeostasis WP3286	Mar-52	0.002057	0.004995	12.93139	79.99735	ADAM17;CCND1;MDM2
Netrin-UNC5B signaling pathway WP4747	Mar-52	0.002057	0.004995	12.93139	79.99735	MAP2K1;PRKCA;MAPK14
The Overlap Between Signal Transduction Pathways that Contribute to a Range of LMNA Laminopathies WP4879	Mar-55	0.002417	0.005783	12.18351	73.40882	CDK4;CTSK;PPARG
Pathogenic Escherichia coli infection WP2272	Mar-55	0.002417	0.005783	12.18351	73.40882	ROCK1;ROCK2;PRKCA
ESC Pluripotency Pathways WP3931	4/116	0.002459	0.005842	7.60023	45.66298	MAP2K1;MDM2;PIK3CD;JAK1
Classical pathway of steroidogenesis with glucocorticoid and mineralocorticoid metabolism WP4523	16-Feb	0.002673	0.006305	29.90827	177.1974	HSD11B1;CYP19A1
Airway smooth muscle cell contraction WP4962	17-Feb	0.003019	0.007024	27.91298	161.9703	ROCK1;ROCK2
Cells and molecules involved in local acute inflammatory response WP4493	17-Feb	0.003019	0.007024	27.91298	161.9703	IL6;ITGAL
T-Cell antigen Receptor (TCR) pathway during Staphylococcus aureus infection WP3863	Mar-62	0.0034	0.007855	10.73422	61.01291	MAP2K1;PAK1;CDK4
Adipogenesis WP236	4/130	0.003705	0.008482	6.750981	37.79247	LIPE;IL6;PPARG;NR3C1
LTF danger signal response pathway WP4478	19-Feb	0.003773	0.008482	24.62663	137.4162	IL6;IRAK4
Nucleotide metabolism WP404	19-Feb	0.003773	0.008482	24.62663	137.4162	POLA1;IMPDH1
Overview of nanoparticle effects WP3287	19-Feb	0.003773	0.008482	24.62663	137.4162	IL6;PIK3CD

PPAR signaling pathway WP3942	Mar-67	0.004232	0.009452	9.893118	54.06608	FABP1;MMP1;PPARG
Sterol regulatory element-binding proteins (SREBP) signaling WP1982	Mar-69	0.004597	0.010081	9.59236	51.63008	CDK8;PPARG;HMGCR
Galanin receptor pathway WP4970	21-Feb	0.004604	0.010081	22.03213	118.5515	IL6;PPARG
Nicotine Activity on Dopaminergic Neurons WP1602	21-Feb	0.004604	0.010081	22.03213	118.5515	CDK5;DRD3
Glucocorticoid Receptor Pathway WP2880	Mar-70	0.004786	0.010411	9.448714	50.47596	NR1I2;PDE4B;NR3C1
Estrogen signaling pathway WP712	23-Feb	0.005512	0.011913	19.93183	103.6627	MAP2K1;MAPK14
Male infertility WP4673	4/146	0.005587	0.011926	5.985461	31.04829	CDK9;AR;PARP1;MDM2
16p11.2 proximal deletion syndrome WP4949	Mar-74	0.005589	0.011926	8.914594	46.23952	PPP2CA;PPARG;NR3C1
NAD Metabolism in Oncogene-Induced Senescence and Mitochondrial Dysfunction-Associated Senescence WP5046	24-Feb	0.005994	0.012709	19.02488	97.35026	IL6;PARP1
EPO Receptor Signaling WP581	26-Feb	0.007014	0.014778	17.43772	86.48872	MAP2K1;JAK2
TLR4 Signaling and Tolerance WP3851	28-Feb	0.008107	0.016973	16.09474	77.49748	IL6;IRAK4
GPCRs, Class A Rhodopsin-like WP455	5/257	0.008328	0.017328	4.238052	20.29251	CCR1;CXCR1;DRD3;HCRTR2;HCRTR1
Sphingolipid pathway WP1422	Feb-30	0.009271	0.019171	14.94361	69.94972	PPP2CA;ASAH1
Tumor suppressor activity of SMARCB1 WP4204	Feb-31	0.009879	0.020057	14.42759	66.61737	CDK6;CDK4
GABA receptor Signaling WP4159	Feb-31	0.009879	0.020057	14.42759	66.61737	GABRB3;GABRA2
SARS coronavirus and innate immunity WP4912	Feb-31	0.009879	0.020057	14.42759	66.61737	TYK2;JAK1
White fat cell differentiation WP4149	Feb-32	0.010504	0.021072	13.94596	63.53726	PPARG;NR3C1
IL17 signaling pathway WP2112	Feb-32	0.010504	0.021072	13.94596	63.53726	JAK2;JAK1
LncRNA involvement in canonical Wnt signaling and CRC WP4258	Mar-94	0.010782	0.021499	6.948328	31.47535	CDK8;CDK6;CCND1
Signal transduction through IL1R WP4496	Feb-33	0.011147	0.021585	13.49542	60.68317	IL6;MAPK14
Alpha 6 Beta 4 signaling pathway WP244	Feb-33	0.011147	0.021585	13.49542	60.68317	PRKCA;MAPK14

Endothelin Pathways WP2197	Feb-33	0.011147	0.021585	13.49542	60.68317	MAP2K1;PRKCA
MAPK Cascade WP422	Feb-33	0.011147	0.021585	13.49542	60.68317	MAP2K1;MAPK14
Nuclear Receptors in Lipid Metabolism and Toxicity WP299	Feb-33	0.011147	0.021585	13.49542	60.68317	NR1I2;PPARG
B Cell Receptor Signaling Pathway WP23	Mar-97	0.011736	0.022473	6.725555	29.89548	MAP2K1;SYK;MAPK14
Signaling of Hepatocyte Growth Factor Receptor WP313	Feb-34	0.011807	0.022473	13.07303	58.03231	PAK1;MAP2K1
p38 MAPK Signaling Pathway WP400	Feb-34	0.011807	0.022473	13.07303	58.03231	RPS6KA5;MAPK14
Overview of leukocyte-intrinsic Hippo pathway functions WP4542	Feb-35	0.012483	0.023626	12.67624	55.56479	ITGAL;MAPK14
Target Of Rapamycin (TOR) Signaling WP1471	Feb-36	0.013176	0.024659	12.30279	53.26316	PRKCA;HMGCR
Host-pathogen interaction of human coronaviruses - MAPK signaling WP4877	Feb-36	0.013176	0.024659	12.30279	53.26316	MAP2K1;MAPK14
Type II interferon signaling (IFNG) WP619	Feb-37	0.013885	0.025842	11.95068	51.11209	JAK2;JAK1
Thermogenesis WP4321	3/108	0.015644	0.028955	6.017629	25.01916	LIPE;PPARG;MAPK14
TNF related weak inducer of apoptosis (TWEAK) Signaling Pathway WP2036	Feb-42	0.017672	0.032351	10.45421	42.19068	IL6;MAPK14
Common Pathways Underlying Drug Addiction WP2636	Feb-42	0.017672	0.032351	10.45421	42.19068	MAP2K1;PRKCA
Wnt signaling WP428	3/115	0.018468	0.033625	5.639533	22.51126	CCND1;ROCK2;PRKCA
Notch Signaling WP268	Feb-45	0.02013	0.036256	9.723378	37.97486	ADAM17;PSEN2
Prostaglandin Synthesis and Regulation WP98	Feb-45	0.02013	0.036256	9.723378	37.97486	HSD11B1;PPARG
DNA Repair Pathways Full Network WP4946	3/120	0.020648	0.036793	5.397163	20.94178	PARP1;PRKDC;CHEK1
Hippo-Merlin Signaling Dysregulation WP4541	3/120	0.020648	0.036793	5.397163	20.94178	PAK1;CCND1;ITGAL
Aryl Hydrocarbon Receptor Netpath WP2586	Feb-46	0.02098	0.037187	9.501914	36.71722	MAP2K1;CDK2
Fragile X Syndrome WP4549	3/121	0.0211	0.037203	5.351154	20.64734	MAP2K1;PRKCA;PIK3CB
Energy Metabolism WP1541	Feb-47	0.021844	0.038313	9.290292	35.52447	PPARG;MAPK14

Differentiation Pathway WP2848	Feb-48	0.022723	0.039647	9.087872	34.39202	IL6;CXCR1
Phosphoinositides metabolism WP4971	Feb-49	0.023616	0.040991	8.894065	33.31568	PIK3CD;PIK3CB
TCA Cycle Nutrient Utilization and Invasiveness of Ovarian Cancer WP2868	05-Jan	0.024018	0.041475	51.82031	193.2352	JAK1
Synaptic signaling pathways associated with autism spectrum disorder WP4539	Feb-50	0.024523	0.041915	8.708333	32.29161	PIK3CD;PIK3CB
Vitamin B12 metabolism WP1533	Feb-50	0.024523	0.041915	8.708333	32.29161	IL6;MPO
Benzene metabolism WP3891	06-Jan	0.028753	0.048647	41.45417	147.1217	MPO
Metastatic brain tumor WP2249	06-Jan	0.028753	0.048647	41.45417	147.1217	CDK6
Hematopoietic Stem Cell Differentiation WP2849	Feb-55	0.029269	0.049272	7.884806	27.843	IL6;PIM1
Mevalonate pathway WP3963	07-Jan	0.033465	0.056053	34.5434	117.353	HMGCR
Mesodermal commitment pathway WP2857	3/147	0.034756	0.057926	4.379211	14.71156	PPP2CA;CCND1;JAK2
HIF1A and PPARG regulation of glycolysis WP2456	08-Jan	0.038154	0.063275	29.60714	96.70056	PPARG
Nonalcoholic fatty liver disease WP4396	3/155	0.039687	0.065265	4.147046	13.3814	IL6;PIK3CD;PIK3CB
Pathways affected in adenoid cystic carcinoma WP3651	Feb-65	0.039743	0.065265	6.629908	21.38354	PRKDC;CHEK1
SARS-CoV-2 innate immunity evasion and cell-specific immune response WP5039	Feb-66	0.040858	0.066769	6.525987	20.86776	IL6;JAK1
Sudden Infant Death Syndrome (SIDS) Susceptibility Pathways WP706	3/158	0.041623	0.067688	4.066163	12.92673	AR;IL6;NR3C1
ATR Signaling WP3875	09-Jan	0.042821	0.06831	25.90495	81.61948	CHEK1
Biotin Metabolism (including IEMs) WP5031	09-Jan	0.042821	0.06831	25.90495	81.61948	HLCS
Eicosanoid metabolism via cytochrome P450 monooxygenases (CYP) pathway WP4720	09-Jan	0.042821	0.06831	25.90495	81.61948	PPARG
Role of Altered Glycolysation of MUC1 in Tumour Microenvironment WP4480	09-Jan	0.042821	0.06831	25.90495	81.61948	IL6
RAC1/PAK1/p38/MMP2 Pathway WP3303	Feb-68	0.043124	0.068467	6.327592	19.89189	PAK1;MAPK14
IL-18 signaling pathway WP4754	4/272	0.043443	0.068648	3.15118	9.883065	IL6;PARP1;MMP1;PRKCA

Folate Metabolism WP176	Feb-69	0.044274	0.069633	6.232836	19.42996	IL6;MPO
Ethanol metabolism resulting in production of ROS by CYP2E1 WP4269	10-Jan	0.047465	0.073276	23.02546	70.176001	MAP2K1
Interleukin-1 Induced Activation of NF-kappa-B WP3656	10-Jan	0.047465	0.073276	23.02546	70.176001	PRKCZ
Non-homologous end joining WP438	10-Jan	0.047465	0.073276	23.02546	70.176001	PRKDC
SARS-CoV-2 and COVID-19 Pathway WP4846	10-Jan	0.047465	0.073276	23.02546	70.176001	CTSL
Chromosomal and microsatellite instability in CRC WP4216	Feb-73	0.048987	0.075278	5.880504	17.73683	MAP2K1;CCND1
Mevalonate arm of cholesterol biosynthesis pathway WP4190	11-Jan	0.052087	0.079677	20.72188	61.22967	HMGCR
Nanoparticle triggered regulated necrosis WP2513	12-Jan	0.056687	0.086319	18.83712	54.06641	PARP1
Vitamin D Receptor Pathway WP2877	3/182	0.058774	0.089092	3.5167	9.966517	CCND1;CDK2;CCNC
Transcriptional cascade regulating adipogenesis WP4211	13-Jan	0.061265	0.090813	17.26649	48.21747	PPARG
Dopamine metabolism WP2436	13-Jan	0.061265	0.090813	17.26649	48.21747	PPP2CA
Neuroinflammation WP4919	13-Jan	0.061265	0.090813	17.26649	48.21747	MAPK14
Osteopontin Signaling WP1434	13-Jan	0.061265	0.090813	17.26649	48.21747	MAP2K1
Purine metabolism WP4792	13-Jan	0.061265	0.090813	17.26649	48.21747	IMPDH1
Pyrimidine metabolism WP4022	Feb-85	0.06413	0.094641	5.027267	13.80913	POLA1;TK1
Selenium Micronutrient Network WP15	Feb-89	0.069486	0.100293	4.79516	12.78691	IL6;MPO
Allograft Rejection WP2328	Feb-89	0.069486	0.100293	4.79516	12.78691	LRRK2;PRKCZ
Cholesterol Biosynthesis Pathway WP197	15-Jan	0.070355	0.100293	14.79836	39.27787	HMGCR
COVID-19 adverse outcome pathway WP4891	15-Jan	0.070355	0.100293	14.79836	39.27787	IL6
ERK Pathway in Huntington's Disease WP3853	15-Jan	0.070355	0.100293	14.79836	39.27787	RPS6KA5
FOXP3 in COVID-19 WP5063	15-Jan	0.070355	0.100293	14.79836	39.27787	IL6

Mammary gland development pathway - Embryonic development (Stage 1 of 4) WP2813	15-Jan	0.070355	0.100293	14.79836	39.27787	CCND1
Phytochemical activity on NRF2 transcriptional activation WP3	15-Jan	0.070355	0.100293	14.79836	39.27787	PRKCA
Amino Acid metabolism WP3925	Feb-91	0.072218	0.10208	4.686931	12.31758	IARS;GLUL
GPCRs, Other WP117	Feb-91	0.072218	0.10208	4.686931	12.31758	CXCR1;DRD3
SREBF and miR33 in cholesterol and lipid homeostasis WP2011	16-Jan	0.074867	0.103638	13.81111	35.79899	HMGCR
ID signaling pathway WP53	16-Jan	0.074867	0.103638	13.81111	35.79899	CDK2
MAPK pathway in congenital thyroid cancer WP4928	16-Jan	0.074867	0.103638	13.81111	35.79899	MAP2K1
NAD+ metabolism WP3644	16-Jan	0.074867	0.103638	13.81111	35.79899	PARP1
Osteoclast Signaling WP12	16-Jan	0.074867	0.103638	13.81111	35.79899	CTSK
ACE Inhibitor Pathway WP554	17-Jan	0.079357	0.107631	12.94727	32.80569	NR3C2
Canonical and non-canonical TGF-B signaling WP3874	17-Jan	0.079357	0.107631	12.94727	32.80569	MAPK14
Drug Induction of Bile Acid Pathway WP2289	17-Jan	0.079357	0.107631	12.94727	32.80569	NR1I2
Leptin Insulin Overlap WP3935	17-Jan	0.079357	0.107631	12.94727	32.80569	JAK2
MAP3K1 role in promoting and blocking gonadal determination WP4872	17-Jan	0.079357	0.107631	12.94727	32.80569	ROCK1
Pathways Regulating Hippo Signaling WP4540	Feb-98	0.082044	0.110826	4.34364	10.86127	PRKCA;PRKCZ
4-hydroxytamoxifen, Dexamethasone, and Retinoic Acids Regulation of p27 Expression WP3879	18-Jan	0.083826	0.11188	12.18505	30.20683	MAP2K1
Transcription co-factors SKI and SKIL protein partners WP4533	18-Jan	0.083826	0.11188	12.18505	30.20683	MERTK
Fatty acid transporters WP5061	18-Jan	0.083826	0.11188	12.18505	30.20683	FABP1
TP53 network WP1742	19-Jan	0.088274	0.116884	11.50752	27.93235	MDM2
Extracellular vesicles in the crosstalk of cardiac cells WP4300	19-Jan	0.088274	0.116884	11.50752	27.93235	IL6
Serotonin Receptor 2 and ELK-SRF/GATA4 signaling WP732	20-Jan	0.0927	0.121782	10.90132	25.92756	MAP2K1

Imatinib and Chronic Myeloid Leukemia WP3640	20-Jan	0.0927	0.121782	10.90132	25.92756	PIM1
Host-pathogen interaction of human coronaviruses - apoptosis WP4864	21-Jan	0.097105	0.126576	10.35573	24.14921	MAPK14
Pathogenesis of SARS-CoV-2 Mediated by nsp9-nsp10 Complex WP4884	21-Jan	0.097105	0.126576	10.35573	24.14921	IL6
Type II diabetes mellitus WP1584	22-Jan	0.101488	0.129766	9.862103	22.56263	PRKCZ
FGF23 signaling in hypophosphatemic rickets and related disorders WP4790	22-Jan	0.101488	0.129766	9.862103	22.56263	CCND1
Glycerolipids and Glycerophospholipids WP4722	22-Jan	0.101488	0.129766	9.862103	22.56263	PLA2G1B
NAD+ biosynthetic pathways WP3645	22-Jan	0.101488	0.129766	9.862103	22.56263	PARP1
Purine metabolism and related disorders WP4224	22-Jan	0.101488	0.129766	9.862103	22.56263	IMPDH1
NRF2-ARE regulation WP4357	23-Jan	0.105851	0.134829	9.413352	21.13979	PRKCA
Sphingolipid Metabolism (general overview) WP4725	24-Jan	0.110192	0.137741	9.003623	19.85773	ASAH1
Angiogenesis WP1539	24-Jan	0.110192	0.137741	9.003623	19.85773	MAPK14
Triacylglyceride synthesis WP325	24-Jan	0.110192	0.137741	9.003623	19.85773	LIPE
miRNA regulation of p53 pathway in prostate cancer WP3982	24-Jan	0.110192	0.137741	9.003623	19.85773	MDM2
Photodynamic therapy-induced NFE2L2 (NRF2) survival signaling WP3612	24-Jan	0.110192	0.137741	9.003623	19.85773	MAPK14
Signal Transduction of S1P Receptor WP26	25-Jan	0.114513	0.14052	8.628038	18.69752	ASAH1
Sphingolipid Metabolism (integrated pathway) WP4726	25-Jan	0.114513	0.14052	8.628038	18.69752	ASAH1
Differentiation of white and brown adipocyte WP2895	25-Jan	0.114513	0.14052	8.628038	18.69752	PPARG
Hypothesized Pathways in Pathogenesis of Cardiovascular Disease WP3668	25-Jan	0.114513	0.14052	8.628038	18.69752	MAPK14
Physiological and pathological hypertrophy of the heart WP1528	25-Jan	0.114513	0.14052	8.628038	18.69752	MAPK14
Cytokines and Inflammatory Response WP530	26-Jan	0.118813	0.144736	8.2825	17.6434	IL6
Wnt/beta-catenin signaling pathway in leukemia WP3658	26-Jan	0.118813	0.144736	8.2825	17.6434	CCND1

7-oxo-C and 7beta-HC pathways WP5064	27-Jan	0.123093	0.148331	7.963542	16.68218	HSD11B1
Canonical and non-canonical Notch signaling WP3845	27-Jan	0.123093	0.148331	7.963542	16.68218	PSEN2
Eicosanoid Synthesis WP167	27-Jan	0.123093	0.148331	7.963542	16.68218	PLA2G2A
Interactions between immune cells and microRNAs in tumor microenvironment WP4559	28-Jan	0.127351	0.152913	7.66821	15.80269	IRAK4
Selective expression of chemokine receptors during T-cell polarization WP4494	29-Jan	0.13159	0.154675	7.393973	14.99548	CCR1
Statin inhibition of cholesterol production WP430	29-Jan	0.13159	0.154675	7.393973	14.99548	HMGCR
T-Cell Receptor and Co-stimulatory Signaling WP2583	29-Jan	0.13159	0.154675	7.393973	14.99548	PRKCA
Cannabinoid receptor signaling WP3869	29-Jan	0.13159	0.154675	7.393973	14.99548	MAPK14
Lipid Metabolism Pathway WP3965	29-Jan	0.13159	0.154675	7.393973	14.99548	LIPE
RAS and bradykinin pathways in COVID-19 WP4969	29-Jan	0.13159	0.154675	7.393973	14.99548	ROCK1
Cell migration and invasion through p75NTR WP4561	30-Jan	0.135807	0.15797	7.138649	14.25244	PAK1
Matrix Metalloproteinases WP129	30-Jan	0.135807	0.15797	7.138649	14.25244	MMP1
PI3K-AKT-mTOR signaling pathway and therapeutic opportunities WP3844	30-Jan	0.135807	0.15797	7.138649	14.25244	PIK3CB
16p11.2 distal deletion syndrome WP4950	31-Jan	0.140005	0.161174	6.900347	13.56661	JAK2
Base Excision Repair WP4752	31-Jan	0.140005	0.161174	6.900347	13.56661	PARP1
Toll-like Receptor Signaling related to MyD88 WP3858	31-Jan	0.140005	0.161174	6.900347	13.56661	IRAK4
Development and heterogeneity of the ILC family WP3893	Jan-32	0.144183	0.16302	6.677419	12.93199	IL6
Hair Follicle Development: Organogenesis - Part 2 of 3 WP2839	Jan-32	0.144183	0.16302	6.677419	12.93199	CCND1
Initiation of transcription and translation elongation at the HIV-1 LTR WP3414	Jan-32	0.144183	0.16302	6.677419	12.93199	CDK9
Monoamine Transport WP727	Jan-32	0.144183	0.16302	6.677419	12.93199	MAPK14
SARS-CoV-2 mitochondrial interactions WP5038	Jan-32	0.144183	0.16302	6.677419	12.93199	CTSL

Ectoderm Differentiation WP2858	2/138	0.14453	0.16302	3.059907	5.918719	PIM1;PDE7A
Fluoropyrimidine Activity WP1601	Jan-33	0.14834	0.164549	6.468424	12.34337	TK1
Monoamine GPCRs WP58	Jan-33	0.14834	0.164549	6.468424	12.34337	DRD3
Oxidative Stress WP408	Jan-33	0.14834	0.164549	6.468424	12.34337	MAPK14
Pregnane X receptor pathway WP2876	Jan-33	0.14834	0.164549	6.468424	12.34337	NR1I2
Purinergic signaling WP4900	Jan-33	0.14834	0.164549	6.468424	12.34337	P2RX7
BDNF-TrkB Signaling WP3676	Jan-34	0.152477	0.167475	6.272096	11.79618	MAP2K1
Type 2 papillary renal cell carcinoma WP4241	Jan-34	0.152477	0.167475	6.272096	11.79618	CTSK
Fatty acid beta-oxidation WP143	Jan-34	0.152477	0.167475	6.272096	11.79618	LIPE
Melatonin metabolism and effects WP3298	Jan-37	0.16477	0.179845	5.748553	10.36581	PRKCA
Calcium Regulation in the Cardiac Cell WP536	2/150	0.164813	0.179845	2.8101	5.066444	PRKCA;PRKCZ
Amyotrophic lateral sclerosis (ALS) WP2447	Jan-38	0.168829	0.183629	5.592905	9.949054	MAPK14
Splicing factor NOVA regulated synaptic proteins WP4148	Jan-42	0.184868	0.199777	5.04624	8.518625	PRKCZ
Tryptophan metabolism WP465	Jan-42	0.184868	0.199777	5.04624	8.518625	CYP19A1
Hedgehog Signaling Pathway WP4249	Jan-44	0.192772	0.207649	4.811047	7.920164	CCND1
Cholesterol metabolism (includes both Bloch and Kandutsch-Russell pathways) WP4718	Jan-46	0.200601	0.214017	4.596759	7.384411	HMGCR
Envelope proteins and their potential roles in EDMD physiopathology WP4535	Jan-46	0.200601	0.214017	4.596759	7.384411	MAP2K1
Oxysterols derived from cholesterol WP4545	Jan-46	0.200601	0.214017	4.596759	7.384411	NR1I2
Development of ureteric collection system WP5053	Jan-47	0.204487	0.216098	4.496603	7.137241	CCND1
Mechanoregulation and pathology of YAP/TAZ via Hippo and non-Hippo mechanisms WP4534	Jan-47	0.204487	0.216098	4.496603	7.137241	PAK1
NO/cGMP/PKG mediated Neuroprotection WP4008	Jan-47	0.204487	0.216098	4.496603	7.137241	PDE3A

Rett syndrome causing genes WP4312	Jan-48	0.208354	0.219493	4.400709	6.902583	IMPDH2
Cardiac Progenitor Differentiation WP2406	Jan-53	0.227413	0.23882	3.976563	5.889233	MAPK14
TGF-beta Receptor Signaling WP560	Jan-54	0.23117	0.242007	3.901336	5.713898	JAK1
Proximal tubule transport WP4917	Jan-57	0.242333	0.252902	3.691778	5.23288	CA2
TGF-beta receptor signaling in skeletal dysplasias WP4816	Jan-58	0.246018	0.255158	3.626827	5.086078	JAK1
Pre-implantation embryo WP3527	Jan-58	0.246018	0.255158	3.626827	5.086078	NR3C2
Novel intracellular components of RIG-I-like receptor (RLR) pathway WP3865	Jan-60	0.253336	0.261937	3.503531	4.810488	MAPK14
Oxidation by Cytochrome P450 WP43	Jan-61	0.256968	0.264875	3.444965	4.681034	CYP19A1
Genotoxicity pathway WP4286	Jan-63	0.26418	0.270643	3.333501	4.437307	MDM2
Lung fibrosis WP3624	Jan-63	0.26418	0.270643	3.333501	4.437307	IL6
Primary focal segmental glomerulosclerosis (FSGS) WP2572	Jan-72	0.295786	0.302099	2.909624	3.544268	CTSL
Cytosolic DNA-sensing pathway WP4655	Jan-75	0.30602	0.311601	2.791244	3.305126	IL6
Joubert Syndrome WP4656	Jan-76	0.309398	0.314086	2.753889	3.230657	PARP1
Apoptosis WP254	Jan-84	0.335847	0.339905	2.48745	2.714058	MDM2
ncRNAs involved in Wnt signaling in hepatocellular carcinoma WP4336	Jan-86	0.3423	0.345394	2.428676	2.603702	CCND1
Complement system WP2806	Jan-97	0.376703	0.378965	2.149197	2.098258	PRKCA
Endoderm differentiation WP2853	1/141	0.497384	0.498873	1.470461	1.02696	NR3C1
Metapathway biotransformation Phase I and II WP702	1/183	0.590898	0.590898	1.12872	0.593833	CYP19A1

KEGG pathways

Term	Overlap	P-value	Adjusted P-value	Odds Ratio	Combined Score	Genes

Epstein-Barr virus infection	16/202	2.49E-15	5.43E-13	20.93933	704.1139	SYK;PIK3CD;PIK3CB;TYK2;IRAK4;ITGAL;MAPK14;IL6;CDK6;CCND1;CCNE2;CDK4;CDK2;MDM2;JAK3;JAK1
Cellular senescence	14/156	2.73E-14	2.98E-12	23.4731	733.0774	MAP2K1;PIK3CD;PIK3CB;MAPK14;CDC25A;IL6;CDK6;CCND1;CCNE2;CDK4;CHEK1;CDK2;CDK1;MDM2
Pathways in cancer	21/531	8.34E-14	6.06E-12	10.50704	316.4228	MAP2K1;ROCK1;MMP1;ROCK2;PIK3CD;PRKCA;PIK3CB;AR;IL6;RPS6KA5;CDK6;CCND1;CCNE2;CDK4;CDK2;PIM1;MDM2;PPARG;JAK2;JAK3;JAK1
Hepatitis B	13/162	1.03E-12	5.10E-11	20.5179	566.3587	MAP2K1;PIK3CD;PRKCA;PIK3CB;TYK2;IRAK4;MAPK14;IL6;CCNE2;CDK2;JAK2;JAK3;JAK1
PI3K-Akt signaling pathway	17/354	1.17E-12	5.10E-11	12.33761	338.9558	MAP2K1;SYK;PIK3CD;PRKCA;PIK3CB;PPP2CA;GYS1;IL6;CDK6;CCND1;CCNE2;CDK4;CDK2;MDM2;JAK2;JAK3;JAK1
Measles	12/139	3.38E-12	1.23E-10	21.98351	580.6637	IL6;CDK6;CCND1;CCNE2;CDK4;CDK2;PIK3CD;PIK3CB;TYK2;IRAK4;JAK3;JAK1
Human cytomegalovirus infection	14/225	4.25E-12	1.32E-10	15.74191	412.1885	CCR1;MAP2K1;ROCK1;ROCK2;PIK3CD;PRKCA;PIK3CB;MAPK14;IL6;CDK6;CCND1;CDK4;MDM2;JAK1
Kaposi sarcoma-associated herpesvirus infection	13/193	9.62E-12	2.62E-10	16.95761	430.1705	CCR1;MAP2K1;SYK;PIK3CD;PIK3CB;TYK2;MAPK14;IL6;CDK6;CCND1;CDK4;JAK2;JAK1
Viral carcinogenesis	13/203	1.82E-11	4.41E-10	16.05695	397.0754	SYK;PIK3CD;PIK3CB;CDK6;CCND1;CCNE2;CDK4;CHEK1;CDK2;CDK1;MDM2;JAK3;JAK1
Cell cycle	11/124	2.10E-11	4.58E-10	22.4007	550.7336	CDK6;CCND1;CCNE2;PRKDC;CDK4;CHEK1;CDK2;CDK1;MDM2;CDC7;CDC25A
AGE-RAGE signaling pathway in diabetic complications	10/100	5.41E-11	1.07E-09	25.30396	598.1931	IL6;CCND1;CDK4;PIM1;PIK3CD;PRKCA;PIK3CB;JAK2;MAPK14;PRKCZ
Sphingolipid signaling pathway	10/119	3.08E-10	5.43E-09	20.87314	457.1177	PPP2CA;MAP2K1;ASAH1;ROCK1;ROCK2;PIK3CD;PRKCA;PIK3CB;MAPK14;PRKCZ
Proteoglycans in cancer	12/205	3.24E-10	5.43E-09	14.41756	315.0412	MAP2K1;PAK1;CCND1;ROCK1;CTSL;ROCK2;MDM2;PDCD4;PIK3CD;PRKCA;PIK3CB;MAPK14
Human T-cell leukemia virus 1 infection	12/219	6.91E-10	1.05E-08	13.43291	283.3324	MAP2K1;IL6;CCND1;CCNE2;CDK4;CHEK1;CDK2;PIK3CD;PIK3CB;ITGAL;JAK3;JAK1
Influenza A	11/172	7.24E-10	1.05E-08	15.6841	330.0893	MAP2K1;IL6;CDK6;CDK4;PIK3CD;PRKCA;PIK3CB;TYK2;IRAK4;JAK2;JAK1
Non-small cell lung cancer	Aug-72	2.12E-09	2.87E-08	27.86376	556.5378	MAP2K1;CDK6;CCND1;CDK4;PIK3CD;PRKCA;PIK3CB;JAK3
Chemokine signaling pathway	11/192	2.32E-09	2.87E-08	13.93691	277.0755	CCR1;MAP2K1;PAK1;ROCK1;CXCR1;ROCK2;PIK3CD;PIK3CB;JAK2;PRKCZ;JAK3
p53 signaling pathway	Aug-73	2.37E-09	2.87E-08	27.43371	544.8725	CDK6;CCND1;CCNE2;CDK4;CHEK1;CDK2;CDK1;MDM2
Glioma	Aug-75	2.95E-09	3.38E-08	26.61211	522.7187	MAP2K1;CDK6;CCND1;CDK4;MDM2;PIK3CD;PRKCA;PIK3CB
MicroRNAs in cancer	13/310	3.37E-09	3.67E-08	10.21637	199.3108	MAP2K1;ROCK1;PIK3CD;PRKCA;PIK3CB;CDC25A;RPS6KA5;CDK6;CCND1;CCNE2;PIM1;MDM2;PDCD4

Hepatitis C	10/157	4.66E-09	4.84E-08	15.44765	296.3376	PPP2CA;MAP2K1;CDK6;CCND1;CDK4;CDK2;PIK3CD;PIK3CB;TYK2;JAK1
Human papillomavirus infection	13/331	7.39E-09	7.32E-08	9.531484	178.4599	MAP2K1;PIK3CD;PIK3CB;TYK2;PRKCZ;PPP2CA;CDK6;CCND1;CCNE2;CDK4;CDK2;MDM2;JAK1
cAMP signaling pathway	11/216	7.97E-09	7.56E-08	12.2903	229.1801	LIPE;MAP2K1;PAK1;PDE10A;ROCK1;ROCK2;PDE4D;PDE3A;PDE4B;PIK3CD;PIK3CB
Osteoclast differentiation	9/127	1.13E-08	1.02E-07	17.14802	313.8517	MAP2K1;SYK;CTSK;PIK3CD;PPARG;PIK3CB;TYK2;MAPK14;JAK1
Morphine addiction	Aug-91	1.39E-08	1.22E-07	21.46474	388.2675	GABRB3;GABRA2;PDE10A;PDE4D;PDE4B;PDE3A;PRKCA;PDE7A
Coronavirus disease	11/232	1.67E-08	1.40E-07	11.39124	203.9772	ADAM17;IL6;SYK;MMP1;PIK3CD;PRKCA;PIK3CB;TYK2;IRAK4;MAPK14;JAK1
Prostate cancer	Aug-97	2.31E-08	1.87E-07	20.01161	351.8336	AR;MAP2K1;CCND1;CCNE2;CDK2;MDM2;PIK3CD;PIK3CB
Progesterone-mediated oocyte maturation	8/100	2.95E-08	2.29E-07	19.35613	335.6461	MAP2K1;CDK2;CDK1;PIK3CD;PGR;PIK3CB;MAPK14;CDC25A
Bladder cancer	Jun-41	4.36E-08	3.28E-07	37.42794	634.3149	MAP2K1;RPS6KA5;CCND1;MMP1;CDK4;MDM2
Melanoma	Jul-72	5.77E-08	4.19E-07	23.73778	395.6554	MAP2K1;CDK6;CCND1;CDK4;MDM2;PIK3CD;PIK3CB
Human immunodeficiency virus 1 infection	10/212	8.16E-08	5.57E-07	11.21031	182.9664	MAP2K1;PAK1;LIMK2;CHEK1;CDK1;PIK3CD;PRKCA;PIK3CB;IRAK4;MAPK14
Chronic myeloid leukemia	Jul-76	8.43E-08	5.57E-07	22.35717	364.1697	MAP2K1;CDK6;CCND1;CDK4;MDM2;PIK3CD;PIK3CB
Pancreatic cancer	Jul-76	8.43E-08	5.57E-07	22.35717	364.1697	MAP2K1;CDK6;CCND1;CDK4;PIK3CD;PIK3CB;JAK1
Lipid and atherosclerosis	10/215	9.31E-08	5.81E-07	11.04458	178.8073	IL6;MMP1;ROCK2;PIK3CD;PRKCA;PPARG;PIK3CB;IRAK4;JAK2;MAPK14
JAK-STAT signaling pathway	9/162	9.33E-08	5.81E-07	13.20187	213.6986	IL6;CCND1;PIM1;PIK3CD;PIK3CB;TYK2;JAK2;JAK3;JAK1
AMPK signaling pathway	8/120	1.23E-07	7.44E-07	15.88363	252.7448	PPP2CA;LIPE;GYS1;CCND1;PIK3CD;PPARG;PIK3CB;HMGCR
Oocyte meiosis	8/129	2.15E-07	1.27E-06	14.69551	225.6114	PPP2CA;AR;MAP2K1;CCNE2;CDK2;CDK1;PGR;MAPK14
FoxO signaling pathway	8/131	2.42E-07	1.37E-06	14.4551	220.2061	MAP2K1;IL6;CCND1;CDK2;MDM2;PIK3CD;PIK3CB;MAPK14
Chemical carcinogenesis	10/239	2.49E-07	1.37E-06	9.875019	150.1503	HSD11B1;AR;MAP2K1;CCND1;PIK3CD;PRKCA;PGR;PIK3CB;JAK2;CDC25A
Axon guidance	9/182	2.52E-07	1.37E-06	11.66382	177.2138	PAK1;CDK5;ROCK1;ROCK2;LIMK2;PIK3CD;PRKCA;PIK3CB;PRKCZ
Small cell lung cancer	Jul-92	3.17E-07	1.69E-06	18.13412	271.3527	CDK6;CCND1;CCNE2;CDK4;CDK2;PIK3CD;PIK3CB

Insulin signaling pathway	8/137	3.42E-07	1.73E-06	13.77859	205.1572	LIPE;GYS1;PTPN1;MAP2K1;PIK3CD;PYGL;PIK3CB;PRKCZ
Yersinia infection	8/137	3.42E-07	1.73E-06	13.77859	205.1572	MAP2K1;IL6;ROCK1;ROCK2;PIK3CD;PIK3CB;IRAK4;MAPK14
Fc gamma R-mediated phagocytosis	Jul-97	4.56E-07	2.26E-06	17.12235	249.9958	MAP2K1;PAK1;SYK;LIMK2;PIK3CD;PRKCA;PIK3CB
C-type lectin receptor signaling pathway	7/104	7.34E-07	3.48E-06	15.8811	224.3226	IL6;PAK1;SYK;MDM2;PIK3CD;PIK3CB;MAPK14
Toll-like receptor signaling pathway	7/104	7.34E-07	3.48E-06	15.8811	224.3226	MAP2K1;IL6;CTSK;PIK3CD;PIK3CB;IRAK4;MAPK14
Acute myeloid leukemia	Jun-67	8.75E-07	4.06E-06	21.44695	299.1671	MAP2K1;CCND1;PIM1;PIK3CD;PIK3CB;MPO
Insulin resistance	7/108	9.48E-07	4.25E-06	15.24906	211.4877	GYS1;PTPN1;IL6;PIK3CD;PYGL;PIK3CB;PRKCZ
Fc epsilon RI signaling pathway	Jun-68	9.56E-07	4.25E-06	21.09996	292.4602	MAP2K1;SYK;PIK3CD;PRKCA;PIK3CB;MAPK14
Prolactin signaling pathway	Jun-70	1.14E-06	4.95E-06	20.43853	279.7607	MAP2K1;CCND1;PIK3CD;PIK3CB;JAK2;MAPK14
Leukocyte transendothelial migration	7/114	1.37E-06	5.84E-06	14.38962	194.3087	ROCK1;ROCK2;PIK3CD;PRKCA;PIK3CB;ITGAL;MAPK14
Neurotrophin signaling pathway	7/119	1.82E-06	7.65E-06	13.74375	181.6177	MAP2K1;RPS6KA5;PSEN2;PIK3CD;PIK3CB;IRAK4;MAPK14
Platelet activation	7/124	2.40E-06	9.88E-06	13.15309	170.1847	SYK;ROCK1;ROCK2;PIK3CD;PIK3CB;MAPK14;PRKCZ
Purine metabolism	7/129	3.13E-06	1.24E-05	12.61084	159.8415	PDE10A;IMPDH1;PDE4D;IMPDH2;PDE3A;PDE4B;PDE7A
Relaxin signaling pathway	7/129	3.13E-06	1.24E-05	12.61084	159.8415	MAP2K1;MMP1;PIK3CD;PRKCA;PIK3CB;MAPK14;PRKCZ
Natural killer cell mediated cytotoxicity	7/131	3.47E-06	1.35E-05	12.40618	155.9771	MAP2K1;PAK1;SYK;PIK3CD;PRKCA;PIK3CB;ITGAL
Neutrophil extracellular trap formation	8/189	3.87E-06	1.48E-05	9.794276	122.0687	MAP2K1;SYK;PIK3CD;PRKCA;PIK3CB;ITGAL;MAPK14;MPO
PD-L1 expression and PD-1 checkpoint pathway in cancer	Jun-89	4.68E-06	1.76E-05	15.74474	193.2365	MAP2K1;PIK3CD;PIK3CB;JAK2;MAPK14;JAK1
Apoptosis	7/142	5.91E-06	2.18E-05	11.38897	137.107	MAP2K1;PARP1;CTSL;CTSK;PIK3CD;PIK3CB;CTSS
Focal adhesion	8/201	6.09E-06	2.21E-05	9.179717	110.2413	MAP2K1;PAK1;CCND1;ROCK1;ROCK2;PIK3CD;PRKCA;PIK3CB
Signaling pathways regulating pluripotency of stem cells	7/143	6.19E-06	2.21E-05	11.30466	135.5691	MAP2K1;PIK3CD;PIK3CB;JAK2;MAPK14;JAK3;JAK1
Breast cancer	7/147	7.42E-06	2.61E-05	10.97944	129.6763	MAP2K1;CDK6;CCND1;CDK4;PIK3CD;PGR;PIK3CB

VEGF signaling pathway	May-59	9.84E-06	3.41E-05	19.97685	230.3135	MAP2K1;PIK3CD;PRKCA;PIK3CB;MAPK14
Chagas disease	6/102	1.03E-05	3.51E-05	13.60371	156.216	PPP2CA;IL6;PIK3CD;PIK3CB;IRAK4;MAPK14
Regulation of actin cytoskeleton	8/218	1.10E-05	3.70E-05	8.42932	96.22786	MAP2K1;PAK1;ROCK1;ROCK2;LIMK2;PIK3CD;PIK3CB;ITGAL
T cell receptor signaling pathway	6/104	1.15E-05	3.80E-05	13.32474	151.5247	MAP2K1;PAK1;CDK4;PIK3CD;PIK3CB;MAPK14
Necroptosis	7/159	1.24E-05	4.04E-05	10.10651	114.1795	PARP1;PYGL;TYK2;JAK2;GLUL;JAK3;JAK1
Th17 cell differentiation	6/107	1.36E-05	4.35E-05	12.92699	144.8927	IL6;TYK2;JAK2;MAPK14;JAK3;JAK1
TNF signaling pathway	6/112	1.76E-05	5.52E-05	12.31412	134.8088	MAP2K1;IL6;RPS6KA5;PIK3CD;PIK3CB;MAPK14
Hepatocellular carcinoma	7/168	1.77E-05	5.52E-05	9.537198	104.3401	MAP2K1;CDK6;CCND1;CDK4;PIK3CD;PRKCA;PIK3CB
Growth hormone synthesis, secretion and action	6/119	2.48E-05	7.63E-05	11.54721	122.4333	MAP2K1;PIK3CD;PRKCA;PIK3CB;JAK2;MAPK14
Thyroid hormone signaling pathway	6/121	2.73E-05	8.26E-05	11.34525	119.2212	MAP2K1;CCND1;MDM2;PIK3CD;PRKCA;PIK3CB
Tuberculosis	7/180	2.76E-05	8.26E-05	8.870263	93.10234	IL6;SYK;IRAK4;JAK2;MAPK14;CTSS;JAK1
Salmonella infection	8/249	2.87E-05	8.46E-05	7.333489	76.6972	MAP2K1;IL6;PAK1;ROCK2;PIK3CD;PIK3CB;IRAK4;MAPK14
Aldosterone-regulated sodium reabsorption	Apr-37	3.04E-05	8.83E-05	25.89769	269.392	PIK3CD;PRKCA;PIK3CB;NR3C2
Vascular smooth muscle contraction	6/133	4.65E-05	1.33E-04	10.26702	102.4265	MAP2K1;ROCK1;ROCK2;PLA2G1B;PLA2G2A;PRKCA
ErbB signaling pathway	May-85	5.84E-05	1.65E-04	13.46671	131.2823	MAP2K1;PAK1;PIK3CD;PRKCA;PIK3CB
Diabetic cardiomyopathy	7/203	5.94E-05	1.66E-04	7.820238	76.09958	GYS1;PARP1;PIK3CD;PRKCA;PIK3CB;MAPK14;PRKCZ
Nitrogen metabolism	17-Mar	7.16E-05	1.98E-04	45.33967	432.7539	CA2;CA7;GLUL
Rap1 signaling pathway	7/210	7.35E-05	2.00E-04	7.547893	71.83908	MAP2K1;PIK3CD;PRKCA;PIK3CB;ITGAL;MAPK14;PRKCZ
Phospholipase D signaling pathway	6/148	8.43E-05	2.27E-04	9.175515	86.08132	MAP2K1;SYK;CXCR1;PIK3CD;PRKCA;PIK3CB
Th1 and Th2 cell differentiation	May-92	8.52E-05	2.27E-04	12.37881	115.9947	TYK2;JAK2;MAPK14;JAK3;JAK1
Gastric cancer	6/149	8.75E-05	2.30E-04	9.110889	85.13595	MAP2K1;CCND1;CCNE2;CDK2;PIK3CD;PIK3CB

Rheumatoid arthritis	May-93	8.97E-05	2.33E-04	12.23752	114.0413	IL6;CTSL;MMP1;CTSK;ITGAL
Cushing syndrome	6/155	1.09E-04	2.79E-04	8.741353	79.78104	MAP2K1;CDK6;CCND1;CCNE2;CDK4;CDK2
Ras signaling pathway	7/232	1.37E-04	3.47E-04	6.802272	60.52016	MAP2K1;PAK1;PLA2G1B;PLA2G2A;PIK3CD;PRKCA;PIK3CB
Tight junction	6/169	1.74E-04	4.37E-04	7.984899	69.10254	PPP2CA;CCND1;ROCK1;CDK4;ROCK2;PRKCZ
Endometrial cancer	Apr-58	1.80E-04	4.47E-04	15.80964	136.2791	MAP2K1;CCND1;PIK3CD;PIK3CB
HIF-1 signaling pathway	5/109	1.90E-04	4.65E-04	10.34647	88.66925	MAP2K1;IL6;PIK3CD;PRKCA;PIK3CB
Shigellosis	7/246	1.96E-04	4.75E-04	6.399256	54.62774	RPS6KA5;ROCK1;ROCK2;MDM2;PIK3CD;PIK3CB;MAPK14
Toxoplasmosis	5/112	2.15E-04	5.16E-04	10.05486	84.89473	TYK2;IRAK4;JAK2;MAPK14;JAK1
Cholinergic synapse	5/113	2.24E-04	5.32E-04	9.961252	83.69157	MAP2K1;PIK3CD;PRKCA;PIK3CB;JAK2
NOD-like receptor signaling pathway	6/181	2.53E-04	5.92E-04	7.432841	61.56699	P2RX7;IL6;TYK2;IRAK4;MAPK14;JAK1
GnRH secretion	Apr-64	2.64E-04	6.13E-04	14.22437	117.1856	MAP2K1;PIK3CD;PRKCA;PIK3CB
Renal cell carcinoma	Apr-69	3.53E-04	8.10E-04	13.12688	104.3447	MAP2K1;PAK1;PIK3CD;PIK3CB
Epithelial cell signaling in Helicobacter pylori infection	Apr-70	3.73E-04	8.47E-04	12.92734	102.0457	ADAM17;PAK1;CXCR1;MAPK14
Pathogenic Escherichia coli infection	6/197	3.98E-04	8.94E-04	6.804672	53.28073	IL6;PAK1;ROCK1;ROCK2;IRAK4;MAPK14
Alzheimer disease	8/369	4.31E-04	9.59E-04	4.865884	37.70427	MAP2K1;ADAM17;IL6;CDK5;PSEN2;PIK3CD;PIK3CB;CDK5R1
Leishmaniasis	Apr-77	5.37E-04	0.001181	11.68361	87.98195	IRAK4;JAK2;MAPK14;JAK1
Autophagy	5/137	5.45E-04	0.001189	8.140234	61.16765	PPP2CA;MAP2K1;CTSL;PIK3CD;PIK3CB
Fluid shear stress and atherosclerosis	5/139	5.82E-04	0.001257	8.017927	59.71997	CTSL;PIK3CD;PIK3CB;MAPK14;PRKCZ
B cell receptor signaling pathway	Apr-81	6.50E-04	0.001389	11.07443	81.27095	MAP2K1;SYK;PIK3CD;PIK3CB
Thyroid cancer	Mar-37	7.62E-04	0.001614	18.6505	133.8931	MAP2K1;CCND1;PPARG
CRC	Apr-86	8.14E-04	0.001707	10.39654	73.95108	MAP2K1;CCND1;PIK3CD;PIK3CB

Oxytocin signaling pathway	5/154	9.25E-04	0.001905	7.205282	50.33445	MAP2K1;CCND1;ROCK1;ROCK2;PRKCA
GABAergic synapse	Apr-89	9.26E-04	0.001905	10.02808	70.04161	GABRB3;GABRA2;PRKCA;GLUL
Non-alcoholic fatty liver disease	5/155	9.52E-04	0.00194	7.156884	49.78886	IL6;PIK3CD;PPARG;PIK3CB;MAPK14
Fat digestion and absorption	Mar-43	0.001186	0.002393	15.84814	106.7759	FABP1;PLA2G1B;PLA2G2A
Choline metabolism in cancer	Apr-98	0.001325	0.002627	9.06383	60.05745	MAP2K1;PIK3CD;PRKCA;PIK3CB
Inflammatory mediator regulation of TRP channels	Apr-98	0.001325	0.002627	9.06383	60.05745	PIK3CD;PRKCA;PIK3CB;MAPK14
Neuroactive ligand-receptor interaction	7/341	0.001362	0.002675	4.556986	30.06977	GABRB3;GABRA2;P2RX7;NR3C1;DRD3;HCRTR2;HCRTR1
Type II diabetes mellitus	Mar-46	0.001443	0.002809	14.74023	96.41427	PIK3CD;PIK3CB;PRKCZ
Amoebiasis	4/102	0.001536	0.002938	8.692122	56.31029	IL6;PIK3CD;PRKCA;PIK3CB
Pancreatic secretion	4/102	0.001536	0.002938	8.692122	56.31029	CA2;PLA2G1B;PLA2G2A;PRKCA
Parathyroid hormone synthesis, secretion and action	4/106	0.00177	0.003355	8.349568	52.91043	MAP2K1;PDE4D;PDE4B;PRKCA
Drug metabolism	4/108	0.001895	0.003562	8.188172	51.32696	IMPDH1;IMPDH2;TK1;MPO
Pathways of neurodegeneration	8/475	0.002178	0.004059	3.74102	22.92961	MAP2K1;IL6;CDK5;LRRK2;PSEN2;PRKCA;MAPK14;CDK5R1
Regulation of lipolysis in adipocytes	Mar-55	0.002417	0.004465	12.18351	73.40882	LIPE;PIK3CD;PIK3CB
Transcriptional misregulation in cancer	5/192	0.002444	0.004477	5.730063	34.46106	CDK9;IL6;MDM2;PPARG;MPO
Herpes simplex virus 1 infection	8/498	0.002913	0.005291	3.561202	20.79284	IL6;SYK;PIK3CD;PIK3CB;TYK2;IRAK4;JAK2;JAK1
MAPK signaling pathway	6/294	0.003098	0.005536	4.490614	25.94259	MAP2K1;PAK1;RPS6KA5;PRKCA;IRAK4;MAPK14
Long-term depression	Mar-60	0.003098	0.005536	11.11198	64.19402	PPP2CA;MAP2K1;PRKCA
Lysosome	4/128	0.003505	0.006213	6.860562	38.78607	ASAH1;CTSL;CTSK;CTSS
Dopaminergic synapse	4/132	0.003912	0.006878	6.644825	36.83643	PPP2CA;PRKCA;MAPK14;DRD3
Estrogen signaling pathway	4/137	0.004465	0.007786	6.393403	34.59828	MAP2K1;PIK3CD;PGR;PIK3CB

Central carbon metabolism in cancer	Mar-70	0.004786	0.00828	9.448714	50.47596	MAP2K1;PIK3CD;PIK3CB
PPAR signaling pathway	Mar-74	0.005589	0.009594	8.914594	46.23952	FABP1;MMP1;PPARG
Retrograde endocannabinoid signaling	4/148	0.00586	0.00998	5.901732	30.33266	GABRB3;GABRA2;PRKCA;MAPK14
Pertussis	Mar-76	0.006019	0.010172	8.669484	44.32543	IL6;IRAK4;MAPK14
Adrenergic signaling in cardiomyocytes	4/150	0.006141	0.010299	5.820298	29.64102	PPP2CA;RPS6KA5;PRKCA;MAPK14
alpha-Linolenic acid metabolism	25-Feb	0.006495	0.010808	18.1968	91.65293	PLA2G1B;PLA2G2A
mTOR signaling pathway	4/154	0.006731	0.011117	5.663943	28.32542	MAP2K1;PIK3CD;PRKCA;PIK3CB
Hippo signaling pathway	4/163	0.008193	0.013428	5.340908	25.66054	PPP2CA;PAK1;CCND1;PRKCZ
Linoleic acid metabolism	Feb-29	0.00868	0.014121	15.49786	73.56468	PLA2G1B;PLA2G2A
cGMP-PKG signaling pathway	4/167	0.008904	0.014378	5.208787	24.59207	MAP2K1;ROCK1;ROCK2;PDE3A
Gap junction	Mar-88	0.009012	0.014446	7.441051	35.04141	MAP2K1;CDK1;PRKCA
GnRH signaling pathway	Mar-93	0.010474	0.016666	7.025887	32.03022	MAP2K1;PRKCA;MAPK14
IL-17 signaling pathway	Mar-94	0.010782	0.017032	6.948328	31.47535	IL6;MMP1;MAPK14
Phosphatidylinositol signaling system	Mar-97	0.011736	0.018407	6.725555	29.89548	PIK3CD;PRKCA;PIK3CB
Viral protein interaction with cytokine and cytokine receptor	3/100	0.012739	0.019836	6.516561	28.43255	CCR1;IL6;CXCR1
Starch and sucrose metabolism	Feb-36	0.013176	0.020371	12.30279	53.26316	GYS1;PYGL
Longevity regulating pathway	3/102	0.013433	0.020623	6.384268	27.51643	PIK3CD;PPARG;PIK3CB
African trypanosomiasis	Feb-37	0.013885	0.021168	11.95068	51.11209	IL6;PRKCA
NF-kappa B signaling pathway	3/104	0.014149	0.02142	6.257215	26.64401	PARP1;SYK;IRAK4
Nicotine addiction	Feb-40	0.01611	0.024221	11.00554	45.43424	GABRB3;GABRA2
Serotonergic synapse	3/113	0.017635	0.026331	5.74265	23.18819	GABRB3;MAP2K1;PRKCA

Carbohydrate digestion and absorption	Feb-47	0.021844	0.032395	9.290292	35.52447	PIK3CD;PIK3CB
Cocaine addiction	Feb-49	0.023616	0.034552	8.894065	33.31568	CDK5;CDK5R1
Ether lipid metabolism	Feb-49	0.023616	0.034552	8.894065	33.31568	PLA2G1B;PLA2G2A
Malaria	Feb-50	0.024523	0.035641	8.708333	32.29161	IL6;ITGAL
Apelin signaling pathway	3/137	0.029072	0.041971	4.708399	16.65828	LIPE;MAP2K1;CCND1
Spinocerebellar ataxia	3/143	0.032418	0.046494	4.505243	15.4487	PIK3CD;PRKCA;PIK3CB
Notch signaling pathway	Feb-59	0.033307	0.047457	7.330009	24.93662	ADAM17;PSEN2
Viral myocarditis	Feb-60	0.034349	0.048623	7.203267	24.28361	CCND1;ITGAL
Arachidonic acid metabolism	Feb-61	0.035403	0.049473	7.080821	23.65675	PLA2G1B;PLA2G2A
Steroid hormone biosynthesis	Feb-61	0.035403	0.049473	7.080821	23.65675	HSD11B1;CYP19A1
Phagosome	3/152	0.037798	0.052484	4.231187	13.85923	CTSL;MPO;CTSS
Long-term potentiation	Feb-67	0.041985	0.057929	6.425263	20.37086	MAP2K1;PRKCA
Prion disease	4/273	0.043931	0.060232	3.139305	9.810761	IL6;PIK3CD;PIK3CB;MAPK14
Wnt signaling pathway	3/166	0.047015	0.064058	3.865031	11.81651	CCND1;ROCK2;PRKCA
Inositol phosphate metabolism	Feb-73	0.048987	0.06633	5.880504	17.73683	PIK3CD;PIK3CB
Gastric acid secretion	Feb-76	0.052635	0.07083	5.641252	16.60996	CA2;PRKCA
Bacterial invasion of epithelial cells	Feb-77	0.053872	0.07205	5.565754	16.25836	PIK3CD;PIK3CB
Antigen processing and presentation	Feb-78	0.05512	0.073269	5.492244	15.9179	CTSL;CTSS
Non-homologous end-joining	13-Jan	0.061265	0.080944	17.26649	48.21747	PRKDC
Taste transduction	Feb-86	0.065455	0.085959	4.967168	13.54244	GABRA2;TAS2R31
Bile secretion	Feb-90	0.070848	0.092484	4.740431	12.54899	CA2;HMGCR

TGF-beta signaling pathway	Feb-94	0.07638	0.099112	4.53341	11.66011	PPP2CA;ROCK1
Circadian entrainment	Feb-97	0.080616	0.10399	4.389584	11.05323	RPS6KA5;PRKCA
Aldosterone synthesis and secretion	Feb-98	0.082044	0.104594	4.34364	10.86127	LIPE;PRKCA
Glycerophospholipid metabolism	Feb-98	0.082044	0.104594	4.34364	10.86127	PLA2G1B;PLA2G2A
Melanogenesis	2/101	0.086375	0.109475	4.211377	10.3139	MAP2K1;PRKCA
Glucagon signaling pathway	2/107	0.095237	0.12001	3.969524	9.333878	GYS1;PYGL
Arginine biosynthesis	22-Jan	0.101488	0.126425	9.862103	22.56263	GLUL
Terpenoid backbone biosynthesis	22-Jan	0.101488	0.126425	9.862103	22.56263	HMGCR
Thermogenesis	3/232	0.103213	0.127843	2.741894	6.226734	LIPE;PPARG;MAPK14
Proximal tubule bicarbonate reclamation	23-Jan	0.105851	0.129684	9.413352	21.13979	CA2
Glutamatergic synapse	2/114	0.105889	0.129684	3.720113	8.353017	PRKCA;GLUL
Collecting duct acid secretion	27-Jan	0.123093	0.149912	7.963542	16.68218	CA2
Endocytosis	3/252	0.123846	0.149992	2.519098	5.261675	CXCR1;MDM2;PRKCZ
Glyoxylate and dicarboxylate metabolism	30-Jan	0.135807	0.163569	7.138649	14.25244	GLUL
Base excision repair	Jan-33	0.14834	0.177682	6.468424	12.34337	PARP1
DNA replication	Jan-36	0.160692	0.191426	5.913095	10.81069	POLA1
Alanine, aspartate and glutamate metabolism	Jan-37	0.16477	0.195217	5.748553	10.36581	GLUL
Primary immunodeficiency	Jan-38	0.168829	0.198944	5.592905	9.949054	JAK3
Cytokine-cytokine receptor interaction	3/295	0.172586	0.202279	2.143435	3.765709	CCR1;IL6;CXCR1
Graft-versus-host disease	Jan-42	0.184868	0.215515	5.04624	8.518625	IL6
Intestinal immune network for IgA production	Jan-48	0.208354	0.241602	4.400709	6.902583	IL6

Sphingolipid metabolism	Jan-49	0.212203	0.244763	4.308811	6.679573	ASAH1
Vibrio cholerae infection	Jan-50	0.216033	0.247869	4.220663	6.467423	PRKCA
Ovarian steroidogenesis	Jan-51	0.219845	0.250922	4.136042	6.265414	CYP19A1
Endocrine and other factor-regulated calcium reabsorption	Jan-53	0.227413	0.258209	3.976563	5.889233	PRKCA
Hedgehog signaling pathway	Jan-56	0.23863	0.268151	3.759091	5.386176	CCND1
Pyrimidine metabolism	Jan-56	0.23863	0.268151	3.759091	5.386176	TK1
Legionellosis	Jan-57	0.242333	0.270916	3.691778	5.23288	IL6
Cytosolic DNA-sensing pathway	Jan-63	0.26418	0.293833	3.333501	4.437307	IL6
Inflammatory bowel disease	Jan-65	0.271323	0.300245	3.229004	4.212063	IL6
Adipocytokine signaling pathway	Jan-69	0.285403	0.311089	3.03845	3.80977	JAK2
Amphetamine addiction	Jan-69	0.285403	0.311089	3.03845	3.80977	PRKCA
Renin secretion	Jan-69	0.285403	0.311089	3.03845	3.80977	PDE3A
RIG-I-like receptor signaling pathway	Jan-70	0.288881	0.313313	2.994263	3.718101	MAPK14
Adherens junction	Jan-71	0.292342	0.315498	2.951339	3.629651	PTPN1
Thyroid hormone synthesis	Jan-75	0.30602	0.328632	2.791244	3.305126	PRKCA
Metabolism of xenobiotics by cytochrome P450	Jan-76	0.309398	0.330632	2.753889	3.230657	HSD11B1
Calcium signaling pathway	2/240	0.324815	0.345413	1.739496	1.956062	P2RX7;PRKCA
Insulin secretion	Jan-86	0.3423	0.36224	2.428676	2.603702	PRKCA
Hypertrophic cardiomyopathy	Jan-90	0.355023	0.373889	2.319054	2.401552	IL6
Salivary secretion	Jan-93	0.364404	0.381923	2.243093	2.264385	PRKCA
Staphylococcus aureus infection	Jan-95	0.370583	0.386541	2.195146	2.179072	ITGAL
mRNA surveillance pathway	Jan-98	0.379741	0.394207	2.126933	2.059439	PPP2CA

Hematopoietic cell lineage	Jan-99	0.382764	0.395462	2.105123	2.021629	IL6
Oxidative phosphorylation	1/133	0.47731	0.490819	1.560211	1.153916	ATP12A
Ubiquitin mediated proteolysis	1/140	0.494917	0.506535	1.481115	1.041765	MDM2
Cell adhesion molecules	1/148	0.514322	0.523935	1.399943	0.930831	ITGAL
Alcoholism	1/186	0.596876	0.605205	1.110248	0.572939	MAP2K1
Parkinson disease	1/249	0.70423	0.71075	0.825563	0.289484	LRRK2
Huntington disease	1/306	0.77669	0.780269	0.669331	0.169149	PPARG
Amyotrophic lateral sclerosis	1/364	0.832368	0.832368	0.560721	0.102881	MAPK14

Table A4.2: Pathway analysis for Targeted protein for Tunicamycin C

Swiss target prediction

Target	Common name	Uniprot ID	ChEMBL ID	Target Class	Known actives (3D/2D)
Cytidine deaminase	CDA	P32320	CHEMBL4502	Enzyme	0 / 2┬á┬á┬á┬á┬á
Protein kinase C alpha	PRKCA	P17252	CHEMBL299	Kinase	2 / 0┬á┬á┬á┬á┬á
Programmed cell death protein 4	PDCD4	Q53EL6	CHEMBL1781868	Unclassified protein	3 / 0┬á┬á┬á┬á┬á
Protein farnesyltransferase	FNTA FNTB	P49354 P49356	CHEMBL2094108	Enzyme	2 / 0┬á┬á┬á┬á┬á
Muscle glycogen phosphorylase	PYGM	P11217	CHEMBL3526	Enzyme	0 / 3┬á┬á┬á┬á┬á
Thymidine kinase, mitochondrial	TK2	O00142	CHEMBL4580	Enzyme	0 / 8┬á┬á┬á┬á┬á
Purinergic receptor P2Y12	P2RY12	Q9H244	CHEMBL2001	Family A G protein-coupled receptor	4 / 0┬á┬á┬á┬á┬á
Adenosine A1 receptor (by homology)	ADORA1	P30542	CHEMBL226	Family A G protein-coupled receptor	0 / 86┬á┬á┬á┬á┬á
Thymidine phosphorylase	TYMP	P19971	CHEMBL3106	Enzyme	0 / 6┬á┬á┬á┬á┬á
Apoptosis regulator Bcl-X	BCL2L1	Q07817	CHEMBL4625	Other ion channel	1 / 0┬á┬á┬á┬á┬á
Apoptosis regulator Bcl-2	BCL2	P10415	CHEMBL4860	Other ion channel	1 / 0┬á┬á┬á┬á┬á
Histamine H3 receptor	HRH3	Q9Y5N1	CHEMBL264	Family A G protein-coupled receptor	1 / 0┬á┬á┬á┬á┬á
Thymidine kinase, cytosolic	TK1	P04183	CHEMBL2883	Transferase	0 / 13┬á┬á┬á┬á┬á

Phospholipase A2 group IIA	PLA2G2A	P14555	CHEMBL3474	Enzyme	1 / 0┬á┬á┬á┬á┬á
Phospholipase A2 group V	PLA2G5	P39877	CHEMBL4323	Enzyme	1 / 0┬á┬á┬á┬á┬á
Group X secretory phospholipase A2	PLA2G10	O15496	CHEMBL4342	Enzyme	1 / 0┬á┬á┬á┬á┬á
Tyrosine-protein kinase receptor FLT3	FLT3	P36888	CHEMBL1974	Kinase	2 / 0┬á┬á┬á┬á┬á
Serine/threonine-protein kinase Aurora-B	AURKB	Q96GD4	CHEMBL2185	Kinase	2 / 0┬á┬á┬á┬á┬á
Ileal bile acid transporter	SLC10A2	Q12908	CHEMBL2778	Electrochemical transporter	4 / 0┬á┬á┬á┬á┬á
Matrix metalloproteinase 13	MMP13	P45452	CHEMBL280	Protease	2 / 0┬á┬á┬á┬á┬á
Matrix metalloproteinase 9	MMP9	P14780	CHEMBL321	Protease	2 / 0┬á┬á┬á┬á┬á
Matrix metalloproteinase 2	MMP2	P08253	CHEMBL333	Protease	2 / 0┬á┬á┬á┬á┬á
Matrix metalloproteinase 8	MMP8	P22894	CHEMBL4588	Protease	2 / 0┬á┬á┬á┬á┬á
Protein kinase C delta	PRKCD	Q05655	CHEMBL2996	Kinase	1 / 0┬á┬á┬á┬á┬á
Squalene synthetase	FDFT1	P37268	CHEMBL3338	Enzyme	3 / 0┬á┬á┬á┬á┬á
Heat shock protein HSP 90-alpha	HSP90AA1	P07900	CHEMBL3880	Other cytosolic protein	1 / 0┬á┬á┬á┬á┬á
Adenosine deaminase (by homology)	ADA	P00813	CHEMBL1910	Hydrolase	0 / 2┬á┬á┬á┬á┬á
Renin	REN	P00797	CHEMBL286	Protease	4 / 0┬á┬á┬á┬á┬á
Leukocyte common antigen	PTPRC	P08575	CHEMBL3243	Enzyme	1 / 0┬á┬á┬á┬á┬á
P-selectin	SELP	P16109	CHEMBL5378	Adhesion	1 / 0┬á┬á┬á┬á┬á
Isoleucyl-tRNA synthetase	IARS	P41252	CHEMBL3235	Enzyme	1 / 0┬á┬á┬á┬á┬á
Methionine aminopeptidase 1	METAP1	P53582	CHEMBL2474	Protease	1 / 0┬á┬á┬á┬á┬á
Cysteinyl leukotriene receptor 2	CYSLTR2	Q9NS75	CHEMBL4330	Family A G protein-coupled receptor	1 / 0┬á┬á┬á┬á┬á
Cyclin-dependent kinase 2/cyclin E	CCNE2 CDK2 CCNE1	O96020 P24941 P24864	CHEMBL2094126	Other cytosolic protein	1 / 0┬á┬á┬á┬á┬á
Protein kinase C epsilon	PRKCE	Q02156	CHEMBL3582	Kinase	1 / 0┬á┬á┬á┬á┬á
Thymidylate synthase (by homology)	TYMS	P04818	CHEMBL1952	Transferase	0 / 7┬á┬á┬á┬á┬á
Maltase-glucoamylase	MGAM	O43451	CHEMBL2074	Hydrolase	0 / 2┬á┬á┬á┬á┬á
Sucrase-isomaltase	SI	P14410	CHEMBL2748	Enzyme	0 / 2┬á┬á┬á┬á┬á
Pancreatic alpha-amylase	AMY2A	P04746	CHEMBL2045	Hydrolase	0 / 4┬á┬á┬á┬á┬á
AMY1C	AMY1A	P04745	CHEMBL2478	Enzyme	0 / 3┬á┬á┬á┬á┬á
Lysosomal alpha-glucosidase	GAA	P10253	CHEMBL2608	Hydrolase	0 / 1┬á┬á┬á┬á┬á
Beta-galactoside alpha-2,6-sialyltransferase 1	ST6GAL1	P15907	CHEMBL3596075	Transferase	0 / 5┬á┬á┬á┬á┬á

Histone-lysine N-methyltransferase SETD2	SETD2	Q9BYW2	CHEMBL3108647	Writer	0 / 1┬á┬á┬á┬á┬á
Histone-arginine methyltransferase CARM1	CARM1	Q86X55	CHEMBL5406	Writer	0 / 1┬á┬á┬á┬á┬á
Histone-lysine N-methyltransferase SETD7	SETD7	Q8WTS6	CHEMBL5523	Writer	0 / 2┬á┬á┬á┬á┬á
Protein-arginine N-methyltransferase 1	PRMT1	Q99873	CHEMBL5524	Writer	0 / 5┬á┬á┬á┬á┬á
Myelin-associated glycoprotein	MAG	P20916	CHEMBL5807	Unclassified protein	0 / 17┬á┬á┬á┬á┬á
cAMP-dependent protein kinase alpha-catalytic subunit	PRKACA	P17612	CHEMBL4101	Kinase	0 / 16┬á┬á┬á┬á┬á
Rho-associated protein kinase 2	ROCK2	O75116	CHEMBL2973	Kinase	0 / 4┬á┬á┬á┬á┬á
Beta-1,4-galactosyltransferase 1	B4GALT1	P15291	CHEMBL4384	Enzyme	0 / 2┬á┬á┬á┬á┬á
Histone-lysine N-methyltransferase, H3 lysine-79 specific	DOT1L	Q8TEK3	CHEMBL1795117	Writer	0 / 3┬á┬á┬á┬á┬á
Adenosylhomocysteinase	AHCY	P23526	CHEMBL2664	Enzyme	0 / 3┬á┬á┬á┬á┬á
Spermidine synthase	SRM	P19623	CHEMBL4232	Enzyme	0 / 1┬á┬á┬á┬á┬á
Pyrimidinergic receptor P2Y6	P2RY6	Q15077	CHEMBL4714	Family A G protein-coupled receptor	0 / 3┬á┬á┬á┬á┬á
UDP-N-acetylglucosamine--peptide N-acetylglucosaminyltransferase 110 kDa subunit	OGT	O15294	CHEMBL5955	Enzyme	0 / 2┬á┬á┬á┬á┬á
Adenosine A2b receptor	ADORA2B	P29275	CHEMBL255	Family A G protein-coupled receptor	0 / 2┬á┬á┬á┬á┬á
Glyceraldehyde-3-phosphate dehydrogenase liver	GAPDH	P04406	CHEMBL2284	Oxidoreductase	0 / 3┬á┬á┬á┬á┬á
S-adenosylmethionine decarboxylase 1	AMD1	P17707	CHEMBL4181	Enzyme	0 / 11┬á┬á┬á┬á┬á
Ectonucleoside triphosphate diphosphohydrolase 2	ENTPD2	Q9Y5L3	CHEMBL5049	Enzyme	0 / 1┬á┬á┬á┬á┬á
Protein-tyrosine phosphatase 1B	PTPN1	P18031	CHEMBL335	Phosphatase	0 / 2┬á┬á┬á┬á┬á
T-cell protein-tyrosine phosphatase	PTPN2	P17706	CHEMBL3807	Phosphatase	0 / 1┬á┬á┬á┬á┬á
Somatostatin receptor 5	SSTR5	P35346	CHEMBL1792	Family A G protein-coupled receptor	0 / 6┬á┬á┬á┬á┬á
Somatostatin receptor 2	SSTR2	P30874	CHEMBL1804	Family A G protein-coupled receptor	0 / 4┬á┬á┬á┬á┬á
Somatostatin receptor 4	SSTR4	P31391	CHEMBL1853	Family A G protein-coupled receptor	0 / 2┬á┬á┬á┬á┬á
Somatostatin receptor 1	SSTR1	P30872	CHEMBL1917	Family A G protein-coupled receptor	0 / 2┬á┬á┬á┬á┬á
Somatostatin receptor 3	SSTR3	P32745	CHEMBL2028	Family A G protein-coupled receptor	0 / 6┬á┬á┬á┬á┬á
Pyrimidinergic receptor P2Y4	P2RY4	P51582	CHEMBL2123	Family A G protein-coupled receptor	0 / 1┬á┬á┬á┬á┬á
Purinergic receptor P2Y2	P2RY2	P41231	CHEMBL4398	Family A G protein-coupled receptor	0 / 1┬á┬á┬á┬á┬á
Serine/threonine-protein kinase AKT	AKT3	Q9Y243	CHEMBL4816	Kinase	0 / 3┬á┬á┬á┬á┬á
5'(3')-deoxyribonucleotidase, mitochondrial	NT5M	Q9NPB1	CHEMBL3751654	Enzyme	0 / 1┬á┬á┬á┬á┬á

P47929	LGALS7	P47929	CHEMBL5008	Other cytosolic protein	0 / 1┬á┬á┬á┬á┬á
Protein kinase C beta	PRKCB	P05771	CHEMBL3045	Kinase	0 / 1┬á┬á┬á┬á┬á
Eukaryotic translation initation factor (by homology)	EIF4E	P06730	CHEMBL4848	Other nuclear protein	0 / 6┬á┬á┬á┬á┬á
Hypoxanthine-guanine phosphoribosyltransferase	HPRT1	P00492	CHEMBL2360	Enzyme	0 / 1┬á┬á┬á┬á┬á
Vascular endothelial growth factor A	VEGFA	P15692	CHEMBL1783	Secreted protein	0 / 1┬á┬á┬á┬á┬á
Acidic fibroblast growth factor	FGF1	P05230	CHEMBL2120	Secreted protein	0 / 1┬á┬á┬á┬á┬á
Basic fibroblast growth factor	FGF2	P09038	CHEMBL3107	Secreted protein	0 / 1┬á┬á┬á┬á┬á
Heparanase	HPSE	Q9Y251	CHEMBL3921	Enzyme	0 / 1┬á┬á┬á┬á┬á
Uridine 5'-monophosphate synthase	UMPS	P11172	CHEMBL5216	Enzyme	0 / 2┬á┬á┬á┬á┬á
Histone-lysine N-methyltransferase, H3 lysine-9 specific 5	EHMT1	Q9H9B1	CHEMBL6031	Writer	0 / 1┬á┬á┬á┬á┬á
Histone-lysine N-methyltransferase, H3 lysine-9 specific 3	EHMT2	Q96KQ7	CHEMBL6032	Writer	0 / 1┬á┬á┬á┬á┬á
DNA polymerase alpha subunit	POLA1	P09884	CHEMBL1828	Transferase	0 / 1┬á┬á┬á┬á┬á
Hexokinase type II	HK2	P52789	CHEMBL2640	Enzyme	0 / 1┬á┬á┬á┬á┬á
Hexokinase type I	HK1	P19367	CHEMBL2688	Enzyme	0 / 1┬á┬á┬á┬á┬á
Non-secretory ribonuclease	RNASE2	P10153	CHEMBL5120	Enzyme	0 / 1┬á┬á┬á┬á┬á
Ribonuclease pancreatic	RNASE1	P07998	CHEMBL5425	Enzyme	0 / 1┬á┬á┬á┬á┬á
Purinergic receptor P2Y14	P2RY14	Q15391	CHEMBL4518	Family A G protein-coupled receptor	0 / 1┬á┬á┬á┬á┬á
Retinoic acid receptor gamma	RARG	P13631	CHEMBL2003	Nuclear receptor	0 / 1┬á┬á┬á┬á┬á
Melanin-concentrating hormone receptor 1	MCHR1	Q99705	CHEMBL344	Family A G protein-coupled receptor	0 / 2┬á┬á┬á┬á┬á
Transmembrane domain-containing protein TMIGD3	TMIGD3	P0DMS9	CHEMBL3712907	Unclassified protein	0 / 1┬á┬á┬á┬á┬á
Adenosine A3 receptor	ADORA3	P0DMS8	CHEMBL256	Family A G protein-coupled receptor	1 / 30┬á┬á┬á┬á┬á
Adenosine A2a receptor	ADORA2A	P29274	CHEMBL251	Family A G protein-coupled receptor	1 / 50┬á┬á┬á┬á┬á
Galectin-3	LGALS3	P17931	CHEMBL4531	Other cytosolic protein	1 / 8┬á┬á┬á┬á┬á
Galectin-4	LGALS4	P56470	CHEMBL1671608	Other cytosolic protein	1 / 1┬á┬á┬á┬á┬á
Galectin-8	LGALS8	O00214	CHEMBL5475	Other cytosolic protein	1 / 1┬á┬á┬á┬á┬á
Glucocorticoid receptor	NR3C1	P04150	CHEMBL2034	Nuclear receptor	1 / 2┬á┬á┬á┬á┬á

Wiki-pathways

Term	Overlap	P-value	Adjusted P-value	Odds Ratio	Combined Score	Genes
GPCRs, Class A Rhodopsin-like WP455	17/257	5.26E-15	1.48E-12	17.63122	579.6787	P2RY12;P2RY14;SSTR1;SSTR2;SSTR3;MCHR1;SSTR4;SSTR5;P2RY6;CYSLTR2;ADORA2A;HRH3;P2RY4;ADORA2B;ADORA3;P2RY2;ADORA1
Nucleotide GPCRs WP80	11-Jul	1.53E-14	2.14E-12	391.2921	12448.48	P2RY6;P2RY4;ADORA2A;ADORA2B;P2RY2;ADORA3;ADORA1
Purinergic signaling WP4900	Sep-33	3.23E-14	3.03E-12	85.68966	2661.845	P2RY12;P2RY6;P2RY4;ADORA2A;ADORA2B;P2RY2;ADORA3;P2RY14;ADORA1
EGFR Tyrosine Kinase Inhibitor Resistance WP4806	Aug-84	6.77E-09	4.18E-07	23.7177	446.157	PRKCB;AKT3;BCL2;PRKCA;FGF2;EIF4E;VEGFA;BCL2L1
Pyrimidine metabolism WP4022	Aug-85	7.44E-09	4.18E-07	23.4085	438.1184	CDA;POLA1;TK2;NT5M;TK1;UMPS;TYMS;TYMP
VEGFA-VEGFR2 Signaling Pathway WP3888	14/432	1.86E-08	8.72E-07	7.959038	141.6612	PTPN1;HSP90AA1;PRKCB;ROCK2;MMP2;PRKCE;PRKCD;PRKCA;PLA2G5;VEGFA;BCL2;GAPDH;EIF4E;BCL2L1
AGE/RAGE pathway WP2324	Jul-66	2.91E-08	1.17E-06	26.45496	459.0945	LGALS3;MMP13;PRKCB;MMP2;PRKCD;PRKCA;MMP9
Translation inhibitors in chronically activated PDGFRA cells WP4566	Jun-46	8.38E-08	2.94E-06	33.10667	539.4853	AKT3;PRKCD;PDCD4;PRKCA;PRKACA;EIF4E
Spinal Cord Injury WP2431	8/118	9.94E-08	3.10E-06	16.35868	263.7694	SELP;LGALS3;MAG;ROCK2;PLA2G2A;PRKCA;PLA2G5;MMP9
Ras signaling WP4223	9/184	2.53E-07	7.11E-06	11.66246	177.1565	FLT3;PRKCB;AKT3;PLA2G10;PLA2G2A;PRKCA;PLA2G5;PRKACA;BCL2L1
Fluoropyrimidine Activity WP1601	May-33	4.89E-07	1.25E-05	39.00314	566.7234	CDA;TK1;TYMS;UMPS;TYMP
Biomarkers for pyrimidine metabolism disorders WP4584	15-Apr	6.53E-07	1.39E-05	78.62846	1119.768	TK2;TYMS;UMPS;TYMP
Oncostatin M Signaling Pathway WP2374	Jun-65	6.86E-07	1.39E-05	22.42373	318.2336	MMP13;PRKCB;PRKCE;PRKCD;PRKCA;VEGFA
PI3K-Akt signaling pathway WP4172	11/340	7.09E-07	1.39E-05	7.699803	109.0197	HSP90AA1;CCNE2;FLT3;AKT3;BCL2;PRKCA;FGF1;FGF2;EIF4E;VEGFA;BCL2L1
IL-18 signaling pathway WP4754	10/272	7.40E-07	1.39E-05	8.71738	123.0567	MMP13;PRKCB;MMP2;PRKCD;BCL2;PRKCA;MMP8;MMP9;VEGFA;BCL2L1
Pyrimidine metabolism and related diseases WP4225	17-Apr	1.13E-06	1.92E-05	66.52508	910.9061	TK2;TYMS;UMPS;TYMP
Kisspeptin/kisspeptin receptor system in the ovary WP4871	May-39	1.16E-06	1.92E-05	32.11054	438.846	PRKCB;PRKCE;PRKCD;PRKCA;MMP9
Pathways Regulating Hippo Signaling WP4540	Jun-98	7.70E-06	1.20E-04	14.35652	169.0329	FLT3;PRKCB;PRKCE;PRKCD;PRKCA;PRKACA
Cell migration and invasion through p75NTR WP4561	30-Apr	1.24E-05	1.71E-04	33.2408	375.5164	MMP2;AKT3;MMP8;MMP9
Matrix Metalloproteinases WP129	30-Apr	1.24E-05	1.71E-04	33.2408	375.5164	MMP13;MMP2;MMP8;MMP9
Lung fibrosis WP3624	May-63	1.29E-05	1.71E-04	18.80068	211.6115	CYSLTR2;MMP2;FGF1;FGF2;MMP9
Endochondral Ossification with Skeletal Dysplasias WP4808	May-64	1.40E-05	1.71E-04	18.4811	206.5809	MMP13;PRKACA;FGF2;MMP9;VEGFA

Endochondral Ossification WP474	May-64	1.40E-05	1.71E-04	18.4811	206.5809	MMP13;PRKACA;FGF2;MMP9;VEGFA
Mammary gland development pathway - Pregnancy and lactation (Stage 3 of 4) WP2817	Apr-32	1.62E-05	1.89E-04	30.86335	340.5006	PTPN1;NR3C1;EIF4E;BCL2L1
Histone Modifications WP2369	May-67	1.75E-05	1.97E-04	17.58419	192.5984	SETD2;EHMT2;SETD7;DOT1L;EHMT1
Gastrin signaling pathway WP4659	6/114	1.83E-05	1.98E-04	12.21975	133.2673	PRKCE;PRKCD;PRKCA;PRKACA;VEGFA;BCL2L1
Osteoblast differentiation WP4787	6/118	2.23E-05	2.32E-04	11.78095	126.1712	PRKCB;PRKCE;PRKCD;PRKCA;FGF1;FGF2
Peptide GPCRs WP24	May-74	2.84E-05	2.85E-04	15.79471	165.3357	SSTR1;SSTR2;SSTR3;SSTR4;SSTR5
Sleep regulation WP3591	Apr-38	3.25E-05	3.15E-04	25.40921	262.6145	AHCY;ADORA2A;ADORA1;ADA
Bladder cancer WP2828	Apr-40	3.99E-05	3.62E-04	23.99517	243.0513	MMP2;MMP9;TYMP;VEGFA
Neural Crest Cell Migration during Development WP4564	Apr-40	3.99E-05	3.62E-04	23.99517	243.0513	MMP2;AKT3;MMP8;MMP9
Circadian rhythm related genes WP3594	7/201	5.22E-05	4.54E-04	7.990849	78.79029	AHCY;ADORA2A;ROCK2;ADORA1;TYMS;OGT;ADA
Neural Crest Cell Migration in Cancer WP4565	Apr-43	5.33E-05	4.54E-04	22.14604	217.9129	MMP2;AKT3;MMP8;MMP9
Pathways in clear cell renal cell carcinoma WP4018	May-85	5.55E-05	4.59E-04	13.61538	133.407	SETD2;GAPDH;HK2;HK1;VEGFA
Corticotropin-releasing hormone signaling pathway WP2355	May-93	8.54E-05	6.67E-04	12.37263	115.9099	HSP90AA1;PRKCB;PRKCD;BCL2;PRKCA
G Protein Signaling Pathways WP35	May-93	8.54E-05	6.67E-04	12.37263	115.9099	PRKCB;PRKCE;PRKCD;PRKCA;PRKACA
Photodynamic therapy-induced AP-1 survival signaling. WP3611	Apr-50	9.69E-05	7.26E-04	18.76938	173.4595	HSP90AA1;MMP2;BCL2;BCL2L1
Nucleotide metabolism WP404	19-Mar	9.82E-05	7.26E-04	40.09677	370.0288	POLA1;HPRT1;SRM
Sudden Infant Death Syndrome (SIDS) Susceptibility Pathways WP706	6/158	1.14E-04	8.09E-04	8.663158	78.65259	SSTR1;NR3C1;PRKACA;SSTR2;GAPDH;VEGFA
Hematopoietic Stem Cell Gene Regulation by GABP alpha/beta Complex WP3657	20-Mar	1.15E-04	8.09E-04	37.73624	342.2435	FLT3;BCL2;BCL2L1
Interferon type I signaling pathways WP585	Apr-54	1.31E-04	8.99E-04	17.26435	154.3284	PTPRC;PRMT1;PDCD4;EIF4E
Methionine De Novo and Salvage Pathway WP3580	22-Mar	1.54E-04	0.001033	33.76061	296.2684	AHCY;AMD1;SRM
Angiogenesis WP1539	24-Mar	2.02E-04	0.001317	30.54224	259.891	MMP9;FGF2;VEGFA
Non-genomic actions of 1,25 dihydroxyvitamin D3 WP4341	Apr-71	3.79E-04	0.002412	12.87281	101.4242	PRKCB;PRKCE;PRKCD;PRKCA
Focal Adhesion WP306	6/198	3.86E-04	0.002412	6.844444	53.78924	PRKCB;ROCK2;AKT3;BCL2;PRKCA;VEGFA
Ethanol effects on histone modifications WP3996	31-Mar	4.37E-04	0.002669	22.89862	177.1363	AHCY;EHMT2;TYMS
Leptin signaling pathway WP2034	Apr-76	4.91E-04	0.002935	11.97585	91.24728	PTPN1;ROCK2;EIF4E;BCL2L1
Photodynamic therapy-induced NF-kB survival signaling WP3617	Mar-35	6.27E-04	0.003673	20.03226	147.7146	MMP2;MMP9;VEGFA

Glioblastoma signaling pathways WP2261	Apr-82	6.55E-04	0.003755	11.05128	81.02035	PRKCB;AKT3;PRKCD;PRKCA
MicroRNAs in cardiomyocyte hypertrophy WP1544	Apr-84	7.17E-04	0.00403	10.77391	78.00777	PRKCB;ROCK2;PLA2G2A;FGF2
Photodynamic therapy-induced HIF-1 survival signaling WP3614	Mar-37	7.40E-04	0.004076	18.85199	135.908	HK1;VEGFA;BCL2L1
Calcium Regulation in the Cardiac Cell WP536	5/150	7.84E-04	0.004238	7.487306	53.54073	PRKCB;PRKCE;PRKCD;PRKCA;PRKACA
Hepatitis B infection WP4666	5/152	8.32E-04	0.004413	7.38469	52.36679	PRKCB;AKT3;BCL2;PRKCA;MMP9
Pancreatic adenocarcinoma pathway WP4263	Apr-89	8.91E-04	0.004636	10.1376	71.19922	AKT3;PRKCD;VEGFA;BCL2L1
Glycogen Synthesis and Degradation WP500	Mar-40	9.31E-04	0.004693	17.32084	120.8886	PYGM;HK2;HK1
Myometrial relaxation and contraction pathways WP289	5/156	9.35E-04	0.004693	7.187614	50.13143	PRKCB;PRKCE;PRKCD;PRKCA;PRKACA
Insulin Signaling WP481	5/160	0.001047	0.005163	7.000709	48.03537	PTPN1;PRKCB;PRKCD;PRKCA;EIF4E
Common Pathways Underlying Drug Addiction WP2636	Mar-42	0.001074	0.005204	16.43093	112.3254	PRKCB;PRKCA;PRKACA
Small cell lung cancer WP4658	Apr-96	0.001182	0.005616	9.362949	63.11502	CCNE2;AKT3;BCL2;BCL2L1
MAPK Signaling Pathway WP382	6/246	0.0012	0.005616	5.462222	36.73415	AKT3;PRKCD;PRKCA;FGF1;PRKACA;FGF2
Glycolysis in senescence WP5049	11-Feb	0.001219	0.005616	47.0331	315.5731	GAPDH;HK1
Glycolysis and Gluconeogenesis WP534	Mar-45	0.001314	0.005955	15.25499	101.212	GAPDH;HK2;HK1
Regulation of Microtubule Cytoskeleton WP2038	Mar-46	0.001401	0.006248	14.89947	97.90008	PRKCA;PRKACA;AURKB
Computational Model of Aerobic Glycolysis WP4629	12-Feb	0.001458	0.006393	42.32766	276.4166	GAPDH;HK1
Wnt signaling pathway and pluripotency WP399	4/102	0.001479	0.006393	8.787045	57.26116	PRKCB;PRKCE;PRKCD;PRKCA
Differentiation Pathway WP2848	Mar-48	0.001585	0.006748	14.23584	91.78044	FGF1;FGF2;VEGFA
IL-3 signaling pathway WP286	Mar-49	0.001683	0.006997	13.92567	88.9491	BCL2;PRKACA;BCL2L1
NO metabolism in cystic fibrosis WP4947	13-Feb	0.001718	0.006997	38.47776	244.9676	PRMT1;CARM1
Purine metabolism WP4792	13-Feb	0.001718	0.006997	38.47776	244.9676	HPRT1;ADA
Cardiac Hypertrophic Response WP2795	Mar-55	0.002347	0.00942	12.31514	74.56497	PLA2G2A;PRKCA;FGF2
Fragile X Syndrome WP4549	4/121	0.002759	0.010918	7.353029	43.33133	PRKCA;PRKACA;MMP9;EIF4E
Kit receptor signaling pathway WP304	Mar-59	0.002868	0.011193	11.43318	66.93149	PRKCB;BCL2;PRKCA
Cori Cycle WP1946	17-Feb	0.002959	0.011389	28.21135	164.2753	GAPDH;HK1
Focal Adhesion-PI3K-Akt-mTOR-signaling pathway WP3932	6/303	0.003411	0.012946	4.401122	25.00111	HSP90AA1;AKT3;FGF1;FGF2;EIF4E;VEGFA
Endometrial cancer WP4155	Mar-63	0.003455	0.012946	10.66882	60.46924	AKT3;FGF1;FGF2

Overview of nanoparticle effects WP3287	19-Feb	0.003697	0.013669	24.88986	139.3896	AKT3;BCL2
Hypertrophy Model WP516	20-Feb	0.004095	0.014944	23.50591	129.2358	EIF4E;VEGFA
Galanin receptor pathway WP4970	21-Feb	0.004512	0.016048	22.26764	120.2686	PRKCD;VEGFA
Host-pathogen interaction of human coronaviruses - apoptosis WP4864	21-Feb	0.004512	0.016048	22.26764	120.2686	BCL2;BCL2L1
Glucocorticoid Receptor Pathway WP2880	Mar-70	0.004649	0.016331	9.550794	51.2976	HSP90AA1;MGAM;NR3C1
Purine metabolism and related disorders WP4224	22-Feb	0.004948	0.016955	21.15319	112.2992	HPRT1;ADA
Regulation of apoptosis by parathyroid hormone-related protein WP3872	22-Feb	0.004948	0.016955	21.15319	112.2992	BCL2;BCL2L1
Non-small cell lung cancer WP4255	Mar-72	0.005031	0.017032	9.273025	49.07462	PRKCB;AKT3;PRKCA
Head and Neck Squamous Cell Carcinoma WP4674	Mar-73	0.005228	0.01749	9.140092	48.01905	AKT3;EIF4E;VEGFA
Estrogen signaling pathway WP712	23-Feb	0.005402	0.017858	20.14488	105.1764	BCL2;PRKACA
Mesodermal commitment pathway WP2857	4/147	0.005517	0.018028	6.008209	31.24176	SETD2;RARG;HPRT1;PRKACA
Regulatory circuits of the STAT3 signaling pathway WP4538	Mar-78	0.006286	0.020098	8.528602	43.23529	PTPRC;PRKCB;SETD7
MTHFR deficiency WP4288	25-Feb	0.006366	0.020098	18.3913	93.00176	EHMT2;EHMT1
Physiological and pathological hypertrophy of the heart WP1528	25-Feb	0.006366	0.020098	18.3913	93.00176	PRKCB;PRKCE
Eicosanoid Synthesis WP167	27-Feb	0.007402	0.022856	16.9183	83.00207	PLA2G2A;PLA2G5
Follicle Stimulating Hormone (FSH) signaling pathway WP2035	27-Feb	0.007402	0.022856	16.9183	83.00207	PRKCA;PRKACA
Chemokine signaling pathway WP3929	4/164	0.008072	0.024648	5.365217	25.85672	PRKCB;ROCK2;AKT3;PRKCD
Acute viral myocarditis WP4298	Mar-86	0.008227	0.024648	7.703459	36.97957	BCL2;MMP9;BCL2L1
Retinoblastoma gene in cancer WP2446	Mar-87	0.008491	0.024648	7.611367	36.29655	POLA1;CCNE2;TYMS
Cannabinoid receptor signaling WP3869	Feb-29	0.008508	0.024648	15.66351	74.66335	ADORA2A;PRKACA
Lipid Metabolism Pathway WP3965	Feb-29	0.008508	0.024648	15.66351	74.66335	AKT3;PRKACA
PDGFR-beta pathway WP3972	Feb-29	0.008508	0.024648	15.66351	74.66335	PRKCB;PRKCA
Oligodendrocyte specification and differentiation, leading to myelin components for CNS WP4304	Feb-30	0.009088	0.025795	15.10334	70.9981	MAG;FGF2
One-carbon metabolism WP241	Feb-30	0.009088	0.025795	15.10334	70.9981	AHCY;TYMS
ErbB signaling pathway WP673	Mar-91	0.009599	0.02668	7.26393	33.74868	PRKCB;AKT3;PRKCA
GPCRs, Other WP117	Mar-91	0.009599	0.02668	7.26393	33.74868	ADORA2A;ADORA3;SSTR2
Trans-sulfuration and one-carbon metabolism WP2525	Feb-31	0.009684	0.02668	14.5818	67.61926	AHCY;TYMS

Monoamine Transport WP727	Feb-32	0.010298	0.028095	14.09504	64.49609	HRH3;ADORA2A
Alpha 6 Beta 4 signaling pathway WP244	Feb-33	0.010928	0.029247	13.63967	61.60202	PRKCD;PRKCA
miRNA regulation of prostate cancer signaling pathways WP3981	Feb-33	0.010928	0.029247	13.63967	61.60202	AKT3;BCL2
B Cell Receptor Signaling Pathway WP23	Mar-97	0.011413	0.029972	6.798216	30.40849	PTPRC;PRKCB;PRKCD
Complement system WP2806	Mar-97	0.011413	0.029972	6.798216	30.40849	SELP;PRKCA;PRKACA
Type 2 papillary renal cell carcinoma WP4241	Feb-34	0.011575	0.030118	13.21277	58.91394	SETD2;VEGFA
Host-pathogen interaction of human coronaviruses - MAPK signaling WP4877	Feb-36	0.012919	0.033305	12.43429	54.0776	BCL2;EIF4E
Amyotrophic lateral sclerosis (ALS) WP2447	Feb-38	0.014327	0.036268	11.74232	49.85354	BCL2;BCL2L1
Nuclear receptors WP170	Feb-38	0.014327	0.036268	11.74232	49.85354	RARG;NR3C1
Wnt signaling WP428	3/115	0.017971	0.045059	5.700461	22.91013	PRKCB;ROCK2;PRKCA
IL-6 signaling pathway WP364	Feb-43	0.01812	0.045059	10.30773	41.34164	PRKCD;BCL2L1
ESC Pluripotency Pathways WP3931	3/116	0.018385	0.045318	5.649729	22.57749	AKT3;FGF1;FGF2
Hedgehog Signaling Pathway WP4249	Feb-44	0.018924	0.046241	10.0618	39.91832	BCL2;PRKACA
Aryl Hydrocarbon Receptor Netpath WP2586	Feb-46	0.020577	0.049846	9.603482	37.29588	HSP90AA1;VEGFA
Hepatitis C and Hepatocellular Carcinoma WP3646	Feb-49	0.023165	0.055635	8.989135	33.8452	VEGFA;BCL2L1
SARS-CoV-2 altering angiogenesis via NRP1 WP5065	05-Jan	0.023773	0.056612	52.36842	195.8165	VEGFA
Wnt Signaling Pathway WP363	Feb-52	0.025879	0.061109	8.448511	30.87361	PRKCB;PRKCA
LncRNA-mediated mechanisms of therapeutic resistance WP3672	06-Jan	0.02846	0.066093	41.89263	149.1067	BCL2L1
Robo4 and VEGF Signaling Pathways Crosstalk WP3943	06-Jan	0.02846	0.066093	41.89263	149.1067	VEGFA
Pathogenic Escherichia coli infection WP2272	Feb-55	0.028715	0.06614	7.969089	28.2928	ROCK2;PRKCA
Endoderm differentiation WP2853	3/141	0.030466	0.069602	4.620383	16.13038	RARG;HPRT1;NR3C1
Glial Cell Differentiation WP2276	07-Jan	0.033125	0.073634	34.90877	118.9508	MAG
MicroRNA for Targeting Cancer Growth and Vascularization in Glioblastoma WP3593	07-Jan	0.033125	0.073634	34.90877	118.9508	VEGFA
SARS-CoV-2 and angiotensin-converting enzyme 2 receptor: molecular mechanisms WP4883	07-Jan	0.033125	0.073634	34.90877	118.9508	REN
Male infertility WP4673	3/146	0.033279	0.073634	4.457704	15.16874	MMP2;BCL2;MMP9
Regulation of Actin Cytoskeleton WP51	3/150	0.035624	0.078207	4.335528	14.4578	ROCK2;FGF1;FGF2
Serine Metabolism WP4688	08-Jan	0.037767	0.081624	29.9203	98.02821	TYMS

HIF1A and PPARG regulation of glycolysis WP2456	08-Jan	0.037767	0.081624	29.9203	98.02821	GAPDH
Breast cancer pathway WP4262	3/154	0.038053	0.081624	4.219825	13.79371	AKT3;FGF1;FGF2
Epithelial to mesenchymal transition in CRC WP4239	3/160	0.04185	0.089089	4.057325	12.87661	MMP2;AKT3;MMP9
EGF/EGFR signaling pathway WP437	3/162	0.043156	0.091128	4.005884	12.59019	PRKCB;PRKCD;PRKCA
Sterol regulatory element-binding proteins (SREBP) signaling WP1982	Feb-69	0.043456	0.091128	6.29946	19.75514	PRKACA;FDFT1
MECP2 and Associated Rett Syndrome WP3584	Feb-72	0.046913	0.095675	6.028571	18.44414	MAG;FGF2
Aspirin and miRNAs WP4707	10-Jan	0.046986	0.095675	23.26901	71.15419	VEGFA
Trans-sulfuration pathway WP2333	10-Jan	0.046986	0.095675	23.26901	71.15419	AHCY
Mammary gland development pathway - Involution (Stage 4 of 4) WP2815	10-Jan	0.046986	0.095675	23.26901	71.15419	MMP9
Chromosomal and microsatellite instability in CRC WP4216	Feb-73	0.048087	0.097213	5.943362	18.03652	AKT3;BCL2
Methionine metabolism leading to sulfur amino acids and related disorders WP4292	11-Jan	0.051563	0.103495	20.94105	62.08911	AHCY
Bile acids synthesis and enterohepatic circulation WP4389	12-Jan	0.056118	0.111838	19.03636	54.83034	SLC10A2
Serotonin and anxiety-related events WP3944	13-Jan	0.060652	0.117539	17.44912	48.90309	PRKCB
Disorders of Folate Metabolism and Transport WP4259	13-Jan	0.060652	0.117539	17.44912	48.90309	TYMS
Dopamine metabolism WP2436	13-Jan	0.060652	0.117539	17.44912	48.90309	PRKACA
Osteopontin Signaling WP1434	13-Jan	0.060652	0.117539	17.44912	48.90309	MMP9
Apoptosis WP254	Feb-84	0.061682	0.118717	5.143228	14.3278	BCL2;BCL2L1
Omega-3/Omega-6 FA synthesis WP4723	14-Jan	0.065163	0.124564	16.10607	43.9834	PLA2G5
Androgen receptor signaling pathway WP138	Feb-90	0.069584	0.128768	4.791103	12.76932	ROCK2;CARM1
Apoptosis Modulation and Signaling WP1772	Feb-90	0.069584	0.128768	4.791103	12.76932	BCL2;BCL2L1
Cholesterol Biosynthesis Pathway WP197	15-Jan	0.069654	0.128768	14.95489	39.8431	FDFT1
Cysteine and methionine catabolism WP4504	15-Jan	0.069654	0.128768	14.95489	39.8431	AHCY
Phytochemical activity on NRF2 transcriptional activation WP3	15-Jan	0.069654	0.128768	14.95489	39.8431	PRKCA
Amino Acid metabolism WP3925	Feb-91	0.070932	0.130274	4.737031	12.53432	IARS;SRM
TNF-alpha signaling pathway WP231	Feb-92	0.072289	0.131904	4.684161	12.30569	HSP90AA1;BCL2L1
Thyroid hormones production and their peripheral downstream signaling effects WP4746	Feb-95	0.076409	0.13545	4.532372	11.65572	AKT3;PRKACA

Serotonin and anxiety WP3947	17-Jan	0.07857	0.13545	13.08421	33.28308	PRKCB
ACE Inhibitor Pathway WP554	17-Jan	0.07857	0.13545	13.08421	33.28308	REN
Airway smooth muscle cell contraction WP4962	17-Jan	0.07857	0.13545	13.08421	33.28308	ROCK2
Amplification and Expansion of Oncogenic Pathways as Metastatic Traits WP3678	17-Jan	0.07857	0.13545	13.08421	33.28308	VEGFA
Cells and molecules involved in local acute inflammatory response WP4493	17-Jan	0.07857	0.13545	13.08421	33.28308	SELP
Glycosaminoglycan degradation WP4815	17-Jan	0.07857	0.13545	13.08421	33.28308	HPSE
NOTCH1 regulation of endothelial cell calcification WP3413	17-Jan	0.07857	0.13545	13.08421	33.28308	VEGFA
Platelet-mediated interactions with vascular and circulating cells WP4462	17-Jan	0.07857	0.13545	13.08421	33.28308	SELP
4-hydroxytamoxifen, Dexamethasone, and Retinoic Acids Regulation of p27 Expression WP3879	18-Jan	0.082997	0.142208	12.31393	30.64876	EIF4E
Integrin-mediated Cell Adhesion WP185	2/101	0.084864	0.144526	4.256394	10.49927	ROCK2;AKT3
Serotonin Receptor 4/6/7 and NR3C Signaling WP734	19-Jan	0.087403	0.146191	11.62924	28.34313	NR3C1
TP53 network WP1742	19-Jan	0.087403	0.146191	11.62924	28.34313	BCL2
Extracellular vesicles in the crosstalk of cardiac cells WP4300	19-Jan	0.087403	0.146191	11.62924	28.34313	MMP9
Hereditary leiomyomatosis and renal cell carcinoma pathway WP4206	20-Jan	0.091787	0.150832	11.01662	26.31079	VEGFA
Metabolism of Spingolipids in ER and Golgi apparatus WP4142	20-Jan	0.091787	0.150832	11.01662	26.31079	B4GALT1
Nanomaterial induced apoptosis WP2507	20-Jan	0.091787	0.150832	11.01662	26.31079	BCL2
Urea cycle and metabolism of amino groups WP497	21-Jan	0.096151	0.155278	10.46526	24.50792	SRM
Globo Sphingolipid Metabolism WP1424	21-Jan	0.096151	0.155278	10.46526	24.50792	ST6GAL1
Nicotine Activity on Dopaminergic Neurons WP1602	21-Jan	0.096151	0.155278	10.46526	24.50792	PRKACA
DNA damage response (only ATM dependent) WP710	2/110	0.098044	0.157431	3.899921	9.056922	AKT3;BCL2
Transcription factor regulation in adipogenesis WP3599	22-Jan	0.100494	0.158645	9.966416	22.8994	NR3C1
Type II diabetes mellitus WP1584	22-Jan	0.100494	0.158645	9.966416	22.8994	PRKCD
Vitamin D in inflammatory diseases WP4482	22-Jan	0.100494	0.158645	9.966416	22.8994	NR3C1
Ebstein-Barr virus LMP1 signaling WP262	23-Jan	0.104816	0.161832	9.512919	21.45681	HSP90AA1

Immune response to tuberculosis WP4197	23-Jan	0.104816	0.161832	9.512919	21.45681	PTPN2
Nanoparticle triggered autophagic cell death WP2509	23-Jan	0.104816	0.161832	9.512919	21.45681	BCL2
NRF2-ARE regulation WP4357	23-Jan	0.104816	0.161832	9.512919	21.45681	PRKCA
Unfolded protein response WP4925	24-Jan	0.109118	0.166643	9.098856	20.1569	BCL2
IL1 and megakaryocytes in obesity WP2865	24-Jan	0.109118	0.166643	9.098856	20.1569	MMP9
Hippo-Merlin Signaling Dysregulation WP4541	2/120	0.113311	0.168599	3.567616	7.768898	FLT3;PRKACA
Signal Transduction of S1P Receptor WP26	25-Jan	0.1134	0.168599	8.719298	18.98049	AKT3
Glycosylation and related congenital defects WP4521	25-Jan	0.1134	0.168599	8.719298	18.98049	B4GALT1
IL-7 signaling pathway WP205	25-Jan	0.1134	0.168599	8.719298	18.98049	BCL2L1
Relationship between inflammation, COX-2 and EGFR WP4483	25-Jan	0.1134	0.168599	8.719298	18.98049	AKT3
Wnt/beta-catenin signaling pathway in leukemia WP3658	26-Jan	0.117661	0.172201	8.370105	17.91161	FLT3
EPO Receptor Signaling WP581	26-Jan	0.117661	0.172201	8.370105	17.91161	PTPRC
Glucuronidation WP698	26-Jan	0.117661	0.172201	8.370105	17.91161	HK1
Nanoparticle-mediated activation of receptor signaling WP2643	28-Jan	0.126122	0.183628	7.749318	16.04501	AKT3
Statin inhibition of cholesterol production WP430	29-Jan	0.130322	0.185566	7.47218	15.22639	FDFT1
T-Cell Receptor and Co-stimulatory Signaling WP2583	29-Jan	0.130322	0.185566	7.47218	15.22639	PRKCA
Eicosanoid metabolism via lipooxygenases (LOX) WP4721	29-Jan	0.130322	0.185566	7.47218	15.22639	CYSLTR2
RAS and bradykinin pathways in COVID-19 WP4969	29-Jan	0.130322	0.185566	7.47218	15.22639	REN
22q11.2 copy number variation syndrome WP4657	2/131	0.130755	0.185566	3.261587	6.635479	MAG;BCL2
Angiopoietin Like Protein 8 Regulatory Pathway WP3915	2/132	0.13237	0.186915	3.236334	6.544359	PTPN1;EIF4E
Eicosanoid metabolism via cyclooxygenases (COX) WP4719	30-Jan	0.134503	0.188036	7.214156	14.47282	PLA2G5
Glycerophospholipid Biosynthetic Pathway WP2533	30-Jan	0.134503	0.188036	7.214156	14.47282	PLA2G2A
16p11.2 distal deletion syndrome WP4950	31-Jan	0.138664	0.192893	6.973333	13.77725	PRMT1
Constitutive Androstane Receptor Pathway WP2875	Jan-32	0.142804	0.195746	6.748048	13.13359	HSP90AA1
White fat cell differentiation WP4149	Jan-32	0.142804	0.195746	6.748048	13.13359	NR3C1

Hair Follicle Development: Organogenesis - Part 2 of 3 WP2839	Jan-32	0.142804	0.195746	6.748048	13.13359	FGF1
Endothelin Pathways WP2197	Jan-33	0.146926	0.1966	6.536842	12.53655	PRKCA
Nuclear Receptors in Lipid Metabolism and Toxicity WP299	Jan-33	0.146926	0.1966	6.536842	12.53655	RARG
Pregnane X receptor pathway WP2876	Jan-33	0.146926	0.1966	6.536842	12.53655	HSP90AA1
Prion disease pathway WP3995	Jan-33	0.146926	0.1966	6.536842	12.53655	BCL2
Resistin as a regulator of inflammation WP4481	Jan-33	0.146926	0.1966	6.536842	12.53655	AKT3
Brain-derived neurotrophic factor (BDNF) signaling pathway WP2380	2/144	0.152097	0.202556	2.961043	5.576341	PRKCD;EIF4E
The influence of laminopathies on Wnt signaling WP4844	Jan-35	0.155109	0.205593	6.151703	11.46448	FNTA
Target Of Rapamycin (TOR) Signaling WP1471	Jan-36	0.159172	0.209987	5.975639	10.98186	PRKCA
Type II interferon signaling (IFNG) WP619	Jan-37	0.163215	0.210382	5.809357	10.53055	PRKCD
Factors and pathways affecting insulin-like growth factor (IGF1)-Akt signaling WP3850	Jan-37	0.163215	0.210382	5.809357	10.53055	EIF4E
Melatonin metabolism and effects WP3298	Jan-37	0.163215	0.210382	5.809357	10.53055	PRKCA
Neovascularisation processes WP4331	Jan-37	0.163215	0.210382	5.809357	10.53055	MMP9
Overview of interferons-mediated signaling pathway WP4558	Jan-37	0.163215	0.210382	5.809357	10.53055	PRKCA
Integrated breast cancer pathway WP1984	2/152	0.165553	0.212422	2.801986	5.039263	BCL2;VEGFA
Parkinson's disease pathway WP2371	Jan-38	0.167239	0.21361	5.652063	10.10777	CCNE2
G13 Signaling Pathway WP524	Jan-39	0.171244	0.217735	5.503047	9.711048	ROCK2
IL-5 signaling pathway WP127	Jan-40	0.17523	0.220805	5.361673	9.338205	BCL2
Oxidative Damage WP3941	Jan-40	0.17523	0.220805	5.361673	9.338205	BCL2
Vitamin D-sensitive calcium signaling in depression WP4698	Jan-41	0.179196	0.222786	5.227368	8.987274	BCL2
Nucleotide-binding Oligomerization Domain (NOD) pathway WP1433	Jan-41	0.179196	0.222786	5.227368	8.987274	HSP90AA1
TNF related weak inducer of apoptosis (TWEAK) Signaling Pathway WP2036	Jan-42	0.183144	0.222786	5.099615	8.656499	MMP9
Tryptophan metabolism WP465	Jan-42	0.183144	0.222786	5.099615	8.656499	PRMT1
DNA Replication WP466	Jan-42	0.183144	0.222786	5.099615	8.656499	POLA1
Fas ligand pathway and stress induction of heat shock proteins WP314	Jan-42	0.183144	0.222786	5.099615	8.656499	BCL2
IL-2 signaling pathway WP49	Jan-42	0.183144	0.222786	5.099615	8.656499	BCL2

Metabolic reprogramming in colon cancer WP4290	Jan-42	0.183144	0.222786	5.099615	8.656499	GAPDH
Vitamin A and carotenoid metabolism WP716	Jan-43	0.187073	0.225612	4.977945	8.3443	RARG
Genes controlling nephrogenesis WP4823	Jan-43	0.187073	0.225612	4.977945	8.3443	VEGFA
Heart Development WP1591	Jan-44	0.190984	0.226441	4.861934	8.049253	VEGFA
Integrated Cancer Pathway WP1971	Jan-44	0.190984	0.226441	4.861934	8.049253	BCL2
Interleukin-11 Signaling Pathway WP2332	Jan-44	0.190984	0.226441	4.861934	8.049253	BCL2
Renin-angiotensin-aldosterone system (RAAS) WP4756	Jan-44	0.190984	0.226441	4.861934	8.049253	REN
ATM Signaling Network in Development and Disease WP3878	Jan-45	0.194876	0.230084	4.751196	7.770074	AURKB
Aryl Hydrocarbon Receptor Pathway WP2873	Jan-46	0.198749	0.232702	4.64538	7.505598	HSP90AA1
Cholesterol metabolism (includes both Bloch and Kandutsch-Russell pathways) WP4718	Jan-46	0.198749	0.232702	4.64538	7.505598	FDFT1
Development of ureteric collection system WP5053	Jan-47	0.202604	0.233327	4.544165	7.25477	RARG
Endoplasmic reticulum stress response in coronavirus infection WP4861	Jan-47	0.202604	0.233327	4.544165	7.25477	BCL2
Energy Metabolism WP1541	Jan-47	0.202604	0.233327	4.544165	7.25477	PRMT1
NO/cGMP/PKG mediated Neuroprotection WP4008	Jan-47	0.202604	0.233327	4.544165	7.25477	BCL2
Structural Pathway of Interleukin 1 (IL-1) WP2637	Jan-49	0.210259	0.241154	4.354386	6.790303	EIF4E
Synaptic signaling pathways associated with autism spectrum disorder WP4539	Jan-50	0.214059	0.244514	4.265306	6.57499	AKT3
Translation Factors WP107	Jan-52	0.221605	0.250084	4.097626	6.174551	EIF4E
Netrin-UNC5B signaling pathway WP4747	Jan-52	0.221605	0.250084	4.097626	6.174551	PRKCA
One-carbon metabolism and related pathways WP3940	Jan-52	0.221605	0.250084	4.097626	6.174551	TYMS
Cardiac Progenitor Differentiation WP2406	Jan-53	0.225351	0.252285	4.018623	5.988141	FGF2
Phosphodiesterases in neuronal function WP4222	Jan-53	0.225351	0.252285	4.018623	5.988141	ADORA2A
The Overlap Between Signal Transduction Pathways that Contribute to a Range of LMNA Laminopathies WP4879	Jan-55	0.232789	0.259579	3.869396	5.640114	FNTA
MET in type 1 papillary renal cell carcinoma WP4205	Jan-59	0.247455	0.274841	3.601815	5.030028	AKT3
T-Cell antigen Receptor (TCR) pathway during Staphylococcus aureus infection WP3863	Jan-62	0.258272	0.285726	3.424159	4.635426	PTPRC
G1 to S cell cycle control WP45	Jan-64	0.265398	0.292458	3.315121	4.397592	CCNE2

Pathways affected in adenoid cystic carcinoma WP3651	Jan-65	0.268935	0.295198	3.263158	4.285455	SETD2
Association Between Physico-Chemical Features and Toxicity Associated Pathways WP3680	Jan-66	0.272456	0.297899	3.212794	4.177528	ROCK2
p53 transcriptional gene network WP4963	Jan-67	0.27596	0.300561	3.163955	4.073596	ADORA2B
DNA damage response WP707	Jan-68	0.279447	0.30086	3.116575	3.973459	CCNE2
Melanoma WP4685	Jan-68	0.279447	0.30086	3.116575	3.973459	AKT3
RAC1/PAK1/p38/MMP2 Pathway WP3303	Jan-68	0.279447	0.30086	3.116575	3.973459	MMP2
Folate Metabolism WP176	Jan-69	0.282917	0.303434	3.070588	3.876929	AHCY
miRNA regulation of DNA damage response WP1530	Jan-71	0.289808	0.309643	2.982556	3.694001	CCNE2
16p11.2 proximal deletion syndrome WP4949	Jan-74	0.300023	0.319342	2.859553	3.442607	NR3C1
Prolactin Signaling Pathway WP2037	Jan-76	0.306751	0.325272	2.783018	3.288741	PTPN1
Alzheimer's disease WP2059	Jan-83	0.329802	0.348399	2.544544	2.822572	GAPDH
Allograft Rejection WP2328	Jan-89	0.348954	0.367251	2.370335	2.495525	VEGFA
T-cell receptor (TCR) signaling pathway WP69	Jan-90	0.352093	0.369172	2.343584	2.446374	PRKCD
Neural Crest Differentiation WP2064	1/101	0.385649	0.402852	2.084632	1.986297	FGF2
Toll-like Receptor Signaling Pathway WP75	1/103	0.391562	0.407515	2.04355	1.916055	AKT3
7q11.23 copy number variation syndrome WP4932	1/104	0.394498	0.409055	2.023608	1.882242	GAPDH
Senescence and Autophagy in Cancer WP615	1/105	0.397419	0.410569	2.004049	1.849262	BCL2
Thermogenesis WP4321	1/108	0.406101	0.418001	1.947565	1.755056	PRKACA
Cell cycle WP179	1/120	0.439606	0.450836	1.750111	1.438376	CCNE2
Nuclear Receptors Meta-Pathway WP2882	2/319	0.454389	0.463904	1.314652	1.036999	HSP90AA1;NR3C1
mRNA Processing WP411	1/126	0.45565	0.463904	1.6656	1.309214	PRMT1
Adipogenesis WP236	1/130	0.466092	0.472823	1.613627	1.231798	NR3C1
Ectoderm Differentiation WP2858	1/138	0.486386	0.491635	1.518786	1.094668	OGT
Regulation of toll-like receptor signaling pathway WP1449	1/139	0.488869	0.492373	1.507704	1.079005	AKT3
NRF2 pathway WP2884	1/146	0.505917	0.507723	1.43441	0.977383	HSP90AA1
Nonalcoholic fatty liver disease WP4396	1/155	0.527011	0.527011	1.349966	0.864699	AKT3

KEGG pthway

Term	Overlap	P-value	Adjusted P-value	Odds Ratio	Combined Score	Genes
Neuroactive ligand-receptor interaction	17/341	5.37E-13	1.12E-10	13.00438	367.3997	P2RY14;SSTR1;NR3C1;SSTR2;SSTR3;MCHR1;SSTR4;SSTR5;P2RY6;CYSLTR2;ADORA2A;HRH3;P2RY4;ADORA2B;ADORA3;P2RY2;ADORA1
Starch and sucrose metabolism	13/363	5.67E-12	5.90E-10	64.53247	1671.134	MGAM;AMY2A;AMY1A;SI;GAA;PYGM;HK2;HK1
Vascular smooth muscle contraction	11/133	4.04E-11	2.80E-09	20.9838	502.2142	ADORA2A;PRKCB;ADORA2B;ROCK2;PRKCE;PRKCD;PLA2G10;PLA2G2A;PRKCA;PLA2G5;PRKACA
Carbohydrate digestion and absorption	17/380	5.64E-11	2.93E-09	46.30536	1092.717	MGAM;AMY2A;AMY1A;PRKCB;SI;AKT3;HK2;HK1
Ras signaling pathway	12/232	1.18E-09	4.92E-08	12.78182	262.745	FLT3;PRKCB;AKT3;PLA2G10;PLA2G2A;PRKCA;PLA2G5;FGF1;PRKACA;FGF2;VEGFA;BCL2L1
HIF-1 signaling pathway	9/109	2.65E-09	9.19E-08	20.4869	404.589	PRKCB;AKT3;BCL2;PRKCA;GAPDH;EIF4E;HK2;HK1;VEGFA
Proteoglycans in cancer	11/205	4.13E-09	1.23E-07	13.14797	253.8105	PRKCB;ROCK2;MMP2;AKT3;PDCD4;PRKCA;HPSE;PRKACA;FGF2;MMP9;VEGFA
Galactose metabolism	11/475	6.98E-09	1.81E-07	53.01067	995.5833	MGAM;B4GALT1;SI;GAA;HK2;HK1
Pyrimidine metabolism	20/637	9.00E-09	2.08E-07	31.86998	590.43	CDA;TK2;NT5M;TK1;UMPS;TYMS;TYMP
AGE-RAGE signaling pathway in diabetic complications	8/100	2.71E-08	5.64E-07	19.57708	341.0823	PRKCB;MMP2;PRKCE;AKT3;PRKCD;BCL2;PRKCA;VEGFA
Pathways in cancer	15/531	3.41E-08	6.45E-07	6.958082	119.6296	HSP90AA1;FLT3;PRKCB;ROCK2;MMP2;PRKCA;FGF1;FGF2;MMP9;VEGFA;CCNE2;AKT3;BCL2;PRKACA;BCL2L1
Growth hormone synthesis, secretion and action	8/119	1.06E-07	1.70E-06	16.21048	260.3153	PRKCB;AKT3;PRKCA;SSTR1;PRKACA;SSTR2;SSTR3;SSTR5
Sphingolipid signaling pathway	8/119	1.06E-07	1.70E-06	16.21048	260.3153	PRKCB;ROCK2;ADORA3;PRKCE;AKT3;ADORA1;BCL2;PRKCA
Pancreatic secretion	7/102	5.99E-07	8.90E-06	16.40012	234.9819	AMY2A;AMY1A;PRKCB;PLA2G10;PLA2G2A;PRKCA;PLA2G5
Insulin resistance	7/108	8.83E-07	1.23E-05	15.42118	214.9617	PTPN1;PRKCB;PRKCE;AKT3;PRKCD;PYGM;OGT
PI3K-Akt signaling pathway	11/354	1.05E-06	1.37E-05	7.380244	101.5767	HSP90AA1;CCNE2;FLT3;AKT3;BCL2;PRKCA;FGF1;FGF2;EIF4E;VEGFA;BCL2L1
Calcium signaling pathway	9/240	2.32E-06	2.84E-05	8.810121	114.2841	CYSLTR2;ADORA2A;PRKCB;ADORA2B;PRKCA;FGF1;PRKACA;FGF2;VEGFA
Relaxin signaling pathway	7/129	2.92E-06	3.37E-05	12.75318	162.5328	MMP13;MMP2;AKT3;PRKCA;PRKACA;MMP9;VEGFA
Estrogen signaling pathway	7/137	4.35E-06	4.53E-05	11.96353	147.6852	HSP90AA1;MMP2;AKT3;PRKCD;BCL2;PRKACA;MMP9
Insulin signaling pathway	7/137	4.35E-06	4.53E-05	11.96353	147.6852	PTPN1;AKT3;PYGM;PRKACA;EIF4E;HK2;HK1
Diabetic cardiomyopathy	8/203	6.06E-06	6.00E-05	9.188345	110.3883	PRKCB;MMP2;AKT3;PRKCD;PRKCA;REN;MMP9;GAPDH

Fc gamma R-mediated phagocytosis	35/582	7.26E-06	6.73E-05	14.51502	171.7602	PTPRC;PRKCB;PRKCE;AKT3;PRKCD;PRKCA
Inflammatory mediator regulation of TRP channels	35/947	7.70E-06	6.73E-05	14.35652	169.0329	PRKCB;PRKCE;P2RY2;PRKCD;PRKCA;PRKACA
Rap1 signaling pathway	8/210	7.77E-06	6.73E-05	8.866787	104.3214	ADORA2A;PRKCB;ADORA2B;AKT3;PRKCA;FGF1;FGF2;VEGFA
Lipid and atherosclerosis	8/215	9.23E-06	7.63E-05	8.650417	100.2892	SELP;HSP90AA1;ROCK2;AKT3;BCL2;PRKCA;MMP9;BCL2L1
cAMP signaling pathway	8/216	9.54E-06	7.63E-05	8.608392	99.51074	ADORA2A;ROCK2;AKT3;ADORA1;SSTR1;PRKACA;SSTR2;SSTR5
Lysine degradation	23/132	1.29E-05	9.97E-05	18.80068	211.6115	SETD2;EHMT2;SETD7;DOT1L;EHMT1
Drug metabolism	6/108	1.35E-05	1.00E-04	12.94248	145.1469	CDA;TK2;TK1;HPRT1;UMPS;TYMP
Chemical carcinogenesis	8/239	1.98E-05	1.42E-04	7.742227	83.82888	HSP90AA1;PRKCB;AKT3;BCL2;PRKCA;PRKACA;FGF2;VEGFA
Shigellosis	8/246	2.44E-05	1.69E-04	7.511841	79.77968	ROCK2;PRKCE;AKT3;PRKCD;BCL2;HK2;HK1;BCL2L1
Bladder cancer	15/67	4.40E-05	2.96E-04	23.34548	234.1596	MMP2;MMP9;TYMP;VEGFA
Fluid shear stress and atherosclerosis	6/139	5.61E-05	3.65E-04	9.910276	97.00186	HSP90AA1;MMP2;AKT3;BCL2;MMP9;VEGFA
Type II diabetes mellitus	16/893	6.97E-05	4.39E-04	20.56108	196.7993	PRKCE;PRKCD;HK2;HK1
GnRH signaling pathway	34/90	8.54E-05	4.96E-04	12.37263	115.9099	PRKCB;MMP2;PRKCD;PRKCA;PRKACA
Salivary secretion	34/90	8.54E-05	4.96E-04	12.37263	115.9099	AMY2A;AMY1A;PRKCB;PRKCA;PRKACA
MAPK signaling pathway	8/294	8.58E-05	4.96E-04	6.235855	58.38813	FLT3;PRKCB;AKT3;PRKCA;FGF1;PRKACA;FGF2;VEGFA
Prostate cancer	35/551	1.04E-04	5.86E-04	11.8323	108.4811	HSP90AA1;CCNE2;AKT3;BCL2;MMP9
MicroRNAs in cancer	8/310	1.24E-04	6.78E-04	5.900662	53.08758	CCNE2;PRKCB;PRKCE;PDCD4;BCL2;PRKCA;MMP9;VEGFA
Hepatitis B	6/162	1.31E-04	6.88E-04	8.439316	75.46376	CCNE2;PRKCB;AKT3;BCL2;PRKCA;MMP9
Longevity regulating pathway	5/102	1.32E-04	6.88E-04	11.21955	100.197	EHMT2;AKT3;EHMT1;PRKACA;EIF4E
Parathyroid hormone synthesis, secretion and action	5/106	1.59E-04	8.04E-04	10.77304	94.25888	MMP13;PRKCB;BCL2;PRKCA;PRKACA
VEGF signaling pathway	21/641	1.85E-04	9.18E-04	15.69091	134.8386	PRKCB;AKT3;PRKCA;VEGFA
Cholinergic synapse	5/113	2.14E-04	0.001032	10.07123	85.10348	PRKCB;AKT3;BCL2;PRKCA;PRKACA
Leukocyte transendothelial migration	5/114	2.23E-04	0.001032	9.978324	83.90854	PRKCB;ROCK2;MMP2;PRKCA;MMP9
Neomycin, kanamycin and gentamicin biosynthesis	44/597	2.26E-04	0.001032	141.1418	1184.965	HK2;HK1
alpha-Linolenic acid metabolism	44/645	2.28E-04	0.001032	29.15249	244.44	PLA2G2A;PLA2G10;PLA2G5
Linoleic acid metabolism	44/649	3.58E-04	0.001554	24.66253	195.7187	PLA2G2A;PLA2G10;PLA2G5
Central carbon metabolism in cancer	25/659	3.59E-04	0.001554	13.06851	103.6761	FLT3;AKT3;HK2;HK1
Focal adhesion	6/201	4.18E-04	0.001776	6.73812	52.4154	PRKCB;ROCK2;AKT3;BCL2;PRKCA;VEGFA

Gastric acid secretion	27/851	4.91E-04	0.002042	11.97585	91.24728	PRKCB;PRKCA;PRKACA;SSTR2
Autophagy	5/137	5.20E-04	0.002121	8.230103	62.23363	AKT3;PRKCD;BCL2;PRKACA;BCL2L1
Human cytomegalovirus infection	6/225	7.57E-04	0.002986	5.99239	43.06116	PRKCB;ROCK2;AKT3;PRKCA;PRKACA;VEGFA
Gastric cancer	5/149	7.61E-04	0.002986	7.539683	54.14253	CCNE2;AKT3;BCL2;FGF1;FGF2
Morphine addiction	33/329	9.68E-04	0.003729	9.903548	68.73231	PRKCB;ADORA1;PRKCA;PRKACA
Small cell lung cancer	33/695	0.001008	0.003814	9.790514	67.54835	CCNE2;AKT3;BCL2;BCL2L1
Fat digestion and absorption	15/766	0.001151	0.004274	16.01935	108.4088	PLA2G2A;PLA2G10;PLA2G5
cGMP-PKG signaling pathway	5/167	0.001267	0.004503	6.695835	44.66803	ROCK2;ADORA3;PRKCE;AKT3;ADORA1
Aldosterone synthesis and secretion	35/886	0.001275	0.004503	9.162812	61.06504	PRKCB;PRKCE;PRKCA;PRKACA
Salmonella infection	6/249	0.001277	0.004503	5.393964	35.94065	HSP90AA1;PTPRC;ROCK2;AKT3;BCL2;GAPDH
Other types of O-glycan biosynthesis	17/227	0.001491	0.005169	14.56012	94.76035	ST6GAL1;B4GALT1;OGT
Ether lipid metabolism	17/958	0.001683	0.005737	13.92567	88.9491	PLA2G10;PLA2G2A;PLA2G5
Glucagon signaling pathway	4/107	0.001763	0.005889	8.358379	52.99649	PRMT1;AKT3;PYGM;PRKACA
Cysteine and methionine metabolism	18/323	0.001784	0.005889	13.62869	86.25608	AHCY;AMD1;SRM
Endocrine and other factor-regulated calcium reabsorption	19/419	0.00211	0.006857	12.80903	78.91737	PRKCB;PRKCA;PRKACA
Chemokine signaling pathway	5/192	0.002336	0.007396	5.793324	35.10362	PRKCB;ROCK2;AKT3;PRKCD;PRKACA
Regulation of lipolysis in adipocytes	20/149	0.002347	0.007396	12.31514	74.56497	AKT3;ADORA1;PRKACA
Thyroid hormone signaling pathway	4/121	0.002759	0.008564	7.353029	43.33133	PRKCB;AKT3;PRKCA;PRKACA
Platelet activation	4/124	0.003013	0.009217	7.168116	41.60881	P2RY12;ROCK2;AKT3;PRKACA
Arachidonic acid metabolism	22/341	0.003153	0.009505	11.03782	63.57044	PLA2G10;PLA2G2A;PLA2G5
Purine metabolism	4/129	0.003473	0.010319	6.879652	38.95834	ENTPD2;NT5M;HPRT1;ADA
Human immunodeficiency virus 1 infection	5/212	0.003575	0.010437	5.228274	29.45467	PRKCB;AKT3;BCL2;PRKCA;BCL2L1
GnRH secretion	23/437	0.003613	0.010437	10.49339	59.00739	PRKCB;AKT3;PRKCA
Dopaminergic synapse	4/132	0.00377	0.010742	6.717391	37.4877	PRKCB;AKT3;PRKCA;PRKACA
Glycolysis / Gluconeogenesis	24/532	0.004111	0.011402	10	54.9406	GAPDH;HK2;HK1
Long-term potentiation	24/532	0.004111	0.011402	10	54.9406	PRKCB;PRKCA;PRKACA
Amphetamine addiction	25/263	0.004465	0.012063	9.695992	52.46875	PRKCB;PRKCA;PRKACA
Renin secretion	25/263	0.004465	0.012063	9.695992	52.46875	ADORA1;REN;PRKACA

Measles	4/139	0.00453	0.01208	6.366828	34.36223	CCNE2;AKT3;BCL2;BCL2L1
Melanoma	26/359	0.005031	0.01308	9.273025	49.07462	AKT3;FGF1;FGF2
Non-small cell lung cancer	26/359	0.005031	0.01308	9.273025	49.07462	PRKCB;AKT3;PRKCA
p53 signaling pathway	26/724	0.005228	0.013426	9.140092	48.01905	CCNE2;BCL2;BCL2L1
Glioma	27/454	0.005637	0.014127	8.885305	46.01125	PRKCB;AKT3;PRKCA
Thyroid hormone synthesis	27/454	0.005637	0.014127	8.885305	46.01125	PRKCB;PRKCA;PRKACA
Pancreatic cancer	27/820	0.005849	0.014483	8.763146	45.05592	AKT3;VEGFA;BCL2L1
Adrenergic signaling in cardiomyocytes	4/150	0.005922	0.014492	5.883859	30.17873	AKT3;BCL2;PRKCA;PRKACA
Oxytocin signaling pathway	4/154	0.006492	0.01552	5.725797	28.84213	PRKCB;ROCK2;PRKCA;PRKACA
mTOR signaling pathway	4/154	0.006492	0.01552	5.725797	28.84213	PRKCB;AKT3;PRKCA;EIF4E
JAK-STAT signaling pathway	4/162	0.007738	0.018289	5.433682	26.41657	AKT3;BCL2;PTPN2;BCL2L1
ErbB signaling pathway	31/107	0.007967	0.018619	7.797797	37.68251	PRKCB;AKT3;PRKCA
Insulin secretion	31/472	0.008227	0.018804	7.703459	36.97957	PRKCB;PRKCA;PRKACA
Taste transduction	31/472	0.008227	0.018804	7.703459	36.97957	ENTPD2;P2RY4;PRKACA
Wnt signaling pathway	4/166	0.008416	0.019028	5.298443	25.31394	PRKCB;ROCK2;PRKCA;PRKACA
Gap junction	32/203	0.008761	0.019404	7.521442	35.63267	PRKCB;PRKCA;PRKACA
Hepatocellular carcinoma	4/168	0.008769	0.019404	5.233298	24.78753	PRKCB;AKT3;PRKCA;BCL2L1
GABAergic synapse	32/568	0.009035	0.019782	7.433608	34.98719	PRKCB;PRKCA;PRKACA
IL-17 signaling pathway	34/394	0.010483	0.022714	7.023396	32.01249	HSP90AA1;MMP13;MMP9
Fructose and mannose metabolism	12/086	0.010928	0.023434	13.63967	61.60202	HK2;HK1
NOD-like receptor signaling pathway	4/181	0.011303	0.023979	4.845738	21.7219	HSP90AA1;PRKCD;BCL2;BCL2L1
Circadian entrainment	35/490	0.011413	0.023979	6.798216	30.40849	PRKCB;PRKCA;PRKACA
Choline metabolism in cancer	35/855	0.011733	0.024163	6.726316	29.9008	PRKCB;AKT3;PRKCA
Glycerophospholipid metabolism	35/855	0.011733	0.024163	6.726316	29.9008	PLA2G10;PLA2G2A;PLA2G5
Progesterone-mediated oocyte maturation	3/100	0.012389	0.025263	6.586964	28.92314	HSP90AA1;AKT3;PRKACA
Melanogenesis	3/101	0.012724	0.025696	6.519421	28.45231	PRKCB;PRKCA;PRKACA
Amoebiasis	3/102	0.013065	0.0259	6.453242	27.99294	PRKCB;PRKCA;PRKACA
Neutrophil extracellular trap formation	4/189	0.013075	0.0259	4.634313	20.09941	SELP;PRKCB;AKT3;PRKCA

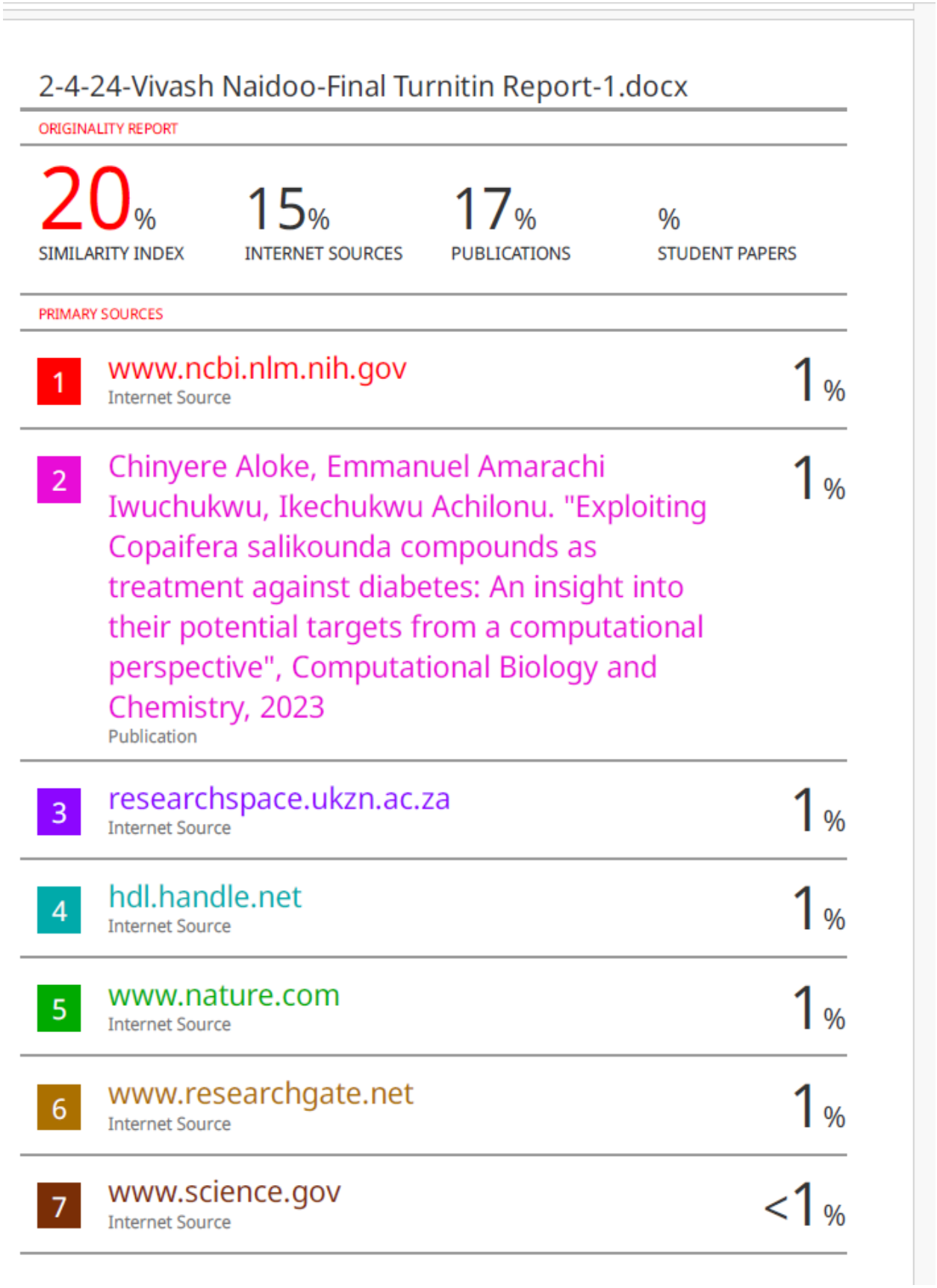
African trypanosomiasis	13/547	0.013615	0.0263	12.07842	51.89612	PRKCB;PRKCA
Aldosterone-regulated sodium reabsorption	13/547	0.013615	0.0263	12.07842	51.89612	PRKCB;PRKCA
NF-kappa B signaling pathway	3/104	0.013762	0.0263	6.324816	27.10706	PRKCB;BCL2;BCL2L1
Transcriptional misregulation in cancer	4/192	0.013782	0.0263	4.559667	19.5354	FLT3;DOT1L;MMP9;BCL2L1
Primary immunodeficiency	13/912	0.014327	0.02709	11.74232	49.85354	PTPRC;ADA
Toxoplasmosis	3/112	0.01676	0.031406	5.858242	23.95295	AKT3;BCL2;BCL2L1
Serotonergic synapse	3/113	0.017158	0.031866	5.804692	23.59764	PRKCB;PRKCA;PRKACA
Glutamatergic synapse	3/114	0.017562	0.032327	5.752107	23.25011	PRKCB;PRKCA;PRKACA
Neurotrophin signaling pathway	3/119	0.01966	0.03587	5.502781	21.62143	AKT3;PRKCD;BCL2
Human T-cell leukemia virus 1 infection	4/219	0.021255	0.038443	3.981598	15.33385	CCNE2;AKT3;PRKACA;BCL2L1
Amino sugar and nucleotide sugar metabolism	17/564	0.022288	0.039965	9.185014	34.93712	HK2;HK1
Arginine and proline metabolism	18/295	0.024056	0.042047	8.801418	32.80628	AMD1;SRM
N-Glycan biosynthesis	18/295	0.024056	0.042047	8.801418	32.80628	ST6GAL1;B4GALT1
Vibrio cholerae infection	18/295	0.024056	0.042047	8.801418	32.80628	PRKCA;PRKACA
FoxO signaling pathway	3/131	0.025236	0.043742	4.983871	18.33811	PRMT1;SETD7;AKT3
Apelin signaling pathway	3/137	0.028311	0.048666	4.759268	16.9645	PRKCE;AKT3;PRKACA
Hedgehog signaling pathway	20/486	0.029688	0.050615	7.821119	27.5071	BCL2;PRKACA
Apoptosis	3/142	0.031018	0.052454	4.586911	15.93114	AKT3;BCL2;BCL2L1
Spinocerebellar ataxia	3/143	0.031576	0.052966	4.553917	15.73544	PRKCB;AKT3;PRKCA
Long-term depression	21/947	0.033704	0.055892	7.280264	24.68105	PRKCB;PRKCA
Breast cancer	3/147	0.033858	0.055892	4.426523	14.98637	AKT3;FGF1;FGF2
Cell adhesion molecules	3/148	0.034441	0.055967	4.395773	14.80713	SELP;MAG;PTPRC
Retrograde endocannabinoid signaling	3/148	0.034441	0.055967	4.395773	14.80713	PRKCB;PRKCA;PRKACA
Necroptosis	3/159	0.041204	0.065931	4.08354	13.02331	HSP90AA1;BCL2;PYGM
Acute myeloid leukemia	24/504	0.041207	0.065931	6.493944	20.71014	FLT3;AKT3
Fc epsilon RI signaling pathway	24/869	0.042326	0.067204	6.395229	20.224	AKT3;PRKCA
Renal cell carcinoma	25/235	0.043456	0.068476	6.29946	19.75514	AKT3;VEGFA
Tight junction	3/169	0.047889	0.074895	3.8356	11.65586	ROCK2;PRKCE;PRKACA

Influenza A	3/172	0.049993	0.077601	3.76694	11.28527	PRKCB;AKT3;PRKCA
Chronic myeloid leukemia	27/791	0.051674	0.079616	5.701553	16.89258	AKT3;BCL2L1
B cell receptor signaling pathway	29/618	0.057856	0.088485	5.339348	15.2161	PRKCB;AKT3
Alcoholism	3/186	0.060394	0.091692	3.476291	9.757505	ADORA2A;ADORA2B;PRKACA
CRC	31/444	0.06428	0.096886	5.020263	13.77814	AKT3;BCL2
Kaposi sarcoma-associated herpesvirus infection	3/193	0.065945	0.09868	3.347029	9.100346	AKT3;FGF2;VEGFA
Bile secretion	32/905	0.069584	0.103382	4.791103	12.76932	SLC10A2;PRKACA
Epstein-Barr virus infection	3/202	0.073415	0.1083	3.194197	8.342066	CCNE2;AKT3;BCL2
Human papillomavirus infection	4/331	0.075199	0.110151	2.602978	6.73551	CCNE2;AKT3;PRKACA;VEGFA
Phosphatidylinositol signaling system	35/462	0.079196	0.115194	4.436506	11.25024	PRKCB;PRKCA
Glycosaminoglycan degradation	44/580	0.087403	0.125626	11.62924	28.34313	HPSE
Regulation of actin cytoskeleton	3/218	0.087576	0.125626	2.954089	7.193941	ROCK2;FGF1;FGF2
C-type lectin receptor signaling pathway	2/104	0.089194	0.126206	4.13058	9.983378	AKT3;PRKCD
T cell receptor signaling pathway	2/104	0.089194	0.126206	4.13058	9.983378	PTPRC;AKT3
One carbon pool by folate	44/581	0.091787	0.128133	11.01662	26.31079	TYMS
Steroid biosynthesis	44/581	0.091787	0.128133	11.01662	26.31079	FDFT1
Terpenoid backbone biosynthesis	44/583	0.100494	0.138277	9.966416	22.8994	FNTA
Coronavirus disease	3/232	0.100839	0.138277	2.771517	6.358498	SELP;PRKCB;PRKCA
TNF signaling pathway	2/112	0.101048	0.138277	3.828627	8.775815	AKT3;MMP9
Mannose type O-glycan biosynthesis	44/584	0.104816	0.14157	9.512919	21.45681	B4GALT1
Renin-angiotensin system	44/584	0.104816	0.14157	9.512919	21.45681	REN
Parkinson disease	3/249	0.117951	0.158283	2.57776	5.509928	ADORA2A;PRKACA;BCL2L1
Oocyte meiosis	2/129	0.127537	0.17005	3.313285	6.823198	CCNE2;PRKACA
Natural killer cell mediated cytotoxicity	2/131	0.130755	0.173229	3.261587	6.635479	PRKCB;PRKCA
Yersinia infection	2/137	0.140517	0.184984	3.115682	6.114306	ROCK2;AKT3
Signaling pathways regulating pluripotency of stem cells	2/143	0.150431	0.19679	2.982194	5.649021	AKT3;FGF2
Nicotinate and nicotinamide metabolism	12/785	0.155109	0.201642	6.151703	11.46448	NT5M

Phospholipase D signaling pathway	2/148	0.158798	0.204368	2.879335	5.29833	AKT3;PRKCA
DNA replication	13/150	0.159172	0.204368	5.975639	10.98186	POLA1
Cushing syndrome	2/155	0.170653	0.217187	2.746628	4.856371	CCNE2;PRKACA
Various types of N-glycan biosynthesis	14/246	0.171244	0.217187	5.503047	9.711048	B4GALT1
Cellular senescence	2/156	0.172359	0.217277	2.728654	4.797451	CCNE2;AKT3
Vasopressin-regulated water reabsorption	16/72	0.190984	0.239305	4.861934	8.049253	PRKACA
Pathways of neurodegeneration	4/475	0.194464	0.241275	1.793871	2.93748	PRKCB;BCL2;PRKCA;BCL2L1
Glycosphingolipid biosynthesis	16/438	0.194876	0.241275	4.751196	7.770074	B4GALT1
Protein processing in endoplasmic reticulum	2/171	0.198257	0.244008	2.484578	4.020524	HSP90AA1;BCL2
Cocaine addiction	17/899	0.210259	0.257258	4.354386	6.790303	PRKACA
Tuberculosis	2/180	0.214018	0.258862	2.357877	3.635124	AKT3;BCL2
Malaria	18/264	0.214059	0.258862	4.265306	6.57499	SELP
Axon guidance	2/182	0.217538	0.260407	2.331442	3.556338	ROCK2;PRKCA
Ovarian steroidogenesis	18/629	0.217841	0.260407	4.179789	6.369963	PRKACA
Glycosaminoglycan biosynthesis	19/360	0.225351	0.267845	4.018623	5.988141	B4GALT1
Glutathione metabolism	20/821	0.240157	0.283822	3.730827	5.321881	SRM
Endometrial cancer	21/186	0.243815	0.285215	3.665189	5.17285	AKT3
Pathogenic Escherichia coli infection	2/197	0.244078	0.285215	2.150464	3.032731	ROCK2;GAPDH
Viral carcinogenesis	2/203	0.25474	0.296011	2.085636	2.852133	CCNE2;PRKACA
Cortisol synthesis and secretion	23/743	0.268935	0.31077	3.263158	4.285455	PRKACA
Mitophagy	24/838	0.279447	0.321132	3.116575	3.973459	BCL2L1
Adipocytokine signaling pathway	25/204	0.282917	0.323334	3.070588	3.876929	AKT3
Prolactin signaling pathway	25/569	0.286371	0.325493	3.025934	3.783832	AKT3
Adherens junction	25/934	0.289808	0.32761	2.982556	3.694001	PTPN1
Leishmaniasis	28/126	0.310092	0.348644	2.74626	3.215561	PRKCB
Antigen processing and presentation	28/491	0.313416	0.350487	2.710458	3.144738	HSP90AA1
PD-L1 expression and PD-1 checkpoint pathway in cancer	32/509	0.348954	0.388141	2.370335	2.495525	AKT3
Rheumatoid arthritis	33/97	0.36142	0.399869	2.266819	2.306973	VEGFA

Staphylococcus aureus infection	34/70	0.367565	0.404516	2.218365	2.220264	SELP
Dilated cardiomyopathy	35/65	0.370615	0.405726	2.194903	2.178643	PRKACA
Prion disease	2/273	0.377862	0.411318	1.541415	1.500145	PRKCD;PRKACA
Hematopoietic cell lineage	36/161	0.379678	0.411318	2.12739	2.060231	FLT3
Chagas disease	1/102	0.388612	0.418816	2.063887	1.95073	AKT3
Toll-like receptor signaling pathway	1/104	0.394498	0.422967	2.023608	1.882242	AKT3
Th17 cell differentiation	1/107	0.403221	0.430102	1.966038	1.785695	HSP90AA1
Herpes simplex virus 1 infection	3/498	0.429297	0.45558	1.264842	1.069559	AKT3;BCL2;BCL2L1
AMPK signaling pathway	1/120	0.439606	0.464152	1.750111	1.438376	AKT3
Cell cycle	1/124	0.450353	0.473098	1.692854	1.35043	CCNE2
Osteoclast differentiation	1/127	0.458279	0.479005	1.652297	1.28925	AKT3
Lysosome	1/128	0.460896	0.479332	1.639204	1.2697	GAA
Amyotrophic lateral sclerosis	2/364	0.523898	0.541999	1.148584	0.742512	BCL2;BCL2L1
Non-alcoholic fatty liver disease	1/155	0.527011	0.541999	1.349966	0.864699	AKT3
Alzheimer disease	2/369	0.531254	0.541999	1.132645	0.716416	AKT3;GAPDH
Hepatitis C	1/157	0.531576	0.541999	1.332524	0.842034	AKT3
Hippo signaling pathway	1/163	0.545012	0.552987	1.282781	0.778581	FGF1
RNA transport	1/186	0.593073	0.598831	1.121991	0.58617	EIF4E
Thermogenesis	1/232	0.67463	0.677889	0.896468	0.352842	PRKACA
Olfactory transduction	1/440	0.882429	0.882429	0.466731	0.058377	PRKACA

Appendix 5: Plagiarism report



2-4-24-Vivash Naidoo-Final Turnitin Report-1.docx

ORIGINALITY REPORT

20%	15%	17%	%
SIMILARITY INDEX	INTERNET SOURCES	PUBLICATIONS	STUDENT PAPERS

PRIMARY SOURCES

1	www.ncbi.nlm.nih.gov Internet Source	1%
2	Chinyere Aloke, Emmanuel Amarachi Iwuchukwu, Ikechukwu Achilonu. "Exploiting Copaifera salikounda compounds as treatment against diabetes: An insight into their potential targets from a computational perspective", Computational Biology and Chemistry, 2023 Publication	1%
3	researchspace.ukzn.ac.za Internet Source	1%
4	hdl.handle.net Internet Source	1%
5	www.nature.com Internet Source	1%
6	www.researchgate.net Internet Source	1%
7	www.science.gov Internet Source	<1%